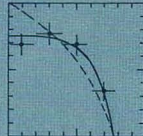
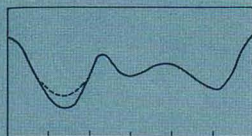


FRONTIERS IN PHYSICS

COLLIDER PHYSICS

UPDATED EDITION



Vernon D. Barger
Roger J.N. Phillips

S 34.1
BAR

Collider Physics

Updated Edition

Vernon D. Barger
University of Wisconsin-Madison

Roger J. N. Phillips

Reg. F. C.
25488



ADDISON-WESLEY PUBLISHING COMPANY
The Advanced Book Program



*Reading, Massachusetts • Menlo Park, California • New York
Don Mills, Ontario • Harlow, England • Amsterdam
Bonn • Sydney • Singapore • Tokyo • Madrid • San Juan
Paris • Seoul • Milan • Mexico City • Taipei*

Many of the designations used by manufacturers and sellers to distinguish their products are claimed as trademarks. Where those designations appear in this book and Addison-Wesley was aware of a trademark claim, the designations have been printed in initial capital letters.

Library of Congress Cataloging-in-Publication Data

Barger, V. (Vernon), 1938-

Collider physics / Vernon Barger, Roger Phillips. —Updated ed.

p. cm. — (Frontiers in physics ; v. 71)

Includes bibliographical references and index.

ISBN 0-201-14945-1

1. Colliders (Physics) 2. Particles (Nuclear physics) 3. Nuclear reactions. I. Phillips, Roger. II. Title. III. Series.

QC787.C59B37 1996

539.7'2—dc21

96-39421

CIP

Copyright © 1987, 1997 by Addison-Wesley Publishing Company, Inc.

All rights reserved. No part of this publication may be reproduced, stored in a retrieval system, or transmitted, in any form or by any means, electronic, mechanical, photocopying, recording, or otherwise, without prior written permission of the publisher. Printed in the United States of America.

Cover design by Lynne Reed

This book was originally typeset in T_EX using a VMS-based T_EX system running on a Micro VAX II computer. Camera-ready output from an Imagen 8/300 Laser Printer.

1 2 3 4 5 6 7 8 9 10-MA-0100999897

First printing, December 1996

*To the honor and memory of our parents
Joseph Frank and Olive Barger
Edward and Enid Phillips*

Preface

During the last twenty years or so there have been astonishing advances in discovering and understanding the fundamental particles and forces of Nature, from which the universe is built. Even the general public has become aware of this progress, as the news media carry occasional items about the discovery of new quarks or leptons or gauge bosons (names that have come to sound familiar) or about new theories to explain submicroscopic physics.

The way was opened by a series of accelerators constructed in many different laboratories around the world to study particle collisions at higher and higher energies. In quantum theory high energies imply short wavelengths, which are essential for probing small-scale phenomena. The latest of these accelerator projects are “colliders,” based on the principle of colliding particle beams, which is now the most economical way to achieve the highest energies. Future plans are centered on colliders as the best way forward.

This book offers an introduction to fundamental particles and their interactions at the level of a lecture course for graduate students, with particular emphasis on the aspects most closely related to colliders—past, present and future. Our intent is that it serve a dual purpose as textbook and handbook for collider physics phenomenology. The emphasis is on fundamental hard scattering processes in e^+e^- , ep , $\bar{p}p$ and pp collisions; two photon processes in e^+e^- and diffractive processes in $\bar{p}p$, pp are not covered. Representative references are given at the end of the book as an introductory guide to the vast literature on collider physics.

We wish to gratefully acknowledge assistance from many colleagues and graduate students in the preparation of this book. T. Han

provided invaluable physics input and editing. W.-Y. Keung contributed Appendix B and suggested several techniques used in early chapters. G. Ross, X. Tata and K. Whisnant gave advice on supersymmetry and superstrings, S. Willenbrock and D. Zeppenfeld on W -pair production, T. Gottschalk and R. Roberts on QCD. M. G. Olson, C. J. Suchyta and R. Marshall each supplied a figure. We also benefited from research collaborations and discussions with many others, at the University of Wisconsin, at the Rutherford Appleton Laboratory, and elsewhere. Parts of the manuscript were developed at the University of Hawaii and at the Aspen Center for Physics. The manuscript was set in \TeX by Brenda Sprecher who deserves our thanks for her excellent work.

Contents

Chapter 1. Introduction

1.1	Fundamental Forces and Particles	1
1.1.1	Four forces	1
1.1.2	The subnuclear world: leptons and quarks	4
1.1.3	The structure of hadrons	6
1.1.4	Color, confinement and jets	9
1.1.5	Gauge theories	11
1.1.6	Higher symmetries, more unification	16
1.1.7	New physics below 1 TeV	21
1.2	Colliders	22
1.2.1	High energies and the collider principle	22
1.2.2	Progress of colliders	24
1.2.3	Typical apparatus	29
1.3	Future Outlook	32

Chapter 2. The Standard Electroweak Gauge Model

2.1	Quantum Electrodynamics	34
2.2	Yang-Mills Fields: $SU(2)$ Symmetry	37
2.3	The Unbroken $SU(2)_L \times U(1)_Y$ Model	40
2.4	The Higgs Mechanism	44
2.5	The Effective Four-Fermion Interaction Lagrangian	48
2.6	Parameters of the Gauge Sector	50
2.7	Radiative Corrections	51
2.8	Lepton Masses	52
2.9	Quark Masses and Mixing	53
2.10	Mixing Matrix Parameterization	57
2.11	Experimental Determination of Mixing	60
2.12	Weak Currents	62
2.13	Chiral Anomalies	65

Chapter 3. Lepton and Heavy Quark Decays

3.1	$V - A$ Semileptonic Decay Rates	67
3.2	Muon Decay	70
3.3	Heavy Neutrino Decay	75
3.4	Charm and Bottom Decay Distributions	78
3.4.1	Spectator approximation	78
3.4.2	Charm lifetime and branching fractions	80
3.4.3	Bottom lifetime and branching fractions	82
3.5	General $V \pm A$ Decay Rate	85
3.6	Semileptonic Decay Distributions	86
3.7	Characteristics of Heavy Quark Decays	91
3.7.1	Electron and muon signals	91
3.7.2	Cascade decays	93
3.7.3	Kinematics: lepton isolation and jet p_T	94
3.7.4	Decay neutrinos and missing p_T	100
3.8	Quark Decays to Real W Bosons	101
3.9	Leptonic Decays	104

Chapter 4. Basic e^+e^- and νe^- Processes

4.1	Cross Sections for Fermion-Antifermion Scattering	109
4.2	$e^+e^- \rightarrow \mu^+\mu^-$	112
4.3	Bhabha Scattering	118
4.4	$e^+e^- \rightarrow$ Massive Fermions	119
4.5	Heavy Neutrino Production	121
4.6	$e^+e^- \rightarrow$ Hadrons	125
4.7	Neutrino-Electron Elastic Scattering	130

Chapter 5. Partons and Scaling Distributions

5.1	The Parton Model	134
5.2	Electron (Muon) Deep Inelastic Scattering	136
5.3	Charged Current Deep Inelastic Scattering	143
5.4	Neutrino Neutral Current Scattering	149
5.5	General Form of Structure Functions	150

5.6	Parameterizations of Quark Distributions	155
5.7	Parton Model for Hadron-Hadron Collisions	157
5.8	Drell-Yan Lepton Pair Production	161
5.9	Gluon Distribution	164

Chapter 6. Fragmentation

6.1	Fragmentation Functions	169
6.2	Example: $e^+e^- \rightarrow \bar{p}X$	175
6.3	Heavy Quark Fragmentation	177
6.4	Independent Quark Jet Fragmentation	180
6.5	1 + 1 Dimensional String Model	183
6.6	Gluon Jets	188

Chapter 7. Quantum Chromodynamics (QCD)

7.1	The QCD Lagrangian	193
7.2	The Renormalization Group Equations (RGE)	195
7.3	The Running Coupling	197
7.4	Leading Log Perturbation Theory	202
7.5	Deep Inelastic Structure Function in QCD	204
7.6	Infrared Cancellation	211
7.7	Altarelli-Parisi Equations	215
7.8	Solving the Altarelli-Parisi Equations	219
7.9	Solutions of the A-P Equations	225
7.10	QCD Corrections to Fragmentation	228
7.11	QCD and the Drell-Yan Process	230
7.12	Direct Photons	235

Chapter 8. Weak Boson Production and Decay

8.1	W Decays	236
8.2	Z^0 Decays	242
8.3	Hadronic W -Production	247
8.4	Hadronic Z -Production	251
8.5	$W \rightarrow e\nu$ Production	253
8.6	Transverse Mass	259

8.7	Transverse Motion of W	263
8.8	Weak Boson Decay Angular Distributions	266
8.9	W, Z Pair Production	268
8.10	Effective W, Z Approximation	275

Chapter 9. Jets

9.1	e^+e^- Collisions	279
9.1.1	Two-jet production	279
9.1.2	Three-jet production	286
9.2	Lepton-Nucleon Collisions	294
9.3	Hadron-Hadron Collisions	296
9.3.1	Two-jet production	296
9.3.2	Three-jet production	311
9.3.3	Minijets and multijets	315
9.4	Monte Carlo Shower Simulations	319
9.4.1	Final state showers	319
9.4.2	Some refinements	325
9.4.3	Initial state showers	328

Chapter 10. Heavy Quark Production

10.1	e^+e^- Collisions	331
10.1.1	Quarkonia	331
10.1.2	Open flavor production	339
10.1.3	Flavor oscillations	343
10.2	Leptoproduction	355
10.2.1	Introduction	355
10.2.2	Current-Gluon fusion	356
10.2.3	Charged current cross section	358
10.2.4	Electromagnetic cross section	360
10.2.5	Gluon bremsstrahlung	363
10.2.6	Leptoquarks	365
10.3	Hadroproduction	370
10.3.1	Quarkonia	370
10.3.2	Open flavor production	374

10.3.3	Lepton signals	383
10.3.4	Signatures for top	388
10.3.5	CP Violation	392
10.3.6	W^+W^- signals	395

Chapter 11. Monte Carlo Simulations

11.1	Introduction	397
11.2	First Example: $c \rightarrow se\nu$ Decay	404
11.3	$B\bar{B}$ Production with Cascade Decays	412
11.4	Stratified Sampling	415
11.5	Many-Body Phase Space	416
11.6	$p\bar{p} \rightarrow e^+e^-X$ Drell-Yan Pair Production	422

Chapter 12. Higgs Boson

12.1	Renormalizability	428
12.2	Mass Bounds	430
12.3	Decays of the Higgs Boson	432
12.3.1	Higgs decays to fermions	432
12.3.2	Higgs decay to gluons	432
12.3.3	Higgs decay to two photons	435
12.3.4	Higgs decays to weak bosons	436
12.3.5	Higgs branching fractions	437
12.4	Higgs Boson Production	438
12.4.1	Heavy quarkonium decay	438
12.4.2	Bremsstrahlung from Z or W^\pm bosons	440
12.4.3	Gluon fusion	443
12.4.4	WW and ZZ fusion	445
12.5	Higgs Searches	446
12.5.1	Low mass Higgs ($m_H < M_Z$)	447
12.5.2	Intermediate mass Higgs ($M_Z < m_H < 2M_W$)	447
12.5.3	High mass Higgs ($2M_W < m_H < 1 \text{ TeV}$)	448
12.6	Two Higgs Doublet Model	452
12.7	Majorons	457
12.8	The Technicolor Alternative	460

Chapter 13. A Fourth Generation

- 13.1 Mass Bounds 467
- 13.2 Neutrino Counting 469
- 13.3 Heavy Leptons from W -Decay 473
 - 13.3.1 Leptonic signal 473
 - 13.3.2 Missing p_T signal 475
- 13.4 $e^+e^- \rightarrow L\bar{L}$ Signals 477
 - 13.4.1 Dilepton signals from $\bar{L}L$ 479
 - 13.4.2 Lepton + jets signals from $\bar{L}L$ 480
 - 13.4.3 Four jet + missing energy signal from $\bar{L}L$ 480
- 13.5 Unstable ν_4 480
 - 13.5.1 $W \rightarrow L\nu_L$ limit revisited 481
 - 13.5.2 $e^+e^- \rightarrow L^+L^-$ limit revisited 482
 - 13.5.3 Experimental limits on ν_4 483
- 13.6 Quark Mixing and Decays 485
- 13.7 Decays to Real W -Bosons 489
 - 13.7.1 Superheavy leptons 489
 - 13.7.2 Superheavy quarks 491
 - 13.7.3 e^+e^- Supercollider search 493
- 13.8 Superheavy Quarkonia 496

Chapter 14. Higher Symmetries

- 14.1 Grand Unification 499
- 14.2 Running Couplings 503
- 14.3 Running Masses 506
- 14.4 $SO(10)$ GUTS 509
- 14.5 The Hierarchy Problem 514
- 14.6 Supersymmetry (SUSY) 515
 - 14.6.1 Concept 515
 - 14.6.2 SUSY mass spectrum 521
 - 14.6.3 SUSY searches 526
 - e^+e^- colliders 527
 - $p\bar{p}$ colliders 528
 - supercolliders 531

14.7 SUSY GUTS	532
14.8 Superstrings	533
14.8.1 Strings as particles	533
14.8.2 E_6 GUT classification symmetry	535
14.8.3 Gauge Bosons from E_6	539
14.8.4 Z' mass and mixing constraints	541

Appendix A: Conventions and Feynman Rules

A.1 Four-Vectors and Scalar Product	549
A.2 Gamma Matrices	549
A.3 Trace Theorems and Tensor Contractions	550
A.4 Dirac Spinors	551
A.5 Hermitian Conjugate of Matrix Elements	552
A.6 Fierz-Michael Reordering Transformation	552
A.7 Feynman Rules for Tree Graphs	553
A.8 Phase Space, Cross Sections, Decays	558
A.9 Heavy Quarkonium Matrix Elements	560

Appendix B: Phase Space

B.1 Two-Body Phase Space	561
B.2 Three-Body Phase Space	564
B.2.1 $\pi^- \rightarrow e\bar{\nu}\pi^0$	565
B.2.2 $\mu \rightarrow e\nu_\mu\bar{\nu}_e$	566
B.3 Multiparticle Phase Space	570

Appendix C: Helicity Projection Techniques

C.1 Helicity Basis	571
C.2 $V \pm A$ Interactions	574
C.3 Application: L Production	
via $d\bar{u} \rightarrow W^- \rightarrow L\bar{\nu}_L$ with $L \rightarrow \nu_L e\bar{\nu}_e$	576

Collider Physics

Chapter 1

Introduction

1.1 Fundamental Forces and Particles

1.1.1 Four forces.

The universe appears to be governed by four kinds of forces: strong, electromagnetic, weak and gravitational. Strong forces – also known as nuclear forces – act only at very short distances; they bind quarks together to make nucleons (protons and neutrons) and bind nucleons together to make nuclei. Electromagnetic forces provide the attractions between electrons and nuclei that build atoms and molecules; they control chemistry and the physics of materials. Weak forces lie behind processes like beta-decay, which allows protons to transmute into neutrons and vice versa; they are vital for the synthesis of heavy elements in the early universe and in stellar cores and for the fusion power cycles in stars. Gravitational forces are by far the weakest; they are important for large bodies but negligible for nuclear and sub-nuclear particles, compared to the other forces.

These forces are transmitted by specific fields or particles which are equivalent concepts in relativistic quantum theory. For example, we can describe electromagnetic interactions in terms of photons which are the quantum states of the electromagnetic field. Electron-electron scattering comes from the emission and reabsorption of *virtual* photons as shown in Figure 1.1. The intermediate state

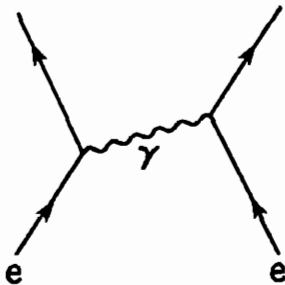


Fig. 1.1. Electron-electron scattering via the emission and reabsorption of a virtual photon.

$e + e + \gamma$ has more energy than the initial or final state and only exists fleetingly on borrowed energy, thanks to the Heisenberg Uncertainty Principle; it is therefore said to be virtual rather than real. The potential energy of such an interaction depends on the couplings at the emission and absorption vertices and on the mass m of the exchanged particle; it falls exponentially with distance r as $\exp(-mr)/r$, but for massless particle exchange this is simply an inverse power law $1/r$ *.

A major achievement of recent years is the discovery that these apparently quite different forces have an underlying unity. It now appears that the fundamental strong forces are transmitted by massless spin-1 gluons, while the weak forces are transmitted by massive spin-1 W and Z bosons, all closely analogous to the photon of electromagnetism. These ideas have been tested and checked in many ways, including the discovery of the gluon in electron-positron collisions and the W and Z in proton-antiproton collisions. The quantum treatment of gravity is still an open question, but the Einstein field equations indicate that it is transmitted by massless spin-2 gravitons. These forces are all described by *gauge theories* (see below); the transmitting particles are *gauge bosons*. Table 1.1 summarizes the fundamental forces and the properties of their gauge bosons.

Figure 1.2 compares the strength and range of the different fundamental forces between a typical pair of particles. Electromagnetism and gravity have massless gauge bosons with $1/r$ behavior for the

* Here and henceforth we use units $\hbar = c = 1$ for convenience.

Table 1.1. *Fundamental forces and gauge bosons. Electric charge is in units of the proton charge, mass is in units GeV for which the proton mass is 0.938.*

<u>Force</u>	<u>boson name</u>	<u>symbol</u>	<u>charge</u>	<u>spin</u>	<u>mass</u>
Strong	gluon	g	0	1	0
Electromagnetic	photon	γ	0	1	0
Weak	{ W-boson	W^\pm	± 1	1	81
	{ Z-boson	Z^0	0	1	92
Gravitational	graviton	G	0	2	0

potential energy, and hence the familiar inverse square law for the force given by the gradient of the potential. Electromagnetic screening does not usually occur at the very small distances illustrated here.

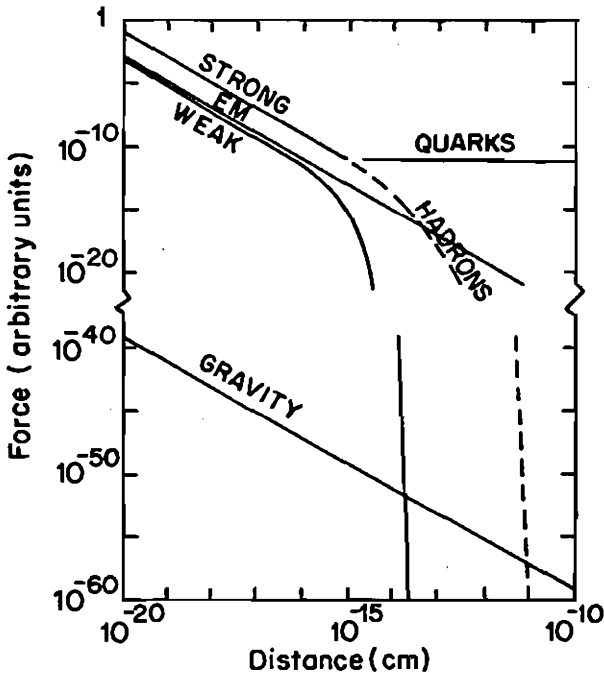


Fig. 1.2. The four fundamental types of force, between a typical pair of particles. (Note the break in the vertical scale.)

Weak interactions have an exponential damping factor $\exp(-mr)$ where $m = M_W$ or M_Z , which cuts them off sharply beyond $r = 2 \times 10^{-16}$ cm. Since strong interactions are mediated by massless gluons, this potential might be expected to fall as $1/r$ but actually behaves quite differently at large r , depending on whether the interaction is between basic quarks or composite hadrons; this is due to the effects of *color* (see below). These advances in understanding basic forces would have been impossible without simultaneous advances in understanding nuclear substructure – that we now come to.

1.1.2 The subnuclear world: leptons and quarks.

When atomic nuclei and the forces within them are probed by high energy collisions, many new particles appear. They are unstable and decay into more familiar particles (protons, electrons, photons, *etc.*), which explains why they did not show up sooner in physics or chemistry. They are very numerous and it is vital to introduce some order into this diversity.

Two particles called μ and τ seem to be simply heavier replicas of the electron. Each has an associated light neutrino and they all have spin- $\frac{1}{2}$. They are known collectively as *leptons* and have no strong interactions.

Apart from the leptons and the γ , W and Z gauge bosons, all other observed particles have strong interactions and are called *hadrons*. They include protons and neutrons, but display much variety in their electric charges, spins and other properties. There is now strong evidence that hadrons are made out of subnuclear constituents called *quarks*, held together by strong forces. There are several different sorts of quark (popularly called *flavors*), which accounts for much of the richness and variety of the hadrons that can be made; see Table 1.2. It is far more economical to tabulate these few quarks than the hundreds of hadrons that can be built from them. The u , c and t flavors of quark have electric charge $\frac{2}{3}$ while d , s and b quarks have charge $-\frac{1}{3}$; all have spin- $\frac{1}{2}$ like the leptons. The t quark was not conclusively established experimentally until 1994, but there had

Table 1.2. Three generations of fundamental spin- $\frac{1}{2}$ particles (units as in Table 1.1).

	<u>name</u>	<u>symbol</u>	<u>charge</u>	<u>mass</u>	<u>type</u>
first generation	up	u	$\frac{2}{3}$	4×10^{-3}	quark
	down	d	$-\frac{1}{3}$	7×10^{-3}	quark
	e -neutrino	ν_e	0	$< 7 \times 10^{-9}$	lepton
	electron	e	-1	5.1×10^{-4}	lepton
second generation	charm	c	$\frac{2}{3}$	1.5	quark
	strange	s	$-\frac{1}{3}$	0.2	quark
	μ -neutrino	ν_μ	0	$< 2.7 \times 10^{-4}$	lepton
	muon	μ	-1	0.106	lepton
third generation	top (truth)	t	$\frac{2}{3}$	~ 175	quark
	bottom (beauty)	b	$-\frac{1}{3}$	4.7	quark
	τ -neutrino	ν_τ	0	$< 2.4 \times 10^{-2}$	lepton
	tau	τ	-1	1.78	lepton

long been strong reasons to believe it existed. The quarks, leptons and gauge bosons listed in Tables 1.1 and 1.2, plus the Higgs particle that we describe later, are the basis of the present understanding of the physical world.

These six quarks and six leptons can be grouped into three *generations* (also called *families*) as shown in Table 1.2. Why Nature chooses to repeat itself like this and whether any more generations remain to be discovered, are still open questions.

Each of the quarks, leptons and gauge bosons above has an associated antiparticle, with the same mass and spin but opposite charge. Thus the antiparticle of the electron e (or e^-) is the positron \bar{e} (or e^+). The antiquarks are denoted \bar{u} , \bar{d} , etc. The antiparticle of W^+ is W^- . The photon, Z^0 and gluon are identical to their antiparticles.

1.1.3 The structure of hadrons.

Two classes of hadrons are found: baryons and mesons. Baryons are fermions (half-integral spins); mesons are bosons (integral spins). Each baryon consists essentially of three quarks; for example, the proton has two u plus one d and the neutron has two d plus one u :

$$p = (uud), \quad n = (ddu).$$

Interchanging u and d quarks has the effect of interchanging protons and neutrons. The neutron-proton symmetry in conventional nuclear physics has its origin in this quark symmetry.

Each meson consists essentially of one quark and one antiquark. For example, the pi meson occurs in three different charge states π^+ , π^- , π^0 which are composed, respectively, of $u\bar{d}$, $d\bar{u}$ and a quantum superposition of $u\bar{u}$ and $d\bar{d}$:

$$\pi^+ = (u\bar{d}), \quad \pi^- = (d\bar{u}), \quad \pi^0 = \left(\frac{u\bar{u} - d\bar{d}}{\sqrt{2}} \right).$$

Other mesons and baryons are excited states of these simple systems or other combinations of quark flavors.

These (qqq) and $(q\bar{q})$ configurations (where q denotes a generic quark) establish the charge and other quantum numbers of baryons and mesons. They are called the *valence* quarks. In addition, a fluctuating cloud (or *sea*) of virtual gluons and neutral $q\bar{q}$ pairs is expected to be present in each hadron, from the laws of quantum mechanics; they do not affect the hadron's quantum numbers but can play a role in high energy collisions as we see in later chapters.

Hadron interactions arise through the interactions of their quark and gluon components. Figure 1.3 shows an electron interacting with a proton by exchanging a photon with one of the quarks. Repeated interactions of this kind are responsible for binding an electron in a hydrogen atom. In high-energy electron-proton collisions however, this kind of interaction can disintegrate the proton; it was in such

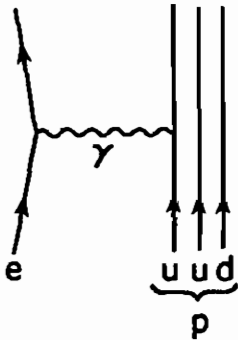


Fig. 1.3. Electron-proton electromagnetic interaction transmitted by a photon.

deep inelastic collisions that the first direct experimental evidence for quarks was found.

Figure 1.4 shows an electron-positron collision producing a J/ψ meson (henceforth abbreviated to ψ) composed of c plus \bar{c} quarks. The initial e^+e^- pair annihilates via a virtual photon to form a $c\bar{c}$ pair which can form ψ when the e^+e^- energy equals m_ψ . Since ψ is unstable it has a finite width and its production is actually a resonance effect around $E = m_\psi$. The discovery of the ψ resonance in e^+e^- annihilation (and simultaneously in proton-nucleus scattering) was one of the first experimental indications that charm quarks exist. This case illustrates $c\bar{c}$ creation but clearly e^+e^- annihilation can create pairs of any fundamental particle that has an electric charge and therefore couples to the photon. The τ lepton was discovered through the creation of $\tau^+\tau^-$ pairs in e^+e^- collisions.

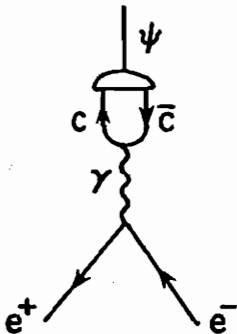


Fig. 1.4. Electromagnetic process $e^+e^- \rightarrow \psi$.

In these figures quarks and leptons have arrows pointing forward in time, antiquarks and antileptons have arrows pointing backwards. This notation brings out the important point that both Figures 1.3 and 1.4 have the same basic vertices where quarks or leptons couple to photons (u and c quarks have the same electric charge and therefore the same coupling to photons). Widely different phenomena are controlled by a few basic interactions.

Figure 1.5 shows neutron beta-decay, $n \rightarrow pe\bar{\nu}_e$, arising from the quark process $d \rightarrow ue\bar{\nu}_e$, with the weak interaction transmitted by a W boson. There is not enough energy in neutron decay to materialize a real W boson, so here it only exists very briefly as a virtual particle. However it is now possible to materialize real W bosons in very high energy collisions; this was first done at the CERN proton-antiproton collider, where the W bosons were detected by their decays into electrons and neutrinos. This process is shown in Fig. 1.6, with the recombination of the final quarks into physical hadrons omitted for simplicity. Here W appears as a resonance in the subprocess $d\bar{u} \rightarrow e\bar{\nu}_e$ at the energy $E = M_W$. Notice that the quark- W and lepton- W vertices of Fig. 1.5 also determine the interaction in Fig. 1.6.

Hadrons containing heavy quarks can decay by processes like Fig. 1.5 in which a heavy quark is transmuted into a lighter one. For example, c changes into d or s , emitting a virtual W^+ which materializes as $e^+\nu_e$, $\mu^+\nu_\mu$, $u\bar{d}$ or $u\bar{s}$.

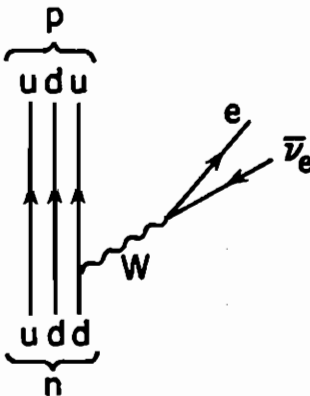


Fig. 1.5. Neutron beta-decay transmitted by a virtual W boson.

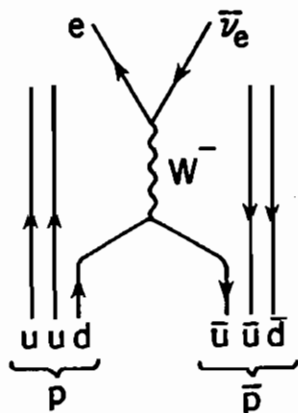


Fig. 1.6. W boson production and decay in $p\bar{p}$ collision.

1.1.4 Color, confinement and jets.

Quarks and gluons alone experience and transmit strong forces. To describe these forces requires a new theoretical concept called *color*. Each quark is supposed to have one of three possible colors: red, blue or green, let us say. Antiquarks are anti-red, anti-blue or anti-green. Gluons carry *two* labels, one color and one anticolor, such that color is conserved at each quark-quark-gluon vertex. For example, a blue quark can turn into a red quark by emitting a blue-anti-red gluon. Only colored particles can emit or absorb a gluon; the corresponding theory of strong forces is called Quantum Chromodynamics or QCD. Leptons and the other gauge bosons are colorless.

Because of color, the strong forces transmitted by gluons differ significantly from the electromagnetic forces transmitted by photons. For example, gluons can couple directly to other gluons whereas photons cannot couple directly to photons. The most striking consequence is color confinement; experiment and theory both suggest that only colorless states are allowed as physical hadrons. In electromagnetic terms, this is like allowing only neutral atoms to exist and forbidding all ionization. The potential energy required to separate two quarks increases linearly with their distance r as implied by Fig. 1.2, due to vacuum polarization that changes the inverse square force law at large r , making the color ionization potential infinite.

Confinement means that neither quarks nor gluons can appear in isolation, they can only exist within colorless (color-neutral) composite hadrons. The strong forces between these hadrons are then like the residual Van der Waals forces between electrically neutral atoms, which are suppressed at large distances. The different behaviors of the interquark and inter-hadron cases shown in Fig. 1.2 are due to confinement and color screening.

The effect of injecting energy into a hadron is not to separate the quarks but to create new quark-antiquark pairs and hence new hadrons, as pictured in Fig. 1.7. Breaking a hadron is somewhat like breaking a bar magnet; the result is not isolated N and S monopoles but the creation of a new pair of poles at the break.

Since they cannot be isolated, quarks and gluons must be studied indirectly. For example, if an electron scatters off a quark, we can get information about the quark by studying the recoiling electron. Also, when a quark or gluon recoils energetically from a hard collision, the broken lines of force behind it lead to a jet of hadrons; from studying the jet one learns about the initiating quark or gluon.

The simplest colorless configurations of quarks are

- (a) three quarks (one red, one blue, one green) and
- (b) quark + antiquark (symmetrical superposition of red + anti-red, blue + anti-blue, green + anti-green).

Remarkably, these are exactly the valence quark combinations that describe the known baryons and mesons.

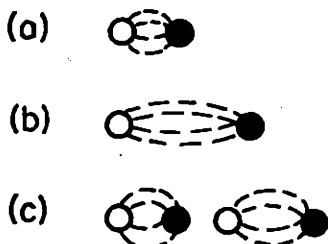


Fig. 1.7. Typical effects of breaking a hadron: (a) original quark-antiquark pair held by color lines of force; (b) lines of force are stretched; (c) lines of force break with the creation of a new quark-antiquark pair.

Colorless configurations can also be made out of gluons alone. QCD studies suggest that hadrons like this (*glueballs*) may exist, but none have yet been conclusively identified and this remains an open question.

1.1.5 Gauge theories.

Quantum electrodynamics (QED) has the vital property that the various unphysical infinite contributions that routinely arise in quantum field theories can all be consistently eliminated; it is said to be *renormalizable*. This can be traced to the fact that it is a *local gauge theory*. Much of the recent progress has come from constructing similar theories for the weak and strong interactions.

QED is a local gauge theory because the Lagrangian function that describes it is unchanged by the following *local gauge transformation* of the electron field $\psi(x)$ and the photon field $A_\mu(x)$ at all space-time points x :

$$\begin{aligned}\psi(x) &\rightarrow \exp[ie\Lambda(x)]\psi(x), \\ A_\mu(x) &\rightarrow A_\mu(x) + \partial\Lambda(x)/\partial x_\mu,\end{aligned}$$

with arbitrary $\Lambda(x)$, where e is the electron-photon coupling (other charged spin- $\frac{1}{2}$ fields transform similarly to ψ). In other words, we can alter $\psi(x)$ by an arbitrary phase factor provided that we simultaneously adjust $A_\mu(x)$ in a suitable way. The photon field plays an intrinsic part; there could be no local gauge invariance without it. Hence if we take the postulate of this local gauge invariance for spin- $\frac{1}{2}$ particles as a starting point, the existence of gauge bosons (in this case photons) is required and in fact their coupling to fermions is specified, too. For exact gauge invariance the gauge bosons must be massless.

The phase factors $\exp[i\Lambda(x)]$ above belong to the symmetry group $U(1)$ of unitary transformations in one dimension. The generalization of QED to other forces is made by looking for other possible symmetry groups and using them as the basis of more general gauge transformations.

For example, we may choose to regard the electron and neutrino as a doublet (ν_e, e) , i.e. as two members of the same family, since both are light spin- $\frac{1}{2}$ particles. We can then describe this doublet by a two-component field $\psi = (\psi_\nu, \psi_e)$ and introduce gauge transformations where Λ is a 2×2 hermitian matrix operating on ψ . We can put the other leptons and the quarks, too, in doublets (ν_μ, μ) , (ν_τ, τ) , (u, d) , etc. and subject them to similar gauge transformations. These transformations are much more than phase factors, since the off-diagonal elements of Λ can change one member of a doublet into the other; they belong to the symmetry group $SU(2)$ of unitary unimodular transformations in two dimensions. Local gauge invariance in this case requires the introduction of three massless spin-1 gauge bosons W^+ , W^- and W^0 , where the superscript is the electric charge. If this is combined with a simultaneous $U(1)$ symmetry (bringing in one more gauge boson B^0), we get the $SU(2)_L \times U(1)$ Glashow-Salam-Weinberg theory of electroweak interactions. The gauge bosons cannot all be massless, experiment excludes this, so the symmetry cannot be exact. The symmetry is broken *spontaneously*, in a way that retains renormalizability; the result is one massless gauge boson γ (made from a linear combination $W^0 \sin \theta_w + B^0 \cos \theta_w$) plus three massive gauge bosons W^+ , W^- and Z^0 (the orthogonal combination $W^0 \cos \theta_w - B^0 \sin \theta_w$). The angle θ_w is a parameter of this unified electroweak theory.

The subscript L on $SU(2)_L$ above indicates that the $SU(2)$ gauge transformations operate only on *left-handed* particles. This is because processes like beta-decay are observed to involve quarks and leptons with left-handed spins relative to their motions. The remaining right-handed states are singlets that do not change under $SU(2)_L$ gauge transformations; for antiquarks and antileptons, interchange L and R . The first-generation spin- $\frac{1}{2}$ particles can be classified in doublet and singlet representations of $SU(2)_L$ as follows:

$$\begin{aligned} & (u_L, d_L), (\nu_{eL}, e_L), \bar{u}_L, \bar{d}_L, \bar{e}_L, \\ & (\bar{d}_R, \bar{u}_R), (\bar{e}_R, \nu_{eR}), u_R, d_R, e_R. \end{aligned}$$

There is no right-handed neutrino (nor left-handed antineutrino) state here; there is no need for such states to exist if the neutrino is massless. Thus we have 15 left-handed (and 15 right-handed) fermion states in each generation counting three colors for each quark flavor, in this gauge theory of electroweak interactions.

The gauge bosons W^+ and W^- transmit *charged current* weak interactions in which one unit of charge is exchanged, as for example in Figs. 1.5-1.6. They transmute one member of a fermion doublet into the other. If each doublet were confined to one generation, they would only give transitions within a generation, such as $u \leftrightarrow d$, $c \leftrightarrow s$, $t \leftrightarrow b$. However, *generation mixing* occurs; the quark doublets in nature appear to be (u_L, d'_L) , (c_L, s'_L) , (t_L, b'_L) where d'_L , s'_L and b'_L are mixtures of d_L , s_L and b_L . As a result, W -couplings allow any of the charge-changing transitions (u or c or t) \leftrightarrow (d or s or b). The heavier quarks can therefore decay by $s \rightarrow u$, $c \rightarrow s$ or d , etc. with the emission of a virtual W that materializes as lighter quarks or leptons. Generation mixing for leptons is an open question and can exist only if neutrinos have masses; the heavier leptons decay via $\mu \rightarrow \nu_\mu$, $\tau \rightarrow \nu_\tau$ transitions; it is not known how or whether any of the neutrinos decay.

Z^0 bosons transmit *neutral current* weak interactions with no change of charge. Celebrated examples are neutrino scattering by quarks or electrons, measurements of which played a vital part in establishing the electroweak theory. Figure 1.8 contrasts neutrino-quark scattering by charged and neutral currents. Z^0 boson interactions transmute singlets and the upper and lower members of doublets into themselves, preserving quark and lepton flavors. During the sixties, however, when only u , d and s quarks were known, the only left-handed quark doublet that could be constructed was $(u_L, d'_L = d_L \cos \theta_C + s_L \sin \theta_C)$ where the *Cabibbo angle* θ_C parameterizes the d - s mixing, leaving the orthogonal state $s'_L = s_L \cos \theta_C - d_L \sin \theta_C$ to be a singlet. This caused a severe difficulty. Given this set of quarks, Z^0 exchange mediates $d'_L \rightarrow d'_L$ (doublet) transitions

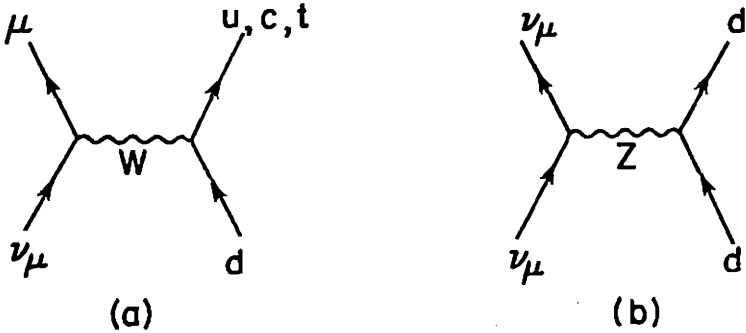


Fig. 1.8. Examples of neutrino-quark scattering via (a) charged current (W -exchange) and (b) neutral current (Z -exchange).

with strength $(\frac{1}{3} \cos^2 \theta_w - \frac{1}{2})$ but $s'_L \rightarrow s'_L$ (singlet) transitions with a different strength $(\frac{1}{3} \cos^2 \theta_w)$; adding them together gives $d \rightarrow d$ and $s \rightarrow s$ transitions plus some *flavor-changing neutral current* $d \rightarrow s$ and $s \rightarrow d$ transitions. The latter are almost completely absent experimentally, flatly contradicting this theory. The solution proposed by Glashow, Iliopoulos and Maiani (GIM) is that a charm quark exists; there is then a second doublet (c_L, s'_L) . The $d' \rightarrow d'$ and $s' \rightarrow s'$ transitions now both refer to doublet members and have equal strengths; when they are added, the offending $d \rightarrow s$ and $s \rightarrow d$ contributions cancel precisely. This GIM mechanism generalizes for any number of quark generations; flavor-changing couplings of Z are absent provided that all quarks have partners, all left-handed components are in doublets and all right-handed components are in singlets. Stringent experimental upper limits on $b \rightarrow d$ and $b \rightarrow s$ neutral current decays indicate that the GIM mechanism is at work here as well and hence that b has a charge $\frac{2}{3}$ partner t , *i.e.* the top quark exists.

In so-called *chiral* theories, where gauge bosons have different couplings to left- and right-handed fermion states (as in the electroweak example above) a new problem arises – typically for the interaction of three gauge bosons via a closed loop of fermions as shown in Fig. 1.9. When the L and R fermion couplings are unequal at one (or three) of the vertices, as is the case in the standard electroweak theory,

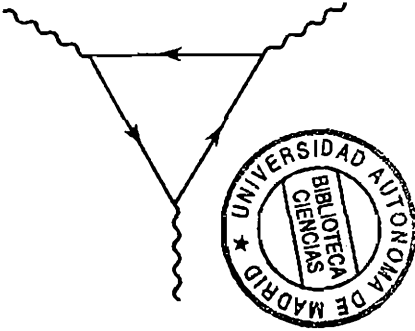


Fig. 1.9. Example of triangle diagram giving chiral anomaly. The external gauge bosons are attached to a fermion loop.

the calculated interaction becomes infinite in an awkward way, that upsets the usual procedures for removing infinities. Each fermion makes a separate contribution to such a *chiral anomaly*. In practice we can only proceed if the sum of fermion contributions exactly cancels in each case, making the theory *anomaly-free*. In the standard electroweak theory above, the fermion contributions from each generation cancel among themselves; it turns out in this case that cancellation requires the electric charges in each generation to sum to zero – which incidentally requires three colors of quark and also demands the existence of a top quark to complete the cancellation in the third generation.

We now turn to strong interactions. Since each quark has three possible colors, we can describe any particular quark flavor by a three-component field $\psi(x) = [\psi(\text{red}, x), \psi(\text{blue}, x), \psi(\text{green}, x)]$ and can consider local gauge transformations where $\Lambda(x)$ is a 3×3 hermitian matrix operating on ψ . These transformations can change the color; they belong to the symmetry group $SU(3)$. To achieve local gauge invariance in this case *requires* the introduction of eight massless gauge bosons which carry pairs of color labels and are precisely the gluons mentioned earlier. This gauge theory is QCD. Combining it with the previous example gives an $SU(3) \times SU(2) \times U(1)$ gauge invariant theory of the strong and electroweak forces, commonly called *the Standard Model*.

With each of these gauge groups ($SU(3)$, $SU(2)$ and $U(1)$) there

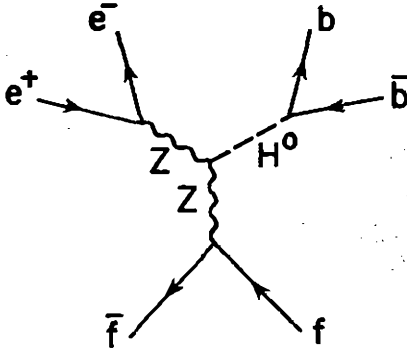


Fig. 1.10. A possible way of producing a Higgs boson H^0 in association with Z^0 . The initial fermion pair $\bar{f}f$ can be e^+e^- or $\bar{q}q$ (quarks from a hadron collision). Decays such as $Z^0 \rightarrow e^+e^-$ and $H^0 \rightarrow b\bar{b}$ could identify these states.

is associated a characteristic coupling strength $\alpha_3, \alpha_2, \alpha_1$ analogous to the fine-structure constant α of electrodynamics. They are sometimes called *coupling constants* but this is a misnomer because their numerical values change logarithmically with the energy scale of the interaction (usually denoted Q) due to renormalization; the name *running couplings* is therefore usually used.

These renormalizable gauge theories allow the presence of spin 0 (*scalar*) particles, too. In fact the usual formulation of the Standard Model requires at least one of these, the Higgs scalar boson, arising from the mechanism for spontaneously breaking the $SU(2) \times U(1)$ electroweak symmetry and giving masses to the weak gauge bosons and to the leptons and quarks. This mechanism is a vital part of the Standard Model. The predicted Higgs scalar would couple most strongly to the heaviest particles and can therefore be produced in association with W or Z and heavy quarks or leptons; Fig. 1.10 shows an example. A major aim of the next collider experiments is to discover the Higgs scalar or scalars.

1.1.6 Higher symmetries, more unification.

Grand Unified Theories (GUTS) postulate that the $SU(3)$, $SU(2)$ and $U(1)$ symmetry groups of the Standard Model have a common origin as subgroups of some larger symmetry group G . At sufficiently large energy scales this symmetry is supposed to be unbroken, all

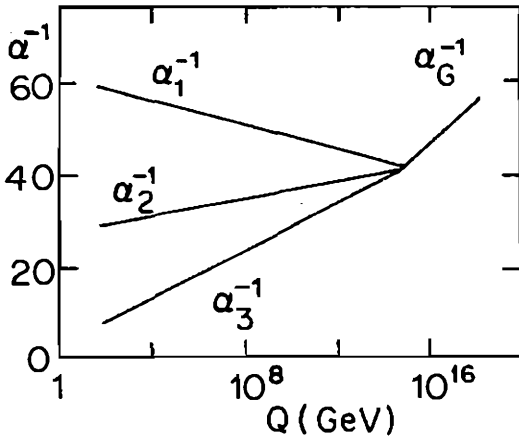


Fig. 1.11. Evolution of the inverse couplings α_i^{-1} with energy according to typical GUT models.

interactions are described by the corresponding local gauge theory and all running couplings coincide $\alpha_3 = \alpha_2 = \alpha_1 = \alpha_G$. Below some critical energy scale Q_{GUT} , G is spontaneously broken and the three α_i become independent, explaining why they differ widely at the much lower energies where they are measured.

This approach also unifies the treatment of quarks and leptons, and may explain why they occur in families. The generators $\Lambda(x)$ of the gauge transformations on spin- $\frac{1}{2}$ particles now operate on multi-component fields $\psi(x)$, that are made up from both quarks and leptons; the details depend on G .

The Lie groups $SU(5)$, $SO(10)$ and E_6 are among those suggested as candidate GUT symmetries. In these examples, the predicted evolution of the running couplings α_3 , α_2 , α_1 upward from the low energy scales where they can be measured is roughly consistent with grand unification somewhere around $Q_{\text{GUT}} = 10^{15}$ GeV. Figure 1.11 sketches this evolution.

GUT models often predict larger families, *i.e.* more quarks and leptons in each generation. For example, the lowest non-trivial representation of $SO(10)$ has 16 members; if we identify such a multiplet of states with the first generation of left-handed fermions, we find that they include all the 15 left-handed states of the standard model above – plus one additional neutrino \bar{N}_L (whose antiparticle N_R could

be interpreted as the hitherto missing right-handed neutrino state). This could explain why the generations occur like this. If instead we take E_6 to be the GUT symmetry, the fundamental representation has 27 members; identifying them with left-handed fermions, we find that 15 correspond precisely with the standard model while 12 are new states:

$$(E_L, \nu_{EL}), (\bar{E}_L, \bar{N}_{EL}), h_L, \bar{h}_L, n_L, \bar{N}_L.$$

Here E is a new charge -1 fermion without color but unlike the electron since both E and \bar{E} are in doublets; h is a new charge $-\frac{1}{3}$ fermion with 3 colors. The appearance of \bar{E} in a doublet and h in a singlet breaks the GIM mechanism and could cause flavor-changing neutral currents if they mix with other leptons and quarks. The additional fermions ν_E, \bar{N}_E, n and \bar{N} are neutral.

GUT models always predict more gauge bosons, since W, Z, γ and g are not enough to secure local gauge invariance with a larger group. Some of these new gauge bosons might have masses of a few hundred GeV, in which case they could be produced and studied experimentally in the near future while others will have masses of the order of the GUT scale. These heavy gauge bosons might be detected indirectly. For example, some GUT gauge bosons transmit exotic new forces which transmuted quarks into leptons or antiquarks, quite unlike the forces transmitted by g, γ, W or Z which preserve the number of quarks minus antiquarks and the number of leptons minus antileptons. Figure 1.12 shows how the processes $uu \rightarrow \bar{d}e^+$ and $ud \rightarrow \bar{u}e^+$ may be mediated by an exotic X -boson with charge $\frac{4}{3}$, leading to proton and neutron decays $p \rightarrow \pi^0 e^+, n \rightarrow \pi^- e^+$. The latter would affect neutrons in stable nuclei where beta-decay is forbidden by energy conservation. This kind of nuclear instability has never been seen but would have striking implications: all nuclear matter would eventually disintegrate into photons and leptons. GUT theories predict that such X -bosons would have enormous masses (comparable to the GUT scale) and hence that nucleon decay via these or other

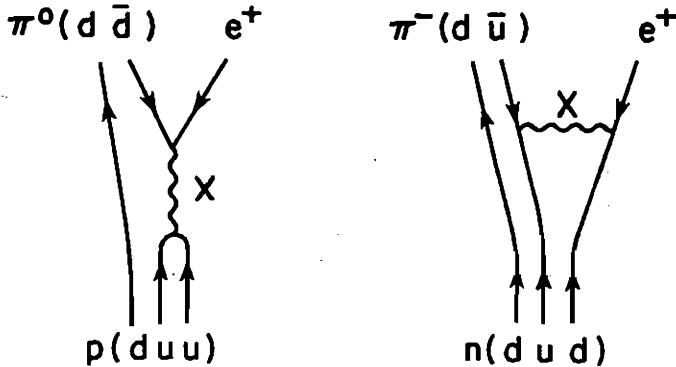


Fig. 1.12. Possible proton and neutron decays mediated by an exotic GUT gauge boson X .

exotic mechanisms would be extremely slow, with mean lifetimes of 10^{30} years or more. This is tantalizingly right in the region of present experimental limits. Large underground detectors containing typically 1000 tons of water or iron (around 10^{33} protons and neutrons) are being used to look for these decays and have set lower limits on the proton lifetime of order 10^{31} years.

GUT models also bring problems, in particular the *hierarchy problem*: how can relatively light mass scales like M_W or M_Z arise naturally in a theory where the basic scale Q_{GUT} is so much larger? A possible answer is Supersymmetry (SUSY), a theoretical idea that goes beyond the quark/lepton and gauge boson unifications of GUTs and attempts to unify the treatment of particles with different spins. It resolves the hierarchy problem and also seems to promise that the spin-2 graviton can be unified with all the other particles (*Supergravity*). It requires every fundamental particle to have a partner, with the same electric charge and other properties like color but with spin differing by half a unit. Thus the leptons and quarks are partnered by spin 0 sleptons and squarks, the photon, gluon, W and Z have spin- $\frac{1}{2}$ photino, gluino, wino and zino partners and so on; see Table 1.3. None of these superpartners have yet been found, but their

Table 1.3. SUSY Particles.

<u>Particle</u>	<u>Spin</u>	<u>Sparticle</u>	<u>Spin</u>
quark q_L, q_R	$\frac{1}{2}$	squark \tilde{q}_L, \tilde{q}_R	0
lepton ℓ_L, ℓ_R	$\frac{1}{2}$	slepton $\tilde{\ell}_L, \tilde{\ell}_R$	0
photon γ	1	photino $\tilde{\gamma}$	$\frac{1}{2}$
gluon g	1	gluino \tilde{g}	$\frac{1}{2}$
W	1	wino \tilde{W}	$\frac{1}{2}$
Z	1	zino \tilde{Z}	$\frac{1}{2}$
Higgs H	0	shiggs \tilde{H}	$\frac{1}{2}$

possible existence is taken seriously since SUSY has powerful theoretical attractions. They may be accessible to discovery with the upcoming colliders.

The huge GUT energy scales are approaching the Planck mass

$$M_{\text{Planck}} = (G_N)^{-\frac{1}{2}} = 1.2 \times 10^{19} \text{ GeV} ,$$

where G_N is Newton's gravitational coupling constant. Here the quantum effects of gravity become important, which makes it essential to include gravity in the theory at such scales.

The latest theoretical developments concern supersymmetric strings (*superstrings*). In string theory the fundamental objects are one-dimensional strings rather than points in space. A string can have excitations (vibrational, *etc.*); the zero mass modes can represent fundamental particle states, both bosons and fermions. Superstring theories have some remarkable properties, for example their quantization requires 10 space-time dimensions and their anomalies are cancelled with fermions appearing in chiral representations only if the gauge symmetry is $E_8 \times E_8$. It is postulated that the extra dimensions are spontaneously *compactified*, *i.e.* they curl up on themselves

on a tiny length scale of order $1/M_{\text{Planck}}$ that makes them invisible, leaving a residual gauge symmetry and a spectrum of particles as their only detectable legacy. A major attraction of superstring theory is its inflexibility; it is not susceptible to arbitrary adjustments. The only room for maneuver at present is in the compactification, but there is hope that this too may turn out to be unique. Superstrings may eventually be a theory of everything.

1.1.7 New physics below 1 TeV.

We have seen that the tally of fundamental particles in Tables 1.1 and 1.2 may well be incomplete, even if we include the t quark. The standard model symmetry breaking mechanism requires at least one Higgs scalar. Alternative proposals such as *Technicolor*, with dynamical symmetry breaking through a new set of interactions, lead to a spectrum of scalar states including leptoquarks – exotic particles that could be produced by lepton-quark fusion. There may be more than three quark/lepton generations. If the replication of generations comes from a new horizontal gauge symmetry, there will be new gauge bosons. GUT models allow the possibility of more fermions in each generation and always predict more gauge bosons. SUSY requires many new particles. Another line of thought suggests that the “fundamental” particles in Tables 1.1 and 1.2 may really be composites, made out of yet more basic particles (*preons*).

The discovery of any new particle would provide invaluable information about the underlying dynamics. Sometimes, as in the case of the W and Z bosons, it can be precisely predicted where the particles should be found – if they exist. A similar situation prevails today for at least two central questions, the Higgs mechanism and supersymmetry. Measurements up to the mass scale 1 TeV will conclusively settle some important issues.

The Higgs mechanism not only provides symmetry breaking and particle masses but also controls the high energy behavior of weak interactions; the mass of the Higgs scalar determines the energy at which weak cross sections stop rising and flatten out. If the Higgs

mass is below 1 TeV it will be detected directly. If not, the interactions between weak bosons are expected to become strong at TeV energies. Similar arguments apply to the Technicolor alternative, where composite particles play a similar role.

Supersymmetry is motivated as a solution to the hierarchy problem. Intimate cancellations between particles and their SUSY partners are an essential part of this picture, but if this is to be effective their mass differences cannot be very large. If this is the correct explanation, at least some of the SUSY partners must have masses below 1 TeV.

For these reasons there is particular interest and emphasis on the mass range up to 1 TeV that will be progressively opened to experiment by present and future colliders.

1.2 Colliders

1.2.1 High energies and the collider principle.

Rutherford's famous experiment of scattering alpha particles from atomic targets was the first dramatic demonstration of scattering techniques in nuclear physics. He was able to show from the angular distribution of the scattered particles that atoms have small massive nuclei at their centers. Further studies established that these nuclei are made of protons and neutrons. Many decades later, electron scattering experiments at much higher energies showed that protons and neutrons themselves contain small hard constituents, the quarks. Higher energies opened the way to deeper understanding.

In optical language, the space resolution that can be achieved in studying the scattering of one particle from another is limited by the wavelength λ of their relative motion: $\lambda = 2\pi/k$ where k is their relative momentum. To probe small distances requires large k which implies high energy in the center-of-mass frame of reference (where their center of mass is at rest and only relative motion remains).

Another reason to ask for high energy is new particle production. A heavy particle of mass m can be materialized only if there is enough spare energy ($E = mc^2$) available in the center-of-mass frame. When the Bevatron was built at Berkeley in the fifties, a major aim was to discover the antiproton; it had been predicted by Dirac but previous accelerators had not provided enough energy to make it in the laboratory. More recently, the CERN $p\bar{p}$ collider project at Geneva was motivated to search for the W and Z bosons predicted by the electroweak theory of Glashow, Salam and Weinberg; previous machines could not provide enough energy to materialize such heavy particles.

Very high energy collisions occur naturally in cosmic ray interactions; they also occurred in the early moments of our universe according to big-bang cosmology. Both these sources provide useful information but they cannot compare with systematic experimentation at accelerator laboratories when this is possible.

When particle 1 in a high-energy beam meets particle 2 in a stationary target, their relative momentum k and their total energy E_{cm} in the center-of-mass frame are

$$E_{cm} = \sqrt{m_1^2 + m_2^2 + 2E_1 m_2} \approx \sqrt{2E_1 m_2}, \quad \left(\begin{array}{l} \text{fixed} \\ \text{target} \end{array} \right)$$

$$k \approx \frac{1}{2} E_{cm},$$

assuming that $E_1 \gg m_1, m_2$. To get high E_{cm} with a fixed target, we need both high beam energy E_1 and substantial target mass m_2 ; hence the target is usually a nucleon. However, E_{cm} increases only as the square root of E_1 . Regrettably, in either linear or circular accelerators of a given design, the construction and operating costs both increase at least linearly with the beam energy, *i.e.* with the square of E_{cm} .

On the other hand, if particle 1 in one beam meets particle 2 in another beam moving in the opposite direction, the available energy becomes

$$E_{cm} = \sqrt{m_1^2 + m_2^2 + 2E_1 E_2 + 2p_1 p_2} \approx \sqrt{4E_1 E_2} \quad \left(\begin{array}{l} \text{colliding} \\ \text{beams} \end{array} \right)$$

where p_1, p_2, E_1, E_2 are the two beam momenta and energies and $k \approx \frac{1}{2}E_{cm}$ as before. This is much better. The particle masses are now immaterial and E_{cm} rises linearly with the beam energies, assuming both are increased together, offering a less expensive route upwards.

The post-war years saw a rapid increase in the energy attainable for proton beams. In the fifties the synchrotron at Berkeley reached 6 GeV; in the sixties the alternating gradient synchrotrons at CERN and Brookhaven reached 30 GeV and the Serpukhov machine gave 70 GeV; by the early seventies the new proton synchrotrons at CERN and Fermilab were running at 400 GeV. These machines also generated secondary hadron beams ($\pi, K, etc.$) to illuminate different aspects of strong interactions, muon and photon beams to probe electromagnetic phenomena and neutrino beams to probe weak scattering processes. They were complemented by a range of electron synchrotrons and the Stanford electron linac giving beams up to 20 GeV. But already in 1971 the highest E_{cm} was to be found at a pp collider; at about the same time, e^+e^- colliders started to produce surprising new results. The colliding beam approach to high energy physics was beginning to pay dividends.

The other major consideration beside energy is luminosity \mathcal{L} , the product of incident beam flux (particles per second) with mean target density (particles per unit area). If the cross section for a particular type of event is σ , the product $\mathcal{L}\sigma$ gives the corresponding event rate. Many important non-strong interaction processes have rather small cross sections and need large luminosities for their detection. Luminosity is a central problem for collider design but happily there have been great advances here, too.

1.2.2 Progress of colliders.

Although we plainly get more E_{cm} and k for given beam energy with colliders, there are also disadvantages and many practical difficulties to overcome.

The obvious disadvantage is low luminosity, low event rate. A normal solid or liquid fixed target has a high density of nucleons and can be made many meters long if necessary, to give a better chance of observing the less probable types of collision. In a colliding beam the "target" particles are more like a low-density gas. This can be partly offset by pinching the beams down to very small size at the crossing points and also (in circular colliders) by bringing the beams around repeatedly to get multiple crossings. Another limitation, coming from the need to store and manipulate the beam particles, is that only charged and stable particles can be used. This restricts the choice to e^- , e^+ , p and \bar{p} beams, but fortunately it does not much restrict the physics potential.

The practical problems should not be underestimated. Many technical difficulties attend the collecting, cooling, stacking and general manipulation of bunches of particles, in a colliding beam system. There are limitations, some apparently fundamental, on the densities of particles that can be stored and on how sharply they can be focused at a collision point. Nevertheless, after three decades of study and development, colliders have become established tools of high energy physics.

The earliest studies at Stanford, Novosibirsk, Frascati and Orsay led first to a number of e^+e^- machines, where bunches of electrons and positrons circulate in opposite directions and collide at regular intervals within a common ring of magnets. By the early seventies, the principles were well understood and center-of-mass energies of many GeV were attained, but this was not all. Electron-positron colliders opened a new window: it had never previously been possible to study e^+e^- annihilation at high E_{cm} because of the limitations of fixed-target kinematics (small m_e). Various spin-1 mesons can be studied in a new way as e^+e^- resonances. The production of a new quark or lepton via $e^+e^- \rightarrow c\bar{c}$, $b\bar{b}$, $\tau\bar{\tau}$ etc. is much simpler theoretically and easier to analyze experimentally than production with a hadron beam and target, because the latter involves five or six

incoming valence quarks. Thus e^+e^- colliders offer new perspectives on particle physics and illustrate the fact that E_{cm} and \mathcal{L} – though very important – are not the only considerations.

The first hadron collider was the Intersecting Storage Rings at CERN that reached $E_{cm} = 63$ GeV for pp collisions (and later for $p\bar{p}$, too). If we think about collisions between participating quarks, however, E_{cm} is much lower: a valence quark carries only about 15% on average (and rarely more than 50%) of the proton energy and a typical antiquark in a proton carries even less (coming only from the small sea of quark-antiquark pairs). The ISR therefore fell far short of making real W or Z bosons via $u\bar{d} \rightarrow W^+$, $u\bar{u} \rightarrow Z^0$, etc. The next step forward was the adaptation of the CERN Super Proton Synchrotron to work as a collider, with p and \bar{p} bunches circulating in the same ring. The SPS collider began running in 1981 with $E_{cm} = 540$ GeV; W and Z bosons were discovered there during the next two years. It has run for brief periods up to 900 GeV but routine operation is limited to 630 GeV by magnet cooling requirements.

The near future offers an exciting range of colliders of all kinds; see Table 1.4. The Fermilab Tevatron has been adapted as a $p\bar{p}$ collider and experiments will run in 1987 with E_{cm} of order 2 TeV (2000 GeV); for quark-antiquark collisions this will effectively explore up to 400 GeV – the highest energy of fundamental particle interactions that will be available anywhere for many years. In the e^+e^- sector, the TRISTAN storage ring in Japan will be going up to 60 GeV. The upcoming Stanford Linear Collider (SLC) has a single-pass layout; a linear accelerator will take alternate e^+ and e^- bunches up to near 50 GeV each and collide them once. Although the particles get only one chance to interact, this is partly compensated by tuning E_{cm} to the Z^0 resonance: $e^+e^- \rightarrow Z^0$. A “ Z^0 factory” such as this will have immense potential to uncover new physics, since Z^0 couples to all particles that have weak interactions. Later the Large Electron-Positron storage ring (LEP) at CERN is scheduled to run, initially up to $E_{cm} = 110$ GeV and eventually to higher energies

Table 1.4 Recent and future colliders. Maximum beam and cm energies are given in GeV; luminosities are given in $\text{cm}^{-2}\text{s}^{-1}$; these are approximate values since running conditions can be changed.

Name	Place	Beams and Energies		E_{cm}	\mathcal{L}
DCI	Orsay	e^+e^-	1.7×1.7	3.4	$2 \cdot 10^{30}$
BEPC	Beijing	"	2.2×2.2	4.4	10^{31}
SPEAR	Stanford	"	4×4	8	10^{31}
DORIS	Hamburg	"	5.6×5.6	11	$3 \cdot 10^{31}$
VEPP 4	Novosibirsk	"	6×6	12	$5 \cdot 10^{31}$
CESR	Cornell	"	6×6	12	$3 \cdot 10^{32}$
PEP	Stanford	"	15×15	30	$6 \cdot 10^{31}$
PETRA	Hamburg	"	23×23	46	$2 \cdot 10^{31}$
TRISTAN	Tsukuba	"	32×32	64	$4 \cdot 10^{31}$
SLC	Stanford	"	50×50	100	10^{30}
LEP I	CERN	"	55×55	110	10^{31}
LEP II	CERN (1996)	"	95×95	190	10^{31}
CLIC	CERN (?)	"	1000×1000	2000	10^{33}
HERA	Hamburg	ep	30×820	315	$2 \cdot 10^{31}$
LHC	CERN (?)	"	50×7000	1200	$2 \cdot 10^{32}$
SPS	CERN	$p\bar{p}$	315×315	630	$6 \cdot 10^{30}$
TEVATRON	FNAL	$p\bar{p}$	1000×1000	2000	10^{31}
ISR	CERN	pp	32×32	63	10^{31}
UNK	Serpukhov (?)	pp	400×3000	2200	10^{33}
LHC	CERN (2003?)	pp	7000×7000	$1.4 \cdot 10^4$	10^{34}
SSC	USA (cancelled 1993)	pp	$2 \cdot 10^4 \times 2 \cdot 10^4$	$4 \cdot 10^4$	10^{33}

where processes like $e^+e^- \rightarrow W^+W^-$ become possible. To complement these machines there will be an ep collider HERA at Hamburg going up to $E_{cm} = 315$ GeV, which will effectively give up to 140 GeV for fundamental lepton-quark scattering.

For the more distant future, a possible next generation of colliders is under discussion. The Superconducting Super-Collider (SSC) project in the USA envisaged $E_{cm} = 40$ TeV with colliding proton

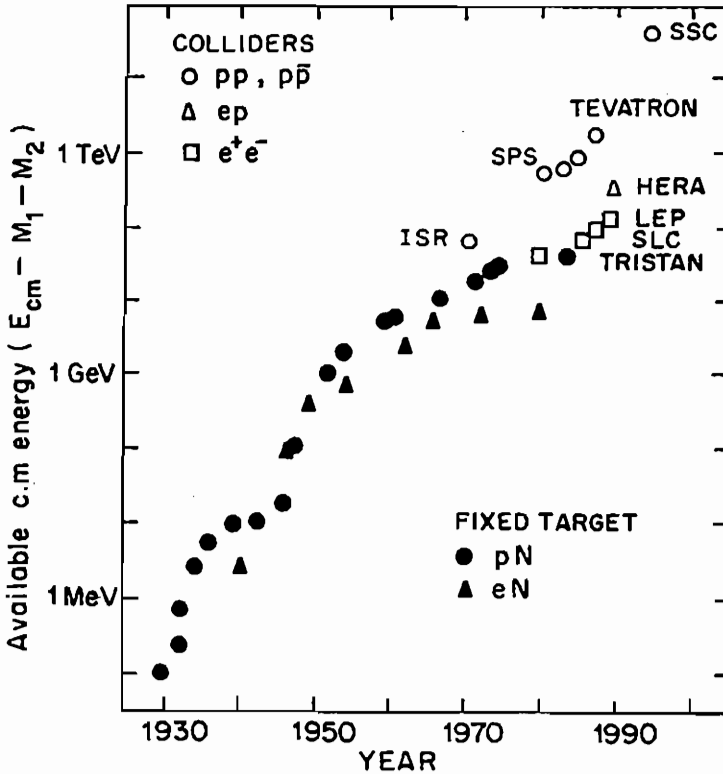


Fig. 1.13. Maximum available center of mass energy as a function of time, for various types of scattering.

rings (but cancelled 1993). In Europe a Large Hadron Collider (LHC) is planned, based on pp rings in the LEP tunnel with collisions in the 14 TeV range; ep collisions would also be possible in such a complex. In the Soviet Union, the possible UNK project includes a 400 GeV proton ring feeding a 3 TeV superconducting ring, initially for fixed target work but with the possibility of colliding the two beams later. In the e^+e^- sector, the feasibility of higher-energy single-pass colliders is being studied and prospects for a 1-2 TeV machine are being discussed by physicists at CERN, SLAC, and TRISTAN.

It is remarkable that the highest attainable energy has been rising approximately exponentially with time since 1930, as one accelerator

technique has succeeded another. Figure 1.13 shows the maximum available c.m. energy ($E_{cm} - m_1 - m_2$) versus time for proton and electron beams in fixed-target and collider experiments. Colliders are the latest chapter in this story.

1.2.3 Typical apparatus.

The bunches of beam particles collide in a vacuum pipe. The apparatus to detect and measure their interactions is assembled around this point. Although details differ from one case to another, detector systems usually have most of the following features, illustrated schematically in Fig. 1.14.

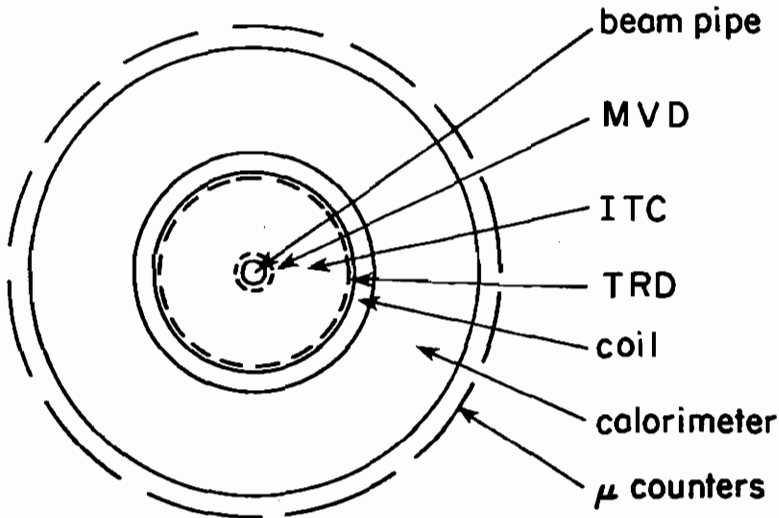


Fig. 1.14. Typical detector system at a collider, looking along the beam; the end-caps contain similar elements.

Beam pipe: made thin to minimize scattering of particles coming out from the interaction. Sometimes detectors are placed inside it.

Microvertex detector (MVD): high resolution detector, as close as possible to the primary vertex, to resolve secondary vertices from short-lived particles that travel a few tens or hundreds of microns before decaying.

Inner tracking chamber (ITC): typically a drift chamber or time-projection chamber recording charged-particle tracks.

Transition radiation detector (TRD): efficient electron identifier (not universally used).

Magnet coils: to give a magnetic field (usually solenoidal) in the ITC. Track curvatures then measure particle momenta. These coils usually form part of the calorimeter.

Calorimeter: alternating layers of material and detectors in which particles make showers which deposit energy and are sampled via their ionization. Total energy deposition is inferred. The pattern of deposition versus depth shows whether the initiating particle is a hadron or electromagnetic (e, γ).

Muon counters: muons are the only charged particles likely to penetrate the iron and other dense material in the calorimeter behind which these counters stand.

High energy collisions frequently produce a large number of particles. An apparatus like that above is well adapted to this situation. It cannot identify many of the individual hadrons emerging from a collision but it can measure a number of things very well, including many things of interest in fundamental quark/lepton/gluon interactions. It can identify and measure the following.

- 1) A high energy jet: seen as a localized peak of hadron energy in a small group of adjoining calorimeter cells, interpreted as originating in a quark or gluon with the corresponding energy and direction (or possibly several nearly collinear quarks and gluons). Calorimetry integrates over the petty details of which hadrons were protons or pions or whatever and gives what theorists really want, the momentum vector of the original fundamental particle(s).
- 2) An electron e^\pm : seen as a charged track in ITC (curvature gives the momentum and sign of charge) plus a TRD signal and/or characteristic pattern in calorimeter. The TRD and calorime-

ter signals are ambiguous or illegible if the e^\pm is accompanied by hadrons in the same angular cells. Hence, e^\pm must be somewhat isolated to be identified. It is hard to spot e^\pm in the middle of a jet.

- 3) A muon μ^\pm : seen as a charged track in ITC (curvature gives momentum and sign) matching with a muon counter. There is a small chance that a π or K meson, decaying in flight to $\mu\nu$, will fake this signal (less likely for faster muons).
- 4) A photon: calorimeter signal like e^\pm but no track in ITC. Any number of photons falling in the same calorimeter cell give the same signal (*e.g.* π^0 meson decaying $\pi^0 \rightarrow \gamma\gamma$).
- 5) Missing transverse momentum. The momentum components of all hadrons, e^\pm , μ^\pm and γ transverse to the beam axis can be measured: (particles that escape down the beam pipe have small transverse momentum). Any significant imbalance in transverse momentum p_T can be attributed to penetrating neutrals which have passed undetected; the latter are usually expected to be one or more neutrinos, but some exotic particles like photinos could also give a missing p_T signature.
- 6) Heavy quarks or leptons: τ leptons and hadrons containing c , b or t quarks could give specific topological signatures in a MVD.

To measure a particular type of interaction, it must be selected and separated from all the other possible interactions. A *trigger* is usually used; only interactions that satisfy specific pre-conditions are fully measured and recorded. Further *selection cuts* are then made to refine the sample of events. For rare events this selection process may be very severe; in the search for $q\bar{q} \rightarrow Z^0 \rightarrow e^+e^-$ events at CERN, less than one event was retained out of every 10^9 interactions. This illustrates an important point about searching for new physics: until you know what you are looking for, you have little chance of finding it. The most systematic way to look for unexpected new effects is to measure very accurately pieces of standard physics that

can be precisely predicted; any significant discrepancy then points to something new.

1.3 Future Outlook

These introductory paragraphs have shown that many questions still remain. For example, why do quarks and leptons appear in generations? Are there more members in each generation? What is the systematics of their masses? Where is the Higgs scalar? Is there more than one? How many more gauge bosons are there? What gauge symmetries lie behind them? Is there a GUT to unify strong with electroweak forces? Where does gravity come in? What about supersymmetry or superstrings? Are there preons?

Particle physics cannot advance without new observations and for this we look to the next round of high energy machines and experiments. They will test present theories still more stringently, seeking discrepancies that point to new physics. They will search for new particles – quarks, leptons, Higgses, SUSY partners, *etc.* – and new types of interaction. Z^0 factories will open a new window on particle production. Studies of $e^+e^- \rightarrow W^+W^-$ will test basic gauge-theory couplings. Electron-proton collisions will probe quark and gluon substructure far more deeply than before; this is where new W bosons or leptoquarks may be found. The $\bar{p}p$ and possible pp colliders will provide interactions between quarks, antiquarks and gluons at previously unattainable energies. Interactions at c.m. energies of order 1 TeV must uncover some new physics, as previously remarked, because there are problems here with present theories unless new ingredients come in. The Higgs scalar, or whatever alternative mechanism causes spontaneous symmetry breaking, must appear. If Supersymmetry is the answer to the hierarchy problem, then SUSY partners should appear, too. The e^+e^- collisions at LEP II and quark and gluon collisions at the Tevatron collider will begin to approach this critical 1 TeV region; supercolliders of the next generation would be

able to explore it thoroughly. The next ten to fifteen years are rich in promise for both experiment and theory.

Chapter 2

The Standard Electroweak Gauge Model

2.1 Quantum Electrodynamics (QED)

Gauge invariance is a central feature of modern field theories, because it ensures that calculated observables are finite (*i.e.*, the amplitudes in a perturbation expansion are renormalizable). QED was the first gauge theory and it is the simplest.

The Lagrangian \mathcal{L} for the massless electromagnetic field A_μ interacting with a spin- $\frac{1}{2}$ field ψ of bare mass m is

$$\mathcal{L} = -\frac{1}{4} F_{\mu\nu} F^{\mu\nu} + \bar{\psi}(i\gamma^\mu D_\mu - m)\psi.$$

Here, $F_{\mu\nu}$ is the electromagnetic field tensor

$$F_{\mu\nu} = \partial_\mu A_\nu - \partial_\nu A_\mu$$

and D_μ is the covariant derivative

$$D_\mu = \partial_\mu + ieA_\mu Q$$

where e is the unit of electric charge and Q is the charge operator (*i.e.* $Q\psi = -\psi$ for an electron). This Lagrangian is invariant under

local gauge transformations

$$\psi(x) \rightarrow U(x)\psi(x), \quad A_\mu(x) \rightarrow A_\mu(x) + \partial_\mu\alpha(x),$$

with

$$U(x) = \exp(-ieQ\alpha(x))$$

and arbitrary $\alpha(x)$. For infinitesimal $\alpha(x)$,

$$\psi(x) \rightarrow (1 - ieQ\alpha(x))\psi(x).$$

It is sufficient to discuss infinitesimal transformations, since finite transformations can be made from them by integration.

Exercise. Demonstrate the invariance of \mathcal{L} under this gauge transformation. (Retain only lowest order in $\alpha(x)$.)

Local gauge invariance demands that there be a *gauge field* A_μ which interacts with fermions in a prescribed way. Had we started from non-interacting ψ fields, the Lagrangian would already have been invariant under global transformations (U independent of x) but local gauge invariance would have required the existence of A_μ fields plus the interaction term

$$\mathcal{L}_{\text{int}} = -eJ_{em}^\mu A_\mu, \quad \text{where } J_{em}^\mu = \bar{\psi}\gamma^\mu Q\psi,$$

and J_{em}^μ is the electromagnetic current.

The Euler-Lagrange equation,

$$\partial_\mu [\partial\mathcal{L}/\partial(\partial_\mu\phi_r)] = \partial\mathcal{L}/\partial\phi_r,$$

obtained from the requirement of stationary action for any field ϕ_r ,

yields the following equations of motion for electromagnetism:

$$\partial_\nu F^{\mu\nu} = J_{em}^\mu, \quad (i\gamma^\mu D_\mu - m)\psi = 0.$$

The electromagnetic current is conserved, $\partial_\mu J_{em}^\mu = 0$, implying conservation of electric charge q , where

$$q = \int J_{em}^0 d^3x.$$

This is an example of Noether's Theorem, that for each continuous symmetry,

$$\phi_r \rightarrow \phi_r - i\epsilon\lambda_{rs}\phi_s,$$

with ϵ an infinitesimal parameter and λ_{rs} constant coefficients, there is a conserved current

$$J_\mu(x) = -i\lambda_{rs}\phi_s \partial\mathcal{L}/\partial(\partial_\mu\phi_r).$$

In the language of group theory, the gauge transformations above with scalar phase $\alpha(x)$ belong to a unitary group $U(1)$ and the full Lagrangian is said to have the symmetry $U(1)_Q$ with the charge operator Q as the generator.

The *minimal coupling* of the photon to spinors above is introduced through the covariant derivative $D_\mu\psi$ and is determined purely by the transformation properties of ψ under the gauge group. Other gauge invariant couplings can be constructed (e.g., $\bar{\psi}\sigma_{\mu\nu}F^{\mu\nu}\psi$) but they are not renormalizable.

2.2 Yang-Mills Fields: SU(2) Symmetry

Gauge transformations can also involve internal degrees of freedom. Consider, for example, an internal symmetry group SU(2) such as isospin under which spin- $\frac{1}{2}$ fields ψ transform as doublets. Their free-field Lagrangian is

$$\mathcal{L} = \bar{\psi}(i\gamma^\mu\partial_\mu - m)\psi,$$

where $\bar{\psi}$ is a row vector and ψ is a column vector in isospin space.

In analogy with QED, we now require invariance under the infinitesimal local gauge transformation

$$\psi(x) \rightarrow [1 - ig \alpha(x) \cdot T]\psi(x),$$

where $\alpha(x)$ is an arbitrary infinitesimal vector in isospin space and $T = (T_1, T_2, T_3)$ is the isospin operator whose components T_i are the generators of SU(2) symmetry transformations. The T_i do not commute,

$$[T_i, T_j] = i\epsilon_{ijk}T_k,$$

and the gauge group is said to be non-abelian. Operating on isospin doublets, the matrix representation is $T_i = \frac{1}{2}\tau_i$ where τ_i are the Pauli matrices.

The ψ -field part of the Lagrangian can be made gauge invariant by introducing an appropriate covariant derivative D_μ :

$$\mathcal{L}_\psi = \bar{\psi}(i\gamma^\mu D_\mu - m)\psi, \quad D_\mu = \partial_\mu + ig\mathbf{W}_\mu \cdot \mathbf{T},$$

provided that an isospin triplet of Yang-Mills gauge fields $W_{i\mu}$ ($i = 1, 2, 3$) exist and transforms simultaneously as

$$W_\mu(x) \rightarrow W_\mu(x) + \partial_\mu\alpha(x) + g\alpha(x) \times W_\mu(x).$$

This transformation on the gauge field is more complicated than in the QED case, because of the non-abelian property. The third term

is needed because the isospin operators in the infinitesimal transformations on $\bar{\psi}$ and ψ do not commute with the isospin operator in D_μ . The gauge invariance of \mathcal{L}_ψ is evident upon inspection.

It remains to choose a gauge-invariant form for the W -field part of the Lagrangian. This can be achieved by taking

$$\mathcal{L}_W = -\frac{1}{4}W_{\mu\nu} \cdot W^{\mu\nu} ,$$

where

$$W_{\mu\nu} = \partial_\mu W_\nu - \partial_\nu W_\mu - gW_\mu \times W_\nu .$$

In addition to the normal kinetic energy terms, this introduces cubic and quartic self-couplings of the W_μ fields. They are essential for gauge invariance.

It is not immediately obvious that \mathcal{L}_W is gauge invariant. The proof brings in general arguments that can be applied to any non-abelian gauge group. We therefore briefly digress to the general case, where the T_i are the generators of some unspecified group, satisfying the commutation relations

$$[T_i, T_j] = i f_{ijk} T_k .$$

The coefficients f_{ijk} are the *structure constants* of the group. In any given representation, the T_i are traceless and normalized by $\text{Tr}(T_i T_j) = c\delta_{ij}$, where c is a constant depending on the representation. There is a gauge field $W_{i\mu}$ for each independent generator T_i and the Lagrangian is defined by

$$\mathcal{L} = -\frac{1}{4}W_{i\mu\nu}W_i^{\mu\nu} + \bar{\psi}(i\gamma^\mu D_\mu - m)\psi ,$$

where

$$W_{i\mu\nu} = \partial_\mu W_{i\nu} - \partial_\nu W_{i\mu} - g f_{ijk} W_{j\mu} W_{k\nu} ,$$

$$D_\mu = \partial_\mu + igW_{i\mu}T_i .$$

We want to show that \mathcal{L} is invariant under the infinitesimal gauge

transformations

$$\begin{aligned}\psi(x) &\rightarrow [1 - ig\alpha_i(x)T_i]\psi(x), \\ W_{i\mu}(x) &\rightarrow W_{i\mu}(x) + \partial_\mu\alpha_i(x) + gf_{ijk}\alpha_j(x)W_{k\mu}(x).\end{aligned}$$

The preliminary steps we suggest as exercises.

Exercise. Show that $\text{Tr}(T_i[T_j, T_k]) = icf_{ijk}$ and hence that f_{ijk} is antisymmetric under the interchange of any pair of indices.

Exercise. Show that the invariance of the $\bar{\psi}\cdots\psi$ terms follows directly from the commutation rules for T_i .

Exercise. From the identity $[T_i, [T_j, T_k]] + (\text{cyclic permutations}) \equiv 0$, derive the Jacobi identities

$$f_{ijm}f_{klm} + (\text{cyclic permutations of } ijk) \equiv 0.$$

Exercise. From these properties of the structure constants, show that $W_{\mu\nu}$ transforms under the gauge transformations as

$$W_{i\mu\nu}(x) \rightarrow W_{i\mu\nu}(x) + gf_{ijk}\alpha_j(x)W_{k\mu\nu}(x).$$

The proof is now simple. The $\bar{\psi}\cdots\psi$ terms in \mathcal{L} are gauge invariant by inspection. $W_{i\mu\nu}$ is not by itself gauge invariant, but the product $W_{i\mu\nu}W_i^{\mu\nu}$ is gauge invariant because f_{ijk} is antisymmetric.

Exercise. Show that a mass term $M^2W^\mu \cdot W_\mu$ would not be gauge invariant, and hence that the W field must be massless for gauge invariance in this model.

We now return to the specific case of SU(2) gauge symmetry. The conserved current of this gauge model is an isovector

$$J^\mu = \bar{\psi}\gamma^\mu\mathbf{T}\psi + \mathbf{W}^{\mu\nu} \times \mathbf{W}_\nu.$$

There are three conserved “charges,” corresponding to the three isospin components of the current \mathbf{J} .

An $SU(2)$ gauge model is a candidate for weak interaction theory, since the isospin triplet W could consist of W^+ , W^0 , W^- bosons to transmit the weak force, with

$$W_\mu^\pm = \frac{1}{\sqrt{2}} (W_{1\mu} \mp iW_{2\mu}) , \quad W_\mu^0 = W_{3\mu} ,$$

where the field operators W_μ^\pm are defined to annihilate W^\pm bosons. However, this model is unsatisfactory for a variety of reasons. Most importantly, the effective low-energy form of weak interactions implies that the charged bosons must be very massive, and also implies a left-handed structure for charged-current couplings. Moreover, it would be desirable to unify weak and electromagnetic interactions in a single gauge theory. The introduction of left-handed fermions and the unification with electromagnetism are carried out in the next section; the generation of masses via spontaneous symmetry breaking is addressed later.

2.3 The Unbroken $SU(2)_L \times U(1)_Y$ Model

To generate the left-handed structure of charged-current weak interactions, an $SU(2)$ gauge symmetry is applied to left-handed fermion fields ψ_L only, where left- and right-handed fields are defined as

$$\psi_L = \frac{1}{2}(1 - \gamma_5)\psi , \quad \psi_R = \frac{1}{2}(1 + \gamma_5)\psi .$$

The fermion mass term $m\bar{\psi}\psi$ is not invariant under $SU(2)_L$, however, since $\bar{\psi}\psi = \bar{\psi}_L\psi_R + \bar{\psi}_R\psi_L$. Therefore, at this stage, we take massless fermions. The conserved quantum number is *weak isospin* T_L ; for notational convenience we shall often omit the subscript L on T_L .

In addition to $SU(2)_L$, an independent $U(1)_Y$ gauge symmetry is introduced whose conserved quantum number Y is called *weak hypercharge*. The $U(1)_Y$ symmetry is essential in order to incorporate

the electric charge Q and unify the weak and electromagnetic interactions in a common gauge structure. The weak hypercharges are specified according to the formula

$$Q = T_3 + \frac{1}{2}Y$$

in analogy with the Gell-Mann-Nishijima formula for strong interaction quantum numbers. Right-handed fermions are assigned to transform under $U(1)_Y$ only; no right-handed neutrino is introduced. Left-handed fermions transform non-trivially under both $SU(2)_L$ and $U(1)_Y$. The weak quantum numbers for the first generation of quarks and leptons are:

	T	T_3	$\frac{1}{2}Y$	Q
ν_{eL}	$\frac{1}{2}$	$\frac{1}{2}$	$-\frac{1}{2}$	0
e_L	$\frac{1}{2}$	$-\frac{1}{2}$	$-\frac{1}{2}$	-1
u_L	$\frac{1}{2}$	$\frac{1}{2}$	$\frac{1}{6}$	$\frac{2}{3}$
d_L	$\frac{1}{2}$	$-\frac{1}{2}$	$\frac{1}{6}$	$-\frac{1}{3}$
e_R	0	0	-1	-1
u_R	0	0	$\frac{2}{3}$	$\frac{2}{3}$
d_R	0	0	$-\frac{1}{3}$	$-\frac{1}{3}$

It is a mystery of the standard model that Y takes these values such that the lepton and quark charges are obtained. With equal numbers of quarks and leptons and three quark colors, these quantum numbers lead to the cancellation of divergent chiral anomaly diagrams; (see §2.13).

The massless gauge fields in this model are an isotriplet W_μ for $SU(2)_L$ and a singlet B_μ for $U(1)_Y$. The Lagrangian is

$$\mathcal{L} = -\frac{1}{4} W^{\mu\nu} \cdot W_{\mu\nu} - \frac{1}{4} B^{\mu\nu} B_{\mu\nu} + \bar{\psi} i \gamma^\mu D_\mu \psi$$

with a separate fermion term for each field ψ_L and ψ_R . The field

tensor $W_{\mu\nu}$ is defined as in the previous section and

$$B_{\mu\nu} = \partial_\mu B_\nu - \partial_\nu B_\mu.$$

The covariant derivative is

$$D_\mu = \partial_\mu + igW_\mu \cdot \mathbf{T} + ig'\frac{1}{2}B_\mu Y.$$

The Lagrangian is invariant under the infinitesimal local gauge transformations for $SU(2)_L$ and $U(1)_Y$ independently:

$SU(2)_L$	$U(1)_Y$
$\psi_L \rightarrow [1 - ig\mathbf{T} \cdot \boldsymbol{\alpha}(x)]\psi_L$	$\psi_L \rightarrow [1 - ig'\frac{1}{2}Y\beta(x)]\psi_L$
$\psi_R \rightarrow \psi_R$	$\psi_R \rightarrow [1 - ig'\frac{1}{2}Y\beta(x)]\psi_R$
$W_\mu \rightarrow W_\mu + \partial_\mu \boldsymbol{\alpha}(x) + g\boldsymbol{\alpha}(x) \times W_\mu$	$W_\mu \rightarrow W_\mu$
$B_\mu \rightarrow B_\mu$	$B_\mu \rightarrow B_\mu + \partial_\mu \beta(x)$

Applied to the isodoublet field ψ_L , the weak isospin operator \mathbf{T} can be represented as $\boldsymbol{\tau}/2$ in terms of the Pauli matrices. We define isospin raising and lowering operators $T^\pm = (T_1 \pm iT_2)/\sqrt{2}$ and hence, $W \cdot \mathbf{T} = W^+T^+ + W^-T^- + W_3T_3$. (Note the sign difference between the conventions in defining W^\pm and T^\pm .)

For the electromagnetic interaction to be unified with the weak interaction in this model, the electromagnetic term $ieQA$ must be contained in the neutral term $i(gW_{3\mu}T_3 + g'\frac{1}{2}B_\mu Y)$ of the covariant derivative. Therefore, the W_3 and B fields must be linear combinations of A and another neutral field Z ; since all the vector boson fields have the same normalization, we can write this relation as

$$\begin{pmatrix} W_3 \\ B \end{pmatrix} = \begin{pmatrix} \cos \theta_w & \sin \theta_w \\ -\sin \theta_w & \cos \theta_w \end{pmatrix} \begin{pmatrix} Z \\ A \end{pmatrix},$$

where θ_w is the electroweak mixing angle. Hence,

$$\begin{aligned} igW_3T_3 + ig'\frac{1}{2}BY &= iA[g \sin \theta_w T_3 + g' \cos \theta_w \frac{1}{2}Y] \\ &+ iZ[g \cos \theta_w T_3 - g' \sin \theta_w \frac{1}{2}Y]. \end{aligned}$$

For the coefficient of A to equal $i\epsilon Q = ie(T_3 + \frac{1}{2}Y)$, we need

$$g = e/\sin \theta_w, \quad g' = e/\cos \theta_w,$$

and hence, $1/g^2 + 1/g'^2 = 1/e^2$. The Z term of the covariant derivative can then be written as

$$D_\mu^Z = ig_Z Z_\mu (T_3 - x_w Q),$$

where we have defined

$$g_Z = \frac{e}{\sin \theta_w \cos \theta_w} \quad \text{and} \quad x_w = \sin^2 \theta_w.$$

The interaction of gauge bosons with any fermion field ψ arises from the term $\bar{\psi} i \gamma^\mu D_\mu \psi$ in \mathcal{L} which can be written as

$$-\mathcal{L}' = eJ_{em}^\mu A_\mu + \frac{g}{\sqrt{2}} \left(J_L^{+\mu} W_\mu^+ + J_L^{-\mu} W_\mu^- \right) + g_Z J_Z^\mu Z_\mu,$$

where

$$\begin{aligned} J_L^{\pm\mu} &= \sqrt{2} \bar{\psi} \gamma^\mu T_L^\pm \psi, \\ J_Z^\mu &= \bar{\psi} \gamma^\mu [T_{3L} - x_w Q] \psi, \\ J_{em}^\mu &= \bar{\psi} \gamma^\mu Q \psi. \end{aligned}$$

The T_L operations vanish on ψ_R and have the representation $T_L = \frac{1}{2}\tau$ on ψ_L isodoublets.

The angle θ_w is a parameter of the model. For given θ_w , all gauge couplings are determined by the electric charge e ; the weak and electromagnetic interactions are thereby unified.

The deficiency of this model as it stands is that the W^\pm and Z bosons and the fermions are all massless. The problem is to generate the required masses while preserving the renormalizability of the gauge theory. This is achieved by spontaneous symmetry breaking, where the gauge symmetry of the Lagrangian remains but is “hidden” by the appearance of a preferred direction in weak isospin space, as described in the following section.

In the unbroken theory, where all gauge bosons are massless, the identification of A and Z as linear combinations of B and W_3 is a purely formal exercise; there is no physical reason to use one pair of fields rather than the other. In the broken theory however, A and Z are the physically distinct mass eigenstates. At momentum transfers $q^2 \gg M_Z^2, M_W^2$ the fermion and gauge boson masses become irrelevant and physical scattering amplitudes are essentially the same as in the unbroken theory; in this sense the symmetry is restored at large q^2 .

2.4 The Higgs Mechanism

In the standard model an $SU(2)$ doublet of scalar fields Φ is introduced. Its self-interactions provide the mechanism for spontaneous symmetry breaking (SSB), giving masses to gauge and fermion fields. It also gives rise to a new neutral scalar particle, the Higgs boson. The additions to the Lagrangian are \mathcal{L}_Φ and \mathcal{L}_Φ^F where

$$\mathcal{L}_\Phi = |D_\mu \Phi|^2 - V(|\Phi|^2),$$

where $|\Phi|^2$ denotes $\Phi^\dagger \Phi$ and \mathcal{L}_Φ^F is the Yukawa coupling of Φ to fermions, which will be discussed later. The most general renormalizable form for the scalar potential V is

$$V = \mu^2 |\Phi|^2 + \lambda |\Phi|^4.$$

We specify the isodoublet to be

$$\Phi = \begin{pmatrix} \phi^+ \\ \phi^0 \end{pmatrix},$$

where ϕ^+ and ϕ^0 are each complex fields with the following quantum numbers:

	T	T_3	$\frac{1}{2}Y$	Q
ϕ^+	$\frac{1}{2}$	$\frac{1}{2}$	$\frac{1}{2}$	1
ϕ^0	$\frac{1}{2}$	$-\frac{1}{2}$	$\frac{1}{2}$	0

In a classical theory with $\mu^2 < 0$ the ground state of $|\Phi|^2$ occurs at $|\Phi|^2 = -\frac{1}{2}\mu^2/\lambda$, as illustrated in Fig. 2.1. The quantum analog is a non-vanishing expectation value of $|\Phi|^2$ in the physical vacuum state. The appearance of this non-vanishing vacuum expectation value selects a preferred direction in weak isospin plus hypercharge space and thereby “spontaneously breaks” the $SU(2) \times U(1)$ symmetry.

It is convenient to introduce the modulus $v/\sqrt{2} = (-\mu^2/2\lambda)^{\frac{1}{2}}$ of the vacuum expectation value (vev) of $|\Phi|$. Since conventional perturbation theory is formulated for fields with zero vev, it is appropriate

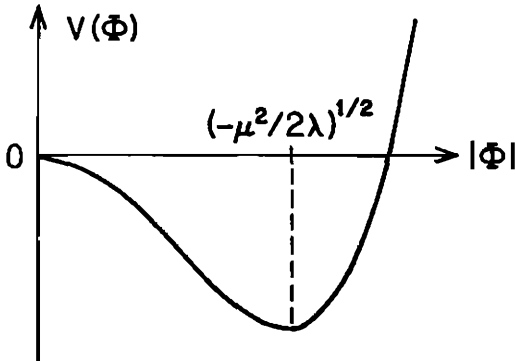


Fig. 2.1. Classical potential of scalar field with $\mu^2 < 0$, $V = \lambda \left(|\Phi|^2 - \frac{1}{2}v^2 \right)^2 - \frac{1}{4}v^4$.

to separate out the vev and to redefine the scalar doublet Φ as

$$\Phi(x) = \exp\left(\frac{i\xi(x) \cdot \tau}{2v}\right) \begin{pmatrix} 0 \\ (v + H(x))/\sqrt{2} \end{pmatrix},$$

where the real fields $\xi_1(x)$, $\xi_2(x)$, $\xi_3(x)$, and $H(x)$ have zero vev. By a finite gauge transformation under $SU(2)_L$ with $\alpha(x) = \xi(x)/v$, we can remove the above phase factor from $\Phi(x)$, eliminating the explicit appearance of $\xi(x)$ in the Lagrangian. In this “unitary gauge” the ξ degrees of freedom seem to vanish but essentially reappear as the longitudinal components of W^\pm and Z when they acquire masses; they have been “eaten” by the gauge fields.

The Goldstone Theorem states that massless spin-0 particles appear in a theory whenever a continuous symmetry is spontaneously broken; physically they embody the zero-energy excitations that were previously described by symmetry transformations. For global symmetry breaking such *Goldstone bosons* are inescapable but in gauge symmetry breaking by the Higgs mechanism something special happens. There are three Goldstone bosons in the present case, that we can represent by the ξ degrees of freedom. These degrees of freedom are gauged away from the scalar sector but essentially reappear (with masses) in the gauge field sector, where they provide the longitudinal modes for W^\pm and Z^0 .

The covariant derivative operation on an isodoublet field expressed in terms of the physical A , W^\pm , and Z fields is

$$D = \partial + ieQA + i\frac{1}{\sqrt{2}}g(\tau^+W^+ + \tau^-W^-) + ig_Z(\frac{1}{2}\tau_3 - x_wQ)Z,$$

where the space-time index μ has been suppressed and we have defined $\tau^+ = \sqrt{2}T^+ = \begin{pmatrix} 0 & 1 \\ 0 & 0 \end{pmatrix}$ and $\tau^- = \sqrt{2}T^- = \begin{pmatrix} 0 & 0 \\ 1 & 0 \end{pmatrix}$. In the unitary gauge $\Phi(x)$ has only a neutral component

$$\Phi(x) = \frac{1}{\sqrt{2}} \begin{pmatrix} 0 \\ v + H(x) \end{pmatrix}$$

and

$$D\Phi = \frac{1}{\sqrt{2}} \begin{pmatrix} \frac{1}{\sqrt{2}} igW^+(v+H) \\ \partial H - \frac{1}{2} ig_Z Z(v+H) \end{pmatrix}.$$

Exercise. Show that the Lagrangian \mathcal{L}_Φ becomes

$$\mathcal{L}_\Phi = \frac{1}{2}(\partial H)^2 + \frac{1}{4}g^2 W^+W^-(v+H)^2 + \frac{1}{8}g_Z^2 ZZ(v+H)^2 - V\left[\frac{1}{2}(v+H)^2\right].$$

The v^2 terms provide W and Z boson mass terms

$$M_W^2 W^+W^- + \frac{1}{2}M_Z^2 ZZ$$

with

$$M_W = \frac{1}{2}gv, \quad M_Z = \frac{1}{2}g_Z v = \frac{M_W}{\cos\theta_w},$$

while the photon remains massless.

Exercise. Show that the kinetic and potential terms in \mathcal{L}_Φ give

$$\frac{1}{2}(\partial H)^2 - \frac{1}{2}(-2\mu^2)H^2 + \frac{1}{4}\mu^2 v^2 \left[-1 + \frac{4H^3}{v^3} + \frac{H^4}{v^4} \right],$$

describing a physical Higgs scalar boson of mass

$$m_H = \sqrt{-2\mu^2}$$

with cubic and quartic self-interactions.

H has no electromagnetic interaction; its interactions with the other gauge fields are given by the cubic and quartic terms

$$\left(\frac{1}{4}g^2 W^+W^- + \frac{1}{8}g_Z^2 ZZ \right) (H^2 + 2vH),$$

which are completely specified by the gauge couplings. We will return to consider the physical implications of these Higgs particle interactions in a later chapter.

Exercise. Show that SSB based instead on a vacuum expectation value for ϕ^+ would have unacceptable physical consequences.

In physical terms, the final result of the Higgs mechanism is that the vacuum everywhere can emit or absorb a neutral colorless quantum of the Higgs field, that carries weak isospin and hypercharge. As a result, the fermions and the W and Z bosons that couple to such a quantum effectively acquire masses, but the photon and gluon that cannot couple to it remain massless.

2.5 The Effective Four-Fermion Interaction Lagrangian

The preceding sections have demonstrated that the $SU(2)_L \times U(1)_Y$ gauge model with SSB unifies the interactions of massive W^\pm and Z bosons with the electromagnetic interaction. The effective four-fermion interaction arising from single boson or photon exchanges in this model has the form

$$-\mathcal{L}_{\text{eff}} = \frac{-\frac{1}{2}e^2 (J_{em}^\mu)^2}{q^2} - \frac{\frac{1}{2}g^2 J_L^{+\mu} J_{L\mu}^-}{q^2 - M_W^2} - \frac{\frac{1}{2}g_Z^2 (J_Z^\mu)^2}{q^2 - M_Z^2},$$

where the electromagnetic current J_{em} , charged currents J_L^\pm and weak neutral current J_Z are as defined in Section 2.3 and q^2 is the invariant square of momentum transfer between the two currents. The factors $\frac{1}{2}$ in front of the J_{em}^2 and J_Z^2 terms appear in order to compensate for the two orderings of fermion currents that can contribute; the factor $\frac{1}{2}$ in front of $J_L^+ J_L^-$ comes from the appearance of $g/\sqrt{2}$ in the local Lagrangian. In the above form for \mathcal{L}_{eff} we omitted weak boson propagator terms $q_\mu q_\nu / M_W^2$ and $q_\mu q_\nu / M_Z^2$; their contributions are proportional to external lepton (or quark) masses and can therefore be neglected in processes involving first or second generation leptons or quarks in one of the currents.

At low energies where q^2 is much less than M_W^2 or M_Z^2 , the second term in \mathcal{L}_{eff} reduces to the standard $V-A$ charged-current interaction

which is known to describe low energy phenomena, provided that g and M_W are related to the Fermi coupling constant G_F by

$$\frac{G_F}{\sqrt{2}} = \frac{g^2}{8M_W^2}.$$

We introduce a parameter ρ , defined as

$$\rho = \left(\frac{g_Z^2}{M_Z^2} \right) / \left(\frac{g^2}{M_W^2} \right),$$

which measures the ratio of neutral current to charged current strengths in \mathcal{L}_{eff} . In the standard model with one Higgs doublet, $\rho = 1$.

Exercise. Show that for a sum of general Higgs multiplets with weak isospins T_i , T_{i3} , and vevs v_i , the ρ -parameter is

$$\rho = \frac{\sum_i [T_i(T_i + 1) - T_{i3}^2] v_i^2}{\sum_i 2T_{i3}^2 v_i^2}.$$

The low-energy four-fermion effective Lagrangian is then

$$-\mathcal{L}_{\text{eff}} = \frac{-\frac{1}{2} e^2 (J_{em}^\mu)^2}{q^2} + \frac{4G_F}{\sqrt{2}} J_L^{+\mu} J_{L\mu}^- + \rho \frac{4G_F}{\sqrt{2}} (J_Z^\mu)^2.$$

The weak neutral current interaction is an important prediction of the $SU(2)_L \times U(1)_Y$ gauge model. The low-energy phenomenology of the effective Lagrangian is taken up in later chapters.

2.6 Parameters of the Gauge Sector

Three basic parameters g , g' and v determine the gauge field masses and interactions in the standard model. However, it is customary to work instead with other more convenient sets of parameters. For low energy electroweak interactions $\alpha = e^2/(4\pi)$, G_F and $\sin^2\theta_w$ are commonly used because the first two are very accurately known, leaving $\sin^2\theta_w$ as the single parameter (characteristic of unification) to be pinned down. The basic parameters are related by $g = e/\sin\theta_w$, $g' = e/\cos\theta_w$ and

$$v = 2M_W/g = \left(\sqrt{2}G_F\right)^{-\frac{1}{2}} = 246 \text{ GeV},$$

and the weak boson masses are

$$\begin{aligned} M_W &= A/\sin\theta_w, \\ M_Z &= A/\sin\theta_w \cos\theta_w, \end{aligned}$$

where

$$A = (\pi\alpha/\sqrt{2}G_F)^{\frac{1}{2}} = 37.2802 \text{ GeV},$$

with G_F determined by the muon lifetime with certain radiative corrections.

Alternatively, instead of $\sin^2\theta_w$ as the third parameter, we could equally well use M_W or M_Z or their ratio. Indeed the experimental accuracy on the W and Z masses is already comparable to the accuracy with which $\sin^2\theta_w$ can be determined by low energy neutral current experiments. In the near future, e^+e^- collisions at the Z resonance will make M_Z the most accurately determined third parameter; it will then be much more appropriate to use α , G_F and M_Z .

2.7 Radiative Corrections

The tree-level results above are modified by higher-order diagrams containing loops; different possible choices then arise for the definition of $\sin^2\theta_w$. In this section we adopt the definition

$$\sin^2\theta_w \equiv 1 - M_W^2/M_Z^2$$

and hence $\rho \equiv 1$. The W and Z mass formulas are then

$$M_W = A/(\sin\theta_w\sqrt{1-\Delta r}), \quad M_Z = M_W/\cos\theta_w,$$

where $\sin^2\theta_w = 0.23 \pm 0.01$ is determined from neutrino neutral-current scattering with radiative corrections and $\Delta r \simeq 1 - \alpha/\alpha(M_Z) - 3G_F m_t^2/(8\sqrt{2}\pi^2 \tan^2\theta_w)$. Thus the Δr correction comes mostly from the running of α up to the electroweak scale and from the effects of large m_t in top-quark loops. Smaller loop effects include a term depending logarithmically on m_H . The net effect is $\Delta r = 0.0475 \pm 0.0009$ for $m_t = 150$ GeV and $m_H = 300$ GeV.

The radiatively corrected formula with $\sin^2\theta_w$ and Δr values above gives

$$M_W = 79.6 \pm 1.7 \text{ GeV}, \quad M_Z = 90.8 \pm 1.4 \text{ GeV}.$$

These predictions are in reasonable accord with 1986 results from the UA1 and UA2 experiments at the CERN $p\bar{p}$ collider,

$$M_W = 83.5 \pm \frac{1.1}{1.0} \pm 2.7 \text{ GeV}, \quad M_Z = 93.0 \pm 1.4 \pm 3.0 \text{ GeV} \quad (\text{UA1})$$

$$M_W = 80.2 \pm 0.6 \pm 1.4 \text{ GeV}, \quad M_Z = 91.5 \pm 1.2 \pm 1.7 \text{ GeV} \quad (\text{UA2})$$

where the first quoted error is statistical and the second is systematic. [Compare 1994 particle data averages $M_W = 80.1 \pm 0.4$, $M_Z = 91.188 \pm 0.007$ GeV, including LEP, SLC and Tevatron data.]

The radiatively-corrected neutrino scattering data give $\rho = 0.998 \pm 0.0086$ with the present definition of $\sin^2\theta_w$, consistent with the model.

The radiative corrections depend only logarithmically on the Higgs mass m_H but depend quadratically on the top quark mass m_t . When calculations are compared with very accurate experimental determinations of M_W , M_Z , ρ , *etc.*, they offer another way to constrain the Standard Model and possibly to discover new physics.

2.8 Lepton Masses

Spontaneous symmetry breaking will generate an electron mass if we add a Yukawa interaction of lepton and Φ fields, which is renormalizable and invariant under $SU(2)_L \times U(1)$ gauge transformations

$$\mathcal{L} = -G_e \left[\bar{e}_R (\Phi^\dagger \ell_L) + (\bar{\ell}_L \Phi) e_R \right].$$

Here G_e is a further coupling constant and

$$\ell_L = \begin{pmatrix} \nu_e \\ e \end{pmatrix}_L, \quad \Phi = \begin{pmatrix} \phi^+ \\ \phi^0 \end{pmatrix}.$$

Substituting the unitary gauge form of $\Phi(x)$, we find

$$\mathcal{L} = -(G_e v / \sqrt{2}) \bar{e} e - (G_e / \sqrt{2}) H \bar{e} e.$$

Thus the electron acquires a mass

$$m_e = (G_e v / \sqrt{2})$$

and also a coupling to the Higgs boson. Replacing G_e by $\sqrt{2} m_e / v$ and using $v = (\sqrt{2} G_F)^{-\frac{1}{2}}$, the Higgs boson coupling to the electron is

$$\mathcal{L} = -\frac{m_e}{v} H \bar{e} e = -2^{\frac{1}{4}} \sqrt{G_F} m_e H \bar{e} e.$$

This coupling is very small, $G_e = 2.9 \times 10^{-6}$. Applying similar arguments for the second and third generation leptons, the Yukawa terms

are

$$\mathcal{L} = -2^{\frac{1}{2}} \sqrt{G_F} (m_e H \bar{e} e + m_\mu H \bar{\mu} \mu + m_\tau H \bar{\tau} \tau).$$

The Higgs couplings to leptons are “semi-weak”, since $\sqrt{G_F}$ is involved.

This Higgs mechanism for generating masses introduces an arbitrary coupling parameter for each fermion mass, and hence provides no fundamental understanding of mass values.

The neutrinos cannot acquire masses or couplings to the H field in an analogous way, since by fiat there are no ν_R fields in the standard model.

In the standard model the three generations of leptons are

$$\begin{array}{cc} \text{weak isospin doublets} & \text{weak isospin singlets} \\ \left(\begin{array}{c} \nu_e \\ e \end{array} \right)_L & \left(\begin{array}{c} \nu_\mu \\ \mu \end{array} \right)_L & \left(\begin{array}{c} \nu_\tau \\ \tau \end{array} \right)_L & e_R, \mu_R, \tau_R \end{array}$$

In the scalar interaction with leptons above we have not considered couplings that mix generations because for massless neutrinos mixing among the three neutrino states has no meaning. In this circumstance ν_e is by definition the partner of e , ν_μ of μ , and ν_τ of τ .

2.9 Quark Masses and Mixing

Quark masses are also generated by Yukawa couplings to the scalars. We assume that the fundamental weak eigenstates of the unbroken gauge theory are

$$D_{jL} \equiv \left(\begin{array}{c} u_j \\ d_j \end{array} \right)_L, \quad u_{jR}, \quad d_{jR}, \quad (j = 1, 2, 3),$$

where D_{jL} is an $SU(2)_L$ doublet with $Y = \frac{1}{3}$ and u_{jR} , d_{jR} are $SU(2)_L$ singlets with $Y = \frac{4}{3}$, $-\frac{2}{3}$, respectively; j is a generation index with 3 generations assumed.

In order to generate quark mass terms for both u -type and d -type quarks we need not only the doublet Φ with $Y = 1$, but also the conjugate multiplet

$$\tilde{\Phi} = i\tau_2 \Phi^* = \begin{pmatrix} \phi^{0*} \\ -\phi^- \end{pmatrix}$$

which transforms as a doublet with $Y = -1$. The most general $SU(2)_L \times U(1)$ invariant Yukawa interaction is

$$\mathcal{L} = - \sum_{i=1}^3 \sum_{j=1}^3 \left[\tilde{G}_{ij} \overline{u_{iR}} (\tilde{\Phi}^\dagger D_{jL}) + G_{ij} \overline{d_{iR}} (\Phi^\dagger D_{jL}) \right] + \text{h.c.}$$

where we have allowed inter-generation couplings. This interaction depends on 18 different complex couplings \tilde{G}_{ij} , G_{ij} . From the vevs of Φ and $\tilde{\Phi}$ we obtain mass terms for the charge $\frac{2}{3}$ and charge $-\frac{1}{3}$ quarks,

$$\overline{(u_1, u_2, u_3)_R} \mathcal{M}^u \begin{pmatrix} u_1 \\ u_2 \\ u_3 \end{pmatrix}_L + \text{h.c.},$$

$$\overline{(d_1, d_2, d_3)_R} \mathcal{M}^d \begin{pmatrix} d_1 \\ d_2 \\ d_3 \end{pmatrix}_L + \text{h.c.},$$

where $\mathcal{M}_{ij}^u = \frac{v}{\sqrt{2}} \tilde{G}_{ij}$ and $\mathcal{M}_{ij}^d = \frac{v}{\sqrt{2}} G_{ij}$ are quark mass matrices in generation space, each depending on 9 complex parameters. These matrices are, in general, not Hermitian.

Any unitary transformation on the quark fields will preserve their anticommutation relations. Moreover, any complex matrix can be transformed to a diagonal matrix by multiplying it on the left and right by appropriate unitary matrices. Thus, by unitary transformations on the fundamental quark states of the unbroken electroweak

theory,

$$\begin{pmatrix} u_1 \\ u_2 \\ u_3 \end{pmatrix}_{L,R} = U_{L,R} \begin{pmatrix} u \\ c \\ t \end{pmatrix}_{L,R}, \quad \begin{pmatrix} d_1 \\ d_2 \\ d_3 \end{pmatrix}_{L,R} = D_{L,R} \begin{pmatrix} d \\ s \\ b \end{pmatrix}_{L,R},$$

we can transform M^u and M^d to diagonal forms

$$U_R^{-1} M^u U_L = \begin{pmatrix} m_u & 0 & 0 \\ 0 & m_c & 0 \\ 0 & 0 & m_t \end{pmatrix},$$

$$D_R^{-1} M^d D_L = \begin{pmatrix} m_d & 0 & 0 \\ 0 & m_s & 0 \\ 0 & 0 & m_b \end{pmatrix},$$

where U_R , U_L , D_R and D_L are unitary matrices and the diagonal entries are the quark masses. The weak eigenstates u_1 , u_2 , u_3 are linear superpositions of the mass eigenstates u , c , t and likewise d_1 , d_2 , d_3 are superpositions of d , s , b , with separate relations for the L and R components.

In the charged-current weak interaction we encounter the bilinear terms $\overline{u_1 L} \gamma^\mu d_{1L}$, $\overline{u_2 L} \gamma^\mu d_{2L}$, $\overline{u_3 L} \gamma^\mu d_{3L}$ whose sum can be represented as an inner product of vectors in generation space

$$\overline{(u_1, u_2, u_3)_L} \gamma_\mu \begin{pmatrix} d_1 \\ d_2 \\ d_3 \end{pmatrix}_L = \overline{(u, c, t)_L} U_L^\dagger D_L \gamma_\mu \begin{pmatrix} d \\ s \\ b \end{pmatrix}_L.$$

There will therefore generally be generation mixing of the mass eigenstates, described by the matrix

$$V \equiv U_L^\dagger D_L.$$

In the neutral-current interaction of the standard model we en-

counter instead bilinear forms such as

$$\overline{(u_1, u_2, u_3)_L} \begin{pmatrix} u_1 \\ u_2 \\ u_3 \end{pmatrix}_L = \overline{(u, c, t)_L} U_L^\dagger U_L \begin{pmatrix} u \\ c \\ t \end{pmatrix}_L,$$

but since $U_L^\dagger U_L = 1$, there is no mixing in this case. The u_R , d_L , d_R neutral-current bilinear terms are similarly unmixed.

Like the mass matrix itself, the mixing of quark flavors in the charged-current weak interaction has no fundamental explanation here, though theoretical attempts to predict the mixing angles have been made in extended gauge models. If all quark masses were zero (or equal), weak mixing phenomena would not exist.

In terms of the above general mixing matrix V , the charged weak currents for quarks are

$$J_{L\mu}^+ = \overline{(u, c, t)_L} \gamma_\mu V \begin{pmatrix} d \\ s \\ b \end{pmatrix}_L.$$

By convention, the mixing is ascribed completely to the $T_3 = -\frac{1}{2}$ states by defining

$$\begin{pmatrix} d' \\ s' \\ b' \end{pmatrix}_L = V \begin{pmatrix} d \\ s \\ b \end{pmatrix}_L.$$

Then the quark weak eigenstates are

weak isospin doublets

$$\begin{pmatrix} u \\ d' \end{pmatrix}_L, \begin{pmatrix} c \\ s' \end{pmatrix}_L, \begin{pmatrix} t \\ b' \end{pmatrix}_L$$

weak isospin singlets

$$u_R, c_R, t_R; d_R, s_R, b_R.$$

Remember however, that any linear combination of doublets (singlets) is also a doublet (singlet). An important prediction of the

gauge theory is that all fermion doublets and singlets, whether leptons or quarks, enter in the weak interaction with the same electroweak coupling strengths g and g' . This universality of quark and lepton interactions is very well borne out experimentally.

2.10 Mixing Matrix Parameterization

The unitary 3×3 matrix V can be specified by 9 independent parameters; the 18 complex parameters of a general 3×3 matrix are reduced to 9 by the unitarity constraints $V_{\alpha\beta}^\dagger V_{\beta\gamma} = \delta_{\alpha\gamma}$. However, we have the freedom to absorb a phase into each left-handed field,

$$q_L \rightarrow e^{i\alpha(q_L)} q_L ,$$

which removes an arbitrary phase from each row or column of V , reducing the degrees of freedom. But since V is unchanged by a common phase transformation of all the q_L , only $6 - 1 = 5$ phase degrees of freedom can be removed in this way. Therefore V can be expressed in terms of only $9 - 5 = 4$ physically independent parameters.

Exercise. Show that for N generations the quark mixing matrix contains $(N - 1)^2$ physically independent parameters. Show also that a general $N \times N$ real unitary matrix (i.e., orthogonal matrix) has $N(N - 1)/2$ independent parameters and hence that V contains $(N - 1)(N - 2)/2$ independent phase angles.

Note that CP violation requires a complex phase in \mathcal{L} which can be realized in the quark sector through V only if there are 3 or more generations.

For three generations the mixing matrix can be parameterized by a product of three rotation matrices R and a phase insertion matrix

D as

$$V = R_2(-\theta_2)R_1(-\theta_1)D(\delta - \pi)R_2(\theta_3),$$

where

$$R_1(\theta_i) = \begin{pmatrix} c_i & s_i & 0 \\ -s_i & c_i & 0 \\ 0 & 0 & 1 \end{pmatrix}, \quad R_2(\theta_i) = \begin{pmatrix} 1 & 0 & 0 \\ 0 & c_i & s_i \\ 0 & -s_i & c_i \end{pmatrix},$$

$$D(\delta) = \begin{pmatrix} 1 & 0 & 0 \\ 0 & 1 & 0 \\ 0 & 0 & e^{i\delta} \end{pmatrix},$$

and $c_i = \cos \theta_i$, $s_i = \sin \theta_i$. This construction leads to the Kobayashi-Maskawa (KM) form

$$V = \begin{pmatrix} c_1 & -s_1 c_3 & -s_1 s_3 \\ s_1 c_2 & c_1 c_2 c_3 - s_2 s_3 e^{i\delta} & c_1 c_2 s_3 + s_2 c_3 e^{i\delta} \\ s_1 s_2 & c_1 s_2 c_3 + c_2 s_3 e^{i\delta} & c_1 s_2 s_3 - c_2 c_3 e^{i\delta} \end{pmatrix}.$$

By suitable choices of the signs of the quark fields, we can restrict the angles to the ranges

$$0 \leq \theta_i \leq \pi/2, \quad 0 \leq \delta \leq 2\pi.$$

The phase δ gives rise to CP-violating effects. An alternative form of the KM matrix sometimes used in the literature replaces δ above by $\delta + \pi$ and θ_1 by $-\theta_1$. The KM parameters are not predicted by the standard model.

In the limit $\theta_2 = \theta_3 = 0$, $\delta = \pi$, V reduces to the Cabibbo rotation

$$V = R_1(-\theta_1) = \begin{pmatrix} c_1 & -s_1 & 0 \\ s_1 & c_1 & 0 \\ 0 & 0 & 1 \end{pmatrix},$$

which mixes the first and second generations only.

Some other constructions of the mixing matrix have advantages in parameterizing the experimental data. One such parameterization inserts the phase via a matrix

$$R_3(\theta, \delta') = \begin{pmatrix} c & 0 & se^{-i\delta'} \\ 0 & 1 & 0 \\ -se^{i\delta'} & 0 & c \end{pmatrix}$$

with $V = R_2(\theta_{23})R_3(\theta_{13}, \delta')R_1(\theta_{12})$. Here θ_{ij} is the angle describing the mixing of generation i with j . This construction yields

$$V = \begin{pmatrix} c_{12}c_{13} & s_{12}c_{13} & s_{13}e^{-i\delta'} \\ -c_{23}s_{12} - c_{12}s_{23}s_{13}e^{i\delta'} & c_{12}c_{23} - s_{12}s_{23}s_{13}e^{i\delta'} & c_{13}s_{23} \\ s_{12}s_{23} - c_{12}c_{23}s_{13}e^{i\delta'} & -c_{12}s_{23} - c_{23}s_{12}s_{13}e^{i\delta'} & c_{13}c_{23} \end{pmatrix}.$$

Experimentally the diagonal elements of V are of order 1 and the off-diagonal elements are small. When all θ_{ij} are small this mixing matrix becomes

$$V \simeq \begin{pmatrix} 1- & s_{12} & s_{13}e^{-i\delta'} \\ -s_{12} & 1- & s_{23} \\ -s_{13}e^{i\delta'} & -s_{23} & 1- \end{pmatrix}$$

and every element is approximated by a single term which is not the case in the small angle limit of the KM parameterization. Note that the diagonal values are slightly less than unity as required by unitarity.

2.11 Experimental Determination of Mixing

The matrix elements of V are labelled by the quarks that they link, as follows

$$V = \begin{pmatrix} V_{ud} & V_{us} & V_{ub} \\ V_{cd} & V_{cs} & V_{cb} \\ V_{td} & V_{ts} & V_{tb} \end{pmatrix} .$$

The most accurately known mixing matrix element is V_{ud} . It is determined by comparing superallowed nuclear beta decays to muon decay. Its value, including radiative and isospin corrections, is

$$|V_{ud}| = 0.9744 \pm 0.0010 .$$

The V_{us} matrix element can be found from $K \rightarrow \pi e \nu$ decays or from hyperon decays. The hyperon decay data analysis has larger theoretical uncertainty because of first-order SU(3) symmetry-breaking in the axial vector couplings. The averaged result from K_{e3} and hyperon decay data is

$$|V_{us}| = 0.2205 \pm 0.0018 .$$

From data on charm production in neutrino collisions, $(\bar{\nu}_\mu^-) N \rightarrow \mu + \text{charm} + X$, plus charm semileptonic decay data the following matrix elements are determined:

$$|V_{cd}| = 0.204 \pm 0.017 , \quad |V_{cs}| = 1.01 \pm 0.18 .$$

The decays of B -mesons proceed predominantly through the $b \rightarrow c$ transition. The measured partial width for $\bar{B} \rightarrow D \ell \bar{\nu}$ yields

$$|V_{cb}| = 0.040 \pm 0.005 .$$

The ratio $|V_{ub}/V_{cb}|$ can be obtained from the upper end of the lepton spectrum in B -meson semileptonic decays, $B \rightarrow \ell \nu X$; the

$b \rightarrow u$ transitions have a higher endpoint than $b \rightarrow c$. Fitting the lepton energy spectrum as a sum of $b \rightarrow u$ and $b \rightarrow c$ contributions, leads to the result

$$\frac{|V_{ub}|}{|V_{cb}|} = 0.08 \pm 0.02.$$

The preceding results for V_{ud} , V_{us} and V_{ub} are consistent with unitarity of the mixing matrix, with three generations of quarks:

$$|V_{ud}|^2 + |V_{us}|^2 + |V_{ub}|^2 = 0.9981 \pm 0.0027.$$

However the existence of a fourth generation of quarks (a, v) with

$$|V_{uv}| \lesssim 0.068, \quad |V_{cv}| \lesssim 0.55, \quad |V_{ad}| \lesssim 0.13, \quad |V_{as}| \lesssim 0.54,$$

is not excluded.

Assuming just 3 generations of quarks, the unitarity of the mixing matrix can be combined with the experimental constraints above to derive bounds on the other matrix elements. The moduli of the matrix elements lie in the ranges (90% confidence)

$$V = \begin{pmatrix} 0.9747 - 0.9759 & 0.218 - 0.224 & 0.000 - 0.005 \\ 0.218 - 0.224 & 0.9738 - 0.9752 & 0.032 - 0.048 \\ 0.004 - 0.015 & 0.030 - 0.048 & 0.9988 - 0.9995 \end{pmatrix}.$$

Information about the CP-violating phase δ can be inferred from theoretical calculations of the ϵ -parameter in the $K^0-\bar{K}^0$ system. These studies suggest that the phase δ is in the range $30^\circ \lesssim \delta \lesssim 177^\circ$.

The empirical results for the $|V_{ij}|$ suggest an approximate form

$$V = \begin{pmatrix} 1 & \theta & \theta^3 e^{-i\delta'} \\ -\theta & 1 & \theta^2 \\ -\theta^3 e^{i\delta'} & -\theta^2 & 1 \end{pmatrix}$$

to order θ^2 for the diagonal elements. Here θ is the Cabibbo angle ($\theta \simeq 13^\circ$, $\sin \theta = 0.23$). The weak $SU(2)_L$ doublets in this convenient approximation to the mixing matrix are

$$\begin{pmatrix} u \\ d + \theta s + \theta^3 e^{-i\delta'} b \end{pmatrix}_L, \begin{pmatrix} c \\ s - \theta d + \theta^2 b \end{pmatrix}_L, \begin{pmatrix} t \\ b - \theta^2 s - \theta^3 e^{i\delta'} d \end{pmatrix}_L.$$

The charged weak current transitions are increasingly suppressed as the generation separation increases and as the quark mass difference increases.

2.12 Weak Currents

For the $SU(2)_L \times U(1)$ assignments of the leptons and quarks introduced previously, we can directly write down the form of the charged, neutral, and electromagnetic currents. The charged current involves only the $SU(2)_L$ doublets

$$J_L^{+\alpha} = \sqrt{2} \bar{\psi} \gamma^\alpha T_L^+ \psi = \bar{\psi}_L \gamma^\alpha \tau^+ \psi_L = \frac{1}{2} \bar{\psi} \gamma^\alpha (1 - \gamma_5) \tau^+ \psi,$$

where $\tau^+ = \begin{pmatrix} 0 & 1 \\ 0 & 0 \end{pmatrix}$. For three generations the currents are

$$J_L^{+\alpha} = \bar{\nu}_e \gamma^\alpha e_L + \bar{\nu}_\mu \gamma^\alpha \mu_L + \bar{\nu}_\tau \gamma^\alpha \tau_L + \bar{u} \gamma^\alpha d'_L + \bar{c} \gamma^\alpha s'_L + \bar{t} \gamma^\alpha b'_L$$

and

$$\begin{aligned} J_L^{-\alpha} &= (J_L^{+\alpha})^\dagger \\ &= \bar{e} \gamma^\alpha \nu_{eL} + \bar{\mu} \gamma^\alpha \nu_{\mu L} + \bar{\tau} \gamma^\alpha \nu_{\tau L} + \bar{d}' \gamma^\alpha u_L + \bar{s}' \gamma^\alpha c_L + \bar{b}' \gamma^\alpha t_L, \end{aligned}$$

where the symbol for a particle is used to denote its field.

The weak neutral current of the Z boson is the linear combination

$$J_Z^\alpha = J_L^{3\alpha} - x_w J_{em}^\alpha$$

of the third component of the $SU(2)_L$ current $J_L^{3\alpha} = \frac{1}{2}\bar{\psi}\gamma^\alpha\tau^3\psi_L$ and the electromagnetic current J_{em} . We recall that $J_L^{3\alpha}$ is independent of the mixing matrix V , since

$$\bar{\psi}'_L\gamma^\alpha\psi'_L = \bar{\psi}_L V^\dagger V\gamma^\alpha\psi_L = \bar{\psi}_L\gamma^\alpha\psi_L,$$

where ψ' denotes $\begin{pmatrix} d' \\ s' \\ b' \end{pmatrix}$ and ψ denotes $\begin{pmatrix} d \\ s \\ b \end{pmatrix}$. As a consequence, the Z neutral current has no flavor-changing transition, like $d \rightarrow s$. This cancellation of flavor-changing transitions, which only occurs in general if all left-handed quark states appear in doublets, is known as the Glashow-Iliopoulos-Maiani (GIM) mechanism. These authors pointed out that the existence of a charm quark would explain the observed extreme suppression of the strangeness-changing $s \rightarrow d$ current (in $K^0 \rightarrow \bar{K}^0$ transitions and in $K_L^0 \rightarrow \mu^+\mu^-$ decay), at a time when only u, d, s quarks were known.

Exercise. Evaluate the neutral current Lagrangian resulting from the following doublet and singlet

$$\begin{pmatrix} u \\ d \cos \theta + s \sin \theta \end{pmatrix}_L, \quad (s \cos \theta - d \sin \theta)_L,$$

and note the flavor changing $s_L \rightarrow d_L$ component.

The first generation terms in the J_L^3 and J_{em} currents are

$$J_L^{3\alpha} = \frac{1}{2}\bar{\nu}_e\gamma^\alpha\nu_{eL} - \frac{1}{2}\bar{e}\gamma^\alpha e_L + \frac{1}{2}\bar{u}\gamma^\alpha u_L - \frac{1}{2}\bar{d}\gamma^\alpha d_L$$

and

$$J_{em}^\alpha = -\bar{e}\gamma^\alpha e + \frac{2}{3}\bar{u}\gamma^\alpha u - \frac{1}{3}\bar{d}\gamma^\alpha d.$$

Table 2.1 *Z*-boson couplings to fermions.

	g_L	g_R	g_V	g_A
ν_e, ν_μ, ν_τ	$\frac{1}{2}$	0	$\frac{1}{4}$	$-\frac{1}{4}$
e, μ, τ	$-\frac{1}{2} + x_w$	x_w	$-\frac{1}{4} + x_w$	$\frac{1}{4}$
u, c, t	$\frac{1}{2} - \frac{2}{3}x_w$	$-\frac{2}{3}x_w$	$\frac{1}{4} - \frac{2}{3}x_w$	$-\frac{1}{4}$
d, s, b	$-\frac{1}{2} + \frac{1}{3}x_w$	$\frac{1}{3}x_w$	$-\frac{1}{4} + \frac{1}{3}x_w$	$\frac{1}{4}$

Using the relation $\bar{\psi}\gamma^\alpha\psi = \bar{\psi}_L\gamma^\alpha\psi_L + \bar{\psi}_R\gamma^\alpha\psi_R$, the *Z*-current is

$$\begin{aligned} J_Z^\alpha &= \sum_f \left(g_L^f \bar{f} \gamma^\alpha f_L + g_R^f \bar{f} \gamma^\alpha f_R \right) \\ &= \sum_f \left(g_V^f \bar{f} \gamma^\alpha f + g_A^f \bar{f} \gamma^\alpha \gamma_5 f \right) \end{aligned}$$

summed over fermion fields f . The couplings g_L , g_R and g_V , g_A are listed in Table 2.1; note that $g_V = \frac{1}{2}(g_L + g_R)$, $g_A = \frac{1}{2}(g_R - g_L)$.

With the above charged and neutral currents we are now in a position to calculate the amplitudes of electroweak processes, which is the subject of the succeeding chapters. Before proceeding, we note that neutrinos appear in the currents only as $(1 - \gamma_5)\nu$ and are therefore two-component. For massless particles, we recall that

$$\frac{1}{2}(1 - \gamma_5)u(p, \lambda = \pm\frac{1}{2}) = u(p, -\frac{1}{2})\delta_{\lambda, -\frac{1}{2}},$$

where $u(p, \lambda)$ is the particle spinor and λ labels the eigenvalue of the helicity operator $H = \frac{1}{2}\gamma_5\boldsymbol{\gamma} \cdot \boldsymbol{s}$, which gives the spin component along the direction of motion. Thus massless neutrinos have negative helicity and are left-handed. By CP conjugation, antineutrinos are

right-handed:

$$\begin{array}{ll}
 \leftarrow & \\
 \longrightarrow \bar{p} & \text{neutrino} \\
 \Rightarrow & \\
 \longrightarrow \bar{p} & \text{antineutrino}
 \end{array}$$

In the limit that the electron (or muon) mass can be neglected, only its left-handed states take part in the charged current weak interaction, but the electromagnetic and weak neutral current interactions involve both left and right-handed states.

2.13 Chiral Anomalies

In chiral theories, where some gauge bosons couple differently to left- and right-handed fermions, difficulties can arise from the divergence of triangle diagrams like Fig. 1.9 with three external gauge bosons. In general the loop integral diverges as $\int d^4p/p^3$, breaking some generalized Ward identities and invalidating the standard renormalization arguments. There is no problem in electrodynamics; the integral vanishes for all-vector couplings (VVV) because these couplings are odd under charge conjugation. However, VVA and AAA couplings that arise in chiral theories do not vanish by themselves. We then have to appeal to cancellations between different fermion contributions; the divergent term is the same for each fermion (regardless of mass), apart from the gauge boson couplings.

Let us denote the fermion coupling strengths at the three vertices by O^a , O^b , O^c . When the fermions form multiplets under a symmetry group (in this case $SU(2)$), the O^a are matrices in the multiplet space and the sum of divergent contributions over a multiplet contains the factor

$$\text{Trace} \left[\left(O^a O^b + O^b O^a \right) O^c \right]$$

including both possible orderings of vertices. In the present case,

the couplings are multiples of T^+ , T^- and linear combinations of T_3 and Y .

Exercise. Show that the cases of $T^a T^b T^c$ and $T^a Y Y$ couplings cancel within each $SU(2)$ doublet. Show that the remaining cases of $T^a T^b Y$ and $Y Y Y$ couplings cancel between quarks and leptons, provided there are corresponding numbers of leptons and quarks and each quark comes in three colors.

Chapter 3

Lepton and Heavy Quark Decays

3.1 $V-A$ Semileptonic Decay Rates

A direct consequence of weak interactions is the decay of the heavier leptons and quarks into lighter particles. Decays are important not only as a test of the standard electroweak model but also as a means to detect and identify heavy particles produced in experiments. The discovery of a new lepton or quark would have important implications; it could signal the presence of a fourth generation of basic fermions, or indicate that there are more members in each generation. In this chapter we first consider a generic example $a \rightarrow b\ell\bar{\nu}_\ell$ with standard $V-A$ interaction, and then apply the results to μ -decay, τ -decay, heavy neutrino decay and the decay of hadrons containing heavy quarks.

Consider the semileptonic decay transition

$$a \rightarrow b\ell^-\bar{\nu}_\ell,$$

where ℓ^- is a negatively charged lepton (e^- , μ^- , τ^-) and $\bar{\nu}_\ell$ is the corresponding antineutrino. The momenta of the particles will be labeled by the particle symbols; see Fig. 3.1. Thus the energy-momentum conservation relation is $a = b + \ell + \bar{\nu}$. We calculate the decay rate in the effective four-fermion interaction approximation, assuming that all masses and the momentum transfer are much smaller than M_W .

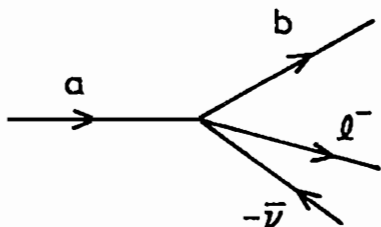


Fig. 3.1. Feynman diagram for semileptonic decay $a \rightarrow b l^- \bar{\nu}_l$.

With G_F strength V - A currents, the Feynman amplitude for the decay process is

$$\mathcal{M} = \frac{G_F}{\sqrt{2}} \bar{u}(b) \gamma^\alpha (1 - \gamma_5) u(a) \bar{u}(\ell) \gamma_\alpha (1 - \gamma_5) v(\bar{\nu}).$$

Taking the square, summing over spins, and replacing the spinor products by projection operators

$$\sum_s u(p) \bar{u}(p) = \not{p} + m, \quad \sum_s v(p) \bar{v}(p) = \not{p} - m,$$

where $\not{p} = p \cdot \gamma$, we obtain

$$\begin{aligned} \sum |\mathcal{M}|^2 = \frac{1}{2} G_F^2 \text{Tr} \left\{ \gamma^\alpha (1 - \gamma_5) (\not{p} + m_a) \gamma^\beta (1 - \gamma_5) (\not{p} + m_b) \right\} \\ \cdot \text{Tr} \left\{ \gamma_\alpha (1 - \gamma_5) \not{p} \gamma_\beta (1 - \gamma_5) (\not{p} + m_\ell) \right\}. \end{aligned}$$

This can be simplified to

$$\sum |\mathcal{M}|^2 = 2G_F^2 [\gamma^\alpha (1 - \gamma_5)]_{\lambda\rho} [\not{p} \gamma^\beta \not{p}]_{\rho\lambda} [\gamma_\alpha (1 - \gamma_5)]_{\mu\sigma} [\not{p} \gamma_\beta \not{p}]_{\sigma\mu}.$$

Exercise. Show why the mass terms do not contribute.

With the help of the Fierz transformation

$$[\gamma^\alpha (1 - \gamma_5)]_{\lambda\rho} [\gamma_\alpha (1 - \gamma_5)]_{\mu\sigma} = -[\gamma^\alpha (1 - \gamma_5)]_{\mu\rho} [\gamma_\alpha (1 - \gamma_5)]_{\lambda\sigma},$$

the above expression becomes a single trace

$$\sum |\mathcal{M}|^2 = -4G_F^2 \text{Tr} \left\{ (1 + \gamma_5) \gamma^\alpha \not{p} \gamma^\beta \not{p} \gamma_\alpha \not{p} \gamma_\beta \not{p} \right\}.$$

Then using the identities

$$\gamma^\alpha \not{a} \gamma^\beta \not{b} \gamma_\alpha = -2 \not{b} \gamma^\beta \not{a}, \quad \gamma^\beta \not{a} \not{b} \gamma_\beta = 4 a \cdot b,$$

we obtain for the $(V-A) \times (V-A)$ interaction

$$\sum |\mathcal{M}|^2 = 128 G_F^2 (a \cdot b)(c \cdot d).$$

Exercise. Show that the same result is obtained for $(V+A) \times (V+A)$ interaction.

Exercise. Show that for $V+A$ coupling at the $a \rightarrow b$ vertex and $V-A$ coupling at the $\bar{\ell} \bar{\nu}$ vertex

$$\sum |\mathcal{M}|^2 = 128 G_F^2 (a \cdot d)(b \cdot c).$$

Exercise. Use the identity

$$\text{Tr} \left\{ \gamma^\rho \gamma^\beta \gamma^\lambda \gamma^\alpha (1 + \gamma_5) \right\} = 4 \left(g^{\rho\beta} g^{\lambda\alpha} + g^{\rho\alpha} g^{\beta\lambda} - g^{\rho\lambda} g^{\beta\alpha} - i \epsilon^{\rho\beta\lambda\alpha} \right)$$

to evaluate $\sum |\mathcal{M}|^2$ directly from the product of the two traces above, without using the Fierz transformation.

It is sometimes convenient to introduce a square bracket symbol

$$[A, B]_{\alpha\beta} = A_\alpha B_\beta + B_\alpha A_\beta - g_{\alpha\beta} A \cdot B - i \epsilon_{\alpha\beta\gamma\delta} A^\gamma B^\delta$$

which arises in many trace calculations and has the property

$$[A, B]_{\alpha\beta} [C, D]^{\alpha\beta} = 4(A \cdot C)(B \cdot D).$$

In this notation, $\sum |\mathcal{M}|^2 = 32 G_F^2 [a, b]^{\alpha\beta} [\ell, \nu]_{\alpha\beta}$ for $(V-A) \times (V+A)$.

An easy mnemonic for recalling the momentum dot products in $|\mathcal{M}|^2$ is the following:

- (i) For $(V-A)^2$ or $(V+A)^2$, the two momenta associated with incoming arrows in the Feynman diagram are dotted, likewise the two with outgoing arrows.
- (ii) For $(V-A) \times (V+A)$ mixed interactions, the momentum with incoming arrow at one W vertex is dotted with the momentum with outgoing arrow at the other W vertex.

If the polarization of a given particle is known or to be measured, we need the projection operators

$$u\bar{u} = \frac{1}{2}(\not{p} + m)(1 + \lambda\gamma_5\not{S}), \quad v\bar{v} = \frac{1}{2}(\not{p} - m)(1 + \lambda\gamma_5\not{S}),$$

where $\lambda = \pm 1$ is twice the helicity and S is the covariant spin vector of the particle in question,

$$S_\mu = (|\mathbf{p}|/m, E\mathbf{p}/(m|\mathbf{p}|)).$$

Exercise. Show that the squared matrix element for $a \rightarrow b\ell\nu$ decay with $(V-A)^2$ interaction is

$$\sum |\mathcal{M}|^2 = 32G_F^2 (a - \lambda_a m_a S^a) \cdot \bar{\nu} (\ell - \lambda_\ell m_\ell S^\ell) \cdot b$$

if a and ℓ helicities are measured.

3.2 Muon Decay

The spin-averaged differential decay rate for $\mu^- \rightarrow \nu_\mu e^- \bar{\nu}_e$ is

$$d\Gamma = \frac{1}{2\mu^0} \frac{1}{2} \sum |\mathcal{M}|^2 (2\pi)^{4-9} \frac{d^3 e}{2e^0} d_2(\text{PS}),$$

where μ^0 and e^0 denote the particle energies, $\sum |\mathcal{M}|^2 = 128 G_F^2 (\mu \cdot \bar{\nu}) (\nu \cdot e)$ and $d_2(\text{PS})$ is the invariant phase space of ν and $\bar{\nu}$,

$$d_2(\text{PS}) = \delta^4(\mu - e - \nu - \bar{\nu}) \frac{d^3 \nu}{2\nu^0} \frac{d^3 \bar{\nu}}{2\bar{\nu}^0}.$$

Note that $\mu^0 \Gamma$ is a Lorentz invariant. Thus the invariant decay dis-

tribution for the electron is

$$\mu^0 e^0 \frac{d\Gamma}{d^3e} = \frac{G_F^2}{2\pi^5} \int [\mu \cdot \bar{\nu} \nu \cdot e] d_2(\text{PS}) .$$

Exercise. Show that the phase space integral of $\bar{\nu}^\alpha \nu^\beta$ is

$$\int d_2(\text{PS}) \bar{\nu}^\alpha \nu^\beta = \frac{\pi}{24} \left\{ g^{\alpha\beta} X^2 + 2X^\alpha X^\beta \right\} ,$$

where $X^\alpha = \mu^\alpha - e^\alpha = \nu^\alpha + \bar{\nu}^\alpha$. (Show from Lorentz covariance that the most general form is $A g^{\alpha\beta} X^2 + B X^\alpha X^\beta$ and then evaluate the integral in the $\nu + \bar{\nu}$ c.m. frame.)

Neglecting the electron mass, the decay distribution is

$$\mu^0 e^0 \frac{d\Gamma}{d^3e} = \frac{G_F^2 m_\mu^4}{96\pi^4} x(3 - 2x) ,$$

where x is the “scaled” electron energy variable

$$x = \frac{2e \cdot \mu}{m_\mu^2} = \frac{2e^0}{m_\mu}$$

and the second equality applies only in the μ rest frame. Now $2e \cdot \mu = \mu^2 + e^2 - (e - \mu)^2 = m_\mu^2 - (\nu + \bar{\nu})^2$ where $(\nu + \bar{\nu})^2$ is the invariant mass squared of the $\nu + \bar{\nu}$ system, which ranges from 0 to m_μ^2 for m_e set to zero. Hence x ranges from 0 to 1. When $x = 1$ and the electron has its maximum energy, it is back-to-back with both ν_e and ν_μ ,

$$\begin{array}{ccc} e & \longrightarrow & \bar{\nu}_e \\ \longleftarrow & & \longrightarrow \nu_\mu \end{array} .$$

Exercise. From the CP invariance of the interaction, or by direct calculation, show that the positron distributions from $\mu^+ \rightarrow e^+ \nu_e \bar{\nu}_\mu$ are identical to the electron distributions above.

We henceforth work in the muon rest frame, where $x = 2e^0/m_\mu$. The distribution becomes

$$\frac{1}{\Gamma} \frac{d\Gamma}{dx} = 2x^2(3 - 2x),$$

where Γ is the total width

$$\Gamma = \frac{G_F^2 m_\mu^5}{192\pi^3}.$$

$d\Gamma/dx$ peaks at $x = 1$ (the electrons from μ decay have a "hard" energy spectrum). Figure 3.2 compares the experimental spectrum of positrons from $\mu^+ \rightarrow e^+ \nu_e \bar{\nu}_\mu$ with the predicted $V-A$ spectrum, including electromagnetic corrections. Experimentally it is easier to study μ^+ decays, because when μ^- are brought to rest in a block of material their interactions with nuclei via $\mu^- p \rightarrow \nu_\mu n$ compete with decay.

Exercise. If the decaying muon has helicity $\frac{1}{2}\lambda_\mu$, show that the x -dependent factor in the invariant distribution becomes $x(3 - 2x) + 2(2x - 1)\lambda_\mu S^\mu \cdot e/m_\mu$. Hence show that if there is a polarized muon source with mean spin vector $\langle S \rangle$, the electron angular distribution in the muon rest frame is

$$d\Gamma/d\cos\theta dx = \Gamma x^2(3 - 2x)(1 - \alpha \cos\theta),$$

where $\cos\theta = \langle S \rangle \cdot e/e^0$ and $\alpha = (2x - 1)/(3 - 2x)$ is the muon asymmetry parameter.

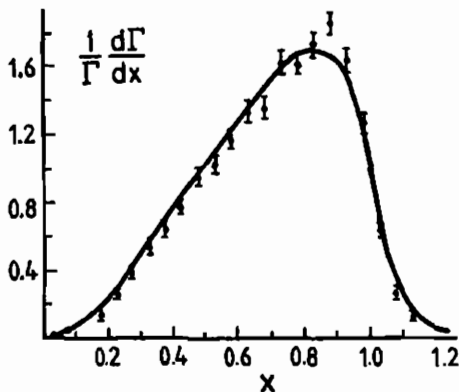


Fig. 3.2. Positron decay spectrum from muon decay; data from Phys. Rev. **119**, 1400 (1960). The theoretical curve includes radiative corrections and experimental resolution; the latter explains the tail above $x = 1$.

Exercise. Show that if m_e is not neglected, the muon decay width is

$$\Gamma = \frac{G_F^2 m_\mu^5}{192\pi^3} I\left(\frac{m_e^2}{m_\mu^2}\right),$$

where $I(x) = 1 - 8x + 8x^3 - x^4 + 12x^2 \ln\left(\frac{1}{x}\right)$.

Exercise. Show that a $(V+A) \times (V-A)$ interaction would yield a different electron decay distribution of the form $\frac{1}{\Gamma} \frac{d\Gamma}{dx} = 12x^2(1-x)$ but give the same lifetime.

Measuring the muon mean lifetime $\tau_\mu = \Gamma_\mu^{-1}$ is the most precise way to determine G_F . First- and second-order electromagnetic radiative corrections and m_μ^2/M_W^2 corrections to the amplitude must be taken into account. The radiative diagrams contributing to order α are shown in Fig. 3.3; the interference of the loop diagram with the Born diagram of Fig. 3.1 contributes in the same order as the first and second diagrams. This radiatively corrected decay width is

$$\Gamma^{\text{rad}} = \Gamma \left[1 + \frac{\alpha}{2\pi} \left(\frac{25}{4} - \pi^2 \right) \left(1 + \frac{2\alpha}{3\pi} \ln \frac{m_\mu}{m_e} \right) \right] \left[1 + \frac{3m_\mu^2}{5M_W^2} \right] I\left(\frac{m_e^2}{m_\mu^2}\right).$$

From the measured μ mean lifetime

$$\tau_\mu = (2.19709 \pm 0.00005) \times 10^{-6} \text{ s},$$

the value of the Fermi constant is determined to be

$$G_F = (1.16637 \pm 0.00002) \times 10^{-5} \text{ GeV}^{-2}.$$

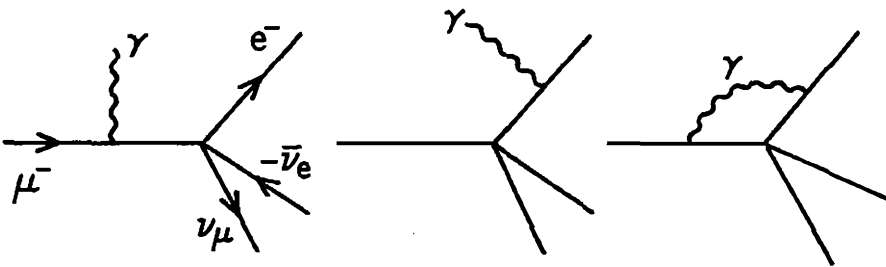


Fig. 3.3. Radiative corrections to order α in muon decay.

Since the Fermi constant has dimensions, it is frequently given in terms of the proton mass m_p . That numerical value is

$$G_F = 1.02679 \times 10^{-5} / m_p^2.$$

If we allow general scalar, pseudoscalar, tensor, vector and axial vector interactions, the distribution of electrons from muon decays has the form

$$\langle d\Gamma \rangle = \lambda x^2 dx d\cos\theta \left\{ 3(1-x) + 2\rho\left(\frac{4}{3}x-1\right) - \xi \cos\theta \left[(1-x) + 2\delta\left(\frac{4}{3}x-1\right) \right] \right\},$$

where λ , ρ , ξ and δ depend on the S , P , T , V , A coupling constants (ρ is known as the Michel parameter). The experimental averages for the parameters ρ , δ , ξ are compared below with the $V-A$ theory

	<u>Experiment</u>	<u>$V-A$ Prediction</u>
ρ	0.752 ± 0.003	$3/4$
δ	0.755 ± 0.009	$3/4$
ξ	0.972 ± 0.013	1

The agreement is excellent, possibly excepting the ξ determination which differs by two standard deviation from the prediction.

For τ -lepton decays, if we sum the $\tau \rightarrow \nu_\tau e \bar{\nu}_e$, $\nu_\tau \mu \bar{\nu}_\mu$ leptonic modes and approximate the hadronic modes by $\tau \rightarrow \nu_\tau d \bar{u}$ bare-quark transitions (with three quark colors and mixing matrix element $V_{ud} \simeq 1$), the τ lifetime is predicted to be

$$\tau_\tau \simeq (m_\mu/m_\tau)^5 \tau_\mu / 5 = 3.2 \times 10^{-13} \text{ s},$$

which agrees reasonably well with the experimental value $(2.96 \pm 0.3) \times 10^{-13} \text{ s}$.

Decays of a possible fourth-generation charged heavy lepton L into light final particles $L \rightarrow \nu_L (e \bar{\nu}_e, \mu \bar{\nu}_\mu, \tau \bar{\nu}_\tau, d \bar{u}, s \bar{c})$ are similar to the τ decay examples, except that the W -propagator factor $M_W^2 / [(L - \nu_L)^2 - M_W^2 + i\Gamma_W M_W]$ in the amplitude may no longer be negligible. For heavy final particles, see §3.5.

3.3 Heavy Neutrino Decay

Possible new neutrinos can be detected in various ways at colliders. If such a new neutrino is light, it will be detected indirectly by experiments which count the number of light neutrino species, which we discuss in a later chapter. If the new neutrino is heavy it will be unstable and may be detected directly through its decay products. We consider here the possibility that a new heavy neutrino N is produced at colliders. If N is the heavier member of an $SU(2)_L$ doublet, it will decay to its charged partner L through a virtual W in a manner analogous to μ decay. If N is the lighter member of a doublet or is a singlet, it can decay through a virtual W via mixing with ν_e, ν_μ, ν_τ neutrino members of doublets; see Fig. 3.4. The decay modes in this case are $N \rightarrow e(\nu_e\bar{e}, \nu_\mu\bar{\mu}, \nu_\tau\bar{\tau}, u\bar{d}, c\bar{s}, \text{etc.})$ and similarly for $N \rightarrow \mu$ and $N \rightarrow \tau$. The $(V-A) \times (V-A)$ matrix element squared for the channel $N \rightarrow e\nu_\mu\bar{\mu}$ for example, is

$$\sum_{\text{spins}} |\mathcal{M}|^2 = 128G_F^2 |V_{Ne}|^2 (N \cdot \bar{\mu})(e \cdot \nu),$$

where V_{Ne} is the mixing matrix element analogous to quark mixing. The calculations of lifetimes and decay spectra closely parallel those of the previous section. In the massless approximation for all final state particles and taking the quark mixing matrix to be diagonal,

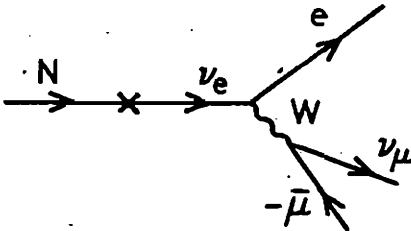


Fig. 3.4. Decay of a heavy neutrino N via mixing, schematically indicated by a cross.

the partial width for $N \rightarrow e f \bar{f}'$ decays via a virtual W is

$$\Gamma(N \rightarrow e) = 9|V_{Ne}|^2 \left(\frac{G_F^2 m_N^5}{192\pi^3} \right),$$

summing over nine final states $f \bar{f}' = \nu_e \bar{\nu}_e, \nu_\mu \bar{\nu}_\mu, \nu_\tau \bar{\nu}_\tau, u \bar{d}, c \bar{s}$. The N lifetime is then

$$\tau_N = [\Gamma(N \rightarrow e) + \Gamma(N \rightarrow \mu) + \Gamma(N \rightarrow \tau)]^{-1}.$$

Because of the observed $e - \mu - \tau$ universality, it is expected that $|V_{N\ell}| \ll 1$ for $\ell = e, \mu$ or τ . The lifetime will therefore be much longer than that of a lepton of comparable mass which can decay without mixing. The decay vertex may be experimentally resolvable, if the mean decay length ℓ_N lies in the range tens of microns up to tens of meters. ℓ_N is given by

$$\ell_N = \beta \gamma \tau_N,$$

where β is the N velocity in the laboratory and $\gamma = (1 - \beta^2)^{-1/2}$. If for example $\bar{N}N$ pairs are produced through $Z \rightarrow \bar{N}N$ decays at an $e^+e^- \rightarrow Z$ factory, then $\beta\gamma = [M_Z^2/(4m_N^2) - 1]^{1/2}$.

Exercise. Show that the mean decay length ℓ_N for neutrinos of multi-GeV mass produced via $e^+e^- \rightarrow Z \rightarrow \bar{N}N$ is approximately

$$\ell_N(\text{cm}) \simeq 40 \left(1 - 4m_N^2/M_Z^2\right)^{1/2} (15 \text{ GeV}/m_N)^6 (10^{-8}/|V|^2),$$

where $|V|^2 = |V_{Ne}|^2 + |V_{N\mu}|^2 + |V_{N\tau}|^2$. Note the approximate scaling $\ell_N \sim |V|^{-2} m_N^{-6}$ for $m_\tau \ll m_N \ll M_Z$.

The above discussion has assumed that N is a Dirac neutrino with conserved lepton number 1 such that it can mix with ν_e, ν_μ or ν_τ . Another possibility is that N has lepton number -1 and mixes with ν_e^c, ν_μ^c and ν_τ^c instead; the resulting decay modes of N are the charge conjugates of those discussed above and the decay widths are the same, just as μ^- and μ^+ decays have the same lifetimes and e^- and e^+ distributions.

For the case that N is a Majorana fermion (*i.e.* N and \bar{N} are identical and have no lepton number), it mixes equally with ν_e and ν_e^c ; then $N \rightarrow e^-$ and $N \rightarrow e^+$ transitions at the W vertex occur with equal probability. This doubles the decay rate, halving the lifetime and decay length.

Decays of $\bar{N}N$ pairs produced at the Z resonance have the following important properties:

- (i) The decay products always contain visible particles including a charged lepton e , μ or τ . Majorana neutrinos give leptons of either charge with equal rates; like-sign dileptons would be particularly striking.
- (ii) The clearest signature is a pair of back-to-back decay cones, separated by gaps from the production vertex. Another signature is one such cone with missing momentum opposite it, when one neutrino decays outside the detector. An interesting special case is the decay $N \rightarrow e^\pm \mu^\mp \nu$ which is distinctive even if the lifetime is too short for a gap to be visible.
- (iii) One can reconstruct the neutrino mass from a sample of N decays.
- (iv) The spatial distribution of events and the branching fractions into e , μ , τ modes determine the lifetime and the moduli of the neutrino mixing matrix elements V_{Ne} , $V_{N\mu}$, $V_{N\tau}$.
- (v) The lifetime and event rate determine the $\bar{N}N$ cross section. Comparison with the predicted $Z^0 \rightarrow \bar{N}N$ rate (see Chapter 4) tests whether N belongs to a doublet and whether it is a Dirac or Majorana particle.

Figure 3.5 displays the mean decay length ℓ_N versus the mass m_N for $e^+e^- \rightarrow \bar{N}N$ production at the Z resonance for various mixing parameters $|V|$. The mass determines the cross section, which is also shown here expressed as a multiple of the $e^+e^- \rightarrow Z \rightarrow \mu^+\mu^-$ cross section, assuming N is a doublet member.

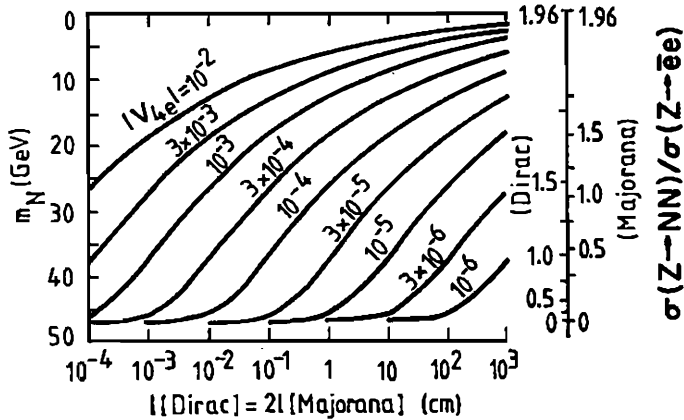


Fig. 3.5. Mean decay length of heavy neutrino N produced via $e^+e^- \rightarrow Z^0 \rightarrow \bar{N}N$ at the Z resonance, versus its mass m_N , for various values of the mixing parameter $|V|$. The corresponding cross section is also indicated on the vertical axis.

3.4 Charm and Bottom Decay Distributions

3.4.1 Spectator approximation.

In this section we consider the weak decays of a hadron containing one heavy quark constituent where this heavy quark turns into a lighter one. Since the energy released by the heavy quark is much bigger than typical quark binding energies, it is plausible to assume that the heavy quark decays independently of the other constituents—which act only as passive spectators. These quarks, together with possible other quark-antiquark pairs, form hadrons with unit probability. This is the *spectator approximation*, illustrated in Fig. 3.6.

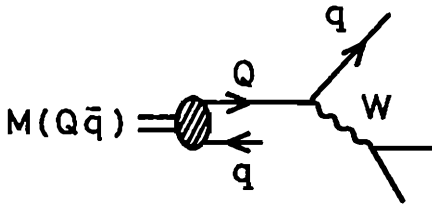


Fig. 3.6. Diagram for weak decay of a meson $M(Q\bar{q})$ with a heavy quark constituent Q in the spectator approximation.

An immediate consequence of the spectator model is that all hadrons containing one heavy quark of a particular flavor should have the same lifetime. In the case of charm this is not precisely true: for example for $D^0(c\bar{u})$, $D^+(c\bar{d})$ and $\Lambda_c^+(cud)$ the measured lifetimes are

$$\begin{aligned}\tau(D^0) &= 4.15 \pm 0.04 \times 10^{-13} \text{ s}, \\ \tau(D^+) &= 10.57 \pm 0.15 \times 10^{-13} \text{ s}, \\ \tau(\Lambda_c^+) &= 2.00 \pm 0.11 \times 10^{-13} \text{ s}.\end{aligned}$$

Nevertheless, these lifetimes are of the same order. Also the energy release in c -quark decay is only about 1 GeV, so the argument above is marginal in this case. It is expected that the spectator approximation becomes better the heavier the quark and that deviations from it are due to small effects of the other constituents. Various additions have been considered, including QCD effects, W -exchange and annihilation diagrams (see Fig. 3.7), interference, color matching, final state interactions and Pauli principle effects. For example, there are calculable non-spectator contributions to the decay of Λ_c which explain why it has a shorter lifetime than the D -mesons; however, there is no consensus about the relative importance of the various corrections in other cases. Aside from QCD corrections, however, these complications mainly affect the non-leptonic decay modes; the semileptonic decays are relatively clean.



Fig. 3.7. Typical W -exchange and annihilation diagrams in heavy quark decay.

3.4.2 Charm lifetime and branching fractions.

As a first approximation, the simple spectator model predictions provide a useful guide. To be specific, consider charm quark decays, illustrated in Fig. 3.8. Of the $c \rightarrow sW^+$ and $c \rightarrow dW^+$ transitions (where W is virtual), the mixing matrix of §2.11 indicates that $c \rightarrow sW^+$ is dominant.

Similarly at the other vertex, $W^+ \rightarrow u\bar{d}$ dominates over $W^+ \rightarrow u\bar{s}$. In the approximation $|V_{cs}| \approx |V_{ud}| \approx 1$ for the mixing matrix elements, there are five decay possibilities,

$$c \rightarrow s(e^+\nu_e \text{ or } \mu^+\nu_\mu \text{ or } u\bar{d})$$

with three color options for $u\bar{d}$. All five have the same matrix element, which is closely analogous to that of $\mu^+ \rightarrow \nu_\mu e^+ \nu_e$ decay; since this matrix element is symmetrical between ν_μ and e^+ , the effect of strange-quark mass in the former case is identical to the effect of electron mass in the latter. Hence the total charm decay width is

$$\Gamma(c \rightarrow \text{all}) \simeq \frac{5G_F^2 m_c^5}{192 \pi^3} I(m_s^2/m_c^2),$$

the charm lifetime can be expressed in terms of the muon lifetime

$$\tau_c \simeq \frac{\tau_\mu}{5} \left(\frac{m_\mu}{m_c} \right)^5 / I \left(\frac{m_s^2}{m_c^2} \right),$$

and the semileptonic branching fraction is

$$B(c \rightarrow e) = \Gamma(c \rightarrow e) / \Gamma(c \rightarrow \text{all}) = 1/5.$$

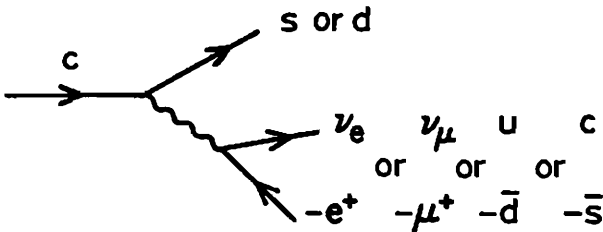


Fig. 3.8. Charm quark decays.

The lifetime prediction depends sensitively on the values assumed for m_c and m_s and to a lesser extent on the masses m_u and m_d that we have neglected. One possibility is to use (i) $m_c = m_D \simeq 1.87$ GeV and $m_s = m_K \simeq 0.50$ GeV to get the correct kinematical limits for D -meson decay, $D \rightarrow Ke\nu$, $D \rightarrow K\pi$, etc. Another possibility is to take (ii) $m_c = \frac{1}{2}m_\psi \sim 1.55$ GeV and $m_s = \frac{1}{2}m_\phi \simeq 0.50$ GeV, based on the $c\bar{c}$, $s\bar{s}$ structure of these mesons. The results are

$$\tau_c \simeq 4 \times 10^{-13} \text{ s} \quad (i), \quad 14 \times 10^{-13} \text{ s} \quad (ii),$$

which are in the right ball park.

The measured semileptonic branching fractions

$$B(D^\pm \rightarrow e) = 0.172 \pm 0.019, \quad B(D^0 \rightarrow e) = 0.077 \pm 0.012,$$

are consistent with the spectator model prediction in the case of D^\pm , but suggest an enhancement of non-leptonic modes in the D^0 case. It is possible to side-step the question of non-leptonic modes by examining the semileptonic width alone, which is experimentally given by $\Gamma(D \rightarrow e) = B(D \rightarrow e)/\tau_D$. The D^\pm and D^0 values are closely similar, as expected in the spectator model

$$\Gamma(D^\pm \rightarrow e) = (1.63 \pm 0.18) \times 10^{11} \text{ s}^{-1},$$

$$\Gamma(D^0 \rightarrow e) = (1.86 \pm 0.29) \times 10^{11} \text{ s}^{-1}.$$

The calculated values, for the quark mass choices above, are

$$\Gamma(c \rightarrow e) = 4.7 \times 10^{11} \text{ s}^{-1} \quad (i), \quad 1.5 \times 10^{11} \text{ s}^{-1} \quad (ii).$$

The agreement with experiment is better for choice (ii).

Another approach to the quark mass question is to regard the decaying hadron such as D^+ as a c -quark plus a massless \bar{d} -quark, each with momentum k in the D rest frame. A Gaussian distribution

of this Fermi momentum may be assumed, with $\langle k \rangle$ of order a few hundred MeV. Introducing k has two consequences: (i) the charm quark lifetime is lengthened by the Lorentz factor of its motion and (ii) the mass of c for each k is determined by energy conservation, $m_D = k + (k^2 + m_c^2)^{1/2}$ giving $m_c^2 = m_D^2 - 2km_D$. The resulting lifetime depends on $\langle k \rangle$.

3.4.3 Bottom lifetime and branching fractions.

It is expected that the spectator approximation will be better for bottom than for charm decays, because of the larger mass. At the b -quark vertex, only $b \rightarrow c$ and $b \rightarrow u$ transitions are allowed kinematically; evidence from the semileptonic decay spectrum indicates that $b \rightarrow c$ dominates. There are then 9 principal decay modes

$$b \rightarrow c(e\bar{\nu}_e \text{ or } \mu\bar{\nu}_\mu \text{ or } \tau\bar{\nu}_\tau \text{ or } d\bar{u} \text{ or } s\bar{c})$$

counting three colors for the quark channels, closely analogous to $\mu^- \rightarrow \nu_\mu e\bar{\nu}_e$ with the charm mass in b -decay playing a similar role to the e mass in μ -decay. The $\tau\bar{\nu}_\tau$ and $s\bar{c}$ channels suffer extra phase-space suppression of order 1/5 to 1/10 relative to the others (exact formulas are given in §3.5). For the following semi-quantitative discussion we shall assume a suppression factor 1/5 for these modes, which should be accurate to the 10% level. The b -quark lifetime is then approximately

$$\tau_b \simeq \frac{\tau_\mu}{5.8|V_{cb}|^2} \left(\frac{m_\mu}{m_b} \right)^5 / I(m_c^2/m_b^2)$$

and the branching fraction for the first-stage semileptonic decay $b \rightarrow ce\bar{\nu}_e$ is

$$B(b \rightarrow e) \simeq 1/5.8 \simeq 0.17.$$

We note that second-stage leptons from $b \rightarrow c \rightarrow se\nu$, etc. have a softer energy spectrum and can be separated experimentally.

For calculations we consider two mass assignments (i) $m_b = m_B \simeq 5.27$ GeV, $m_c = m_D \simeq 1.87$ GeV and (ii) $m_b = \frac{1}{2}m_\Upsilon \simeq 4.73$ GeV, $m_c = \frac{1}{2}m_\psi = 1.55$ GeV, which give

$$\tau_b = 1.2 \times 10^{-12} \times \left(\frac{0.05}{|V_{cb}|} \right)^2 s \quad (i), \quad 1.8 \times 10^{-12} \times \left(\frac{0.05}{|V_{cb}|} \right)^2 s \quad (ii).$$

The measured B -meson mean lifetimes are

$$\tau_{B^+} = (1.54 \pm 0.11) \times 10^{-12} s, \quad \tau_{B^0} = 1.50 \pm 0.11 \times 10^{-12} s.$$

Comparison of the spectator model calculation with experiment determines $|V_{cb}|$, but the result clearly depends somewhat on the assumed quark mass values.

The B^\pm and B^0 meson semileptonic branching fractions have not yet been separately determined. The measurements of the mean branching fractions for the first-stage decays are

$$B(B \rightarrow e) = 0.104 \pm 0.004, \quad B(B \rightarrow \mu) = 0.103 \pm 0.005.$$

Again, since these are smaller than the spectator model value 0.17, non-leptonic enhancements seem to be indicated. A cleaner measure of $|V_{cb}|$ may therefore result from comparing theory and experiment for the semileptonic partial width. Ignoring possible differences in the B^\pm and B^0 lifetimes and branching fractions, the experimental value is

$$\Gamma(B \rightarrow e) = (0.68 \pm 0.06) \times 10^{11} s^{-1}$$

to be compared with the theoretical values

$$\Gamma(B \rightarrow e) = 1.2 \times 10^{11} \times \left(\frac{|V_{cb}|}{0.05} \right)^2 \quad (i), \quad 0.8 \times 10^{11} \times \left(\frac{|V_{cb}|}{0.05} \right)^2 \quad (ii).$$

It is clear that $|V_{cb}|$ is of order 0.04–0.05 and that the quark mass choice is not very critical.

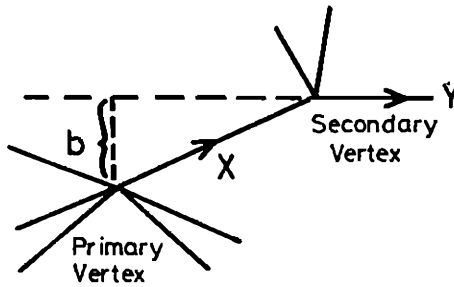


Fig. 3.9. Impact parameter b for a track from a secondary vertex.

Exercise. Estimate the lifetime and semileptonic branching fraction for a t -quark of mass 40 GeV .

In order to measure the lifetime of a very short-lived particle such as D or B , one must be able to distinguish the production and decay points and measure the gap between them. In collider experiments this is accomplished by measuring charged particle tracks emerging from an interaction and extrapolating them back, either to the primary interaction vertex or to possible secondary decay vertices. High resolution microvertex detectors (*e.g.* silicon strips, CCD's—charge-coupled devices, *etc.*) are used to resolve short decay gaps. In establishing whether a track emanates from the primary vertex (which usually has many outgoing tracks) an impact parameter b is defined as the shortest distance between the track and the primary vertex; see Fig. 3.9. If the impact parameter is significantly larger than the experimental resolution (typically some tens of microns, one micron = 10^{-4}cm) a secondary vertex is indicated.

Exercise. Suppose that the shortlived particle X has velocity β and Lorentz factor $\gamma = (1 - \beta^2)^{-1/2}$ in the lab frame. In the rest-frame of X , reached by boosting along the X -momentum, suppose that X lives for time τ and that the secondary particle Y has energy Y^0 and momentum components Y_L, Y_T along and perpendicular to the X -direction. The decay length of X is therefore $\beta\gamma\tau$. Show that the angle θ between the X and Y tracks in the lab is

$$\theta = \arctan \left[Y_T / (\beta\gamma Y^0 + \gamma Y_L) \right]$$

and hence that the impact parameter for relativistic X ($\gamma \gg 1$) is

$$b = \beta \tau Y_T / (\beta Y^0 + Y_L) \simeq \tau Y_T / (Y^0 + Y_L).$$

If X is spinless or unpolarized, so that its rest-frame decay is isotropic, show that the mean value of b is

$$\langle b \rangle = \frac{1}{2} \pi \tau_X,$$

where τ_X is the mean lifetime (assuming Y is relativistic in the X rest frame). Thus the distribution of b is insensitive to the γ -factor of the decaying particle X , and directly measures the lifetime.

3.5 General $V \pm A$ Decay Rate

For completeness, we give the general form of the rate for the decay

$$a \rightarrow bc\bar{d}$$

via an effective Lagrangian with $V \pm A$ weak currents and arbitrary masses,

$$\mathcal{L}_{\text{eff}} = (G_L \bar{b}_L \gamma^\mu a_L + G_R \bar{b}_R \gamma^\mu a_R) (g_L \bar{c}_L \gamma_\mu d_L + g_R \bar{c}_R \gamma_\mu d_R).$$

The transition probability, summed over spins, is

$$\begin{aligned} \sum |\mathcal{M}|^2 = & 16 \left[(G_L^2 g_L^2 + G_R^2 g_R^2) (a \cdot \bar{d})(b \cdot c) \right. \\ & + (G_L^2 g_R^2 + G_R^2 g_L^2) (a \cdot c)(b \cdot \bar{d}) \\ & - G_L G_R (g_L^2 + g_R^2) m_a m_b (c \cdot \bar{d}) \\ & + (G_L^2 + G_R^2) g_L g_R (a \cdot b) m_c m_d \\ & \left. - 4 G_L G_R g_L g_R m_a m_b m_c m_d \right]. \end{aligned}$$

The two-body phase space of any pair of outgoing particles can be integrated over using Appendix B results. Clustering $c\bar{d}$ first, we note

that as $\int c^\mu \bar{d}^\nu d_2$ (PS of $c\bar{d}$) is symmetric in $\mu\nu$ indices, the integrals of the $(a \cdot \bar{d})(b \cdot c)$ and $(a \cdot c)(b \cdot \bar{d})$ terms will be the same. The final result for the partial width is

$$\Gamma = \frac{m_a^5}{128\pi^3} [(G_L^2 + G_R^2)(g_L^2 + g_R^2)I_1 + G_L G_R(g_L^2 + g_R^2)I_2 + (G_L^2 + G_R^2)g_L g_R I_3 + G_L G_R g_L g_R I_4],$$

where

$$I_1 = \int dz (z - x_c^2 - x_d^2)(1 + x_b^2 - z)f,$$

$$I_2 = -2 \int dz (z - x_c^2 - x_d^2)x_b f,$$

$$I_3 = 2 \int dz (1 + x_b^2 - z)x_c x_d f,$$

$$I_4 = -16 \int dz x_b x_c x_d f.$$

Here $x_i = m_i/m_a$, $(x_c + x_d)^2 \leq z < (1 - x_b)^2$ and $f = \lambda^{1/2}(1, z, x_b^2)\lambda^{1/2}(z, x_c^2, x_d^2)/z$. We remark that $I_1(x_a, x_b, x_c)$ is independent of a, b, c ordering and $I_1(0, 0, 0) = 1/12$.

3.6 Semileptonic Decay Distributions

We can qualitatively infer some features of lepton spectra from c and b decays from our earlier discussion of μ decay. The squared matrix elements for the semileptonic decays are

$$\begin{aligned} \mu^- \rightarrow \nu_\mu e^- \bar{\nu}_e & \quad \sum |\mathcal{M}|^2 \propto (\mu^- \cdot \bar{\nu}_e)(\nu_\mu \cdot e^-), \\ c \rightarrow s e^+ \nu_e & \quad \sum |\mathcal{M}|^2 \propto (c \cdot e^+)(s \cdot \nu_e), \\ b \rightarrow c e^- \bar{\nu}_e & \quad \sum |\mathcal{M}|^2 \propto (b \cdot \bar{\nu}_e)(c \cdot e^-). \end{aligned}$$

Thus the following decay spectra will be similar:

$$\begin{array}{ll} \mu^- \rightarrow e^- & \text{down} \rightarrow \text{down} \\ c \rightarrow \nu_e & \text{up} \rightarrow \text{up} \\ b \rightarrow e^- & \text{down} \rightarrow \text{down} \end{array}$$

and likewise

$$\begin{array}{ll}
 \mu^- \rightarrow \bar{\nu}_e & \text{down} \rightarrow \overline{\text{up}} \\
 c \rightarrow e^+ & \text{up} \rightarrow \overline{\text{down}} \\
 b \rightarrow \bar{\nu}_e & \text{down} \rightarrow \overline{\text{up}}
 \end{array}$$

will be similar, up to corrections involving masses of final particles; here up and down refer to the location in the doublet. It was noted previously that the $\mu^- \rightarrow e^-$ spectrum was hard, with event rate peaking at the upper end-point; a similar feature exists for $b \rightarrow e^-$, which as we shall see later, enhances the electron signal from b -decays compared to c -decays at colliders. Corresponding results hold for the antiparticle decays, by CP symmetry. The decays $c \rightarrow s\mu^+\nu_\mu$ and $b \rightarrow c\mu^-\bar{\nu}_\mu$ are essentially the same as the corresponding decays to electrons, since both electron and muon masses are negligible here.

To be more quantitative, the invariant single-particle distributions from charm decay are

$$E_i \frac{d\Gamma}{d^3p_i} = \frac{|V_{cs}|^2 G_F^2}{2c^0\pi^5} \int [c \cdot e^+ s \cdot \nu_e] d_2(\text{PS}) \equiv g_i(X_i^2),$$

where $i = e^+, s,$ or ν_e and

$$X_i = c - p_i.$$

In the c rest frame $X_i^2 = m_c^2 + m_i^2 - 2m_c E_i$. The phase-space integral is over the other two final-state particles ($j, k \neq i$). The integrals can be evaluated using formulas of Appendix B.

Exercise. Show that the invariant distributions are given by

$$g_e(X_e^2) = \frac{6K(X_e^2 - s^2)^2(c^2 - X_e^2)}{X_e^2},$$

$$g_\nu(X_\nu^2) = \frac{K(X_\nu^2 - s^2)^2(c^2 - X_\nu^2)[2X_\nu^4 + X_\nu^2(c^2 + s^2) + 2c^2s^2]}{X_\nu^6},$$

$$g_s(X_s^2) = K[(c^2 - s^2)^2 + X_s^2(c^2 + s^2) - 2X_s^4],$$

where $K = |V_{cs}|^2 G_F^2 / (96\pi^4 c^0)$. Neglecting also the strange quark

mass, find the corresponding distributions $\Gamma^{-1}d\Gamma/dx_i$ where $x_i = 2E_i/m_c$ in the c rest frame and compare with μ decay results.

Exercise. Show that the physical ranges of the X_i^2 are

$$(m_j + m_k)^2 \leq X_i^2 \leq (m_c - m_i)^2, \quad i \neq j \neq k,$$

and that the corresponding ranges of the decay particle energies in the charm rest frame are

$$0 \leq E_e \text{ (or } E_\nu) \leq (m_c^2 - m_s^2)/(2m_c),$$

$$m_s \leq E_s \leq (m_c^2 + m_s^2)/(2m_c).$$

These energy distributions can be readily calculated from the above invariant distributions using $E_i d\Gamma/d^3p_i = (4\pi p_i)^{-1} d\Gamma/dE_i$. The results in the “scaled” energy variables $x_i = 2E_i/m_c$ are shown in Fig. 3.10 for masses $m_c = 1.87$ and $m_s = 0.5$ GeV. We note that the ν_e energy distribution is harder than the e^+ energy distribution. The s quark takes a higher fraction of the energy, due to its mass (compare the formulas above for the kinematic ranges of the energies). The energy of the final quark is not directly measurable because of fragmentation, which is discussed in a later chapter.

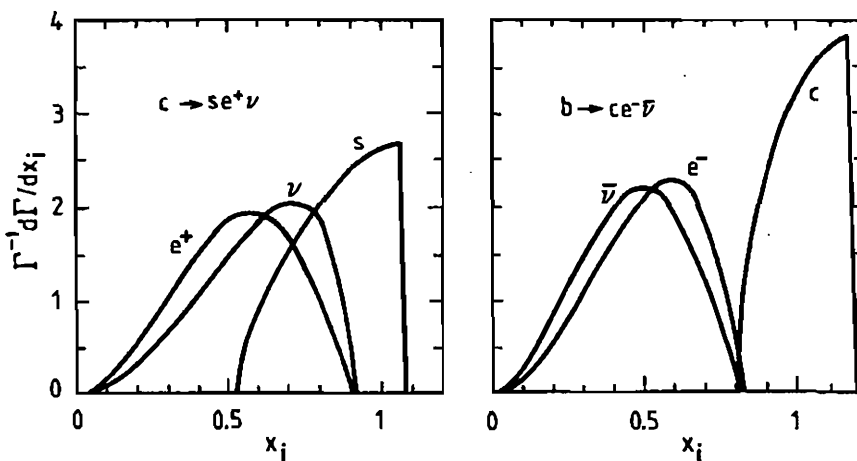


Fig. 3.10. Fractional energy spectra $x_i = 2E_i/m_Q$ of decay leptons and quarks from $Q = c, b$ semileptonic decay.

The corresponding distributions for $b \rightarrow c e^- \bar{\nu}_e$ decay can be obtained from those for charm decay by making the following substitutions in the preceding equations:

$$c \rightarrow b, \quad s \rightarrow c, \quad \nu_e \rightarrow e^-, \quad e^+ \rightarrow \bar{\nu}_e.$$

The scaled energy distributions in the b rest frame are also shown in Fig. 3.10 for masses $m_b = 5.27$ GeV and $m_c = 1.87$ GeV, with $x_i = 2E_i/m_b$. The energy spectra of the electron and the neutrino are qualitatively interchanged in going from c to b decay and a harder charged lepton energy distribution is obtained in b decay (analogous to μ decay). This enhances the electron signal from b -quarks relative to that from c -quarks, in high energy collider experiments, since the more energetic electrons are more likely to survive acceptance cuts.

Exercise. Show that the different behavior of $d\Gamma/dE_e$ in c and b decays near the endpoints can be understood as a consequence of angular momentum conservation. For decays with the parent particle at rest, the maximum electron energy occurs when the other two particles recoil together against it. In the massless approximation for all final-state particles, this configuration is allowed in b decay but is forbidden in c decay.

The relative contributions of the $b \rightarrow c e^- \bar{\nu}_e$ and $b \rightarrow u e^- \bar{\nu}_e$ decay channels can be experimentally determined from the shape of the electron spectrum near its upper endpoint. For electron energy in the range,

$$\frac{m_b^2 - m_c^2}{2m_b} \leq E_e \leq \frac{m_b^2 - m_u^2}{2m_b},$$

only the $b \rightarrow u e^- \bar{\nu}_e$ channel can contribute. In studies of the electron spectrum from B mesons produced nearly at rest in e^+e^- collisions at CESR, it is found that the spectrum cuts off sharply near the endpoint for $b \rightarrow c e^- \bar{\nu}_e$, as shown in Fig. 3.11. This is the source of the experimental limit on the mixing matrix element $|V_{ub}|$.

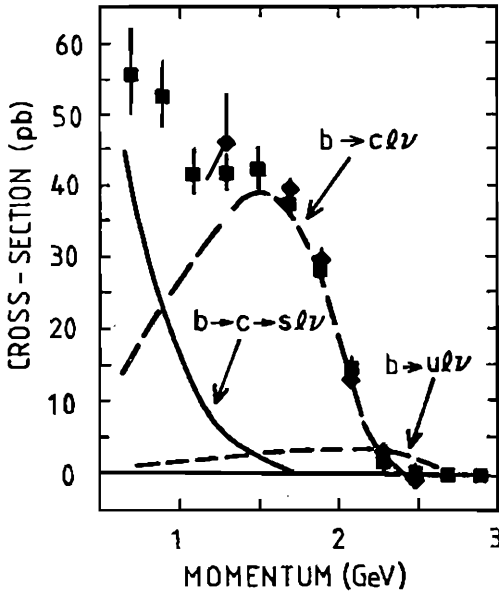


Fig. 3.11. The measured spectra of electrons (squares) and muons (diamonds) from B decay. The curves represent the shapes of primary $b \rightarrow c\ell\nu$ and $b \rightarrow u\ell\nu$ contributions along with the secondary $b \rightarrow c \rightarrow s\ell\nu$ component.

Exercise. Show that if $V_{ub} = 0$ exactly, there is no CP violating phase in the quark mixing matrix for three generations.

We have hitherto concentrated attention on cases with $m_a \ll M_W$, approximating the W -propagator factor in the amplitude by

$$(-g_{\mu\nu} + q_\mu q_\nu / M_W^2) / (q^2 - M_W^2 + iM_W \Gamma_W) \simeq g_{\mu\nu} / M_W^2,$$

where $q = a - b = c + \bar{d}$ is the momentum carried by W . However, the results above can be generalized to $m_a \sim M_W$ by including the W -denominator factor $|1 - zm_a^2 / (M_W^2 - i\Gamma_W M_W)|^{-2}$ in the integrands of $I_1 \cdots I_4$ above, since $q^2 = zm_a^2$. The $q_\mu q_\nu / M_W^2$ term in the numerator can still be neglected, so long as c and \bar{d} are light compared to W .

3.7 Characteristics of Heavy Quark Decays

3.7.1 Electron and muon signals.

The problem of finding heavy quarks through their decay products is that there are large backgrounds from conventional quark and gluon sources. Although in principle the heavy hadron could be identified and its mass measured from peaks in the invariant mass distributions of its decay products, in practice these backgrounds obscure such signals unless there is some other tag for heavy quark events.

The presence of leptons is a powerful way to tag final states containing heavy quarks. The latter have substantial semileptonic branching fractions, of order 10% for e and 10% for μ ; this is known experimentally for c and b , and expected theoretically for t on the basis of counting lepton and quark decay modes. Among hadrons containing light quarks, only $\pi \rightarrow \mu\nu$, $K \rightarrow \mu\nu$, $K \rightarrow \pi e\nu$ and $\pi^0 \rightarrow e^+e^-\gamma$ are substantial sources of leptons, but these can be separated in various ways. For example, the first three cases have long decay paths and give kinks in the charged particle track at the decay point, because the incoming π^\pm or K^\pm momentum does not match the outgoing μ^\pm or e^\pm momentum in magnitude or direction; the fourth case gives low-mass e^+e^- pairs. Notice that π and K decay backgrounds are not the same for electrons and muons; in particular $\pi \rightarrow e\nu$ and $K \rightarrow e\nu$ are essentially absent.

The expectation that t -quarks and possible heavier quarks Q have semileptonic branching fraction of order 10% into electrons is based on decay via W -bosons only. In extensions of the standard model with more than one scalar multiplet (e.g. two scalar doublets), there are additional decays into charged Higgs scalar particles, e.g. $Q \rightarrow H^+q$, via Yukawa couplings; see Fig. 3.12. If $m_{H^+} < m_Q < M_W$, this decay width is of order $G_F m_Q^3$, which dominates over the $G_F^2 m_Q^5$ contribution from virtual W -bosons. H^+ in turn is expected to decay into the heaviest kinematically accessible fermion-antifermion channel, so that $H^+ \rightarrow e\nu$ or $\mu\nu$ are highly suppressed. In this case of

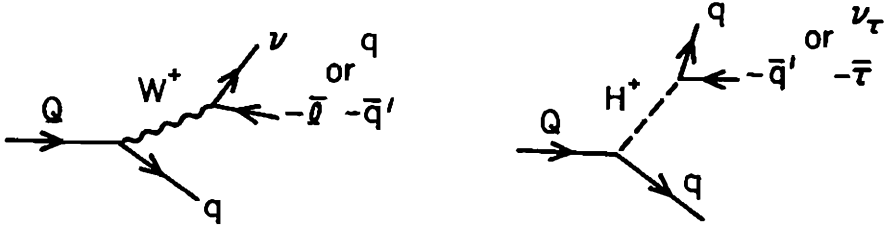


Fig. 3.12. Dominant contributions to heavy quark decay from virtual W and real charged Higgs bosons.

real H^+ emission, there is essentially no lepton signal for Q from primary semileptonic decays. The fact that B -mesons have semileptonic decays shows that there is no charged Higgs particle with $m_H < m_B$.

Exercise. Assuming the coupling of H^+ to $t\bar{b}$ has the form

$$\mathcal{L} = \left(2\sqrt{2} G_F\right)^{\frac{1}{2}} m_t \cot \beta H^+ \bar{t}_R b_L + \text{h.c.}$$

(which is the dominant term in the two-doublet model (§12.6) if $\cot^2 \beta \gg m_b/m_t$), show that the partial width for $t \rightarrow bH^+$ is

$$\Gamma(t \rightarrow bH^+) = \sqrt{2} G_F m_t^3 \cot^2 \beta (1 - m_H^2/m_t^2)^2 / (16\pi)$$

ignoring m_b^2/m_t^2 terms, and hence that the ratio to the sum of virtual W mediated decays is

$$\begin{aligned} \Gamma(t \rightarrow bH^+) / \Gamma(t \rightarrow bq\bar{q} + b\bar{l}\nu) &= 4\sqrt{2} \pi^2 \cot^2 \beta (1 - m_H^2/m_t^2)^2 / (3G_F m_t^2) \\ &\sim 1.6 \times 10^6 [\text{GeV}]^2 \cot^2 \beta / m_t^2. \end{aligned}$$

Exercise. Assume that H^+ has the following dominant couplings to $\nu\bar{\tau}$ and $c\bar{s}$ decay channels, as in the two-doublet model (§12.6) with $|V_{cs}| \simeq 1$

$$\begin{aligned} \mathcal{L} &= (2\sqrt{2} G_F)^{\frac{1}{2}} H^+ [m_\tau \tan \beta \bar{\nu}_{\tau L} \tau_R + m_s \tan \beta \bar{c}_L s_R + m_c \cot \beta \bar{c}_R s_L] \\ &+ \text{h.c.} \end{aligned}$$

Neglecting m_s/m_H corrections, show that the partial decay widths are

$$\Gamma(H^+ \rightarrow \tau^+ \nu) = \frac{\sqrt{2}G_F}{8\pi} m_H \left(1 - \frac{m_\tau^2}{m_H^2}\right)^2 m_\tau^2 \tan^2 \beta,$$

$$\Gamma(H^+ \rightarrow c \bar{s}) = \frac{3\sqrt{2}G_F}{8\pi} m_H \left(1 - \frac{m_c^2}{m_H^2}\right)^2 (m_c^2 \cot^2 \beta + m_s^2 \tan^2 \beta),$$

and hence that the branching fractions are approximately (taking $m_c \simeq m_\tau$ and $m_s \simeq 0$)

$$B(H^+ \rightarrow \tau^+ \nu) \simeq 1/(1 + 3 \cot^4 \beta), \quad B(H^+ \rightarrow c \bar{s}) \simeq 3/(\tan^4 \beta + 3).$$

3.7.2 Cascade decays.

Because of the nearly-diagonal character of the quark mixing matrix, the most favored route for a heavy quark charged-current decay is either to the same generation (*e.g.* $c \rightarrow s$) or—if this is kinematically impossible—to the nearest generation (*e.g.* $b \rightarrow c$). As a result, heavy quark decays go preferentially via a cascade:

$$\begin{aligned} c &\rightarrow s, \\ b &\rightarrow c \rightarrow s, \\ t &\rightarrow b \rightarrow c \rightarrow s, \end{aligned}$$

with real or virtual W emission at each stage.

One consequence is multilepton production: there is a possibility of producing an $\ell^- \bar{\nu}_\ell$ or $\ell^+ \nu_\ell$ pair at each step of the cascade. Figure 3.13 shows schematically how up to two charged leptons can be produced in b -decay and up to three in t -decay, along the main cascade sequence. The full possibilities are many:

$$\begin{aligned} t &\rightarrow b(\bar{e}\nu, \bar{\mu}\nu, \bar{\tau}\nu, c\bar{s}, u\bar{d}), \\ b &\rightarrow c(e\bar{\nu}, \mu\bar{\nu}, \tau\bar{\nu}, \bar{c}s, \bar{u}d), \\ c &\rightarrow s(\bar{e}\nu, \bar{\mu}\nu, u\bar{d}), \\ \tau &\rightarrow \nu(e\bar{\nu}, \mu\bar{\nu}, \bar{u}d), \end{aligned}$$

involving many options at each stage, with sometimes a side-branch as in $b \rightarrow c\tau\bar{\nu}$ where both c and τ go on to decay. However, the

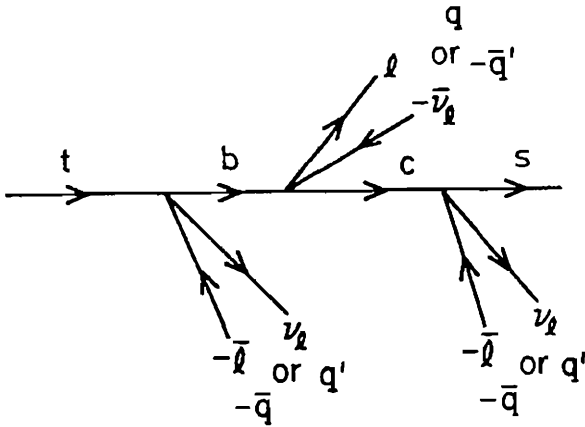


Fig. 3.13. Multi-lepton and multi-quark possibilities in t -quark cascade decays.

leptons from later cascade stages typically carry less energy, which makes them more difficult to detect in experiments with acceptance cuts on momenta.

Exercise. Including principal side-branches, show that the maximum number of charged leptons remains 2 for b , 3 for t decays.

Another consequence of cascade decays is more secondary decay vertices close to the primary quark production vertex. Bottom-quarks give typically two such vertices, one from b and one from c decay, but with modes like $b \rightarrow c\tau\bar{\nu}$ there is a third. Top-quarks are too short-lived to have resolvable decay vertices, but the subsequent cascade gives two and side-branches can give two more. These multiple decay vertices provide a valuable way to identify heavy-quark events experimentally.

3.7.3 Kinematics: lepton isolation and jet p_T .

The kinematics of decay of a hadron ($Q\bar{q}$) or (Qqq) containing a heavy quark Q are essentially the kinematics of Q decay. For simplicity the following discussion refers to Q , but it should be understood that it is the heavy hadron which decays and that the decay products of interest are hadrons and leptons. The dominant feature of Q decay is its large energy release.

The most immediate consequence is that the decay products have large invariant mass. If their four-momenta are labelled p_i , then $(\sum p_i)^2 = m_Q^2$. In principle this property could identify heavy quarks and measure their mass m_Q . In practice however, there are usually many hadrons in an event which makes it difficult to single out those which come from hadronic decays of Q and semileptonic decays have the problem of a missing neutrino.

A useful consequence of the large energy release is that the final particles from heavy quark decay are distributed over a wider solid angle than the decay products from lighter quarks of the same energy. As a simple example, when heavy quarks Q are produced near threshold via $e^+e^- \rightarrow Q\bar{Q}$, they are moving slowly and their decay products are distributed rather isotropically, quite unlike the situation with light quarks q produced via $e^+e^- \rightarrow q\bar{q}$ at the same energy, which lead to narrow back-to-back pairs of jets. Hence concentrating attention on isotropic events here makes it easier to detect a new heavy quark threshold.

As another example, a fast lepton from b or c decay is necessarily accompanied closely by hadrons. Figure 3.14 shows a B -meson which produces a \bar{D} -meson when it decays semileptonically. If the final electron is very energetic, kinematics require that the initial B was also energetic and hence that the decay products are mostly collimated in the forward direction.

Exercise. By requiring that the invariant mass of e^+ plus \bar{D} in Fig. 3.14 is less than m_B , show that the angle between e^+ and \bar{D} and the momentum of \bar{D} are constrained in any given frame by

$$\sin \theta_{eD} < \frac{m_B^2 - m_D^2}{2p_e m_D}, \quad p_D > \frac{4m_D^2 p_e^2 - (m_B^2 - m_D^2)^2}{4p_e(m_B^2 - m_D^2)}.$$

Hint: For given p_e and θ_{eD} , first find the upper and lower bounds on p_D . At what value of θ_{eD} do these bounds meet? What is the lowest lower bound?

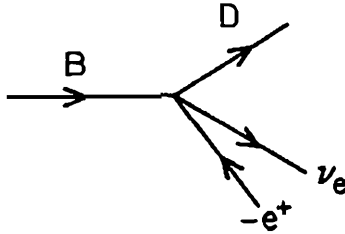


Fig. 3.14. Sketch of $B \rightarrow \bar{D}e^+\nu_e$ decay.

These bounds are extreme limits: most events will satisfy them by a comfortable margin. They bite hard when $p_e > m_B^2/m_D = 14 \text{ GeV}$ which requires $\sin\theta_{eD} < \frac{1}{2}(1 - m_D^2/m_B^2)$ and $p_D > \frac{3}{4}m_D/(1 - m_D^2/m_B^2)$. The physical consequence is that a very energetic lepton from b -decay (or c -decay, which is similar) cannot appear in isolation: there must be energetic hadrons nearby in angle. On the other hand, for a 175 GeV t -quark, the analogous constraint for t -flavored meson $T \rightarrow Be\nu$ decay does not bite hard until $p_e \sim m_T^2/m_B \sim 6 \text{ TeV}$. Figure 3.15 illustrates the difference between t and b quark decay kinematics.

Exercise. For a massless particle emitted in 3-body decay of a moving heavy quark, show that there is no constraint on its angle of emission but there is a severe constraint on its energy for backward angles.

Thus *lepton isolation* offers a way to distinguish the contributions of t or other very heavy quarks from b and c contributions. If we set a suitable threshold for their momenta, leptons coming from the heavier quark decays have a good chance to be isolated from hadrons, while those coming from b and c decays are not isolated. This property has been used in t -quark searches at the CERN $p\bar{p}$ collider.

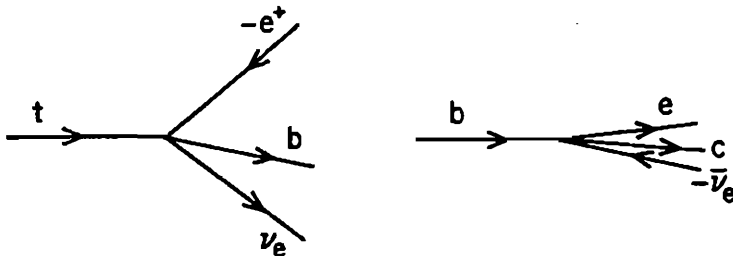


Fig. 3.15. Qualitative comparison of collimation of decay particles from t and b quarks, for primary quark momentum $p_Q \approx m_t \gg m_b$.

Exercise. For a t -quark of mass 40 GeV produced with 300 GeV momentum at a supercollider, within what angular cone about the t -direction can a 100 GeV electron be emitted?

Another useful application of Q -decay kinematics is flavor-tagging of jets. When an energetic light quark turns into hadrons, these hadrons form a narrow jet collimated along the original quark direction. Such jets are a familiar feature of e^+e^- experiments, where $e^+e^- \rightarrow \bar{q}q$ reactions lead typically to pairs of back-to-back jets originated by q and \bar{q} . However, it is not generally possible to determine experimentally which flavor of light quark originated a given jet (or whether it came from a gluon instead). With a heavy quark Q it is different; the jet contains the decay products of Q which dominate its properties.

For example, semileptonic decay of Q can give a muon in the Q jet. Although Q itself has momentum collimated with its jet axis (defined by the summed momenta in the Q jet or the back-to-back \bar{Q} jet) the muon can have momentum component transverse to this axis up to the limit $p_T^\mu \lesssim \frac{1}{2}m_Q$, which is quite distinctive. Thus for example c -decays give $p_T^\mu \lesssim 0.9$ GeV and b -decays give $p_T^\mu \lesssim 2.3$ GeV. This provides an effective way to tag heavy flavors. In e^+e^- experiments at PEP and PETRA samples of b -jets have been selected by choosing jets containing muons with $p_T^\mu > 1$ GeV; going one step further, the sign of the decay μ^\pm establishes whether b or \bar{b} is the parent.

This technique can also be used in the search for heavier quark flavors. Figure 3.16 compares the electron or muon p_T spectra calculated from semileptonic decays of b quarks and hypothetical fourth-generation charge $-\frac{1}{3}$ v quarks of mass 40 GeV, produced in $e^+e^- \rightarrow Z \rightarrow b\bar{b}$ and $v\bar{v}$. Both primary electrons from $b \rightarrow c$ or $v \rightarrow c$ transitions and secondary electrons from $c \rightarrow s\bar{e}\nu_e$ and $\tau \rightarrow \nu_\tau e\bar{\nu}_e$ are included. The v -decay electrons have a p_T distribution dramatically harder than in b decay. We emphasize the importance of using the jet axis as a reference direction in heavy quark tagging; distributions relative to the beam axis owe more to the angular distribution of quark

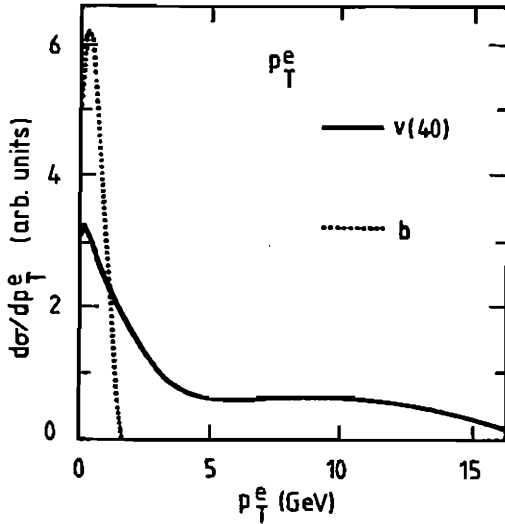


Fig. 3.16. Distributions of electron momentum transverse to the heavy quark axis in $e^+e^- \rightarrow Z \rightarrow Q\bar{Q}$ with $Q = b, v$.

production (broadly similar for all flavors) than to decay kinematics, and are therefore less distinctive.

We can also consider the sum $\sum p_T^i$ over all particles from a single Q -decay. Figure 3.17 shows the calculated distributions for the $e^+e^- \rightarrow Z \rightarrow b\bar{b}, v\bar{v}$ scenario described above. If the final products of the full cascade Q decay process have negligible masses, the mean value of $\sum p_T^i$ can be evaluated analytically.

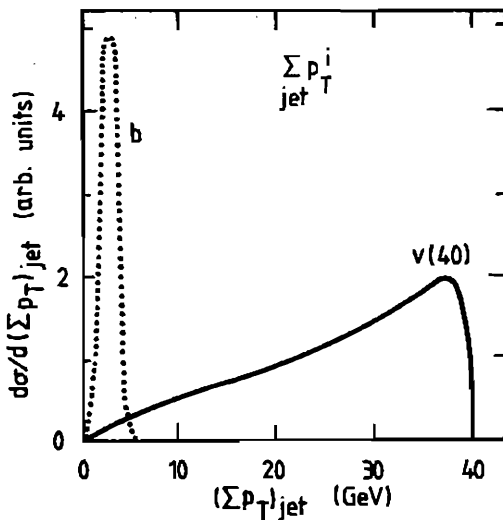


Fig. 3.17. Distributions of the summed momenta of all decay products of a given heavy quark Q transverse to the Q quark axis in $e^+e^- \rightarrow Z \rightarrow b\bar{b}, v\bar{v}$.

We first boost longitudinally to the Q rest frame, which leaves p_T unchanged. Assuming the decay distribution is isotropic (*i.e.* if the Q -hadron is spinless or unpolarized), the average value of each contribution p_T^i is

$$\langle p_T^i \rangle = \langle p^i \rangle \langle \sin \theta \rangle = \frac{1}{4}\pi \langle p^i \rangle ,$$

where θ is the polar angle relative to the jet axis. Energy conservation fixes the sum of the momenta

$$\sum_i p^i = m_Q .$$

Hence

$$\left\langle \sum_i p_T^i \right\rangle = \frac{1}{4}\pi m_Q .$$

Here we have summed only over decay products of Q , but the result is approximately true for the complete jet. Thus selecting jets with large transverse momentum sum can help to select heavy quark events and this sum can help to measure m_Q .

Exercise. If p_\perp^i denotes particle momenta normal to a plane containing the Q momentum, show that

$$\left\langle \sum_i |p_\perp^i| \right\rangle = \frac{1}{2}m_Q .$$

Such kinematic considerations are also useful in identifying decays of light particles such as the τ lepton. The hadronic decay products of τ are characterized by low multiplicity and low invariant mass $< m_\tau$. Narrow jets of hadrons from energetic isolated τ decays therefore look very different from QCD jets, which are typically broader and of higher multiplicity. On the basis of this difference, events of $W \rightarrow \tau\nu$ origin have been identified at the CERN $p\bar{p}$ collider.

3.7.4 Decay neutrinos and missing p_T .

Along with electrons and muons, the heavy quark decays also give neutrinos. In collider experiments these neutrinos are not directly detected but give an apparent imbalance in energy and momentum. Experimentally the balance of momentum along the beam axis cannot be evaluated, because some final particles can escape undetected down the beam pipe. However, the transverse momentum p_T of all particles except neutrinos can be measured to test for p_T imbalance. Such “missing p_T ” larger than expected from measurement errors is a signal for decay neutrinos of heavy quarks or other interesting physics. Other sources of missing p_T include $W \rightarrow e\bar{\nu}$, $Z \rightarrow \nu\bar{\nu}$, $ep \rightarrow \nu X$ and decays of new particles from Supersymmetry such as $\tilde{g} \rightarrow q\bar{q}\tilde{\gamma}$ where the photino $\tilde{\gamma}$ is undetected.

Heavy quark decays can also provide neutrino beams. Conventional neutrino beams are made by taking π^+ and K^+ (or π^- and K^-) beams from a primary proton interaction, allowing them to decay down a flight tube and then stopping all hadrons and muons with a shield: this gives primarily ν_μ (or $\bar{\nu}_\mu$) beams with some contamination from ν_e and $\bar{\nu}_e$. Alternatively, if a primary proton beam is stopped in a “beam dump” (a target followed directly by a shield) the produced π and K are mostly absorbed before they can decay. The dominant source of neutrinos is then the prompt decay of very short-lived heavy quarks, mainly charm. In this case equal numbers of ν_μ and ν_e are produced; the $\bar{\nu}/\nu$ ratio depends on the relative momentum distributions of c and \bar{c} quarks, which may differ. High luminosity hadron supercolliders will copiously produce c and b quarks and hence there is a possibility of obtaining neutrino beams from their decays.

3.8 Quark Decays to Real W Bosons

A heavy quark with mass $m_Q > M_W + m_q$ will decay into a real W boson and a lighter quark q , as illustrated in Fig. 3.18. Likewise a heavy charged lepton L with mass $m_L > M_W + m_{\nu_L}$ will decay into a real W boson plus ν_L ; similar considerations apply in both cases. The matrix element for this decay in the quark case is

$$\mathcal{M} = -\frac{ig}{2\sqrt{2}} V_{Qq} \bar{u}(q) \gamma^\alpha (1 - \gamma_5) u(Q) \epsilon_\alpha^*(W).$$

The spin-averaged matrix element squared, $\frac{1}{2} \sum_{\text{spins}} |\mathcal{M}|^2$, is

$$\begin{aligned} & \frac{g^2}{16} |V_{Qq}|^2 \text{Tr} \left\{ (\not{q} + m_q) \gamma^\alpha (1 - \gamma_5) (\not{Q} + M_Q) \gamma^\beta (1 - \gamma_5) \right\} \left(-g_{\alpha\beta} + \frac{W_\alpha W_\beta}{M_W^2} \right) \\ &= \frac{g^2}{16} |V_{Qq}|^2 8 (q^\alpha Q^\beta + Q^\alpha q^\beta - g^{\alpha\beta} q \cdot Q - i \epsilon^{\rho\alpha\lambda\beta} q_\rho Q_\lambda) \left(-g_{\alpha\beta} + \frac{W_\alpha W_\beta}{M_W^2} \right) \\ &= \frac{g^2}{2} |V_{Qq}|^2 \left(q \cdot Q + \frac{2q \cdot W \cdot Q \cdot W}{M_W^2} \right). \end{aligned}$$

To take into account the running of the couplings with the mass scale, which is M_W in this case, we introduce

$$G = \frac{g^2 \sqrt{2}}{8M_W^2} = \frac{\pi \alpha(M_W^2)}{\sqrt{2} x_W (M_W^2) M_W^2},$$

where $\alpha(M_W^2) \approx 1/128$ and $x_W(M_W^2) \approx 0.23$.

The dot products can be expressed in terms of the masses as $q \cdot Q = \frac{1}{2}(Q^2 + q^2 - W^2)$, $q \cdot W = \frac{1}{2}(Q^2 - q^2 - W^2)$, $Q \cdot W = \frac{1}{2}(Q^2 - q^2 + W^2)$,

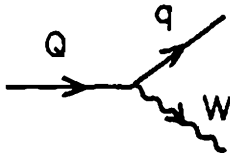


Fig. 3.18. Heavy quark decay to a real W boson.

giving

$$\frac{1}{2} \sum |\mathcal{M}|^2 = \frac{2G}{\sqrt{2}} |V_{Qq}|^2 [(Q^2 - q^2)^2 + W^2(Q^2 + q^2) - 2W^4] .$$

The decay rate is

$$\Gamma = \frac{1}{2Q^0} \left(\frac{1}{2} \sum |\mathcal{M}|^2 \right) (2\pi)^{4-6} \frac{\pi}{2} \lambda^{\frac{1}{2}} \left(1, \frac{W^2}{Q^2}, \frac{q^2}{Q^2} \right),$$

where $\lambda(a, b, c) = a^2 + b^2 + c^2 - 2ab - 2ac - 2bc$. In the Q rest frame we obtain

$$\Gamma = \frac{Gm_Q^3}{8\pi\sqrt{2}} |V_{Qq}|^2 \lambda^{\frac{1}{2}} \left(1, \frac{W^2}{Q^2}, \frac{q^2}{Q^2} \right) \left[\left(1 - \frac{q^2}{Q^2} \right)^2 + \frac{W^2}{Q^2} \left(1 + \frac{q^2}{Q^2} \right) - 2 \frac{W^4}{Q^4} \right].$$

In the case that $q^2/Q^2 \ll 1$, this simplifies to

$$\Gamma = \frac{Gm_Q^3}{8\pi\sqrt{2}} |V_{Qq}|^2 \left(1 - \frac{M_W^2}{m_Q^2} \right)^2 \left(1 + \frac{2M_W^2}{m_Q^2} \right).$$

This rate is semiweak ($\sim G_F$) and therefore much bigger than for the four-fermion processes ($\sim G_F^2$) which describe decays with a virtual W . This difference arises because a real W decays with unit probability, without costing an extra factor G_F .

In an exercise in §3.7.1 the decay rate for $Q \rightarrow qH^+$ was given for a particular coupling; in the two Higgs doublet model (§12.6) with $\tan\beta = 1$, there is an additional factor of $|V_{Qq}|^2$. The ratio of the Higgs and W decay widths is then

$$\frac{\Gamma(Q \rightarrow qH^+)}{\Gamma(Q \rightarrow qW^+)} = \frac{(1 - m_H^2/m_Q^2)^2}{(1 - M_W^2/m_Q^2)^2 (1 + 2M_W^2/m_Q^2)}$$

neglecting m_q^2/m_Q^2 . Thus if the H and W masses are comparable, these decay rates may be comparable.

Next we consider the sequential decay

$$Q \rightarrow q + W$$

$$\quad \quad \quad \downarrow$$

$$\quad \quad \quad e\nu$$

where the W may be either real or virtual. The matrix element is given by the four-fermion effective interaction, multiplied by a W propagator factor:

$$\mathcal{M} = \mathcal{M}(M_W \rightarrow \infty) \frac{-M_W^2}{W^2 - M_W^2 + iM_W\Gamma_W}.$$

Integrating the differential decay rate over the $e^+\nu_e$ phase space gives the invariant q -quark distribution

$$E_q \frac{d\Gamma}{d^3q} = \frac{g_q(X_q^2)M_W^4}{(X_q^2 - M_W^2)^2 + M_W^2\Gamma_W^2},$$

where $g_q(X_q^2)$ has the same functional form as the s -quark distribution function from charm decay or the c -quark distribution from bottom decay (which are the same) and $X_q^2 = (Q - q)^2$.

The total rate in the Q rest frame can be obtained by integrating over $dE_q = -dX_q^2/2Q^0$

$$\Gamma = \frac{\pi}{Q^2} \int dX_q^2 \frac{\sqrt{(Q^2 + q^2 - X_q^2)^2 - 4Q^2q^2}}{\left[\left(1 - \frac{X_q^2}{M_W^2}\right)^2 + \frac{\Gamma_W^2}{M_W^2} \right]} g_q(X_q^2).$$

Figure 3.19 shows the integrated partial rate *versus* m_Q for $m_q = 0$ and $|V_{Qq}| = 1$. The change from the m_Q^5 dependence for $m_Q < M_W + m_q$ to the m_Q^3 dependence for $m_Q > M_W + m_q$ is evident.

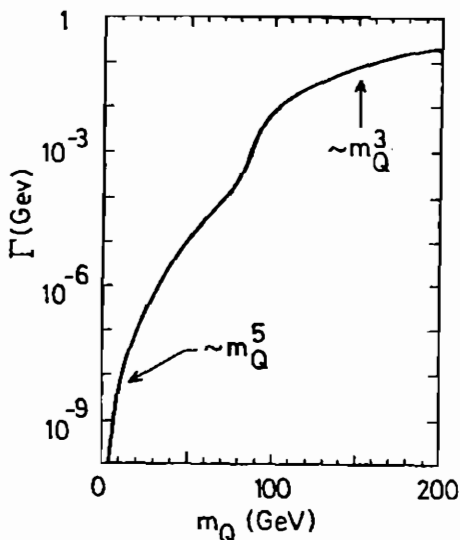


Fig. 3.19. Dependence of partial width for $Q \rightarrow qe\nu$ on m_Q .

3.9 Leptonic Decays

Pseudoscalar mesons $X^-(\bar{Q}q)$ can decay to $e\bar{\nu}$, $\mu\bar{\nu}$, $\tau\bar{\nu}$ through the annihilation process in Fig. 3.20. In addition to the well-known $\pi^-(\bar{u}d)$ and $K^-(\bar{u}s)$ leptonic decays, other possibilities include $D^-(\bar{c}d)$, $D_s^-(\bar{c}s)$, $B_u^-(\bar{b}u)$, $B_c^-(\bar{b}c)$, etc. The effective Lagrangian for the $X^- \rightarrow \ell^- \bar{\nu}_\ell$ transition with $m_X^2 \ll M_W^2$ is

$$\mathcal{L}_{\text{eff}} = \frac{G_F}{\sqrt{2}} V_{Qq} \langle 0 | \bar{v}(\bar{Q}) \gamma^\mu (1 - \gamma_5) u(q) | X \rangle \bar{u}(\ell) \gamma^\mu (1 - \gamma_5) v(\bar{\nu}).$$

The hadronic matrix element must be of the form

$$\langle 0 | \bar{v}(\bar{Q}) \gamma_\mu (1 - \gamma_5) u(q) | X \rangle = f_X X_\mu,$$

where f_X is a real constant, since X_μ is the only four vector in the initial state. Since the X meson is pseudoscalar, only the axial current contributes. Using the Dirac equation, and assuming that the neutrino is massless, \mathcal{M} simplifies to

$$\mathcal{M} = \frac{G_F}{\sqrt{2}} V_{Qq} f_X m_\ell \bar{u}(\ell) (1 - \gamma_5) v(\bar{\nu}),$$

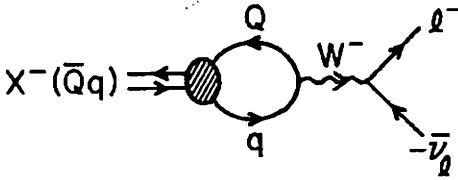


Fig. 3.20. Pseudoscalar meson leptonic decay $X^- \rightarrow \ell^- \bar{\nu}_\ell$.

whose spin-summed square is

$$\sum |\mathcal{M}|^2 = 2G_F^2 |V_{Qq}|^2 f_X^2 m_\ell^2 (m_X^2 - m_\ell^2).$$

In the X rest frame, the decay width is

$$d\Gamma = \frac{1}{2m_X} \sum |\mathcal{M}|^2 (2\pi)^4 d_2(\text{PS})$$

giving

$$\Gamma = \frac{G_F^2 |V_{Qq}|^2 f_X^2}{8\pi} m_X m_\ell^2 \left(1 - \frac{m_\ell^2}{m_X^2}\right)^2.$$

The decay width is proportional to the lepton mass squared.

Exercise. Show that the vanishing of $\Gamma(\pi \rightarrow \ell \bar{\nu})$ for $m_\ell = 0$ is a consequence of angular momentum conservation.

For π decays the ratio of e to μ partial widths is

$$\frac{\Gamma(\pi^- \rightarrow e \bar{\nu}_e)}{\Gamma(\pi^- \rightarrow \mu \bar{\nu}_\mu)} = \left(\frac{m_e}{m_\mu}\right)^2 \left(\frac{m_\pi^2 - m_e^2}{m_\pi^2 - m_\mu^2}\right)^2 = 1.283 \times 10^{-4}.$$

Radiative corrections corresponding to the conditions of the experimental measurement change this prediction to 1.228×10^{-4} , to be compared with the measured value of $(1.230 \pm 0.004) \times 10^{-4}$. This is the most accurate test of $e - \mu$ universality (i.e. that $e \bar{\nu}_e$ and $\mu \bar{\nu}_\mu$ have the same weak coupling strength).

From the charged pion lifetime

$$\tau_\pi = \frac{1}{\Gamma_\pi} = 2.6 \times 10^{-8} \text{ s}$$

and the mixing matrix element $|V_{ud}| = 0.974$, the value of the pion decay constant is deduced to be

$$f_\pi = 131 \text{ MeV} = 0.94 m_\pi .$$

From the measured partial width for $K \rightarrow \mu\bar{\nu}$ decay, $\Gamma(K_{\mu 2}) = 5.15 \times 10^3 \text{ s}^{-1}$, and $|V_{us}| = 0.221$, the K -decay constant is found to be

$$f_K = 160 \text{ MeV} = 1.15 m_\pi .$$

The decay constants for mesons containing heavy quarks have not been accessible to experiment thus far. There is an upper limit $f_D < 310 \text{ MeV}$ from $B(D^+ \rightarrow \mu^+ \nu_\mu) < 7.2 \times 10^{-4}$. Some theoretical estimates suggest that

$$f_X \lesssim f_\pi ,$$

but this question is controversial. The f_B constant is important because it is needed in order to predict $B^0 - \bar{B}^0$ mixing.

In the case of charm (and heavier flavors), the dominant leptonic modes are into $\tau\nu_\tau$ because m_τ is the largest lepton mass:

$$D_s^-(\bar{c}s) \rightarrow \tau^- \bar{\nu}_\tau , \quad D^-(\bar{c}d) \rightarrow \tau^- \bar{\nu}_\tau .$$

The Cabibbo-allowed $D_s \rightarrow \tau\bar{\nu}_\tau$ decay offers a potential means for producing ν_τ neutrinos which could then be detected through the reaction $\nu_\tau N \rightarrow \tau + \text{hadrons}$.

As the mass of X increases, the leptonic branching fraction decreases, since

$$\Gamma(\text{leptonic}) \propto m_X , \quad \Gamma(\text{semileptonic}) \propto m_X^5 .$$

Thus the prospects of finding leptonic decays of B or higher mass mesons become much less favorable. Moreover, in the B -meson case,

the weak current element $|V_{ub}|$ is known to be small, which suppresses the leptonic decay of $\bar{B}(b\bar{u})$; the $\bar{B}(b\bar{c})$ state with coupling $|V_{cb}|$ remains as a possibility.

The decay of the τ fermion to a pion

$$\tau \rightarrow \pi\nu_\tau$$

is described by the same effective Lagrangian.

Exercise. Show that the partial width for this decay is

$$\Gamma = \frac{G_F^2 |V_{ud}|^2}{16\pi} f_\pi^2 m_\tau^3 \left(1 - \frac{m_\pi^2}{m_\tau^2}\right)^2.$$

The predicted ratio of

$$\Gamma(\tau \rightarrow \pi\nu)/\Gamma(\tau \rightarrow \nu_\tau e\bar{\nu}_e) = 0.63$$

is in good accord with the measured value of 0.58 ± 0.13 .

The decays of the τ into a hadronic state of spin -1 can be similarly calculated. For example, the partial width for the decay into the rho meson

$$\tau \rightarrow \rho\nu_\tau$$

is given by

$$\Gamma = \frac{G_F^2 |V_{ud}|^2 f_\rho^2}{16\pi} \frac{m_\tau^3}{m_\rho^2} \left(1 - \frac{m_\rho^2}{m_\tau^2}\right)^2 \left(1 + \frac{2m_\rho^2}{m_\tau^2}\right).$$

The ρ -decay constant is determined from the isovector part of the electromagnetic form factor; see Fig. 3.21. The prediction for $\tau \rightarrow \rho\nu_\tau$ agrees with the measured branching fraction.

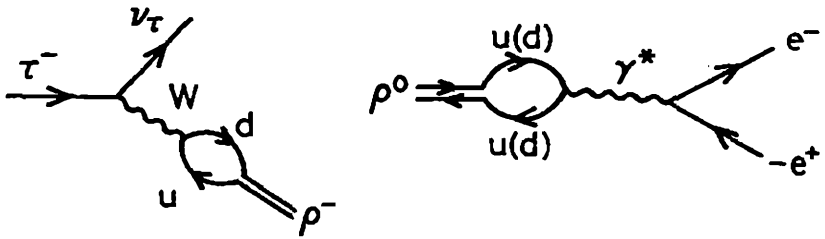


Fig. 3.21. Illustration of the underlying similarity between $\tau \rightarrow \nu_\tau \rho^-$ and $\rho^0 \rightarrow e^+ e^-$ decay; only conserved vector currents contribute in each case.

Chapter 4

Basic e^+e^- and νe^- Processes

4.1 Cross Sections for Fermion-Antifermion Scattering

Lepton-lepton scattering offers opportunities to study electroweak interactions rather cleanly, since leptons have no strong interactions. We start this chapter by deriving the formulas for a general fermion-antifermion scattering at tree level via gauge-boson exchanges; in later sections we apply these formulas to particular cases. The e^+e^- interactions via the Z^0 gauge boson are of special interest, in the era of “ Z factories” at the SLC and LEP colliders.

To calculate fermion-antifermion scattering it is convenient to use the chirality basis for spinors (*i.e.* left- and right-handed projections) which are physically distinct helicity states in the massless limit. Consider a general process $\ell\bar{\ell} \rightarrow f\bar{f}$ with particle symbols used to denote the four-momenta, as illustrated in Fig. 4.1. Here $\bar{\ell}$ (\bar{f}) is not necessarily the antiparticle of ℓ (f) as *e.g.*, in the case $\ell = e$, $\bar{\ell} = \bar{\nu}_e$. The invariant kinematical variables are

$$\begin{aligned} s &= (\ell + \bar{\ell})^2 = (f + \bar{f})^2, \\ t &= (f - \ell)^2 = (\bar{f} - \bar{\ell})^2, \\ u &= (\bar{f} - \ell)^2 = (f - \bar{\ell})^2. \end{aligned}$$

Gauge boson exchanges can occur in either the s or t channels (*i.e.*, where the virtual gauge boson momentum squared is either s or t).

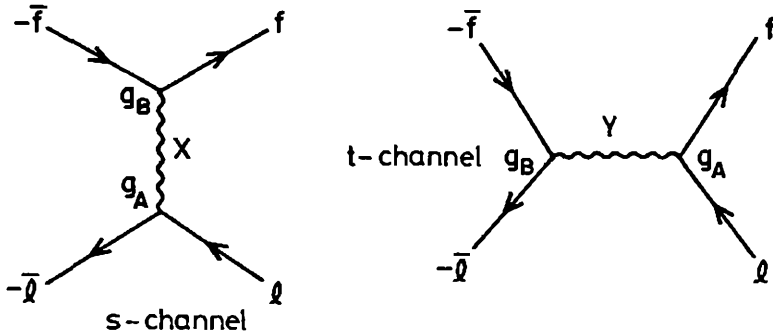


Fig. 4.1. Gauge boson exchange diagrams for fermion-antifermion scattering.

The transition amplitude for the sum of s -channel exchanges is

$$\mathcal{M}_{AB}^{(s)} = G_{AB}(s) [\bar{u}_B(f) \gamma^\alpha v_B(\bar{f})] [\bar{v}_A(\bar{\ell}) \gamma_\alpha u_A(\ell)],$$

where A, B denote L, R chiralities and G_{AB} represents the product of couplings g_i and propagator factors

$$G_{AB}(s) = \sum_X \frac{g_A(X \rightarrow \bar{\ell} \ell) g_B(X \rightarrow f \bar{f})}{s - M_X^2 + i M_X \Gamma_X}$$

summed over all contributing gauge bosons $X = \gamma, Z^0, W^\pm$. The amplitude for t -channel exchanges is

$$\mathcal{M}_{AB}^{(t)} = -G_{AB}(t) [\bar{v}_B(\bar{\ell}) \gamma^\alpha v_B(\bar{f})] [\bar{u}_A(f) \gamma_\alpha u_A(\ell)]$$

with

$$G_{AB}(t) = \sum_Y \frac{g_A(Y \rightarrow \bar{\ell} f) g_B(Y \rightarrow \bar{f} \ell)}{t - M_Y^2}$$

summed over contributing gauge bosons Y . The overall minus sign comes from the different orderings of the anticommuting fermion operators in the s - and t -channel cases, with an odd number of interchanges to go from the ordering in one case to the other. Notice

our conventions here; the labels A and B in G_{AB} refer always to the L, R couplings of the *fermion* ℓ and the *fermion* f , as listed in §2.12. A fermion coupled to a g_L vertex has L chirality but an antifermion coupled to such a vertex has R chirality.

Consider first the case of all left-handed fermions. By the Fierz transformation of the fermion spinors

$$[\bar{u}_L(f)\gamma^\alpha u_L(\ell)] [\bar{v}_L(\bar{\ell})\gamma_\alpha v_L(\bar{f})] = -[\bar{u}_L(f)\gamma^\alpha v_L(\bar{f})] [\bar{v}_L(\bar{\ell})\gamma_\alpha u_L(\ell)] ,$$

so the s - and t -exchange amplitudes can be combined to give

$$\mathcal{M}(\bar{\ell}_L \ell_L \rightarrow \bar{f}_L f_L) = [G_{LL}(s) + G_{LL}(t)] [\bar{u}_L(f)\gamma^\alpha v_L(\bar{f})] [\bar{v}_L(\bar{\ell})\gamma_\alpha u_L(\ell)] .$$

The square of \mathcal{M} can be evaluated as in the μ -decay calculation

$$\begin{aligned} |\mathcal{M}(\bar{\ell}_L \ell_L \rightarrow \bar{f}_L f_L)|^2 &= 16 (\ell \cdot \bar{f})(\bar{\ell} \cdot f) |G_{LL}(s) + G_{LL}(t)|^2 \\ &= 4 u^2 |G_{LL}(s) + G_{LL}(t)|^2 . \end{aligned}$$

The final expression is based on a massless approximation for initial- and final-state fermions.

Similarly, for an interaction involving only right-handed fermions,

$$|\mathcal{M}(\bar{\ell}_R \ell_R \rightarrow \bar{f}_R f_R)|^2 = 4 u^2 |G_{RR}(s) + G_{RR}(t)|^2 .$$

Exercise. Show that in transitions involving mixed handedness, only the s - or t -channel contributes, and hence that

$$|\mathcal{M}(\bar{\ell}_L \ell_L \rightarrow \bar{f}_R f_R)|^2 = 4 t^2 |G_{LR}(s)|^2 ,$$

$$|\mathcal{M}(\bar{\ell}_R \ell_R \rightarrow \bar{f}_L f_L)|^2 = 4 t^2 |G_{RL}(s)|^2 ,$$

$$|\mathcal{M}(\bar{\ell}_L \ell_L \rightarrow \bar{f}_L f_R)|^2 = 4 s^2 |G_{RL}(t)|^2 ,$$

$$|\mathcal{M}(\bar{\ell}_R \ell_L \rightarrow \bar{f}_R f_L)|^2 = 4 s^2 |G_{LR}(t)|^2 .$$

Combining these contributions, the spin-averaged differential cross

section is

$$\frac{d\sigma}{dt}(\bar{\ell}\ell \rightarrow \bar{f}f) = \frac{1}{16\pi s^2} \left\{ u^2 [|G_{LL}(s) + G_{LL}(t)|^2 + |G_{RR}(s) + G_{RR}(t)|^2] \right. \\ \left. + t^2 [|G_{LR}(s)|^2 + |G_{RL}(s)|^2] + s^2 [|G_{LR}(t)|^2 + |G_{RL}(t)|^2] \right\}.$$

Exercise. Show that the cross sections for an unpolarized $\bar{\ell}$ and a L or R polarized ℓ are, respectively,

$$\frac{d\sigma_L}{dt} = \frac{1}{8\pi s^2} \left\{ u^2 |G_{LL}(s) + G_{LL}(t)|^2 + t^2 |G_{LR}(s)|^2 + s^2 |G_{LR}(t)|^2 \right\}, \\ \frac{d\sigma_R}{dt} = \frac{1}{8\pi s^2} \left\{ u^2 |G_{RR}(s) + G_{RR}(t)|^2 + t^2 |G_{RL}(s)|^2 + s^2 |G_{RL}(t)|^2 \right\}.$$

The corresponding results for fermion-fermion scattering $\ell f' \rightarrow \ell' f$ can be obtained by crossing ($f' = -\bar{f}$, $\ell' = -\bar{\ell}$) with the replacements $s \leftrightarrow u$ in $|\mathcal{M}|^2$. The result is

$$\frac{d\sigma}{dt}(\ell f' \rightarrow \ell' f) = \frac{1}{16\pi s^2} \left\{ s^2 [|G_{LL}(t) + G_{LL}(u)|^2 + |G_{RR}(t) + G_{RR}(u)|^2] \right. \\ \left. + u^2 [|G_{LR}(t)|^2 + |G_{RL}(t)|^2] + t^2 [|G_{LR}(u)|^2 + |G_{RL}(u)|^2] \right\}.$$

It is straightforward to derive polarized cross section formulas, too. We will apply these general expressions to specific examples in the following sections and in Chapter 5.

4.2 $e^+e^- \rightarrow \mu^+\mu^-$

In the standard model there are only γ , Z^0 exchanges in the s channel. The effective Lagrangian of the standard model gives

$$G_{AB}(s) = \frac{e^2}{s} + \frac{8G_F}{\sqrt{2}} g_A g_B R(s),$$

where

$$g_L = g_V - g_A = x_w - 1/2, \quad g_R = g_V + g_A = x_w,$$

$$R(s) = \frac{M_Z^2}{s - M_Z^2 + iM_Z\Gamma_Z}.$$

In an extended gauge theory having additional Z bosons there will be additional contributions to $G_{AB}(s)$. The differential cross section is

$$\frac{d\sigma}{dt} = \frac{1}{16\pi s^2} \left\{ u^2 (|G_{LL}(s)|^2 + |G_{RR}(s)|^2) + t^2 (|G_{LR}(s)|^2 + |G_{RL}(s)|^2) \right\}$$

in the massless e, μ approximation. Hence, we obtain

$$\begin{aligned} \frac{d\sigma}{dt} = \frac{1}{16\pi s^2} \left\{ \frac{2e^4(t^2 + u^2)}{s^2} + \frac{2e^2}{s} \left(\frac{8G_F}{\sqrt{2}} \right) [(g_L^2 + g_R^2) u^2 + 2g_L g_R t^2] \Re e R \right. \\ \left. + \left(\frac{8G_F}{\sqrt{2}} \right)^2 [(g_L^4 + g_R^4) u^2 + 2g_L^2 g_R^2 t^2] |R|^2 \right\}. \end{aligned}$$

Using the relations

$$t = -\frac{1}{2}s(1 - \cos\theta), \quad u = -\frac{1}{2}s(1 + \cos\theta),$$

the QED contribution alone is

$$\frac{d\sigma}{d\cos\theta} = \frac{\pi\alpha^2}{2s} (1 + \cos^2\theta).$$

Integrating $d\sigma/dt$ over the full kinematic range $0 \leq \theta \leq \pi$, we obtain

$$\begin{aligned} \sigma(e^+e^- \rightarrow \mu^+\mu^-) &= \frac{s}{48\pi} \left\{ |G_{LL}(s)|^2 + |G_{RR}(s)|^2 + 2|G_{LR}(s)|^2 \right\} \\ &= \frac{4\pi\alpha^2}{3s} + \frac{4\alpha}{3} \frac{G_F}{\sqrt{2}} (g_L + g_R)^2 \Re e R + \frac{4s}{3\pi} \left(\frac{G_F}{\sqrt{2}} \right)^2 (g_L^2 + g_R^2)^2 |R|^2. \end{aligned}$$

For $s \ll M_Z^2$, where the Z contribution is negligible, the QED μ -pair

production cross section is

$$\sigma(e^+e^- \rightarrow \gamma^* \rightarrow \mu^+\mu^-) = \frac{4\pi\alpha^2}{3s} \equiv \sigma_{\text{QED}} = 21.7 \text{ nb}/[E(\text{GeV})]^2,$$

where $E = \sqrt{s}/2$ is the beam energy. An improved $s \ll M_Z^2$ approximation retains the leading γ^* , Z^* interference term

$$\sigma \simeq \frac{4\pi\alpha^2}{3s} \left[1 - \frac{4G_F s}{\sqrt{2}\pi\alpha} \left(x_w - \frac{1}{4} \right)^2 \right].$$

The ratio of the integrated $e^+e^- \rightarrow \mu^+\mu^-$ cross sections, including both γ^* and Z contributions, to the pure QED value is given as a function of \sqrt{s} in Fig. 4.2. The Z pole gives an enhancement of two orders of magnitude at $\sqrt{s} = M_Z$ over the γ^* cross section.

At the Z resonance, the Z contribution alone is a good approximation, given by

$$\sigma_Z \equiv \sigma(e^+e^- \rightarrow Z \rightarrow \mu^+\mu^-) = \frac{4}{3\pi} \left(\frac{G_F M_Z^2}{\sqrt{2}} \right)^2 \frac{s(g_L^2 + g_R^2)^2}{(s - M_Z^2)^2 + M_Z^2 \Gamma_Z^2}.$$

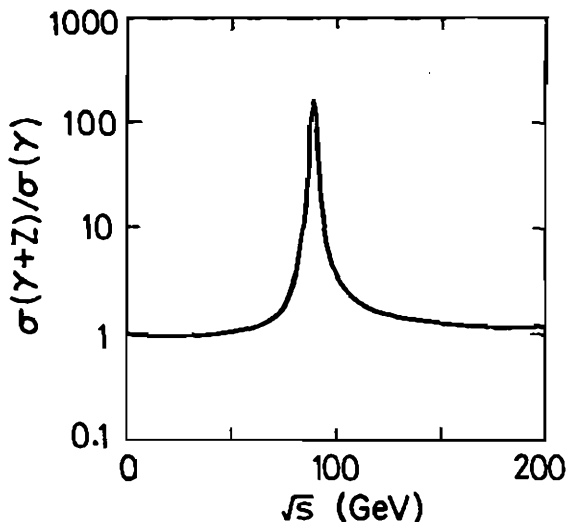


Fig. 4.2. Energy dependence of the $e^+e^- \rightarrow (\gamma^*, Z) \rightarrow \mu^+\mu^-$ cross section, relative to the QED cross section.

This can be expressed in terms of the partial widths for Z -leptonic decays (derived in a later chapter)

$$\Gamma_{\mu\mu} = \Gamma_{ee} = \frac{G_F}{\sqrt{2}} \frac{M_Z^3 (g_L^2 + g_R^2)}{3\pi}$$

as

$$\sigma_Z = \frac{12\pi (s/M_Z^2) \Gamma_{ee} \Gamma_{\mu\mu}}{(s - M_Z^2)^2 + M_Z^2 \Gamma_Z^2},$$

which is a relativistic Breit-Wigner resonance formula. At the Z resonance energy $s = M_Z^2$, the ratio of the resonance contribution (peak minus background) to the electromagnetic background is

$$\frac{\sigma(e^+e^- \rightarrow Z \rightarrow \mu^+\mu^-)}{\sigma(e^+e^- \rightarrow \gamma^* \rightarrow \mu^+\mu^-)} = \frac{9}{\alpha^2} B_{ee} B_{\mu\mu} = 1.47 \times 10^5 B_{\mu\mu},$$

where $B_{\mu\mu} = \Gamma(Z \rightarrow \mu^+\mu^-)/\Gamma_Z$ is the $\mu^+\mu^-$ branching fraction and $\alpha = \alpha(M_Z^2) \simeq 1/128$ (§7.3). This offers a direct way to measure $B_{\mu\mu}$. These expressions hold more generally for the production of any $J^P = 1^-$ resonant state, such as ψ or Υ .

Exercise. Show that in the narrow width approximation,

$$\frac{1}{(s - M_Z^2)^2 + M_Z^2 \Gamma_Z^2} \approx \frac{\pi}{M_Z \Gamma_Z} \delta(s - M_Z^2).$$

In the narrow width approximation the cross section formula becomes

$$\sigma_Z = 12\pi^2 B_{ee} B_{\mu\mu} \frac{\Gamma_Z}{M_Z} \delta(s - M_Z^2).$$

The integrated Z -resonance contribution is then

$$\int d\sqrt{s} \sigma_Z = 6\pi^2 B_{ee} B_{\mu\mu} \frac{\Gamma_Z}{M_Z}.$$

This offers a way to measure Γ_Z , given a determination of $B_{\mu\mu} = B_{ee}$ above.



With polarized electron beams the cross sections σ_L and σ_R for the scattering of left-handed and right-handed electrons on unpolarized positrons can be separately measured. A left-right polarization asymmetry A_{LR} is defined as

$$A_{LR} = \frac{\sigma_L - \sigma_R}{\sigma_L + \sigma_R}.$$

Exercise. Show that for $e^+e^- \rightarrow \mu^+\mu^-$,

$$A_{LR} = \frac{|G_{LL}|^2 - |G_{RR}|^2}{|G_{LL}|^2 + |G_{RR}|^2 + 2|G_{LR}|^2},$$

and can be approximated at the Z resonance by

$$A_{LR} \simeq -2g_V^e g_A^e / [(g_V^e)^2 + (g_A^e)^2],$$

where g_V^e and g_A^e are the couplings to electrons or muons. Find the corresponding result on Z resonance for $e^+e^- \rightarrow f\bar{f}$.

We now consider the angular distribution of the cross section. The QED contribution alone has $(1 + \cos^2\theta)$ shape, but the full cross section has a term linear in $\cos\theta$ from interference between the γ^* or Z vector coupling and the axial vector Z coupling. Figure 4.3 gives typical experimental e^+e^- experimental angular distributions showing this effect; the solid curve is based on $x_w = 0.23$.

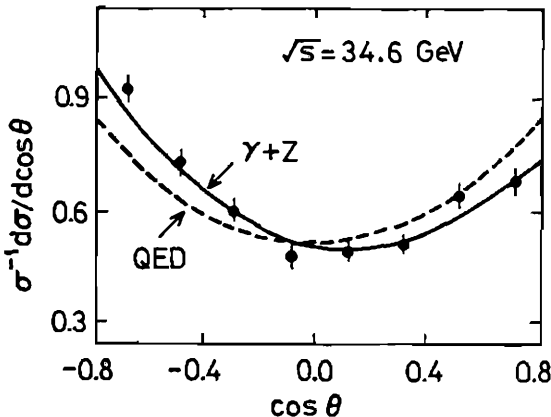


Fig. 4.3. Angular distribution of $e^+e^- \rightarrow \mu^+\mu^-$ scattering, showing the asymmetry from QED-weak interference. (PETRA data).

The forward-backward asymmetry in the $e^+e^- \rightarrow \mu^+\mu^-$ reaction for unpolarized beams is defined to be the number of μ^+ at c.m. scattering angle θ minus the number of μ^+ at angle $\pi - \theta$ divided by the sum

$$A_{FB}(\theta) = \frac{d\sigma(\theta) - d\sigma(\pi - \theta)}{d\sigma(\theta) + d\sigma(\pi - \theta)}.$$

The integrated asymmetry is

$$A_{FB} = \frac{\int_0^{\pi/2} [d\sigma(\theta) - d\sigma(\pi - \theta)]}{\sigma} = \frac{N(\text{forward}) - N(\text{backward})}{N(\text{forward}) + N(\text{backward})}.$$

From the preceding cross section expressions we find

$$A_{FB} = \frac{3 (|G_{LL}|^2 + |G_{RR}|^2 - 2|G_{LR}|^2)}{4 (|G_{LL}|^2 + |G_{RR}|^2 + 2|G_{LR}|^2)}.$$

Figure 4.4 compares the standard model prediction with the data. The asymmetry reaches a minimum value of about -0.7 below $\sqrt{s} = M_Z$, due to large γ^* , Z interference; see Fig. 4.5.

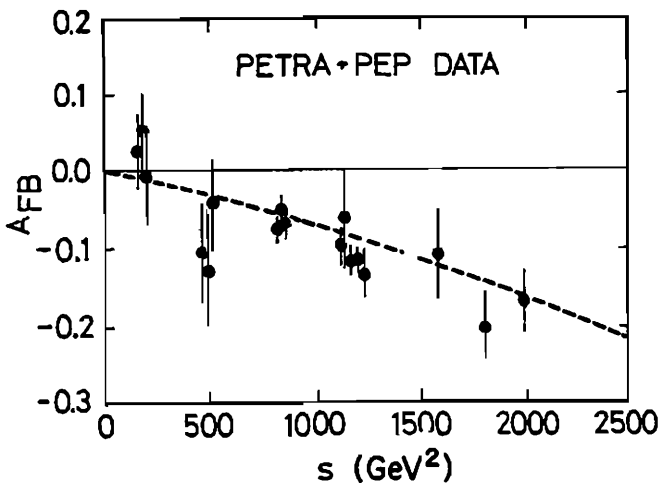


Fig. 4.4. Comparison of data on the integrated $e^+e^- \rightarrow \mu^+\mu^-$ asymmetry with the standard model prediction for $x_w = 0.23$.

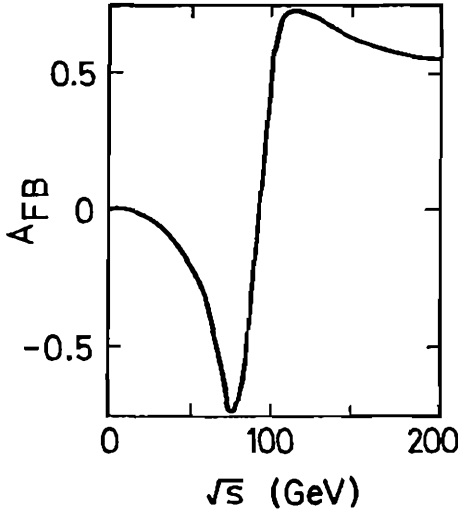


Fig. 4.5. Prediction of integrated $e^+e^- \rightarrow \mu^+\mu^-$ asymmetry A_{FB} as a function of \sqrt{s} .

Exercise. For $e^+e^- \rightarrow \bar{f}f$ scattering at the Z resonance, show that

$$A_{FB} \simeq 3 \frac{g_A^e g_V^e}{(g_A^e)^2 + (g_V^e)^2} \cdot \frac{g_A^f g_V^f}{(g_A^f)^2 + (g_V^f)^2},$$

neglecting m_f/m_Z . Hence for $e^+e^- \rightarrow \mu^+\mu^-$ show that $A_{FB} = \frac{3}{4} A_{LR}^2$ on the Z resonance.

4.3 Bhabha Scattering

In the elastic process $e^+e^- \rightarrow e^+e^-$ both direct-channel and cross-channel poles contribute, as illustrated below.

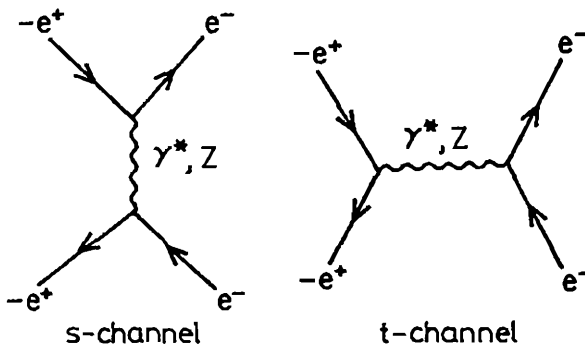


Fig. 4.6. s - and t -channel exchanges contributing to Bhabha scattering.

The general cross section formula of §4.1 applies in terms of $G_{AB}(s)$ and $G_{AB}(t)$ where both have the same functional form given in §4.2 for $e^+e^- \rightarrow \mu^+\mu^-$. The Bhabha cross section can be used for further tests of the standard model but is also useful experimentally as a luminosity monitor, as is $e^+e^- \rightarrow \mu^+\mu^-$.

4.4 $e^+e^- \rightarrow$ Massive Fermions

There are many $e^+e^- \rightarrow \bar{f}f$ channels of interest where the masses \bar{m} and m of the final state fermions cannot be neglected. To treat these cases the formalism of §4.1 must be generalized. The chirality amplitudes $G_{AB}(s)$, $G_{AB}(t)$ can still be used, but some interference terms now appear because chirality is not conserved for f and \bar{f} ; also the masses appear explicitly. The differential cross section formula becomes

$$\begin{aligned} \frac{d\sigma}{dt}(e^+e^- \rightarrow \bar{f}f) &= \frac{1}{16\pi s^2} \left\{ (t-\bar{m}^2)(t-m^2) [|G_{LR}(s)|^2 + |G_{RL}(s)|^2] \right. \\ &+ (u-\bar{m}^2)(u-m^2) [|G_{LL}(s)+G_{LL}(t)|^2 + |G_{RR}(s)+G_{RR}(t)|^2] \\ &+ s(s-\bar{m}^2-m^2) [|G_{LR}(t)|^2 + |G_{RL}(t)|^2] \\ &\left. + 2s\bar{m}m \operatorname{Re} \{ [G_{LL}(s)+G_{LL}(t)]G_{LR}^*(s) + [G_{RR}(s)+G_{RR}(t)]G_{RL}^*(s) \} \right\}. \end{aligned}$$

To obtain the cross section formula for $L(R)$ polarized electrons on unpolarized positrons, multiply by 2 and retain only the G_{AB} for which $A = L$ ($A = R$).

Exercise. Use the general form of $|M|^2$ given in §3.5 for $a \rightarrow bcd$ decay, with suitable crossing, to confirm the s -channel exchange contributions in $d\sigma/dt$.

Exercise. For the case of equal masses $m = \bar{m}$ and s -channel exchanges only, show that the angular distribution and total cross sec-

tion are

$$\frac{d\sigma}{d\cos\theta} = \frac{\beta s}{128\pi} \left\{ (|G_{LL}|^2 + |G_{RR}|^2)(1 + \beta \cos\theta)^2 + (|G_{LR}|^2 + |G_{RL}|^2)(1 - \beta \cos\theta)^2 + 2(1 - \beta^2) \operatorname{Re}(G_{LL}G_{LR}^* + G_{RR}G_{RL}^*) \right\},$$

$$\sigma = \frac{\beta s}{64\pi} \left\{ (|G_{LL}|^2 + |G_{RR}|^2 + |G_{LR}|^2 + |G_{RL}|^2) \left(1 + \frac{1}{3}\beta^2\right) + 2(1 - \beta^2) \operatorname{Re}(G_{LL}G_{LR}^* + G_{RR}G_{RL}^*) \right\}.$$

Here $\beta = (1 - 4m^2/s)^{1/2}$ is the velocity of the final state fermions.

Exercise. From the preceding results, show that the left-right polarization asymmetry and the forward-backward angular asymmetry, for equal f and \bar{f} masses and only s -channel exchanges, are given by

$$A_{LR} = \frac{(|G_{LL}|^2 + |G_{LR}|^2 - |G_{RR}|^2 - |G_{RL}|^2) \left(1 + \frac{1}{3}\beta^2\right) + 2 \operatorname{Re}(G_{LL}G_{LR}^* - G_{RR}G_{RL}^*) (1 - \beta^2)}{(|G_{LL}|^2 + |G_{LR}|^2 + |G_{RR}|^2 + |G_{RL}|^2) \left(1 + \frac{1}{3}\beta^2\right) + 2 \operatorname{Re}(G_{LL}G_{LR}^* + G_{RR}G_{RL}^*) (1 - \beta^2)},$$

$$A_{FB} = \frac{(|G_{LL}|^2 + |G_{RR}|^2 - |G_{LR}|^2 - |G_{RL}|^2) \beta}{(|G_{LL}|^2 + |G_{RR}|^2 + |G_{LR}|^2 + |G_{RL}|^2) \left(1 + \frac{1}{3}\beta^2\right) + 2 \operatorname{Re}(G_{LL}G_{LR}^* + G_{RR}G_{RL}^*) (1 - \beta^2)}.$$

An immediate application is tau lepton pair production, $e^+e^- \rightarrow \tau^+\tau^-$, for which $G_{AB}(s)$ has the same form as in $e^+e^- \rightarrow \mu^+\mu^-$. Tau pairs may be recognized from their decay products, for example by the appearance of acoplanar $e^\pm\mu^\pm$ events with missing energy from double semileptonic decays. Near threshold where we can neglect the Z pole, $G_{AB} = e^2/s = 4\pi\alpha/s$ and the total cross section is

$$\sigma(e^+e^- \rightarrow \tau^+\tau^-) = \left(\frac{4\pi\alpha^2}{3s}\right) \frac{\beta(3 - \beta^2)}{2} = \sigma_{\text{QED}} \frac{\beta(3 - \beta^2)}{2}.$$

Thus, the cross section vanishes at threshold as $\sigma \propto \beta$ where $\beta = p/E = (1 - 4m_\tau^2/s)^{1/2}$ is the τ velocity. The threshold dependence of the $\tau^+\tau^-$ cross section was used in the initial determination of the τ mass.

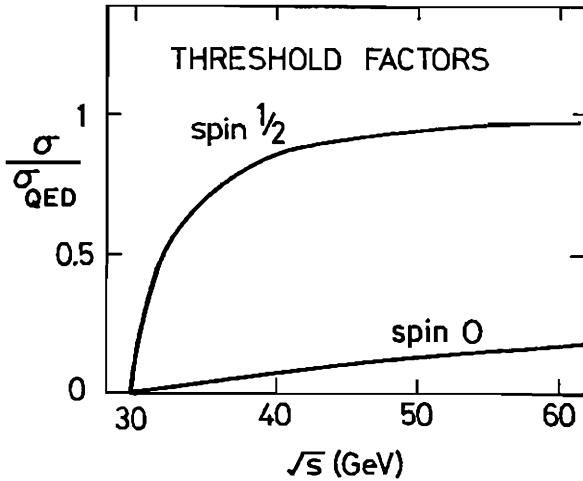


Fig. 4.7. Comparison of spin-0 and spin- $\frac{1}{2}$ particle pair production in e^+e^- collisions, for particles of mass $m = 15$ GeV.

Exercise. For the production of point-like spin zero particles via the interaction Lagrangian $\mathcal{L} = -ie [\phi^+(\partial_\mu\phi) - (\partial_\mu\phi^+)\phi] A^\mu$, show that the cross section is

$$\sigma(e^+e^- \rightarrow \gamma^* \rightarrow \phi^+\phi^-) = \frac{1}{4}\beta^3 \left(\frac{4\pi\alpha^2}{3s} \right).$$

Hence scalar particle production is more suppressed at threshold and its value at high s is $1/4$ of that for μ -pair production. This is illustrated in Fig. 4.7.

4.5 Heavy Neutrino Production

Another interesting class of lepton processes in which final state masses are important is the production in e^+e^- collisions of a possible heavy neutral lepton N in e^+e^- collisions via the diagrams in Fig. 4.8. With a neutral fermion such as N the question always arises, is it a Dirac or Majorana particle? If Dirac, the particle and antiparticle are distinct $N \neq \bar{N}$; if Majorana, they are identical $N = \bar{N}$. For light (essentially massless) neutrinos in the standard model, this question usually makes no difference, since what we normally call “neutrinos” are produced and detected only through left-handed couplings involving helicity $-\frac{1}{2}$ states while “antineutrinos” occur only in helicity $+\frac{1}{2}$

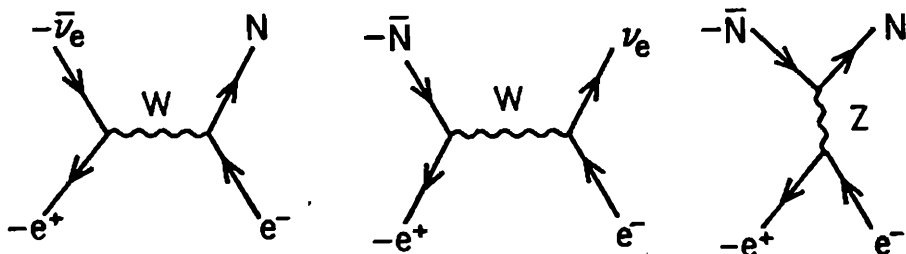


Fig. 4.8. Diagrams for the production of a heavy neutrino N in e^+e^- collisions.

states. These states are physically distinct because of their helicities, whether or not $\nu = \bar{\nu}$. If we rewrite the standard model replacing $\bar{\nu}$ by ν everywhere it will make no difference to semileptonic decay or neutrino scattering predictions. The only changes for light neutrinos arise when more than one of a given flavor is present, as for example in $e^+e^- \rightarrow Z \rightarrow \nu_e \bar{\nu}_e$; if ν_e is Majorana the amplitude must be suitably antisymmetrized, but in fact the cross section is unchanged (see below). In this section we shall start by assuming that N is a Dirac neutrino, since the preceding formulas cover this case; later we shall see what differences arise in the Majorana case.

Consider first $e^+e^- \rightarrow \bar{\nu}_e N$ which proceeds via W -exchange by a mixing matrix element V_{Ne} in the lepton sector, analogous to quark mixing matrix elements.

Exercise. Show that the only contributing chirality amplitude is $G_{LL}(t) = [-4G_F V_{Ne}/\sqrt{2}]/[(1 - t/M_W^2)]$ so that

$$\frac{d\sigma}{dt}(e^+e^- \rightarrow \bar{\nu}_e N) = \frac{d\sigma}{dt}(e^+e^- \rightarrow \bar{N}\nu_e) = \frac{1}{16\pi s^2} |G_{LL}(t)|^2 u(u - m_N^2)$$

and hence that the cross section at low s is

$$\sigma(e^+e^- \rightarrow \bar{\nu}_e N) = \sigma(e^+e^- \rightarrow \bar{N}\nu_e) = \frac{G_F^2 s |V_{Ne}|^2}{6\pi} \left(1 - \frac{m_N^2}{s}\right)^2 \left(1 + \frac{m_N^2}{2s}\right).$$

Pair production of $\bar{N}N$ is possible through s -channel Z exchange as well as t -channel W exchange. The W exchange contribution is suppressed by $|V_{Ne}|^4$ whereas the Z contribution will be unsuppressed by mixing if N belongs to an $SU(2)_L$ doublet (for example, if N is a fourth-generation heavy neutrino).

Exercise. Since the N neutral-current coupling is left-handed, show that the only contributing s -channel chirality amplitudes to $e^+e^- \rightarrow \bar{N}N$ are

$$G_{LL}(s) = \sqrt{2}G_F(2x_w - 1)R(s), \quad G_{RL}(s) = \sqrt{2}G_F(2x_w)R(s),$$

where $R(s)$ is given in §4.2. Hence show that the differential and total cross sections are

$$\frac{d\sigma}{dt}(e^+e^- \rightarrow \bar{N}N) = \frac{G_F^2 |R|^2}{8\pi s^2} [(t - m_N^2)^2 (2x_w)^2 + (u - m_N^2)^2 (2x_w - 1)^2],$$

$$\sigma(e^+e^- \rightarrow \bar{N}N) = \frac{G_F^2 s}{24\pi} \beta \left(\frac{3 + \beta^2}{4} \right) (1 - 4x_w + 8x_w^2) |R(s)|^2.$$

Note that this cross section is not suppressed by a mixing matrix element.

The formulas above assume that N and ν_e are Dirac neutrinos. It is possible that one or both are Majorana fermions, for which particle and antiparticle are identical. Unless both ν_e and N are Majorana fermions, the processes $e^+e^- \rightarrow \bar{\nu}_e N$ and $e^+e^- \rightarrow \bar{N}\nu_e$ are physically distinct and the cross section formulas are as given above. If both are Majorana fermions, the two processes lead to the same final state except that ν_e has right-handed helicity in the first case and left-handed helicity in the second, due to the $V - A$ structure of the interaction. The two contributions are therefore incoherent and the cross section for $e^+e^- \rightarrow \nu_e N$ is given by their sum; then

$$\frac{d\sigma}{dt}(e^+e^- \rightarrow \nu_e N) = \frac{1}{16\pi s^2} \left\{ |G_{LL}(t)|^2 u(u - m_N^2) + |G_{LL}(u)|^2 t(t - m_N^2) \right\}$$

and at low energy,

$$\sigma(e^+e^- \rightarrow \nu_e N) = \frac{G_F^2 s |V_{Ne}|^2}{3\pi} \left(1 - \frac{m_N^2}{s}\right)^2 \left(1 + \frac{m_N^2}{2s}\right).$$

For $e^+e^- \rightarrow \bar{N}N$ production with Majorana N , we have to antisymmetrize the amplitude between the two identical fermions in the final state, and integrate only over half the phase space. The vector coupling of Z to $N\bar{N}$ gives $J^{PC} = 1^{--}$ states which are symmetrical between N and \bar{N} ; the axial vector coupling gives $J^{PC} = 1^{++}$ states which are antisymmetrical. Therefore the effect of antisymmetrization is to cancel out the vector $ZN\bar{N}$ coupling and to double the axial vector coupling.

Exercise. Show that the contributing chirality amplitudes for $e^+e^- \rightarrow NN$ with Majorana N are

$$\begin{aligned} G_{LL}(s) &= -G_{LR}(s) = \sqrt{2}G_F(2x_w - 1)R(s), \\ G_{RL}(s) &= -G_{RR}(s) = \sqrt{2}G_F(2x_w)R(s), \end{aligned}$$

and that the cross section formulas become

$$\begin{aligned} \frac{d\sigma}{dt}(e^+e^- \rightarrow NN) &= \frac{G_F^2 |R|^2}{8\pi s^2} (1 - 4x_w + 8x_w^2) \\ &\quad \times [(t - m_N^2)^2 + (u - m_N^2)^2 - 2sm_N^2], \\ \sigma(e^+e^- \rightarrow NN) &= \frac{G_F^2 s}{24\pi} \beta^3 (1 - 4x_w + 8x_w^2) |R(s)|^2. \end{aligned}$$

Note there is more suppression near threshold for Majorana N compared to Dirac N , but the cross sections become the same at high energy.

Exercise. Evaluate $\sigma(e^+e^- \rightarrow \bar{N}N)$ at the Z resonance for both Dirac and Majorana cases. Hence using the general resonance formula of §4.2 show that

$$\Gamma(Z \rightarrow \bar{N}N) = \frac{G_F M_Z^3}{12\sqrt{2}\pi} \times \begin{cases} \beta(3 + \beta^2)/4 & \text{Dirac} \\ \beta^3 & \text{Majorana} \end{cases}$$

4.6 $e^+e^- \rightarrow$ Hadrons

The experimental cross section ratio of $e^+e^- \rightarrow \gamma^* \rightarrow$ hadrons relative to $e^+e^- \rightarrow \gamma^* \rightarrow \mu^+\mu^-$ provides direct evidence for the color quantum number. In the parton model (§5.1) the hadronic cross section at high Q^2 is given by the sum of the quark cross sections, since quarks are presumed to fragment to hadrons with unit probability. Figure 4.9 shows the basic quark model diagram. The integrated quark cross section from QED is

$$\sigma(e^+e^- \rightarrow \gamma^* \rightarrow \bar{q}q) = N_c e_q^2 \left(1 - \frac{4m_q^2}{s}\right)^{1/2} \left(1 + \frac{2m_q^2}{s}\right) \cdot \sigma(e^+e^- \rightarrow \gamma^* \rightarrow \mu^+\mu^-) \theta(s - 4m_q^2),$$

where e_q is the quark charge in units of e . Hence the ratio of cross sections at s values not close to quark thresholds is

$$R = \frac{\sigma(e^+e^- \rightarrow \gamma^* \rightarrow \text{hadrons})}{\sigma(e^+e^- \rightarrow \gamma^* \rightarrow \mu^+\mu^-)} = \frac{\sum_q \sigma(e^+e^- \rightarrow \gamma^* \rightarrow q\bar{q})}{\sigma(e^+e^- \rightarrow \gamma^* \rightarrow \mu^+\mu^-)} = N_c \sum_q e_q^2,$$

where the sum is over quarks with $m_q < \sqrt{s}/2$, e_q is the quark charge in units of $|e|$ and N_c is the number of types (called color) of each quark flavor. For $N_c = 3$, we have

R	q
2	d, u, s
10/3	d, u, s, c
11/3	d, u, s, c, b
15/3	d, u, s, c, b, t

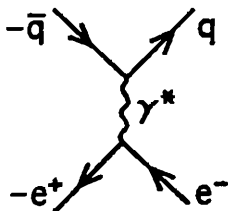


Fig. 4.9. Diagram for $e^+e^- \rightarrow \gamma^* \rightarrow q\bar{q}$ production.

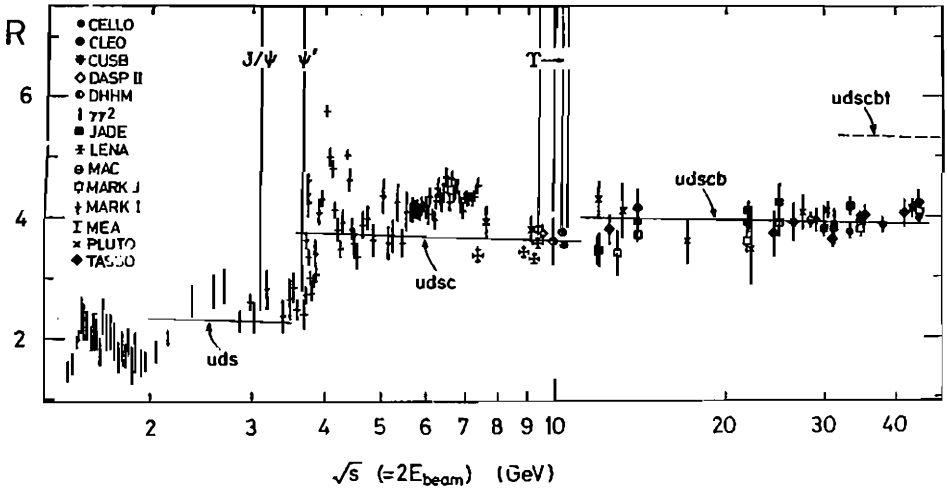


Fig. 4.10. Ratio R of cross sections $\sigma(e^+e^- \rightarrow \text{hadrons})/\sigma(e^+e^- \rightarrow \mu^+\mu^-)$.

The steps in the data are consistent with this quark interpretation provided that each quark flavor has three colors; see Fig. 4.10.

To include first-order QCD corrections the above contributions to R are multiplied by a factor $1 + \alpha_s/\pi$ where $\alpha_s = g_s^2/4\pi$ is the QCD coupling at scale \sqrt{s} .

The cross section well above the $q\bar{q}$ threshold, including both γ^* and Z^0 contributions, is given by

$$\sigma(e^+e^- \rightarrow q\bar{q}) \simeq \frac{s}{16\pi} \left\{ |G_{LL}(s)|^2 + |G_{RR}(s)|^2 + |G_{LR}(s)|^2 + |G_{RL}(s)|^2 \right\}$$

with

$$G_{AB}(s) = -\frac{e_q 4\pi\alpha}{s} + \frac{8G_F}{\sqrt{2}} g_A(Z \rightarrow e\bar{e}) g_B(Z \rightarrow q\bar{q}) R(s).$$

At the Z -resonance energy, the ratio of the resonance contribution

(peak minus background) to the electromagnetic background is

$$R = \frac{\sigma(e^+e^- \rightarrow Z \rightarrow \text{hadrons})}{\sigma(e^+e^- \rightarrow \gamma^* \rightarrow \mu^+\mu^-)} = \frac{9}{\alpha^2} B_{ee} B_h,$$

where B_{ee} is the $Z \rightarrow e^+e^-$ branching fraction and B_h is the $Z \rightarrow$ hadrons branching fraction. The integrated Z -resonance contribution above background is

$$\int d\sqrt{s} \sigma(e^+e^- \rightarrow Z \rightarrow \text{hadrons}) = 6\pi^2 B_{ee} B_h \Gamma_Z / M_Z^2.$$

These two formulas apply equally to any narrow spin-1 resonance (for instance to the ψ and Υ).

A left-right polarization asymmetry A_{LR} and a forward-backward asymmetry A_{FB} can be defined for each quark flavor. Explicit expressions can easily be derived from the general formulas that appear in §4.4. These asymmetries can be measured experimentally in cases where the quark flavor can be tagged, *e.g.* c and b quarks by their semileptonic decay characteristics, and provide independent determinations of Z couplings.

The total cross section for e^+e^- annihilation into hadrons is qualitatively shown in Fig. 4.11. The small peaks at the left are the ψ and Υ resonance regions, following which the cross section falls steadily through the $\sqrt{s} = 10$ -60 GeV region covered by the PEP, PETRA and TRISTAN colliders. Beyond this valley the cross section soars to a peak of about 40 nb at the Z^0 resonance, which is around 1000 times the QED cross section there. The attraction of doing physics at Z^0 factories is plain to see. At the luminosities of the SLC and LEP I colliders, 10^{30} - 10^{31} cm^2s^{-1} , this cross section corresponds to about $10^4 Z^0$ events per day. Such high event rates allow precision tests of the standard model and sensitive searches for possible new particles produced in Z^0 decays.

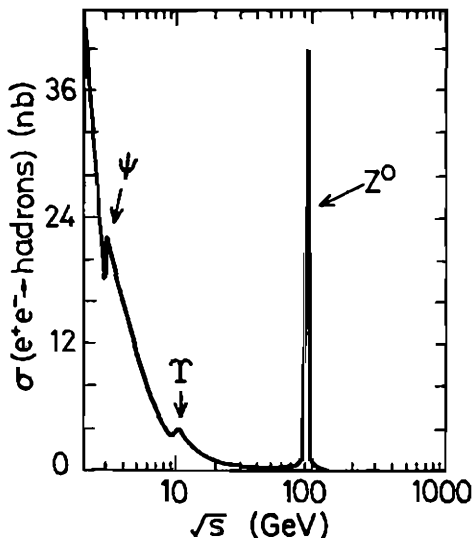


Fig. 4.11. Qualitative features of the total $e^+e^- \rightarrow \text{hadrons}$ cross section.

For heavy quark production at the Z resonance, both threshold and first-order QCD corrections need to be included. The Z exchange cross section formula with threshold factors can be written as

$$\sigma(e^+e^- \rightarrow Z \rightarrow \bar{Q}Q) = \frac{\beta s G_F^2 M_Z^4 (1 - 4x_w + 8x_w^2)}{4\pi [(s - M_Z^2)^2 + \Gamma_Z^2 M_Z^2]} [2g_V^2 (3 - \beta^2) + 4g_A^2 \beta^2],$$

where g_V and g_A are the Z couplings of Q . The effect of first-order QCD corrections is to introduce the following extra factors

$$g_V^2 \rightarrow g_V^2 \left\{ 1 + \frac{4}{3} \alpha_s \left[\frac{\pi}{2\beta} - \frac{3 + \beta}{4} \left(\frac{\pi}{2} - \frac{3}{4\pi} \right) \right] \right\},$$

$$g_A^2 \rightarrow g_A^2 \left\{ 1 + \frac{4}{3} \alpha_s \left[\frac{\pi}{2\beta} - \left(\frac{19}{10} - \frac{22}{5} \beta + \frac{7}{2} \beta^2 \right) \left(\frac{\pi}{2} - \frac{3}{4\pi} \right) \right] \right\},$$

where α_s is the QCD running coupling, which is of order $\alpha_s(M_Z^2) \simeq 0.13$ at the Z mass scale. Note that the correction factors approach $(1 + \alpha_s/\pi)$ as $\beta \rightarrow 1$ but are singular at $\beta = 0$ where higher order effects must be taken into account. Figure 4.12 shows these QCD corrections to the $e^+e^- \rightarrow Z \rightarrow \bar{t}t$ rate as a function of m_t . Figure 4.13 compares the total cross sections for $e^+e^- \rightarrow Z \rightarrow \bar{f}f$ production of various heavy fermion pairs.

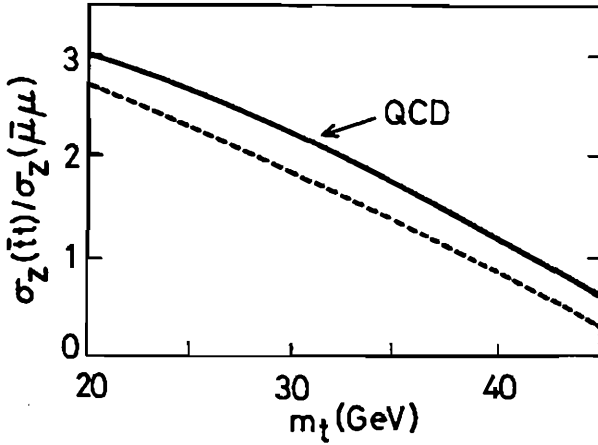


Fig. 4.12. Cross section for $e^+e^- \rightarrow Z \rightarrow \bar{t}t$ production versus m_t , with and without first-order QCD corrections, relative to $e^+e^- \rightarrow Z \rightarrow \mu^+\mu^-$.

Exercise. Evaluate $\Gamma(Z \rightarrow \bar{f}f)/\Gamma(Z \rightarrow e^+e^-)$ for $f = b$ and $f = c$ in the approximation $\beta \simeq 1$.

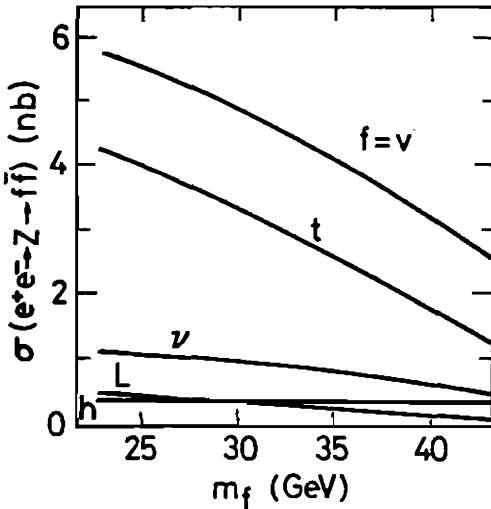


Fig. 4.13. Cross sections for $e^+e^- \rightarrow Z \rightarrow \bar{f}f$ production of heavy fermion pairs, for $f = t$, $f = \nu$ (doublet quark with charge $-\frac{1}{3}$), $f = \nu$ (doublet Dirac neutrino), $f = L$ (doublet heavy charged lepton) and $f = h$ (singlet fermion of charge $-\frac{1}{3}$). For comparison $\sigma(e^+e^- \rightarrow Z \rightarrow \mu^+\mu^-) = 1.8 \text{ nb}$.

4.7 Neutrino-Electron Elastic Scattering

Neutrino-electron scattering is a basic process free from the complications of strong interactions and can be used to determine the weak angle θ_w . Although the measurements are made in fixed-target experiments, we include a discussion for completeness. The general cross section formula derived in the previous section for $\ell f \rightarrow \ell f$ applies to $\nu e \rightarrow \nu e$ scattering and the formula for $\bar{\ell}\ell \rightarrow \bar{f}f$ applies to $\bar{\nu}e \rightarrow \bar{\nu}e$ scattering, except that the spin-average factors of $1/4$ in $d\sigma/dt$ must be replaced by $1/2$ (since the ν or $\bar{\nu}$ has only one helicity component). Since ν has only left-hand couplings, we obtain

$$\frac{d\sigma}{dt}(\nu e \rightarrow \nu e) = \frac{1}{8\pi s^2} \left\{ s^2 |G_{LL}(t) + G_{LL}(u)|^2 + u^2 |G_{LR}(t)|^2 + t^2 |G_{LR}(u)|^2 \right\},$$

$$\frac{d\sigma}{dt}(\bar{\nu}e \rightarrow \bar{\nu}e) = \frac{1}{8\pi s^2} \left\{ u^2 |G_{LL}(s) + G_{LL}(t)|^2 + t^2 |G_{LR}(s)|^2 + s^2 |G_{LR}(t)|^2 \right\},$$

where the electron mass is neglected and the $\bar{\nu}e$ result is obtained by $s \leftrightarrow u$ crossing. Following our convention from §4.1, the labels A and B in G_{AB} refer to the coupling of *fermions* ν and e , respectively; thus $A = L$ refers to ν states with L chirality or $\bar{\nu}$ states with R chirality.

The elastic process $\nu_\mu e^- \rightarrow \nu_\mu e^-$ proceeds via Z^0 exchange in the t channel as illustrated in Fig. 4.14.

Exercise. For $Q^2 \ll M_Z^2$ show that the amplitudes G_{AB} are

$$G_{LL}(t) = \frac{-4G_F}{\sqrt{2}} \left(x_w - \frac{1}{2}\right), \quad G_{LR}(t) = \frac{-4G_F}{\sqrt{2}} x_w.$$

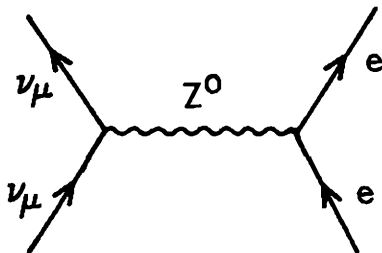


Fig. 4.14. Elastic $\nu_\mu e$ scattering.

The differential cross section is

$$\frac{d\sigma}{dt}(\nu_\mu e) = \frac{G_F^2}{\pi s^2} \left[s^2 \left(x_w - \frac{1}{2}\right)^2 + u^2 x_w^2 \right].$$

Introducing the dimensionless variable,

$$y = -\frac{t}{s} = 1 + \frac{u}{s} = -\frac{(e - e')^2}{s},$$

the cross section expression becomes

$$\frac{d\sigma}{dy}(\nu_\mu e) = \frac{G_F^2 s}{\pi} \left[\left(x_w - \frac{1}{2}\right)^2 + x_w^2 (1 - y)^2 \right].$$

In the laboratory frame $s = 2m_e E_\nu$ and $y = E'_e/E_\nu$, and hence y has the kinematic range 0 to 1. The $(1 - y)^2$ term is associated with the $Z^0 \bar{e}_R e_R$ current. The vanishing of this contribution at $y = 1$ is a consequence of angular momentum conservation. At $y = 1$ ($\cos \theta_{\text{cm}} = -1$) the final particles are reversed from the corresponding initial particles. The resulting configuration of helicities and momenta in the c.m. frame for $m_e = 0$ are given in Fig. 4.15. The net helicity of the initial state differs from that of the final state, which is forbidden for this collinear configuration.

A similar calculation applies for the process $\bar{\nu}_\mu e^- \rightarrow \bar{\nu}_\mu e^-$ with the same amplitudes $G_{AB}(t)$, with the result

$$\frac{d\sigma}{dy}(\bar{\nu}_\mu e^-) = \frac{G_F^2 s}{\pi} \left[x_w^2 + \left(x_w - \frac{1}{2}\right)^2 (1 - y)^2 \right].$$

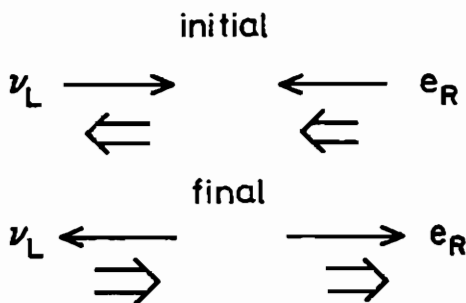


Fig. 4.15. Helicity configurations for backward $\nu_L e_R$ scattering in the c.m. frame.

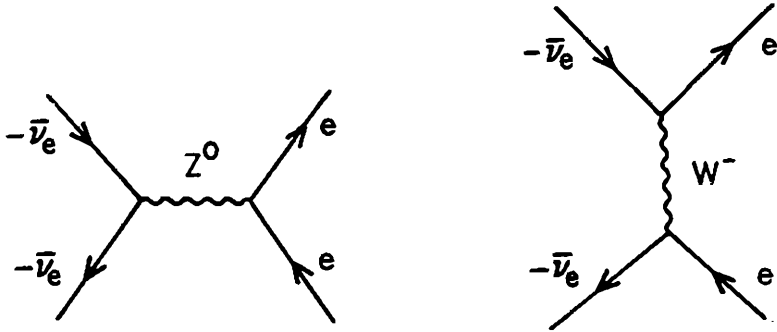


Fig. 4.16. Diagrams for $\bar{\nu}_e e$ elastic scattering.

For the elastic process $\bar{\nu}_e e^- \rightarrow \bar{\nu}_e e^-$ both Z and W exchanges contribute, as illustrated in Fig. 4.16.

The G_{AB} for the t -channel Z^0 exchange are as before; for the s -channel W exchange we have

$$G_{LL}(s) = \frac{-4G_F}{\sqrt{2}}.$$

Thus the differential cross section is

$$\frac{d\sigma}{dt}(\bar{\nu}_e e) = \frac{G_F^2}{\pi s^2} [x_w^2 s^2 + (x_w + \frac{1}{2})^2 u^2]$$

or, equivalently,

$$\frac{d\sigma}{dy}(\bar{\nu}_e e) = \frac{G_F^2 s}{\pi} [x_w^2 + (x_w + \frac{1}{2})^2 (1-y)^2].$$

Exercise. Show that

$$\frac{d\sigma}{dy}(\nu_e e) = \frac{G_F^2 s}{\pi} \left[(x_w + \frac{1}{2})^2 + x_w^2 (1-y)^2 \right].$$

The cross sections integrated over y are

$$\sigma(\nu_\mu e^-) = \frac{G_F^2 s}{4\pi} \left(1 - 4x_w + \frac{16}{3} x_w^2 \right) = 0.16 \times 10^{-43} \text{cm}^2 (E/10 \text{ MeV}),$$

$$\sigma(\bar{\nu}_\mu e^-) = \frac{G_F^2 s}{4\pi} \left(\frac{1}{3} - \frac{4}{3} x_w + \frac{16}{3} x_w^2 \right) = 0.13 \times 10^{-43} \text{cm}^2 (E/10 \text{ MeV}),$$

$$\sigma(\nu_e e) = \frac{G_F^2 s}{4\pi} \left(1 + 4x_w + \frac{16}{3}x_w^2\right) = 0.93 \times 10^{-43} \text{ cm}^2 (E/10 \text{ MeV}),$$

$$\sigma(\bar{\nu}_e e^-) = \frac{G_F^2 s}{4\pi} \left(\frac{1}{3} + \frac{4}{3}x_w + \frac{16}{3}x_w^2\right) = 0.39 \times 10^{-43} \text{ cm}^2 (E/10 \text{ MeV}).$$

The cross sections grow linearly with $s \simeq 2m_e E_\nu$ for energies $s \ll M_Z^2$ (Z and W propagator damping effects are neglected in the above expressions). The order of magnitude of these cross sections is set by

$$G_F^2 m_e / (2\pi) = 4.3 \times 10^{-42} \text{ cm}^2 / \text{GeV}.$$

Since the cross sections are so small, only integrated rates have been used thus far in determining x_w . For example, present neutrino-electron data give $x_w = 0.212 \pm 0.023$. The next generation of $\nu_\mu e$ and $\bar{\nu}_\mu e$ experiments will yield hundreds of events. It should then be possible to use the differential as well as the total cross sections in determining x_w .

Exercise. In νe scattering show that the c.m. scattering angle θ^* and the electron recoil angle θ are related by

$$\tan \theta = 2m_e \sqrt{s} (s + m_e^2)^{-1} \cot \left(\frac{1}{2}\theta^*\right).$$

Derive the cross section formula

$$\frac{d\sigma}{d\cos\theta} = \frac{8m_e^2 s (1 - m_e^2/s)^2 \cos\theta}{D^2} \frac{d\sigma}{dy},$$

with $y = 4m_e^2(1 - m_e^2/s)^2 \cos^2\theta / D$ where the denominator factor $D = s^{-1}(s + m_e^2)^2 \sin^2\theta + 4m_e^2 \cos^2\theta$ becomes very small at small θ and generates a cross section peak there.

Exercise. Show that the cross section for $e^+e^- \rightarrow \nu\bar{\nu}$ is

$$\sigma(e^+e^- \rightarrow \nu\bar{\nu}) = \frac{G_F^2 s}{6\pi} \left\{ 1 + (1 - 2x_w) \text{Re} R + \frac{n}{8} [1 + (1 - 4x_w)^2] |R|^2 \right\},$$

where n is the number of light left-handed neutrino generations and $R(s)$ is defined in §4.2.

Chapter 5

Partons and Scaling Distributions

5.1 The Parton Model

In deep inelastic electron-proton scattering $ep \rightarrow eX$, the exchange of an energetic virtual photon or Z^0 with large transverse momentum squared disintegrates the proton into hadrons. The final electron energy and angle are measured, but the inclusive hadronic final state X is not necessarily studied. Experiments showed that the structure functions, which describe the hadronic vertex, exhibit approximate scaling in a dimensionless variable. The interpretation of the approximate scaling behavior is that the photon or Z^0 interacts with pointlike constituents (called partons by Feynman, which we now know to be quarks) within the proton target; see Fig. 5.1.

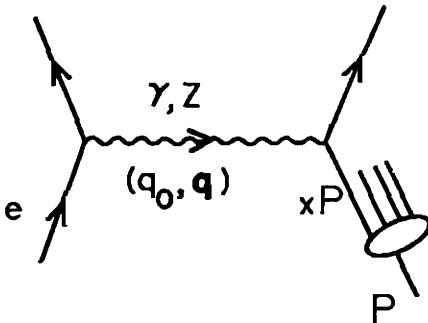


Fig. 5.1. Parton model description of deep inelastic electron-proton scattering.

We imagine the proton as constantly dissociating into virtual states of free partons. By the uncertainty principle, the lifetime of a virtual state is of order $\tau_{\text{vir}} \sim 1/\Delta E$, where ΔE is the energy difference between the virtual state and the proton. Similarly, the time duration of a collision during which the photon or Z^0 energy q^0 is absorbed by the proton is of order $\tau_{\text{coll}} \sim 1/q^0$. If the collision time is much shorter than the virtual state lifetime, we may treat the partons as free during the collision. These time scales depend on the Lorentz frame we use; the justification for the parton model is made in a frame where the proton is moving very fast so that by relativistic time dilation its clock runs very slowly. We must establish, however, that $\tau_{\text{coll}} \ll \tau_{\text{vir}}$ in this frame.

It is convenient to work in the electron-proton c.m. frame, where the proton momentum \mathbf{P} is large in high energy collisions. Suppose that the proton dissociates virtually into a parton of momentum $x\mathbf{P}$ and mass m_1 plus a group of partons of momentum $(1-x)\mathbf{P}$ and invariant mass m_2 . Then

$$\begin{aligned} \Delta E &= [x^2 P^2 + m_1^2]^{1/2} + [(1-x)^2 P^2 + m_2^2]^{1/2} - [P^2 + M^2]^{1/2} \\ &\simeq \left[\frac{m_1^2}{2x} + \frac{m_2^2}{2(1-x)} - \frac{M^2}{2} \right] / |\mathbf{P}|, \end{aligned}$$

where M is the proton mass. Before evaluating q^0 we remark that the quantities $q^2 = -Q^2$ and $q \cdot \mathbf{P} = M\nu$ are both large ($\gg M^2$) in deep inelastic scattering. Here q is the photon or Z^0 four-momentum, Q^2 is the invariant momentum transfer squared and ν is the energy carried by the virtual photon or Z^0 in the proton rest frame. In the electron-proton c.m. frame the four-momenta are $(|\mathbf{P}|, -\mathbf{P})$ for the initial electron and $(|\mathbf{P}| - q^0, -\mathbf{P} - \mathbf{q})$ for the final electron, in the massless electron approximation; the mass shell condition for the final electron gives $q^2 - 2q^0|\mathbf{P}| - 2\mathbf{P} \cdot \mathbf{q} = 0$. Using $\mathbf{P} \cdot \mathbf{q} = q^0\sqrt{P^2 + M^2} - \mathbf{P} \cdot \mathbf{q}$ to eliminate $\mathbf{P} \cdot \mathbf{q}$ we obtain

$$q^0 = \frac{\mathbf{P} \cdot \mathbf{q} + \frac{1}{2}q^2}{\sqrt{P^2 + M^2} + |\mathbf{P}|} \simeq \frac{2M\nu - Q^2}{4|\mathbf{P}|}$$

so that the ratio of time scales is

$$\tau_{\text{coll}}/\tau_{\text{vir}} \sim \Delta E/q^0 \simeq [2m_1^2/x + 2m_2^2/(1-x) - 2M^2] / [2M\nu - Q^2] ,$$

which is small in deep inelastic scattering where both $2M\nu$ and $Q^2 \gg M^2$. Note that $Q^2 = 2M\nu$ corresponds to elastic electron-proton scattering, which is not a deep inelastic process.

The above arguments justify the *impulse approximation* in which the partons are treated as free during the collision. Hence the partons scatter incoherently and the virtual-boson-nucleon cross section is a sum of the parton cross sections. After scattering, the partons are assumed to recombine into hadrons with probability 1.

Approximate scaling behavior was also observed in deep inelastic neutrino scattering and in the production of lepton pairs in hadron-hadron collisions. The extraction of the quark (and gluon) scaling distributions from various experiments is discussed in this chapter. Scaling violations due to QCD radiation of gluons will be considered in Chapter 7.

5.2 Electron (Muon) Deep Inelastic Scattering

Consider the process $ep \rightarrow eX$, where p is a proton target and X is an inclusive hadronic final state. Only the final electron is detected, and the hadrons in the system X are summed over. Parton model calculations must be made in a frame where the proton has a very large momentum (*infinite momentum frame*) and all its partons are traveling in the same direction. The results are subsequently Lorentz transformed to the laboratory frame relevant to the experiment. For fixed-target experiments the lab frame is the proton rest frame while for collider experiments it is a frame where neither the electron nor the proton is at rest.

Suppose that $q(x)$ is the *probability distribution* for finding a parton q with momentum fraction $x = (\text{parton momentum})/(\text{proton$

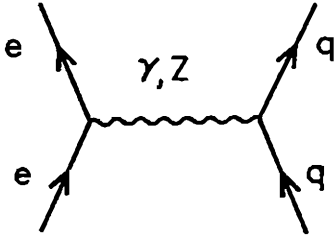


Fig. 5.2. Electron-quark scattering.

momentum). Then the inclusive cross section is given by the cross section for scattering from the parton times $q(x) dx$, summed over all partons q and integrated over dx . The Feynman diagram for scattering from the point-like quark partons is shown in Fig. 5.2. From formulas in §4.1 for lepton-fermion scattering with t -channel exchanges only, the $eq \rightarrow eq$ differential cross section is

$$\frac{d\hat{\sigma}}{d\hat{t}}(eq \rightarrow eq) = \frac{1}{16\pi\hat{s}^2} \left\{ \hat{s}^2 [|G_{LL}(\hat{t})|^2 + |G_{RR}(\hat{t})|^2] + \hat{u}^2 [|G_{LR}(\hat{t})|^2 + |G_{RL}(\hat{t})|^2] \right\},$$

where

$$G_{AB}(\hat{t}) = \frac{e_q e^2}{\hat{t}} + \frac{8G}{\sqrt{2}} g_A^e g_B^q R(\hat{t}).$$

Here e_q is the charge of q and \hat{s} , \hat{t} , \hat{u} are the invariants for the subprocess. G corresponds to the Fermi coupling at low \hat{t} and has a definition for large \hat{t} analogous to that given in §3.8; $R(\hat{t})$ is the Z -propagator factor, $R(\hat{t}) = M_Z^2 / (M_Z^2 - \hat{t})$ which is essentially unity in the regime $-\hat{t} \ll M_Z^2$.

Exercise. For electron scattering on u -quarks at $\hat{t} = -M_Z^2$, estimate the importance of the Z exchange contribution.

At small \hat{t} the Z exchange contribution is negligible compared to the photon exchange. In the following we specialize to the photon dominance region where

$$\frac{d\hat{\sigma}}{d\hat{t}}(eq \rightarrow eq) = e_q^2 \frac{\hat{s}^2 + \hat{u}^2}{8\pi\hat{s}^2} \left(\frac{e^2}{\hat{t}} \right)^2.$$

We introduce the dimensionless variable

$$y = -\hat{t}/\hat{s}$$

and rewrite the above result using $1 - y = -\hat{u}/\hat{s}$ as

$$\frac{d\hat{\sigma}}{dy} = e_q^2 \frac{2\pi\alpha^2\hat{s}}{Q^4} [1 + (1 - y)^2],$$

where $Q^2 = -\hat{t}$. Notice that $y = \sin^2(\frac{1}{2}\hat{\theta})$, where $\hat{\theta}$ is the electron-quark c.m. scattering angle, in the massless approximation for electrons and quarks. Also,

$$\begin{aligned} s &= (e + P)^2 = M^2 + 2e \cdot P, \\ \hat{s} &= (e + k)^2 = 2e \cdot k = x(2e \cdot P), \end{aligned}$$

where k is the incident electron momentum. Hence

$$\hat{s} \simeq xs.$$

Then the inclusive deep inelastic cross section in the parton model obtained by multiplying the parton subprocess cross sections by $q(x)dx$ is

$$\frac{d\sigma}{dx dy} = \frac{2\pi\alpha^2 s}{Q^4} [1 + (1 - y)^2] \sum_q e_q^2 xq(x).$$

Note that aside from the $(Q^2)^{-2}$ photon propagator factor, the differential cross section is a function only of x and y and does not depend on Q^2 . This scaling behavior in x was first observed in fixed-target experiments at SLAC in 1968.

Thus far x and y have been defined in terms of electron-quark scattering variables. These scaling variables are related to the observed deep inelastic electron-proton scattering variables ν , Q^2 and s as follows. Denote the initial and final quark momenta by k and

k' ; let P and q denote the proton and virtual photon momenta as in §5.1. Then $k' = k + q$ and the massless condition for the final quark gives

$$0 = k'^2 = (k + q)^2 = q^2 + 2k \cdot q.$$

Substituting $k = xP$, $q^2 = -Q^2$ and $P \cdot q = M\nu$ we obtain

$$x = \frac{-q^2}{2P \cdot q} = \frac{Q^2}{2M\nu},$$

which is the Bjorken scaling variable for deep inelastic scattering. This identification of the quark momentum fraction x with the quantity $Q^2/(2M\nu)$ is a consequence of quark kinematics. Since

$$\hat{s} = 2xe \cdot P = 2xME,$$

where E is the laboratory energy of the electron for a proton target at rest (related to s by $s = 2ME + M^2$), we obtain

$$y = \frac{-\hat{t}}{\hat{s}} = \frac{Q^2}{2xME} = \frac{\nu}{E} \simeq \frac{2P \cdot q}{s}.$$

The invariant mass W of the hadronic system is

$$W^2 = (P + q)^2 = M^2 - Q^2 + 2M\nu.$$

Exercise. Show that the physical region defined by $s \geq W^2 \geq M^2$ together with $0 \leq \hat{\theta} \leq \pi$ for electron-quark scattering gives the kinematic limits,

$$0 \leq x \leq 1, \quad 0 \leq y \leq 1, \quad 0 \leq Q^2 \leq 2M\nu, \quad 0 \leq \nu \leq (s - M^2)/2M.$$

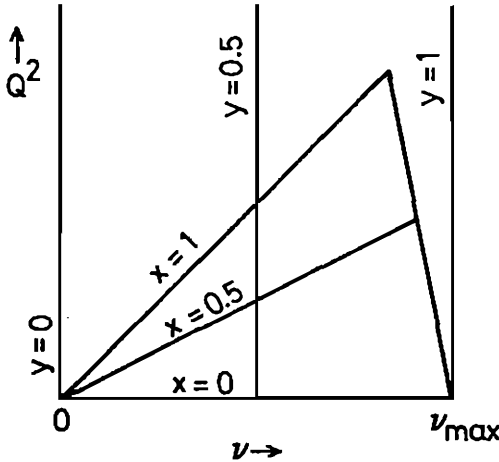


Fig. 5.3. The physical region of ep inelastic scattering in the ν, Q^2 plane. Constant x corresponds to a slanted straight line passing through the origin. Constant y corresponds to a vertical straight line.

Figure 5.3 shows the complete physical region in the ν, Q^2 plane with lines of constant x and constant y . The boundaries are the horizontal line $Q^2 = 0$ ($x = 0$), the sloping line $Q^2 = 2M\nu$ ($x = 1$) and the line $Q^2 = 4\nu_{\max}(\nu_{\max} - \nu)$ where $\nu_{\max} = (s - M^2)/2M$. This third line is approximately vertical for $s \gg M^2$ and represents the limit $\cos \theta = -1$ in the proton rest-frame. Notice that electron-quark kinematics gives instead the boundary $\cos \hat{\theta} = -1$ which is $\nu = \nu_{\max}$, a precisely vertical line, illustrating the slight mismatch between the kinematics of the true ep and idealized eq situations.

In fixed-target experiments, Q^2 and ν are related to the initial and final electron energies E_e and E'_e , and to the electron scattering angle θ , by

$$Q^2 = 4E_e E'_e \sin^2 \frac{\theta}{2}, \quad \nu = E_e - E'_e.$$

In ep collider experiments, Q^2 and ν are given by

$$Q^2 = 4E_e E'_e \sin^2 \frac{\theta}{2},$$

$$M\nu = \frac{1}{2}(s - M^2) - E'_e(E_p + p_p \cos \theta) \simeq \frac{1}{2}s [1 - (E'_e/E_e) \cos^2 \frac{\theta}{2}].$$

Exercise. Show that in the ν, Q^2 plane fixed scattering angle θ corresponds to a straight line passing through the point $\nu = \nu_{\max}, Q^2 = 0$

for fixed-target experiments. Show that a similar result holds for collider experiments.

Exercise. Show that the various differential cross sections are related by

$$\begin{aligned} \frac{d\sigma}{d\nu dQ^2} &= \frac{2M}{(s-M^2)^2 y} \frac{d\sigma}{dx dy} = \frac{\pi}{E_e E'_e} \frac{d\sigma}{dE'_e d\Omega'_e} \quad \left(\begin{array}{l} \text{fixed-} \\ \text{target} \end{array} \right) \\ &= \frac{2\pi M}{E'_e (s-M^2)} \frac{d\sigma}{dE'_e d\Omega'_e} \quad (\text{collider}) . \end{aligned}$$

We label the u, d, c, s, \dots quark densities in a *proton* by $u(x), d(x), c(x), s(x), \dots$ (For a neutron interchange $u(x)$ and $d(x)$.) In order to reproduce the proton quantum numbers for charm, strangeness, isospin and baryon number, the following integral conditions must be satisfied:

$$\begin{aligned} C = 0 &= \int_0^1 dx [c(x) - \bar{c}(x)] , & S = 0 &= \int_0^1 dx [s(x) - \bar{s}(x)] , \\ I_3 = \frac{1}{2} &= \int_0^1 dx \left\{ \frac{1}{2} [u(x) - \bar{u}(x)] - \frac{1}{2} [d(x) - \bar{d}(x)] \right\} , \\ B = 1 &= \int_0^1 dx \frac{1}{3} [u(x) - \bar{u}(x) + d(x) - \bar{d}(x) + s(x) - \bar{s}(x) + c(x) - \bar{c}(x)] . \end{aligned}$$

These conditions give

$$\int_0^1 dx [u(x) - \bar{u}(x)] = 2 \quad \text{and} \quad \int_0^1 dx [d(x) - \bar{d}(x)] = 1 .$$

In other words, the proton contains two *valence* up quarks and one *valence* down quark which carry the quantum numbers, plus a *sea* of $q\bar{q}$ pairs with zero quantum numbers. These are the quark-parton model sum rules. When QCD radiation of gluons from the partons is taken into account, the quark distributions become functions of both x and Q^2 and the sum rules above hold at fixed Q^2 .

We separate the quark densities $q(x)$ into valence parts $q_v(x)$ and sea components $\xi_q(x)$:

$$u(x) = u_v(x) + \xi_u(x), \quad \bar{u}(x) = \xi_u(x),$$

$$d(x) = d_v(x) + \xi_d(x), \quad \bar{d}(x) = \xi_d(x),$$

$$s(x) = \xi_s(x), \quad \bar{s}(x) = \xi_s(x),$$

$$c(x) = \xi_c(x), \quad \bar{c}(x) = \xi_c(x).$$

The valence components must satisfy

$$\int_0^1 u_v(x) dx = 2 \quad \text{and} \quad \int_0^1 d_v(x) dx = 1.$$

There are some theoretical arguments on the qualitative x dependence to be expected for the valence and sea distributions. Correspondence of deep inelastic scattering for large ν and small fixed Q^2 with Regge behavior of the total cross sections for virtual photon scattering on a nucleon target gives the behaviors

$$q_v(x) \sim x^{-1/2}, \quad \xi(x) \sim x^{-1}.$$

Here the valence distributions are identified with Regge exchanges associated with observed particles (f^0 , A_2) while the sea is identified with the Pomeron exchange which carries the quantum numbers of the vacuum. Correspondence as $x \rightarrow 1$ with elastic γ^*p scattering leads to the behavior

$$q_v(x) \sim (1-x)^3.$$

A faster fall-off for the sea distribution as $x \rightarrow 1$ is deduced empirically from the deep inelastic data and the sum rules. Typically fits to the deep inelastic data give

$$\xi(x) \sim (1-x)^8.$$

Parameterizations of the quark distributions are discussed in §5.6.

Exercise. When $R \simeq 1$ and heavy quark components in the nucleon are ignored, show that

$$\frac{d\sigma}{dx}(ep \rightarrow eX) = \frac{8\pi\alpha^2 s}{3Q^4} x \left\{ \frac{4}{9} [u(x) + \bar{u}(x)] + \frac{1}{9} [d(x) + \bar{d}(x) + s(x) + \bar{s}(x)] \right\},$$

$$\frac{d\sigma}{dx}(en \rightarrow eX) = \frac{8\pi\alpha^2 s}{3Q^4} x \left\{ \frac{4}{9} [d(x) + \bar{d}(x)] + \frac{1}{9} [u(x) + \bar{u}(x) + s(x) + \bar{s}(x)] \right\}.$$

5.3 Charged Current Deep Inelastic Scattering

The parton substructure of the proton and neutron can also be probed by W boson exchange deep inelastic processes

$$\begin{aligned} e^- p &\rightarrow \nu_e X, & \bar{\nu}_\ell p &\rightarrow \ell^+ X, \\ e^+ p &\rightarrow \bar{\nu}_e X, & \nu_\ell p &\rightarrow \ell^- X, \end{aligned}$$

where $\ell = e$ or μ . The early experimental work was done with neutrino beams on fixed targets, but future work at very high Q^2 will be done with electron-proton colliders where neutrino production will be recognized from missing transverse momentum. In either case the kinematic variables are as described in the preceding section, with appropriate identification of incoming and outgoing leptons.

The underlying parton subprocesses for electron charged current (CC) deep inelastic scattering are shown in Fig. 5.4. The neutrino scattering subprocesses are simply related to these by crossing.

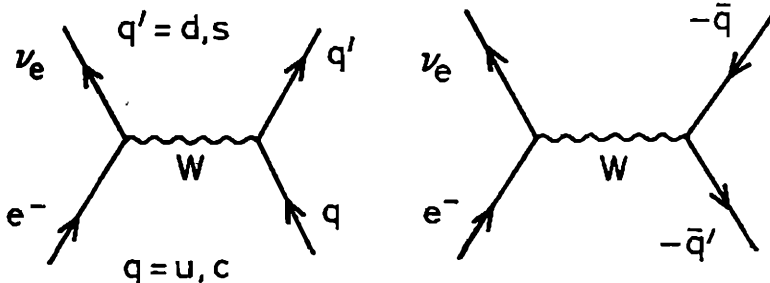


Fig. 5.4. Electron-quark charged current scattering subprocesses.

From formulas derived in §4.1, the subprocess differential cross sections in the massless quark approximation are

$$\frac{d\hat{\sigma}}{dy}(e^-q \rightarrow \nu_e q') = \frac{1}{2} \frac{d\hat{\sigma}}{dy}(\nu_\ell q' \rightarrow \ell^- q) = \frac{G_F^2 \hat{s}}{2\pi} |V_{qq'}|^2 R^2(Q),$$

$$\frac{d\hat{\sigma}}{dy}(e^- \bar{q}' \rightarrow \nu_e \bar{q}) = \frac{1}{2} \frac{d\hat{\sigma}}{dy}(\nu_\ell \bar{q} \rightarrow \ell^- \bar{q}') = \frac{G_F^2 \hat{s}}{2\pi} |V_{qq'}|^2 (1-y)^2 R^2(Q),$$

where $V_{qq'}$ is the weak mixing matrix element and $R(Q^2) = M_W^2 / (M_W^2 + Q^2)$. The factor $\frac{1}{2}$ difference between eq and νq cases arises from the initial spin average (neutrinos have only one helicity but electrons have two). The e^+ and $\bar{\nu}$ cross sections have similar forms, with the interchanges $e^+ \leftrightarrow e^-$, $\bar{\nu} \leftrightarrow \nu$, $\bar{q} \leftrightarrow q$.

Exercise. Show that the vanishing of the $e^- \bar{q}' \rightarrow \nu_e \bar{q}$ cross section at $y = 1$ is a consequence of angular momentum conservation.

The inclusive cross sections on a proton target are obtained by multiplying the parton cross sections by $q(x)dx$.

$$\frac{d\sigma^{CC}}{dxdy}(e^-p) = \frac{G_F^2 s}{2\pi} \sum_{q,q'} |V_{qq'}|^2 x [q(x) + (1-y)^2 \bar{q}'(x)] R^2(Q^2),$$

$$\frac{d\sigma^{CC}}{dxdy}(e^+p) = \frac{G_F^2 s}{2\pi} \sum_{q,q'} |V_{qq'}|^2 x [\bar{q}(x) + (1-y)^2 q'(x)] R^2(Q^2).$$

The scale of these cross sections is

$$\frac{G_F^2 M}{\pi} = 1.58 \times 10^{-38} \text{ cm}^2/\text{GeV}.$$

Note that these cross sections scale in x and y if $Q^2 \ll M_W^2$ so that $R \simeq 1$, provided the quark distributions depend on x alone (i.e. are *scaling* distributions). It then follows that the total deep inelastic cross sections and the average value of Q^2 grow linearly with s , $\langle Q^2 \rangle \propto s$, $\sigma \propto s$. Figure 5.5 shows this property in neutrino

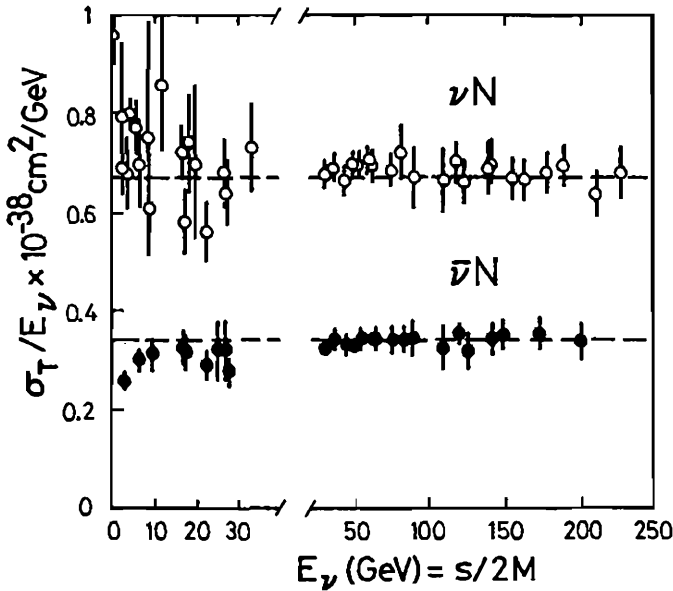


Fig. 5.5. Linear rise of νN and $\bar{\nu} N$ total cross sections with s .

and antineutrino total cross sections. However, at high Q^2 the W -propagator factor slows this growth; also the Q^2 dependences of the quark distributions become important. In the scaling approximation at low Q^2 with only valence contributions retained, the y dependences have the forms

$$\frac{d\sigma^{CC}}{dy}(e^+p) \sim \frac{d\sigma^{CC}}{dy}(\bar{\nu}_l p) \sim (1-y)^2,$$

$$\frac{d\sigma^{CC}}{dy}(e^-p) \sim \frac{d\sigma^{CC}}{dy}(\nu_l p) \sim \text{constant}.$$

The distributions measured in fixed target ν_μ and $\bar{\nu}_\mu$ deep inelastic scattering experiments are in qualitative accord with this behavior.

Exercise. In valence dominance approximation and putting $|V_{ud}| \simeq 1$, show that

$$\begin{aligned} d\sigma(\nu p \rightarrow \mu X)/dx &= (G_F^2 s/\pi) x d(x), \\ d\sigma(\bar{\nu} n \rightarrow \mu X)/dx &= (G_F^2 s/\pi) x u(x), \end{aligned}$$

and hence that

$$F_2^{\nu D}(x) = \frac{18}{5} F_2^{eD}(x), \quad \text{where}$$

$$F_2^{\nu D} = \left(\frac{2\pi}{G_F^2 s} \right) \left[\frac{d\sigma}{dx}(\nu p \rightarrow \mu X) + \frac{d\sigma}{dx}(\nu n \rightarrow \mu X) \right],$$

$$F_2^{eD} = \left(\frac{3Q^4}{8\pi\alpha^2 s} \right) \left[\frac{d\sigma}{dx}(ep \rightarrow eX) + \frac{d\sigma}{dx}(en \rightarrow eX) \right].$$

This relation is a test of the quark charges. The experimental values show equality in the valence region; see Fig. 5.6.

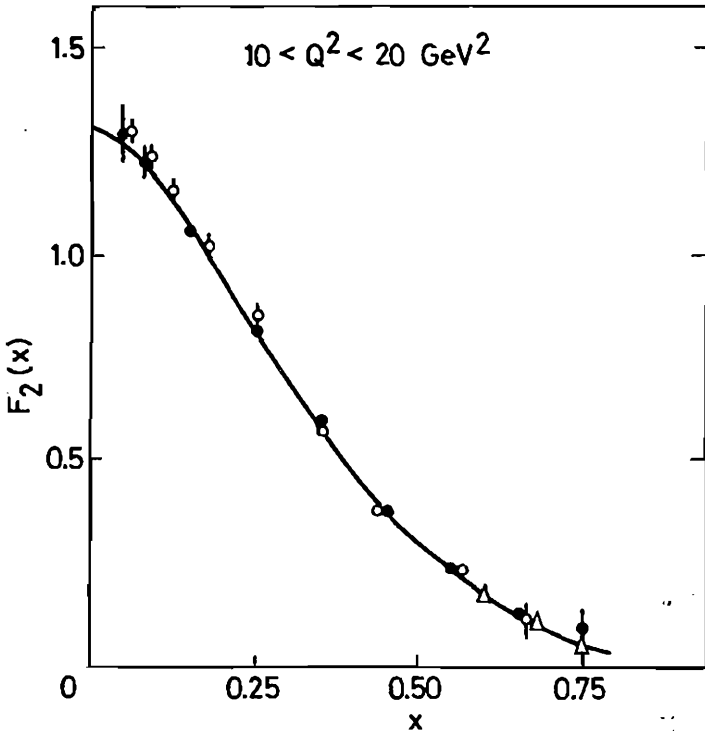


Fig. 5.6. Comparison of F_2 for electron, muon and neutrino data. Solid circles are CDHS neutrino data [Z. Phys. C17, 283 (1983)], open circles are EMC muon data [Phys. Lett. 105B, 322 (1981)], triangles are SLAC-MIT data [Phys. Rev. D20, 1471 (1979)].

For production of a heavy quark Q from a light quark q , the heavy quark mass modifies the scaling variable of the quark distribution. If k is the initial quark momentum and $q = e - \nu$ is the momentum transfer to the quark, the m_Q mass shell constraint gives

$$m_Q^2 = (k + q)^2 = q^2 + 2k \cdot q = 2x'P \cdot q - Q^2.$$

Hence we obtain the *slow rescaling* variable

$$x' = \frac{Q^2 + m_Q^2}{2M\nu} = x + \frac{m_Q^2}{2MEy},$$

which is the quark momentum fraction appropriate to absorb the virtual W described by ν and Q^2 . Figure 5.7 shows the relationship of the x and x' variables. Clearly only a part of the range $0 \leq x' \leq 1$ is in the physical region $Q^2 \geq 0$; the whole of the line $x' = 0$, for example, is unphysical. In terms of parton kinematics, $x' = 1$ is a kinematical boundary for heavy quark production; it translates into a bound on hadronic invariant mass $W^2 \geq M^2 + m_Q^2$. This is not precisely the physical threshold $W \gtrsim M + m_Q$, but for large m_Q the difference is not very important; we therefore regard $x' = 1$ as approximating this threshold. The threshold and $Q^2 \geq 0$ requirements then give the limits

$$m_Q^2/(2M\nu) \leq x' \leq 1.$$

Since the small x' region can not contribute, there is a suppression of the cross section near threshold. The vanishing of the struck parton distribution as $x' \rightarrow 1$ gives a smooth threshold region.

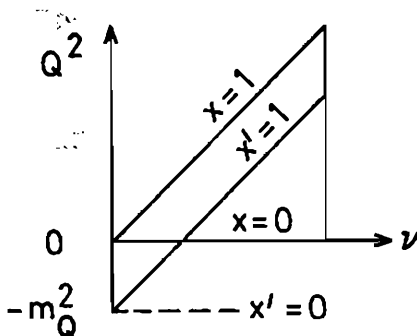


Fig. 5.7. Comparison of the variables x and x' in the ν, Q^2 plane.

Exercise. Use the massive-fermion results of §4.4 to derive expressions for $d\hat{\sigma}/d\hat{t}(\nu q' \rightarrow lq)$ and $d\hat{\sigma}/dy'$ where $y' = -\hat{t}/\hat{s} = Q^2/(2ME'x')$. Show that the Jacobian $\partial(x', y')/\partial(x, y) = 1$. Hence derive the following cross section formulas for charm production by neutrinos, assuming $c(x) = \bar{c}(x) = 0$:

$$\frac{d\sigma}{dx dy}(\nu p \rightarrow \mu^- cX) = \frac{G_F^2 s}{\pi} \left(x' - \frac{m_c^2}{s}\right) [|V_{cs}|^2 s(x') + |V_{cd}|^2 d(x')] R^2,$$

$$\frac{d\sigma}{dx dy}(\bar{\nu} p \rightarrow \mu^+ \bar{c}X) = \frac{G_F^2 s}{\pi} \left(x' - \frac{m_c^2}{s}\right) [|V_{cs}|^2 \bar{s}(x') + |V_{cd}|^2 \bar{d}(x')] R^2.$$

Exercise. Derive similar formulas for bottom quark production:

$$\frac{d\sigma}{dx dy}(\nu p \rightarrow \mu^- \bar{b}X) = \frac{G_F^2 s}{\pi} \left(x' - x'y' - \frac{m_b^2}{s}\right) (1 - y') \bar{u}(x') |V_{ub}|^2 R^2,$$

$$\frac{d\sigma}{dx dy}(\bar{\nu} p \rightarrow \mu^+ bX) = \frac{G_F^2 s}{\pi} \left(x' - x'y' - \frac{m_b^2}{s}\right) (1 - y') u(x') |V_{ub}|^2 R^2.$$

Exercise. Derive similar formulas for producing heavy quarks Q with charge $\frac{2}{3}$ or Q' with charge $-\frac{1}{3}$ at an ep collider:

$$\frac{d\sigma}{dx dy}(ep \rightarrow \nu_e \bar{Q}X) = \frac{G_F^2 s}{2\pi} \left(x' - x'y' - \frac{m_Q^2}{s}\right) (1 - y') \sum_{q'} \bar{q}'(x') |V_{Qq'}|^2 R^2,$$

$$\frac{d\sigma}{dx dy}(ep \rightarrow \nu_e Q'X) = \frac{G_F^2 s}{2\pi} \left(x' - \frac{m_{Q'}^2}{s}\right) \sum_q q(x') |V_{qQ'}|^2 R^2.$$

Notice that for ν , Q^2 regions far above threshold we have $x' \simeq x$ and $y' \simeq y$ so that the original light-quark formulas are approximately valid once more.

Analogous quark mass-shell arguments do *not* give a satisfactory slow rescaling variable for heavy-to-light transitions such as $\nu \bar{c} \rightarrow \mu \bar{s}$ (which materializes a spectator c quark from the $c\bar{c}$ sea) nor for

heavy-to-heavy electromagnetic or neutral current transitions. The quark parton model does not adequately describe the kinematics in these cases. A more satisfactory description can be made using current-gluon fusion; see Chapter 10.

5.4 Neutrino Neutral Current Scattering

The scattering of neutrinos by weak neutral currents is a particularly clean way of probing Z couplings. The experimental signature of NC events is the production of hadrons *with no charged lepton*. The cross section formulas are given by the Z exchange components of §5.2 with an additional factor 2 from the difference in initial spin averaging. We therefore obtain, for any neutrino flavor,

$$\frac{d\hat{\sigma}}{dy}(\nu q \rightarrow \nu q) = \frac{G_F^2 \hat{s}}{\pi} [(g_L^q)^2 + (g_R^q)^2(1-y)^2] R^2(Q^2),$$

$$\frac{d\hat{\sigma}}{dy}(\bar{\nu} q \rightarrow \bar{\nu} q) = \frac{G_F^2 \hat{s}}{\pi} [(g_R^q)^2 + (g_L^q)^2(1-y)^2] R^2(Q^2),$$

where now $R(Q^2) = M_Z^2/(M_Z^2 + Q^2)$. Hence

$$\frac{d\sigma^{\text{NC}}(\nu p)}{dx dy} = \frac{G_F^2 s x}{\pi} \sum_q q(x) [(g_L^q)^2 + (g_R^q)^2(1-y)^2] R^2(Q^2),$$

$$\frac{d\sigma^{\text{NC}}(\bar{\nu} p)}{dx dy} = \frac{G_F^2 s x}{\pi} \sum_q q(x) [(g_R^q)^2 + (g_L^q)^2(1-y)^2] R^2(Q^2),$$

where the sum is understood to include antiquarks too, but the latter have g_L and g_R interchanged, $g_{L,R}(\bar{q}) = g_{R,L}(q)$.

Exercise. In valence approximation show that the ratio $R = \sigma^{\text{NC}}/\sigma^{\text{CC}}$ of neutral current to charge current cross sections in neutrino deep

inelastic scattering are

$$R^{\text{NC}}(\nu N) = \frac{1}{2} - x_w + \frac{20}{27} x_w^2,$$

$$R^{\text{NC}}(\bar{\nu} N) = \frac{1}{2} - x_w + \frac{20}{9} x_w^2,$$

where N is an isoscalar nuclear target with equal numbers of neutrons and protons. Make a sketch of $R^{\text{NC}}(\bar{\nu} N)$ versus $R^{\text{NC}}(\nu N)$, varying x_w between 0 and 1. Comparison of the measured R values is used in determining the Weinberg parameter x_w .

Neutrino NC scattering presents measurement problems. The initial neutrino direction is known but its energy cannot be estimated from the final particles because these include an undetected neutrino (unlike the CC case). The energy of the recoil hadron jet measures ν and its recoil angle gives one more parameter, but without additional information one cannot extract ν , Q^2 and E_ν for each event. In these circumstances one is limited to measuring spectrum-averaged cross sections (the neutrino spectrum and flux is known), usually integrated over Q^2 or over Q^2 and ν . However, with "narrow-band" neutrino beams (derived from $\pi, K \rightarrow \mu\nu$ decays of collimated monoenergetic pions and kaons) there is a kinematic correlation between the neutrino energy and its angle relative to the meson beam. Using this additional information one can determine all three parameters ν , Q^2 and E_ν approximately for each event and hence measure $d\sigma/dx dy$ as a function of x , y and s ; the price is lower statistics since narrow-band beams have lower intensity.

5.5 General Form of Structure Functions

The general form of the amplitude for lepton-nucleon scattering by the exchange of a gauge boson is

$$M(\ell p \rightarrow \ell' X) = \frac{g^2}{D} [\bar{u}(\ell') \gamma^\alpha O u(\ell)] \langle X | J_\alpha | p \rangle,$$

where g^2 denotes some coupling constants, D is the denominator of the gauge boson propagator, O is an appropriate (V, A) coupling

operator at the lepton vertex and J_α is the appropriate hadronic current. The $q_\alpha q_\beta/m^2$ term from the boson propagator has vanished because the leptons are assumed massless. When the matrix element is squared and summed over spins and final hadrons there appear lepton and hadron tensors $L^{\alpha\beta}$ and $W_{\alpha\beta}$

$$L^{\alpha\beta} = \frac{1}{n_\ell} \sum_{\text{spins}} [\bar{u}(\ell') \gamma^\alpha O u(\ell)] [\bar{u}(\ell') \gamma^\beta O u(\ell)]^*,$$

$$W_{\alpha\beta} = \frac{1}{2} \sum_{\text{spins}} \int \langle X | J_\alpha | p \rangle \langle X | J_\beta | p \rangle^* (2\pi)^{3-3n} \frac{d_n(PS)}{2E_p},$$

where $n_\ell = 2$ (electrons or muons) or 1 (neutrinos) is the number of initial lepton spin states to be averaged and $d_n(PS)$ is the n -body phase space of the final hadrons. In terms of these tensors the inclusive spin-averaged cross section is

$$E_{\ell'} \frac{d\sigma}{d^3 \ell'} = \frac{1}{16\pi^2 E_\ell} \frac{g^4}{|D|^2} L^{\alpha\beta} W_{\alpha\beta}.$$

The lepton tensor can be evaluated explicitly for any case of interest.

Exercise. Show that for electron scattering by γ exchange ($O = 1$), neutrino scattering by W exchange ($O = \frac{1-\gamma_5}{2}$) and antineutrino scattering by W exchange ($O = \frac{1+\gamma_5}{2}$) the lepton tensors are, respectively

$$L^{\alpha\beta} = 2(\ell^\alpha \ell'^\beta + \ell'^\alpha \ell^\beta - g^{\alpha\beta} \ell \cdot \ell'),$$

$$L^{\alpha\beta} = 2(\ell^\alpha \ell'^\beta + \ell'^\alpha \ell^\beta - g^{\alpha\beta} \ell \cdot \ell' + i\epsilon^{\alpha\beta\gamma\delta} \ell_\gamma \ell'_\delta),$$

$$L^{\alpha\beta} = 2(\ell^\alpha \ell'^\beta + \ell'^\alpha \ell^\beta - g^{\alpha\beta} \ell \cdot \ell' - i\epsilon^{\alpha\beta\gamma\delta} \ell_\gamma \ell'_\delta).$$

Show the second formula also describes $e \rightarrow \nu_e$ within a factor 1/2.

The form of the hadronic tensor is constrained by general arguments. It must be describable in terms of the four-momenta p and $q = \ell - \ell'$ alone; see Fig. 5.8. There are thus at most two independent scalar arguments $q^2 = -Q^2$ and $p \cdot q = M\nu$. The most general

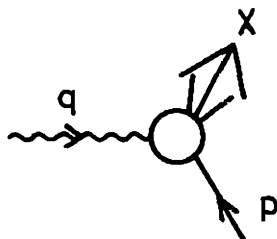


Fig. 5.8. The hadron tensor depends on p and q only.

tensor (α, β) form that can be constructed is a linear combination of $g_{\alpha\beta}$, $p_\alpha p_\beta$, $q_\alpha q_\beta$, $p_\alpha q_\beta$, $q_\alpha p_\beta$ and $\epsilon_{\alpha\beta\gamma\delta} p^\gamma q^\delta$. However, q_α or q_β contracted with $L^{\alpha\beta}$ gives zero (a consequence of massless leptons) so only three terms survive, giving the most general form

$$W_{\alpha\beta} = -g_{\alpha\beta}W_1 + \frac{p_\alpha p_\beta}{M^2} W_2 - \frac{i\epsilon_{\alpha\beta\gamma\delta} p^\gamma q^\delta}{2M^2} W_3,$$

where the structure functions W_1 , W_2 , W_3 depend on ν and Q^2 . The coefficients of W_1 and W_2 are even under parity (space reflection); the coefficient of W_3 is parity-odd and therefore forbidden for photon exchange, but it can appear for W or Z exchange through V, A interference.

Hence the most general forms of ep scattering by photon exchange or $\nu, \bar{\nu}$ scattering by W exchange are, in the proton rest frame,

$$\frac{d^2\sigma}{d\Omega' dE'}(ep) = \frac{4\alpha^2 E'^2}{Q^4} \left\{ 2W_1^e \sin^2 \frac{\theta}{2} + W_2^e \cos^2 \frac{\theta}{2} \right\},$$

$$\frac{d^2\sigma^{CC}}{d\Omega' dE'}(\nu p) = \frac{G_F^2 E'^2}{2\pi^2} \left\{ 2W_1^{\nu, \bar{\nu}} \sin^2 \frac{\theta}{2} + W_2^{\nu, \bar{\nu}} \cos^2 \frac{\theta}{2} \mp \frac{E+E'}{M} W_3^{\nu, \bar{\nu}} \sin^2 \frac{\theta}{2} \right\},$$

where the difference between ν and $\bar{\nu}$ cases arises from the sign of the ϵ term in $L^{\alpha\beta}$. Putting $2MW_1 = F_1$, $\nu W_2 = F_2$ and $\nu W_3 = F_3$,

this implies

$$\begin{aligned} \frac{d\sigma}{dx dy}(ep) &= \frac{2\pi\alpha^2 s}{Q^4} \{F_1^e xy^2 + 2F_2^e(1-y)\}, \\ \frac{d\sigma^{CC}}{dx dy}(\nu p) &= \frac{G_F^2 s}{4\pi} \{F_1^\nu xy^2 + 2F_2^\nu(1-y) - F_3^\nu xy(2-y)\}, \\ \frac{d\sigma^{CC}}{dx dy}(\bar{\nu} p) &= \frac{G_F^2 s}{4\pi} \{F_1^\nu xy^2 + 2F_2^\nu(1-y) + F_3^\nu xy(2-y)\}. \end{aligned}$$

The parton model results of previous sections at once imply that F_1 , F_2 and F_3 depend on x alone (Bjorken scaling) and that

$$F_2(x) = xF_1(x),$$

known as the *Callan-Gross relation*.

Exercise. Assuming the Callan-Gross relation, show that neutrino cross sections have the form

$$\frac{d\sigma^{CC}}{dx dy}(\nu p) = \frac{G_F^2 sx}{4\pi} [F_1 \mp F_3 + (F_1 \pm F_3)(1-y)^2].$$

Hence show that in the quark parton model

$$\begin{aligned} F_1(ep) &= \frac{4}{9}(u + \bar{u}) + \frac{1}{9}(d + \bar{d} + s + \bar{s}), \\ F_1^{CC}(\nu p) &= 2(\bar{u} + d \cos^2 \theta_C + s \sin^2 \theta_C), \\ F_1^{CC}(\bar{\nu} p) &= 2(u + \bar{d} \cos^2 \theta_C + \bar{s} \sin^2 \theta_C), \\ F_3^{CC}(\nu p) &= 2(\bar{u} - d \cos^2 \theta_C - s \sin^2 \theta_C), \\ F_3^{CC}(\bar{\nu} p) &= 2(-u + \bar{d} \cos^2 \theta_C + \bar{s} \sin^2 \theta_C), \end{aligned}$$

ignoring heavy quark production, where $|V_{ud}| = \cos \theta_C$ and $|V_{us}| = \sin \theta_C$. What changes occur when we go far above charm production threshold?

Exercise. Either by approximating $\theta_C \simeq 0$ or by including charm production in the limit $x' \simeq x$, show that the parton model sum rules of §5.2 give

$$\int \left[F_1^{CC}(\bar{\nu}p) - F_1^{CC}(\nu p) \right] dx = 2.$$

This is the Adler sum rule (first proved from current algebra).

Exercise. Similarly show that the parton model predicts

$$\int \left[F_3^{CC}(\bar{\nu}p) + F_3^{CC}(\nu p) \right] dx = -6,$$

which is the Gross-Llewellyn Smith sum rule.

Exercise. Show that the parton model in the limit $\theta_C \simeq 0$ gives charge-symmetry relations for F_i ($i = 1, 2, 3$):

$$F_i^{CC}(\nu p) = F_i^{CC}(\bar{\nu}n), \quad F_i^{CC}(\nu n) = F_i^{CC}(\bar{\nu}p).$$

Exercise. Show that the charged-current structure functions of $ep \rightarrow \nu_e X$ scattering are identical to those of $\bar{\nu}p \rightarrow \bar{\mu} X$ scattering and that

$$\frac{d\sigma^{CC}}{dx dy}(ep) = \frac{G_F^2 s}{8\pi} \left\{ F_1^\nu xy^2 + 2F_2^\nu(1-y) - F_3^\nu xy(2-y) \right\}.$$

Exercise. Show that the cross section formulas of $ep \rightarrow \nu_e X$ scattering are like those of $\nu_e p \rightarrow eX$ scattering, but with the roles of $T_3 = \pm \frac{1}{2}$ quarks interchanged plus an extra factor $\frac{1}{2}$.

5.6 Parameterizations of Quark Distributions

The quark distributions $q(x)$ are empirically determined from data on electron and neutrino deep inelastic scattering at low Q^2 . The parameterizations are required to satisfy the normalizations $\int_0^1 u_v(x) dx = 2$ and $\int_0^1 d_v(x) dx = 1$. In addition the parameterizations are chosen to reproduce Regge behavior as $x \rightarrow 0$ and to correspond to elastic scattering behavior as $x \rightarrow 1$. Two representative parameterizations in common use are (A) Duke and Owens (DO), (B) Eichten *et al.* (EHLQ). The $q(x)$ values obtained with different parameterizations are largely similar, with differences mainly attributable to minor inconsistencies between electron and neutrino data in the framework of the quark parton model. Below we reproduce these two parameterizations, including the gluon distribution whose determination is discussed later.

$$\begin{aligned} \text{Parameterization A: } x(u_v + d_v) &= 1.874x^{0.419}(1-x)^{3.46}(1+4.4x) \\ x d_v &= 2.775x^{0.763}(1-x)^4 \\ x\bar{u} = x\bar{d} = x\bar{s} &= 0.2108(1-x)^{8.05} \\ xg(x) &= 1.56(1-x)^6(1+9x) \end{aligned}$$

$$\begin{aligned} \text{Parameterization B: } x u_v &= 1.78x^{0.5}(1-x^{1.51})^{3.5} \\ x d_v &= 0.67x^{0.4}(1-x^{1.51})^{4.5} \\ x\bar{u} = x\bar{d} &= 0.182(1-x)^{8.54} \\ x\bar{s} &= 0.081(1-x)^{8.54} \\ xg(x) &= (2.62 + 9.17x)(1-x)^{5.90} \end{aligned}$$

Data on charm production by neutrinos suggest that $\bar{s}/\bar{u} \sim \frac{1}{2}$; although this constraint is not taken into account in parameterization A, it should not be critical in most applications. Figure 5.9 illustrates some of the minor differences in data fitting, showing (a) the ratio of electromagnetic structure functions $F_2(en)/F_2(ep)$ and (b) the valence ratio $d_v(x)/u_v(x)$ extracted from neutrino data. Parameterization A fits (a) better than (b); with parameterization B it is the other way round.

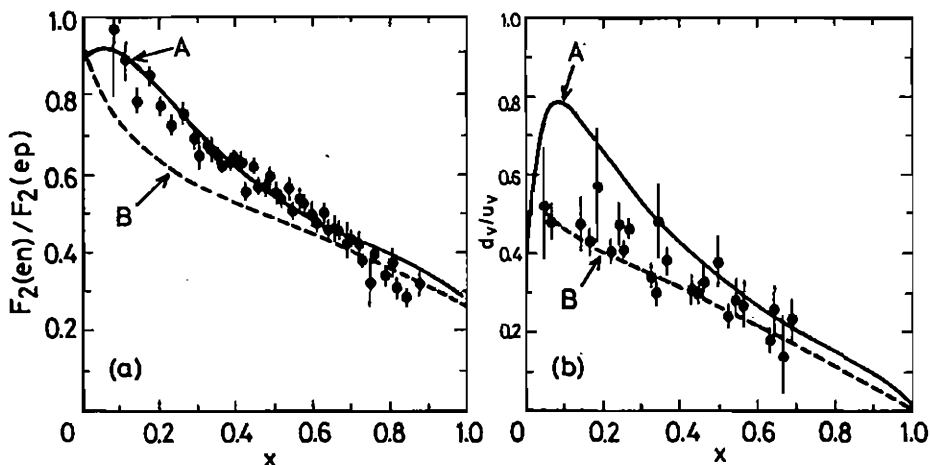


Fig. 5.9. Illustration of some minor differences in data fitting (a) $F_2(en)/F_2(ep)$ data [Phys. Rev. D20, 1471 (1979)], (b) $d_v(x)/u_v(x)$ data [Proc. Neutrino Conference, Nordkirchen, p. 422 (1984)].

The valence and sea distributions of parameterization B are plotted in Fig. 5.10. Note that the peak values of xu_v and xd_v occur near $x = 0.15-0.20$. As $x \rightarrow 1$, d_v/u_v vanishes like $1 - x$.

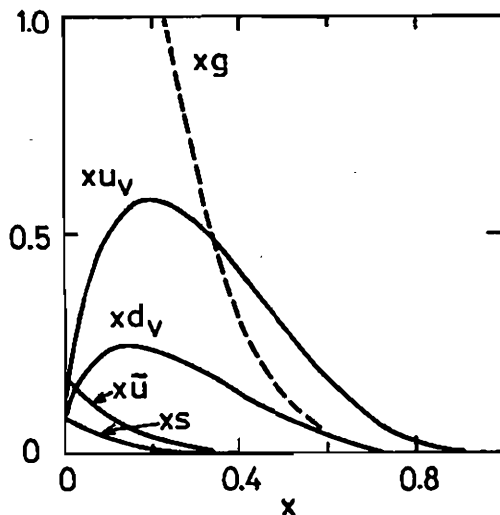


Fig. 5.10. Quark and gluon distributions from parameterization B.

The total fraction of the proton momentum carried by the quarks and antiquarks, as found from the fits to the deep inelastic scattering data, is

$$\int_0^1 dx x [u(x) + \bar{u}(x) + d(x) + \bar{d}(x) + s(x) + \bar{s}(x)] = 0.5 .$$

This is the quark contribution to the *momentum sum rule*; the observation that it does not equal 1 was one of the first indications that gluons have real dynamical meaning. Since the remaining 50% of the proton momentum must be carried by the neutral constituents, the gluons, this is the normalization requirement imposed on the gluon distribution

5.7 Parton Model for Hadron-Hadron Collisions

Hadronic collisions which involve a hard scattering (*i.e.* high Q^2) subprocess can also be described by the parton model. An incoming hadron of momentum P is represented by partons i carrying longitudinal momentum fractions x_i ($0 \leq x_i \leq 1$). Transverse momenta of the partons are neglected. The parton scattering representation of a hadron-hadron collision is illustrated in Fig. 5.11. Here A and B are the incident hadrons. The various scattered and spectator partons are assumed to fragment to final state hadrons with probability 1.

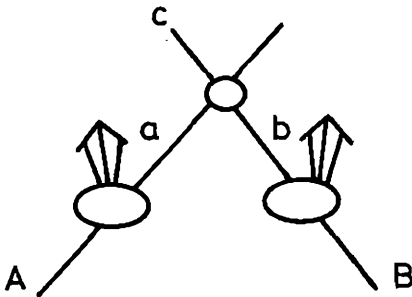


Fig. 5.11. Hadron-hadron scattering via a hard parton subprocess.

We shall denote the longitudinal momentum fraction of parton a in hadron A by x_a and the parton density of a in A by $f_{a/A}(x_a)$. The cross section for producing a quark or lepton c in the inclusive reaction

$$A + B \rightarrow c + \text{anything}$$

is obtained by multiplying the subprocess cross section $\hat{\sigma}$ for

$$a + b \rightarrow c + \text{anything}$$

by $dx_a f_{a/A}(x_a)$ and $dx_b f_{b/B}(x_b)$, summing over parton and antiparton types a, b and integrating over x_a and x_b ; also an average must be made over the colors of a and b . The resulting relation is

$$\sigma(AB \rightarrow cX) = \sum_{a,b} C_{ab} \int dx_a dx_b \cdot [f_{a/A}(x_a) f_{b/B}(x_b) + (A \leftrightarrow B \text{ if } a \neq b)] \hat{\sigma}(ab \rightarrow cX).$$

In this formula $\hat{\sigma}$ is *summed over* initial and final colors; the initial color-averaging factor C_{ab} appears separately. The color-average factors for quarks and gluons are

$$C_{qq} = C_{q\bar{q}} = \frac{1}{9}, \quad C_{qg} = \frac{1}{24}, \quad C_{gg} = \frac{1}{64}.$$

In a Lorentz frame in which masses can be neglected compared with three-momenta, the four-momenta relations

$$a = x_a A \quad \text{and} \quad b = x_b B,$$

lead to

$$\hat{s} = x_a x_b s = \tau s,$$

where $\sqrt{\hat{s}}$ is the invariant mass of the ab system, \sqrt{s} is the invariant mass of the AB system and we have introduced a convenient

variable τ

$$\tau = x_a x_b .$$

Changing to x_a and τ as independent variables the cross section expression becomes

$$\sigma = \sum_{a,b} C_{ab} \int_0^1 d\tau \int_{\tau}^1 \frac{dx_a}{x_a} [f_{a/A}(x_a) f_{b/B}(\tau/x_a) + (A \leftrightarrow B \text{ if } a \neq b)] \hat{\sigma}(\hat{s} = \tau s).$$

Thus we can write

$$\frac{d\sigma}{d\tau} = \sum_{a,b} \frac{d\mathcal{L}_{ab}}{d\tau} \hat{\sigma}(\hat{s} = \tau s)$$

with

$$\frac{d\mathcal{L}_{ab}(\tau)}{d\tau} = C_{ab} \int_{\tau}^1 \frac{dx_a}{x_a} [f_{a/A}(x_a) f_{b/B}(\tau/x_a) + (A \leftrightarrow B \text{ if } a \neq b)] .$$

The quantity $d\mathcal{L}_{ab}/d\tau$ is called the *parton luminosity* since multiplying the parton cross section $\hat{\sigma}$ by $d\mathcal{L}/d\tau$ gives the particle cross section $d\sigma/d\tau$ in hadron collisions.

In hard scattering processes at high energy, where the only dimensional scale is \hat{s} , the subprocess cross section has the form

$$\hat{\sigma}(\hat{s}) = c/\hat{s} = c/(\tau s) ,$$

where c is a dimensionless constant. Then, for scaling parton distributions (*i.e.* the f depend only on x), the quantity $s d\sigma/d\tau$ scales with τ , *i.e.* it depends on τ alone:

$$s \frac{d\sigma}{d\tau} = G(\tau)$$

with the form of the scaling function $G(\tau)$ depending on the parton distributions $f(x)$.

For $2 \rightarrow 2$ subprocesses such as $\bar{q}q \rightarrow \mu^+\mu^-$ or $\bar{q}q \rightarrow \bar{q}q$ in which both final-state particles from the hard scattering subprocess are measured (as a pair of leptons or a pair of jets), the longitudinal momentum p of the ab system is an observable. In the AB c.m. frame,

$$p = a_3 + b_3 = (x_a - x_b)A_3 \simeq (x_a - x_b)\sqrt{s}/2 \equiv x\sqrt{s}/2,$$

where

$$x = x_a - x_b$$

is the longitudinal momentum fraction of ab . The momentum fractions x_a, x_b are related to the variables x, τ by

$$x_{a,b} = \frac{1}{2} [(x^2 + 4\tau)^{\frac{1}{2}} \pm x].$$

The Jacobian transformation from x_a, x_b to x, τ gives

$$\frac{d\sigma}{dx d\tau} = \frac{1}{\sqrt{x^2 + 4\tau}} \frac{d\sigma'}{dx_a dx_b}.$$

An alternative to the variable x is the *rapidity* y of the ab system in the AB c.m. frame, defined by

$$y = \frac{1}{2} \ln \left(\frac{a_0 + b_0 + a_3 + b_3}{a_0 + b_0 - a_3 - b_3} \right) = \frac{1}{2} \ln \frac{x_a}{x_b}.$$

In obtaining the latter form we used $a_0 = a_3$ and $b_0 = -b_3$. The transformation from x_a, x_b to y, τ is

$$x_{a,b} = \sqrt{\tau} e^{\pm y}.$$

The Jacobian transformation from x_a, x_b to y, τ variables is

$$\frac{d\sigma}{dy d\tau} = \frac{d\sigma}{dx_a dx_b} = \sum_{a,b} C_{ab} [f_{a/A}(x_a) f_{b/B}(x_b) + (A \leftrightarrow B \text{ if } a \neq b)] \hat{\sigma}.$$

At $y = 0, x_a = x_b = \sqrt{\tau}$ and

$$\left. \frac{d\sigma}{dy d\tau} \right|_{y=0} = \sum_{a,b} C_{ab} [f_{a/A}(\sqrt{\tau}) f_{b/B}(\sqrt{\tau}) + (A \leftrightarrow B \text{ if } a \neq b)] \hat{\sigma}.$$

This cross section form will be the basis for our discussion of the Drell-Yan process in the next section.

Exercise. For scattering regions where x_a or x_b (or both) are small, show that pp and $p\bar{p}$ collisions are essentially equivalent.

Finally a word of caution. Notice that the gluon and quark-antiquark sea distributions become very large at very small x and that this may invalidate the formulas above at sufficiently high energy. Up to the present, the relevant x -values have been limited typically to $x > 10^{-3}$ by the available collider energies and the requirement that the parton subprocess energy is high enough (many GeV). With future supercolliders however, very much smaller x values will be probed and much larger hard-scattering cross sections will be predicted; see for example the case of minijets in §9.3. When these cross sections approach the geometrical size of the proton, our naive prescription of simply adding parton cross sections incoherently must break down; interactions between partons in the same hadron, multiple scattering and shadowing effects must all be introduced. This is an important problem, currently being addressed by many theorists.

5.8 Drell-Yan Lepton Pair Production

In hadronic collisions, electrons or muons are pair-produced when quarks and antiquarks annihilate to produce a virtual photon, or a Z^0 , which decays to a lepton pair. This inclusive hadronic reaction

$$A + B \rightarrow e^+e^- + \text{anything (or } \mu^+\mu^- + \text{anything)}$$

is known as the *Drell-Yan process*. Measurements have been made in pp , $\pi^\pm p$, $K^\pm p$ and $p\bar{p}$ collisions. The quark-antiquark subprocess is illustrated in Fig. 5.12. The parton distributions which enter the calculations of p or \bar{p} cross sections are

$$\text{proton} \quad f_{u/p}(x) = u(x) \quad f_{\bar{u}/p}(x) = \bar{u}(x)$$

$$\text{antiproton} \quad f_{\bar{u}/\bar{p}}(x) = u(x) \quad f_{u/\bar{p}}(x) = \bar{u}(x)$$

$$\text{nucleus} \quad f_{u/A}(x) = Zu(x) + Nd(x) \quad f_{\bar{u}/A}(x) = Z\bar{u}(x) + N\bar{d}(x)$$

and similarly for d , \bar{d} , s , \bar{s} distributions.

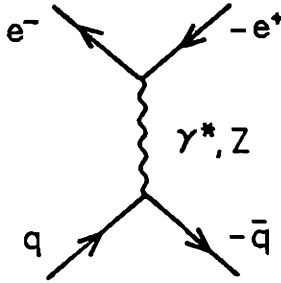


Fig. 5.12. Drell-Yan subprocess.

For $\hat{s} \ll M_Z^2$ the color-summed subprocess cross section is

$$\hat{\sigma}(\bar{q}q' \rightarrow e^+e^-) = 3\delta_{qq'} e_q^2 \left(\frac{4\pi\alpha^2}{3\hat{s}} \right).$$

The factor of 3 is from color (each color of incident quarks can annihilate). Thus the differential distribution of lepton pairs is

$$\frac{d\sigma}{dy d\tau} = \frac{1}{3} \left(\frac{4\pi\alpha^2}{3s} \right) \sum_{q=u,d,s} x_q^{-1} x_{\bar{q}}^{-1} [e_q^2 f_{q/A}(x_q) f_{\bar{q}/B}(x_{\bar{q}}) + (A \leftrightarrow B)].$$

For proton-proton scattering at $y = 0$, where $x_q = x_{\bar{q}} = \sqrt{\tau}$, the quark distribution factor is

$$\frac{8}{9} u(\sqrt{\tau}) \bar{u}(\sqrt{\tau}) + \frac{2}{9} d(\sqrt{\tau}) \bar{d}(\sqrt{\tau}) + \frac{2}{9} s(\sqrt{\tau}) \bar{s}(\sqrt{\tau}).$$

The τ distribution depends critically on the antiquark distribution and the cross section falls off at high τ like the antiquark sea. Approximate scaling behavior of $s d\sigma/d\tau dy$ at $y = 0$ is observed in pp collisions at \sqrt{s} values between 19 and 63 GeV. Moreover, the observed cross section agrees roughly with the Drell-Yan prediction based on quark distributions from deep inelastic scattering.

For antiproton-proton collisions the quark distribution factor in the differential cross section at $y = 0$ is

$$\begin{aligned} \frac{4}{9} [u(\sqrt{\tau}) u(\sqrt{\tau}) + \bar{u}(\sqrt{\tau}) \bar{u}(\sqrt{\tau})] + \frac{1}{9} [d(\sqrt{\tau}) d(\sqrt{\tau}) + \bar{d}(\sqrt{\tau}) \bar{d}(\sqrt{\tau})] \\ + \frac{1}{9} [s(\sqrt{\tau}) s(\sqrt{\tau}) + \bar{s}(\sqrt{\tau}) \bar{s}(\sqrt{\tau})]. \end{aligned}$$

Here the valence components dominate for $\sqrt{\tau} > 0.1$ and the cross section at high $x_q = \sqrt{\tau}$ is less suppressed than in the pp case. This was part of the motivation for building $p\bar{p}$ colliders to produce W and Z bosons.

Exercise. Show that the parton model with scaling distributions predicts that $m^3 d\sigma/dm$ and $m^3 d\sigma/dm dy (y=0)$ both depend on τ alone for given incident hadrons, where m is the dimuon mass ($m^2 = \tau s$).

Figures 5.13 and 5.14 illustrate this scaling effect with pp and πp data. Finally we note that πp and Kp Drell-Yan data enable one to determine approximately the quark distributions in π and K .

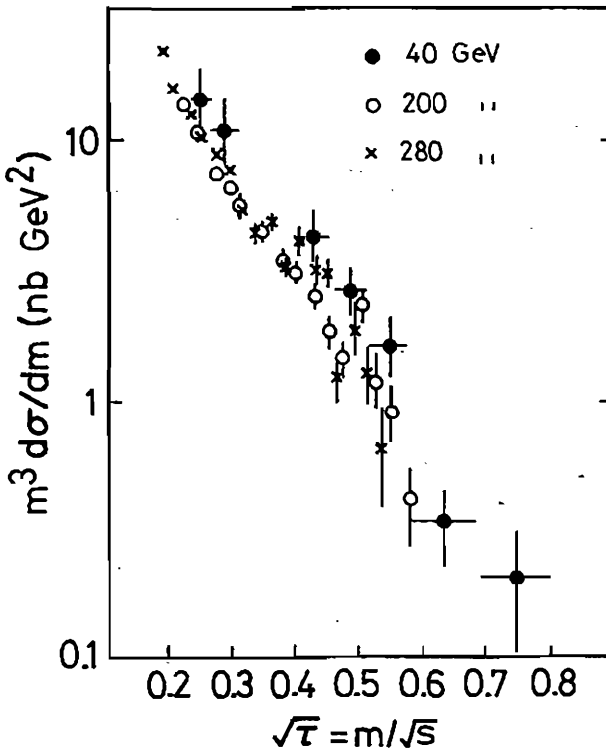


Fig. 5.13. Approximate scaling of $m^3 d\sigma/dm$ for Drell-Yan pair production in $\pi^- p$ scattering with lab momentum from 40 to 280 GeV [Phys. Lett. 96B, 417 (1980)].

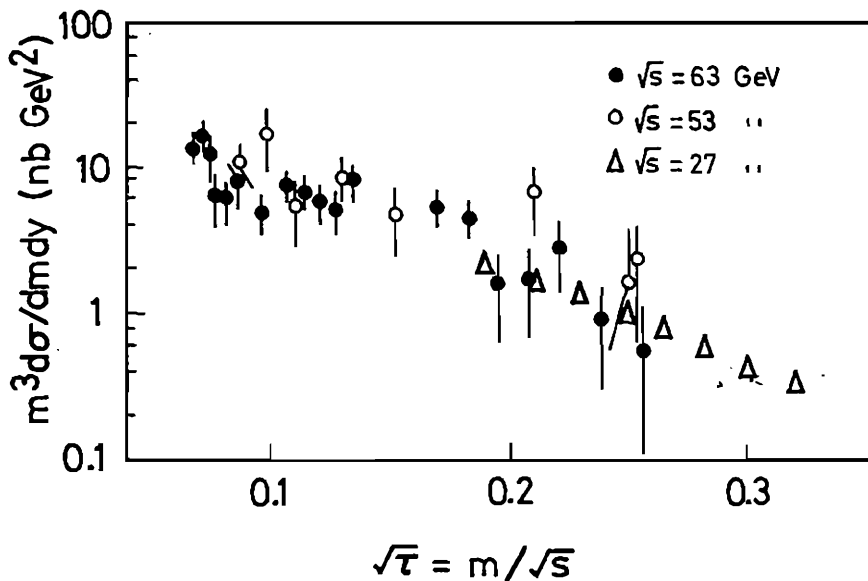


Fig. 5.14. Approximate scaling of $m^3 d\sigma/dm dy(y = 0)$ for Drell-Yan pair production in pp scattering [Phys. Lett. **91B**, 475 (1980)].

5.9 Gluon Distribution

Since the gluon has no electromagnetic or weak interactions, its distribution does not enter the lowest-order electroweak inelastic or Drell-Yan cross sections. Its presence as a parton constituent of the nucleon is signalled indirectly through the momentum sum rule (§5.6). However, there is a process,

$$\gamma N \rightarrow \psi + \text{anything},$$

where the gluon distribution enters in lowest order and can be directly determined from experiment. The lowest-order parton subprocesses $\gamma g \rightarrow c\bar{c}$ are illustrated in Fig. 5.15.

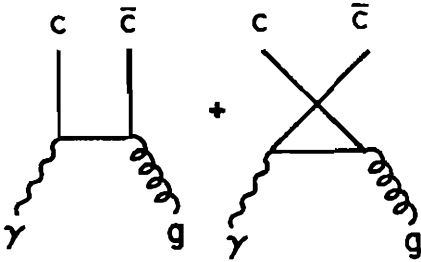


Fig. 5.15. Photon-gluon fusion production of charmed quark pairs.

These diagrams describe both bound-state and free charmed hadron pair production. The cross section for producing $c\bar{c}$ quark pairs in the invariant mass range $2m_c < m(c\bar{c}) < 2m_D$ (where m_c and m_D are the charmed quark and lightest charmed meson masses) is plausibly identified with the production of bound $c\bar{c}$ states, and a fixed fraction F is attributed to ψ production (including ψ from cascade decays of other $c\bar{c}$ bound states). The process $\gamma g \rightarrow c\bar{c}$ actually produces a color-octet $c\bar{c}$ system; the hadronization $c\bar{c} \rightarrow \psi$ is supposed to include the radiation of a soft gluon to give colorless ψ . We then have

$$\sigma(\gamma N \rightarrow \psi X) = \frac{F}{8} \int_{x_1}^{x_2} dx g(x) \hat{\sigma}(\gamma g \rightarrow c\bar{c}),$$

where $x = \hat{s}/s = m^2/s$ and the factor $\frac{1}{8}$ is the color average for initial gluons. The limits are $x_1 = 4m_c^2/s$ and $x_2 = 4m_D^2/s$ with $s \simeq 2ME_\gamma$ at high photon energy. Since the range of x integration above is small, we can approximately replace $g(x)$ by its value at the midpoint $\bar{x} = 2(m_c^2 + m_D^2)/s$, obtaining

$$\begin{aligned} \sigma(\gamma N \rightarrow \psi X) &\approx g(\bar{x}) \frac{F}{8} \int_{x_1}^{x_2} dx \hat{\sigma}(\gamma g \rightarrow c\bar{c}) \\ &= \frac{\bar{x}g(\bar{x})}{2(m_c^2 + m_D^2)} \frac{F}{8} \int_{4m_c^2}^{4m_D^2} dm^2 \hat{\sigma}(\gamma g \rightarrow c\bar{c}) = \bar{x}g(\bar{x}) \cdot (\text{constant}). \end{aligned}$$

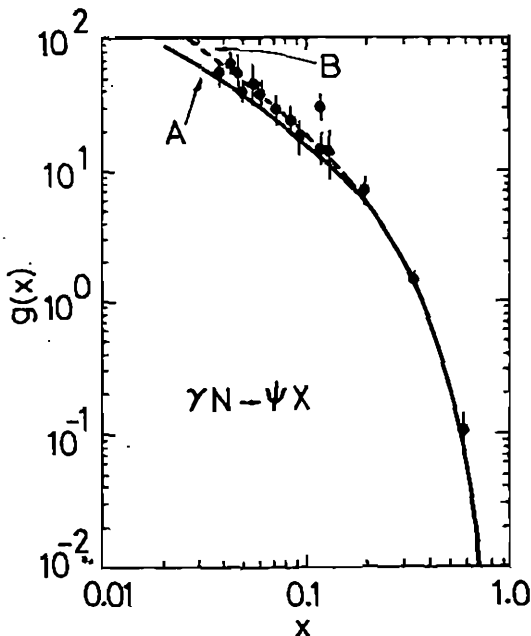


Fig. 5.16. Determination of the gluon distribution $g(x)$ from data on $\gamma N \rightarrow \psi X$ cross section data [Phys. Lett. **91B**, 253 (1980)]. Parameterizations A and B are shown for comparison.

Hence we can read the x dependence of $xg(x)$ directly from the s dependence of $\sigma(\gamma N \rightarrow \psi X)$, as shown in Fig. 5.16. (The data shown are actually for “elastic” ψ production where $E_{\text{had}} < 5$ GeV, but the total cross section behavior is similar.) The curves represent the gluon parameterizations A and B discussed in §5.6.

There are analogous mechanisms in the hadroproduction of ψ . Take for example $pp \rightarrow \psi X$: the contributing parton subprocesses are $q\bar{q} \rightarrow c\bar{c}$ and $gg \rightarrow c\bar{c}$ as illustrated in Fig. 5.17. The $pp \rightarrow \psi X$ cross section at ψ rapidity $y = 0$ has the form (see §5.7)

$$\frac{d\sigma}{dy}(y=0) = F \int_{\tau_1}^{\tau_2} d\tau \left\{ \frac{2}{9} \sum q(\sqrt{\tau}) \bar{q}(\sqrt{\tau}) \hat{\sigma}(q\bar{q} \rightarrow c\bar{c}; \tau s) + \frac{1}{64} [g(\sqrt{\tau})]^2 \hat{\sigma}(gg \rightarrow c\bar{c}; \tau s) \right\},$$

where $\tau = \hat{s}/s$, $\tau_1 = 4m_c^2/s$, $\tau_2 = 4m_D^2/s$, $y = \frac{1}{2} \ln[(E_\psi + p_{z\psi})/(E_\psi - p_{z\psi})]$, and the factors $\frac{1}{9}$ and $\frac{1}{64}$ are for color averaging. Replacing the

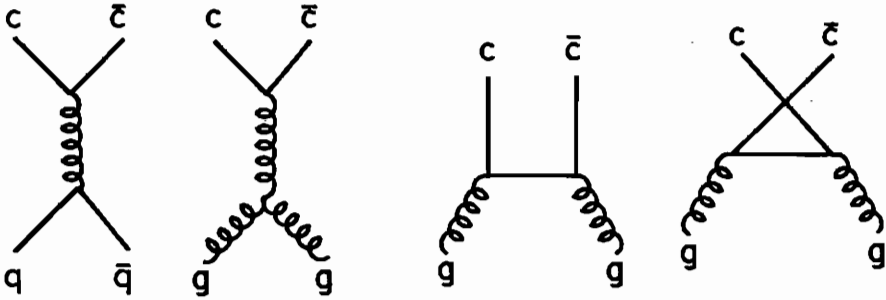


Fig. 5.17. Parton subprocesses for $c\bar{c}$ production in hadronic collisions.

parton densities by their values at $\bar{x} = \bar{r}^{1/2} = [(2m_c^2 + 2m_D^2)/s]^{1/2}$, which is the narrow-window approximation, we obtain

$$\frac{d\sigma}{dy}(y=0) = F \left\{ \sum \bar{x}^2 q(\bar{x}) \bar{q}(\bar{x}) \int dm^2 \frac{2}{9} \hat{\sigma}(q\bar{q}) + [\bar{x}g(\bar{x})]^2 \int dm^2 \frac{1}{64} \hat{\sigma}(gg) \right\} / (2m_c^2 + 2m_D^2).$$

In practice the $q\bar{q}$ term is found to be much smaller than the gg term, assuming $g(x)$ is roughly given by the preceding parameterization. Neglecting therefore the $q\bar{q}$ term, we obtain $\bar{x}g(\bar{x})$ to within an overall normalization constant:

$$[\bar{x}g(\bar{x})]^2 = \frac{d\sigma}{dy}(pp \rightarrow \psi X; y=0) \cdot (\text{constant}).$$

The data again give a gluon distribution that is well described by the same parameterizations, as shown in Fig. 5.18.

Analogous results can be obtained for asymmetrical situations ($y \neq 0$) and for other pairs of incident hadrons. In particular, analysis of $\pi N \rightarrow \psi X$ and $KN \rightarrow \psi X$ data can be used to extract the gluon distributions in π and K .

It turns out that different production channels ($\gamma N \rightarrow \psi X$, $\pi p \rightarrow \psi X$, etc.) are best fitted with different empirical fractions F . This

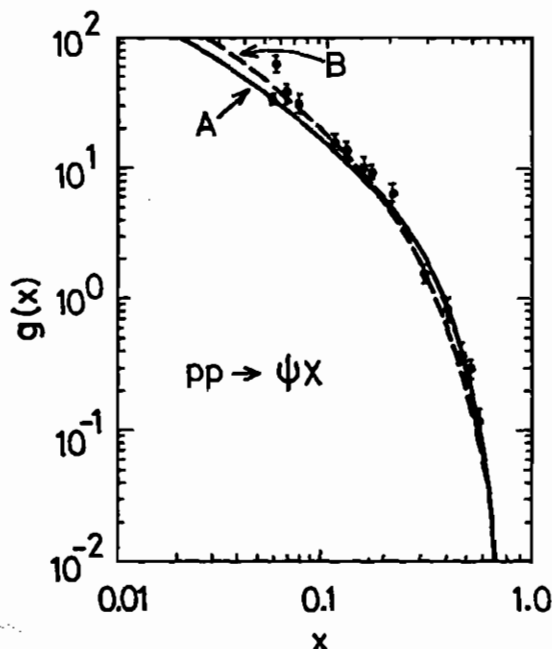


Fig. 5.18. Determination of the gluon distribution from $pp \rightarrow \psi X$ cross section data [Phys. Lett. 91B, 253 (1980)].

can be accommodated by remarking that not all $c\bar{c}$ pairs produced below threshold (with $m(c\bar{c}) < 2m_D$) necessarily appear as bound $c\bar{c}$ states; quarks or gluons produced at other vertices can provide energy to form charmed hadrons. Also the relative production of ψ and χ states can depend on the process. This depends on details of fragmentation which change from process to process; it affects the fraction F of $c\bar{c}$ pairs available to form ψ .

The determinations of the scaling form of the gluon distribution in this section do not take into account the variation with Q^2 expected in QCD. This will be addressed in Chapter 7.

Chapter 6

Fragmentation

6.1 Fragmentation Functions

Colored quarks and gluons can be regarded as free during a hard collision, but subsequently color forces will organize them into colorless hadrons; this is called *fragmentation* or *hadronization*. Typically it involves the creation of additional quark-antiquark pairs by the color force field. Figure 6.1 shows an example for deep inelastic ep scattering, where the struck quark and the spectator diquark combine with many quark-antiquark pairs to form a multi-hadron final state.

Fragmentation is governed by soft non-perturbative processes that cannot be calculated from scratch. (We explicitly exclude hard gluon or $q\bar{q}$ radiation, which we regard as part of the initial hard-scattering

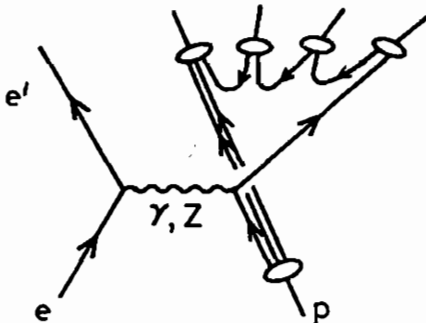


Fig. 6.1. Example of fragmentation in ep deep inelastic scattering.

process.) We have to describe it semi-empirically, guided by general principles and physical ideas, just as we do for parton distributions in the initial hadrons. A complete description of the final state requires a complete description of fragmentation, but sometimes an incomplete description is enough. As an extreme example, for inclusive cross sections such as lepton scattering $\ell p \rightarrow \ell' X$ or Drell-Yan pair production $p\bar{p} \rightarrow \ell\bar{\ell} X$ where all hadronic final states X are summed, the parton model allows us to ignore the fragmentation completely; so long as it takes place over a long timescale, with probability 1 and without interfering with the hard scattering, it adds nothing that we need to know here. Another example is semi-inclusive cross sections, where one measures the spectrum of one particular type of hadron h produced say in $ep \rightarrow ehX$ or $e^+e^- \rightarrow hX$, but sums over all other hadrons X . This requires only a partial description of the hadronization process, in the form of single-particle fragmentation functions—the subject of this section. More complete descriptions of hadronization require explicit jet models, addressed in later sections.

Since the total color of the final hadrons is neutral, the color charge of a scattered quark is exactly balanced by the color charge of the recoiling system (an antiquark or diquark or whatever). We imagine the quark and recoiling system as well separated but joined by color flux lines; these flux lines stretch and break, materializing $q\bar{q}$ pairs as sketched in Fig. 6.2, and the various colored components regroup into colorless hadrons. In the c.m. frame (or any other frame where the initial quark and recoil systems travel fast in opposite directions) these hadrons form jets of particles—one quark jet and one recoil jet, at least for simple recoil systems. Provided that the regrouping into hadrons takes place *locally*, this picture suggests that the properties of the quark jet depend only on the quark (its color charge, its momentum, its quantum numbers). Thus each fast parton fragments independently, as a first approximation.



Fig. 6.2. Color flux lines break to materialize $q\bar{q}$ pairs.

Consider a fast parton k with energy E_k , producing a hadron h with energy fraction z ,

$$z = E_h/E_k, \quad 0 \lesssim z \lesssim 1,$$

among its fragmentation products. The probability of finding h in the range z to $z + dz$ is defined to be $D_k^h(z)dz$, where D_k^h is called the k -to- h fragmentation function. If the parton energy is very large compared to participating masses and transverse momenta (and if we assume there is no other scale in the physics), z is plausibly the only significant variable. If D indeed depends on z alone, it is said to obey *Feynman scaling*. Some physicists use longitudinal momentum p_L (along the quark direction of motion) or the light-cone variable $(E + p_L)$ instead of E in defining z ,

$$z = p_{hL}/p_{kL} \quad \text{or} \quad z = (E_h + p_{hL})/(E_k + p_{kL}).$$

The light-cone choice has the merit of being invariant under longitudinal boosts, but all definitions coincide for relativistic hadrons h traveling close to the direction of the parent parton k .

The cross section for inclusive h production is related through D_k^h to the cross sections for producing possible parent partons k ;

$$\frac{d\sigma}{dE_h}(AB \rightarrow hX) = \sum_k \int \frac{d\sigma}{dE_k}(AB \rightarrow kX) D_k^h(E_h/E_k) \frac{dE_k}{E_k},$$

since $dz = E_k^{-1}dE_h$. For example, in ep charged-current scattering the dominant subprocess $eu \rightarrow \nu_e d$ gives a recoiling d quark jet;

hence the production and z -distribution of hadrons h in the recoil jet is described by the simple factorized formula

$$\frac{d\sigma}{dx dy dz} (\bar{e}p \rightarrow \nu_e h X) = \frac{d\sigma}{dx dy} (ep \rightarrow \nu_e X) D_d^h(z)$$

for x values where the $q\bar{q}$ sea is negligible and ignoring small $u \rightarrow s$ contributions. The recoil quark energy is the total energy of the recoil jet (distinguished by direction from the "beam jet" made by the spectator diquark ud), so $D_d^h(z)$ can be extracted experimentally for any given incident energy and x, y bin. The independent fragmentation hypothesis says that all these measurements of $D_d^h(z)$ —and any measurements in other reactions—should agree. Figure 6.3 compares results for the fragmentation function $D_u^{\pi^+}$ extracted from deep inelastic muon scattering with the exponential form $D(z) \sim \exp(-8z)$ that approximates results for $e^+e^- \rightarrow \pi X$ with $z > 0.2$. Results for $D_d^{\pi^-}$ obtained from $\bar{\nu}p$ scattering are also shown.

Exercise. What kind of experiments are needed to measure the fragmentation functions of u, s, c, b quarks? What about gluons?

Integrating $D_k^h(z)$ over a range z_1 to z_2 gives the probability of finding a hadron h here; *i.e.* it gives the average number of hadrons h in this range. Hence the integral of $D_k^h(z)$ over the full physical range of z is the average number of hadrons h (the *mean multiplicity* of h) in the complete jet arising from parton k ,

$$\langle n_k^h \rangle = \int_{z_{\min}}^1 dz D_k^h(z),$$

where the lower limit is the kinematical bound for given parton energy E_k

$$z_{\min} = m_h/E_k.$$

Hence the behavior of the hadron multiplicity at high energy is controlled by the behavior of $D(z)$ at small z (if we continue to believe

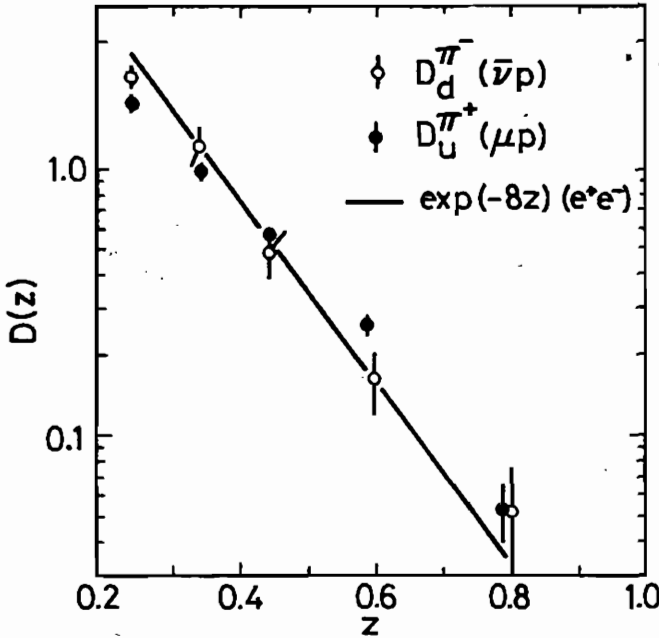


Fig. 6.3. Comparison of fragmentation function results from different sources. Solid points denote $D_U^{\pi^+}(z)$ extracted from muon scattering [Phys. Lett. **160B**, 417 (1985)]. The solid line represents an exponential approximation to the corresponding results from a large number of e^+e^- experiments. Open circles denote $D_d^{\pi^-}(z)$ obtained from $\bar{\nu}p$ scattering [Phys. Lett. **91B**, 470 (1980)].

the independent fragmentation picture in this limit). $D(z)$ is often parameterized in the form

$$D(z) = f(1-z)^n/z.$$

Here f is a constant, the factor $(1-z)^n$ parameterizes the behavior at large z and the factor z^{-1} is chosen to give a logarithmic increase in mean multiplicity per parton k at high energy as observed,

$$\langle n_k^h \rangle \simeq f \ln(E_k/m_h) \text{ as } E_k \rightarrow \infty.$$

Exercise. Show that energy conservation among the totality of fragmentation products h of a given parton k leads to the constraint

$$\sum_h \int_0^1 z D_k^h(z) dz = 1.$$

Strictly speaking, the lower limit of integration should be $z_{\min}(h)$, but since the integral converges here we can replace it approximately by 0.

Exercise. Show that charge conjugation and isospin symmetry lead to many relations, including the following

$$\begin{aligned} D_d^{\pi^-} &= D_u^{\pi^+} = D_{\bar{u}}^{\pi^-} = D_{\bar{d}}^{\pi^+}, \\ D_c^{D^+} &= D_c^{D^0} = D_{\bar{c}}^{D^0} = D_{\bar{c}}^{D^-}, \\ D_g^{\pi^+} &= D_g^{\pi^-} = D_g^{\pi^0}, \end{aligned}$$

and notice a test of the top line in Fig. 6.3.

There is a close analogy between fragmentation functions $D_k^h(z)$ and parton distribution functions $f_{k/h}$ shown pictorially in Fig. 6.4. One is the probability density for finding hadron h among the fragmentation products of parton k ; the other is the probability density for finding parton k within hadron h . The mean multiplicity integral of D above corresponds to the parton multiplicity in a hadron. The energy conservation relation corresponds to the momentum sum-rule for partons in a hadron. The charge-conjugation and isospin relations correspond to similar relations between parton distributions. When we come to QCD radiative corrections, the analogy still persists.

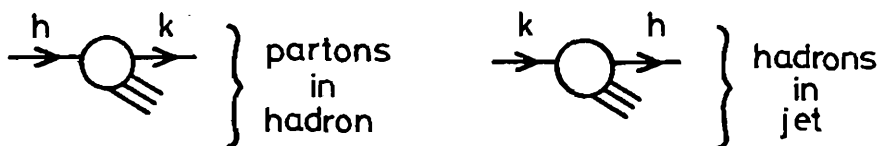


Fig. 6.4. Analogy between parton components of a hadron and hadron components of a (parton) jet.

6.2 Example: $e^+e^- \rightarrow \bar{p}X$

The analogy between fragmentation functions and structure functions is particularly transparent in the case of $e^+e^- \rightarrow \bar{p}X$ inclusive antiproton production, since this reaction is simply the crossed counterpart of $ep \rightarrow eX$ deep inelastic scattering; see Fig. 6.5. The similarity of the diagrams is striking. Let q and \bar{p} be the momentum vectors of the time-like virtual photon (or Z) and the antiproton, respectively. Convenient variables to describe $e^+e^- \rightarrow \bar{p}X$ are then q^2 and $\bar{\nu}$ defined by $M\bar{\nu} = q \cdot \bar{p}$. Since q^2 is the total c.m. energy squared and $\frac{1}{2}\sqrt{q^2}$ is the energy of each quark q_k in a typical production channel $e^+e^- \rightarrow q_k\bar{q}_k$, the ratio $z = 2M\bar{\nu}/q^2$ is precisely the energy fraction $E_{\bar{p}}/E_{q_k}$ that arises when discussing $q_k \rightarrow \bar{p}$ fragmentation in the c.m. frame.

The cross sections can be written in terms of structure functions $\bar{F}_1(\bar{\nu}, q^2)$ and $\bar{F}_2(\bar{\nu}, q^2)$ that are formally related to the analogous structure functions $F_1(\nu, Q^2)$ and $F_2(\nu, Q^2)$ of $ep \rightarrow e'X$ scattering. (See Chapter 5 and recall that $Q^2 = -q^2$ and $\nu = q \cdot p/M = -\bar{\nu}$ by crossing.)

$$\begin{aligned}\bar{F}_1(\bar{\nu}, q^2) &= -F_1(\nu = -\bar{\nu}, Q^2 = -q^2), \\ \bar{F}_2(\bar{\nu}, q^2) &= F_2(\nu = -\bar{\nu}, Q^2 = -q^2).\end{aligned}$$

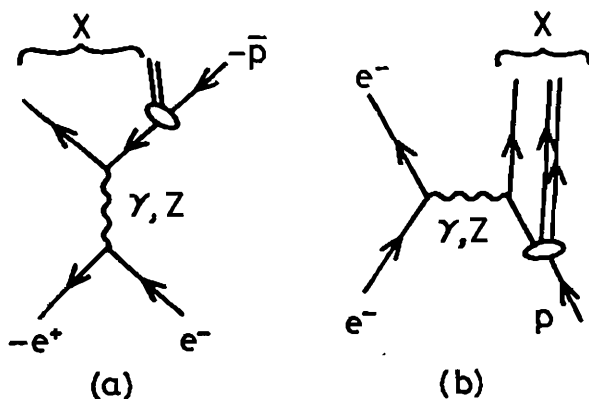


Fig. 6.5. Diagrams for (a) $e^+e^- \rightarrow \bar{p}X$ and (b) $ep \rightarrow eX$ scattering.

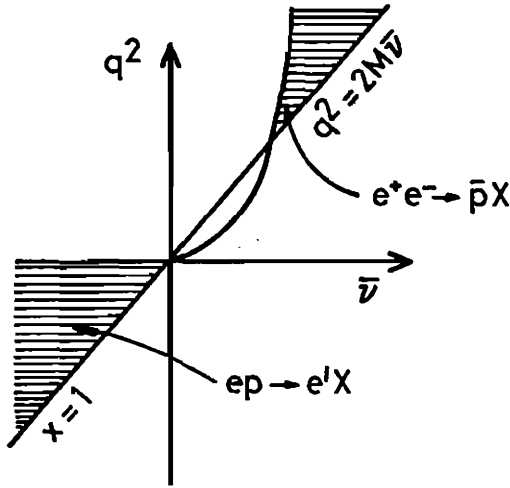


Fig. 6.6. Comparison of physical regions for the crossed channels $e^+e^- \rightarrow \bar{p}X$ and $ep \rightarrow e'X$.

The Bjorken variable $x = Q^2/2M\nu$ and $z = 2M\bar{\nu}/q^2$ are formally related through crossing by $x = 1/z$. These relationships are not immediately profitable, however, since the physical region of \bar{F}_1 and \bar{F}_2 does not overlap with that of F_1 and F_2 ; see Fig. 6.6. In the annihilation channel the parabolic limit is $E_{\bar{p}} \geq M$, and the line $q^2 = 2M\bar{\nu}$ corresponds to the limit $E_{\bar{p}} \leq \frac{1}{2}\sqrt{q^2}$.

In the Bjorken limit $\nu, q^2 \rightarrow \infty$ with z fixed ($0 < z < 1$), the cross section has the form

$$\frac{d\sigma(e^+e^- \rightarrow \bar{p}X)}{dz d\cos\theta} = \frac{\pi\alpha^2}{q^2} \left(z\bar{F}_1 + \frac{1}{2}z^2\bar{F}_2 \sin^2\theta \right),$$

where θ is the \bar{p} c.m. angle relative to the e^+e^- beam axis.

Exercise. Using the results of Chapter 4, show that the parton model predicts

$$\frac{d\sigma}{dz d\cos\theta} = \frac{\pi\alpha^2}{2q^2} (1 + \cos^2\theta) \sum_k 3e_k^2 (D_k^{\bar{p}} + D_k^{\bar{n}}),$$

where the suffix k stands for quark flavors (with electric charges e_k).

Comparing these formulas, we see that the parton model predicts

- i) A relation $z\bar{F}_2 = -\bar{F}_1$, the analog of the Callan-Gross relation $F_2 = xF_1$ (Chapter 5).
- ii) An interpretation of \bar{F}_1 and \bar{F}_2 as fragmentation functions

$$z\bar{F}_1 = -z^2\bar{F}_2 = \sum_k 3e_k^2 \left[D_k^p(z) + D_{\bar{k}}^p(z) \right]$$

analogous to $F_1 = \sum_k e_k^2 [q_k(x) + \bar{q}_k(x)]$ in the scattering channel. The factor 3 arises because colors are summed in the annihilation channel but averaged in the scattering channel.

- iii) In the scaling parton picture, the D -functions and hence \bar{F}_1, \bar{F}_2 depend on z alone.

6.3 Heavy Quark Fragmentation

A quark and antiquark are most likely to combine into a meson when they have about the same velocity. If the fragmenting parton is a heavy quark Q , it needs to lose only a small fraction of its energy in order to materialize a number of light quark pairs with comparable velocity. If Q then combines with one or more of these light quarks, the resulting heavy-flavored hadron H_Q will carry a large fraction of the original energy: $z = E_H/E_Q \sim 1$. We therefore expect qualitatively that the fragmentation of heavy quarks into heavy hadrons will have hard distributions, concentrated at large values of z , and that this property will become more marked as the quark mass increases, approaching a δ -function for very heavy quarks, $D_Q^H \sim \delta(1-z)$. This expectation contrasts sharply with the fragmentation of light quarks into light hadrons, typified by the results in Fig. 6.3 which peak at small z .

An explicit model (originated by *Peterson et al.*) displays this general feature. Consider the transition from an initial heavy quark Q to the heavy hadron $H(Q\bar{q})$ plus spectator light quark q , by $q\bar{q}$ production in the color force field; see Fig. 6.7. Using time-ordered



Fig. 6.7. Fragmentation of heavy quark Q to heavy hadron $H(Q\bar{q})$.

perturbation theory in an infinite-momentum frame, the energy denominator for this process is

$$\Delta E = E_Q - E_H - E_q \simeq \frac{m_Q^2}{2p} - \frac{M_H^2}{2zp} - \frac{m_q^2}{2(1-z)p} \sim 1 - \frac{1}{z} - \frac{m_q^2/m_Q^2}{(1-z)},$$

where p is the initial Q momentum, $m_Q \simeq m_H$ is assumed, z is the H momentum fraction and $1 - z$ is the q momentum fraction. Strictly speaking, the squared masses here denote $m^2 + p_T^2$, including the effects of small transverse momenta that will be integrated. The Peterson model assumes that the transition probability, which gives the $Q \rightarrow H$ fragmentation function, is dominated by the energy denominator $(\Delta E)^{-2}$. All other factors are approximated by constants, apart from a factor z^{-1} for longitudinal phase space, which arises from counting states:

$$d^3 p_H / E_H \simeq \pi dp_{HT}^2 dp_{HL} / p_{HL} = \pi dp_T^2 dz / z.$$

This gives

$$D_Q^H(z) = (\text{constant}) z^{-1} \left[1 - \frac{1}{z} - \frac{\epsilon_Q}{1-z} \right]^{-2},$$

where $\epsilon_Q = \langle m_q^2 + p_{qT}^2 \rangle / \langle m_Q^2 + p_{QT}^2 \rangle$ is a parameter, expected to be proportional to m_Q^{-2} . As ϵ_Q decreases, the peak of D_Q^H moves closer to $z = 1$.

Figure 6.8 shows typical $c \rightarrow D^*$ and $b \rightarrow B$ fragmentation results from the ARGUS and MARK-J experiments respectively, with arbitrary normalization. For comparison, Peterson model calculations

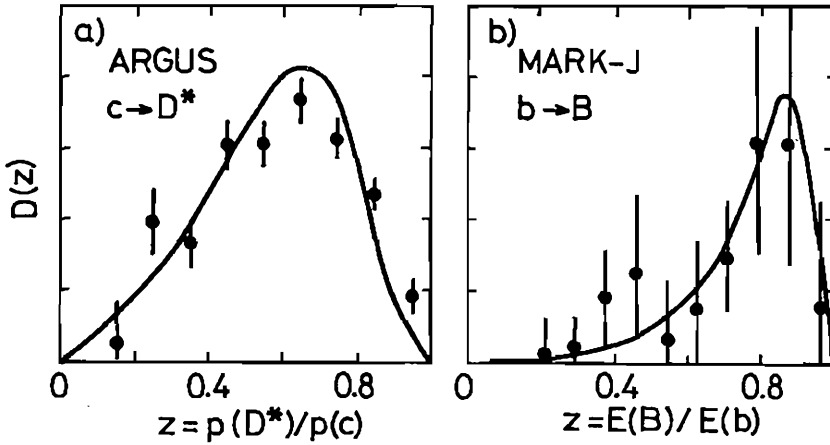


Fig. 6.8. $c \rightarrow D^*$ and $b \rightarrow B$ fragmentation functions from the Argus and Mark-J experiments (Bari Conference 1985) compared to Peterson model calculations for $\epsilon = 0.18$ and $\epsilon = 0.018$, respectively.

are shown for $\epsilon = 0.18$ and $\epsilon = 0.018$, respectively (the ratio 10 : 1 being suggested by the predicted m_Q^{-2} dependence). Notice however that one experiment uses momentum fraction while the other uses energy fraction to define z . Values of ϵ in the ranges 0.1-0.4 for c fragmentation and 0.003-0.04 for b -fragmentation are quoted in the literature, with the empirical ϵ values depending on the experiment and on the definition of z employed.

Figure 6.9 compares Peterson model predictions for c , b and t quark fragmentation, assuming ϵ is proportional to m_Q^{-2} and $m_t = 40$ GeV, with common normalization $\int D(z) dz = 1$.

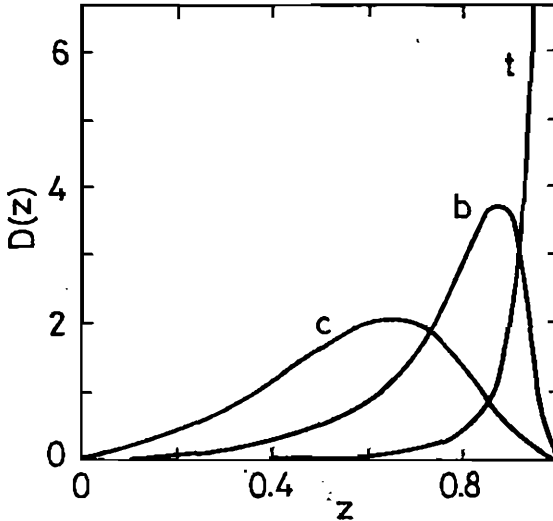


Fig. 6.9. Comparison of Peterson model predictions for $Q = c, b, t$ fragmentation, assuming $\epsilon = 0.40 \text{ GeV}^2/m_Q^2$ with $m_c = 1.5$, $m_b = 4.7$ and $m_t = 40 \text{ GeV}$.

6.4 Independent Quark Jet Fragmentation

A more detailed picture of the jet of produced hadrons can be obtained by an explicit Monte Carlo construction, based on a recursion principle. The first such model was due to Feynman and Field.

Suppose an initial quark q_0 creates a color field in which a new light pair $q_1 \bar{q}_1$ are produced; a meson ($q_0 \bar{q}_1$) is formed with a fraction z_1 of the q_0 momentum, leaving a quark q_1 in place of q_0 , and so on. A one-dimensional “chain decay” picture results; see Fig. 6.10. If we neglect transverse momenta and flavor and spin indices for a moment, such a process is completely specified by one arbitrary function $f(z)$, normalized to $\int f(z) dz = 1$ (since the total probability for each step to happen with some value of z is 1).

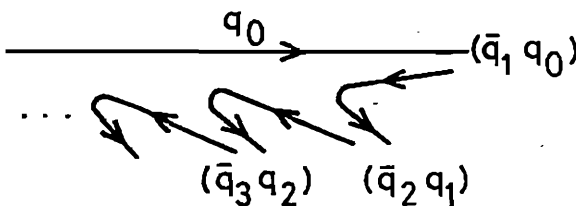


Fig. 6.10. Chain decay picture of jet fragmentation.

This kind of model describes the complete jet, including the single-particle fragmentation functions. If $D(z)$ is the probability density for producing any meson with momentum fraction z , then D satisfies the integral equation

$$D(z) = f(z) + \int_z^1 f(1-z')D(z/z') dz'/z'.$$

This states that the meson is either the first in the chain (probability $f(z)$) or is part of a similar chain initiated by q_1 , which carries a fraction z' of the q_0 momentum with probability $f(1-z')$. Such integral equations are typical of recursive processes.

Exercise. Show that the form $f(z) = (n+1)(1-z)^n$ implies

$$D(z) = (n+1)(1-z)^n/z.$$

For a heavy quark fragmenting to a heavy meson, only the first step of the chain contributes and $D(z) = f(z)$ in this approach.

Such models lend themselves to direct Monte Carlo jet simulations. It is straightforward to take some account of flavors, spins and transverse momenta, for example as discussed below. Starting from an initial quark q_0 of given flavor and momentum, the instructions could be:

- i) Select a value z_1 of the random variable z , with probability distribution $f(z)$.
- ii) Select a quark pair $q_1\bar{q}_1 = u\bar{u}$, $d\bar{d}$ or $s\bar{s}$ with some preassigned relative probability; the meson $(q_0\bar{q}_1)$ then has longitudinal momentum $z_1 p_0$ and the quark q_1 has longitudinal momentum $p_1 = (1-z_1)p_0$.
- iii) Attribute a small (bounded) transverse momentum p_T to the quark q_1 and $-p_T$ to \bar{q}_1 , with some preassigned probability distribution.

- iv*) Select a mass and spin 0 or 1 (or higher) with preassigned probabilities for the meson $q_0\bar{q}_1$.
- v*) Repeat this cycle for the next $q\bar{q}$ pair and continue until the momentum $p_n = (1 - z_n)p_{n-1}$ of the n th quark falls below a cutoff value and the recursion stops.

This procedure generates a chain of mesons $(q_i\bar{q}_{i+1})$ with longitudinal momenta $z_i p_{i-1}$ and transverse momenta $(p_{iT} - p_{i+1T})$, with specified flavors, masses and spins; those that are not π or K mesons already can be decayed into lighter mesons following the particle data tables. When the recursion stops after n steps, there remains a slow quark q_n that has not yet been assigned to a hadron; at this point the various jets can no longer be treated in isolation. The unpaired quarks from all jets must together be turned into hadrons by some prescription; if we are working in the lab frame these hadrons are slow and would play little part in determining jet properties in an experiment. Finally, since the Monte Carlo chains conserve momentum for each jet but not energy, it is necessary to rescale all momenta slightly in each complete event to ensure the correct final energy.

Such a Monte Carlo jet prescription contains an arbitrary function $f(z)$ plus other input parameters for the flavor/spin/mass options at each step. The procedure is to determine these parameters by comparing with data and thereafter to use them predictively. The underlying physical assumptions are that the fragmentation process is

- i*) independent of other jets,
- ii*) local (pairing of adjacent quarks in the chain), and
- iii*) universal (process-independent).

What we have sketched above is just an outline, the details are not fixed. One can identify z with energy fraction or $E + p_L$ fraction instead. The $q_i\bar{q}_{i+1}$ pairs can be identified with low-mass hadron clusters instead of single mesons. Baryon production can be included. But we must remember it is only a framework for parameterization.

It is not quantum mechanical and includes neither interference effects nor identical-particle symmetrization effects (such as Bose-Einstein correlations among pions).

In fact the original Feynman-Field parametrization used the variable $E + p_L$ and took

$$f(z) = 1 - a + 3a(1 - z)^2$$

with $a = 0.77$ determined from data. They assumed that $u\bar{u}$, $d\bar{d}$, $s\bar{s}$ probabilities are 0.4, 0.4, 0.2 and that an equal mix of low-mass spin 0 and spin 1 mesons are formed. The quarks have Gaussian p_T distribution with $\sigma^2 = (0.35 \text{ GeV})^2$.

6.5 1 + 1 Dimensional String Model

When a color-neutral $\bar{q}q$ pair is produced, for example via a $e^+e^- \rightarrow \bar{q}q$ collision, a color force field is created between them. It is believed that for a confining theory like QCD the color lines of force are mostly concentrated in a narrow tube connecting q with \bar{q} , acting like a string with constant tension (independent of the separation between q and \bar{q}). This picture is consistent with Regge phenomenology, heavy quarkonium spectroscopy and lattice QCD, which indicate a value of the string tension,

$$\kappa \simeq 1 \text{ GeV}/fm \simeq 0.2 \text{ GeV}^2,$$

where $fm = \text{femtometer (or fermi)} = 10^{-13} \text{ cm}$. As the quarks fly apart they are decelerated by the string tension, accelerated back together and then fly apart once more, executing periodic oscillations (known as *yo-yo modes*); see Fig. 6.11.

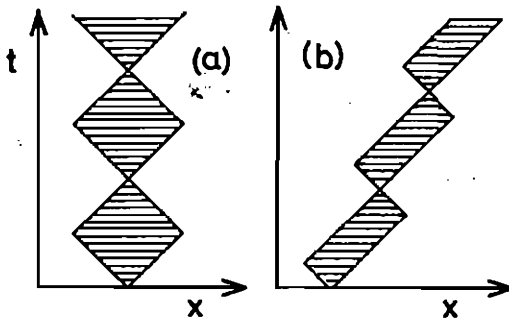


Fig. 6.11. Space-time picture of yo-yo modes of one-dimensional string connecting massless quarks: (a) in $q\bar{q}$ rest frame, (b) for moving $q\bar{q}$.

The equations of motion for the end-points of this relativistic string, in one space and one time dimension, are

$$dp/dt = \pm \kappa,$$

where p is the momentum of the end-point quark and the $+$ ($-$) sign refers to the left (right) end of the string.

Exercise. Using $p = \beta\gamma m$ where $\beta = dx/dt$, $\gamma = 1/\sqrt{1-\beta^2}$ and m is the quark mass, show that the solution for the motion of the right-hand quark (up to the moment when the quarks cross and it becomes the left-hand quark) is

$$p = p_0 - \kappa t, \quad \kappa x = \sqrt{p_0^2 + m^2} - \sqrt{p^2 + m^2}.$$

Notice that the trajectory is a hyperbola in general, becoming two straight-line segments in the limit $m \rightarrow 0$ (illustrated in Fig. 6.11).

Each quark initially travels outward, steadily losing momentum, until its momentum goes to zero. At this time it starts accelerating back in the opposite direction, steadily picking up momentum until the string shrinks to zero and the ends cross. It then starts losing momentum once more.

Exercise. By boosting this trajectory to another 2-dimensional space-time frame, show that the string tension κ is the same in all frames.

In this model the string carries stored energy (equal to κ times its length) but no momentum. The motion of a quark at one endpoint is independent of what happens at the other endpoint, up to the moment when the ends cross over.

A new element is now introduced. The color force field may materialize a massless $q\bar{q}$ pair of zero energy-momentum at a point on the string. Suppose there is a red quark at the right-hand end of the string and an anti-red antiquark at the left-hand end. Then if a red-anti-red $q\bar{q}$ pair is created at an intermediate point, the color lines of force from the right-hand quark can terminate on the intermediate \bar{q} (and similarly the lines from the left-hand antiquark can terminate on the intermediate q). The string then separates into two independent color-neutral strings. One can make an analogy with the case of a constant uniform electric field coupled to particles, which suggests that the probability for string breaking is uniform in space and time

$$d(\text{Probability})/dx dt = (\text{constant}) \exp(-\pi m^2/\kappa),$$

where m is the mass of the created quarks; this is like a tunneling probability through a potential barrier. The motion of the string is now a statistical question. As time develops it breaks randomly into smaller pieces carrying smaller fractions of the original energy, all executing yo-yo modes in the intervals between breaks; see Fig. 6.12. When the invariant mass of a string piece gets small enough, it is identified as a hadron (or a cluster of hadrons) and the breaking stops within that piece. Thus the whole system eventually evolves into hadrons. This approach was pioneered by the Lund group.

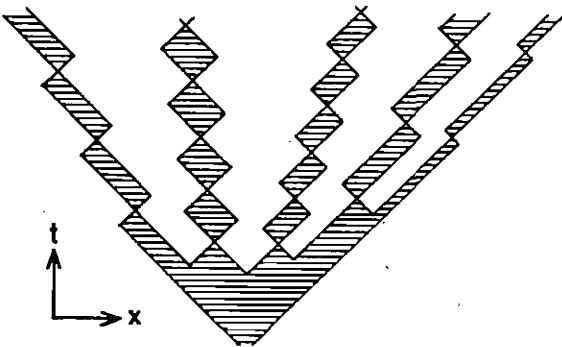


Fig. 6.12. Example of string breaking.

The evolution can be expressed as a stochastic process if we add an assumption. Consider initial massless quarks q_0 moving to the right, \bar{q}_0 moving left, and suppose that n $q\bar{q}$ massless pairs are created at space-time points $(x_1t_1), (x_2t_2), \dots, (x_nt_n)$ starting from the right-hand end of the string. If we assume that all these breaks occur during the first expanding phase of the yo-yo modes, then all q_i are moving left, all \bar{q}_i are moving right ($i > 0$).

Exercise. In these circumstances show that the i th meson $q_{i-1}\bar{q}_i$ has momentum and energy

$$p_i = \kappa(t_{i-1} - t_i), \quad E_i = \kappa(x_{i-1} - x_i).$$

(Take whichever of t_{i-1}, t_i is the later time. What are the endpoint quark momenta at this time? Show that the length of the string at this time is $x_{i-1} - x_i - |t_{i-1} - t_i|$.)

Exercise. Show that the above meson invariant mass squared is $2\kappa^2$ times the area enclosed by its yo-yo mode indicated in Fig. 6.13. (Find the lengths of the sides of the yo-yo rectangle, projected on the x or t axis.)

These formulas also include the end-point quarks if we regard them as “created” at the turning points where their momenta first go to zero. Then if break-point (x_{i-1}, t_{i-1}) and the required mass m_i are specified, the next break-point must lie on a well defined hyperbola in space-time. The setting-up of the chain of breaks can then be

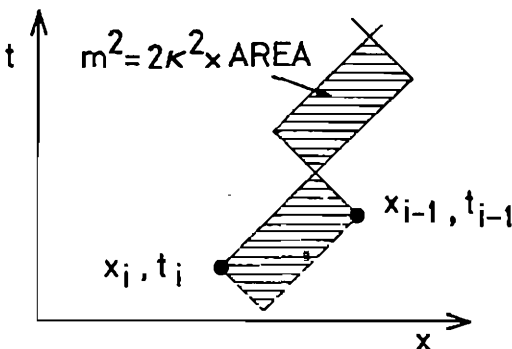


Fig. 6.13. Relation between mass and area of yo-yo mode.

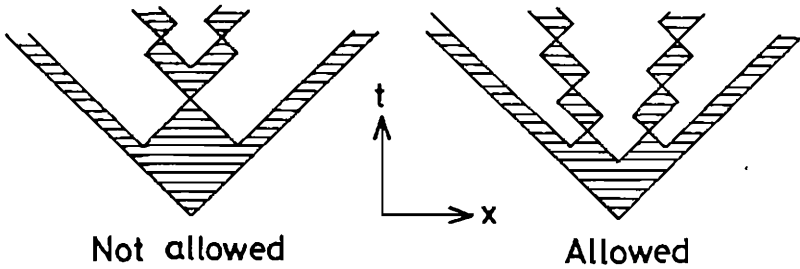


Fig. 6.14. Examples of string-breaking patterns that are allowed and not allowed in the stochastic picture.

viewed as a stochastic process (starting at either end) since each step depends only on random variables and on the end-point of the previous step. But to get this stochastic picture we have assumed that all breaks occur during the first expansion of the yo-yo in question; some breaking patterns are therefore not allowed; see Fig. 6.14.

The stochastic process is conveniently described using light-cone variables $x^\pm = t \pm x$. Starting from the $(i - 1)$ break-point, the step to the next break in the x^+ direction is chosen by

$$\Delta x^+ \equiv (x_{i-1}^+ - x_i^+) = z_i x_{i-1}^+, \quad 0 \leq z_i \leq 1$$

with some probability distribution $f(z)$ for z_i . The step in the x^- direction is then fixed by the mass m_i :

$$\Delta x^- \equiv (x_{i-1}^- - x_i^-) = -m_i^2 / (\kappa^2 \Delta x^+),$$

since the area of the yo-yo rectangle is $\frac{1}{2} \Delta x^+ \Delta x^-$. The initial and final boundary conditions are $x_0^+ = 2E_0/\kappa$, $x_0^- = 0$ and $x_{n+1}^+ = 0$, $x_{n+1}^- = 2\bar{E}_0/\kappa$ where E_0 and \bar{E}_0 are the initial energies of the original pair q_0 and \bar{q}_0 . The chain of points x_i^\pm can be generated from the right (as above) or from the left or from both ends (choosing left or right at random each time), with some empirical adjustment for the final boundary matching. There is qualitative similarity to the Feynman-Field approach, with $f(z)$ playing a similar role in each case, but the specific string picture here is new.

The Lund group originally chose $f(z) = 1$ but later moved to the *symmetric Lund* form

$$f_{\alpha\beta}(z) = N_{\alpha\beta} z^{a_\alpha - a_\beta - 1} (1 - z)^{a_\beta},$$

where $N_{\alpha\beta}$, a_α and a_β are parameters and α and β are the quark and antiquark flavors. This form has the merit of generating left-right symmetrical jets whatever end one starts from, which is desirable since quarks and antiquarks are expected to fragment in similar ways. One must also parameterize the meson transverse momenta, for example by a Gaussian probability distribution $d\sigma/dp_T^2 \sim \exp(-bp_T^2)$, and the meson spins. Previous references to m^2 must then be interpreted as $m^2 + p_T^2$. As a first approximation, the choices $a = 1$ for all light flavors and $b = (1.5 \text{ GeV})^{-2}$ give reasonable fits to data, but the parameters are constantly being refined.

Heavy quark pairs cannot simply be materialized at a point because of energy conservation; instead they are created at a separation $\Delta x = 2m/\kappa$ and this length of string is annihilated to provide their rest-energy. Following the previous analogy with the case of a uniform electric field, the probability for producing a $Q\bar{Q}$ pair with masses m_Q is taken to be proportional to $\exp(-\pi m_Q^2/\kappa)$. With conservative mass choices $m_s \simeq 0.25 \text{ GeV}$, $m_c \simeq 1.2 \text{ GeV}$ this gives the relative probabilities of $u\bar{u} : d\bar{d} : s\bar{s} : c\bar{c}$ to be $1 : 1 : 0.37 : 10^{-10}$, so in this model essentially nothing heavier than strange quarks is pair produced along the string. Heavy quark to heavy meson fragmentation occurs only at the first step with $D(z) = f(z)$.

6.6 Gluon Jets

We have hitherto dealt only with quark jets. Since gluons carry two color labels (one color, one anticolor), a possible approximation is to replace an initial gluon by a collinear massless quark plus antiquark carrying these color labels, with the momentum divided between them (e.g. weighted by the QCD $g \rightarrow q\bar{q}$ splitting function of

Chapter 7). This is a simple extension of the independent quark jet picture of §6.4.

Exercise. Show by examples that this prescription gives a higher meson multiplicity with a softer z -distribution for the gluon jet, compared to a quark jet of the same energy.

Another approach is to follow the classical string picture a little further and ask where the color lines of force will lie. Take for example a color-neutral $\bar{q}qg$ system, which may be produced in e^+e^- collisions. One simple way to connect up the color lines of force between them is by a single string (flux tube) running from q to g to \bar{q} . Hitherto we have attached massless particles only to the ends of the string; now we attach a massless gluon to a point in the middle. Consider any frame (not necessarily the c.m. frame) where the q , \bar{q} and g momenta are coplanar and all three fly outward with the velocity of light from a common origin O ; see Fig. 6.15. As time passes the string gets longer and absorbs energy from q , \bar{q} and g . Consider first the quark q : in time δt it travels a distance δt and the string gets longer (at the q -end) by $\delta t \cos \theta$. If it were at rest this new piece of string would contain energy $\kappa \delta t \cos \theta$, but since it is moving sideways with velocity $\beta = \sin \theta$ its total energy is $\gamma \kappa \delta t \cos \theta = \kappa \delta t$, where $\gamma = 1/\sqrt{1 - \beta^2} = 1/\cos \theta$ is the appropriate Lorentz factor. This energy is extracted from q by a force of strength κ acting against the direction of motion, *i.e.* along AO in Fig. 6.15. This retarding force can be understood as the sum of a reduced string tension $\kappa \cos \theta$ along AB (a moving string has time dilated by γ and tension correspondingly reduced) and an inertial component $\kappa \sin \theta$ orthogonal to AB . Similarly \bar{q} experiences a retarding force κ directed along CO and g experiences a force 2κ along BO . Hence the motion of the three massless particles at A , B and C is completely specified.

We now add string breaking along the segments AB and BC . This leads to two chains of mesons, similar to what one would get from two $q\bar{q}$ strings except that one of the mesons includes a piece from both segments (the string piece that includes the point B); the latter

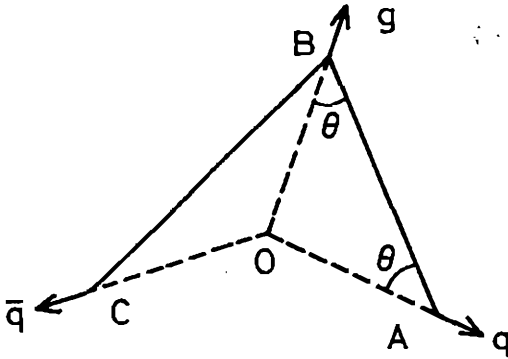


Fig. 6.15. A color-neutral $q\bar{q}g$ system connected by the string ABC.

can be regarded as a colorless $q\bar{q}g$ system rather than a $q\bar{q}$ system. In a frame where O lies on AB, the fragmentation of string segment AB gives a pair of back-to-back jets of hadrons, directed mainly along OA and OB but with a symmetrical p_T distribution about this axis. Similarly for string segment BC, in a frame where O lies on BC. In the c.m. frame, however, these jets are boosted sideways: the resulting hadron distributions are therefore not symmetrically distributed about the parton axes OA, OB, OC (which would be expected for independent jet fragmentation). Instead there is an excess of hadrons in the angular regions AOB and BOC with a corresponding depletion in COA: this has been called the *string effect*; see Fig. 6.16.

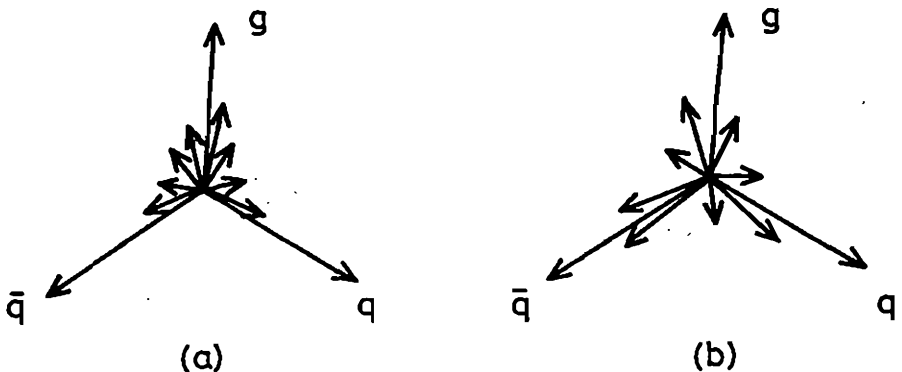


Fig. 6.16. Fragmentation of $q\bar{q}g$ system in (a) string picture and (b) independent jet picture.

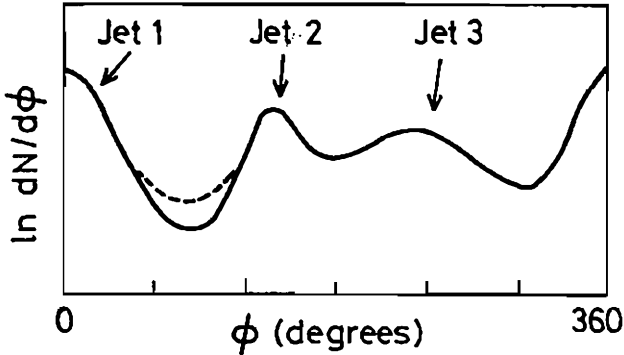


Fig. 6.17. Particle flow versus angle for $e^+e^- \rightarrow q\bar{q}g$ events. The solid curve denotes string fragmentation, the dashed curve denotes independent jet fragmentation: data agree with the former.

There is experimental evidence for such an effect in $e^+e^- \rightarrow 3$ jets events. First one orders the three jets according to their energy; according to QCD, the events are primarily due to $e^+e^- \rightarrow q\bar{q}g$ and the gluon jet is usually the least energetic. String fragmentation then predicts a depletion of hadron production in the angular arc between the two more energetic jets, compared to independent jet fragmentation calculations. Figure 6.17 shows a qualitative plot of the predicted particle flow versus angle in the event plane, when the most energetic jet (jet 1) is fixed at $\phi = 0$ and jets 2 and 3 are ordered in angle by convention. The depletion between jets 1 and 2 is not seen in $e^+e^- \rightarrow q\bar{q}\gamma$ events, confirming that it has something to do with the gluon. The string effect suggests there is real dynamics in the string picture. However, the QCD Monte Carlo shower model of Webber (§9.4) also reproduces the string effect, due apparently to a careful treatment of soft gluons.

In general, before fragmenting a multi-parton state into hadrons, the string approach requires us first to collect the quarks and gluons into colorless clusters. The $q\bar{q}g$ systems discussed above are just one example of colorless clusters. Another interesting case is three-gluon systems, produced for example in $e^+e^- \rightarrow \Upsilon(b\bar{b}) \rightarrow ggg$: here the

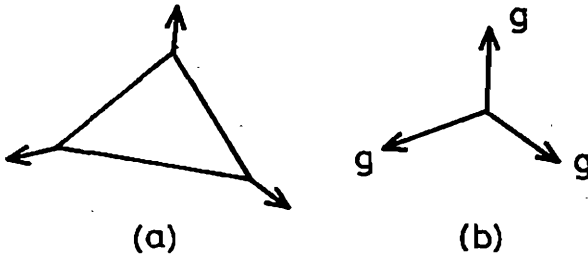


Fig. 6.18. Different pictures of $\Upsilon \rightarrow ggg$ fragmentation: (a) color string and (b) independent jets.

independent jet approach suggests three gluon jets but the string picture suggests a continuous triangular string with three gluons attached at the vertices, as in Fig. 6.18.

In this chapter we have described various ways of parameterizing fragmentation processes. Many different prescriptions are available, with parameters tuned to reproduce a wide range of measured distributions. Interested readers should refer to recent conference reports for references to the latest versions.

Chapter 7

Quantum Chromodynamics (QCD)

7.1 The QCD Lagrangian

Strong interactions are described by a local non-abelian gauge theory of quarks and gluons in which $SU(3)$ is the gauge group and gluons are the gauge bosons. Three colored quarks of each quark flavor form a triplet in the fundamental representation of $SU(3)$ and eight gluons form an octet in the adjoint representation (defined to have the same dimensions as the group). Following the general structure outlined in §2.2, the QCD Lagrangian is

$$\mathcal{L} = -\frac{1}{4}F_a^{\mu\nu}F_{a\mu\nu} + \bar{\psi}_j(i\gamma_\mu D_{jk}^\mu - M_j\delta_{jk})\psi_k,$$

where the indices a, j and k refer to color and assume the values $a = 1, \dots, 8$ and $j, k = 1, 2, 3$. The covariant derivative D acting on a quark field is

$$D_{jk}^\mu = \delta_{jk} \partial^\mu + ig(T_a)_{jk} G_a^\mu,$$

where G_a^μ are the gluon fields, T_a are the $SU(3)$ generators, and g is the strong coupling; M_{jk} is the quark mass matrix. The gluon field tensor is

$$F_a^{\mu\nu} = \partial^\mu G_a^\nu - \partial^\nu G_a^\mu - g f_{abc} G_b^\mu G_c^\nu,$$

where f_{abc} are the structure constants of $SU(3)$, defined by the com-

mutation of the SU(3) generators

$$[T_a, T_b] = i f_{abc} T_c .$$

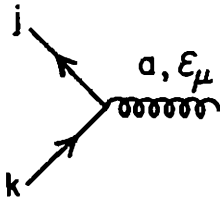
This Lagrangian is invariant under the infinitesimal local gauge transformations

$$\psi(x) \rightarrow [1 - ig \alpha_a(x) T_a] \psi(x) ,$$

$$G_a^\mu(x) \rightarrow G_a^\mu(x) + \partial^\mu \alpha_a(x) + g f_{abc} \alpha_b(x) G_c^\mu(x) ,$$

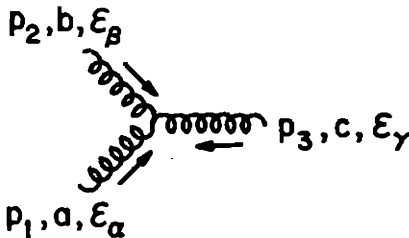
as already demonstrated in §2.2.

This Lagrangian contains a quark-gluon interaction vertex of the form



$$\text{vertex factor} = -ig \gamma^\mu (T_a)_{jk} .$$

In addition, there is a triple gluon coupling



$$\begin{aligned} \text{vertex factor} = & -g f_{abc} [g_{\alpha\beta} (p_1 - p_2)_\gamma \\ & + g_{\beta\gamma} (p_2 - p_3)_\alpha + g_{\gamma\alpha} (p_3 - p_1)_\beta] . \end{aligned}$$

There is also a four-gluon interaction. The gluon self-interactions have no analog in QED; they arise from the non-abelian nature of the theory and are analogous to the W self-interactions in the $SU(2)$ case. The complete QCD Feynman rules are given in Appendix A.

7.2 The Renormalization Group Equations (RGE)

In evaluating Feynman diagrams that contain loops, divergent integrals over loop momenta occur. To make sense of these quantities, the divergent expressions are first made “temporarily finite” by some *regularization* procedure which introduces additional parameters (*e.g.*, a gluon mass m_g , an ultraviolet momentum cut-off Λ , or a fractional space-time dimension $D = 4 - 2\epsilon$). In this way, the divergences of perturbation theory are re-expressed in a well-defined way (though still with divergent limits). These regularized divergences of perturbation theory are then removed by absorbing them into the definitions of physical quantities through a *renormalization* procedure. This is done by some specified (but arbitrary) prescription, which introduces a new dimensional scale μ . Renormalized quantities in the theory, such as the basic vertex coupling strength g , depend explicitly on μ . Different renormalization prescriptions with different μ must all lead to the same observable amplitudes. The transformations of renormalized operators as μ is changed form a Lie group, first recognized by Stueckelberg and Peterman and named by them the *Renormalization Group*. The equations that express the invariance of the physics under changes of the parameter μ are known as the *Renormalization Group Equations* (RGE).

Renormalization is done on the sum of connected Feynman graphs with the external propagators removed (including their self-energy parts). In more technical language, it deals with single-particle-irreducible Green’s functions Γ , which cannot be disconnected by cutting any single internal line. One way to control divergences in Γ

is to introduce an ultraviolet cut-off Λ in the loop momentum integrals, thus obtaining unrenormalized Green's functions $\Gamma_U(p_i, g_0, \Lambda)$, where p_i denotes external particle momenta and g_0 is the basic vertex coupling in the Lagrangian. For a renormalizable theory such as QCD, it is possible to define renormalized Green's functions Γ_R by

$$\Gamma_R(p_i, g, \mu) = Z_\Gamma(g_0, \Lambda/\mu) \Gamma_U(p_i, g_0, \Lambda),$$

which are finite in the $\Lambda \rightarrow \infty$ limit but depend on the prescription parameter μ and a renormalized coupling g . Z_Γ is a product of factors Z_i , one for each external particle i of the Green's function Γ .

Since Γ_U does not depend on μ , we obtain on differentiation,

$$\frac{d\Gamma_U}{d\mu} = \frac{d}{d\mu} [Z_\Gamma^{-1} \Gamma_R] = \frac{\partial Z_\Gamma^{-1}}{\partial \mu} \Gamma_R + Z_\Gamma^{-1} \left(\frac{\partial}{\partial \mu} + \frac{\partial g}{\partial \mu} \frac{\partial}{\partial g} \right) \Gamma_R = 0,$$

which is usually written

$$\left(\mu \frac{\partial}{\partial \mu} + \beta \frac{\partial}{\partial g} + \gamma_\Gamma \right) \Gamma_R(p_i, g, \mu) = 0,$$

where the beta function $\beta(g)$ and the "anomalous dimension" $\gamma(g)$ have been defined by:

$$\beta = \mu \frac{\partial g}{\partial \mu}, \quad \gamma_\Gamma = -\frac{\mu}{Z_\Gamma} \frac{\partial Z_\Gamma}{\partial \mu}.$$

Here Λ is held constant in the differentiation and subsequently the limit $\Lambda \rightarrow \infty$ is taken. The beta function is universal; the γ function depends on the Green's function. If Z_Γ is expressed as a product of renormalization factors, γ may be expressed as a sum of the corresponding contributions.

Consider the case in which there is a single large momentum scale Q . All momenta p_i can then be expressed as fixed fractions x_i of Q .

Introducing the variable

$$t = \frac{1}{2} \ln \left(\frac{Q^2}{\mu^2} \right),$$

the RGE is

$$\left(-\frac{\partial}{\partial t} + \beta(g) \frac{\partial}{\partial g} + \gamma_\Gamma(g) \right) \Gamma(t, g, x_i) = 0.$$

We define a “running coupling” $g(t)$ through the equation

$$\frac{dg(t)}{dt} = \beta(g(t))$$

with $g(t=0) = g$, the coupling constant appearing in the RGE. Then

$$t = \int_{g(0)}^{g(t)} \frac{dg'}{\beta(g')}, \quad \frac{dg(t)}{dg(0)} = \frac{\beta(g(t))}{\beta(g(0))},$$

and the general solution to the RGE is

$$\Gamma(t, g(0), x_i) = \Gamma(0, g(t), x_i) \exp \int_{g(0)}^{g(t)} dg' \frac{\gamma_\Gamma(g')}{\beta(g')}.$$

This shows that the whole Q^2 dependence of Γ arises through $g(t)$.

7.3 The Running Coupling

In practice Γ , γ_Γ and β can only be calculated in perturbation series in the coupling $g(0)$. Let us denote by $\Gamma^{n,m}$ the renormalized, truncated QCD Green's functions with n gluon and m quark external legs. The lowest order diagrams contributing to $\Gamma^{2,0}$, $\Gamma^{0,2}$ and $\Gamma^{1,2}$ are shown in Fig. 7.1 (where a gluon loop is shown, it is understood that the appropriate ghost loop is added; see Appendix A).

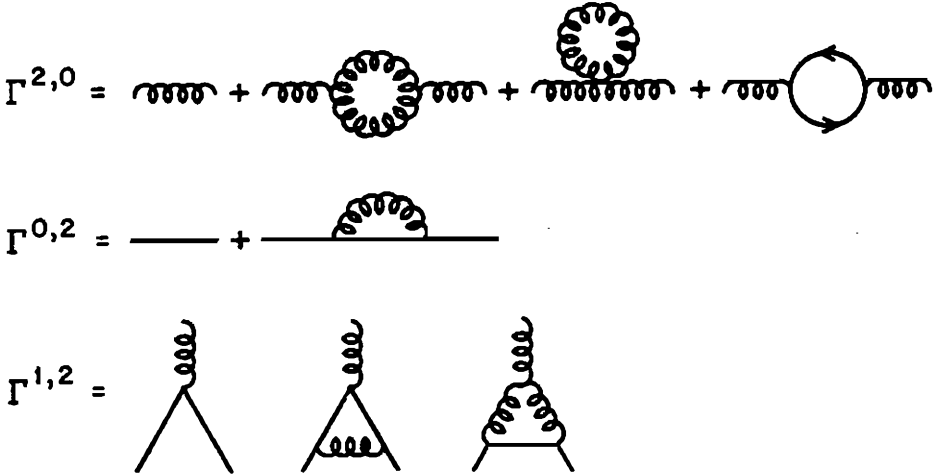


Fig. 7.1. Diagrams contributing to Green's functions.

The perturbative expansions to order g^2 are

$$\Gamma^{2,0} = (p_\mu p_\nu - g_{\mu\nu} p^2) \left\{ 1 + \left[\frac{13}{6} C_2(G) - \frac{4}{3} T(R) \right] \frac{g^2}{16\pi^2} \ln \left(\frac{-p^2}{\mu^2} \right) \right\},$$

$$\Gamma^{0,2} = \not{p} + O(g^4),$$

$$\Gamma^{1,2} = g\gamma_\mu T_i \left[1 - \frac{3}{4} C_2(G) \frac{g^2}{16\pi^2} \ln \left(\frac{-p^2}{\mu^2} \right) \right],$$

with incoming momentum configurations $(p, -p)$ for the two-leg and $(0, -p, p)$ for the three-leg cases normalized at $p^2 = -\mu^2$. We have used the Landau gauge, where the gluon propagator is $-i\delta_{ab}(g_{\mu\nu} p^2 - p_\mu p_\nu)/p^4$. $C_2(G)$ and $T(R)$ depend on the gauge group G and the representation R corresponding to the quarks; they are defined by

$$C_2(G)\delta_{ab} = \sum_{c,d} f_{acd} f_{bcd}, \quad T(R)\delta_{ab} = \text{Tr}(T_a T_b).$$

They arise from the gluon and quark loops shown in Fig. 7.2, and their values for QCD are $C_2(G) = 3$, $T(R) = \frac{1}{2}f$ including an implicit

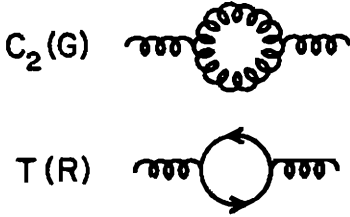


Fig. 7.2. Gluon and quark loops give rise to coefficients $C_2(G)$ and $T(R)$, respectively.

summation over f quark flavors. These Green's functions satisfy the RGE:

$$\begin{aligned} \left(\mu \frac{\partial}{\partial \mu} + \beta \frac{\partial}{\partial g} + 2\gamma_G \right) \Gamma^{2,0} &= 0, \\ \left(\mu \frac{\partial}{\partial \mu} + \beta \frac{\partial}{\partial g} + 2\gamma_Q \right) \Gamma^{0,2} &= 0, \\ \left(\mu \frac{\partial}{\partial \mu} + \beta \frac{\partial}{\partial g} + 2\gamma_Q + \gamma_G \right) \Gamma^{1,2} &= 0, \end{aligned}$$

where γ_G and γ_Q are the contributions for each gluon or quark leg.

Exercise. By substituting the perturbative expressions for $\Gamma^{n,m}$ in these RGE, show that in the Landau gauge,

$$\gamma_G = \left[\frac{13}{6} C_2(G) - \frac{4}{3} T(R) \right] \frac{g^2}{16\pi^2} + O(g^4),$$

$$\gamma_Q = 0 + O(g^4),$$

$$\beta = - \left[\frac{11}{3} C_2(G) - \frac{4}{3} T(R) \right] \frac{g^3}{16\pi^2} + O(g^5),$$

The results above show that $\beta(g)$ arises from the loop diagrams in Fig. 7.2 and that its expansion in powers of g begins in general

$$\beta(g) = -bg^3(1 + b'g^2 + \dots)$$

with, for the QCD case,

$$b_{\text{QCD}} = \frac{1}{48\pi^2} (33 - 2f),$$

where f is the number of quark flavors contributing in the loops. The

positive contribution in b_{QCD} is from gluon loops. Although β and γ can in general depend on the choice of renormalization scheme and gauge, the first two coefficients b and b' are always the same, as the following exercise shows.

Exercise. Suppose g^2 and \bar{g}^2 are the results of two different renormalization schemes, related by $\bar{g}^2 = g^2 + a_1 g^4 + a_2 g^6 + \dots$ with some coefficients a_i . By transforming the expansion of β from one scheme to the other, show that the coefficients b and b' are unchanged.

The lowest order approximation $\beta = -bg^3$ is called the one-loop approximation since b arises from single loop diagrams.

Exercise. Integrate the one-loop equation $dg/dt = -bg^3$ to obtain

$$g^2(t) = \frac{g^2(0)}{1 + 2bg^2(0)t}.$$

Exercise. Integrate the two-loop equation $dg/dt = -bg^3(1 + b'g^2)$ to obtain

$$\frac{1}{g^2(t)} - \frac{1}{g^2(0)} + b' \ln \left[\frac{b' + 1/g^2(0)}{b' + 1/g^2(t)} \right] = 2bt.$$

Hence show that the leading logarithmic approximation (LLA) for $g^2(t)/g^2(0)$, where only terms of order $[g^2(0)t]^n$ are retained, is given by the one-loop approximation above.

We shall henceforth confine our discussion mainly to the LLA (one-loop approximation) for $g^2(t)$. With $f \leq 16$ flavors b_{QCD} is positive and $g^2(t) \rightarrow 0$ as $t \rightarrow \infty$. This property that the running coupling goes to zero as $Q^2 \rightarrow \infty$ is known as *asymptotic freedom* and allows RGE-improved perturbation theory calculations at large Q^2 . It is convenient to use

$$\alpha_s(Q^2) \equiv \frac{g^2(Q^2)}{4\pi} = \frac{g^2(0)}{4\pi[1 + bg^2(0) \ln(Q^2/\mu^2)]}$$

and to introduce the parameter $\Lambda = \mu \exp \{ -[2bg^2(0)]^{-1} \}$ so that

$$\alpha_s(Q^2) = \frac{1}{4\pi b \ln(Q^2/\Lambda^2)} = \frac{12\pi}{(33 - 2f) \ln(Q^2/\Lambda^2)}.$$

The parameter Λ is to be determined by experiment. The theory is applicable only for $Q^2 \gg \Lambda^2$ for which α_s is small. The number f of participating flavors depends on Q^2 ; in general, a quark i of mass m_i is expected to contribute to the loops only when $|Q^2| \geq 4m_i^2$. At a new quark threshold, where f increases by 1, the value of Λ must change in order that $\alpha_s(Q^2)$ be continuous.

Exercise. If $\Lambda_4 = 0.2 \text{ GeV}$ is the value of Λ for $f = 4$ flavors, what is the value of Λ_5 if the $f = 5$ threshold is at $Q^2 = 4m_b^2 = 100 \text{ GeV}^2$? Show that the modified formula

$$\alpha_s(Q^2) = 12\pi / \left[25 \ln \left(\frac{Q^2}{\Lambda_4^2} \right) - \sum_{i>4} 2\theta(Q^2 - 4m_i^2) \ln \left(\frac{Q^2}{4m_i^2} \right) \right]$$

gives the desired behavior of α_s through the fifth and subsequent thresholds, where the θ function is $\theta(x) = 1$ (0), for $x > 0$ (≤ 0).

As introduced here in the LLA context, Λ has a precise operational meaning (it fixes $\alpha_s(Q^2)$ with which we calculate) but its theoretical basis is somewhat subtle. If we added a non-leading log term, by changing the denominator factor from $\ln(Q^2/\Lambda^2)$ to $\ln(Q^2/\Lambda^2) + X$, it would be equivalent to changing $\Lambda \rightarrow \Lambda' = \Lambda \exp(-\frac{1}{2}X)$. Thus if we determine Λ from a particular experiment, using LLA formulas, the resulting empirical value of Λ parameterizes to some extent the non-leading terms that we have neglected. These non-leading terms arise from the higher-loop contributions to both $\beta(g)$ and $\gamma(g)$; see the general RGE solution in the previous section. Although $\beta(g)$ is universal, the relevant $\gamma(g)$ depends on the experimental measurements in question. Hence the empirical value of Λ found from data fitting with LLA formulas will depend in general on the class of data being used. To determine whether these different values of Λ are consistent with a common QCD interpretation, one must consistently include non-leading log terms in the formulas.

In QCD the second coefficient b' is given by

$$bb' = (102 - 38f/3)/(16\pi^2)^2$$

and the two term solution can be written

$$\alpha_s(Q^2) = \frac{1}{4\pi b \ln(Q^2/\Lambda^2)} \left\{ 1 - \frac{b'}{b} \frac{\ln[\ln(Q^2/\Lambda^2)]}{\ln(Q^2/\Lambda^2)} \right\}.$$

In QED there is no analog to the gluon loops, so $C_2(G) = 0$ and $T(R) = \sum_i e_i^2$, summed over all fermions (with charges e_i) appearing in the fermion loops. Hence

$$b_{QED} = -\frac{1}{12\pi^2} \sum_i e_i^2$$

and the QED running coupling in one-loop approximation is

$$\alpha(Q^2) = \frac{\alpha}{1 - (\alpha/3\pi) \sum_i e_i^2 \theta(Q^2 - 4m_i^2) \ln(Q^2/4m_i^2)}.$$

Here we have made the choice $\mu = m_e$ and introduced $\alpha = \alpha(m_e^2) \simeq 1/137$ rather than a mass scale Λ to fix the normalization. QED is not asymptotically free, but the small value of α allows the use of perturbation theory up to very large values of Q^2 .

Exercise. By evolving α_{QED} in steps from $\alpha(m_e^2) = 1/137$ (approximating $m_u = m_d = 10 \text{ MeV}$, $m_s = m_\mu = 100 \text{ MeV}$, $m_c = m_\tau = 1.8 \text{ GeV}$, $m_b = 5 \text{ GeV}$, $m_t = 40 \text{ GeV}$) show that $\alpha(Q^2 = M_W^2) \simeq 1/128$.

7.4 Leading Log Perturbation Theory

In conventional perturbation calculations, loop integrations lead to large logarithms and hence convergence requires both $g^2(0) \ll 1$ and $g^2(0) \ln(Q^2/\mu^2) \ll 1$. The RGE however permit us to include all leading-log terms (i.e. powers $[g^2 \ln Q^2]^n$ for all n) directly through the running coupling constant $g(Q^2)$, when β and γ are calculated to one-loop level. Convergence then requires only that $g^2(Q^2) \ll 1$.

To see this, the exponential factor in the RGE solution can be evaluated in a perturbation series. As we saw in §7.3, the expansion of γ begins with $\gamma = \gamma_1 g^2 + \gamma_2 g^4 + \dots$ and hence

$$\frac{\gamma}{\beta} = - \left(\frac{\gamma_1}{b} \right) \frac{1}{g} + c_2 g + c_3 g^3 + \dots$$

The RGE solution involves the integral

$$\int_{g(0)}^{g(t)} dg' \frac{\gamma}{\beta} = \ln \left(\frac{g(0)}{g(t)} \right)^{\gamma_1/b} + \frac{1}{2} c_2 [g^2(t) - g^2(0)] + \dots$$

With the LLA to $g(t)$,

$$g^2(t) - g^2(0) = \frac{2b g^4(0) t}{1 + 2b g^2(0) t},$$

it is clear that $\frac{1}{2} c_2 [g^2(t) - g^2(0)]$, and higher terms in the above expansion give non-leading contributions in $\ln Q^2$, i.e. $(g^2(0))^n t^{n-1}$ with $n = 2, 3, \dots$. In LLA these terms are dropped and the general RGE solution is of the form

$$\Gamma(t, g(0)) = \Gamma(0, g(t)) \left(\frac{g^2(0)}{g^2(t)} \right)^{\gamma_1/2b}$$

in which all the t -dependence enters through $g(t)$ and only the one-loop values of β and γ are involved.

7.5 Deep Inelastic Structure Functions in QCD

In calculating the QCD corrections to the scaling of parton distributions, we shall separate the hadronic vertex from the leptonic vertex and calculate the former from Feynman rules for gluon emission processes. For illustration we take the case of electron-proton deep inelastic scattering (DIS) $ep \rightarrow e'X$ via a virtual photon. We recall from §5.5 that the tensor $W^{\alpha\beta}$ describing the hadronic vertex is

$$W_{\alpha\beta} = \frac{1}{8\pi M} \sum_{\text{spins}} \int h_{\alpha} h_{\beta}^* \left[\prod_f \frac{d^3 f}{(2\pi)^3 2f_0} \right] (2\pi)^4 \delta^4(\gamma^* + P - \Sigma f),$$

where $h_{\alpha} = \langle X | J_{\alpha} | p \rangle$ is the hadronic matrix element, f denotes the final hadrons summed in X , and P is the proton momentum. The most general form of $W_{\alpha\beta}$ can be written

$$W_{\alpha\beta} = \left(-g_{\alpha\beta} + \frac{q_{\alpha} q_{\beta}}{q^2} \right) \frac{F_1(x, y)}{2M} + \left(P_{\alpha} - \frac{P \cdot q}{q^2} q_{\alpha} \right) \left(P_{\beta} - \frac{P \cdot q}{q^2} q_{\beta} \right) \frac{F_2(x, y)}{M^2 \nu},$$

where $q = e - e'$ is the photon momentum, $x = Q^2/(2M\nu)$, and $M\nu = q \cdot P$, as usual. In this general form we have included q_{α} and q_{β} terms (which vanish when contracted with a massless lepton tensor and were therefore omitted in §5.5) in order that the coefficients of F_1 and F_2 shall be manifestly gauge invariant. From these expressions we can extract the structure functions F_1 and F_2 for any given QCD subprocess at the hadron vertex.

We denote the momentum fraction carried by the struck parton by w . It is necessary to distinguish w from $x = Q^2/(2M\nu)$ since they are not equal when QCD radiation occurs (equality is special to $\gamma^* + q \rightarrow q'$ transitions and does not apply to $\gamma^* + q \rightarrow q' + g$, etc.). In evaluating the DIS cross section above in the parton model, the flux factor $1/(2s)$ appropriate for a proton target must be replaced by $1/(2\hat{s}) = 1/(2ws)$ for a parton of fractional momentum w which introduces a factor $1/w$ in $W_{\alpha\beta}$ (equivalently, this kinematical factor

can be introduced by treating the parton as a particle of mass wM at rest in the proton rest frame). Also the parton cross sections must be weighted by the probability $q(w)dw$ and a color factor (depending on the subprocess) from summing final and averaging initial colors.

The lowest-order calculation for $\gamma^* q \rightarrow q'$ gives $h_\alpha = e_q \langle p' | \gamma_\alpha | p \rangle$ for each quark.

Exercise. Show that in this order

$$W_{\alpha\beta} = \sum_q \frac{e_q^2}{2M} \int_0^1 \frac{dw}{w} q(w) \left[-x g_{\alpha\beta} + \frac{p_\alpha p'_\beta + p'_\alpha p_\beta}{M\nu} \right] \delta(x-w),$$

where $p = wP$ and $p' = wP + q$ are the initial and final quark momenta, and hence that the structure functions are

$$F_1(x, y) = x^{-1} F_2(x, y) = \sum_q e_q^2 \int dw q(w) \delta(x-w) = \sum_q e_q^2 q(x),$$

as found previously in §5.5.

In the next order there are $\gamma^*(q) + q(p) \rightarrow q(p') + g(k)$ subprocesses with gluon emission, as in Fig. 7.3. These give the hadronic matrix element

$$h_\alpha = e_q e g_s \left[\frac{\langle p' | \gamma_\alpha (\not{p}' - \not{q}) \not{\epsilon}^* | p \rangle}{(p' - q)^2} + \frac{\langle p' | \not{\epsilon}^* (\not{p} + \not{q}) \gamma_\alpha | p \rangle}{(p + q)^2} \right] T_{ij}^a,$$

where g_s and ϵ are the gluon coupling and polarization vector, respectively, and i, j, a are the color indices of the SU(3) matrix T . Squaring, summing over spins, and evaluating the phase space gives $\tilde{W}_{\alpha\beta}$, defined by

$$W_{\alpha\beta} = \sum_q e_q^2 \int_x^1 \frac{dw}{w} q(w) \tilde{W}_{\alpha\beta},$$

where the limit $w \geq x$ comes from the constraint $\hat{s} = 2Mw\nu - Q^2 \geq 0$.

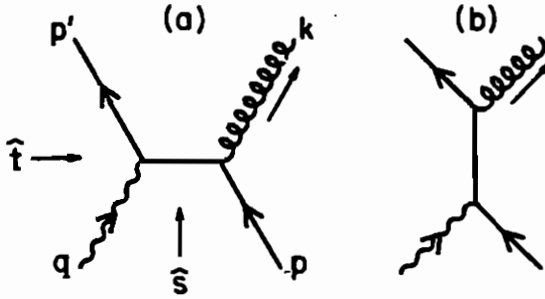


Fig. 7.3. Gluon radiation diagrams in photon-quark interaction.

Exercise. Show that in this order,

$$\begin{aligned} \tilde{W}_{\alpha\beta} = \frac{4C\alpha_s}{M} \int d(PS) \frac{1}{\hat{s}\hat{t}} & \left[(\hat{u} - Q^2) \{p', p\}_{\alpha\beta} + (\hat{u} + \hat{t}) \{k, p\}_{\alpha\beta} \right. \\ & \left. - (\hat{u} + \hat{s}) \{p', k\}_{\alpha\beta} + \hat{s} \{p, p\}_{\alpha\beta} + \hat{t} \{p', p'\}_{\alpha\beta} \right], \end{aligned}$$

where $\alpha_s = g_s^2/4\pi$, $\hat{s} = (p+q)^2$, $\hat{t} = (p'-q)^2$, $\hat{u} = (p'-p)^2$, the color factor is $C = \frac{1}{3} \sum_{a,b} \text{Tr}(T^a T^b) = \frac{4}{3}$, and the bracket symbol is defined by

$$\{a, b\}_{\alpha\beta} = a_\alpha b_\beta + b_\alpha a_\beta - g_{\alpha\beta} a \cdot b.$$

The differential two-body phase space above is

$$d(PS) = \frac{d^4 k}{(2\pi)^3} \frac{d^4 p'}{(2\pi)^3} (2\pi)^4 \delta^4(p+q-p'-k) \delta^+(k^2) \delta^+(p'^2),$$

where $\delta^+(k^2) = \delta(k^2) \theta(k_0)$.

Exercise. By integrating out the delta functions and the azimuthal angle, show that this can be simplified to

$$d(PS) = \frac{d \cos \theta}{16\pi} = \frac{d\hat{t}}{8\pi(\hat{s} + Q^2)}.$$

To extract F_1 and F_2 from $W_{\alpha\beta}$ (or equivalently their kernels \tilde{F}_1 and \tilde{F}_2 defined in a similar way to $\tilde{W}_{\alpha\beta}$), we contract separately with $g^{\alpha\beta}$ and $P^\alpha P^\beta$.

Exercise. Show that the first-order gluon radiation diagrams give

$$Mg^{\alpha\beta}\tilde{W}_{\alpha\beta} = \left[-\frac{3}{2}\tilde{F}_1 + \frac{\tilde{F}_2}{2x} \right] = \frac{16}{3}\alpha_s \int d(PS)(\hat{t}^2 + \hat{s}^2 - 2\hat{u}Q^2)/(\hat{s}\hat{t}),$$

$$MP^\alpha P^\beta \tilde{W}_{\alpha\beta} = \frac{Q^2}{8x^2} \left[-\tilde{F}_1 + \frac{\tilde{F}_2}{x} \right] = \frac{16}{3}\alpha_s \int d(PS)(-\hat{u})/(2w^2),$$

$$\tilde{F}_1 = \frac{16}{3}\alpha_s \int d(PS) \left(\frac{-\hat{t}^2 - \hat{s}^2 + 2\hat{u}Q^2}{\hat{s}\hat{t}} - \frac{2x^2}{w^2} \frac{\hat{u}}{Q^2} \right),$$

$$\tilde{F}_2 = \frac{16}{3}x\alpha_s \int d(PS) \left(\frac{-\hat{t}^2 - \hat{s}^2 + 2\hat{u}Q^2}{\hat{s}\hat{t}} - \frac{6x^2}{w^2} \frac{\hat{u}}{Q^2} \right).$$

Thus the contributions to xF_1 and F_2 are no longer equal, differing by a non-singular term which we henceforth neglect for simplicity.

The Q^2 -dependence of the structure functions F_1 and F_2 above can be interpreted in terms of Q^2 -dependent parton densities $q(w, Q^2)$. We do this by *defining*

$$x^{-1}F_2(x, Q^2) \equiv \sum_q e_q^2 q(x, Q^2).$$

F_2 is chosen (in preference to F_1) because it satisfies the Adler sum rule in all orders for any Q^2 , consistent with the parton model sum rules. Since F_2 no longer equals xF_1 precisely, there is no simple parton interpretation for the latter and henceforth we focus attention on F_2 .

The expression for $x^{-1}F_2$ becomes, omitting the sum over quarks,

$$x^{-1}F_2 = 4e_q^2\alpha_s \int_x^1 \frac{dw}{w} q(w) \int d(PS) \frac{4}{3} \left[\frac{\hat{s}}{-\hat{t}} + \frac{-\hat{t}}{\hat{s}} + \frac{2\hat{u}Q^2}{\hat{s}\hat{t}} \right],$$

where $q(w)$ is a bare quark distribution, from which the full Q^2 -dependent distribution will be generated. In the lowest order the

Bjorken variable $x = Q^2/(2P \cdot q)$ was the same as the parton momentum fraction w . In this order x and w are independent. It is convenient to introduce a variable z which is their ratio

$$z = \frac{x}{w} = \frac{Q^2}{2p \cdot q} = \frac{Q^2}{\hat{s} + Q^2}.$$

We now change the variable of integration from w to z and express the integrand in terms of \hat{t} , z and Q^2 :

$$x^{-1}F_2(x, Q^2) = \frac{e_q^2 \alpha_s}{2\pi} \int_x^1 \frac{dz}{z} q(x/z) \int_0^{Q^2/z} d(-\hat{t}) \frac{4}{3} \left[\frac{1}{-\hat{t}} \frac{1+z^2}{1-z} - \frac{z^2(\hat{t} + 2Q^2)}{(1-z)Q^4} \right].$$

The lower limit $z = x$ comes from $w \leq 1$. Formally this expression is divergent; there are two types of singularities. The $dz/(1-z)$ integration has a *soft singularity* at $z = 1$ which corresponds to $\hat{s} = Q^2(1-z)/z = 0$; this is the physical threshold with emitted gluon momentum $k = 0$. This *infrared* divergence is cancelled by contributions from one-loop vertex corrections, as we will discuss later; for now we regularize this divergence with a cut-off at $z_{\max} < 1$. The $d\hat{t}/\hat{t}$ integration has a *mass singularity* at $\hat{t} = 0$; this corresponds to the incident quark emitting a collinear gluon (which can be energetic) while itself remaining on mass-shell, which can occur only because they are both massless.

Exercise. Suppose a quark of momentum p and mass m splits into a collinear real quark and real massless gluon. Show that the propagator denominator $(p^2 - m^2)$ of the original quark vanishes only if $m = 0$ or the gluon momentum vanishes.

The *collinear singularity* can be regularized in various ways, for example by a cut-off at $\hat{t} = -\mu^2$ at the lower limit of integration; it will later be absorbed into the definition of the bare quark distribution.

With the above cut-off regularization prescription,

$$x^{-1}F_2 = \frac{e_q^2 \alpha_s}{2\pi} \int_x^{z_{\max}} \frac{dz}{z} q\left(\frac{x}{z}\right) \left[\frac{4}{3} \frac{1+z^2}{1-z} \ln\left(\frac{Q^2}{\mu^2}\right) + f(z) + O\left(\frac{1}{Q^2}\right) \right].$$

For large Q^2 , the $\ln Q^2$ term dominates and $f(z)$ is irrelevant. We can in fact interpret this expression more generally, with μ being any convenient reference mass scale; changing from μ to μ' is equivalent to adding $(4/3)(1+z^2)/(1-z) \ln(\mu'^2/\mu^2)$ to $f(z)$.

The coefficient of the $\ln Q^2$ term in the square brackets is not only independent of the regularization prescription, but also occurs universally in any process where a quark radiates a gluon. It is known as the *quark \rightarrow quark splitting function*

$$P_{qq}(z) = \frac{4}{3} \left(\frac{1+z^2}{1-z} \right).$$

In terms of P_{qq} the leading-logarithm approximation of this contribution to F_2 can be written as

$$\begin{aligned} x^{-1} F_2 &= \frac{e_q^2 \alpha_s}{2\pi} \int_z^{z_{\max}} \frac{dz}{z} q\left(\frac{x}{z}\right) P_{qq}(z) \int_{\mu^2}^{Q^2} \frac{d(-\hat{t})}{-\hat{t}} \\ &= \frac{e_q^2 \alpha_s}{2\pi} \int_{x/z_{\max}}^1 \frac{dw}{w} q(w) P_{qq}\left(\frac{x}{w}\right) \ln\left(\frac{Q^2}{\mu^2}\right). \end{aligned}$$

Adding this to the lowest-order term, we get

$$x^{-1} F_2 = e_q^2 \int \frac{dw}{w} q(w) \left[\delta\left(1 - \frac{x}{w}\right) + \frac{\alpha_s}{2\pi} P_{qq}\left(\frac{x}{w}\right) \ln\left(\frac{Q^2}{\mu^2}\right) \right],$$

where the first term represents direct absorption of γ^* on a quark and the second term represents absorption on a quark which has first radiated a gluon, *i.e.* the t -channel pole diagram of Fig. 7.3. The splitting function P_{qq} describes the probability of a quark turning into a quark (with emission of a gluon).

In order to give a physical picture, we go to the *Breit frame* at

large Q where the photon is purely spacelike and

$$\begin{aligned} q &= (0, 0, 0, -Q), \\ P &= (\tfrac{1}{2}Q/x, 0, 0, \tfrac{1}{2}Q/x), \\ p &= wP = (\tfrac{1}{2}Q/z, 0, 0, \tfrac{1}{2}Q/z). \end{aligned}$$

Since the dominant contribution to F_2 is at small \hat{t} ($\ll Q^2$) due to the $1/\hat{t}$ singularity, the virtual quark remains nearly on mass-shell and all momenta are essentially collinear. In the t -channel exchange diagram (Fig. 7.3(a)) the incident quark splits into a virtual quark plus a collinear real gluon $p \rightarrow p_{\text{vir}} + k$; this virtual quark absorbs the photon to become the final real quark $p_{\text{vir}} + \gamma^* \rightarrow p'$.

Exercise. Show from energy-momentum conservation and mass-shell constraints that

$$\begin{aligned} p_{\text{vir}} &= (\tfrac{1}{2}Q, 0, 0, \tfrac{1}{2}Q) = xP = zp, \\ p' &= (\tfrac{1}{2}Q, 0, 0, -\tfrac{1}{2}Q), \\ k &= (\tfrac{1}{2}Q \frac{1-x}{z}, 0, 0, \tfrac{1}{2}Q \frac{1-x}{z}) = (1-z)p. \end{aligned}$$

Thus in the leading diagram with the \hat{t} -channel pole, the initial quark turns into a virtual quark with momentum fraction z plus a gluon with momentum fraction $1-z$, in this infinite-momentum frame; see Fig. 7.4.

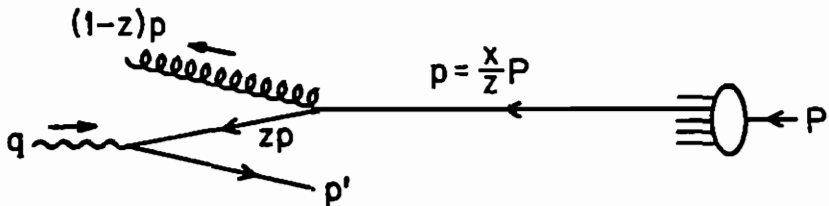


Fig. 7.4. Parton momentum fractions in $\gamma^*q \rightarrow gq$ scattering, for the t -channel diagram in the Breit frame.

7.6 Infrared Cancellation

To see the cancellation of soft divergences between diagrams, a regularization scheme is needed. An elegant scheme is dimensional regularization, introduced by 't Hooft and Veltman, in which Feynman diagrams are evaluated in $D = 4 - 2\epsilon$ dimensions and the singularities in integrated expressions are extracted as poles in $1/\epsilon^2$ and $1/\epsilon$ in the physical limit $\epsilon \rightarrow 0$. In a finite theory the singularities from various diagrams either cancel or can be absorbed in the definitions of physical quantities. In $D \neq 4$ dimensions, the coupling g acquires a dimension which can be explicitly extracted by the replacement $g \rightarrow g\mu^\epsilon$ where μ is an arbitrary mass parameter and the new g is dimensionless. The Dirac algebra in D dimensions is

$$\begin{aligned} \{\gamma^\mu, \gamma^\nu\} &= 2g^{\mu\nu}, & \text{Tr}(\gamma^\mu \gamma^\nu) &= 4g^{\mu\nu}, \\ g_\mu^\mu &= D, & \gamma^\mu \gamma_\mu &= D \mathbf{1}. \end{aligned}$$

Integrals over a virtual momentum become $d^D k = k^{D-1} dk d\Omega_D$ with the angular part $d\Omega_D$ appropriately extended to D dimensions,

$$\begin{aligned} d\Omega_2 &= d\theta_1, \\ d\Omega_3 &= \sin\theta_2 d\theta_2 d\theta_1, \\ d\Omega_D &= \sin^{D-2}\theta_{D-1} \sin^{D-3}\theta_{D-2} \dots \sin\theta_2 d\theta_{D-1} \dots d\theta_1. \end{aligned}$$

For any D , the solid angle is

$$\int d\Omega_D = \frac{2(\pi)^{D/2}}{\Gamma(D/2)}.$$

In $D = 4 - 2\epsilon$ dimensions with the approximation of neglecting the $1/Q^2$ contribution (and hence taking $F_2 = xF_1$), the kernel \tilde{F}_2 from real gluon radiation is

$$x^{-1} \tilde{F}_2|_{\text{rad}} = \frac{16}{3} \alpha_s (\mu^2)^\epsilon (1-\epsilon) \int d(PS) \left[(1-\epsilon) \left(\frac{\hat{s}}{-\hat{t}} + \frac{-\hat{t}}{\hat{s}} \right) + \frac{2\hat{u}Q^2}{\hat{s}\hat{t}} + 2\epsilon \right].$$

The D -dimensional phase space is

$$\begin{aligned} \int d(P S) &= \int \frac{d^D p'}{(2\pi)^{D-1}} \int \frac{d^D k}{(2\pi)^{D-1}} (2\pi)^D \delta^D(p+q-p'-k) \delta^+(p'^2) \delta^+(k^2) \\ &= \frac{1}{8\pi} \left(\frac{4\pi}{\hat{s}} \right)^\epsilon \frac{1}{\Gamma(1-\epsilon)} \int_0^1 \frac{dv}{[v(1-v)]^\epsilon}, \end{aligned}$$

where all variables have been integrated except for the polar angle θ in the $\gamma^* q$ c.m. frame, which is replaced by the variable $v = \frac{1}{2}(1 + \cos \theta)$. The v integration over the $1/\hat{t}$ singularity is finite for small negative ϵ and yields the result as $\epsilon \rightarrow 0$ from negative values

$$\begin{aligned} x^{-1} \tilde{F}_2 \Big|_{\text{rad}} &= \frac{\alpha_s}{2\pi} \left(\frac{4\pi\mu^2}{Q^2} \right)^\epsilon \frac{\Gamma(1-\epsilon)}{\Gamma(1-2\epsilon)} z^\epsilon (1-z)^{-\epsilon} \\ &\quad \times \frac{4}{3} \left(-\frac{1}{\epsilon} \frac{1+z^2}{1-z} + 3 - z - \frac{3}{2} \frac{1}{1-z} - \frac{7}{2} \frac{\epsilon}{1-z} \right). \end{aligned}$$

For the factor $z^\epsilon (1-z)^{-1-\epsilon}$ we use the identity

$$z^\epsilon (1-z)^{-1-\epsilon} \equiv -\frac{1}{\epsilon} \delta(1-z) + \frac{1}{(1-z)_+} + O(\epsilon),$$

where the “+ prescription” defines $1/(1-z)_+$ etc. as distributions

$$\int_0^1 dz \frac{h(z)}{(1-z)_+} \equiv \int_0^1 dz \frac{h(z) - h(1)}{1-z}.$$

The effect is to remove the singularity from $1/(1-z)$ and to express it as $\epsilon^{-1} \delta(1-z)$.

Exercise. Using this definition of the + prescription confirm the above expansion for $z^\epsilon (1-z)^{-1-\epsilon}$.

With these expansions, \tilde{F}_2 becomes

$$\begin{aligned} x^{-1} \tilde{F}_2 \Big|_{\text{rad}} &= \frac{4}{3} \frac{\alpha_s}{2\pi} \left(\frac{4\pi\mu^2}{Q^2} \right)^\epsilon \frac{\Gamma(1-\epsilon)}{\Gamma(1-2\epsilon)} \\ &\quad \times \left\{ \frac{2}{\epsilon^2} \delta(1-z) - \frac{1}{\epsilon} \frac{1+z^2}{(1-z)_+} + \frac{3}{2\epsilon} \delta(1-z) + \text{finite terms as } \epsilon \rightarrow 0 \right\}. \end{aligned}$$

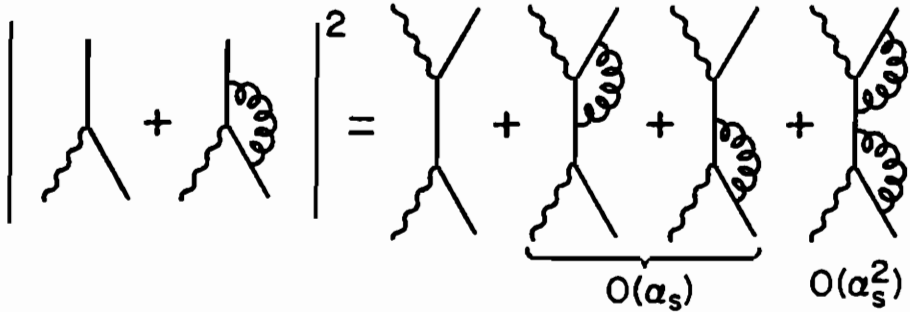


Fig. 7.5. Contributions of vertex diagrams.

The interference of the lowest-order vertex diagram with the virtual-gluon vertex diagram also gives a contribution of order α_s ; see Fig. 7.5. These contributions must be included as well as external quark wave function renormalizations in the lowest-order diagram shown in Fig. 7.6. It is convenient to calculate in the Landau gauge, where ultraviolet divergences are absent from both the vertex correction and the quark self-energy. The sum of the Born term and all the virtual gluon contributions is found to be

$$x^{-1} \tilde{F}_2|_{\text{vir}} = \delta(1-z) \left[1 + \frac{\alpha_s}{2\pi} \left(\frac{4\pi\mu^2}{Q^2} \right)^\epsilon \frac{\Gamma(1-\epsilon)}{\Gamma(1-2\epsilon)} \frac{4}{3} \left(-\frac{2}{\epsilon^2} - \frac{3}{\epsilon} + \text{finite pieces} \right) \right].$$

When Born and virtual gluon contributions are added to the radiative

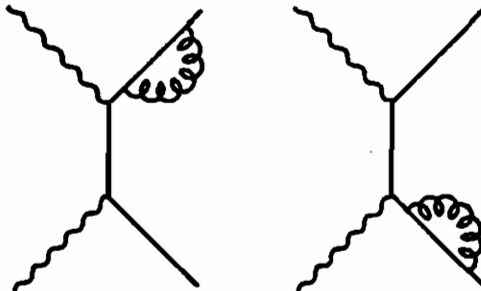


Fig. 7.6. External wave function renormalizations.

contribution, the $1/\epsilon^2$ infrared singularity cancels and we are left with

$$x^{-1} \tilde{F}_2(z, Q^2) = \delta(1-z) - \frac{1}{\epsilon} \frac{\alpha_s}{2\pi} P_{qq}(z) \left(\frac{4\pi\mu^2}{Q^2} \right)^\epsilon \frac{\Gamma(1-\epsilon)}{\Gamma(1-2\epsilon)} + \text{finite terms},$$

where $P_{qq}(z)$ is given by

$$P_{qq}(z) = \frac{4}{3} \frac{1+z^2}{(1-z)_+} + 2\delta(1-z).$$

Exercise. Show that the splitting function can be rewritten as

$$P_{qq}(z) = \frac{4}{3} \left(\frac{1+z^2}{1-z} \right)_+.$$

Noting that

$$-\frac{1}{\epsilon} \left(\frac{\mu^2}{Q^2} \right)^\epsilon = -\frac{1}{\epsilon} + \ln \left(\frac{Q^2}{\mu^2} \right) + O(\epsilon),$$

the $\epsilon \rightarrow 0$ limit of \tilde{F}_2 is

$$x^{-1} \tilde{F}_2(z, Q^2) = \delta(1-z) + \frac{\alpha_s}{2\pi} P_{qq}(z) \left[\ln \left(\frac{Q^2}{\mu^2} \right) - \frac{1}{\epsilon} \right] + \text{finite terms}.$$

The remaining $1/\epsilon$ collinear singularity is independent of Q^2 and must be absorbed into the quark distribution $q(x/z)$. It is a general feature that soft (infrared) singularities are explicitly cancelled by other diagrams and that collinear (mass) singularities are factored out into the bare parton distributions.

The removal of the ϵ^{-1} singularity proceeds as follows in order α_s (it can be done in all orders but is more complicated). The full

equation for F_2 in this order is

$$\frac{F_2(x, Q^2)}{x} = \sum_q e_q^2 \int_x^1 \frac{dz}{z} q\left(\frac{x}{z}\right) \left\{ \delta(1-z) + \frac{\alpha_s}{2\pi} P_{qq} \left[\ln\left(\frac{Q^2}{\mu^2}\right) - \frac{1}{\epsilon} \right] + \alpha_s f_q^{F_2}(z) \right\},$$

where the finite non-leading-log terms $f_q^{F_2}(z)$ are shown explicitly and "higher-twist" contributions of order $1/Q^2$ are neglected. If we redefine the bare quark distributions to be

$$q'(x) = q(x) + \int_x^1 \frac{dz}{z} q\left(\frac{x}{z}\right) \left[\alpha_s f_q^{F_2}(z) - \frac{\alpha_s}{2\pi} P_{qq}(z) \frac{1}{\epsilon} \right],$$

then both ϵ^{-1} and $f_q^{F_2}$ will vanish from the equation for F_2 , in this order. Henceforth we use the redefined bare distributions $q'(x)$, but suppress the prime for simplicity of notation. Note that there is some arbitrariness in choosing whether to absorb some finite terms in addition to the ϵ^{-1} term; it is a matter of convention. The choice made above gives a particularly simple result for $x^{-1}F_2$ but a less simple result for F_1 , which has different non-leading contributions.

7.7 Altarelli-Parisi Equations

The previous sections have shown that the inclusion of gluon radiation from the struck quark introduces an explicit non-scaling Q^2 -dependence into F_2 of the form

$$x^{-1}F_2 = \sum_q e_q^2 \int \frac{dw}{w} q(w) \left[\delta\left(1 - \frac{x}{w}\right) + \frac{\alpha_s}{2\pi} P_{qq}\left(\frac{x}{w}\right) \ln\left(\frac{Q^2}{\mu^2}\right) \right]$$

for large Q^2 (through order α_s) where P_{qq} is defined by the $1/(1-z)_+$ prescription. As mentioned previously, this suggests a redefinition



the quark density at high Q^2 , such that

$$x^{-1} F_2(x, Q^2) = \sum_q e_q^2 q(x, Q^2) = \sum_q e_q^2 [q(x) + \delta q(x, Q^2)]$$

with

$$\delta q(x, Q^2) = \frac{\alpha_s}{2\pi} \ln\left(\frac{Q^2}{\mu^2}\right) \int \frac{dw}{w} q(w) P_{qq}\left(\frac{x}{w}\right).$$

The origin of this Q^2 dependence in the quark density is the Q^2 dependence of the gluon radiation contribution. Physically we can picture it this way: as Q^2 increases, for given x and w , so also the subprocess c.m. energy squared $\hat{s} = Q^2(w/x - 1)$ increases and hence the probability of gluon radiation increases. The virtual photon probe therefore increasingly sees that the quark it is hitting is not simply a point particle, but is capable of becoming a more complex quark-plus-gluon system, which gives non-scaling effects beyond the simple parton model.

Simply adding the contribution of order $\alpha_s \ln Q^2$ to the quark is not enough, since higher terms in the leading logarithmic series $(\alpha_s \ln Q^2)^n$ are important and must be summed. This can be remedied by writing a differential equation for $q(x, Q^2)$,

$$\frac{dq(x, Q^2)}{d(\ln Q^2)} = \frac{\alpha_s}{2\pi} \int_x^1 \frac{dw}{w} q(w, Q^2) P_{qq}\left(\frac{x}{w}\right) + O(\alpha_s^2 \ln Q^2).$$

Solving this equation by iteration will generate contributions to q of order $(\alpha_s \ln Q^2)^n$ from n -fold collinear gluon emission, so these are now implicitly included. These contributions correspond to the *ladder graphs* of Fig. 7.7, when we regard \tilde{F}_2 as the imaginary part of a photon-quark forward scattering amplitude. Thus far we have been using α_s at a fixed renormalization scale μ^2 ; it can be shown that adding the leading log contributions from vertex and propagator

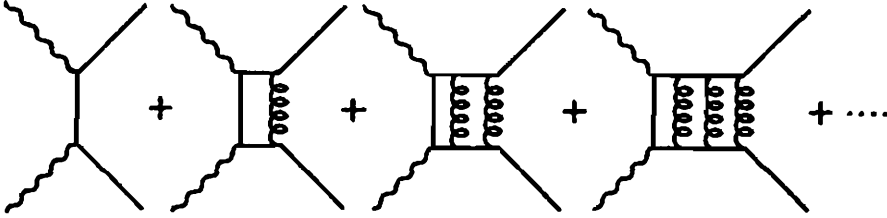


Fig. 7.7. The ladder graphs generated by repeated $q \rightarrow q$ splitting.

insertions in the ladder graphs simply corresponds to replacing α_s by the running coupling $\alpha_s(Q^2)$:

$$\frac{dq(x, Q^2)}{d(\ln Q^2)} = \frac{\alpha_s(Q^2)}{2\pi} \int_x^1 \frac{dw}{w} q(w, Q^2) P_{qq}\left(\frac{x}{w}\right) + O(\alpha_s^2(Q^2)).$$

Since $\alpha_s(Q^2)$ is small at large Q^2 , the $O(\alpha_s^2(Q^2))$ terms can be ignored.

This evolution equation expresses the fact that the quark on which the photon is absorbed could have come from a quark parent with momentum fraction $w > x$. But equally, the struck quark could have come from a gluon parent with $w > x$, via the subprocesses shown in Fig. 7.8. These are related to our previous subprocesses by crossing. Calculation of the corresponding contributions to F_2 leads to a $g \rightarrow q$ splitting function of

$$P_{qg}(z) = \frac{1}{2}[z^2 + (1-z)^2].$$

Adding this contribution from initial gluons and absorbing the ϵ^{-1} singularity into the bare gluon distribution as in the quark case, the quark evolution equation becomes

$$\frac{dq_i(x, Q^2)}{d(\ln Q^2)} = \frac{\alpha_s(Q^2)}{2\pi} \int_x^1 \frac{dw}{w} \left[q_i(w, Q^2) P_{qq}\left(\frac{x}{w}\right) + g(w, Q^2) P_{qg}\left(\frac{x}{w}\right) \right].$$

Here a Q^2 evolution of the gluons is anticipated, although it only

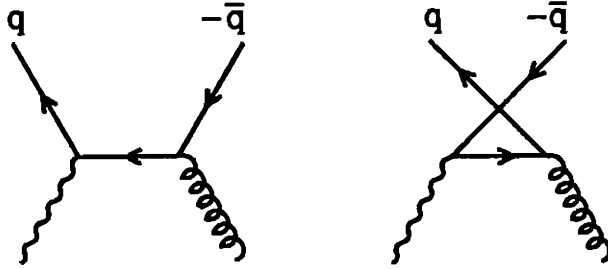


Fig. 7.8. The struck quark could have had a gluon parent.

contributes in order α_s^2 to this equation. An equation of this type applies to each massless quark or antiquark q_i .

Similar considerations apply to gluon evolution. Although photons do not interact with gluons, quark or gluon probes of the gluon distribution at momentum fraction x must take account of the fact that the struck gluon could have come from a parent quark or parent gluon with momentum fraction $w > x$. The quark \rightarrow gluon and gluon \rightarrow gluon splitting functions are found to be

$$P_{gq}(z) = \frac{4}{3} \frac{1 + (1-z)^2}{z},$$

$$P_{gg}(z) = 6 \left[\frac{z}{(1-z)_+} + \frac{1-z}{z} + z(1-z) + \left(\frac{11}{12} - \frac{f}{18} \right) \delta(1-z) \right],$$

where f is the number of quark flavors and the gluon distribution is required to satisfy the momentum sum rule $\int dx x [\sum q(x, Q^2) + g(x, Q^2)] = 1$. The corresponding gluon evolution equation is

$$\frac{dg(x, Q^2)}{d(\ln Q^2)} = \frac{\alpha_s(Q^2)}{2\pi} \int_x^1 \frac{dw}{w} \left[\sum_i q_i(w, Q^2) P_{gq}\left(\frac{x}{w}\right) + g(w, Q^2) P_{gg}\left(\frac{x}{w}\right) \right],$$

where the sum is over both quarks and antiquarks. These equations for the evolution of quark and gluon densities are the *Altarelli-Parisi equations*.

It is interesting to note some properties of the splitting functions. By charge conjugation,

$$P_{\bar{q}q}(z) = P_{qq}(z), \quad P_{g\bar{q}}(z) = P_{gq}(z).$$

Momentum conservation at the splitting vertex gives

$$P_{qg}(z) = P_{qg}(1-z), \quad P_{gg}(z) = P_{gg}(1-z), \quad P_{qq}(z) = P_{qq}(1-z).$$

The integral of $P_{qq}(z)$ over all z vanishes:

$$\int_0^1 P_{qq}(z) dz = 0.$$

Exercise. Show that the vanishing of this integral is necessary and sufficient to guarantee that the quark flavor sum rules $\int (u - \bar{u}) dx = 2$, $\int (d - \bar{d}) dx = 1$, etc. are preserved as Q^2 varies.

Total momentum conservation implies the relations

$$\int_0^1 dz z [P_{qq}(z) + P_{gq}(z)] = 0, \quad \int_0^1 dz z [2f P_{qg}(z) + P_{gg}(z)] = 0.$$

7.8 Solving the Altarelli-Parisi Equations

The Altarelli-Parisi equations allow us to calculate how the parton distributions $q_i(w, Q^2)$ and $g(w, Q^2)$ change with Q^2 , if they are specified at some starting value $Q^2 = Q_0^2$ and $Q^2 \gg \Lambda^2$. This Q^2 dependence explicitly violates Bjorken scaling of structure functions and other scaling predictions of the simple parton model of Chapter 5.

To discuss the solution of these evolution equations, it is conventional to refer the definition of $\alpha_s(Q^2)$ to a scale parameter Λ , as in the leading log form of §7.3 and to define $t = \ln(Q^2/\Lambda^2)$:

$$\alpha_s(Q^2) = \frac{12\pi}{(33 - 2f) \ln(Q^2/\Lambda^2)} = \frac{1}{4\pi b t}.$$

We introduce the symbolic notation

$$P_{qq} \otimes q_i = \int_x^1 \frac{dw}{w} P_{qq}\left(\frac{x}{w}\right) q_i(w, t)$$

and similarly for other convolutions. The equations are then written compactly as

$$\begin{aligned} \frac{dq_i}{dt}(x, t) &= \frac{\alpha_s(t)}{2\pi} [P_{qq} \otimes q_i + P_{qg} \otimes g], \\ \frac{dg}{dt}(x, t) &= \frac{\alpha_s(t)}{2\pi} [P_{gq} \otimes \sum_i q_i + P_{gg} \otimes g]. \end{aligned}$$

To solve these integro-differential equations we need to specify initial conditions at $t = t_0$, chosen such that perturbation theory applies for $t > t_0$. These initial parton distributions are determined from data with Q^2 near $Q_0^2 \sim 2\text{-}5 \text{ GeV}^2$ typically, by fitting them to a “scaling” parametrization. The value of Λ affects the Q^2 dependence predicted by the A-P equations, and can therefore be inferred from experiment. With the first-order form for $\alpha(t)$ above, the analysis of deep inelastic lepton scattering data gives values of order $\Lambda \approx 0.2 \text{ GeV}$ (but the result is sensitive to assumptions about the input gluon distribution).

The equations above assume all quarks are massless. The simplest scheme for taking account of the masses of heavy quarks (such as c and b) is to decouple them from the equations below some effective threshold such as $Q^2 = 4m_c^2$ for charm; *i.e.* $c(x, t) = \bar{c}(x, t) = 0$ for

$t < t_c = \ln(4m_c^2/\Lambda^2)$. One starts with $u, d, s, \bar{u}, \bar{d}, \bar{s}, g$ distributions at t_0 and evolves them up to t_c with $f = 3$ active flavors and a scale parameter Λ_3 . In this regime

$$\alpha_s = 1/(4\pi b_3 t_3),$$

where

$$b_f = (33 - 2f)/(48\pi^2), \quad t_f = \ln(Q^2/\Lambda_f).$$

For $t > t_c$, the c and \bar{c} distributions enter the equations and the evolution proceeds with $f = 4$ flavors. Since $\alpha_s(t)$ must be continuous across the threshold, Λ_4 is determined from Λ_3 via $b_3 \ln(4m_c^2/\Lambda_3^2) = b_4 \ln(4m_c^2/\Lambda_4^2)$. In this simplified treatment, mass effects enter only through thresholds and the massless approximation to the equations is used. More complicated prescriptions for mass effects have been considered in the literature, including mass-dependent terms in the splitting functions, but we do not pursue them here.

A helpful simplification of the equations occurs if we work with the following linear combinations of the quark densities (which are non-singlets or singlets under $SU(f)$ flavor symmetry).

Singlet distribution:

$$q^S(x, t) = \sum_i (q_i + \bar{q}_i)$$

summed over all active flavors $i = 1, 2, \dots, f$.

Non-singlet distributions, generically labeled as $q^{NS}(x, t)$; there are many of these, including

$$u_v = u - \bar{u}, \quad d_v = d - \bar{d}, \quad q_i^{NS} = q_i - (2f)^{-1} q^S,$$

and linear combinations thereof. These satisfy the equations

$$\frac{dq^{NS}}{dt}(x, t) = \frac{\alpha_s(t)}{2\pi} P_{qq} \otimes q^{NS},$$

$$\frac{dq^S}{dt}(x, t) = \frac{\alpha_s(t)}{2\pi} [P_{qq} \otimes q^S + 2f P_{qg} \otimes g],$$

$$\frac{dg}{dt}(x, t) = \frac{\alpha_s(t)}{2\pi} [P_{gq} \otimes q^S + P_{gg} \otimes g].$$

These equations can be solved in various ways, for example by direct numerical integration step-by-step in t , or by inverting moments as we describe below. The non-singlet distributions are decoupled; the singlet and the gluon evolution equations are coupled, however. For numerical integration, it is helpful to reduce the singularity at small x by taking equations for x times the parton distributions.

Exercise. Show that the evolution equation for $p^{NS} = xq^{NS}$ can be written

$$\begin{aligned} \frac{dp(x, t)}{dt} &= \frac{\alpha_s(t)}{2\pi} \int_x^1 dz P_{qq}(z) p(x/z, t) \\ &= \frac{2\alpha_s(t)}{3\pi} \int_x^1 \frac{dz}{1-z} [(1+z^2) p(x/z, t) - 2p(x, t)] \\ &\quad + \frac{\alpha_s(t)}{\pi} \left[1 + \frac{4}{3} \ln(1-x) \right] p(x, t). \end{aligned}$$

Remember that the $+$ prescription refers to integrals from 0 to 1.

We define the n^{th} moment of a parton distribution $p(x, t) = q^{NS}$, q^S or g by

$$p_n(t) = \int_0^1 x^{n-1} p(x, t) dx$$

and denote the integrals of the splitting functions as

$$A_n = \int_0^1 dz z^{n-1} P(z).$$

Then the moments of the A-P equations have a factorized form:

$$\begin{aligned} \frac{dq_n^{NS}}{dt} &= \frac{\alpha_s(t)}{2\pi} A_n^{qq} q_n^{NS}, \\ \frac{dq_n^S}{dt} &= \frac{\alpha_s(t)}{2\pi} [A_n^{qq} q_n^S + 2f A_n^{qg} g_n], \\ \frac{dg_n}{dt} &= \frac{\alpha_s(t)}{2\pi} [A_n^{gq} q_n^S + A_n^{gg} g_n]. \end{aligned}$$

Since $\alpha = 1/(4\pi bt)$, these equations can be simply integrated. For example, the solution for the non-singlet moments is

$$q_n^{NS}(t) = q_n^{NS}(t_0) (t/t_0)^{A_n^{qq}/(8\pi^2 b)} = q_n^{NS}(t_0) [\alpha(t_0)/\alpha(t)]^{A_n^{qq}/(8\pi^2 b)}.$$

The singlet moments have an analogous matrix solution. Notice that this solution has the general form of the LLA solutions to the RGE of §7.4. The moments of the structure functions are physical quantities that satisfy RGE and the moments of the splitting functions such as A_n^{qq} are $4\pi^2$ times the first coefficients γ_1 of their anomalous dimensions. In fact the A-P equations were originally derived starting from the moment equations.

The second moments ($n = 2$) of parton densities are particularly interesting, since they are the corresponding contributions to the momentum sum rule.

Exercise. Show that $A_2^{qq} = -\frac{16}{9}$ and hence that the valence quark contributions to the momentum sum rule tend to zero as $t \rightarrow \infty$.

Exercise. Derive the $n = 2$ singlet equations

$$\begin{aligned}\frac{dq_2^S}{dt} &= \frac{\alpha}{2\pi} \left[-\frac{16}{9} q_2^S + \frac{f}{3} g_2 \right], \\ \frac{dg_2}{dt} &= \frac{\alpha}{2\pi} \left[\frac{16}{9} q_2^S - \frac{f}{3} g_2 \right].\end{aligned}$$

Hence confirm that the momentum sum rule $q_2^S + g_2 = 1$ is independent of t and that the linear combination $\frac{16}{9}q_2^S - \frac{f}{3}g_2$ tends to zero asymptotically. Show that gluons carry a fraction $\frac{16}{(16+3f)}$ of the momentum as $t \rightarrow \infty$, where f is the number of active quark flavors.

Finally the parton x -distributions can be recovered from the moment solution by an inverse Mellin transform, after formally continuing the moment solution analytically into a region of the complex n plane. For example,

$$q^{NS}(x, t) = \frac{1}{2\pi i} \int_{C-i\infty}^{C+i\infty} q_n^{NS}(t) x^{-n} dn,$$

where $C > 2$. Changing variables to $dn = i d\nu$ and $u = -\frac{1}{2\pi} \ln x$, the solution can be written as a Fourier transform

$$q^{NS}(x, t) = \frac{x^{-C}}{2\pi} \int_{-\infty}^{\infty} e^{2\pi i \nu u} q_\nu^{NS}(t) d\nu.$$

There are efficient numerical techniques (fast Fourier transform) for evaluating these integrals.

7.9 Solutions of the A-P Equations

For practical applications, solutions to the A-P equations are sometimes presented in the form of approximate numerical parameterizations, in which the Q^2 -dependence enters through the variable

$$\bar{s} = \ln(t/t_0) = \ln [\ln(Q^2/\Lambda^2) / \ln(Q_0^2/\Lambda^2)],$$

which varies slowly with changing Q^2 .

For example, the Duke-Owens 1 parameterization (which is evolved from the scaling parameterization A of §5.6 at $Q^2 = Q_0^2 = 4 \text{ GeV}^2$) expresses the valence quark distributions as follows:

$$x(u_v + d_v) = N_{ud} x^{\eta_1} (1-x)^{\eta_2} (1 + \gamma_{ud} x),$$

$$x d_v = N_d x^{\eta_3} (1-x)^{\eta_4} (1 + \gamma_d x),$$

where

$$N_{ud} = 3 / \{B(\eta_1, \eta_2 + 1) [1 + \gamma_{ud} \eta_1 / (\eta_1 + \eta_2 + 1)]\},$$

$$N_d = 1 / \{B(\eta_3, \eta_4 + 1) [1 + \gamma_d \eta_3 / (\eta_3 + \eta_4 + 1)]\}.$$

Here $B(\alpha, \beta)$ is the Euler beta function. The coefficients are:

$$\eta_1 = 0.419 + 0.004\bar{s} - 0.007\bar{s}^2, \quad \eta_3 = 0.763 - 0.237\bar{s} + 0.026\bar{s}^2,$$

$$\eta_2 = 3.46 + 0.724\bar{s} - 0.066\bar{s}^2, \quad \eta_4 = 4.00 + 0.627\bar{s} - 0.019\bar{s}^2,$$

$$\gamma_{ud} = 4.40 - 4.86\bar{s} + 1.33\bar{s}^2, \quad \gamma_d = -0.421\bar{s} + 0.033\bar{s}^2.$$

The light quark sea is flavor-independent,

$$x\bar{u} = x\bar{d} = x\bar{s} \equiv xS,$$

and xS , xc , xg are all parameterized as

$$Ax^a(1-x)^b(1 + \alpha x + \beta x^2 + \gamma x^3)$$

with the following coefficients:

$$xS: A = 0.211 - 0.189\bar{s} + 0.049\bar{s}^2$$

$$a = -0.372\bar{s} - 0.029\bar{s}^2$$

$$b = 8.05 + 1.59\bar{s} - 0.153\bar{s}^2$$

$$\alpha = 6.31\bar{s} - 0.273\bar{s}^2$$

$$\beta = -10.5\bar{s} - 3.17\bar{s}^2$$

$$\gamma = 14.7\bar{s} + 9.80\bar{s}^2$$

$$xc: A = 0.135s - 0.075\bar{s}^2$$

$$a = -0.036 - 0.222\bar{s} - 0.058\bar{s}^2$$

$$b = 6.35 + 3.26\bar{s} - 0.909\bar{s}^2$$

$$\alpha = -3.03\bar{s} + 1.50\bar{s}^2$$

$$\beta = 17.4 - 11.3\bar{s}^2$$

$$\gamma = -17.9\bar{s} + 15.6\bar{s}^2$$

$$xg: A = 1.56 - 1.71\bar{s} + 0.638\bar{s}^2$$

$$a = -0.949\bar{s} + 0.325\bar{s}^2$$

$$b = 6.0 + 1.44\bar{s} - 1.05\bar{s}^2$$

$$\alpha = 9.0 - 7.19\bar{s} + 0.255\bar{s}^2$$

$$\beta = -16.5\bar{s} + 10.9\bar{s}^2$$

$$\gamma = 15.3\bar{s} - 10.1\bar{s}^2$$

This parameterization gives reasonable accuracy for most of the x range up to $Q^2 \sim 10^6$ GeV but is unreliable near $x = 1$ and for very small $x \ll 0.01$. The solution of Eichten *et al.* (EHLQ) is evolved from the scaling parameterization B of §5.6 at $Q^2 = Q_0^2 = 5$ GeV². These authors couple heavy quarks $Q = c, b, t$ into the equations above their production thresholds $Q^2(1-z)/z > 4m^2$, with explicit heavy quark mass dependence in the corresponding $g \rightarrow Q$ splitting functions. The results for typical parton distributions $q_i(x, Q^2)$ are presented in the form

$$q_i(x, Q^2) = x^{-1}(1-x)^a \sum_{ijk} c_{ijk} P_j(x) P_k(\ln Q^2),$$

where P_j and P_k are specified polynomials. For $x < 0.1$, polynomials in $\ln x$ are used instead of polynomials in x . There 576 coefficients c_{ijk} per solution; see Rev. Mod. Phys. 56, 579 (1984) and Erratum for the details.

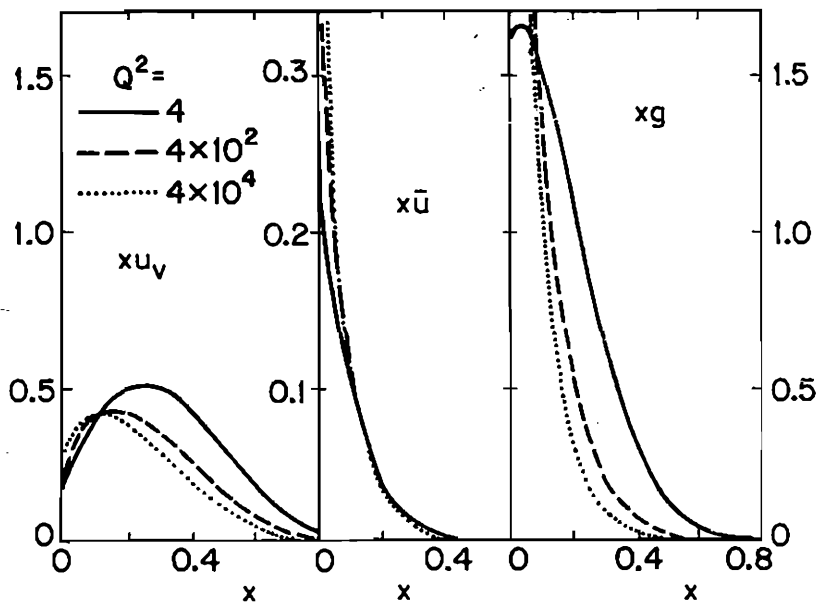


Fig. 7.9 Q^2 -evolution of parton distributions (Duke-Owens solution).

Figure 7.9 illustrates the evolution of parton distributions in the Duke-Owens solution; $xu(x, Q^2)$, $x\bar{u}(x, Q^2)$ and $xg(x, Q^2)$ are shown versus x for $Q^2 = 4, 4 \times 10^2, 4 \times 10^4$ GeV². The area under the curves represents the corresponding contributions to the momentum sum rule; the progressive reduction of the typical valence u_v contribution can be seen. The logarithmic evolution toward softer distributions as Q^2 increases, with sea and gluon dominance, is evident.

Finally we note that at very small x the A-P equations lend themselves to analytic solution, in various approximation. In this region the evolution equations are dominated by the z^{-1} singularities in the splitting functions P_{gq} and P_{gg} .

Exercise. Assuming that $xg^S(x, t) \ll xg(x, t)$ and approximating $P_{gg}(z) = 6/z$, show that the gluon evolution equation at very small x leads to

$$\frac{\partial^2 [xg(x, t)]}{\partial \ln(1/x) \partial \ln t} = \frac{3}{4\pi^2 b} xg(x, t)$$

and that a solution is

$$xg(x, t) = (\text{constant}) \exp \left[\frac{144}{33 - 2f} \ln \left(\frac{x_0}{x} \right) \ln \left(\frac{t}{t_0} \right) \right]^{1/2}$$

so long as $\ln(x_0/x) \ln(t/t_0) \gg 1$.

7.10 QCD Corrections to Fragmentation

The effects of QCD radiative processes on fragmentation functions are closely analogous to their effects on parton distributions. Take for example the production in e^+e^- collisions of a hadron h carrying a fraction z of the incident beam energy. The cross section is described by structure functions \bar{F}_1 and \bar{F}_2 as in §6.2. To zeroth order each quark contribution is simply a multiple of $D_q^h(z)$. However, to first order in α_s the quark can emit a gluon with energy fraction $(1 - z')$ and two new contributions then arise, as shown in Fig. 7.10. (i) The daughter quark can fragment to h with probability $D_q^h(z/z')$ and (ii) the gluon can fragment to h with probability $D_g^h(z/z'')$ where we put $z'' = 1 - z'$. This splitting of a quark into quark plus gluon is most likely in collinear configurations, where the matrix element is singular and the process is described by the same splitting functions P_{qq} and P_{gq} as we encountered in previous sections. The QCD corrections get stronger as the c.m. energy squared $s = q^2$ increases. If we define the

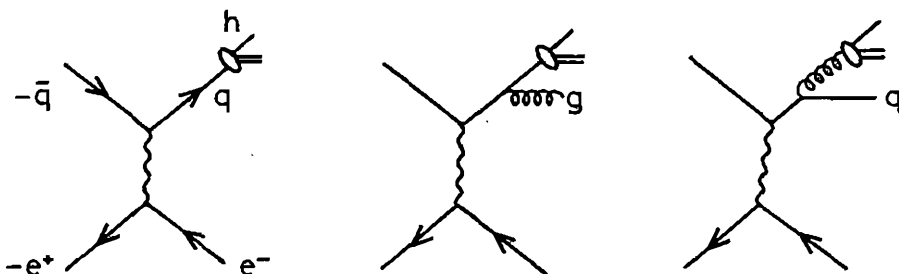


Fig. 7.10. Zeroth and first-order QCD contributions to fragmentation.

q^2 -dependent fragmentation functions $D_k^h(z, q^2)$ by $z^2 \bar{F}_{2k}(z, q^2)$, they obey leading-log evolution equations very similar to the Altarelli-Parisi equations,

$$\frac{dD_q^h(z, t)}{dt} = \frac{\alpha(t)}{2\pi} \int_0^1 \frac{dw}{w} [P_{qq}(w)D_q^h(z/w) + P_{gq}(w)D_g^h(z/w)] ,$$

$$\frac{dD_g^h(z, t)}{dt} = \frac{\alpha(t)}{2\pi} \int_0^1 \frac{dw}{w} \left\{ P_{qg}(w) \sum_i [D_q^h(z/w) + D_g^h(z/w)] + P_{gg}(w)D_g^h(z/w) \right\} ,$$

where $t = \ln(q^2/\Lambda^2)$ and i sums over quark flavors. For heavy flavors the appropriate thresholds are understood.

These evolution equations can be solved explicitly by direct integration or via the inversion of moments, just as for quark distributions. The effect of this evolution is that D -functions become more weighted toward lower z -values as Q^2 increases; see Fig. 7.11. The physical meaning is clear; since the likelihood of radiation increases with Q^2 , the likelihood that the fragmenting parton carries a large fraction of the maximum energy goes down, and the z -distribution of each fragmentation product becomes softer.

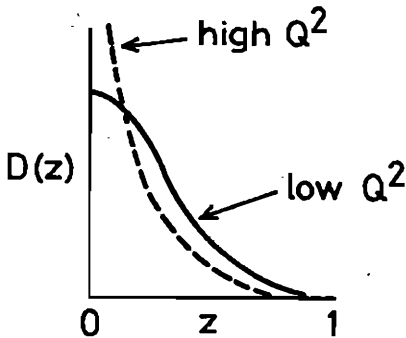


Fig. 7.11. Qualitative Q^2 -evolution of fragmentation functions.

7.11 QCD and the Drell-Yan Process

Let us consider first lepton pairs with mass $m \ll M_Z$ so that we can neglect the virtual Z contribution. To zeroth order in the QCD coupling, the hadronic part of the Drell-Yan process is the annihilation of a $q\bar{q}$ pair to a virtual photon with $q^2 = m^2$. To first order in α_s there are additional terms in which either q or \bar{q} has been radiated from a quark or gluon parent, and also terms in which a virtual gluon has been exchanged, as shown in Fig. 7.12. There is a close analogy between the case of the total cross section $d\sigma^{DY}/dq^2$ and the case of electromagnetic structure functions: the Feynman diagrams are simply related by crossing the γ and \bar{q} lines, and in both cases there is a summation over final hadronic states at fixed q^2 . If the real and virtual gluon terms are evaluated to order α_s , the infrared singularities cancel and the resulting cross section has the form

$$\begin{aligned} \frac{d\sigma^{DY}}{dq^2}(AB \rightarrow \ell\bar{\ell}X) = & \sum_q e_q^2 \int_0^1 dx_a \int_0^1 dx_b \frac{4\pi\alpha^2}{9s^2} \left\{ \left[q^A(x_a)\bar{q}^B(x_b) + A \leftrightarrow B \right] \right. \\ & \cdot \left[\delta(1-z) + \theta(1-z) \frac{\alpha_s}{2\pi} 2P_{qq}(z) \left(-\frac{1}{\epsilon} + \ln \frac{q^2}{\mu^2} \right) + \alpha_s f_q^{DY}(z) \right] \\ & \left. + \left[(q^A(x_a) + \bar{q}^A(x_a))g^B(x_b) + A \leftrightarrow B \right] \left[\theta(1-z) \frac{\alpha_s}{2\pi} P_{qg}(z) \left(-\frac{1}{\epsilon} + \ln \frac{q^2}{\mu^2} \right) + \alpha_s f_g^{DY}(z) \right] \right\}. \end{aligned}$$

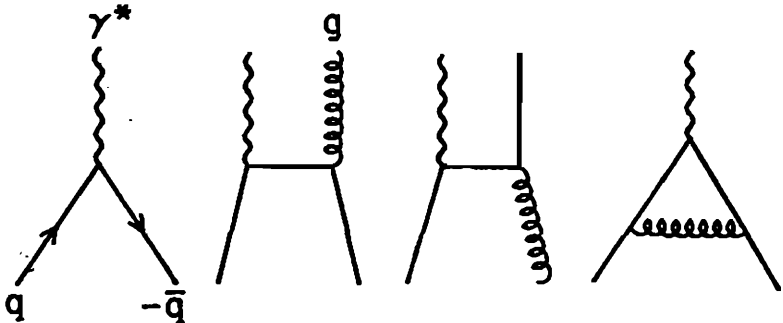


Fig. 7.12 Zeroth and first order QCD contributions to the Drell-Yan process.

Here $z = \tau/(x_a x_b) = q^2/\hat{s}$; q and g are the bare quark and gluon distributions. $P_{qq}(z)$ and $P_{qg}(z)$ are the same splitting functions as in the evaluation of F_2 , (the factor 2 with P_{qq} arises because either incident quark can radiate a quark) but the non-leading terms f_q^{DY} and f_g^{DY} differ from the F_2 case. This expression should be compared to the full equation for F_2 at the end of §7.6 (after adding a gluon contribution to the latter). The $1/\epsilon$ singularities and the leading logarithmic $\alpha_s \ln(q^2/\mu^2)$ terms in $d\sigma/dq^2$ will all be absorbed if we replace $q(x)$ by the full quark contribution to $x^{-1}F_2$, *i.e.* by the Q^2 -dependent quark distribution, evaluated at $Q^2 = q^2$, as follows:

$$\begin{aligned} \frac{d\sigma^{DY}}{dq^2}(AB \rightarrow \ell\bar{\ell}X) &= \sum_q e_q^2 \int_0^1 dx_a \int_0^1 dx_b \left(\frac{4\pi\alpha^2}{9\hat{s}^2} \right) \\ &\cdot \left\{ \left[q^A(x_a, q^2) \bar{q}^B(x_b, q^2) + A \leftrightarrow B \right] \left[\delta(1-z) + \theta(1-z)\alpha_s \left(f_q^{DY} - 2f_q^{F_2} \right) \right] \right. \\ &+ \left. \left[\left(q^A(x_a, q^2) + \bar{q}^A(x_a, q^2) \right) g^B(x_b) + A \leftrightarrow B \right] \theta(1-z)\alpha_s \left(f_g^{DY} - f_g^{F_2} \right) \right\}. \end{aligned}$$

This expression shows that the leading-logarithm corrections to $d\sigma/dq^2$ are taken into account by introducing q^2 -dependent quark distributions into the original Drell-Yan formula of Chapter 5. Note however that the definition of $q(x, Q^2) = x^{-1}F_2(x, Q^2)$ related originally to a spacelike probe ($q^2 < 0$, $Q^2 = -q^2$); we are now using it in connection with a timelike probe, where q^2 is equally large but of the opposite sign ($q^2 > 0$, $Q^2 = q^2$). There remain non-leading corrections, represented by the differences of coefficient functions f , which turn out to be important at q^2 values of present interest. Their explicit forms are

$$\begin{aligned} \alpha_s \left(f_q^{DY} - 2f_q^{F_2} \right) &= \frac{\alpha_s}{2\pi} \frac{4}{3} \left\{ \frac{3}{(1-z)_+} - 6 - 4z + 2(1+z^2) \left[\frac{\ln(1-z)}{1-z} \right]_+ \right. \\ &+ \left. \left(1 + \frac{4\pi^2}{3} \right) \delta(1-z) \right\}, \end{aligned}$$

$$\alpha_s \left(f_g^{DY} - f_g^{F_2} \right) = \frac{\alpha_s}{2\pi} \frac{1}{2} \left\{ [z^2 + (1-z)^2] \ln(1-z) + \frac{9}{2} z^2 - 5z + \frac{3}{2} \right\}.$$

Numerically the important contributions are the last two terms in the f_q case. The first of these, containing $\ln(1-z)$, can be traced to the difference in final two-body phase space between the F_2 and DY cases, for given Q^2 . The other important contribution, containing a factor $\delta(1-z)$, has the effect simply of multiplying the leading Drell-Yan cross section formula by an overall factor; it is dominated by the $4\pi^2/3$ part, which has the following interesting physical origin. In evaluating the virtual gluon contributions to F_2 and $d\sigma^{DY}/dq^2$ to order α_s , we encounter twice the real part of the loop graph amplitude which contains the factor

$$\begin{aligned} & \frac{\alpha_s}{2\pi} \frac{4}{3} \left(\frac{4\pi\mu^2}{-q^2} \right)^\epsilon \frac{\Gamma(1+\epsilon)\Gamma^2(1-\epsilon)}{\Gamma(1-2\epsilon)} \left[-\frac{2}{\epsilon^2} - \frac{3}{\epsilon} - 8 + O(\epsilon) \right], \\ F_2: & \rightarrow \frac{\alpha_s}{2\pi} \frac{4}{3} \left(\frac{4\pi\mu^2}{Q^2} \right)^\epsilon \frac{\Gamma(1-\epsilon)}{\Gamma(1-2\epsilon)} \left[-\frac{2}{\epsilon^2} - \frac{3}{\epsilon} - 8 - \frac{\pi^2}{3} + O(\epsilon) \right], \\ DY: & \rightarrow \frac{\alpha_s}{2\pi} \frac{4}{3} \left(\frac{4\pi\mu^2}{q^2} \right)^\epsilon \frac{\Gamma(1-\epsilon)}{\Gamma(1-2\epsilon)} \left[-\frac{2}{\epsilon^2} - \frac{3}{\epsilon} - 8 + \frac{2\pi^2}{3} + O(\epsilon) \right]. \end{aligned}$$

The $-\pi^2/3$ term in the F_2 case arises from substituting $\Gamma(1-\epsilon)\Gamma(1+\epsilon) = 1 + \epsilon^2\pi^2/6 + O(\epsilon^4)$ and picking up the corresponding correction to the ϵ^{-2} pole. In the DY case there is an additional correction factor $(-1)^\epsilon$, because q^2 is now timelike; $\Re(-1)^\epsilon = 1 - \epsilon^2\pi^2/2 + O(\epsilon^4)$. There is therefore a non-leading correction

$$\alpha_s \left(f_q^{DY} - 2f_q^{F_2} \right) \simeq \frac{\alpha_s}{2\pi} \left(\frac{4\pi}{3} \right)^2 \delta(1-z),$$

which contains the factor $\delta(1-z)$ because it involves only virtual gluons. With the other $\delta(1-z)$ term it gives an overall correction

factor K to the leading-order Drell-Yan cross section, with

$$K = 1 + \frac{\alpha_s}{2\pi} \frac{4}{3} \left(1 + \frac{4}{3} \pi^2 \right),$$

where α_s is understood to mean $\alpha_s(q^2)$ by renormalization group arguments. The complete non-leading correction contains the other terms too and cannot be precisely expressed as a single overall factor. However, it is often approximated in discussions by the factor above (sometimes keeping the π^2 term only). It is commonly referred to as the K -factor. With $\Lambda = 0.2$, $Q^2 = 10$, $f = 4$ we find typically $K = 1.8$, showing a considerable correction.

The preceding discussion applies specifically to $d\sigma^{DY}/dq^2$. In the case of the rapidity distribution $d\sigma^{DY}/dq^2 dy$ a similar discussion can be made but the details will differ. In the $O(\alpha_s)$ subprocesses $q\bar{q} \rightarrow \gamma^* g$ and $qg \rightarrow \gamma^* q$, the lab rapidity y of the massive photon depends on the scattering angle, so the phase-space integrals are not identical with those for $d\sigma^{DY}/dq^2$. However the non-leading $\delta(1-z)$ contributions from the virtual gluon diagram continue to appear as a simple multiplicative correction to the zeroth order approximation. With these delta-function corrections only, we obtain

$$\frac{d\sigma^{DY}}{dy dq^2} = \frac{4\pi\alpha^2 K}{9s^2} \sum_q \frac{e_q^2}{x_a x_b} \left\{ q^A(x_a, q^2) \bar{q}^B(x_b, q^2) + (A \leftrightarrow B) \right\},$$

which is the original parton model formula (§5.8) with quark distributions evolved up to $Q^2 = q^2$ and the same overall multiplicative correction factor K as in $d\sigma^{DY}/dq^2$. The complete non-leading correction contains other terms too, which appear to be numerically unimportant for $\tau = q^2/s < 0.2$.

We now consider momentum components p_T transverse to the hadron beam axis. Although radiative QCD processes can give quarks with non-zero p_T , the Altarelli-Parisi equations concentrate attention on the singular collinear configurations so that the Q^2 -dependent parton distributions evolved from them refer always to partons collinear

with the parent hadrons. Hence the lowest order subprocess $q\bar{q} \rightarrow \gamma^* \rightarrow \ell\bar{\ell}$ always gives lepton pairs with zero p_T . Non-zero p_T arises first in the $O(\alpha_s)$ subprocesses $q\bar{q} \rightarrow \ell\bar{\ell}g$ and $qg \rightarrow \ell\bar{\ell}q$. It is useful to record here the full cross section formulas, in which both leptons are treated as independent particles:

$$d\sigma(q\bar{q} \rightarrow \ell\bar{\ell}g) = \frac{64e_q^2\alpha^2\alpha_s}{9\pi^2m^2\hat{s}\hat{t}\hat{u}} [(\ell \cdot q)^2 + (\ell \cdot \bar{q})^2 + (\bar{\ell} \cdot q)^2 + (\bar{\ell} \cdot \bar{q})^2] \times \prod_{i=\ell,\bar{\ell},g} \frac{d^3p_i}{2E_i} \delta^4(q + \bar{q} - \ell - \bar{\ell} - g),$$

where m is the dilepton mass and $\hat{s}, \hat{t}, \hat{u}$ are the Mandelstam invariants for the subprocess $q\bar{q} \rightarrow \gamma^*g$. The cross section for $qg \rightarrow \ell\bar{\ell}q$ is simply related to this by crossing the matrix element and multiplying by 3/8 for the change in color averaging. Integrating over the internal orientation of the lepton pair then gives

$$\frac{d\sigma}{dm^2 d\hat{t}}(q\bar{q} \rightarrow \ell\bar{\ell}g) = \frac{8e_q^2\alpha^2\alpha_s}{27m^2} \frac{(\hat{t} - m^2)^2 + (\hat{u} - m^2)^2}{\hat{s}^2\hat{t}\hat{u}},$$

where $\hat{s} = (q + \bar{q})^2$, $\hat{t} = (q - g)^2$, $\hat{u} = (\bar{q} - g)^2$ and

$$\frac{d\sigma}{dm^2 d\hat{t}}(qg \rightarrow \ell\bar{\ell}q') = \frac{e_q^2\alpha^2\alpha_s}{9m^2} \frac{(\hat{s} - m^2)^2 + (\hat{u} - m^2)^2}{-\hat{s}^2\hat{u}},$$

where $\hat{s} = (q + g)^2$, $\hat{t} = (q - q')^2$, $\hat{u} = (g - q')^2$. In each case $m^2 = q^2$, $p_T^2 = \hat{t}\hat{u}/\hat{s}$ and $-d\hat{t} = \hat{s}(\hat{t} - \hat{u})^{-1} dp_T^2$. These subprocess cross sections, convoluted with parton distributions, are the leading contributions to $d\sigma^{DY}/dm^2 dp_T^2$. Non-leading contributions have been found to give K -factor enhancements comparable to the case of $d\sigma^{DY}/dq^2$. Both subprocesses contribute $(p_T)^{-2}$ singularities, expressing the fact that the emission of a single soft or collinear light quantum with small p_T diverges as $p_T \rightarrow 0$. This singularity can be averted however by summing multiple small- p_T emissions, for example in a QCD shower calculation.

7.12 Direct Photons

The production of high- p_T real photons is similar to the Drell-Yan process (which gives virtual photons) and in principle offers another way to test QCD predictions. The lowest order subprocesses

$$q\bar{q} \rightarrow \gamma g, \quad gq(\bar{q}) \rightarrow \gamma q(\bar{q}),$$

are shown in Fig. 7.13.

Exercise. Derive the subprocess cross sections

$$\frac{d\sigma}{d\hat{t}}(q\bar{q} \rightarrow \gamma g) = \frac{8\pi\alpha\alpha_s e_q^2}{9} \frac{\hat{t}^2 + \hat{u}^2}{\hat{s}^2 \hat{t} \hat{u}},$$

where $\hat{s} = (q + \bar{q})^2$, $\hat{t} = (q - g)^2$, $\hat{u} = (\bar{q} - g)^2$ and

$$\frac{d\sigma}{d\hat{t}}(gq \rightarrow \gamma q') = \frac{\pi\alpha\alpha_s e_q^2}{3} \frac{\hat{s}^2 + \hat{u}^2}{-\hat{s}^3 \hat{u}},$$

where $\hat{s} = (q + g)^2$, $\hat{t} = (q - q')^2$ and $\hat{u} = (g - q')^2$.

At high p_T the signature for such an event would be a hadron jet (or jets) balancing an electromagnetic shower (no fast hadrons in the central detector). Although an energetic π^0 has the same signature as γ ($\pi^0 \rightarrow \gamma\gamma$ with the photons unresolved), such π^0 are most likely to be formed in a jet and not in isolation.

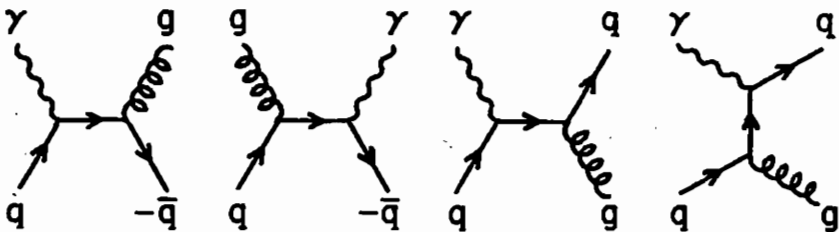


Fig. 7.13. $O(\alpha_s)$ diagrams for direct photon production in hadron-hadron collisions.

Chapter 8

Weak Boson Production and Decay

8.1 W Decays

The experimental discovery of weak bosons at the CERN $p\bar{p}$ collider gave spectacular support to the standard electroweak gauge theory that had predicted them. These bosons are detected by their decays. In the standard model W and Z decay through their fundamental gauge couplings to the basic quarks and leptons. The first detected W decays were the leptonic modes $W \rightarrow e\nu$. The amplitude for $W^- \rightarrow e^- + \bar{\nu}_e$ decay is

$$\mathcal{M} = -i \frac{g}{\sqrt{2}} \epsilon_\alpha^\lambda(P) \bar{u}(\ell) \gamma^\alpha \frac{1}{2} (1 - \gamma_5) v(k),$$

where the momenta are labeled in Fig. 8.1 and g is the charged

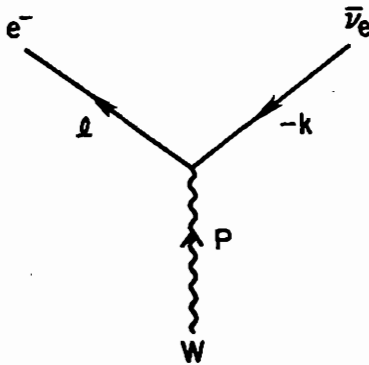


Fig. 8.1. Leptonic decay mode $W^- \rightarrow e^- \bar{\nu}_e$.

current coupling defined in Chapter 2. Averaging $|\mathcal{M}|^2$ over W -polarizations and summing over the fermion spins, we obtain in the massless ν_e, e approximation

$$\begin{aligned} \frac{1}{3} \sum_{\text{spins}} |\mathcal{M}|^2 &= \frac{g^2}{6} \left(-g^{\alpha\beta} + \frac{P^\alpha P^\beta}{M_W^2} \right) \text{Tr} \left(\not{\ell} \gamma_\alpha \not{k} \gamma_\beta \left(\frac{1 - \gamma_5}{2} \right) \right), \\ &= \frac{g^2}{3} \left(-g^{\alpha\beta} + \frac{P^\alpha P^\beta}{M_W^2} \right) (\ell_\alpha k_\beta + k_\alpha \ell_\beta - g_{\alpha\beta} k \cdot \ell), \\ &= \frac{g^2}{3} \left(\ell \cdot k + 2 \frac{P \cdot \ell P \cdot k}{M_W^2} \right) = \frac{1}{3} g^2 M_W^2. \end{aligned}$$

Hence the differential decay rate in the W rest frame is

$$d\Gamma(W \rightarrow e\bar{\nu}_e) = \frac{1}{2M_W} \left(\frac{1}{3} g^2 M_W^2 \right) (2\pi)^{4-6} d_2(PS).$$

Exercise. The gauge boson polarization vectors can be chosen to be

$$\epsilon_0^\mu = (p/M_W, 0, 0, E/M_W),$$

$$\epsilon_\pm^\mu = \frac{1}{\sqrt{2}}(0, 1, \pm i, 0),$$

where ϵ_0^μ is the longitudinal (L) polarization with helicity $h = 0$ and ϵ_\pm^μ are transverse (T) polarizations with helicity $h = \pm 1$. Show that the decay distributions of the electron in the W^- rest frame are

$$d\Gamma_\pm/d\cos\hat{\theta} \sim (1 \mp \cos\hat{\theta})^2, \quad d\Gamma_L/d\cos\hat{\theta} \sim \sin^2\hat{\theta},$$

where $\hat{\theta}$ is the angle of the electron with respect to the longitudinal axis.

The phase space integral is $\int d_2(PS) = \frac{1}{2}\pi \int d\Omega/4\pi = \frac{1}{2}\pi$ leading to a partial decay width

$$\Gamma(W \rightarrow e\bar{\nu}_e) = \frac{1}{48\pi} g^2 M_W = \frac{G_F M_W^3}{\sqrt{2} 6\pi} \equiv \Gamma_W^0$$

since $g^2 = 8M_W^2 G_F/\sqrt{2}$. The numerical value of this partial width

$$\Gamma_W^0 = 0.225 \text{ GeV}.$$

Decays to μ and τ leptons are similar. In the spirit of the parton model, we approximate the total hadronic decay rate by the decay rate to quark-antiquark pairs, assuming that the latter fragment to hadrons with probability 1. Then in the approximation that all fermion masses can be neglected compared to M_W , all lepton and quark decays are related by

$$\begin{aligned} \Gamma(W \rightarrow e\bar{\nu}_e) &= \Gamma(W \rightarrow \mu\bar{\nu}_\mu) = \Gamma(W \rightarrow \tau\bar{\nu}_\tau) = \Gamma_W^0, \\ \Gamma(W \rightarrow q'\bar{q}) &= 3 |V_{qq'}|^2 \Gamma_W^0, \end{aligned}$$

where V is the quark mixing matrix of §2.9. The factor of 3 in the decay rate to quarks comes from summing three colors. Summing over all quark generations N_G ,

$$\sum_{q',q} |V_{qq'}|^2 = \sum_{q'} 1 = N_G = 3,$$

the total hadronic width in the massless fermion approximation is

$$\Gamma(W \rightarrow \text{hadrons}) \simeq 3 \Gamma(W \rightarrow \text{leptons}) \simeq 9 \Gamma_W^0 \simeq 2.1 \text{ GeV}.$$

Thus the total W width is approximately

$$\Gamma(W \rightarrow \text{all}) \simeq 12 \Gamma_W^0 \simeq 2.7 \text{ GeV}.$$

Since $1 \text{ GeV} = 1.52 \times 10^{24} \text{ sec}^{-1}$, the mean lifetime $\tau = 1/\Gamma$ is $\tau(W) \simeq 2 \times 10^{-25} \text{ sec}$. The branching fraction of the W into $e\bar{\nu}_e$ is approximately

$$B(W \rightarrow e\bar{\nu}_e) \simeq \frac{\Gamma(W \rightarrow e\bar{\nu}_e)}{\Gamma(W \rightarrow \text{all})} = \frac{1}{12}.$$

Of the hadronic modes the decays $W \rightarrow \bar{u}d$, $W \rightarrow \bar{c}s$ and $W \rightarrow \bar{t}b$ were expected to give the dominant contributions since

$$|V_{ud}| \approx |V_{cs}| \approx |V_{tb}| \approx 1$$

and all other KM matrix elements are small, (see §2.11).

The $W \rightarrow \bar{t}b$ decay mode was recognized early as a possible place to discover the t -quark at a hadron collider, if $m_t < M_W - m_b$. For heavy quarks like t , we cannot neglect the quark mass in comparison with M_W as we have done above. We must then evaluate $|\mathcal{M}|^2$ and the phase space exactly (see Appendix B).

Exercise. Show that when the quark masses are retained, the partial decay width formula becomes

$$\Gamma(W \rightarrow \bar{t}b) = 3 \Gamma_W^0 |V_{tb}|^2 \lambda^{\frac{1}{2}}(1, r_t, r_b) \left[1 - \frac{1}{2}r_t - \frac{1}{2}r_b - \frac{1}{2}(r_t - r_b)^2 \right],$$

where $r_t = m_t^2/M_W^2$, $r_b = m_b^2/M_W^2$ and $\lambda(a, b, c) = a^2 + b^2 + c^2 - 2ab - 2ac - 2bc$.

Since $r_b \ll 1$, the $W \rightarrow \bar{t}b$ partial width is given to a good approximation by neglecting r_b and setting $|V_{tb}| = 1$. The results for the decay widths, lifetime and $\bar{t}b$ branching fraction then become

$$\Gamma(W \rightarrow \bar{t}b) = 3 \Gamma_W^0 \left[1 - \frac{3}{2}r_t + \frac{1}{2}r_t^3 \right] = 0.37 \text{ GeV},$$

$$\Gamma(W \rightarrow \text{hadrons}) = 9 \Gamma_W^0 \left[1 - \frac{1}{2}r_t + \frac{1}{6}r_t^3 \right] = 1.72 \text{ GeV},$$

$$\Gamma_W \equiv \Gamma(W \rightarrow \text{all}) = 2.39 \text{ GeV},$$

$$B(W \rightarrow \bar{t}b) = \frac{1}{4} \left[\frac{1 - \frac{3}{2}r_t + \frac{1}{2}r_t^3}{1 - \frac{3}{8}r_t + \frac{1}{8}r_t^3} \right] = 0.15,$$

where the numerical values assume a hypothetical top with $m_t = 45$ GeV, $M_W = 80.1$ GeV and three generations.

First order QCD corrections multiply the hadronic width by $1 + \alpha_s(M_W)/\pi$ (neglecting quark masses) where we may take $\alpha_s(M_W) = 0.12$. Table 8.1 summarizes the W partial widths, branching fractions and total width, including the first order QCD correction. The entries in the table are based on the following mixing matrix, which is

TABLE 8.1. *W*-boson partial widths and branching fractions for $M_W = 80.1$ GeV, $m_t > M_W$ and $\alpha_s(M_W) = 0.12$.

Decay	Partial Width	Branching Fraction (%)
$W \rightarrow e\bar{\nu}_e$	0.225	10.8
$\rightarrow \mu\bar{\nu}_\mu$	0.225	10.8
$\rightarrow \tau\bar{\nu}_\tau$	0.225	10.8
$\rightarrow \bar{u}d$	0.666	32.1
$\rightarrow \bar{c}s$	0.664	32.0
$\rightarrow \bar{u}s$	0.035	1.7
$\rightarrow \bar{c}d$	0.035	1.7
$\rightarrow \bar{c}b$	0.001	0.05
$\rightarrow \bar{u}b$	0.000	0.00

Total Width: $\Gamma(W) = 2.08$ GeV

1994 measurements: $\Gamma_W = 2.08 \pm 0.07$ GeV

compatible with the limits discussed in Chapter 2;

$$|V_{ij}| = \begin{pmatrix} 0.975 & 0.222 & 0.003 \\ 0.222 & 0.974 & 0.040 \\ 0.003 & 0.040 & 0.999 \end{pmatrix}$$

Figure 8.2 shows how the $W^+ \rightarrow t\bar{b}$ branching fraction depends on the t -quark mass. The W branching fractions into the important leptonic modes are about 9% for each channel. Also shown is the $Z \rightarrow t\bar{t}$ branching fraction which will be discussed later. Figure 8.3 shows how the total W and Z widths vary with m_t , assuming that only 3 generations of quarks and leptons contribute.

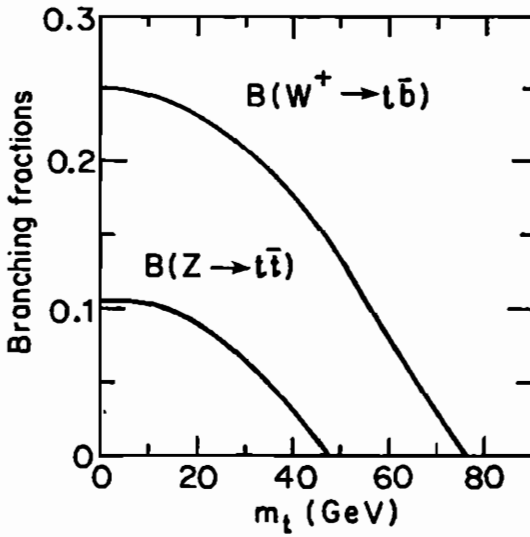


Fig. 8.2. Dependence of the $W^+ \rightarrow t\bar{b}$ and $Z \rightarrow t\bar{t}$ branching fractions on m_t .

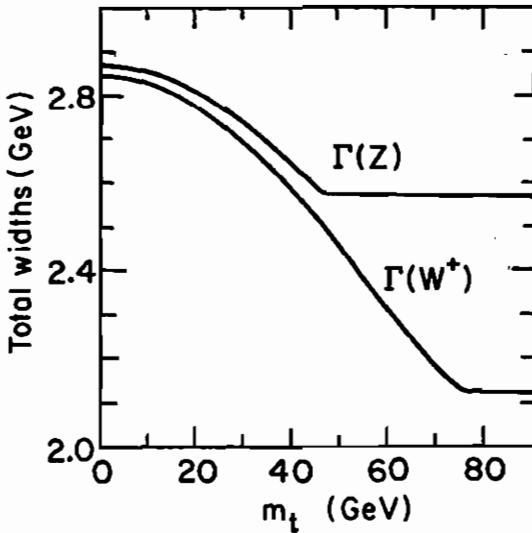


Fig. 8.3. Dependence of W and Z total decay widths on m_t .

8.2 Z Decays

In this section we discuss the decays of Z into quarks and leptons. The Z was first detected through the leptonic decay $Z \rightarrow e^+e^-$. The amplitude for this mode is

$$\mathcal{M} = -ig_Z \epsilon_\alpha^\lambda(P) \bar{u}(\ell) \gamma^\alpha (g_V + g_A \gamma_5) v(k),$$

where the momenta labels are $Z(P) \rightarrow e^+(k)e^-(\ell)$ and the couplings are defined in §2.12.

Exercise. Show that in the massless e approximation, a calculation similar to the $W \rightarrow e\nu$ case gives

$$\Gamma(Z \rightarrow e^+e^-) = \frac{1}{48\pi} \left(2\sqrt{2}g_Z\right)^2 \left(\frac{g_V^2 + g_A^2}{2}\right) M_Z,$$

where $g_Z^2 = \frac{8G_F}{\sqrt{2}} M_Z^2$ and hence

$$\Gamma(Z \rightarrow e^+e^-) = \frac{G_F M_Z^3}{12\pi\sqrt{2}} 8(g_V^2 + g_A^2) \equiv 8(g_V^2 + g_A^2) \Gamma_Z^0.$$

In the massless fermion approximation similar expressions hold for all $\ell\bar{\ell}$ and $q\bar{q}$ partial widths

$$\Gamma(Z \rightarrow \ell\bar{\ell}) = 8 \left[(g_V^\ell)^2 + (g_A^\ell)^2 \right] \Gamma_Z^0,$$

$$\Gamma(Z \rightarrow q\bar{q}) = 24 \left[(g_V^q)^2 + (g_A^q)^2 \right] \Gamma_Z^0,$$

where $\ell = e, \nu_e, \mu, \nu_\mu, \tau, \nu_\tau$ and $q = d, u, s, c, b$ (the approximation is not good for t). The appropriate g_V, g_A must be used in each case.

The extra factor of 3 in the quark cases is due to color. The standard model fermion couplings are

$$g_V^f = \frac{1}{2}T_3^f - Q^f x_w, \quad g_A^f = -\frac{1}{2}T_3^f,$$

and hence

$$\begin{aligned} (g_V^f)^2 + (g_A^f)^2 &= \frac{1}{2}(T_3^f)^2 - T_3^f Q^f x_w + (Q^f)^2 x_w^2 \\ &= \frac{1}{8} (1 - 4|Q^f| x_w + 8(Q^f)^2 x_w^2). \end{aligned}$$

The lowest order partial widths for $x_w = 0.23$ and $M_Z = 91.19$ GeV are then

$$\begin{aligned} \Gamma(Z \rightarrow \bar{\nu}_e \nu_e) &= \Gamma_Z^0 &= 0.17 \text{ GeV}, \\ \Gamma(Z \rightarrow e^+ e^-) &= \Gamma_Z^0 (1 - 4x_w + 8x_w^2) = 0.08 \text{ GeV}, \\ \Gamma(Z \rightarrow \bar{u} u) &= 3 \Gamma_Z^0 (1 - \frac{8}{3}x_w + \frac{32}{9}x_w^2) = 0.29 \text{ GeV}, \\ \Gamma(Z \rightarrow \bar{d} d) &= 3 \Gamma_Z^0 (1 - \frac{4}{3}x_w + \frac{8}{9}x_w^2) = 0.37 \text{ GeV}. \end{aligned}$$

Summing over three generations of quarks and leptons (excluding t), the total Z width in the massless fermion approximation is

$$\Gamma_Z \simeq \Gamma_Z^0 (21 - 40x + \frac{160}{3}x^2) = 2.4 \text{ GeV}.$$

The corresponding Z branching fractions are

$$\begin{aligned} B(Z \rightarrow \nu_e \bar{\nu}_e) &\simeq 0.07, & B(Z \rightarrow \bar{e} e) &\simeq 0.03, \\ B(Z \rightarrow \bar{u} u) &\simeq 0.12, & B(Z \rightarrow \bar{d} d) &\simeq 0.15, \end{aligned}$$

with similar branching fractions to the other generations.

Quark mass effects are more important in Z decays than in W decays, as we now show for hypothetical top quarks with $m_t < \frac{1}{2}M_Z$.

From Appendix B, the $Z \rightarrow t\bar{t}$ partial width in lowest order with m_t included is

$$\Gamma(Z \rightarrow t\bar{t}) = 3\Gamma_Z^0 F(m_t^2/M_Z^2),$$

where

$$\begin{aligned} F(r) &= (1 - 4r)^{\frac{1}{2}} 8 \left[g_V^2(1 + 2r) + g_A^2(1 - 4r) \right] \\ &= (1 - 4r)^{\frac{1}{2}} \left[1 - \frac{8}{3}x_w + \frac{32}{9}x_w^2 - r \left(1 + \frac{16}{3}x_w - \frac{64}{9}x_w^2 \right) \right]. \end{aligned}$$

For $x_w = 0.23$ the expression for $F(r)$ becomes

$$F(r) = (1 - 4r)^{\frac{1}{2}}(0.57 - 1.85r).$$

For $M_Z = 91.19$ GeV, the suppression factor is

$$F(r) = 0.36, 0.19, 0.02 \text{ for } m_t = 25, 35, 45, \text{ respectively.}$$

The total width decreases by 0.18 GeV as m_t changes from 25 to 45 GeV.

The first order QCD correction to the quark decays of the Z is $(1 + \alpha_s(M_Z)/\pi)$, neglecting the quark masses. Table 8.2 summarizes the Z -branching fractions, including this QCD correction with $\alpha_s = 0.12$.

The partial widths are in the ratios

$$\Gamma(\nu_e\bar{\nu}_e) : \Gamma(e^+e^-) : \Gamma(u\bar{u}) : \Gamma(d\bar{d}) = 2.0 : 1.0 : 3.6 : 4.6.$$

The branching fraction for $Z \rightarrow e^+e^-$ is 3.36%. The branching fraction into invisible modes is

$$B(\nu_e\bar{\nu}_e + \nu_\mu\bar{\nu}_\mu + \nu_\tau\bar{\nu}_\tau) = 20.0\%.$$

The total Γ width can be measured directly from the resonant line-shape of the total e^+e^- cross section near $s = M_Z^2$. It is an important

TABLE 8.2. *Z* boson partial widths and branching fractions for $M_Z = 91.19$ GeV, $m_t > \frac{1}{2}M_Z$ and $\alpha_s(M_Z) = 0.12$.

Decay	Partial Width	Branching Fraction (%)
$Z \rightarrow \nu_e \bar{\nu}_e$	0.166	6.7
$\rightarrow \nu_\mu \bar{\nu}_\mu$	0.166	6.7
$\rightarrow \nu_\tau \bar{\nu}_\tau$	0.166	6.7
$\rightarrow e \bar{e}$	0.083	3.4
$\rightarrow \mu \bar{\mu}$	0.083	3.4
$\rightarrow \tau \bar{\tau}$	0.083	3.4
$\rightarrow d \bar{d}$	0.383	15.4
$\rightarrow s \bar{s}$	0.383	15.4
$\rightarrow b \bar{b}$	0.378	15.2
$\rightarrow u \bar{u}$	0.297	12.0
$\rightarrow c \bar{c}$	0.297	11.9
Total Width: $\Gamma(Z) \equiv 2.49$ GeV		
[1994 measurements: $\Gamma_Z = 2.491 \pm 0.007$ GeV]		

window on possible new physics. The visible and invisible parts of Γ_Z can be separated using the peak visible cross sections. Any new particle with non-trivial $SU(2) \times U(1)$ quantum numbers will couple to Z and appear in Z decays (if light enough), revealing its presence through an increase in Γ_Z^{vis} and/or Γ_Z^{inv} above standard model expectations. New neutrinos are an interesting example; any neutrino belonging to an $SU(2)$ doublet contributes 0.17 GeV to Γ_Z^{inv} , so upper limits on Γ_Z^{inv} can be translated into upper limits on the number of new neutrino species [the 1994 result $\Gamma_Z^{\text{inv}} = 0.496 \pm 0.029$ GeV fits $N_\nu = 3.0 \pm 0.2$ doublet neutrinos]. Charged heavy leptons and quarks from the fourth generation, new supersymmetry particles and possible new fermions from higher symmetry schemes (such as E_6 GUTS) might also contribute to Z decay, if they exist and kinematics permit.

Hadron collider experiments do not measure Γ_Z or Γ_W very precisely but they can measure the ratio Γ_Z/Γ_W indirectly through the

ratio

$$R = \frac{\sigma(p\bar{p} \rightarrow W \rightarrow e\nu)}{\sigma(p\bar{p} \rightarrow Z \rightarrow e^+e^-)} = \frac{\sigma(p\bar{p} \rightarrow W)}{\sigma(p\bar{p} \rightarrow Z)} \cdot \frac{\Gamma(W \rightarrow e\nu)}{\Gamma(Z \rightarrow e^+e^-)} \cdot \frac{\Gamma_Z}{\Gamma_W}.$$

The ratio of W and Z production cross sections can be calculated rather accurately, since many of the theoretical uncertainties cancel out, and the leptonic partial widths can be calculated reliably. The results are $\sigma_W/\sigma_Z = 3.3 \pm 0.2$ and $\Gamma(Z \rightarrow e\bar{e})/\Gamma(W \rightarrow e\nu) = 0.37$. Hence Γ_Z/Γ_W is determined from R . The 1986 experimental indications that $R = 7.2 \pm_{1.2}^{1.7}$ translate into

$$\Gamma_Z/\Gamma_W = 0.82 \pm_{0.14}^{0.19} \text{ (stat.)} \pm 0.06 \text{ (theor.)}.$$

At 90% (95%) CL the upper limit is $\Gamma_Z/\Gamma_W < 1.16$ (1.27).

Figure 8.4 shows the standard model prediction for Γ_Z/Γ_W versus the t -quark mass, assuming $N_\nu = 3$ or $N_\nu = 4$ neutrinos. Comparison with the upper bound at 90% CL suggests that $m_t < 70$ GeV for $N_\nu = 3$ but at 95% CL there is no m_t bound.

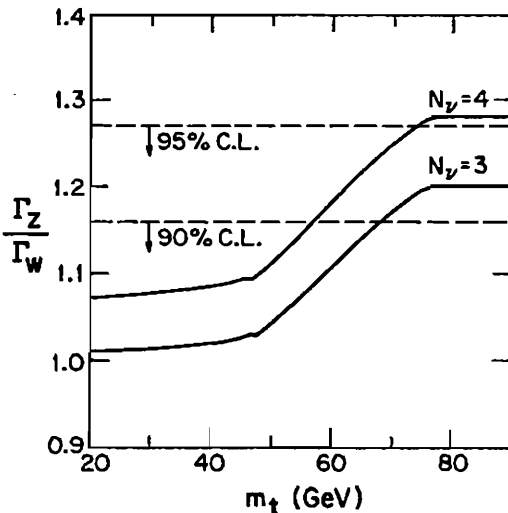


Fig. 8.4. Γ_Z/Γ_W predictions compared with the upper bound from CERN collider data.

Once it is established how many neutrinos contribute to Γ_Z/Γ_W , measurements of Γ_Z/Γ_W can be combined with measurements of Γ_Z from Z -factories to infer Γ_W . This will provide the most accurate measure of Γ_W until W -pairs are produced at LEP II. The present collider data values of Γ_Z/Γ_W will become more accurate with increased statistics and the theoretical uncertainty (second uncertainties on above values) will be reduced by new structure function measurements at low Q^2 .

8.3 Hadronic W -Production

The cross section for W -production

$$A + B \rightarrow W^\pm + \text{anything}$$

is computed in a similar way to the Drell-Yan cross section. The quark subprocess in this case is

$$q\bar{q}' \rightarrow W^+,$$

where q is a 2/3 charge quark (or 1/3 charge antiquark) from hadron A and \bar{q}' is a 1/3 charge anti-quark (or 2/3 charge quark) from hadron B . The matrix element is the same as in W -decay. Labeling the momenta by $q(p_2)\bar{q}'(p_1) \rightarrow W^+(P)$, we have

$$\mathcal{M} = -iV_{qq'} \frac{g}{\sqrt{2}} \epsilon_\alpha^{\lambda*}(P) \bar{v}(p_1) \frac{1}{2} \gamma^\alpha (1 - \gamma_5) u(p_2).$$

Neglecting the quark masses, the spin and W -polarization sum of $|\mathcal{M}|^2$ is

$$\sum_{\text{spins}} |\mathcal{M}|^2 = |V_{qq'}|^2 g^2 M_W^2 = |V_{qq'}|^2 \frac{8G_F}{\sqrt{2}} M_W^4$$

so the subprocess cross section is

$$\hat{\sigma}(q\bar{q}' \rightarrow W^+) = \left(\frac{1}{2}\right)^2 \frac{1}{2\hat{s}} \left(|V_{qq'}|^2 \frac{8G_F}{\sqrt{2}} M_W^4 \right) (2\pi)^{4-3} \int d(PS),$$

where $\hat{s} = (p_1 + p_2)^2$. Evaluating the phase space gives

$$\int \frac{d^3p}{2E_p} \delta(P - p_1 - p_2) = \delta(\hat{s} - M_W^2)$$

and hence

$$\hat{\sigma}(q\bar{q}' \rightarrow W^+) = 2\pi |V_{qq'}|^2 \frac{G_F}{\sqrt{2}} M_W^2 \delta(\hat{s} - M_W^2).$$

The total W^+ cross section is the convolution of $\hat{\sigma}$ with the quark densities, including a color factor of $3 \times \frac{1}{3} \times \frac{1}{3}$,

$$\sigma(AB \rightarrow W^+ X) = \frac{K}{3} \int_0^1 dx_a \int_0^1 dx_b \sum_q q(x_a, M_W^2) \bar{q}'(x_b, M_W^2) \hat{\sigma},$$

where x_a (x_b) is the momentum fraction of q (\bar{q}') in A (B). Here it is assumed that $q^2 = \hat{s} = M_W^2$ is the appropriate scale of the quark distributions. The K -factor includes first order QCD corrections,

$$K \simeq 1 + \frac{8\pi}{9} \alpha_s(M_W^2),$$

similar to the Drell-Yan K -factor of §7.6.

We transform the integration to \hat{s} , y variables (see §5.7)

$$dx_a dx_b = \frac{d\hat{s} dy}{s},$$

where $y = \frac{1}{2} \ln[(E + P_L)/(E - P_L)]$ is the rapidity of the W in the AB c.m. frame. The integral over $d\hat{s}$ takes out the delta function

and we find

$$\frac{d\sigma}{dy}(W^+) = K \frac{2\pi G_F}{3\sqrt{2}} \sum_{q, \bar{q}'} |V_{qq'}|^2 x_a x_b q(x_a, M_W^2) \bar{q}'(x_b, M_W^2),$$

where x_a and x_b are now evaluated at

$$x_{a,b} = \frac{M_W}{\sqrt{s}} e^{\pm y}.$$

For proton-proton scattering the differential cross section in the Cabibbo mixing approximation is

$$\begin{aligned} \frac{d\sigma}{dy}(pp \rightarrow W^+ X) = K \frac{2\pi G_F}{3\sqrt{2}} x_a x_b \left\{ \cos^2 \theta_C [u(x_a) \bar{d}(x_b) + \bar{d}(x_a) u(x_b)] \right. \\ \left. + \sin^2 \theta_C [u(x_a) \bar{s}(x_b) + \bar{s}(x_a) u(x_b)] \right\}, \end{aligned}$$

where it is understood that all quark distributions are evaluated at $q^2 = M_W^2$. In the further approximation of an SU(3) symmetric sea, $\bar{u} = \bar{d} = \bar{s}$, this simplifies to

$$\frac{d\sigma}{dy}(pp \rightarrow W^+ X) = K \frac{2\pi G_F}{3\sqrt{2}} x_a x_b [u(x_a) \bar{d}(x_b) + \bar{d}(x_a) u(x_b)].$$

For $\bar{p}p$ collisions, the W^+ differential cross section is

$$\begin{aligned} \frac{d\sigma}{dy}(p\bar{p} \rightarrow W^+ X) = K \frac{2\pi G_F}{3\sqrt{2}} x_a x_b \left\{ \cos^2 \theta_C [u(x_a) d(x_b) + \bar{d}(x_a) \bar{u}(x_b)] \right. \\ \left. + \sin^2 \theta_C [u(x_a) s(x_b) + \bar{s}(x_a) \bar{u}(x_b)] \right\}. \end{aligned}$$

In the valence dominance approximation for low c.m. energies this is roughly

$$\frac{d\sigma}{dy}(p\bar{p} \rightarrow W^+ X) = K \frac{2\pi G_F}{3\sqrt{2}} x_a x_b u(x_a) d(x_b).$$

Exercise. Show that the corresponding differential cross sections for W^- production are obtained in pp collisions by interchanging quark and antiquark densities, and in $p\bar{p}$ collisions by interchanging x_a with x_b in the arguments of these densities.

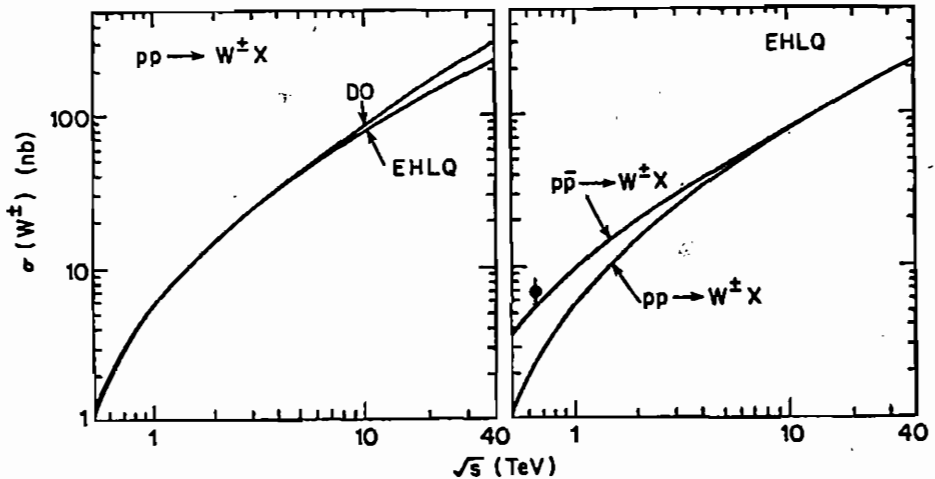


Fig. 8.5 Predicted W^\pm production cross sections versus energy. The measured value at the CERN $p\bar{p}$ collider is shown, assuming $B(W \rightarrow e\nu) = 9\%$.

The total cross sections for W -production are obtained by integration over the full kinematic range of the rapidity. From $x_{a,b} \leq 1$ we obtain the W -rapidity limits

$$-\ln \frac{\sqrt{s}}{M_W} \leq y \leq \ln \frac{\sqrt{s}}{M_W}.$$

Calculations based on the DO and EHLQ distributions from §7.9. are shown versus \sqrt{s} in Fig. 8.5. At the energy $\sqrt{s} = 630$ GeV of the CERN $p\bar{p}$ collider, the predicted cross section is

$$\sigma(\bar{p}p \rightarrow W^+ X) = \sigma(\bar{p}p \rightarrow W^- X) = \begin{cases} 2.8 \text{ nb,} & \text{EHLQ} \\ 3.0 \text{ nb,} & \text{DO} \end{cases}.$$

With the predicted W -branching fraction to electrons $B(W^+ \rightarrow e^+\nu) = 0.09$ we expect an electron yield $\sum_{W^\pm} \sigma_{W^\pm} B(W^\pm \rightarrow e^\pm) = 0.50$ nb (0.54 nb) for the EHLQ (DO) distributions. The measured

rate in the UA1 experiment

$$(\sigma \cdot B)_{W \rightarrow e\nu} = 0.60 \pm 0.05 \pm 0.09 \text{ nb}$$

is in approximate accord with this expectation.

8.4 Hadronic Z-Production

The calculation of the cross section for

$$A + B \rightarrow Z + \text{anything}$$

is like the W calculation of the preceding section. The matrix element squared for the fusion subprocess

$$q\bar{q} \rightarrow Z$$

is

$$|\mathcal{M}|^2 = \left(2\sqrt{2}g_Z\right)^2 \left[\frac{(g_V^q)^2 + (g_A^q)^2}{2}\right] M_Z^2 = 32 \frac{G_F}{\sqrt{2}} [(g_V^q)^2 + (g_A^q)^2] M_Z^4,$$

where g_V and g_A are the couplings to quarks. Hence the subprocess cross section and the resulting color-averaged hadronic cross section are

$$\hat{\sigma}(q\bar{q} \rightarrow Z) = 8\pi \frac{G_F}{\sqrt{2}} [(g_V^q)^2 + (g_A^q)^2] M_Z^2 \delta(\hat{s} - M_Z^2),$$

$$\frac{d\sigma}{dy}(AB \rightarrow ZX) = K \frac{8\pi}{3} \frac{G_F}{\sqrt{2}} \sum_q [(g_V^q)^2 + (g_A^q)^2] x_a x_b q(x_a) \bar{q}(x_b),$$

where the K -factor is evaluated at scale M_Z^2 . For Z production in $p\bar{p}$ collisions, as for example at the CERN $S\bar{p}\bar{p}S$ and Fermilab Tevatron

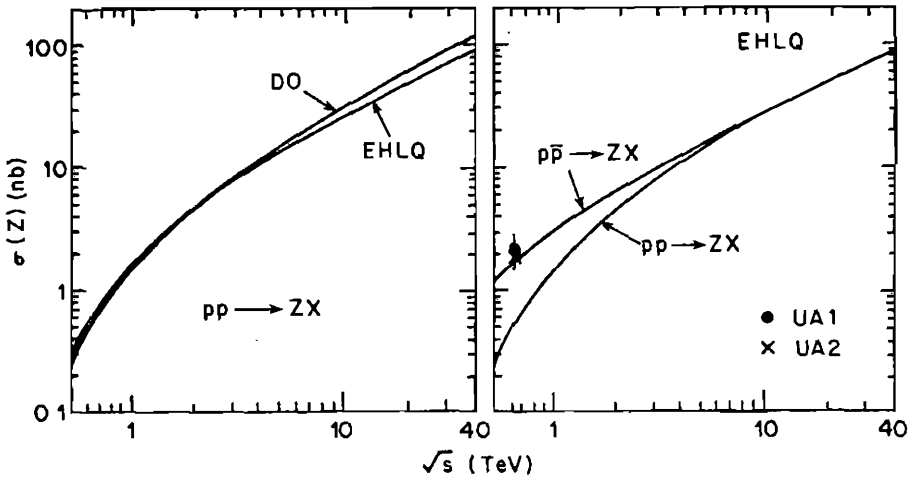


Fig. 8.6. Z production cross sections in pp and $p\bar{p}$ scattering from the leading-order formulas, for DO and EHLQ quark distributions.

colliders, the result is

$$\frac{d\sigma}{dy}(\bar{p}p \rightarrow ZX) = K \frac{\pi G_F}{3\sqrt{2}} x_a x_b \left\{ \left[1 - \frac{8}{3}x_w + \frac{32}{9}x_w^2 \right] \left[u(x_a)u(x_b) + \bar{u}(x_a)\bar{u}(x_b) \right] \right. \\ \left. + \left[1 - \frac{4}{3}x_w + \frac{8}{9}x_w^2 \right] \left[d(x_a)d(x_b) + \bar{d}(x_a)\bar{d}(x_b) + s(x_a)s(x_b) + \bar{s}(x_a)\bar{s}(x_b) \right] \right\}.$$

In pp collisions, as at the future SSC or LHC machines, the cross section from u , d and s quarks is

$$\frac{d\sigma}{dy}(pp \rightarrow ZX) = K \frac{\pi G_F}{3\sqrt{2}} x_a x_b \left\{ \left[1 - \frac{8}{3}x_w + \frac{32}{9}x_w^2 \right] \left[u(x_a)\bar{u}(x_b) + \bar{u}(x_a)u(x_b) \right] \right. \\ \left. + \left[1 - \frac{4}{3}x_w + \frac{8}{9}x_w^2 \right] \left[d(x_a)\bar{d}(x_b) + \bar{d}(x_a)d(x_b) + s(x_a)\bar{s}(x_b) + \bar{s}(x_a)s(x_b) \right] \right\}.$$

Figure 8.6 shows the predicted Z cross sections versus \sqrt{s} .

At $\sqrt{s} = 630$ GeV the predicted $p\bar{p}$ cross section for $M_Z = 92$ GeV

is

$$\sigma(p\bar{p} \rightarrow ZX) \simeq 1.8 \text{ nb},$$

which combined with the $Z \rightarrow e^+e^-$ branching fraction 3.3% gives

$$\sigma(p\bar{p} \rightarrow Z \rightarrow e^+e^-) \simeq 0.06 \text{ nb}.$$

The result is in reasonable agreement with 1986 results from the UA1 and UA2 collaborations at the CERN collider

$$\sigma(p\bar{p} \rightarrow Z \rightarrow e^+e^-) = \begin{cases} 73 \pm 14 \pm 11 \text{ pb}, & \text{UA1} \\ 69 \pm 13 \pm 6 \text{ pb}, & \text{UA2} \end{cases}$$

where the first (second) uncertainty is statistical (systematic).

Because of the smaller production cross section and smaller leptonic branching fraction, the ratio of $Z \rightarrow e^+e^-$ events to $W^\pm \rightarrow e\nu$ events is about $\frac{1}{10}$ at the CERN and Tevatron colliders.

8.5 Hadronic $W \rightarrow e\nu$ Production

In order to predict the distribution of $W \rightarrow e\nu$ decay leptons, we must calculate the complete production and decay subprocess, typically

$$u\bar{d} \rightarrow W^+ \rightarrow e^+\nu_e$$

with momenta labeled as in Fig. 8.7. The matrix element is

$$\mathcal{M} = i \frac{G_F}{\sqrt{2}} M_W^2 V_{ud} \frac{\bar{v}(d)\gamma^\alpha(1-\gamma_5)u(u)\bar{u}(\nu)\gamma_\alpha(1-\gamma_5)v(e^+)}{\hat{s} - M_W^2 + iM_W\Gamma_W}.$$

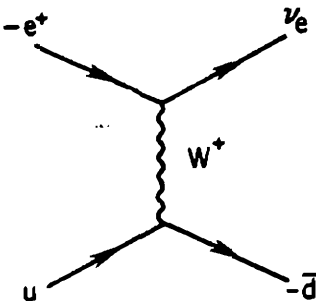


Fig. 8.7. The subprocess $u\bar{d} \rightarrow W^+ \rightarrow e^+\nu_e$.

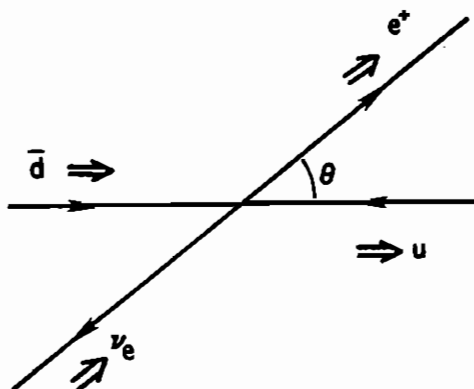


Fig. 8.8. Subprocess for $W^+ \rightarrow e^+\nu$ in W rest-frame. Arrows denote momenta, double arrows denote helicities.

Exercise. Show that squaring and summing spins gives

$$\sum_{\text{spins}} |\mathcal{M}|^2 = 64 |V_{ud}|^2 \left(\frac{G_F M_W^2}{\sqrt{2}} \right)^2 \frac{\hat{u}^2}{(\hat{s} - M_W^2)^2 + (M_W \Gamma_W)^2},$$

neglecting quark and lepton masses. Here \hat{s} and \hat{u} are the subprocess kinematic invariants

$$\hat{s} = (u + \bar{d})^2, \quad \hat{u} = (u - e^+)^2.$$

In the $\bar{e}\nu$ rest frame, the c.m. scattering angle $\hat{\theta}$ is defined as the angle between the \bar{d} and e^+ ; see Fig. 8.8. In this frame, $\hat{u} = -\frac{1}{2}\hat{s}(1 + \cos \hat{\theta})$.

The spin-averaged cross section for the $u\bar{d} \rightarrow e^+\nu$ subprocess is

$$\frac{d\hat{\sigma}}{d\hat{t}} (u\bar{d} \rightarrow e^+\nu) = \frac{|V_{ud}|^2}{\pi \hat{s}^2} \left(\frac{G_F M_W^2}{\sqrt{2}} \right)^2 \frac{\hat{u}^2}{(\hat{s} - M_W^2)^2 + (\Gamma_W M_W)^2}$$

or

$$\frac{d\hat{\sigma}}{d \cos \hat{\theta}} (u\bar{d} \rightarrow e^+\nu) = \frac{|V_{ud}|^2}{8\pi} \left(\frac{G_F M_W^2}{\sqrt{2}} \right)^2 \frac{\hat{s}(1 + \cos \hat{\theta})^2}{(\hat{s} - M_W^2)^2 + (\Gamma_W M_W)^2}.$$

The total cross section is

$$\hat{\sigma} (u\bar{d} \rightarrow e^+\nu) = \frac{|V_{ud}|^2}{3\pi} \left(\frac{G_F M_W^2}{\sqrt{2}} \right)^2 \frac{\hat{s}}{(\hat{s} - M_W^2)^2 + (\Gamma_W M_W)^2}.$$

For $u\bar{s} \rightarrow e^+\nu$ change V_{ud} to V_{us} above. The vanishing of the differential cross section at $\cos\hat{\theta} = -1$ in the typical $u\bar{d} \rightarrow e^+\nu$ case is a consequence of helicity conservation in collinear scattering; see Fig. 8.8. Hence the e^+ is emitted preferentially along the \bar{d} direction. In $p\bar{p}$ collisions below $\sqrt{s} = 1$ TeV, the antiproton is the principal source of \bar{d} and the proton is the principal source of u quarks. Thus the e^+ is preferentially produced in the hemisphere about the antiproton beam direction.

Exercise. For $d\bar{u} \rightarrow e^-\nu$, define the scattering angle $\hat{\theta}$ of the e^- relative to the incident quark d , and show that the differential cross section is given by the same formula above. Correspondingly, in $d\bar{u} \rightarrow W^- \rightarrow e^-\bar{\nu}$ production, the e^- is emitted preferentially along the d direction, i.e. in the hemisphere about the proton beam direction in $p\bar{p}$ collisions.

In terms of the subprocess differential cross section $d\hat{\sigma}$, the inclusive hadronic cross section for $AB \rightarrow e^+\nu X$ has the form

$$d\sigma(AB \rightarrow e^+\nu X) = \frac{1}{3} \sum_{q,q'} \int_0^1 dx_a \int_0^1 dx_b q(x_a) \bar{q}'(x_b) d\hat{\sigma}(q\bar{q}' \rightarrow e^+\nu),$$

where x_a is the momentum fraction of parton q in hadron A , etc. and the summation is over both quarks and antiquarks. The factor $\frac{1}{3}$ is for color. It is understood that the parton distributions are evolved up to $Q^2 = \hat{s} = M_W^2$. For a Monte Carlo calculation of electron and neutrino final state distributions from $AB \rightarrow WX \rightarrow e\nu X$, this formula for folding in the parton distributions combined with the formula above for $d\hat{\sigma}/d\cos\hat{\theta}$ are sufficient. One chooses random x_a and x_b , which define the $q\bar{q}'$ c.m. frame and \hat{s} , and then chooses random $\cos\hat{\theta}$ (and $\hat{\phi}$) in this c.m. frame to define the final state. The integrand factors give the statistical weight (see Chapter 11).

Exercise. Defining the electron rapidity in the $u\bar{d}$ c.m. frame as

$$\hat{y} = \frac{1}{2} \ln [(e_0 + e_L)/(e_0 - e_L)] = \ln \cot \left(\frac{1}{2} \hat{\theta} \right),$$

where subscript L denotes the longitudinal momentum component,

show that

$$\frac{d\hat{\theta}}{d\hat{y}} = \sin^2 \hat{\theta} \frac{d\hat{\theta}}{d \cos \hat{\theta}} \sim \left(\frac{1 + \tanh \hat{y}}{\cosh \hat{y}} \right)^2.$$

Exercise. Show that the electron laboratory momenta and rapidity are related to x_a , x_b and the c.m. scattering angle $\hat{\theta}$ by

$$\begin{aligned} E_e &= \frac{1}{4} \sqrt{s} \left[x_a (1 + \cos \hat{\theta}) + x_b (1 - \cos \hat{\theta}) \right], \\ p_e L &= \frac{1}{4} \sqrt{s} \left[x_a (1 + \cos \hat{\theta}) - x_b (1 - \cos \hat{\theta}) \right], \\ y &= \frac{1}{2} \ln \left[\frac{x_a (1 + \cos \hat{\theta})}{x_b (1 - \cos \hat{\theta})} \right] = \frac{1}{2} \ln \left(\frac{x_a}{x_b} \right) + \hat{y}. \end{aligned}$$

Hence show that the e lab rapidity distribution has the form

$$\frac{d\sigma}{dy}(AB \rightarrow eX) = \frac{1}{3} \sum_{qq'} \int_0^1 dx_a \int_0^1 dx_b q(x_a) \bar{q}'(x_b) \left[\frac{d\hat{\theta}}{d \cos \hat{\theta}} (qq' \rightarrow e\nu) \sin^2 \hat{\theta} \right],$$

where the quantity in square brackets is evaluated at $\hat{y} = y - \frac{1}{2} \ln(x_a/x_b)$ with $\sin \hat{\theta} = (\cosh \hat{y})^{-1}$, $\cos \hat{\theta} = \tanh \hat{y}$.

The transverse momentum distribution of the electron and the neutrino are important in the identification of $W \rightarrow e\nu$ events. In the $u\bar{d} \rightarrow e^+\nu$ subprocess c.m. frame, the transverse momenta \hat{p}_T of the e^+ and ν are back-to-back and have the same magnitude

$$\hat{p}_T^2 = \frac{1}{4} \hat{s} \sin^2 \hat{\theta} = \hat{t} \hat{u} / \hat{s}.$$

To change variables in the differential cross section from $d \cos \hat{\theta}$ to $d\hat{p}_T^2$, using $\cos \hat{\theta} = [1 - 4\hat{p}_T^2/\hat{s}]^{1/2}$, we encounter the Jacobian

$$\frac{d \cos \hat{\theta}}{d\hat{p}_T^2} = -\frac{2}{\hat{s}} \left(1 - \frac{4\hat{p}_T^2}{\hat{s}} \right)^{-\frac{1}{2}} = -\frac{2}{\hat{s} \cos \hat{\theta}}.$$

Since angles $\hat{\theta}$ and $\pi - \hat{\theta}$ contribute to the same \hat{p}_T , linear $\cos \hat{\theta}$ terms

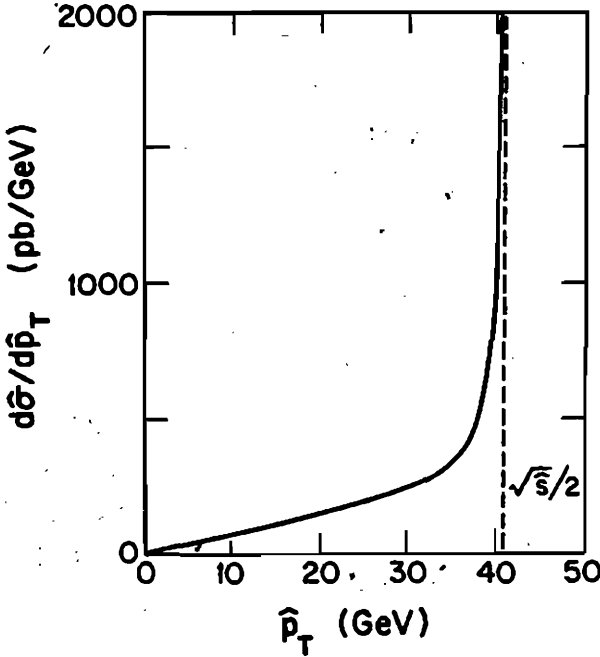


Fig. 8.9. Jacobian peak p_T -distribution in the $u\bar{d} \rightarrow e^+\nu$ subprocess at fixed \hat{s} .

in $d\hat{\sigma}/d\cos\hat{\theta}$ cancel and

$$\frac{d\hat{\sigma}}{d\hat{p}_T^2} = \hat{\sigma} \frac{3}{2} \frac{(1 + \cos^2\hat{\theta})}{\hat{s} |\cos\hat{\theta}|} = \frac{\hat{\sigma}}{\hat{s}} 3 \frac{(1 - 2\hat{p}_T^2/\hat{s})}{(1 - 4\hat{p}_T^2/\hat{s})^{1/2}}.$$

The divergence at $\hat{\theta} = \frac{1}{2}\pi$ which is the upper endpoint $\hat{p}_T = \frac{1}{2}\sqrt{\hat{s}} \simeq \frac{1}{2}M_W$ of the p_T distribution stems from the Jacobian factor and is known as a *Jacobian peak*; it is characteristic of all two-body decays, in this case $W \rightarrow e\nu$. The shape of the distribution is shown in Fig. 8.9.

If we take simply the lowest-order subprocesses $q\bar{q}' \rightarrow W \rightarrow e\nu$, the incident quarks are longitudinal so W is produced longitudinally and the laboratory transverse momentum of e is the subprocess transverse momentum: $p_T = \hat{p}_T$. In this case the p_T -distribution obtained by folding $d\hat{\sigma}/d\hat{p}_T^2$ with the quark distributions is averaged only over the Breit-Wigner \hat{s} dependence of $\hat{\sigma}(q\bar{q}' \rightarrow e\nu)$. This integration over \hat{s} removes the singularity and leaves a Jacobian peak of finite height near $p_T = \frac{1}{2}M_W$.

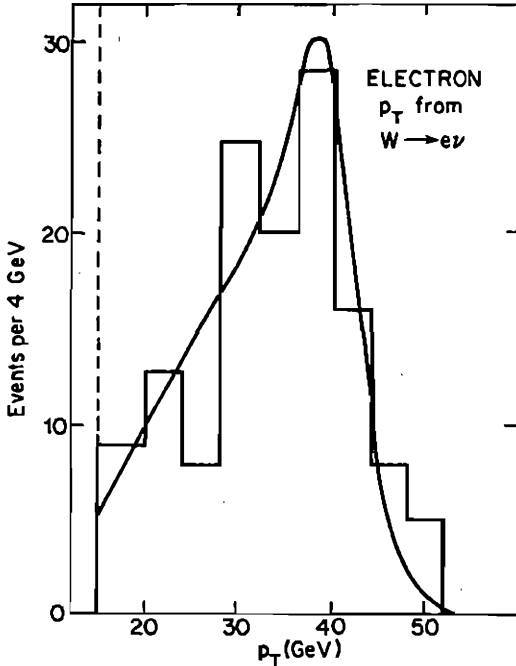


Fig. 8.10. Distribution of electron p_T from $p\bar{p} \rightarrow W \rightarrow e\nu$ events at $\sqrt{s} = 630$ GeV (UA1 data) compared with a calculation folding in the smearing from $p_T(W)$.

Higher order subprocesses, such as $u\bar{d} \rightarrow W^+g$, give the W a transverse momentum distribution which smears out the Jacobian peak in the decay electron p_T distribution. This smearing makes it difficult to obtain an accurate determination of M_W from the p_{eT} distribution alone. Figure 8.10 shows the electron p_T distribution from $p\bar{p} \rightarrow W \rightarrow e\nu$ at $\sqrt{s} = 630$ GeV, compared with a calculation folding in the p_T of the parent W boson.

However it is possible also to exploit information about the neutrino momentum. Since all hadrons and charged leptons with appreciable p_T are detected, the overall p_T imbalance for detected particles gives an approximate measure of the undetected neutrino contribution $p_{\nu T}$. One cannot make a similar determination of the longitudinal momentum component $p_{\nu L}$, since particles can escape undetected down the beam pipe.

An alternative observable quantity, which has a sharp Jacobian peak like p_{eT} and $p_{\nu t}$ but which is *insensitive* to the W transverse momentum distribution, is the transverse mass.

8.6 Transverse Mass

The $e\nu$ transverse mass $m_T(e, \nu)$ is defined by

$$m_T^2(e, \nu) = (|p_{eT}| + |p_{\nu T}|)^2 - (p_{eT} + p_{\nu T})^2.$$

It is analogous, in the transverse momentum subspace, to the $e\nu$ invariant mass $m(e, \nu)$,

$$m^2(e, \nu) = (|p_e| + |p_\nu|)^2 - (p_e + p_\nu)^2.$$

Forming the difference, we find

$$m^2(e, \nu) - m_T^2(e, \nu) = 2 \left[(p_{eT}^2 + p_{eL}^2)^{\frac{1}{2}} (p_{\nu T}^2 + p_{\nu L}^2)^{\frac{1}{2}} - |p_{eT}| |p_{\nu T}| - p_{eL} p_{\nu L} \right] \geq 0.$$

Thus $m_T(e, \nu)$ always lies in the range $0 \leq m_T(e, \nu) \leq m(e, \nu)$ and for $W \rightarrow e\nu$ decay where $m(e, \nu) = M_W$, we have

$$0 \leq m_T(e, \nu) \leq M_W$$

modulo smearing over the intrinsic width of the W resonance. The end-points of the m_T distribution are unchanged by transverse motion of W .

When the W is produced with zero p_T , by the annihilation of longitudinal $q\bar{q}'$ pairs, $m_T(e, \nu)$ is simply given by

$$m_T(e, \nu) = 2 |p_{eT}| = 2 |p_{\nu T}|$$

and the m_T distribution for given \hat{s} is

$$\frac{d\hat{\sigma}}{dm_T^2} = \frac{|V_{qq'}|^2}{4\pi} \left(\frac{G_F M_W^2}{\sqrt{2}} \right)^2 \frac{1}{(\hat{s} - M_W^2)^2 + (\Gamma_W M_W)^2} \frac{2 - m_T^2/\hat{s}}{(1 - m_T^2/\hat{s})^{1/2}}.$$

The m_T distribution is unaffected by longitudinal boosts of the $e\nu$ system, since it depends only on transverse momenta.

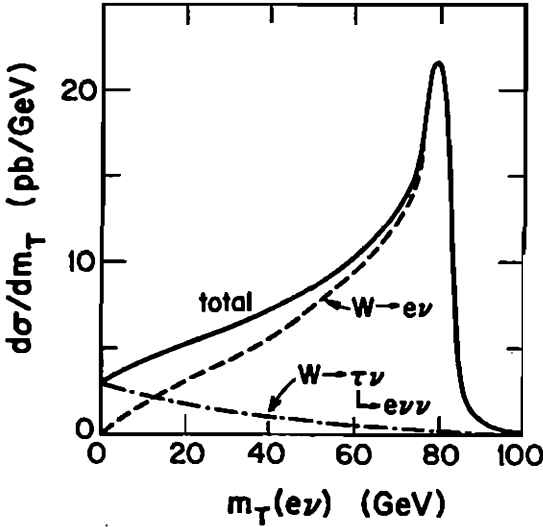


Fig. 8.11. Predicted distribution of transverse mass $m_T(e\nu)$ for $p\bar{p} \rightarrow W^\pm \rightarrow e\nu$ collisions at $\sqrt{s} = 630$ GeV.

Exercise. By boosting the e and ν momenta in a transverse direction, corresponding to a transverse velocity β of the decaying W , show that $m_T(e, \nu)$ is unchanged to order β and contains corrections only of order β^2 .

Including the finite W width, folding in the incident quark distributions and averaging color, the m_T distribution (from the lowest order subprocess) becomes

$$\frac{d\sigma}{dm_T^2}(AB \rightarrow e\nu X) = \frac{K}{3} \sum_{q,q'} \int_0^1 dx_a \int_0^1 dx_b q(x_a, \hat{s}) \bar{q}'(x_b, \hat{s}) \frac{d\hat{\sigma}}{dm_T^2}(q\bar{q}' \rightarrow e\nu),$$

with initial quark distributions evolved up to $Q^2 = \hat{s}$ and correction factor $K \simeq 1 + \frac{8\pi}{9} \alpha_s(M_W^2)$. Figure 8.11 shows the prediction for $p\bar{p}$ collisions at $\sqrt{s} = 630$ GeV, for Duke-Owens quark distributions.

The shape of the m_T distribution close to the endpoint is sensitive to both M_W and Γ_W . The accuracy with which $p_{\nu T}$ can be deter-

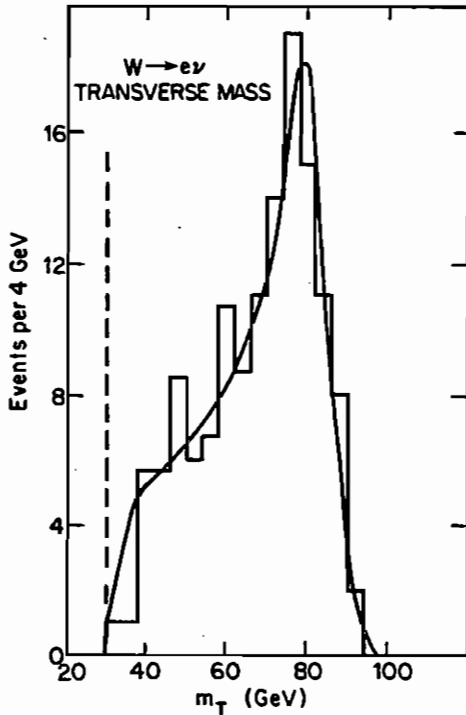


Fig. 8.12. Transverse $e\nu$ mass distribution from the UA1 experiment.

mined is a crucial limiting factor in determining the shape in this region. For each event the uncertainty in $m_T(e, \nu)$ is $\Delta m_T \approx \Delta p_{\nu T}$. If the uncertainty in the missing transverse momentum can be reduced to the order of 1 GeV, which may eventually be feasible, it should become possible to determine Γ_W from the endpoint region of the m_T distribution.

Figure 8.12 shows the measured $m_T(e, \nu)$ distribution from the UA1 experiment indicating a mass $M_W \simeq 83 \pm 4$ GeV. The curve represents a theoretical calculation, including acceptance and efficiency corrections. Only an upper limit $\Gamma_W < 6.5$ GeV has been deduced thus far from the data.

A background to the $W \rightarrow e\nu$ signal comes from the cascade decay $W \rightarrow \tau\nu$, $\tau \rightarrow e\nu\bar{\nu}$. Since the neutrinos are undetected, this process is topologically indistinguishable from $W \rightarrow e\nu$ decay, but has different dynamical distributions. The case $u\bar{d} \rightarrow W^+ \rightarrow \tau^+\nu_\tau \rightarrow e^+\nu_e\nu_\tau\bar{\nu}_\tau$ is illustrated in Fig. 8.13. The matrix element for the process is

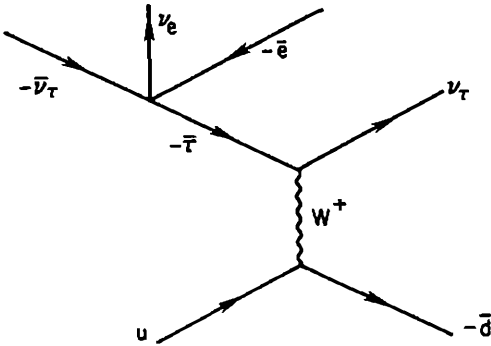


Fig. 8.13. The production/decay chain $u\bar{d} \rightarrow W^+ \rightarrow \tau^+\nu \rightarrow e^+\nu\nu\bar{\nu}$.

$$\begin{aligned} \mathcal{M} = & \left(\frac{G_F}{\sqrt{2}} \right)^2 \frac{M_W^2}{\hat{s} - M_W^2 + iM_W\Gamma_W} \frac{1}{p_\tau^2 - m_\tau^2 + im_\tau\Gamma_\tau} \\ & \times \left[\bar{v}(\bar{d})\gamma^\alpha(1 - \gamma_5)u(u) \right] \left[\bar{u}(\nu_e)\gamma^\beta(1 - \gamma_5)v(\bar{e}) \right] \\ & \times \left[\bar{u}(\nu_\tau)\gamma_\alpha(1 - \gamma_5)(\not{p}_\tau + m_\tau)\gamma_\beta(1 - \gamma_5)v(\bar{\nu}_\tau) \right]. \end{aligned}$$

Squaring and summing over spin states, this can be reduced in the approximation of narrow τ and W widths to

$$\begin{aligned} \sum |\mathcal{M}|^2 = & 2^{14} G_F^4 M_W^4 \left(\frac{\pi}{M_W\Gamma_W} \right) \left(\frac{\pi}{m_\tau\Gamma_\tau} \right) \\ & \times (\nu_\tau \cdot \bar{d} \bar{\tau} \cdot u \bar{\tau} \cdot \nu_e \bar{\nu}_\tau \cdot \bar{e} - \frac{1}{2} m_\tau^2 \nu_\tau \cdot \bar{d} \nu_e \cdot u \bar{\nu}_\tau \cdot e) \\ & \times \delta(\hat{s} - M_W^2) \delta(\tau^2 - m_\tau^2). \end{aligned}$$

We note that Γ_τ^{-1} is the τ lifetime that has been directly measured. The subprocess cross section is given by

$$d\hat{\sigma} = \left(\frac{1}{2} \right)^2 \frac{1}{2\hat{s}} \sum |\mathcal{M}|^2 (2\pi)^{4-12} d_4(PS).$$

After analytically evaluating the delta function integration, the rest of the four-particle phase space integral is best carried out numerically, using Monte Carlo techniques.

Figure 8.11 compares the m_T distribution from $W \rightarrow \tau$ with that from $W \rightarrow e\nu$. We see that the m_T distribution from the $W \rightarrow \tau \rightarrow e$ mode is peaked towards low values.

8.7 Transverse Motion of W

The lowest-order fusion process $q\bar{q}' \rightarrow W$, evaluated with QCD-evolved quark distributions and multiplied by a K -factor for non-leading QCD corrections, gives the total W hadroproduction cross section correctly through order α_s . However, since the Altarelli-Parisi equations are based on a longitudinal approximation, the QCD-evolved distributions do not include the transverse momentum that should accompany the radiation of gluons and quarks. To include transverse momenta from radiated gluons and quarks, one can explicitly evaluate multiple emissions; techniques have been developed to sum the radiated momenta and obtain the net recoil W momentum. Alternatively one can explicitly simulate the radiative events by Monte Carlo methods; this is the Monte Carlo shower approach described in §9.4, which has the advantage of describing the associated hadron jets, too. For the present, we consider a simplified approach based on the $\mathcal{O}(\alpha_s)$ subprocesses shown in Fig. 8.14, with the incident partons in these diagrams evolved up to the scale $Q^2 = M_W^2$ in the folding to obtain hadronic cross sections. At very large p_T , these $\mathcal{O}(\alpha_s)$ subprocesses are expected to dominate; here the argument of α_s is plausibly proportional to p_T^2 , and higher order QCD processes are suppressed by powers of α_s .

Exercise. Derive the spin and color averaged cross section formula for the annihilation subprocess $q\bar{q}' \rightarrow Wg$,

$$\frac{d\hat{\sigma}}{d\hat{t}} = \frac{4}{9} \alpha_s \frac{G_F M_W^2}{\sqrt{2}} \frac{|V_{qq'}|^2}{\hat{s}^2} \left[\frac{\hat{t}^2 + \hat{u}^2 + 2\hat{s}M_W^2}{\hat{t}\hat{u}} \right],$$

where $\hat{s} = (q + \bar{q}')^2$, $\hat{t} = (q - W)^2$ and $\hat{u} = (\bar{q}' - W)^2$.

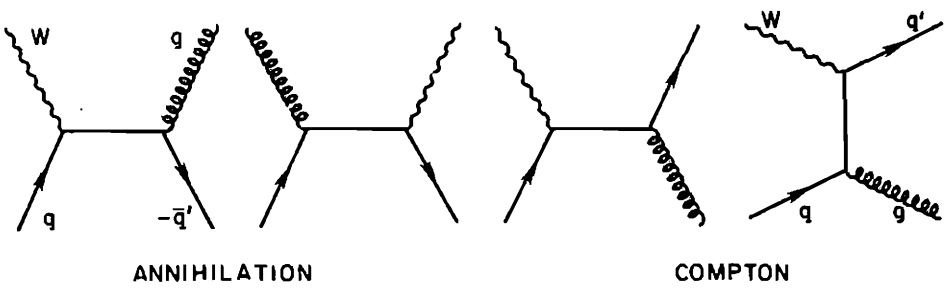


Fig. 8.14. $O(\alpha_s)$ annihilation and Compton subprocesses for W production.

Exercise. Using crossing symmetry, derive the corresponding result for the Compton subprocess $qg \rightarrow Wq'$

$$\frac{d\hat{\sigma}}{d\hat{t}} = \frac{1}{6} \alpha_s \frac{G_F M_W^2}{\sqrt{2}} \frac{|V_{qq'}|^2}{\hat{s}^2} \left[\frac{\hat{s}^2 + \hat{t}^2 + 2\hat{u}M_W^2}{-\hat{t}} \right].$$

In $p\bar{p}$ collisions at c.m. energies below 1 TeV, the cross section contribution from the annihilation subprocess is almost an order of magnitude larger than the Compton contribution. In the following discussion we neglect the Compton contribution.

To obtain the distributions of $W \rightarrow e\nu$ decay products, we need the matrix element for the complete production/decay sequence $q\bar{q}' \rightarrow Wg \rightarrow e\nu g$ containing W polarization effects. This is obtained by crossing from a result in §10.2.3, in a rather simple form:

$$d\sigma(\bar{u}d \rightarrow e\bar{\nu}g) =$$

$$\left(\frac{G_F}{\sqrt{2}}\right)^2 \frac{32\alpha_s W^2 M_W^4 |V_{ud}|^2 [(e \cdot \bar{u})^2 + (\bar{\nu} \cdot d)^2] \delta^4(\bar{u} + d - e - \bar{\nu} - g)}{9\pi^4 \hat{s} \hat{t} \hat{u} [(W^2 - M_W^2)^2 + \Gamma_W^2 M_W^2]} \prod_{j=e,\bar{\nu},g} \frac{d^3 p_j}{2E_j}.$$

The corresponding Compton formulas are again obtained by crossing.

These cross sections have mass and infrared singularities, which cause a divergence at $p_T^2 = 0$. As we saw in Chapter 7, the infrared singularities cancel when loop diagrams are taken into account, while mass singularities are factored out into the parton distributions. In short, this divergence is unphysical and would be explicitly removed in an ideal treatment. Here we shall simply regularize the divergence with a p_T cut-off factor, representing our ignorance of the precise details at small p_T , and multiply by the factor K for non-leading enhancements.

The $\mathcal{O}(\alpha_s)$ calculation alone will provide a useful approximation to the complete $AB \rightarrow WX$ hadronic production process if we adjust this cut-off factor such that the integrated $\mathcal{O}(\alpha_s)$ cross section equals the total $AB \rightarrow WX$ cross section to order α_s . This condition can be written

$$\int d_{ab} \int dp_T^2 f d\sigma_1/dp_T^2 = \int d_{ab} K \sigma_0 ,$$

where $d_{ab} = dx_a dx_b \sum_{q,q'} q(x_a, M_W^2) \bar{q}'(x_b, M_W^2)$, $d\sigma_1/dp_T^2$ is the $\mathcal{O}(\alpha_s) q\bar{q}' \rightarrow Wg$ differential cross section, $f(p_T^2)$ is the cut-off factor, σ_0 is the $q\bar{q}' \rightarrow W$ fusion cross section. We have implicitly neglected a QCD enhancement of the first-order cross section $d\sigma_1/dp_T^2$ which is known to be a reasonable approximation. In this calculational method, the lowest order cross section σ_0 enters only through the normalization condition above. This truncated QCD shower approximation, which we call the "Poor Man's Shower Model," gives both the total cross section and the p_T -dependence at large p_T . The p_T -dependence at small and intermediate p_T (where multiple emissions contribute) is not exactly correct, but its integral is constrained to be correct so the deviations are not expected to be serious.

Figure 8.15 shows a comparison of the Poor Man's Shower (PMS) with $p_T(W)$ distribution measured by the UA1 collaboration at the CERN $p\bar{p}$ collider. Also shown is a full QCD shower calculation.

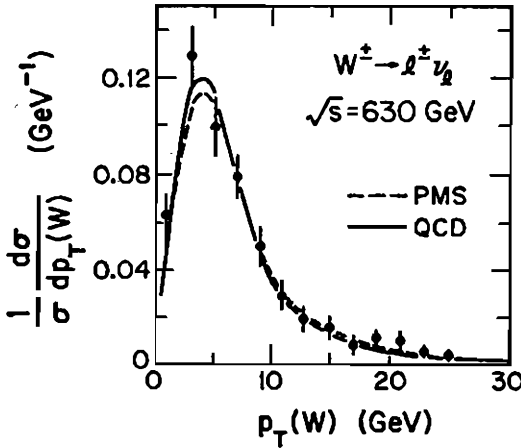


Fig. 8.15. Comparison of the truncated QCD shower prediction (PMS) and full QCD shower prediction with the $p_T(W)$ distribution measured by the UA1 collaboration at CERN $p\bar{p}$ collider.

8.8 Weak Boson Decay Angular Distributions

As shown in §8.5, the $V-A$ interaction causes the electron (positron) from the decay of a W^- (W^+) to be emitted along the incoming quark (antiquark) direction with an angular distribution

$$\frac{d\hat{\sigma}}{d\cos\hat{\theta}} \sim (1 + \cos\hat{\theta})^2,$$

where $\hat{\theta}$ is the emission angle of the electron (positron) with respect to the proton (antiproton) direction in the W rest frame. This angular distribution is shown in Fig. 8.16 for well measured $W \rightarrow e\nu$ events observed by the UA1 collaboration at the CERN $p\bar{p}$ collider in which the sign of the e^\pm are determined. The data agree well with the prediction above.

The spin of the W -boson can be determined from these events using the theoretical relation for $J \neq 0$,

$$\langle \cos\hat{\theta} \rangle = \langle \lambda \rangle \langle \mu \rangle / J(J + 1),$$

where $\langle \mu \rangle$ and $\langle \lambda \rangle$ are the global helicity of the production system ($u\bar{d}$) and decay system ($e^+\nu$), respectively. For $V-A$ interactions

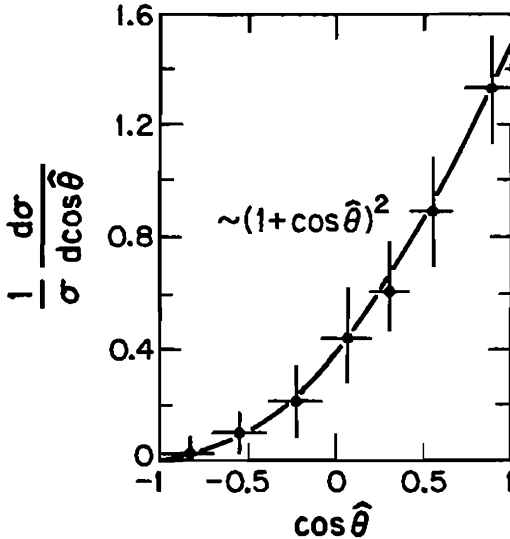


Fig. 8.16. Measured $W \rightarrow e\nu$ decay angular distribution from the UA1 collaboration at the CERN $p\bar{p}$ collider, compared with the predicted distribution for $V-A$ interactions.

$\langle \lambda \rangle = \langle \mu \rangle = -1$ and $J = 1$ leading to the prediction

$$\langle \cos \hat{\theta} \rangle = 0.5,$$

whereas one expects $\langle \cos \hat{\theta} \rangle = 0$ for $J = 0$ and $\langle \cos \hat{\theta} \rangle \leq 1/6$ for $J \geq 2$. The experimental value

$$\langle \cos \hat{\theta} \rangle = 0.43 \pm 0.07$$

agrees with the $J = 1$ assignment for the W and the prediction of maximal helicity at production and decay vertices.

Similar consideration apply to Z production and decay to e^+e^- . The angular distribution there involves both $V-A$ and $V+A$ couplings and can be used to deduce the value of x_w .

Exercise. For $q\bar{q} \rightarrow Z \rightarrow e^+e^-$ show that the angular distribution in the Z rest frame is

$$\frac{d\hat{\sigma}}{d\cos\hat{\theta}} \sim [(g_V^q)^2 + (g_A^q)^2][(g_V^e)^2 + (g_A^e)^2](1 + \cos^2\hat{\theta}) + 8g_A^q g_V^q g_A^e g_V^e \cos\hat{\theta}.$$

Figure 8.17 shows a comparison of experiment and theory for $Z \rightarrow \ell^+\ell^-$ events.

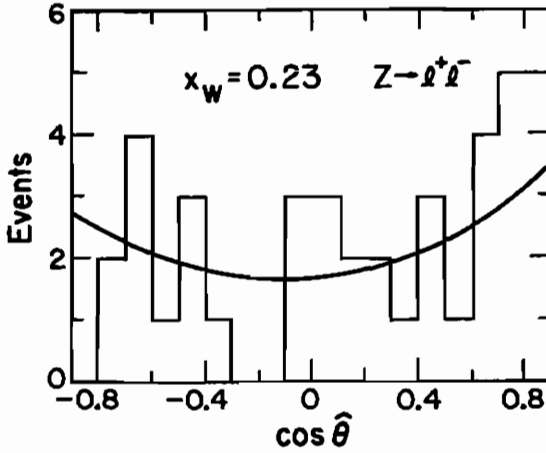


Fig. 8.17. Measured $Z \rightarrow \ell^+ \ell^-$ decay angular distribution from the UA1 collaboration at the CERN $p\bar{p}$ collider, compared with standard model prediction for $x_w = 0.23$.

8.9 W, Z Pair Production

The production of W^+W^- in e^+e^- collisions will lead to a precise determination of W boson properties—its mass, width and couplings to different quark flavors. Single W production via $e^+e^- \rightarrow W e \nu$, is higher order in α than W^+W^- and its cross section is three orders of magnitude smaller. The $e^+e^- \rightarrow W^+W^-$ process provides the best opportunity to measure the $WW\gamma$ and WWZ couplings and test the gauge theory predictions for the Yang-Mills self-interactions. There are cancellations among the three contributing diagrams in Fig. 8.18 and small deviations from the gauge theory couplings would lead to observable effects.

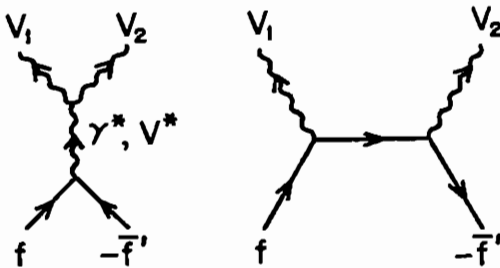


Fig. 8.18. Representative lowest order contributing diagrams for $f \bar{f}' \rightarrow V_1 V_2$.

In pp or $p\bar{p}$ collisions the W^+W^- , $W^\pm Z$ and ZZ final states can be realized. The W^+W^- contribution is an important background to the signal for a heavy Higgs boson (see §12.5). Also gauge boson pairs are backgrounds to the search at hadron supercolliders for new heavy quarks and heavy leptons that decay to W -bosons (§10.3, §13.7).

In the following we denote the incident fermion (antifermion) by f (\bar{f}') and the produced gauge bosons by V_1, V_2 . The amplitude for $f\bar{f}' \rightarrow V_1V_2$ has the general form

$$M(f\bar{f}' \rightarrow V_1V_2) = i\bar{v}(\bar{f}')T^{\mu\nu}u(f)\epsilon_\mu^*(V_2)\epsilon_\nu^*(V_1),$$

where ϵ denotes a polarization vector and the tensor $T^{\mu\nu}$ is process dependent. We shall use the notation

$$\begin{aligned} \ell_1 &= f - V_1, & \ell_2 &= f - V_2, \\ \hat{s} &= (f + \bar{f}')^2, & \hat{t} &= \ell_1^2, & \hat{u} &= \ell_2^2, \end{aligned}$$

and $D_V = (\hat{s} - M_V^2 + iM_V\Gamma_V)^{-1}$. The tensors for W^+W^- , ZZ and WZ production are given by

$$\begin{aligned} T_{\mu\nu}^{W^+W^-} &= e^2 \left(\frac{Q_f}{\hat{s}} + D_Z \frac{g_V^f - g_A^f \gamma_5}{x_w} \right) \\ &\quad \times [g_{\mu\nu}(\not{V}_1 - \not{V}_2) + \gamma_\mu(2V_2 + V_1)_\nu - \gamma_\nu(2V_1 + V_2)_\mu] \\ &\quad - e^2 \frac{(1 + \gamma_5)}{4x_w} \left[\theta(-Q_f) \frac{\gamma_\mu \not{\ell}_1 \gamma_\nu}{\hat{t}} + \theta(Q_f) \frac{\gamma_\nu \not{\ell}_2 \gamma_\mu}{\hat{u}} \right], \\ T_{\mu\nu}^{ZZ} &= -e^2 \frac{(g_V^f)^2 + (g_A^f)^2 - 2g_V^f g_A^f \gamma_5}{x_w(1 - x_w)} \left(\frac{\gamma_\mu \not{\ell}_1 \gamma_\nu}{\hat{t}} + \frac{\gamma_\nu \not{\ell}_2 \gamma_\mu}{\hat{u}} \right), \\ T_{\mu\nu}^{W^-Z} &= e^2 \frac{V_{ff'}(1 + \gamma_5)}{2\sqrt{2} x_w \cos \theta_w} \\ &\quad \times \left\{ D_W(1 - x_w) [g_{\mu\nu}(\not{Z} - \not{W}) + \gamma_\nu(2W + Z)_\mu - \gamma_\mu(2Z + W)_\nu] \right. \\ &\quad \left. - g_L^f \frac{\gamma_\mu \not{\ell}_1 \gamma_\nu}{\hat{t}} - g_L^f \frac{\gamma_\nu \not{\ell}_2 \gamma_\mu}{\hat{u}} \right\}. \end{aligned}$$

For W^+Z production interchange g^f and $-g^{f'}$ and interchange \hat{u} and \hat{t} in the W^-Z expression above.

In writing the differential cross section expressions we use the notation

$$U_T = \hat{u}\hat{t} - M_{V_1}^2 M_{V_2}^2, \quad \beta_V = \left[\left(1 - \frac{M_{V_1}^2 + M_{V_2}^2}{\hat{s}} \right)^2 - \frac{4M_{V_1}^2 M_{V_2}^2}{\hat{s}^2} \right]^{\frac{1}{2}},$$

where β_V is a threshold factor. Also we denote the color average factor by C ($C = \frac{1}{3}$ for $\bar{q}q$ and $C = 1$ for e^+e^-) and the third component of weak isospin by T_3^f . The cross sections are then

$$\begin{aligned} \frac{d\hat{\sigma}(W^+W^-)}{d\hat{t}} &= \frac{\pi\alpha^2 C}{4x_w^2 \hat{s}^2} \left\{ \frac{U_T}{\hat{s}^2} \left[3 - \frac{1}{1-x_w} \frac{g_L^f}{T_3^f} (\hat{s} - 6M_W^2) \mathcal{R}e D_Z \right. \right. \\ &+ \left. \frac{(g_L^f)^2 + (g_R^f)^2}{(1-x_w)^2} \left(\beta_W^2 + \frac{12M_W^4}{\hat{s}^2} \right) \hat{s}^2 |D_Z|^2 \right] - \frac{4g_L^f}{T_3^f} M_Z^2 \mathcal{R}e D_Z \\ &+ 4 \frac{(g_L^f)^2 + (g_R^f)^2}{1-x_w} M_Z^2 \hat{s} \beta_W^2 |D_Z|^2 \\ &+ \theta(-Q_f) \left[2 \left(1 + \frac{g_L^f}{T_3^f} M_Z^2 \mathcal{R}e D_Z \right) \left(\frac{U_T}{\hat{s}\hat{t}} - \frac{2M_W^2}{\hat{t}} \right) + \frac{U_T}{\hat{t}^2} \right] \\ &+ \left. \theta(Q_f) \left[2 \left(1 + \frac{g_L^f}{T_3^f} M_Z^2 \mathcal{R}e D_Z \right) \left(\frac{U_T}{\hat{s}\hat{u}} - \frac{2M_W^2}{\hat{u}} \right) + \frac{U_T}{\hat{u}^2} \right] \right\}, \end{aligned}$$

$$\frac{d\hat{\sigma}(ZZ)}{d\hat{t}} = \frac{\pi\alpha^2 C}{x_w^2 \hat{s}^2} \frac{(g_L^f)^4 + (g_R^f)^4}{(1-x_w)^2} \left[\frac{\hat{t}}{\hat{u}} + \frac{\hat{u}}{\hat{t}} + \frac{4M_Z^2 \hat{s}}{\hat{t}\hat{u}} - M_Z^4 \left(\frac{1}{\hat{t}^2} + \frac{1}{\hat{u}^2} \right) \right],$$

$$\begin{aligned} \frac{d\hat{\sigma}(W^-Z)}{d\hat{t}} &= \frac{\pi\alpha^2 C |V_{ff'}|^2}{2x_w^2 \hat{s}^2} \left\{ \frac{1}{4} \left[(9-8x_w)U_T - (6-8x_w)(M_W^2 + M_Z^2)\hat{s} \right] \right. \\ &\times |D_W|^2 + 2 \left[U_T - (M_W^2 + M_Z^2)\hat{s} \right] \left(\frac{g_L^{f'}}{\hat{t}} - \frac{g_L^f}{\hat{u}} \right) \mathcal{R}e D_W \\ &+ \left. \frac{U_T}{1-x_w} \left[\left(\frac{g_L^{f'}}{\hat{t}} \right)^2 + \left(\frac{g_L^f}{\hat{u}} \right)^2 \right] + \frac{2(M_W^2 + M_Z^2)\hat{s}}{1-x_w} \frac{g^{f'}}{\hat{t}} \frac{g_L^f}{\hat{u}} \right\}, \end{aligned}$$

for W^+Z production, interchange \hat{t} and \hat{u} in the above formula.

The integrated cross sections for $e^+e^- \rightarrow W^+W^-$ and ZZ are shown in Fig. 8.19 versus c.m. energy \sqrt{s} ($=\sqrt{\hat{s}}$ in the above formulas). The s -dependence of W^+W^- production near threshold will be measured at LEP II.

Exercise. Determine the expected value of $R = \sigma(e^+e^- \rightarrow \text{hadrons}) / \sigma(e^+e^- \rightarrow \gamma^* \rightarrow \mu^+\mu^-)$ from $e^+e^- \rightarrow W^+W^-$ with $W^\pm \rightarrow \text{hadrons}$ at $\sqrt{s} = 200 \text{ GeV}$ and $\sqrt{s} = 600 \text{ GeV}$.

The energy dependence of the total cross sections is crucially dependent on gauge cancellations. For example in $e^+e^- \rightarrow W^+W^-$ the contribution of the ν -exchange diagram grows very rapidly with energy

$$\sigma(\nu\text{-exchange}) \simeq \frac{\pi\alpha^2 s}{96x_W^2 M_W^4}$$

but the full standard model result decreases at high energy

$$\sigma(\text{standard model}) \simeq \frac{\pi\alpha^2}{2x_W^2 s} \ln\left(\frac{s}{M_W^2}\right)$$

as illustrated in Fig. 8.19.

In $e^+e^- \rightarrow W^+W^-$ the W^+ is produced preferentially along the e^+ direction. The angular distribution is shown in Fig. 8.20 at c.m. energies $\sqrt{s} = 200 \text{ GeV}$ and 600 GeV . The distribution becomes more sharply peaked forward as the energy increases. This forward peaking will enable the separation of this contribution from possible new physics sources that decay to W^+W^- (Higgs boson, heavy leptons, heavy quarks).

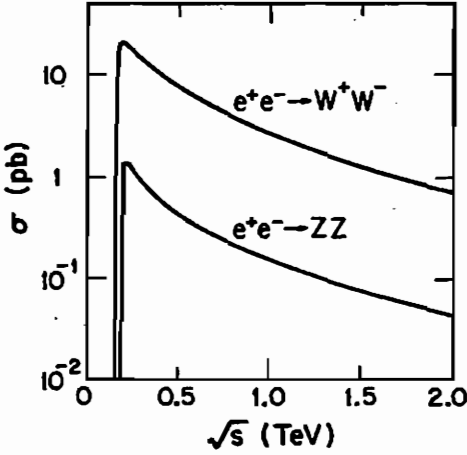


Fig. 8.19. Total cross sections for $e^+e^- \rightarrow W^+W^-$ and ZZ versus the total c.m. energy \sqrt{s} .

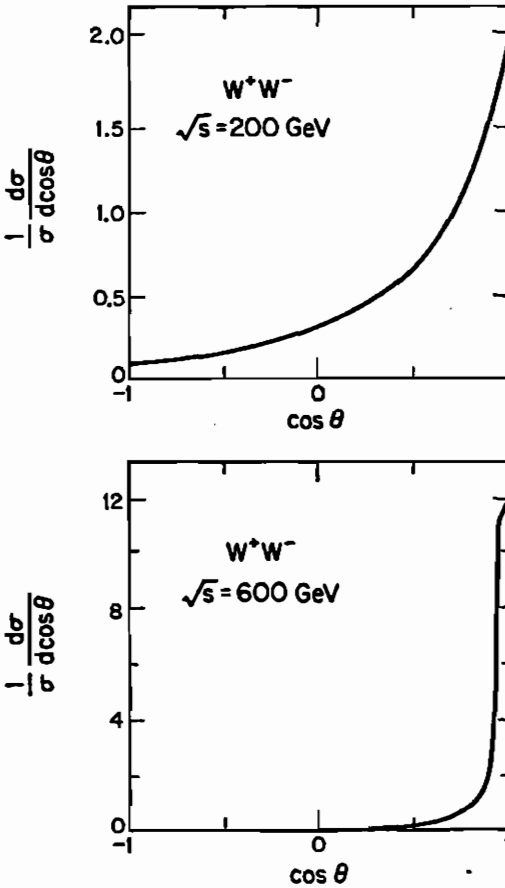


Fig. 8.20. Angular distribution of $e^+e^- \rightarrow W^+W^-$. θ is the angle between W^+ and e^+ .

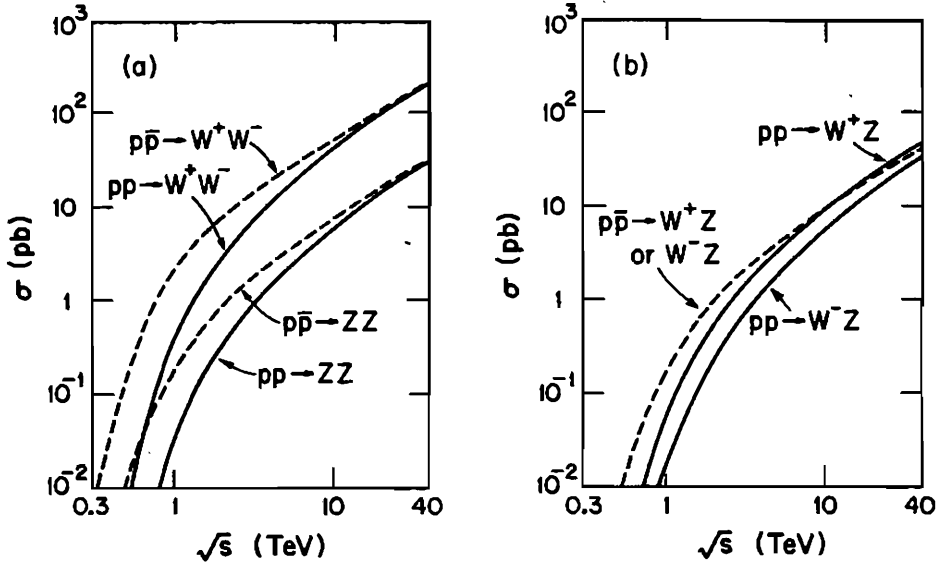


Fig. 8.21. Total cross sections in pp and $p\bar{p}$ collisions for gauge boson pair production versus the total energy \sqrt{s} : (a) W^+W^- and ZZ ; (b) $W^\pm Z$.

In $e^+e^- \rightarrow W^+W^-$ production the boson spins are correlated; this gives correlations between their decay products $W^+ \rightarrow a\bar{b}$, $W^- \rightarrow c\bar{d}$, where a, b, c, d are leptons or quarks (jets). To calculate these effects the full matrix element for $e^+e^- \rightarrow a\bar{b}c\bar{d}$ must be evaluated. There are very many lepton-lepton, lepton-jet and jet-jet correlations that can be studied to test the gauge theory couplings.

The total cross sections for gauge boson pairs produced in pp and $p\bar{p}$ collisions are shown in Fig. 8.21 versus \sqrt{s} . The W^+Z production process has a clean experimental signature with $W^+ \rightarrow e\nu$ and $Z \rightarrow e\bar{e}$ decays.

The W, Z pair production cross sections for transverse and longitudinal polarized vector bosons have also been evaluated in the literature for both e^+e^- and $pp, p\bar{p}$ collisions. At high energies, $\sqrt{s} \gg M_W$, the cross sections for transversely polarized W and Z bosons dominate over those for longitudinal polarizations. Figure 8.22 shows

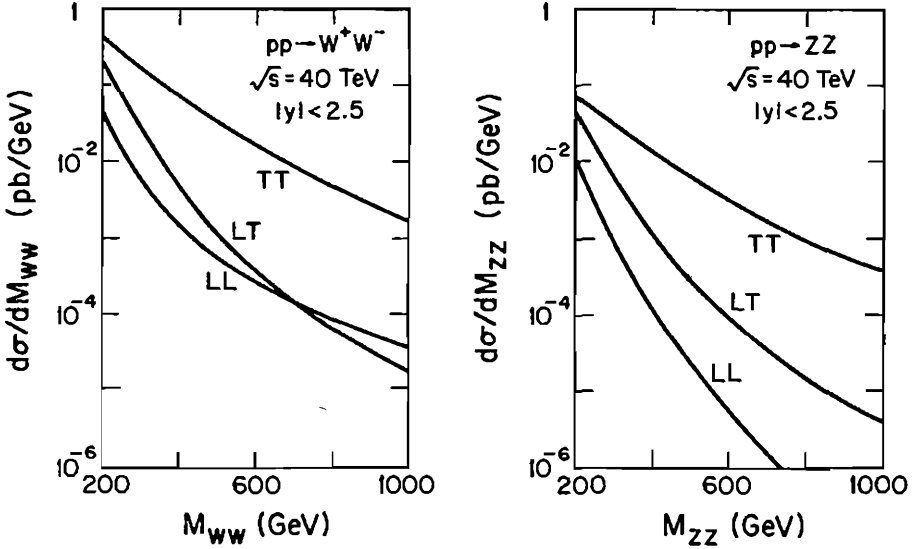


Fig. 8.22. Invariant mass distribution for W^+W^- and ZZ pair production in pp collisions at 40 TeV. T (transverse) and L (longitudinal) refer to the polarizations of the weak bosons.

results for WW and ZZ pair production in pp collisions at 40 TeV. As the energy increases the W, Z mass effects become less important and the weak bosons become transverse.

The Goldstone boson equivalence theorem states that an amplitude involving external longitudinally polarized gauge bosons is equivalent to the amplitude with the external gauge bosons replaced by corresponding Goldstone bosons, up to corrections of order M_V/E_V where E_V is the gauge boson energy. The couplings of the Goldstone bosons are like those of the physical Higgs boson since they belong to the original $SU(2)$ Higgs doublet. Consequently the coupling of longitudinally polarized W and Z bosons to light quarks is suppressed at high energies by a factor of order M_V/E_V . On the other hand, the W and Z bosons that result from the decay of heavy particles are predominantly longitudinally polarized. For example the coupling of Goldstone boson pairs to a Higgs boson, a Z' boson and a

heavy quark are enhanced by factors $(m_H/M_W)^2$, $(M_{Z'}/M_W)^2$ and (m_f/M_W) , respectively. This should help in separating these signals from the continuum backgrounds.

8.10 Effective W, Z Approximation

The parton model with QCD evolved distributions provides a successful description of hadronic interactions at high energies. As the energy increases and the charm, bottom and top thresholds are crossed it is necessary to include their contributions in the parton sea. At still higher energies that will be reached at hadron supercolliders the W and Z gauge bosons will be significant additions to the parton sea. The distributions of W and Z bosons can be calculated in a manner similar to the effective photon approximation for the distribution of photons in an electron. A difference is that a massive gauge boson has both transverse and longitudinal polarizations that must be treated separately. The W and Z distributions can be used to calculate cross sections in the parton model just as quark or gluon distributions are used. Final states reached by VV scattering, where $V = W$ or Z , can be simply estimated with this *effective W, Z approximation* for subprocess c.m. energies $\hat{s} \gg M_V^2 \gg M_V^2$.

In order to obtain the effective W or Z distribution one starts with the process $f_1 + f_2 \rightarrow f'_1 + X$ mediated by a gauge boson V_h of helicity h in the t -channel as illustrated in Fig. 8.23. Here the fermions f can be either leptons or quarks. Then in the approximation that V_h is produced via a collinear transition $f_1 \rightarrow f'_1 + V_h$, the cross section can be written as

$$\sigma(f_1 + f_2 \rightarrow f'_1 + X) = \sum_h \int_{M_V/E_1}^1 dx P_{V/f_1}^h(x) \sigma(V_h + f_2 \rightarrow X),$$

where $P_{V/f_1}^h(x)$ is the distribution function for finding a gauge boson V of helicity h in a fermion f_1 and $x = (E_{f_1} - E_{f'_1})/E_{f_1}$ is the fraction of the f_1 energy carried by V .

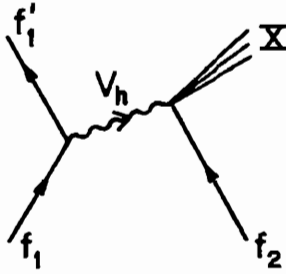


Fig. 8.23. Process of $f_1 + f_2 \rightarrow f_1' + X$, mediated by a gauge boson V_h of polarization h . Here V_h can be taken as a parton inside a fermion f_1 .

In the leading logarithm approximation the distribution of transverse and longitudinal gauge bosons in a fermion f with energy E in the limit $E \gg M_V$ are (note that this prescription is frame-dependent)

$$P_{V/f}^\pm(x) = \frac{C}{16\pi^2 x} \left[(g_V^f \mp g_A^f)^2 + (g_V^f \pm g_A^f)^2 (1-x)^2 \right] \ln \left(\frac{4E^2}{M_V^2} \right),$$

$$P_{V/f}^0(x) = C \frac{(g_V^f)^2 + (g_A^f)^2}{4\pi^2} \left[\frac{1-x}{x} \right],$$

where for W -bosons $C = g^2/8$, $g_V = -g_A = 1$ and for Z -bosons $C = g^2/(1-x_w)$, $g_V = \frac{1}{2}T_3 - Qx_w$, $g_A = -\frac{1}{2}T_3$.

We note in passing that in the effective photon approximation where electron beams are treated as sources of on-shell photons the distributions are

$$P_{\gamma/e}(x) = \frac{\alpha}{\pi} \frac{1 + (1-x)^2}{x} \ln(E_e/m_e),$$

$$P_{e/\gamma}(x) = \frac{\alpha}{\pi} \frac{1 + x^2}{(1-x)} \ln(E_\gamma/m_e),$$

where x is the momentum fraction carried by the emitted particle.

Exercise. Show that the cross section for producing a heavy final state particle X via a pair of gauge bosons V_1 and V_2 of helicities h

and h' is

$$\hat{\sigma}(f_1 f_2 \rightarrow f'_1 f'_2 V_1^h V_2^{h'} \rightarrow f'_1 f'_2 X) = \int d\tau \frac{d\mathcal{L}}{d\tau} \hat{\sigma}(V_1^h V_2^{h'} \rightarrow X),$$

where $\tau = m_X^2/\hat{s}$ with $\hat{s} = (f_1 + f_2)^2$, and the effective luminosity is defined by

$$\frac{d\mathcal{L}}{d\tau} = \int_{\tau}^1 \frac{dx}{x} P_{V_1/f_1}^h(x) P_{V_2/f_2}^{h'}(\tau/x).$$

In the case that X is a spinless particle show that

$$\hat{\sigma}(f_1 f_2 \rightarrow f'_1 f'_2 X) = \frac{16\pi^2}{m_X^3} \Gamma(X \rightarrow V_1^h V_2^{h'}) \tau \frac{d\mathcal{L}}{d\tau},$$

Exercise. Using the expressions for $P_{V/f}^h$ given previously show for a pair of transversely polarized gauge bosons of helicities h and h' that

$$\begin{aligned} \frac{d\mathcal{L}}{d\tau} = & \frac{C^2}{(16\pi^2)^2} \left[\ln\left(\frac{\hat{s}}{M_V^2}\right) \right]^2 \left\{ \frac{1}{\tau} \left[(2+\tau)^2 \ln\left(\frac{1}{\tau}\right) - 2(1-\tau)(3+\tau) \right] G_1 G_2 \right. \\ & + \left[(\tau+4) \ln\left(\frac{1}{\tau}\right) - 4(1-\tau) \right] h h' I_1 I_2 \\ & \left. + \frac{1}{\tau} \left[\tau(4+\tau) \ln\left(\frac{1}{\tau}\right) - 3(1-\tau^2) \right] (h G_1 I_2 + h' G_2 I_1) \right\}, \end{aligned}$$

where $G_i = (g_V^{f_i})^2 + (g_A^{f_i})^2$ and $I_i = 2g_V^{f_i} g_A^{f_i}$. For a pair of longitudinally polarized gauge bosons show that

$$\frac{d\mathcal{L}}{d\tau} = C^2 \frac{G_1 G_2}{16\pi^4 \tau} \left[(1+\tau) \ln\left(\frac{1}{\tau}\right) - 2(1-\tau) \right].$$

In the case that f is a quark in a hadron we obtain the hadronic cross section by convoluting the subprocess cross section with the

quark distributions in the hadrons A and B and sum over all possible contributions from quarks:

$$\begin{aligned} & \sigma(AB \rightarrow V_1 V_2 \rightarrow X + \text{anything}) \\ &= \sum_{h, h'} \sum_{i, j} \int d\tau' \int_{\tau'}^1 \frac{dx'}{x'} f_{q_i/A}(x') f_{q_j/B}\left(\frac{\tau'}{x'}\right) \hat{\sigma}(q_i q_j \rightarrow V_1^h V_2^{h'} \rightarrow q'_i q'_j X), \end{aligned}$$

where $\tau' = \hat{s}/s \geq m_X^2/s$ and s is the total c.m. energy of the AB system, and $f_{q/A}(x)$ is the distribution function of quark q in the hadron A .

Exercise. In the effective W approximation show that the differential cross section for $e^+e^- \rightarrow \bar{\nu}_e \nu_e W^+ W^- \rightarrow \bar{\nu}_e \nu_e X$ scattering to an inclusive final state X is given by

$$\begin{aligned} \frac{d\sigma}{dM_{WW} dM} &= \frac{4MM_{WW}}{s^2[(1 + \tau - \eta)^2 - 4\tau]^{1/2}} \\ &\times \left[P_{W^+/e^+}(x_+) f_{W^-/e^-}(x_-) + P_{W^+/e^+}(x_-) P_{W^-/e^-}(x_+) \right] \hat{\sigma}_{WW}(M_{WW}), \end{aligned}$$

where M is the invariant mass of $\bar{\nu}_e$ and ν_e , $\tau = M_{WW}^2/s$, $\eta = M^2/s$, $x_{\pm} = \frac{1}{2}\{1 + \tau - \eta \pm [(1 + \tau - \eta)^2 - 4\tau]^{1/2}\}$ and $\hat{\sigma}$ is the $WW \rightarrow X$ subprocess cross section.

The effective W, Z approximation has been used in calculations of heavy Higgs boson production, heavy lepton production and heavy quark production at supercollider energies. Exact calculations were later made for these processes and found to give comparable results to the effective W, Z approximation in the kinematic range of its validity. The approximation is now of interest mainly because of its simplicity for making estimates.

Chapter 9

Jets

9.1 e^+e^- Collisions

9.1.1 Two jet production.

Jet production was first observed at e^+e^- colliders in 1975. The lowest order process for producing hadrons here is

$$e^+e^- \rightarrow q\bar{q}$$

with cross section given in §4.6, where the quarks fragment into hadrons. Up to about $Q = E_{cm} = 3$ GeV the dominant feature of the final states is resonance production: $e^+e^- \rightarrow \rho^0, \omega, \phi, \dots, \psi$, but at higher energies the quark-parton ideas discussed in Chapters 5 and 6 suggest that the quarks should usually materialize as a pair of back-to-back jets. The essential assumption of the parton model, leading to the expectation of jets, is that the transverse momenta of quark fragmentation products come mainly from soft processes and remain small, whereas their longitudinal momenta can increase with the quark energy. This jet behavior began to be seen at the top of the SPEAR range ($Q = 6-8$ GeV). When PEP and PETRA energies were reached ($Q = 30-40$ GeV) it was found to be the dominant feature of hadron production, a very striking phenomenon. Figure 9.1 shows a typical two-jet event at $Q = 34$ GeV.

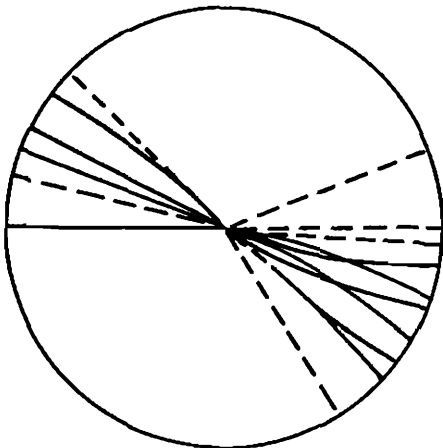


Fig. 9.1. A typical two-jet event at $Q = E_{\text{cm}} = 34$ GeV, projected on a plane normal to the beam axis. The solid (dashed) lines denote charged (neutral) particle tracks, reconstructed in the JADE detector.

To describe and quantify the “jettiness” of an event, new collective variables such as *sphericity*, *aplanarity* and *thrust* have been introduced. For each event we define the *normalized momentum tensor* M_{ab}

$$M_{ab} = \sum_i p_{ia} p_{ib} / \sum_i p_i^2,$$

where a, b run over the three space directions and p_i is the momentum of particle i , summed over final particles i in the event (ideally all particles are summed, but in practice sometimes charged particles only are used). M_{ab} is a symmetric matrix and can be diagonalized, with unit eigenvectors n_1, n_2, n_3 and eigenvalues Q_j that are normalized and ordered by

$$Q_1 + Q_2 + Q_3 = 1, \quad 0 \leq Q_1 \leq Q_2 \leq Q_3.$$

These eigenvalues can be used to quantify the event shape.

Exercise. Show that

- i) for roughly spherical events, $Q_1 \approx Q_2 \approx Q_3$;
- ii) for pancake-shaped (coplanar) events, $Q_1 \ll Q_2$;
- iii) for cigar-shaped (collinear) events, $Q_2 \ll Q_3$.

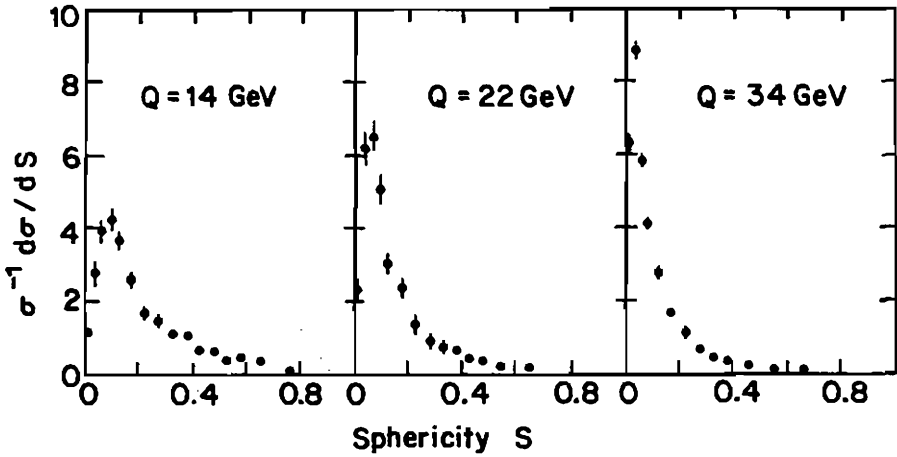


Fig. 9.2. The sphericity distribution becomes more peaked towards small S as the energy Q increases (TASSO data).

Particular combinations of the Q_j have been given names. The *sphericity* S is defined by

$$S = \frac{3}{2} (Q_1 + Q_2) = \frac{3}{2} \min \left[\frac{\sum_j (p_{jT})^2}{\sum_j (p_j)^2} \right],$$

where subscript T denotes momentum component transverse to an axis; the axis which minimizes the sum in the numerator (which is simply n_3) is called the *sphericity axis*. Sphericity lies in the range

$$0 \leq S \leq 1.$$

Events with $S \approx 1$ are rather spherical. Events with $S \ll 1$ are cigar-shaped, looking like a pair of back-to-back jets. Figure 9.2 shows how the sphericity distribution becomes more peaked at small values (*i.e.* the two-jet structure becomes more marked) as energy increases.

The plane of the eigenvectors n_2 and n_3 is called the *event plane*. The *aplanarity* A is defined by

$$A = \frac{3}{2} Q_1,$$

normalized to lie in the range $0 \leq A \leq 1/2$. A is small for coplanar

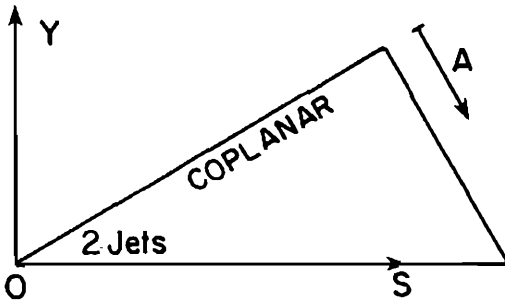


Fig. 9.3. The physical region is a triangle in the (S, Y) plane.

(including collinear) events. It turns out that the events in the high S tails of the sphericity distributions in Fig. 9.2 have small A ; these events are not collinear but they mostly remain coplanar, consistent with a three-jet interpretation (see the next section).

Event distributions are sometimes displayed as a two-dimensional scatter plot, for example in the (S, Y) plane, where

$$Y = \frac{\sqrt{3}}{2}(Q_2 - Q_1).$$

Exercise. Show that the physical region in this plane is a right-angled triangle with vertices at $(0, 0)$, $(1, 0)$, $(3/4, \sqrt{3}/4)$ and that the coordinate parallel to the shortest side is precisely A , as shown in Fig. 9.3. Hence show that two-jet events cluster near the origin, coplanar events are close to the line $S = \sqrt{3}Y$ and non-coplanar events lie in the lower right-hand part of the triangle.

The variables above based on M_{ab} have some shortcomings, however, essentially because M_{ab} has a quadratic form. First, at a purely empirical level, it is unsatisfactory that particles are weighted by the squares of their momenta in their contributions to M_{ab} , since an occasional fast track then has an exaggerated effect. Secondly, from a theoretical point of view, it would be nice to have quantities that could be calculated directly from QCD perturbation theory at the quark-gluon level, without the need for explicit Monte Carlo simulations of the fragmentation process. Now a quark can split into

a collinear quark-gluon pair with high probability (diverging in the massless limit); the final quark plus gluon have the same momentum as the original quark but contribute quite differently to any quadratic function. Quantities like M_{ab} are therefore intrinsically unstable against such collinear splittings, which are a systematic feature of QCD radiation and also appear in fragmentation where a fast parton is replaced by a jet of approximately collinear light hadrons.

A first step toward including radiative corrections in a quark-gluon description of jets was made by Sterman and Weinberg, who showed how to define cross sections free of singularities by integrating over finite ranges of energy and angle. For $e^+e^- \rightarrow q\bar{q}g$ they introduced a quantity $\sigma(Q, \theta, \epsilon, \delta)$ which is the cross section for all events where a fraction $(1 - \epsilon)$ or more of the total energy is emitted within two oppositely directed cones of half-angle δ , making an angle θ with the beam axis; see Fig. 9.4. Both ϵ and δ are $\ll 1$.

They showed that the singularities cancel out, after summing over all diagrams to a given order, leaving the result to order α_s

$$\frac{d\sigma}{d\Omega}(Q, \theta, \epsilon, \delta) = \left(\frac{d\sigma}{d\Omega}\right)_0 \left[1 - \frac{4\alpha_s}{3\pi} \left(3 \ln \delta + 4 \ln \delta \ln 2\epsilon + \frac{\pi^2}{3} - \frac{5}{2} \right) + O(\epsilon, \delta) \right],$$

where $(d\sigma/d\Omega)_0 = (3\alpha^2/4Q^2)(1 + \cos^2\theta)e_q^2$ is the zeroth-order differential cross section for massless $q\bar{q}$ production and e_q is the quark charge.

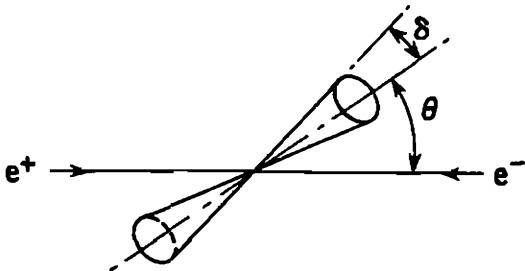


Fig. 9.4. The two cones of half-angle δ used to define the Sterman-Weinberg two-jet cross section.

Exercise. By comparing this result with the total $e^+e^- \rightarrow q\bar{q}$ cross section to order α_s , given in Chapter 7, show that the fraction of events lying within the ϵ and δ cuts above (which may be taken to define a two-jet event) is

$$f(\epsilon, \delta) = 1 - \frac{4}{3} \frac{\alpha_s}{\pi} \left[\ln \delta (4 \ln 2\epsilon + 3) + \frac{\pi^2}{3} - \frac{7}{4} \right].$$

Hence show that, if we keep f and ϵ constant as $Q \rightarrow \infty$, then δ must decrease as a power of Q : i.e. the jets become narrower.

The formulas above are strictly applicable only when δ and ϵ are small (so that their logarithms are large) while at the same time $(\alpha_s/\pi) \ln \delta$ and $(\alpha_s/\pi) \ln \epsilon$ are small. These conditions can just about be met at PEP and PETRA energies.

Exercise. Taking $Q = 35 \text{ GeV}$ and $\epsilon = 0.2$, show that about 70% of $q\bar{q}g$ events lie inside cones with half-angle $\delta = 1^\circ$ and about 80% within $\delta = 5^\circ$ according to the formula above.

These results show that perturbative QCD explicitly leads to jets; this is because QCD radiation is mainly a collinear effect. Hitherto the theoretical expectation of jets was based on the parton-model assumption of restricted p_T in fragmentation. However, the jet opening angles in the exercise above are much smaller than the typical angular spread of jets observed at PEP and PETRA (compare Fig. 9.1), which shows that non-perturbative fragmentation effects are more important in determining the structure of jets at these energies.

Jet variables based on linear sums of particle momenta are stable against collinear splittings and therefore have a chance to be both free of singularities at the quark-gluon level and to be insensitive to fragmentation details. One such variable is *thrust* T defined by

$$T = \max \left[\frac{\sum_i |\mathbf{p}_i \cdot \mathbf{n}|}{\sum_i |\mathbf{p}_i|} \right],$$

where \mathbf{n} is a unit vector chosen to maximize the numerator, which defines the *thrust axis*. Another such variable is the *acoplanarity* A' ,

which measures the flatness of an event:

$$A' = 4 \min \left[\frac{\sum_i |\mathbf{p}_i \cdot \mathbf{n}'|}{\sum_i |\mathbf{p}_i|} \right]^2,$$

where \mathbf{n}' is another unit vector chosen to minimize the numerator.

Exercise. For a spherically distributed multiparticle event, show that $T = 1/2$ and $A' = 1$. For a collinear event show that $T = 1$ and $A' = 0$. Hence show that these variables have the ranges

$$\frac{1}{2} \leq T \leq 1, \quad 0 \leq A' \leq 1.$$

The thrust axis is commonly used to define the jet axis, used in measuring the angular distribution of 2-jet events. The plane normal to \mathbf{n}' provides an alternative definition of the event plane in this linear variable approach. Figure 9.5 shows how the thrust distribution becomes narrower as total energy Q increases, corresponding to the changes of sphericity in Fig. 9.2.

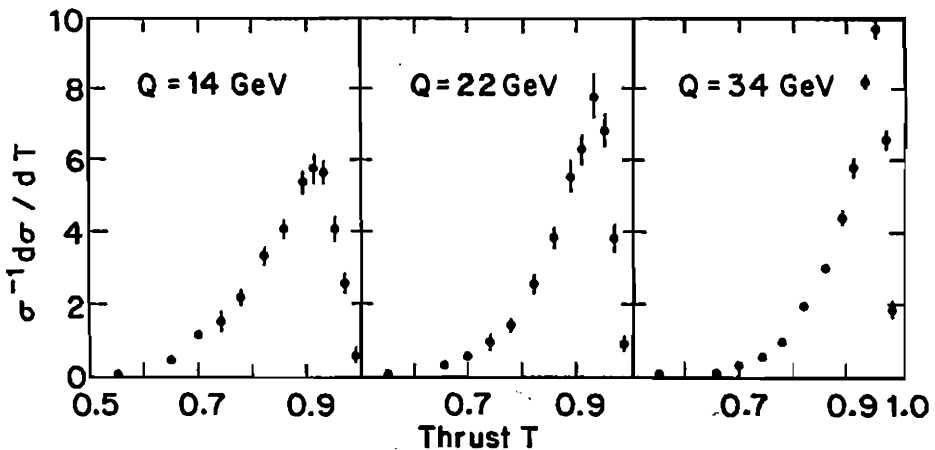


Fig. 9.5. The thrust distribution becomes more peaked toward large T as Q increases (TASSO data).

Other suggested variables include *spherocity* S' , *sphericity* S'' and harmonic moments H_ℓ , defined by

$$S' = (4/\pi)^2 \min \left[\sum_i E_i |\sin \theta_i| \right]^2 / E_{\text{tot}}^2,$$

$$S'' = \min \left[\sum_i E_i \sin^2 \theta_i \right] / E_{\text{tot}},$$

$$H_\ell = \sum_{i,j} E_i E_j P_\ell(\cos \theta_{ij}) / E_{\text{tot}}^2,$$

where E_{tot} is the total energy, θ_i is the angle between \mathbf{p}_i and \mathbf{n} , while θ_{ij} is the angle between \mathbf{p}_i and \mathbf{p}_j .

Finally, note that the discussion of two-jet events above assumes massless quarks or at least mass $\ll Q$. Close above threshold for producing a pair of heavy quarks, the latter will be almost at rest and will give approximately spherical events—an additional background at high S or low T . These effects must be included when comparing with experimental distributions.

9.1.2 Three-Jet production.

The $O(\alpha_s)$ QCD subprocess

$$e^+e^- \rightarrow q\bar{q}g$$

can give three-jet events, when all three final partons have appreciable energy and are well separated in angle. Such events are seen experimentally: they lie in the tails of the sphericity and thrust distributions of Figs. 9.2 and 9.5; a typical example is shown in Fig. 9.6. The observation of such events in 1979 was the first direct evidence for the existence of gluons. The three jets should be coplanar, since their momenta sum to zero by momentum conservation. In practice there is some ambiguity in distinguishing 3-jet from 2-jet configurations, in the regions where two of the jets lie close in angle or one jet is soft. There is a similar problem in the theoretical calculation, too, as we now discuss.

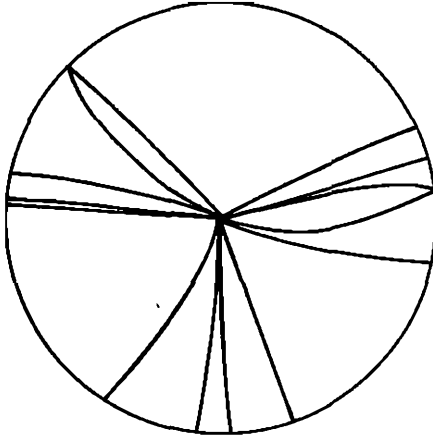


Fig. 9.6. A typical 3-jet event, seen in the TASSO detector (charged tracks shown).

Figure 9.7 shows the diagrams that contribute to hadronic final states through order $\alpha_s(Q^2)$ in the QCD coupling; (a) gives the zeroth order, (b) and (c) contribute to $q\bar{q}g$ states in order α_s , interference of (a) with (d), (e), (f) contributes to $q\bar{q}$ states in order α_s . The zeroth order cross section is

$$\sigma_0(e^+e^- \rightarrow q\bar{q}) = 3e_q^2 \left[\frac{4\pi\alpha^2}{3Q^2} \right],$$

where Q is the total c.m. energy, e_q is the quark charge, 3 is a color factor, and massless quarks are assumed.

To describe $q\bar{q}g$ production we use particle names to denote their 4-momenta and introduce the variables

$$s = (q + \bar{q})^2, \quad t = (q + g)^2, \quad u = (\bar{q} + g)^2.$$

The differential cross section to order $\alpha_s(Q^2)$ is

$$\frac{d^2\sigma(e^+e^- \rightarrow q\bar{q}g)}{dt du} = \left(\frac{4}{3}\right) \left(\frac{\alpha_s}{2\pi}\right) \sigma_0 \left[\frac{t^2 + u^2 + 2sQ^2}{tuQ^4} \right].$$

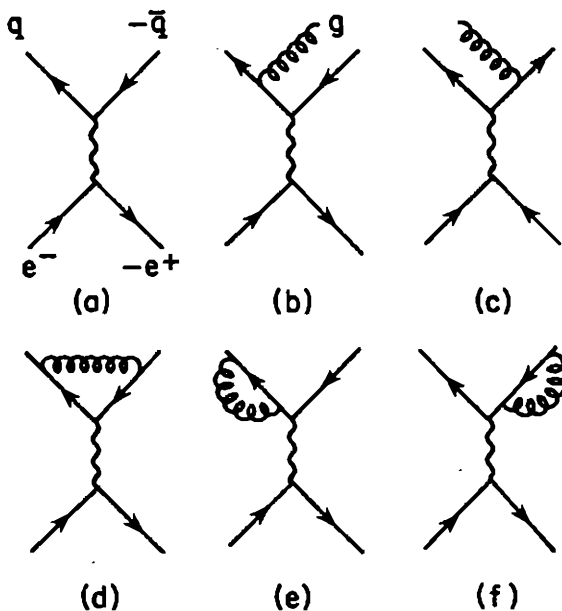


Fig. 9.7. Diagrams that contribute to the hadronic cross section through order α_s .

• *Exercise.* Show that $s + t + u = Q^2$ and that the physical region in the (s, t) plane is a triangle as shown in Fig. 9.8.

This diverges as $t \rightarrow 0$ or $u \rightarrow 0$, that is whenever the gluon momentum goes to zero (infrared divergence) or becomes collinear with q or \bar{q} (mass singularities). The problem is similar to the divergence of structure functions described in Chapter 7, to which it is related by crossing. In the limit where q and g become collinear and $t \rightarrow 0$, the diagram 9.7(b) dominates and we can define z to be the momentum fraction transmitted from the intermediate quark q^* to the final quark q .

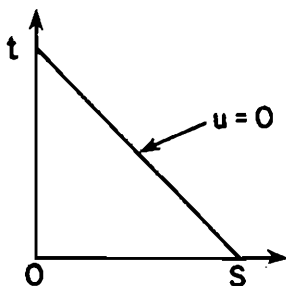


Fig. 9.8. Physical region of $e^+e^- \rightarrow q\bar{q}g$ in the (s, t) plane.

Exercise. In this limit, with $q = zq^*$ and $g = (1-z)q^*$, show that $s = zQ^2$, $u = (1-z)Q^2$. Hence show the cross section can be written

$$d^2\sigma(e^+e^- \rightarrow q\bar{q}g) = \sigma_0 \frac{dt}{t} \left(\frac{\alpha_s}{2\pi} \right) P_{qq}(z) dz,$$

where $P_{qq}(z) = (4/3)(1+z^2)/(1-z)$ is the universal $q \rightarrow q$ splitting function of Chapter 7 (modulo infrared corrections) with a similar result in the $u \rightarrow 0$ limit.

These divergences are unphysical. In the integrated cross section, the infinities cancel against the $O(\alpha_s)$ contribution from the interference of diagram (a) with (d), (e) and (f) in Fig. 9.7, leaving a finite remainder. To control the infinities and separate the finite part unambiguously, one may use dimensional regularization as in Chapter 7. The result is

$$\sigma(e^+e^- \rightarrow q\bar{q}) + \sigma(e^+e^- \rightarrow q\bar{q}g) = \sigma_0(1 + \alpha_s(Q^2)/\pi).$$

Note however that the α_s term is *not* the three-jet cross section, it is simply the net $O(\alpha_s)$ contribution.

In the $e^+e^- \rightarrow q\bar{q}g$ differential distribution, however, the divergences still leave a problem. The cross section still becomes very large as t or u becomes very small; this is cancelled – but not locally – by infinite negative δ -function terms at precisely $t = 0$ and $u = 0$ from the $q\bar{q}$ final state. One possible solution is to introduce smearing in s , t and u , corresponding to some finite resolution function. The Serman-Weinberg approach is one example, where an angle cut is used to remove some 3-jet events into the 2-jet sector. Another possibility is a mass cut, defining $q\bar{q}g$ events to be 3-jet events if they satisfy $s > \lambda^2$, $t > \lambda^2$, $u > \lambda^2$ (where λ is a convenient cutoff such as 5 GeV), but otherwise to be 2-jet events. These have been called “dressed jet” cuts, since the gluon is regarded as belonging to (dressing) the q jet whenever $t < \lambda$, *etc.*; see Fig. 9.9. Some smearing certainly takes place during fragmentation and also

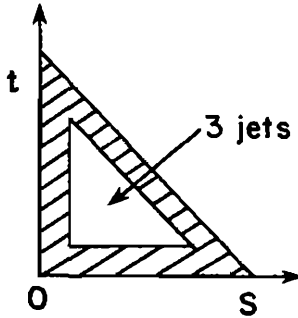


Fig. 9.9. The three-jet region for dressed jet cuts.

during the experimental measurement process, but it is difficult to devise a theoretical smearing procedure that will reliably correspond to these effects. For comparisons between theory and experiment, we must concentrate attention on regions where the cross section is not changing rapidly (to avoid smearing ambiguities) and where none of the produced quanta are close in angle (to avoid two-jet/three-jet ambiguities).

Experimentally the first problem is to determine the three jet axes and energies. This may be done via a generalized sphericity

$$S_N = \min \left[\sum_{j=1}^N \sum_k' (p_{kT})^2 \right] / \left[\sum_k p_k^2 \right],$$

where the particle momenta are partitioned into N jets (in this case $N = 3$). A different unit vector \mathbf{n}_j is assigned to each jet, p_{kT} is the particle momentum component transverse to its jet vector and the prime denotes summation of the particles k within each jet j . To reduce the combinatorial problems of searching all possible partitions, the particle momenta \mathbf{p}_k and jet vectors \mathbf{n}_j are usually replaced by their projections on the event plane.

Alternatively we can define a generalized thrust variable,

$$T_N = \max \left[\sum_{j=1}^N \sum_k' |\mathbf{p}_k \cdot \mathbf{n}_j| \right] / \sum_k |\mathbf{p}_k|,$$

where the N unit vectors \mathbf{n}_j again define jet axes. For the case $N = 3$, T_3 is known as *triplicity*. To reduce the combinatorial problem of

searching all partitions, one usually solves the problem for the high-momentum tracks first, adding the slower tracks one at a time later. For events with low thrust, triplicity is a possible measure of three-jettiness.

Cluster analysis is another approach, which does not decide in advance how many jets are present. One possible prescription is this. Form particle momenta first into preclusters, such that (i) each particle belongs to just one precluster and (ii) two belong to the same precluster if the angle between them is less than some value α (typically 30°). Now define the precluster momenta to be the vector sums of the component momenta and group them into clusters such that (iii) each precluster belongs to just one cluster, and (iv) two belong to the same cluster if the angle between their momenta is less than some value β (typically 45°). Finally choose an energy cut to decide which clusters shall rank as jets.

Once a clean sample of three-jet events is measured, one can compare with theoretical predictions, both to test the latter in general and to investigate particular questions such as

- (a) the value of $\alpha_s(Q^2)$, and
- (b) the spin of the gluon (comparing spin-0 and spin-1 possibilities).

The comparisons are made sometimes with full Monte Carlo fragmentation calculations; this may be as much a test of the fragmentation model as a test of QCD (see the string effect in §6.6). Sometimes the comparisons are made with calculations at the quark-gluon level, in cases with little sensitivity to fragmentation.

A quantity rather insensitive to fragmentation is the *asymmetry of the energy-energy correlation*. The differential energy-energy correlation is defined as

$$\frac{d\Sigma}{d\theta} = \frac{1}{\sigma_{\text{tot}}} \sum_{i,j} dx_i dx_j x_i x_j \frac{d\sigma(e^+e^- \rightarrow ijX)}{dx_i dx_j d\theta},$$

where σ is the inclusive two-body cross section for $e^+e^- \rightarrow i + j +$

anything, $x_i = E_i/Q$ and $x_j = E_j/Q$ are the normalized energies of particles i and j and θ is the angle between their momenta. The sum is over all pairs i, j , including $i = j$ and counting (i, j) , (j, i) separately, and the normalization gives $\int (d\Sigma/d\theta)d\theta = 1$. For $e^+e^- \rightarrow q\bar{q}$ processes (at the quark level) $d\Sigma/d\theta$ receives equal contributions at $\theta = 0$ and 180° only; fragmentation will broaden these into forward and backward peaks. For $e^+e^- \rightarrow q\bar{q}g$ events, however, quite a different distribution is expected; for example, a symmetrical event with equal energy quanta at 120° intervals will contribute only at $\theta = 0$ and $\theta = \pm 120^\circ$ (in the ratio 1 to 2), again broadened by fragmentation. Hence the asymmetry

$$A(\theta) = \frac{d\Sigma}{d\theta}(\pi - \theta) - \frac{d\Sigma}{d\theta}(\theta)$$

is expected to be sensitive to gluon emission and three-jet structure; specific calculations indicate that it is relatively insensitive to fragmentation. The QCD prediction to order $\alpha_s(Q^2)$ can be made by performing suitably weighted integrations of the $d\sigma/dt du$ differential cross section formula above. Calculations to order α_s^2 have also been made, but differ because of different jet resolution criteria. Figure 9.10 shows results for $A(\theta)$ at $Q = 34$ GeV, compared with an $O(\alpha_s^2)$ calculation neglecting fragmentation: the shapes agree well and the normalization in this case gives $\alpha_s(Q) = 0.115 \pm 0.005$. Figure 9.11 compares a number of different determinations of $\alpha_s(34$ GeV); there is evidently still some sensitivity to the choice of fragmentation model and jet resolution criteria.

On the question of determining the gluon spin, three-jet angular distributions have been studied. If the jets are ordered so that $E_1 > E_2 > E_3$ then the angle between jets 1 and 3 in the $(2 + 3)$ rest-frame is labeled $\tilde{\theta}$. Figure 9.12 shows the experimental $\tilde{\theta}$ dependence compared with predictions of vector-gluon (QCD) and scalar-gluon models.

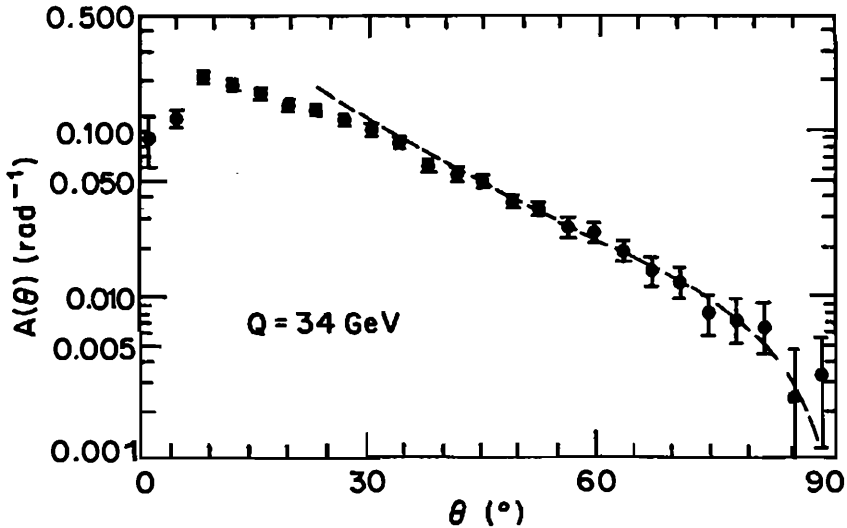


Fig. 9.10. Asymmetry of energy-energy correlation at $Q = 34$ GeV, compared with a QCD calculation neglecting fragmentation (JADE data, *Z. Phys. C*25, 231 (1984)).

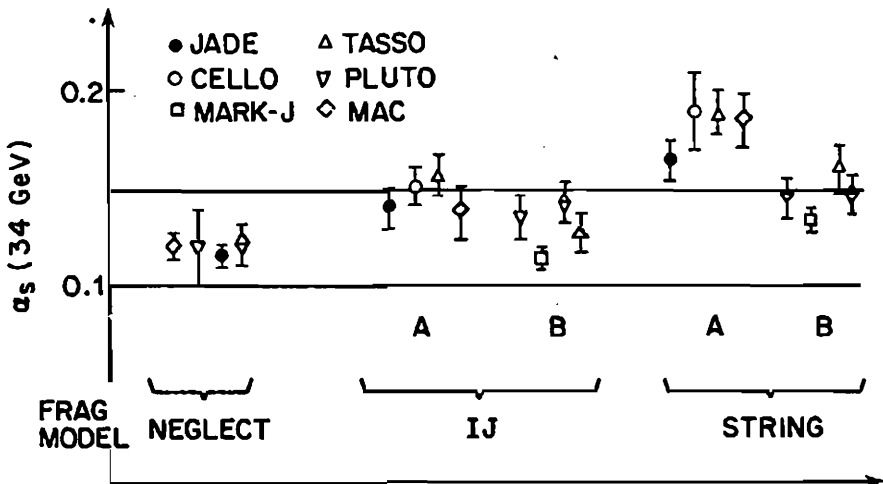


Fig. 9.11. Comparison of various determinations of α_s at $Q = 34$ GeV from energy-energy correlations (adapted from DESY 86-113). A and B denote different $O(\alpha_s^2)$ prescriptions; IJ (independent jet) and string fragmentation alternatives are shown.

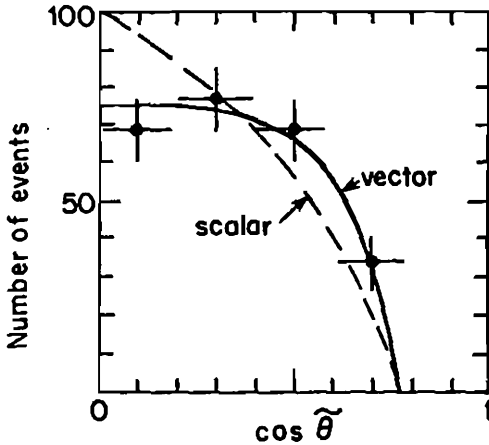


Fig. 9.12. $\tilde{\theta}$ dependence of a sample of 3-jet data compared with predictions of vector and scalar gluon models (TASSO data, Phys. Lett. **97B**, 453 (1980)).

Finally, since one of the three jets is supposedly a gluon jet, there is an opportunity to compare quark and gluon fragmentation. It is impossible to decide which is the gluon jet event-by-event, but Monte Carlo simulations suggest it is likely to be the least energetic, *i.e.* jet 3. A typical simulation of 3-jet production at $Q = 33$ GeV, using string fragmentation, finds the gluon gives jet 3 in 51%, jet 2 in 22% and jet 1 in 12% of events (the remaining 15% coming from $q\bar{q}$ production). To approximate the data with independent fragmentation models, one must ascribe a broader p_T distribution and a softer z distribution to the gluon jet compared to the quark jet.

9.2 Lepton-Nucleon Collisions

In a hard lepton-nucleon collision (with large energy and momentum transfer, see Chapter 5) the basic subprocess is lepton-quark scattering as shown in Fig. 9.13. Final hadrons come from the fragmentation of the recoiling quark and the spectator diquark. When the quark-diquark c.m. energy is big enough we expect these hadrons to appear in jets, just as in the e^+e^- case. One interesting aspect, absent in e^+e^- collisions, is the possibility to study diquark jets. There

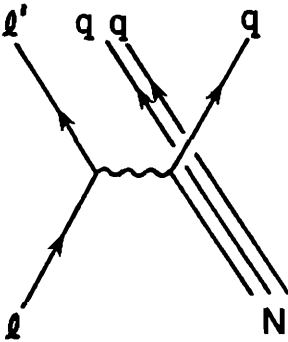


Fig. 9.13. Lepton-nucleon scattering at the quark level.

is also an advantage here over the e^+e^- system, since we know the momentum transfer vector $q = l - l'$ (assuming l and l' are both known) and hence the axis of the two-jet system in its c.m. frame, so there is no need to determine it from sphericity or thrust analysis. On the other hand, the appearance of a collimated bunch of hadrons along the q direction does not by itself imply a quark jet in this case; it could come from soft diffractive scattering as in Fig. 9.14. It is necessary also to specify $Q^2 = |q^2| \gtrsim 2 \text{ GeV}^2$; in this region the diffractive effects become very small and the approximate scaling of structure functions points to a quark-parton mechanism.

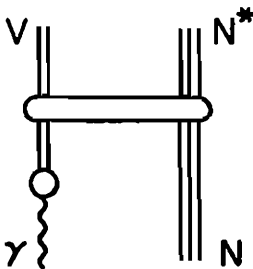


Fig. 9.14. Example of diffractive effect; an incident virtual photon becomes a virtual hadron $V (= \rho, \omega, \phi, \text{ etc.})$ that scatters at small angle from the target nucleon.

QCD adds radiative corrections to this picture, as described in Chapter 7. This leads to additional jet broadening, three-jet production and so on, with opportunities to test QCD. Hitherto, however, QCD tests have been mostly confined to inclusive measurements, the Q^2 -dependence of structure functions (see Chapter 7). Jet studies have mostly been confined to aspects of fragmentation, testing the universality and the Q^2 -dependence for example. This is because experiments have been limited to fixed-target configurations, with muon and neutrino beams up to about 300 GeV, so that the available quark-diquark c.m. energy $E_{\text{had}} = (2M\nu + M^2 - Q^2)^{1/2}$ has been limited to $E_{\text{had}} \sim 10\text{-}20$ GeV at most. This seems scarcely adequate when we recall that jet production was barely discernible at SPEAR (6-8 GeV) while the clean jet signals at PEP and PETRA are at 30-40 GeV in hadronic c.m. energy.

At HERA values up to $E_{\text{had}} \simeq 250$ GeV can be explored (in principle the full ep c.m. energy of 315 GeV could be transferred to the final hadronic system, leaving the final electron at rest in this system, but very heavy QED radiative corrections make this region unsafe). This is well beyond the energy of SLC or LEP I. A full range of jet studies, multijets, energy-energy correlations, *etc.* will be possible.

9.3 Hadron-Hadron Collisions

9.3.1. Two-Jet production.

The bulk of the cross section in hadron-hadron collisions is due to soft processes that cannot be calculated at present from first principles. However in selected kinematic regions one can observe the hard scattering of underlying partons and compare with perturbative QCD predictions. Examples of parton-parton scattering are shown in Fig. 9.15. Such processes can give four jets: one from each of the scattered partons plus two beam jets from the spectator partons that carry on along the beam directions (the latter are partly lost down

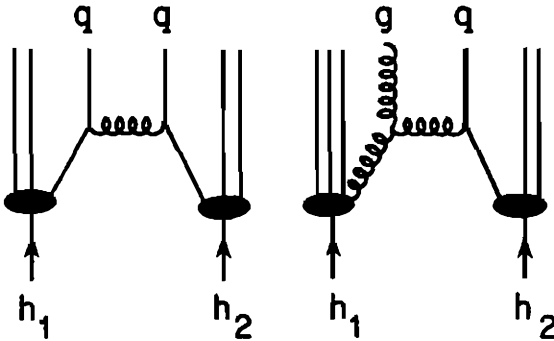


Fig. 9.15. Examples of quark-quark and quark-gluon hard scattering in the collision of two hadrons h_1 and h_2 .

the beam pipes in colliders and we shall not discuss them). From an analogy with the $e^+e^- \rightarrow q\bar{q}$ case, where we already have experience, we expect the hadronization of the scattered system will begin to show two-jet structure when the c.m. energy reaches 6-8 GeV; let us say 10 GeV to be safe, which means 5 GeV per parton. To avoid confusion with the beam jets, we further require a scattered parton to come out at a wide angle relative to the beam axis. Putting these conditions together, we expect jet formation from wide-angle partons with transverse momenta $p_T \gtrsim 5$ GeV relative to the beam axis.

In soft hadronic collisions the mean particle multiplicity rises slowly (logarithmically) with s and the mean p_T depends little on s , so the soft cross section for producing a given sum $\sum_i |p_{iT}|$ rises slowly with s . In hard parton-parton collisions, however, the cross section for producing a given large $\sum |p_T|$ of scattered partons rises very rapidly with s , because in each hadron the required momentum fraction $x \sim (\sum |p_T|)/\sqrt{s}$ gets smaller and therefore the number of hadrons with this x rises rapidly. Hence we expect that hard parton-parton scattering will not only give jets but also dominate the cross section for sufficiently large $\sum |p_T|$, at sufficiently high energy. In calorimeter measurements $\sum |p_T|$ is replaced by its approximate equivalent $\sum E_T$, where $E_T = E \sin \theta$ is called the *transverse energy*.

Since incident quarks and gluons carry typically 20% or less of the parent hadron momentum (and very few carry more than 50%), the total c.m. energy is scaled down by this factor in going from

the hadron-hadron to the parton-parton system. Hence there was little chance of forming parton jets in fixed-target experiments with 400 GeV beams (although attempts were made to find them). At the ISR pp collider with $\sqrt{s} = 63$ GeV the chances were better and jets were eventually detected, when a large $\sum E_T$ trigger was used. At the CERN $p\bar{p}$ collider, with $\sqrt{s} = 540\text{-}630$ GeV, parton-parton encounters at c.m. energies of 50 GeV and more became copious; jet production became the most striking feature of events with large $\sum E_T$.

The signature for a jet is large energy deposition in a localized group of calorimeter cells; when both jets hit the calorimeter they are opposite in azimuth (since their transverse momenta are equal and opposite for longitudinal initial partons). Figure 9.16 displays the pattern of E_T deposition in calorimeter cells versus azimuth ϕ and polar angle θ , for one of the early 2-jet events. In this example the jets have very clean signatures; they also have approximately equal E_T (57 and 60 GeV) and opposite azimuths as expected. In contrast to this, soft hadronic processes (called *minimum bias events* because they are what we get with an unselective trigger) have small E_T in many calorimeter cells but few high p_T tracks and no jet-like clustering.

The lowest-order parton-parton scattering processes that contribute to two-jet production are listed in Table 9.1, together with their squared matrix elements (averaged over spin and color). Lowest order Feynman diagrams are shown in Fig. 9.17. The subprocess cross sections have the form

$$d\hat{\sigma}/d\hat{t}(ab \rightarrow cd) = |\mathcal{M}|^2/(16\pi\hat{s}^2),$$

where $\hat{s} = (a+b)^2$ is the subprocess c.m. energy squared, $\hat{t} = (a-c)^2$ and $\hat{u} = (a-d)^2$, assuming massless quarks. The final column of Table 9.1 shows numerical values at c.m. scattering angle $\hat{\theta} = 90^\circ$

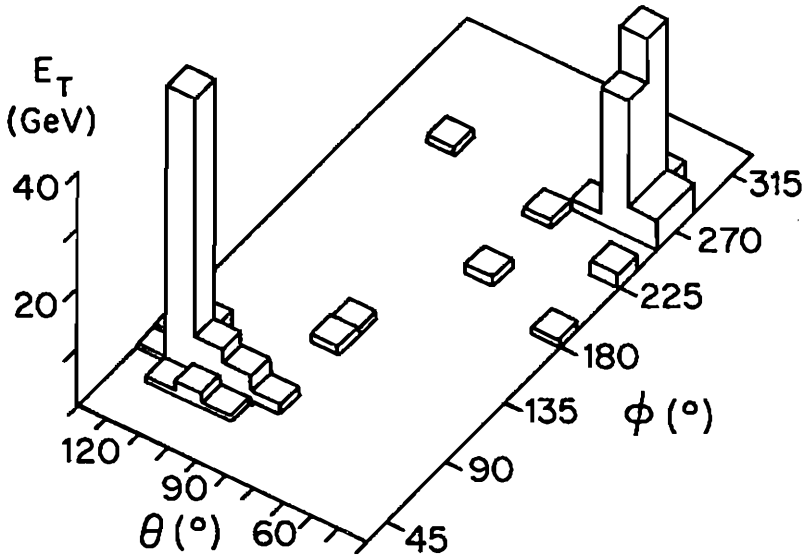


Fig. 9.16. Deposition of transverse energy $E_T = E \sin \theta$ in calorimeter cells for a typical two-jet event, observed in $p\bar{p}$ collisions at $\sqrt{s} = 540$ GeV by the UA2 detector. (Cells with less than 0.4 GeV are not shown.)

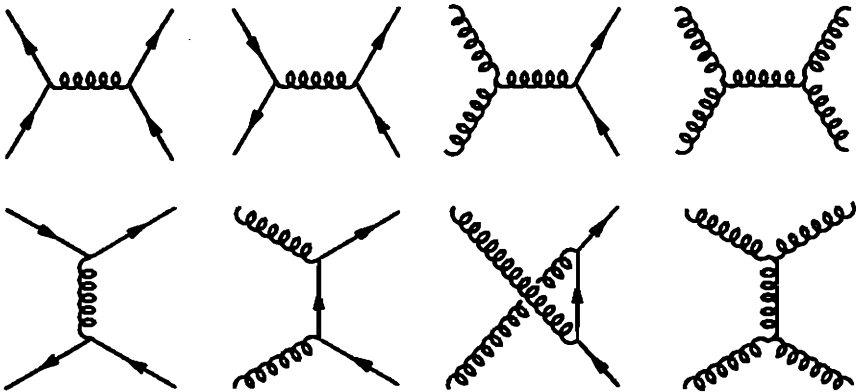


Fig. 9.17. Diagrams for parton-parton scattering to order α_s^2 .

Table 9.1. Squared matrix elements for $2 \rightarrow 2$ subprocesses in QCD (averaged over spin and color): q and q' denote distinct flavors of quark, $g_s^2 = 4\pi\alpha_s$ is the coupling squared. For identical final partons, integrate only half the solid angle.

Subprocess	$ \mathcal{M} ^2/g_s^4$	$ \mathcal{M}(90^\circ) ^2/g_s^4$
$\left. \begin{array}{l} qq' \rightarrow qq' \\ q\bar{q}' \rightarrow q\bar{q}' \end{array} \right\}$	$\frac{4}{9} \frac{\hat{s}^2 + \hat{u}^2}{\hat{t}^2}$	2.2
$qq \rightarrow qq$	$\frac{4}{9} \left(\frac{\hat{s}^2 + \hat{u}^2}{\hat{t}^2} + \frac{\hat{s}^2 + \hat{t}^2}{\hat{u}^2} \right) - \frac{8}{27} \frac{\hat{s}^2}{\hat{u}\hat{t}}$	3.3
$q\bar{q} \rightarrow q'\bar{q}'$	$\frac{4}{9} \frac{\hat{t}^2 + \hat{u}^2}{\hat{s}^2}$	0.2
$q\bar{q} \rightarrow q\bar{q}$	$\frac{4}{9} \left(\frac{\hat{s}^2 + \hat{u}^2}{\hat{t}^2} + \frac{\hat{t}^2 + \hat{u}^2}{\hat{s}^2} \right) - \frac{8}{27} \frac{\hat{u}^2}{\hat{s}\hat{t}}$	2.6
$q\bar{q} \rightarrow gg$	$\frac{32}{27} \frac{\hat{u}^2 + \hat{t}^2}{\hat{u}\hat{t}} - \frac{8}{3} \frac{\hat{u}^2 + \hat{t}^2}{\hat{s}^2}$	1.0
$gg \rightarrow q\bar{q}$	$\frac{1}{6} \frac{\hat{u}^2 + \hat{t}^2}{\hat{u}\hat{t}} - \frac{3}{8} \frac{\hat{u}^2 + \hat{t}^2}{\hat{s}^2}$	0.1
$gg \rightarrow qq$	$\frac{\hat{s}^2 + \hat{u}^2}{\hat{t}^2} - \frac{4}{9} \frac{\hat{s}^2 + \hat{u}^2}{\hat{u}\hat{s}}$	6.1
$gg \rightarrow gg$	$\frac{9}{4} \left(\frac{\hat{s}^2 + \hat{u}^2}{\hat{t}^2} + \frac{\hat{s}^2 + \hat{t}^2}{\hat{u}^2} + \frac{\hat{u}^2 + \hat{t}^2}{\hat{s}^2} + 3 \right)$	30.4

(where $\hat{t} = \hat{u} = -\hat{s}/2$), the angular region that contributes the largest p_T for given \hat{s} ; notice that the largest subprocess cross sections are for elastic scatterings $ab \rightarrow ab$.

The transverse momentum p_T of either scattered parton relative to the beam axis is given by

$$p_T^2 = \hat{u}\hat{t}/\hat{s} = \frac{\hat{s}}{4} \sin^2\hat{\theta},$$

neglecting any small intrinsic p_T of the incident partons. The p_T dependence for each parton and hence for each resulting jet is therefore

$$\frac{d\hat{\sigma}}{dp_T^2} = \frac{d\hat{\sigma}}{d\hat{t}} \frac{1}{\cos \hat{\theta}} = \frac{d\hat{\sigma}}{d\hat{t}} \frac{\hat{s}}{(\hat{t} - \hat{u})}.$$

Summing over all pairs of initial partons ab and subprocess channels $ab \rightarrow cd$ and folding in the parton distributions $f_{a/A}(x_A)$ etc. in the initial hadrons A and B (as in §5.7) the net two-jet cross section is

$$\frac{d\hat{\sigma}}{dp_T^2}(AB \rightarrow 2 \text{ jets}) = \sum_{abcd} \iint dx_A dx_B f_{a/A}(x_A) f_{b/B}(x_B) \frac{d\hat{\sigma}}{dp_T^2}(ab \rightarrow cd).$$

The upper integration limit here is $x_A = x_B = 1$; the lower limit is $x_A x_B \geq 4p_T^2/s$, derived from $\sin^2 \hat{\theta} \leq 1$. This formula gives the lowest order QCD cross section for two jet production.

Higher-order QCD subprocesses give more elaborate configurations of partons; for example gluons will be radiated from the incoming parton lines and outgoing scattered lines. The dominant configurations however are those where there is only one high- p_T scattering and the additional radiation is approximately collimated with the incident or scattered partons. If the experimental definition of a jet is sufficiently broad (*i.e.* the cone over which hadron energy is summed into a single jet is wide enough), the dominant high- p_T configurations again lead to two-jet production. We then expect the two-jet cross section to be predicted by the lowest-order terms, calculated with parton distributions evolved up to a scale of order p_T^2 or \hat{s} , and multiplied by a K -factor of order 1 to 2 for non-leading corrections.

Experimental groups at the CERN $p\bar{p}$ collider have indeed taken rather broad angular definitions for a jet. For example the UA1 *jet algorithm* requires at least one calorimeter cell (in solid angle) to contain $E_T > 2.5$ GeV, after which other such cells are added within $|\Delta\eta|^2 + |\Delta\phi|^2 < 1$, where the pseudorapidity $\eta = \ln \cot \frac{1}{2}\theta$ and azimuth ϕ are coordinates of the cells. Finally cells with $E_T < 2.5$ GeV are added to the nearest cluster if the angle to the cluster axis is less than $\pi/4$ and E_T transverse to the cluster axis is < 1 GeV. The UA2

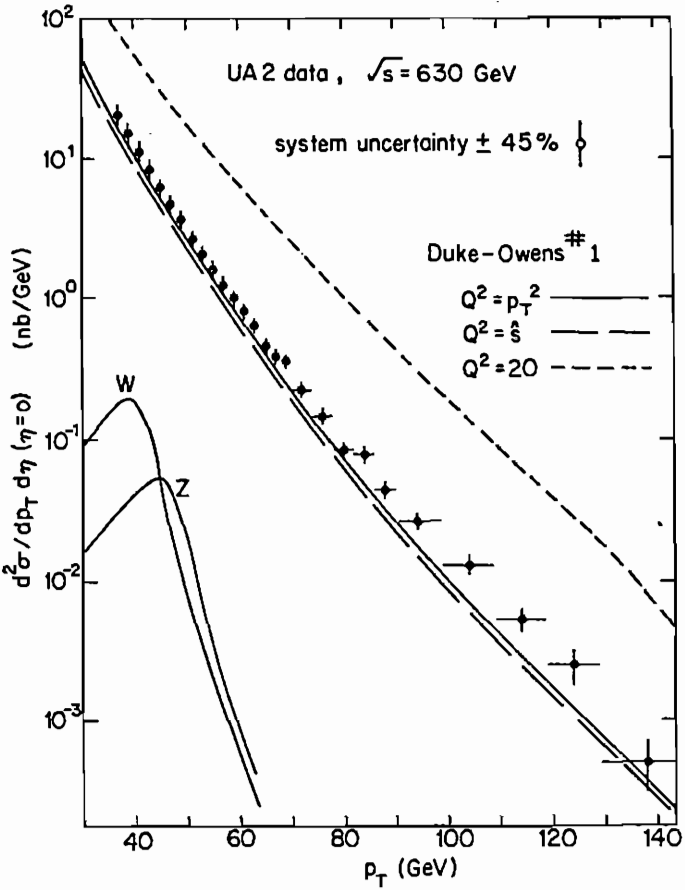


Fig. 9.18. Inclusive $p\bar{p} \rightarrow$ jet cross section at $\sqrt{s} = 630$ GeV, compared with QCD predictions. Data are from the UA2 experiment. The calculations take $K = 1$.

jet algorithm has similar angular resolution. It is therefore reasonable to confront their results with the $O(\alpha_s^2)$ parton cross sections, folded with initial parton distributions.

Figure 9.18 shows the inclusive jet cross section $d\sigma/dp_T d\eta$ averaged over the range $|\eta| < 0.85$ at $\sqrt{s} = 630$ GeV. The data have $\pm 45\%$ overall normalization uncertainty beside the statistical errors shown. The theoretical curves are for the Duke-Owens parton distributions with $K = 1$, evolved up to $Q^2 = \hat{s}$ and $Q^2 = p_T^2$ to show the

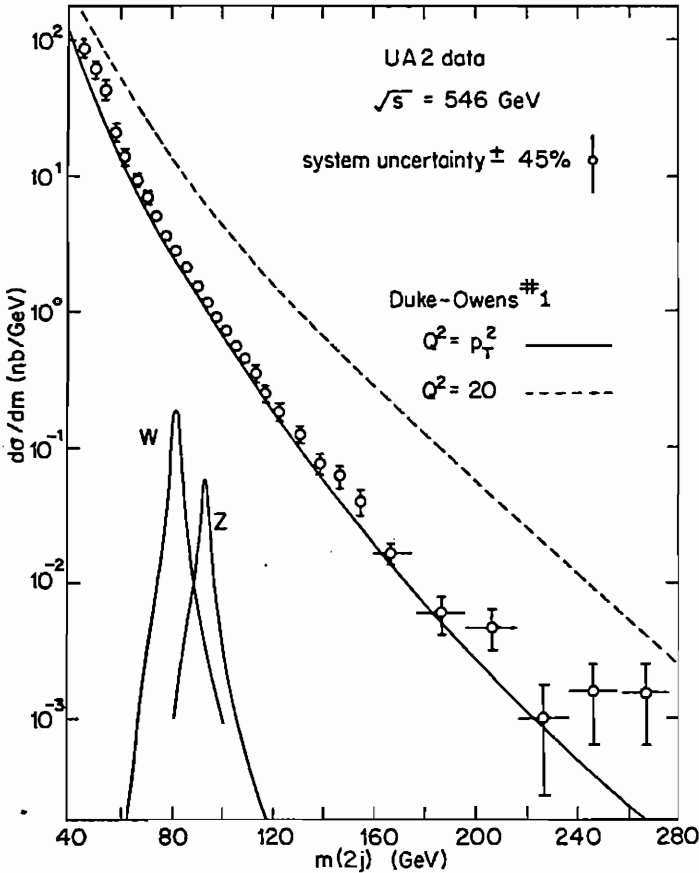


Fig. 9.19. Two-jet invariant mass distribution for $p\bar{p}$ collisions at $\sqrt{s} = 546 \text{ GeV}$, where both jets have $|\eta| < 0.85$ (UA2 data).

scale of uncertainty arising from this question. There is good agreement between theory and experiment, especially in the shape of the distribution which is much better measured than its normalization. In Fig. 9.19 the distribution versus two-jet invariant mass, for events in which both jets have $|\eta| < 0.85$ at $\sqrt{s} = 546 \text{ GeV}$, shows equally good agreement.

There are other lessons from Figs. 9.18 and 9.19. The short-dashed curves, denoting the theoretical predictions for the choice $Q^2 = 20 \text{ GeV}^2$, show the importance of Q^2 -evolution up to a rele-

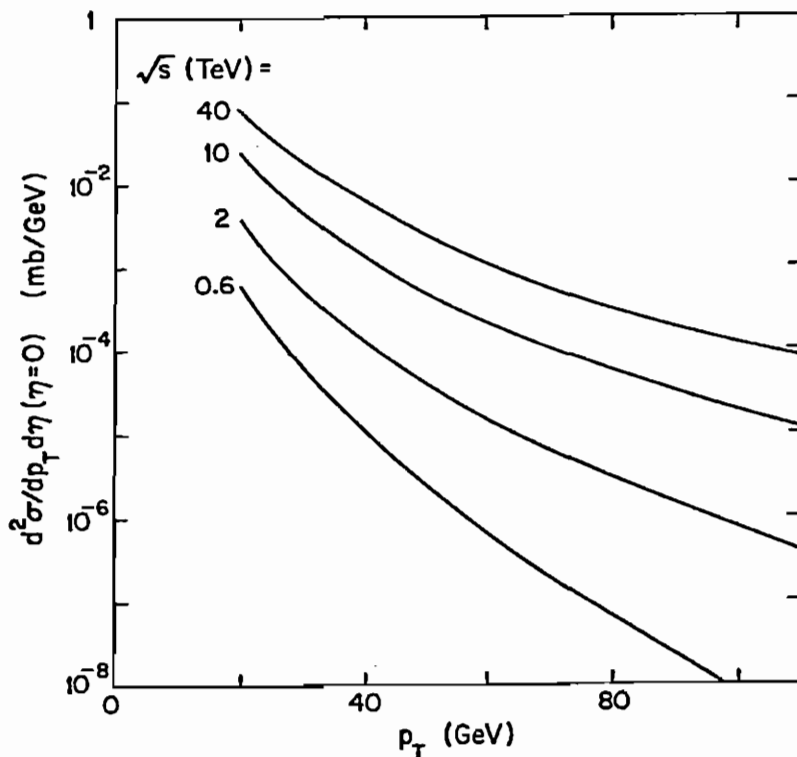


Fig. 9.20. Predicted rise in the inclusive $p\bar{p} \rightarrow$ jet cross section from $\sqrt{s} = 0.6$ to 40 TeV (EHLQ parton distributions); pp results are essentially identical at the higher energies.

vant scale. The curves labelled W and Z are the jet contributions from $q\bar{q} \rightarrow (W, Z) \rightarrow q\bar{q}$ subprocesses (see Chapter 8); they show how difficult it is to detect weak bosons from their two-jet decays in the face of QCD backgrounds, in spite of their sharp peaks versus invariant mass.

Figure 9.20 shows how the high- p_T jet cross section is predicted to rise at higher energies; the rise at any given p_T is due to the rise in the number of contributing partons at the relevant values $x \sim 2p_T/\sqrt{s}$.

Can parton distributions be extracted directly from the data? Since it is impossible to tell whether any particular jet comes from a quark or from a gluon, all the subprocesses in Table 9.1 contribute

on an equal footing. The cross sections for non-identical final partons should be symmetrized (by adding $\hat{t} \leftrightarrow \hat{u}$ terms without dividing by 2) and the two final partons can then be regarded as indistinguishable jets, integrating over half the phase space. We notice that all the important contributions are dominated by the t -channel exchange contributions (coming from the upper row of diagrams in Fig. 9.17), and are therefore equal within color factors to a good approximation.

Exercise. Show that

$$\begin{aligned} |\mathcal{M}(qq \rightarrow jj)|^2 &\simeq |\mathcal{M}(q\bar{q} \rightarrow jj)|^2 \simeq (8/9)g_s^4 f(\chi), \\ |\mathcal{M}(gg \rightarrow jj)|^2 &\simeq 2g_s^4 f(\chi), \\ |\mathcal{M}(gg \rightarrow jj)|^2 &\simeq (9/2)g_s^4 f(\chi), \end{aligned}$$

where j denotes jet, $\chi = \hat{u}/\hat{t} = (\cot \frac{1}{2}\hat{\theta})^2$ and

$$f(\chi) = \chi^2 + \chi + 1 + \chi^{-1} + \chi^{-2}.$$

Exercise. Compare the angular distribution $f(\chi)$, which comes from symmetrizing the $qq' \rightarrow qq'$ cross section, with the case of $ee \rightarrow ee$ elastic electron scattering (§4.1). Show that the dominant pole terms are the same. Why do some other terms differ?

Hence for initial hadrons A and B the $AB \rightarrow jj$ cross section can be written in a factorized form

$$d\sigma(AB \rightarrow jjX) \simeq \int d\sigma(gg \rightarrow gg) F_A(x_A) F_B(x_B) dx_A dx_B / (x_A x_B),$$

where x_A, x_B are parton momentum fractions in the incident hadrons A, B and $F(x)$ is x times the sum of color-weighted parton distributions

$$F(x) = x \left[g(x) + \frac{4}{9} \sum_i (q_i(x) + \bar{q}_i(x)) \right]$$

with a summation over quark flavors i . $F_A(x_A)$ and $F_B(x_B)$ are what we can hope to extract in AB collisions. Note that F is the same for proton and antiproton.

Exercise. Show that the two-jet distribution can be written in the form

$$\frac{d\sigma(AB \rightarrow j_1 j_2 X)}{dp_T^2 dy_1 dy_2} = \frac{9\pi\alpha_s^2}{2x_A^2 x_B^2 s^2} F_A(x_A) F_B(x_B) f(\chi) ,$$

where y_1 and y_2 are the jet rapidities in the AB c.m. frame and s is the AB c.m. energy squared, with

$$\begin{aligned} x_A &= (p_T/\sqrt{s}) [\exp(y_1) + \exp(y_2)] , \\ x_B &= (p_T/\sqrt{s}) [\exp(-y_1) + \exp(-y_2)] . \end{aligned}$$

Note that it is not possible to determine x_A or x_B from one jet alone.

These approximate factorized formulas agree with the complete QCD calculation quite well even at large scattering angles (*e.g.* within 25% for the cases shown in Figs. 9.18-19), and can be used to extract $F(x)$ from two-jet data. The factorization property can serve as a cross-check, by testing if results for $[F_A(x_A)F_B(x_B)]/[F_A(x_A)F_B(x'_B)]$ are independent of x_A , when x_B and x'_B are held fixed. Figure 9.21 shows that the values of $F(x)$ for a proton, extracted assuming $K = 2$ enhancement, agree well with Duke-Owens distributions evolved up to $Q^2 = 2000$ (which is the mean $|t|$ for the data used). The $Q^2 = 20$ curve shows the importance of Q^2 -evolution once again.

The most important feature of Fig. 9.21 is the dashed curve, which gives the effect of omitting gluons. The difference between this and the full curve is the contribution of gg , gq and $g\bar{q}$ scattering, of which the dominant terms come from gluon exchange and rely on the triple-gluon coupling. This shows directly that the gluon gauge symmetry is non-abelian.

It is not surprising that the gluon contribution dominates $F(x)$ at small x ; we have already noted this dominance in §7.9. It means that determinations of $F(x)$ here are essentially determinations of $g(x)$. It also implies that events in which both x_A and x_B are small provide an almost pure sample of gluon jets, whereas events where

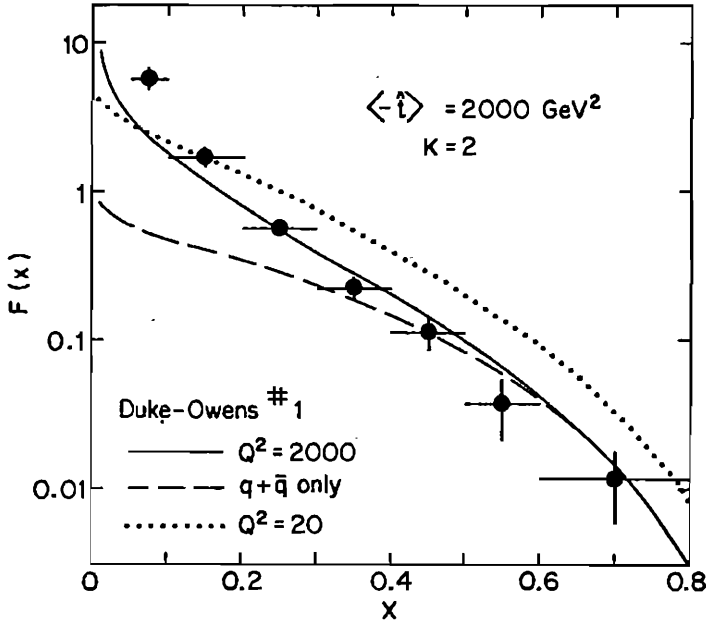


Fig. 9.21. Effective parton distribution $F(x)$ in the proton, extracted from $p\bar{p} \rightarrow 2$ jet data at $\sqrt{s} = 630$ GeV by the UA1 group, compared with Duke-Owens extrapolation to $Q^2 = 2000$.

both x_A and x_B are large provide quark (or antiquark) jets only. Hence samples of quark and gluon jets can be isolated for study.

For quark jets this provides an opportunity to study the Q^2 -evolution of fragmentation at very large Q^2 . Figure 9.22 shows the charged-particle fragmentation function $D(z, Q^2) = dn^c/dz$ where n^c is the multiplicity of charged hadrons in the jet and $z = E_h/E_q$ is the hadron energy fraction. Below $Q^2 = 2000$ the data are for quark jets alone, from $e^+e^- \rightarrow 2$ jet measurements (TASSO experiment); the solid curves are theoretical QCD extrapolations based on these data. The triangular data points are quark jet results from $p\bar{p} \rightarrow 2$ jet measurements (UA1 experiment), which appear to be in reasonable agreement with expectations.

Gluon jets are expected to be softer than quark jets, because the gluon has a stronger color coupling and more readily radiates extra

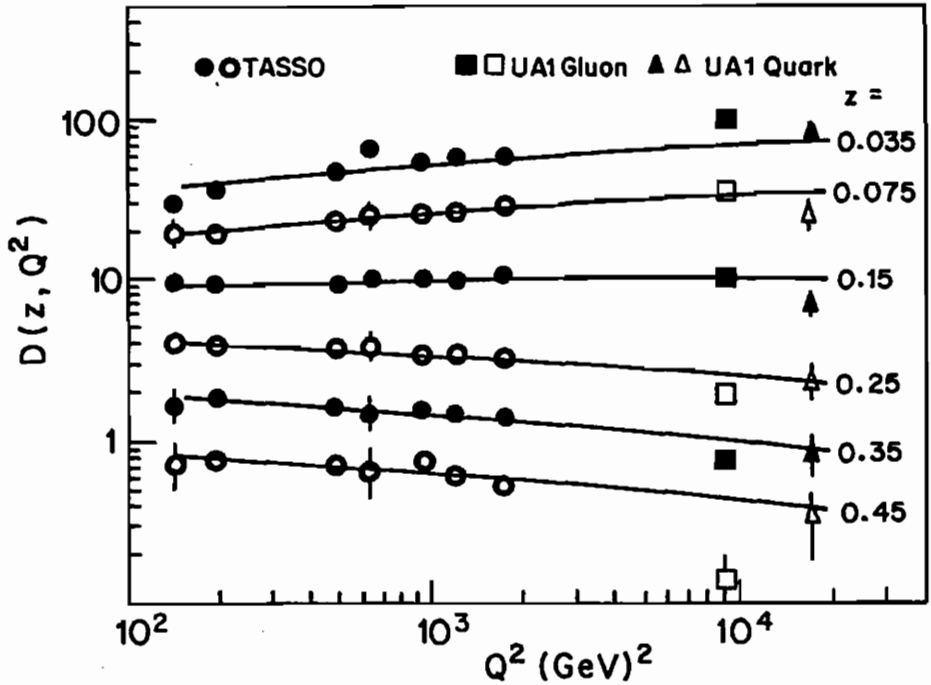


Fig. 9.22. Comparison of quark and gluon fragmentation in two-jet events. $D(z, Q^2)$ is the charged-particle fragmentation function. Circles denote quark results from e^+e^- measurements (TASSO group) and solid curves are a QCD extrapolation. Triangles and squares denote quark and gluon results from $p\bar{p}$ measurements (UA1 group).

gluons (there is an extra factor $9/4$ in the $g \rightarrow g$ splitting function compared to $q \rightarrow g$ at small z ; see Chapter 7). This expectation is qualitatively confirmed by the $D(z)$ results for gluon jets in Fig. 9.22 (at $Q^2 = 9000$, denoted by squares), compared to the quark-jet results at comparable Q^2 ; the fragmentation function for gluons is bigger at small z , smaller at large z .

High- p_T jets also offer ways to test *compositeness*. If quarks and leptons are actually composites of more basic *preons*, an immediate consequence is form factors. Gauge boson-fermion couplings would be modified by factors

$$F(Q^2) = (1 + Q^2/\Lambda^{*2})^{-1},$$

where Λ^* characterizes the compositeness scale, through diagrams like Fig. 9.23(a). Measurements of $e^+e^- \rightarrow \ell^+\ell^-$ and $\bar{q}q$ have set limits $\Lambda^* > 100\text{-}200$ GeV for photon form factors. The precise agreement of theory and experiment for the muon anomalous magnetic moment gives $\Lambda^* > 670$ GeV for the muon. In quark and anti-quark scattering at colliders, the presence of a form factor would suppress gluon exchanges at large p_T . However, compositeness also implies that preons can be exchanged (Fig. 9.23(b) and (c)); there are stringent constraints on such couplings that flip flavor, but little constraint on flavor-conserving terms. It turns out that preon exchange is the dominant effect in high p_T scattering.

Preon exchanges give essentially point-like interactions if $\Lambda^* > \sqrt{\hat{s}}$. The most general point-like quark-quark interaction contains many independent parameters, even after plausible symmetry constraints are applied. Illustrative calculations have usually been made with the simple assumption of color-singlet isoscalar exchanges between left-handed u and d quarks, described by the effective Lagrangian (proposed by Eichten *et al.*)

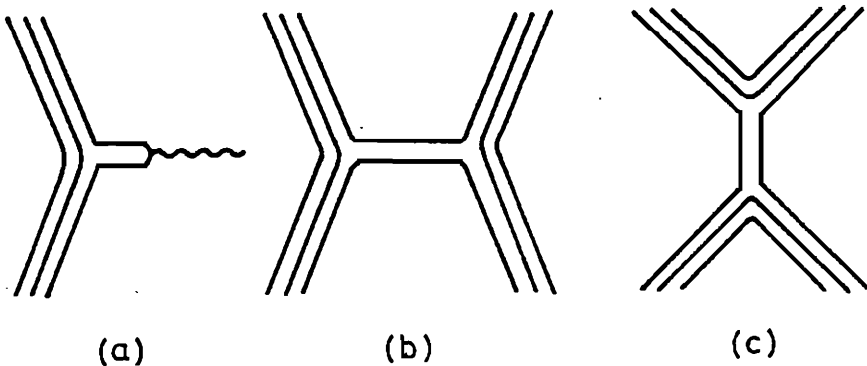


Fig. 9.23. Typical effects of preon substructure for quarks and leptons: (a) form factors, (b) and (c) scattering via preon exchanges.

$$\mathcal{L} = \frac{\eta g^2}{2\Lambda^{*2}} (\bar{u}_L \gamma^\mu u_L + \bar{d}_L \gamma^\mu d_L) (\bar{u}_L \gamma_\mu u_L + \bar{d}_L \gamma_\mu d_L),$$

where $g^2/4\pi = 1$ is assumed, $\eta = \pm 1$ gives the sign and Λ^* parameterizes the coupling strength.

This empirical contact interaction modifies the quark-(anti)quark scattering amplitudes as follows:

$$\begin{aligned} |\mathcal{M}(q\bar{q} \rightarrow q\bar{q})|^2 &= [\text{QCD}] + \frac{8}{9} g_s^2 \frac{4\pi\eta}{\Lambda^{*2}} \left(\frac{\hat{u}^2}{\hat{t}} + \frac{\hat{u}^2}{\hat{s}} \right) + \frac{8}{3} \left(\frac{4\pi\eta\hat{u}}{\Lambda^{*2}} \right)^2, \\ |\mathcal{M}(qq \rightarrow qq)^2 &= [\text{QCD}] + \frac{8}{9} g_s^2 \frac{4\pi\eta}{\Lambda^{*2}} \left(\frac{\hat{s}^2}{\hat{t}} + \frac{\hat{s}^2}{\hat{u}} \right) + \left(\frac{4\pi\eta}{\Lambda^{*2}} \right)^2 \left(\hat{u}^2 + \hat{t}^2 + \frac{2}{3}\hat{s}^2 \right), \\ |\mathcal{M}(q\bar{q} \rightarrow q'\bar{q}')|^2 &= [\text{QCD}] + \left(\frac{4\pi\eta\hat{u}}{\Lambda^{*2}} \right)^2, \\ |\mathcal{M}(qq' \rightarrow qq')|^2 &= |\mathcal{M}(q\bar{q}' \rightarrow q\bar{q}')|^2 = [\text{QCD}] + \left(\frac{4\pi\eta\hat{u}}{\Lambda^{*2}} \right)^2, \end{aligned}$$

where [QCD] denotes the corresponding expression listed in Table 9.1. In regions where the contact terms are small compared to QCD terms, their interference is the main effect; notice that the sign can then be positive or negative depending on η . Figure 9.24 compares predictions of this model, with $\eta = +1$ and $\Lambda^* = 300$ or 460 GeV against inclusive single jet production at $\sqrt{s} = 630$ GeV. Future measurements at the Tevatron and SSC will be able to probe the question of compositeness much more deeply.

Compositeness will also give quark-lepton and lepton-lepton contact terms, leading to new effects in the Drell-Yan process, lepton-nucleon scattering, $e^+e^- \rightarrow \bar{q}q$, $e^+e^- \rightarrow \mu^+\mu^-$, *etc.* at sufficiently high energies.

Finally we note that when subprocess energies become much bigger than the compositeness scale Λ^* , multifermion production will begin, many new channels will open and the previous description of hard scattering will break down dramatically.

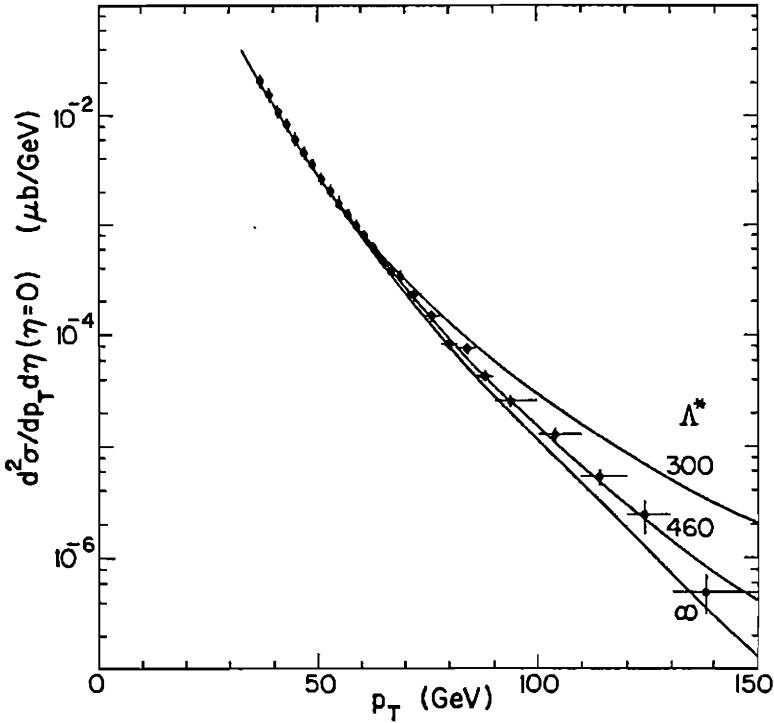


Fig. 9.24. Comparison of inclusive jet production in $p\bar{p}$ scattering at $\sqrt{s} = 630$ GeV (UA2 data) with possible consequences of compositeness. The curves are for $\Lambda^* = 300$ GeV, 460 GeV and ∞ .

9.3.2 Three-jet production.

Three scattered partons with large p_T can be produced by $2 \rightarrow 3$ QCD subprocesses in order α_s^3 . There are very many diagrams; some examples are shown in Fig. 9.25. Table 9.2 lists the various contributing channels and their squared matrix elements, summed (averaged) over final (initial) spins and colors. The various matrix elements M_1 , M_2 , M_3 and M_4 refer to the cases (at tree level)

- 1) $qq' \rightarrow qq'g$ (distinct quark flavors q, q')
- 2) $qq \rightarrow qqg$ (identical quark flavors)
- 3) $q\bar{q} \rightarrow ggg$

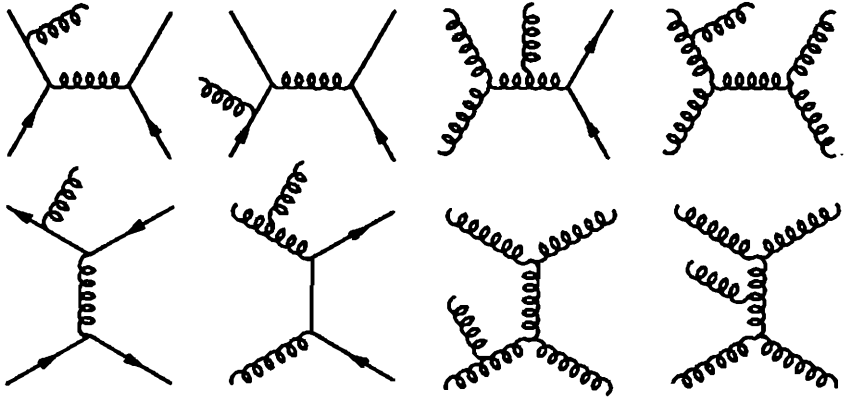


Fig. 9.25. Examples of $2 \rightarrow 3$ parton subprocesses.

4) $gg \rightarrow ggg$

to which all other cases are related by crossing.

Table 9.2. $2 \rightarrow 3$ parton subprocesses and squared matrix elements. Particle momenta are labeled by the convention $k_1 k_2 \rightarrow k_3 k_4 k_5$.

Subprocess	$ \mathcal{M} ^2$
$qq' \rightarrow qq'g$	$ \mathcal{M}_1(k_1, k_2, k_3, k_4, k_5) ^2$
$gg \rightarrow qq'\bar{q}'$	$ \mathcal{M}_1(k_1, -k_5, k_3, k_4, -k_2) ^2 \times (-3/8)$
$q\bar{q}' \rightarrow q\bar{q}'g$	$ \mathcal{M}_1(k_1, -k_4, k_3, -k_2, k_5) ^2$
$q\bar{q} \rightarrow \bar{q}'q'g$	$ \mathcal{M}_1(k_1, -k_3, -k_2, k_4, k_5) ^2$
$qq \rightarrow qqg$	$ \mathcal{M}_2(k_1, k_2, k_3, k_4, k_5) ^2$
$gg \rightarrow qq\bar{q}$	$ \mathcal{M}_2(k_1, -k_5, k_3, k_4, -k_2) ^2 \times (-3/8)$
$q\bar{q} \rightarrow q\bar{q}g$	$ \mathcal{M}_2(k_1, -k_4, k_3, -k_2, k_5) ^2$
$q\bar{q} \rightarrow ggg$	$ \mathcal{M}_3(k_1, k_2, k_3, k_4, k_5) ^2$
$gg \rightarrow qgg$	$ \mathcal{M}_3(k_1, -k_3, -k_2, k_4, k_5) ^2 \times (-3/8)$
$gg \rightarrow q\bar{q}g$	$ \mathcal{M}_3(-k_4, -k_3, -k_1, -k_2, k_5) ^2 \times (9/64)$
$gg \rightarrow ggg$	$ \mathcal{M}_4(k_1, k_2, k_3, k_4, k_5) ^2$

If we label the momenta of the five participating partons by the convention $k_1 k_2 \rightarrow k_3 k_4 k_5$ the matrix element $|\mathcal{M}_1|^2$ can be written

$$|\mathcal{M}_1|^2 = \frac{g_s^6}{27} [(s^2 + s'^2 + u^2 + u'^2)/tt'] [(k_1 \cdot k_5)(k_2 \cdot k_5)(k_3 \cdot k_5)(k_4 \cdot k_5)]^{-1} \\ \times \left\{ 2 [(u + u')(ss' + tt' - uu') + u(st + s't') + u'(st' + s't)] \right. \\ \left. - \frac{1}{4} [(s + s')(ss' - tt' - uu') + 2tt'(u + u') + 2uu'(t + t')] \right\},$$

where

$$s = (k_1 + k_2)^2, \quad t = (k_1 - k_3)^2, \quad u = (k_1 - k_4)^2, \\ s' = (k_3 + k_4)^2, \quad t' = (k_2 - k_4)^2, \quad u' = (k_2 - k_3)^2,$$

and $g_s^2 = 4\pi\alpha_s$ is the QCD coupling squared. With two identical quark flavors the formula becomes

$$|\mathcal{M}_2|^2 = |\mathcal{M}_1|^2 + |\mathcal{M}_1|^2 (t \leftrightarrow u, t' \leftrightarrow u') \\ + \frac{g_s^6}{324} [(s^2 + s'^2)(ss' - tt' - uu')/(tt'uu')] \\ \times [(k_1 \cdot k_5)(k_2 \cdot k_5)(k_3 \cdot k_5)(k_4 \cdot k_5)]^{-1} \\ \times [9(s + s')(ss' - tt' - uu') + 2tt'(u + u') + 2uu'(t + t') \\ - 8s(tu + t'u') - 8s'(tu' + t'u)].$$

For processes with three gluons we have

$$|\mathcal{M}_3|^2 = \frac{2g_s^6}{81} \left[\sum_{i=1}^3 a_i b_i (a_i^2 + b_i^2) \right] (a_1 a_2 a_3 b_1 b_2 b_3)^{-1} \\ \times \left\{ 5s - 9 \left[\frac{a_1 b_2 + a_2 b_1}{(k_3 \cdot k_4)} + \frac{a_2 b_3 + a_3 b_2}{(k_4 \cdot k_5)} + \frac{a_3 b_1 + a_1 b_3}{(k_5 \cdot k_3)} \right] \right. \\ \left. + \frac{162}{s} \left[\frac{a_1 b_1 (a_2 b_3 + a_3 b_2)}{(k_3 \cdot k_4)(k_3 \cdot k_5)} + \frac{a_2 b_2 (a_3 b_1 + a_1 b_3)}{(k_4 \cdot k_5)(k_4 \cdot k_3)} + \frac{a_3 b_3 (a_1 b_2 + a_2 b_1)}{(k_5 \cdot k_3)(k_5 \cdot k_4)} \right] \right\},$$

where $a_i = k_1 \cdot k_{i+2}$ and $b_i = k_2 \cdot k_{i+2}$. All the formulas above are for massless quarks. Finally, the five-gluon amplitude has rather

symmetrical form

$$|\mathcal{M}_4|^2 = \frac{27g_s^6}{16} \left[(12345) + (12354) + (12435) + (12453) + (12534) \right. \\ \left. + (12543) + (13245) + (13254) + (13425) + (13524) + (14235) + (14325) \right] \\ \times \left[\sum_{i < j} (k_i \cdot k_j)^4 \right] / \prod_{i < j} (k_i \cdot k_j),$$

where $(ijklmn) = (k_i \cdot k_j)(k_j \cdot k_l)(k_l \cdot k_m)(k_m \cdot k_n)(k_n \cdot k_i)$.

We can obtain three-jet cross sections from these formulas, in regions of phase space where the jets do not overlap with each other or with the beam jets, as follows. First symmetrize the cross sections between non-identical final partons as in §9.3.1 and regard each final parton as a jet; if we now integrate over the full three-jet phase space we must divide by 3! since the jets are indistinguishable. After folding in the initial parton distributions and summing over initial and final parton channels, the generic formula is

$$d\sigma(AB \rightarrow jjj) = \sum_{abcde} \iint dx_A dx_B f_{a/A}(x_A) f_{b/B}(x_B) d\sigma(ab \rightarrow cde).$$

For a comparison with experiment, we introduce the scaled energy variables and ordering

$$x_i = 2E_i/\sqrt{\hat{s}}, \quad x_3 > x_4 > x_5,$$

for the five participating partons $1+2 \rightarrow 3+4+5$ in their c.m. frame. Let θ_{13} be the c.m. angle between p_1 and p_3 and let ϕ be the angle between the planes (123) and (345). The UA1 group collected a sample of 173 well-separated 3-jet events satisfying the conditions

$$x_3 < 0.9, \quad |\cos \theta_{13}| < 0.6, \quad 30^\circ < \phi < 150^\circ,$$

and found their distributions agreed well with the $O(\alpha_s^3)$ QCD prediction. Figure 9.26 shows the distributions versus x_3 and x_4 . The QCD prediction has some systematic differences from pure phase space that seem to be supported by the data.

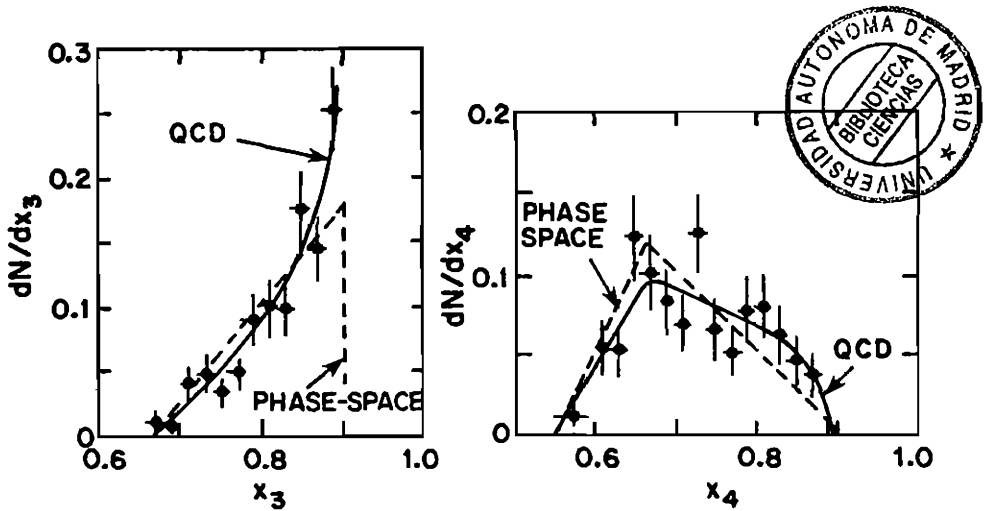


Fig. 9.26. Distributions of three-jet data versus x_3 and x_4 in $p\bar{p}$ collisions at $\sqrt{s} = 630$ GeV, compared with $O(\alpha_s^3)$ QCD and phase space predictions (UA1 data).

The curves in Fig. 9.26 are normalized to the data. In principle the ratio of three-jet to two-jet events at given subprocess energy \hat{s} can be used to determine the QCD coupling $\alpha_s(\hat{s})$, since uncertainties in the parton densities will largely cancel. However, a precise determination would require a knowledge of the K -factor for non-leading corrections to the $2 \rightarrow 3$ cross sections, which is not yet available.

9.3.3 Minijets and multijets.

The early two-jet events at the CERN $p\bar{p}$ collider were triggered on high ΣE_T and the subsequent studies concentrated on large p_T , typically $p_T(\text{jet}) \simeq E_T(\text{jet}) \gtrsim 20$ GeV. However, the analogy with e^+e^- results suggests that recognizable jets may be formed with p_T as low as 5 GeV. (see the discussion in §9.3.1). Such *minijets* were reported by the UA1 group, from data taken with a minimum-bias trigger while the collider was ramped through the range $\sqrt{s} = 200$ –900 GeV. Jets were defined using calorimeter E_T information only; in this study cells with $E_T > 1.5$ GeV initiate a jet and cells with $(\Delta\eta)^2 + (\Delta\phi)^2 < 1$ are associated with it. Jets were retained if

Table 9.3. Averaged charged multiplicity in $|\eta| < 2.5$.

\sqrt{s} (GeV)		200	350	630	900
$\langle n^c \rangle$	jet	26.5 ± 0.2	30.2 ± 0.5	32.2 ± 0.3	32.9 ± 0.1
$\langle n^c \rangle$	no jet	13.8 ± 0.1	14.6 ± 0.1	15.1 ± 0.1	15.9 ± 0.1

they had $|\eta| < 1.5$ and azimuth more than 30° from the vertical (where there is a crack between the two halves of the calorimeter). A significant jet signal was reported right down to $p_T = 5$ GeV.

Complementary information from the central detector confirms that the jet events are qualitatively different from non-jet events. For example, the average charged-particle multiplicity $\langle n^c \rangle$ is twice as large in jet events; see Table 9.3.

Figure 9.27 shows the inclusive jet E_T distribution at $\eta = 0$ for $\sqrt{s} = 900$ GeV compared to a lowest-order QCD calculation based on the EHLQ parton distributions evolved up to $Q^2 = p_T^2$, with $K = 1$. There is reasonable qualitative agreement. In fact some quantitative mismatch is expected here, both because $K > 1$ and because the calorimeter cells where the jet falls receive some E_T (of order 1–2 GeV) from the “underlying event”—*i.e.*, from the soft interactions of all the spectator partons. There is no correction for this in the data shown, so in effect the jets E_T are overestimated and the data points should move a little to the left.

Figure 9.28 shows the total cross section for jet production (including an estimate of the jets falling outside the measured region $|\eta| < 1.5$), with the uncorrected experimental jet threshold $p_T(\text{jet}) > 5$ GeV. For comparison we illustrate QCD calculations (with the same EHLQ parton distributions and $K = 1$) for thresholds $p_T > 5$ GeV and $p_T > 3$ GeV, to show the sensitivity to this threshold. The agreement suggests that minijets are explicable by parton scattering and are not a new phenomenon.

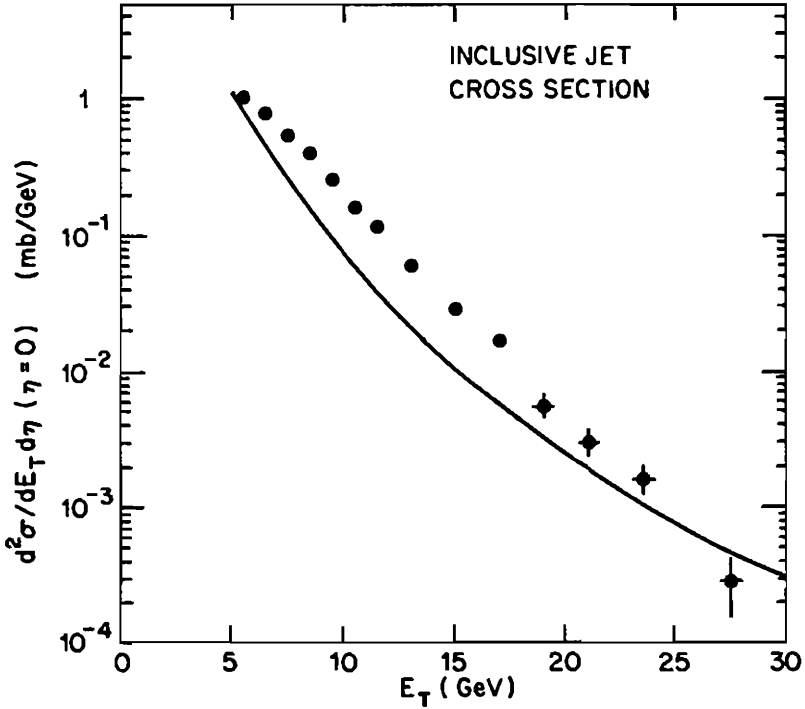


Fig. 9.27. Inclusive jet E_T distribution at $\sqrt{s} = 900$ GeV (UA1 data); the solid curve is a QCD calculation with $K = 1$.

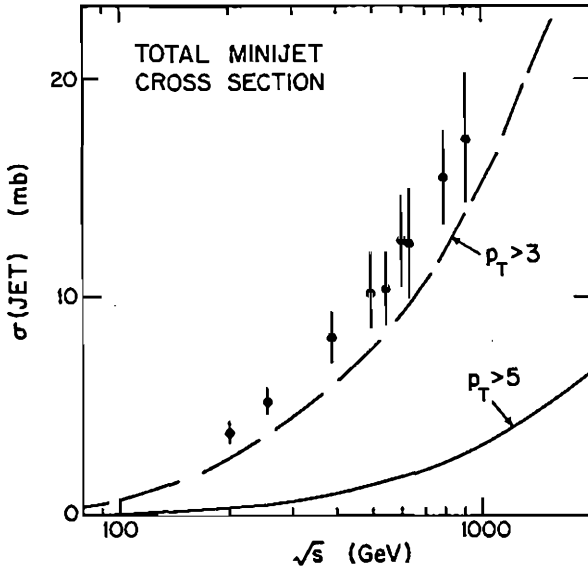


Fig. 9.28. Total jet cross sections (UA1 data) compared with QCD calculations for thresholds $p_T > 5$ GeV (solid curve), $p_T > 3$ GeV (dashed curve).

The rising of the minijet cross section bears some resemblance to the behavior of the total $p\bar{p}$ cross section, which rises by about 10 mb between $\sqrt{s} = 200$ and $\sqrt{s} = 900$ GeV. However, it is premature to make a direct connection between these observations. The latter effect is usually associated with Pomeron exchange (small- p_T diffractive processes) which rises approximately like $s^{0.08}$ all the way from $\sqrt{s} = 5$ GeV.

The predicted total minijet cross section continues to rise at higher energies. Extrapolating to the SSC ($\sqrt{s} = 40$ TeV), the lowest order QCD parton model calculation above gives $\sigma(p_T^{\text{jet}} > 5 \text{ GeV}) \simeq 120$ mb and $\sigma(p_T^{\text{jet}} > 3 \text{ GeV}) \simeq 200$ mb. These are much bigger than the geometrical size of the proton (a disk of radius 10^{-13} cm has area 31 mb) and show that the incoherent addition of parton cross sections cannot be correct. The prediction has become large because the density of partons at small x is very large; however, the total interaction cross section for n partons confined in a box (a hadron) cannot greatly exceed the size of the box itself, no matter how large n may be. A correct treatment cannot simply add parton cross sections here, but must take account of multiple scattering—including shadowing and screening corrections. This in turn requires parton-parton correlations, *i.e.* more detailed information about the hadron wave functions. We do not pursue this question, except to remark that it opens a new window on physics; there will be interesting phenomena arising from multiple interactions where many pairs of incident partons undergo hard scattering in a single event.

Multiple emission of hard gluons and quarks from a single pair of incident partons is a different phenomenon, contained within the incoherent parton approximation, expected from high order-QCD contributions as illustrated in Fig. 9.29. At c.m. energies of order 10-50 GeV in the incident parton-parton system, there is not enough energy available to produce more than a few distinct jets; the extra radiated partons are simply not resolved experimentally and are effectively just a part of the fragmentation process. At parton-parton

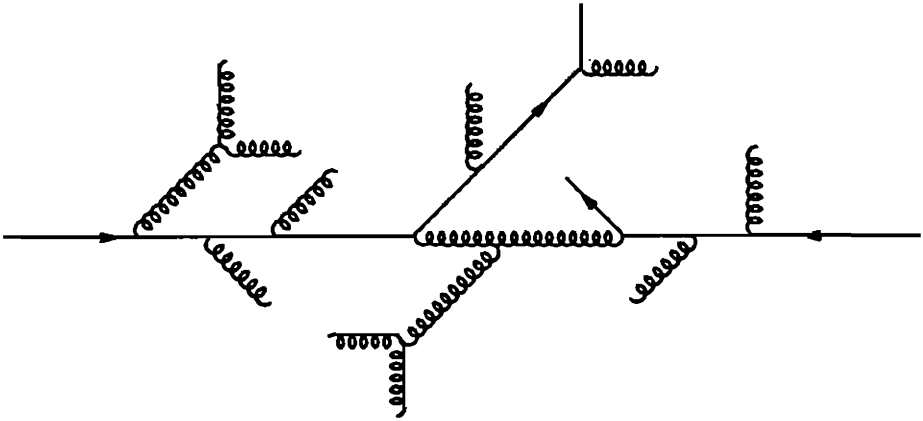


Fig. 9.29. Example of multiparton shower production.

c.m. energies of order hundreds of GeV, however, there is ample energy to make many jets that are narrow enough to be resolved. This situation will be met at the Tevatron collider and even more acutely at the SSC. Multijets will disappear if by fiat one takes a very broad resolution function for jets (integrating for example over cones of large solid angle). However, the challenge will be to exploit the richness of information in multijet data and to devise the best ways to confront the theory. The most promising way to calculate these multijet effects at present is by Monte Carlo showers, described in the next section.

9.4 Monte Carlo Shower Simulations

9.4.1 Final state showers

We are concerned here with the emission of many hard gluons and quarks. Although the exact matrix elements for $2 \rightarrow 3$ and $2 \rightarrow 4$ parton subprocesses have been calculated to low order in perturbative QCD, it is prohibitively difficult to make exact calculations for

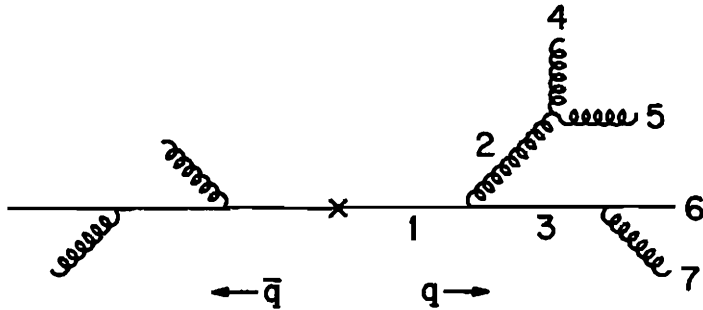


Fig. 9.30. Example of $e^+e^- \rightarrow q\bar{q}$ final state shower.

multiparton processes like Fig. 9.29. The way forward has been via Monte Carlo simulations based on leading logarithm approximations (LLA).

Consider first the case of final state hadron showers, taking for example $e^+e^- \rightarrow q\bar{q}$ as the initial hard process followed by QCD radiation from both q and \bar{q} as in Fig. 9.30 (excluding loop graphs at this stage). Kinematics require that the *virtuality* $t_i = p_i^2$ of each virtual quark or gluon line is positive and ordered down each chain (just as in the decay chains of real particles). For example, for the particles labeled $i = 1, \dots, 7$ in Fig. 9.30 we have

$$Q^2 > t_1 > t_2 > t_4, t_5, \quad t_1 > t_3 > t_6, t_7.$$

The initially produced quark can have virtuality up to Q^2 , the e^+e^- c.m. energy squared in this example. As the shower evolves, the virtualities of the partons diminish but we introduce a minimum cut-off at some value $t_c \gg \Lambda^2$ such that the running coupling $\alpha_s(t_i)$ remains small enough for a perturbative treatment. The evolution of the parton shower beyond this point is soft physics, to be represented by phenomenological fragmentation models or by direct representations of experimental data.

It is best to treat the LLA of multiple small-angle emission using an axial gauge for the gluon propagator, $-i\delta_{ab}[g_{\mu\nu} - (p_\mu\eta_\nu + p_\nu\eta_\mu)/$

$(p \cdot \eta) + \eta^2 p_\mu p_\nu / (p \cdot \eta)^2 \big] / p^2$, where η is some 4-vector orthogonal to transverse polarization vectors ($\eta \cdot \epsilon = 0$). In this gauge interference terms between different Feynman graphs (where the gluons are ordered differently) are subleading and may be dropped. The cross section is then essentially a product of independent emission probabilities. For single gluon emission from a quark line the LLA cross section is

$$d\sigma_1 = \sigma_0 \frac{\alpha_s}{2\pi} \frac{dt}{t} P_{qq}(z) dz,$$

where σ_0 is the initial hard-scattering cross section (this result is exact in the collinear limit $t \rightarrow 0$ as we saw in §9.1.2). Here t is the virtuality of the emitting quark q and z is the energy fraction transferred to the final quark q'

$$z = \frac{E'}{E} = \frac{|p'|}{|p|} = \frac{E' + p'_L}{E + p_L} = \frac{E' + |p'|}{E + |p|} = \frac{(p' + A)^2}{(p + A)^2} = \dots,$$

where A is some reference 4-vector with $A^2 = 0$. All these possible definitions coincide in the collinear limit $t \rightarrow 0$ which dominates the LLA, but for $t > 0$ they differ and give different subleading behaviors. The choice of definition therefore has practical consequences: some choices will work better than others in a given situation. $P_{qq}(z)$ is the $q \rightarrow q$ splitting function introduced in Chapter 7; the infrared singularity from the gluon emission diagram is cancelled by non-emission loop diagrams, such that $\int_0^1 dz P_{qq}(z) = 0$. We now introduce a cut-off parameter $z_c \ll 1$ to represent the limit below which a final parton will be too soft to be resolved; only the range $z_c < z < 1 - z_c$ then gives emission of a resolvable parton.

In the formula for σ_1 above, the factor multiplying σ_0 on the right can be regarded as the probability for emitting a gluon with momentum fraction in the range $1 - z$ to $1 - z - dz$ while the virtuality of the quark evolves from t to $t - dt$. Self-energy corrections replace α_s by the running couplings $\alpha_s(t)$.

Exercise. Show that the $O(\alpha_s)$ contribution to the probability of having no resolvable emission while the quark virtuality evolves from an

initial t_p to the final cutoff t_c is

$$P_1(t_p, t_c; z_c) = \int_{t_c}^{t_p} \frac{dt}{t} \frac{\alpha_s(t)}{2\pi} \left[\int_0^{z_c} + \int_{1-z_c}^1 dz P_{qq}(z) \right] = -\frac{\gamma_0(z_c)}{4\pi b} \ln \left[\frac{\alpha_s(t_c)}{\alpha_s(t_p)} \right]$$

using the LLA form $\alpha_s(t) = [4\pi b \ln(t/\Lambda^2)]^{-1}$ and the definition

$$\gamma_0(z_c) = \frac{1}{2\pi} \int_{z_c}^{1-z_c} dz P_{qq}(z).$$

Notice that P_1 in this exercise is negative. This should not alarm us. It happens because $P_{qq}(z)$ contains negative contributions at $z = 1$ from loop diagrams with no external gluon line, which simply renormalize the zeroth order $e^+e^- \rightarrow q\bar{q}$ contribution.

Similarly the LLA cross section for emitting n gluons from the quark line is

$$d\sigma_n = \sigma_0 \prod_{i=1}^n \left[\frac{\alpha_s(t_i)}{2\pi} \frac{dt_i}{t_i} P_{qq}(z_i) dz_i \right],$$

where the t_i are ordered: $t_1 > t_2 > \dots > t_n > t_c$. The factor multiplying σ_0 on the right can be interpreted as the n -gluon emission probability.

Exercise. Summing over all such processes from $n = 0$ to ∞ , show that the net probability of no resolvable emission while the quark evolves from t_p to t_c is

$$\begin{aligned} \prod(t_p, t_c; z_c) &= \sum_{n=0}^{\infty} \left(\frac{-1}{2\pi} \right)^n \int_{t_c}^{t_p} \frac{\alpha_s(t_1) dt_1}{t_1} \dots \int_{t_c}^{t_{n-1}} \frac{\alpha_s(t_n) dt_n}{t_n} \\ &\quad \times \int_{z_c}^{1-z_c} P_{qq}(z_1) dz_1 \dots \int_{z_c}^{1-z_c} P_{qq}(z_n) dz_n \\ &= \sum_{n=0}^{\infty} \frac{1}{n!} \left\{ -\frac{\gamma_0(z_c)}{4\pi b} \ln \left[\frac{\alpha_s(t_c)}{\alpha_s(t_p)} \right] \right\}^n = \left[\frac{\alpha_s(t_c)}{\alpha_s(t_p)} \right]^{-\gamma_0/4\pi b}, \end{aligned}$$

where γ_0 is defined in the exercise above and the crucial factor $1/n!$ arises from re-arranging the upper limits of all t -integrations to be t_p .

Notice that this expression has the canonical form for a solution of the RGE in LLA (§7.4). If z_c is very small (high resolution) then γ_0 is very large and the probability of no resolved emission is consequently very small.

So far we have only spoken of gluon emission by light quarks but the treatment can easily be generalized. For primary gluons both $g \rightarrow g$ and $g \rightarrow q$ splitting must be considered; in this case we simply replace $P_{qq}(z)$ above by $P_{gg}(z) + \sum_f P_{qg}(z)$ summed over quark flavors f . For heavy quarks it is appropriate to add mass-dependent non-leading terms in P_{gg} and P_{qg} . Thus a shower function Π_i can be derived for each type i of parton, differing only in the coefficient $\gamma_{0i}(z_c)$.

The quantities Π_i are the fundamental functions needed for a Monte Carlo shower simulation. The emission probability density $\Xi_i(t)$, defined such that $\Xi_i(t) dt$ is the probability that parton i emits resolvable radiation between t and $t - dt$, is by definition the derivative of Π_i

$$\Xi(t, z_c) = -\frac{d}{dt} \Pi_i(t, t_c; z_c)$$

$$\Pi_i(t, t_c; z_c) = 1 - \int_{t_c}^t dt' \Xi(t', z_c)$$

at least for the range $t_p > t > t_c$ of present interest. The first step in a shower simulation is to choose a random value of t for the first resolvable emission, with the probability weighting $\Xi_i(t)$; for this however we do not need to introduce $\Xi_i(t)$ explicitly.

Exercise. Show that we can choose random $t < t_p$, with probability weighting $\Xi(t)$ as required as follows. Choose (pseudo-) random numbers x , uniformly distributed in $0 < x < 1$. Then define t as the

solution of

$$x = [\alpha_s(t)/\alpha_s(t_p)]^{-\gamma_{0i}/4\pi b} .$$

If $t < t_c$, it means that no resolvable radiation was emitted between t_p and t_c . Notice that a similar technique can be applied quite generally to select a random variable t according to a probability density $P(t)$, by constructing $Q(t) = \int_{t_{\min}}^t dt' P(t')$ or $\int_t^{t_{\max}} dt' P(t')$ and solving $x = Q(t)$.

A shower calculation begins with the basic hard-scattering process ($e^+e^- \rightarrow q\bar{q}$ or $q\bar{q}g$, for example). Unweighted events are generated by standard Monte Carlo methods as in Chapter 11. In each event we determine the maximum allowed virtuality t_p of each emitted parton. For each parton in turn we then generate a branch of the shower as follows.

- i) Choose t for the first resolvable emission with the appropriate function Π_i as described above. If $t < t_c$ there is no such emission and this branch of the shower ends.
- ii) Choose z in the range $z_c < z < 1 - z_c$ (and the type of splitting if there is a choice) according to the splitting probability weights. Assign maximum virtuality zt and $(1 - z)t$ to the corresponding partons produced by the splitting.
- iii) Repeat this process for all the produced parton lines, until all have virtuality t_c and the showering stops.

At each branching vertex we now know the virtuality t for the incoming parton i and both the outgoing partons j, k (the latter having been determined at their first splittings); hence the c.m. momentum of the transition $i \rightarrow j + k$ is determined. The angle of emission relative to the momentum vector of i is determined by z . Only the azimuthal angle is undetermined and it is usually taken to be uniformly distributed ignoring possible spin effects. The full QCD shower kinematics is now specified for the event in question.

9.4.2 Some refinements.

In the previous subsection we took the resolution cutoff z_c to be fixed. This had the advantage of separating the z and t integrations but is somewhat unrealistic. The kinematic limits on z depend on both t and t_c and also on the particular definition of z .

Exercise. Taking the definition $z = (E' + p'_L)/(E + p_L)$ where the longitudinal direction is along the momentum vector of the initial parton, and taking the virtuality of the final partons to be $\geq t_c$, show that the kinematic limits on z are given by $z_0(t) < z < 1 - z_0(t)$ with

$$z_0(t) = \frac{1}{2} \left[1 - \sqrt{1 - 4t_c/t} \right].$$

Fortunately it is simple to implement a t -dependent cut instead in the Monte Carlo framework. We repeat the previous fixed-cut procedure, with small amendments as follows.

- i) After determining the initial t_p , choose fixed cuts z_c less severe than any possible t -dependent limit:

$$z_c \leq z_{\min}(t), \quad z_{\max}(t) \leq 1 - z_c.$$

- ii) Generate t and z as before.
 iii) Check the t -dependent limits on z . If z is inside the limits, accept the event and proceed as before. If z is outside the limits, the evolution down to t has produced no resolvable radiation; return to step (ii) and continue the evolution (starting now from t).

The definition of z is an important part of the shower prescription. Consider for example the $e^+e^- \rightarrow q\bar{q}g$ cross section (§9.1.2).

Exercise. Show the $e^+e^- \rightarrow q\bar{q}g$ cross section can be written symmetrically as

$$\begin{aligned} d\sigma(q\bar{q}g) &= \frac{4}{3} \frac{\alpha_s}{2\pi} \sigma_0 \left\{ \frac{dt}{t} \frac{du}{Q^2} \left[\frac{u(u+t) + 2sQ^2}{Q^2(u+t)} \right] + \frac{du}{u} \frac{dt}{Q^2} \left[\frac{t(t+u) + 2sQ^2}{Q^2(u+t)} \right] \right\} \\ &= \sigma_0 \left\{ \frac{\alpha_s}{2\pi} \frac{dt}{t} dz \left[P_{qq}(z) - \frac{4t}{3Q^2} \right] + \frac{\alpha_s}{2\pi} \frac{du}{u} dz \left[P_{qq}(z) - \frac{4u}{3Q^2} \right] \right\} \end{aligned}$$

when z is defined symmetrically by

$$1 - z = 1 - \frac{s}{Q^2} = \frac{u + t}{Q^2}.$$

We see from this exercise that the cross section is given (up to the non-leading Q^{-2} terms) by the sum of the branchings of the quark and antiquark lines. Given an unsymmetrical definition of z , however, the shower would develop unsymmetrically. Notice that in the present definition, the branching of q uses the \bar{q} momentum as a reference (and vice versa):

$$z(q^* \rightarrow q) = \frac{(q + \bar{q})^2}{(q^* + \bar{q})^2}, \quad z(\bar{q}^* \rightarrow \bar{q}) = \frac{(\bar{q} + q)^2}{(\bar{q}^* + q)^2}.$$

The probabilistic shower picture above has relied on the absence of interference terms in axial gauges. It is true that these interference terms contain no collinear (mass) singularities and therefore do not contribute to the leading logarithms, but they do contain soft (infra-red) divergences. As a result there is some additional quantum mechanical interference to include. Surprisingly the main effects can be expressed probabilistically in a Monte Carlo shower, simply by imposing an additional angular ordering. For each branching vertex $i \rightarrow j + k$ we introduce the angular variable

$$\xi_i = (p_j \cdot p_k) / (E_j E_k) \simeq 1 - \cos \theta_i,$$

where the second equality applies when the virtualities are small compared to the energies ($p_j^2 \approx E_j^2$, etc.) and θ_i is the branching angle; see Fig. 9.31. The interference effects of soft gluons are taken into account to leading order by requiring the values of ξ to decrease along each branch of the shower. For example, in Fig. 9.32 we require

$$\xi_0 > \xi_1 > \xi_2 \text{ or } \xi_3, \quad \theta_0 > \theta_1 > \theta_2 \text{ or } \theta_3,$$

where ξ_0 and θ_0 refer to the initial hard vertex from which the shower develops. When this ξ -ordering is included we have a *coherent shower* prescription. This ordering was first implemented in the Webber-Marchesini shower model.

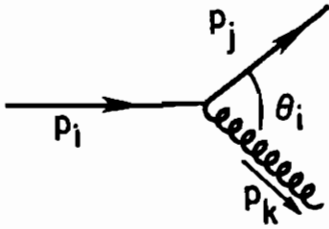


Fig. 9.31. Branching angle θ_i defined at the vertex where parton i branches to $j + k$.

Exercise. Show that the constraints resulting from shower kinematics will usually imply $\xi_0 > \xi_1 > \xi_2, \xi_3$ when the energy is approximately equally divided at each splitting, but that ξ -ordering does not follow when a soft gluon is emitted.

The angular ordering above has a simple physical interpretation. Suppose a soft gluon is emitted at a large angle relative to the rest of the shower (violating the ordering condition). It could have been emitted from any one of many color sources within the shower, but the soft gluon cannot resolve these sources so they must be added coherently. The sum is equivalent to a single parton source (the original parent of the shower), all collinear singularities cancel out and nothing remains in LLA. Thus the regions of phase space that violate ξ -ordering are suppressed.

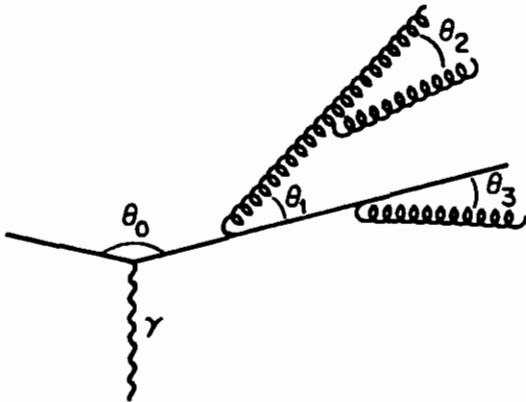


Fig. 9.32. Angular ordering $\theta_0 > \theta_1 > \theta_2, \theta_3$ occurs in a coherent shower.

9.4.3 Initial state showers.

Typical examples of initial state showers are the radiation from the incoming quark lines in $q\bar{q} \rightarrow (Z, \gamma) \rightarrow e^+e^-$ and $q\bar{q}' \rightarrow W \rightarrow e\nu$. These showers generate p_T -distributions for Drell-Yan pairs and heavy bosons, with the appearance of accompanying jets at large p_T . Figure 9.33 shows an example. The kinematics here differ from the previous case.

Exercise. If the initial parton is on mass shell (i.e., virtuality $t_1 = 0$ in Fig. 9.33), show that the emission of real gluons makes subsequent internal parton momenta spacelike ($t_2, t_3 < 0$) but that kinematics alone do not impose an ordering of t_2 and t_3 .

A Monte Carlo shower calculation can be set up if we nevertheless impose an ordering of the virtualities $\dots t_3 < t_2 < t_1$, with t limited by the intrinsic scale of the central hard interaction (e.g., the mass of the e^+e^- pair). We can then set out as before, evolving the virtuality down from an initial t_1 (not zero, to avoid soft QCD effects) with successive branchings. However with this approach, evolving forwards from an initial pair of partons, there is difficulty in matching boundary conditions—i.e., in getting $q + \bar{q}$ with the required invariant mass for the remaining $q + \bar{q}$ at the end. We can simply generate a lot of events and reject unsatisfactory ones, but this is very inefficient.

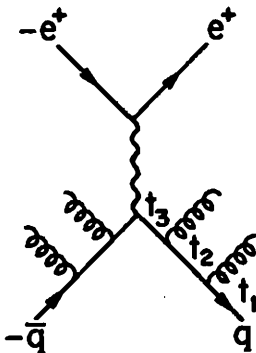


Fig. 9.33. Example of initial state shower in $\bar{q}q \rightarrow e^+e^-$ Drell-Yan process.

A much better approach is to evolve the shower *backwards*, beginning with the central hard collision and working outwards toward the initial partons (t increasing). As with final state showers, we first generate a central hard collision; to each of the participating initial partons we attach a maximum negative virtuality $-t_p$ and calculate the differential probability of branching as t evolves backward toward a minimum negative value $-t_c$. Just as in §9.4.1, the probability of no resolved branching in the range $(-t_p, -t_c)$ is

$$\prod(t_p, t_c; Z_0) = [\ln(t_p/\Lambda^2)/\ln(t_c/\Lambda^2)]^{-\gamma_0/4\pi b}$$

and the branching probability is obtained by differentiation. Different branching possibilities are summed at each step. Any real gluons or quarks that are radiated can themselves start showering, but these branches are treated as normal final-state showers. When the evolution reaches $-t_c$ (for both incident partons) we boost to the center-of-mass of the incident partons; in general the central W or Z or Drell-Yan pair has both longitudinal and transverse momenta in this frame. Finally we must weight the event with the appropriate initial parton densities (this weighting can be partially incorporated in the generation of the central collision), and give it the appropriate distribution of longitudinal boosts to the lab frame.

As in all other Monte Carlo showers, the choice of branching variable z is an important question; the answer depends on the process considered and also on the author. There are also a variety of ways to make the random choices and to impose the kinematics. For more details, see the literature.

Finally, a few remarks. It has been shown that the phase space regions excluded by ordering the initial-state virtualities are not important dynamically, so this is not as artificial as it seemed. Also initial-state kinematics imposes automatically the angular ordering required by soft gluon coherence, so there is no need to impose it separately here. All Monte Carlo shower dynamics is based on LLA, but it

is possible to improve on this somewhat by introducing more dynamics into the central hard collision: *e.g.* we could calculate $q\bar{q} \rightarrow e^+e^-g$ or $gq \rightarrow e^+e^-q$ using *exact* matrix elements and add extra radiation by Monte Carlo, rather than starting with $q\bar{q} \rightarrow e^+e^-$.

Chapter 10

Heavy Quark Production

10.1 e^+e^- Collisions

10.1.1 Quarkonia.

e^+e^- annihilation is the classic channel for producing and studying heavy quarks, because the cross sections are relatively large compared to backgrounds. Quarkonia is the name for $Q\bar{Q}$ bound states with zero net flavor; they are said to have *hidden flavor* and some of them are produced as resonances in e^+e^- collisions. Charm quarks were discovered simultaneously in e^+e^- and p -nucleus collisions via the charmonium resonance $\psi(c\bar{c})$; bottom quarks were discovered via $\Upsilon(b\bar{b})$ resonances, first seen in p -nucleus interactions but explored in detail at e^+e^- colliders. It is possible that an early signature of top quark production at e^+e^- colliders will be the formation of narrow toponium $\theta(t\bar{t})$ resonances.

There are many possible states of a heavy $Q\bar{Q}$ system. In non-relativistic approximation the total angular momentum of a quark-antiquark system is $J = L + S$ with spin states $S = 0$ (antisymmetric) and $S = 1$ (symmetric). The parity and charge conjugation of the system are $P = (-)^{L+1}$ and $C = (-)^{L+S}$; see Table 10.1. The notation ψ , Υ , θ distinguishes the $c\bar{c}$, $b\bar{b}$, $t\bar{t}$ states with $L = 0$, $S = 1$; subscripts c , b , t are used to distinguish other states, *e.g.* η_c , η_b , η_t are the $L = 0$, $S = 0$ states. Of these states, only those with $J^{PC} = 1^{--}$ can be produced via a virtual photon in e^+e^- annihilation. $J^{PC} = 1^{++}$

Table 10.1. Quantum numbers of quarkonium states.

angular momentum	J^{PC}		spectroscopic notation	
	$S = 0$	$S = 1$	$2S+1L_J$	
$L = 0$ (S)	$\eta(0^{-+})$	$\psi, \Upsilon, \theta(1^{--})$	1S_0	3S_1
$L = 1$ (P)	$h(1^{+-})$	$\chi_J(0^{++}, 1^{++}, 2^{++})$	1P_1	3P_J
$L = 2$ (D)	2^{-+}	$1^{--}, 2^{--}, 3^{--}$	1D_2	3D_J

production via virtual Z^0 axial couplings is possible; however, production with $L > 0$ suffers from angular momentum suppression. We therefore concentrate attention on e^+e^- annihilation to 3S_1 states.

Cross section formulas for the production and decay of a spin-1 resonance have been given in Chapter 4. Since the lowest toponium states are expected to be much narrower than the energy resolution of the e^+ and e^- beams, the energy-integrated formulas will be appropriate in this case:

$$\int d\sqrt{s} \sigma(e^+e^- \rightarrow \theta \rightarrow X) = \frac{6\pi^2}{m_\theta^2} \frac{\Gamma_{ee}\Gamma_X}{\Gamma},$$

where X denotes any particular set of final states, Γ_X is the corresponding partial width and Γ is the total width of θ . Notice that the total integrated cross section is proportional to Γ_{ee} .

Quarkonium states with masses above the threshold for producing two heavy mesons will decay strongly into the latter and therefore have large widths. The number of narrow 3S_1 states below this threshold can be estimated in a potential model framework. If we set the zero of energy at $2m_Q$ (where $Q = c, b, t, \dots$ is the heavy quark of interest) then the interquark potential $V(r)$ arising from QCD is independent of flavor. Also the threshold energy $E_T = 2m(Q\bar{q}) - 2m_Q$ for decay into heavy mesons $(Q\bar{q}) + (\bar{Q}q)$ is approximately independent of m_Q , for $m_Q \gg m_q$, since the $Q\bar{q}$ potential and reduced mass are approximately independent of m_Q . The number N_T of bound

energy levels below E_T is given by the number of nodes of the radial wave function at E_T ; in the WKB approximation this is found by integrating $k(r)dr$ from $r = 0$ to r_T (the classical limit):

$$N_T - \frac{1}{4} \simeq \frac{1}{\pi} \int_0^{r_T} dr [m_Q(E_T - V(r))]^{\frac{1}{2}} \simeq (\text{constant})\sqrt{m_Q},$$

where $[k(r)]^2/m_Q = E - V$ and $V(r_T) = E_T$. Recall that the reduced mass in the Schrödinger equation is $m_Q/2$. Scaling this to charmonium (two narrow states ψ and ψ' , $N_T = 2$) gives the rule

$$N_T(Q\bar{Q}) \simeq 2(m_Q/m_c)^{\frac{1}{2}},$$

which correctly predicts three narrow Υ states ($m_b/m_c \simeq 3$) and suggests about 20–25 bound toponium S -states for $m_t = 150\text{--}200$ GeV.

Exercise. For the case of a square well potential, verify explicitly that the number of bound states below any given level E_T is proportional to $\sqrt{m_Q}$.

The production cross sections and annihilation decay widths of 3S_1 quarkonia are determined by the wave function at the origin. The interquark potential has been parameterized as a sum of three contributions

$$V(r) = -\frac{4\alpha_s(r)}{3r} + V_I(r) + ar.$$

The first term is a short-distance Coulomb-like term (the Fourier transform of the one-gluon exchange scattering amplitude) and $\alpha_s(r)$ is the Fourier transform of $\alpha_s(Q^2)$.

Exercise. Derive the factor $4/3$ in the Coulomb term.

As a first approximation α_s can be taken to be fixed, e.g. $\alpha_s = \alpha_s(Q^2 = m_Q^2)$, but the logarithmic behavior of α_s within the Fourier transform can be included. At two-loop order, one obtains

$$\alpha_s(r) = \frac{12\pi}{25t} \left[1 - \frac{462 \ln t}{625 t} + \left(\frac{57}{75} + 2\gamma_E \right) \frac{1}{t} + O(t^{-2}) \right],$$

where $t = -\ln(r^2 \Lambda_{\overline{MS}}^2)$, $\gamma_E = 0.5772\dots$ is Euler's constant and $\Lambda_{\overline{MS}}$ is the QCD scale parameter in the \overline{MS} subtraction scheme.

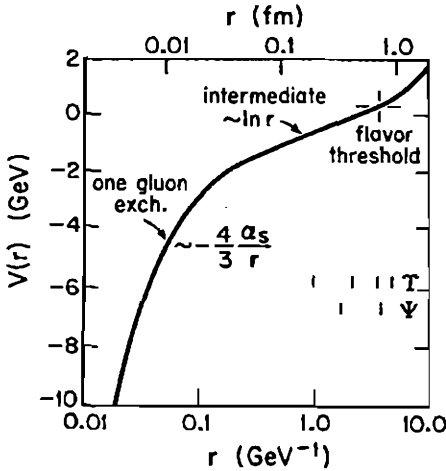


Fig. 10.1. The quarkonium potential. Toponium states in principle probe to smaller distances than $c\bar{c}$ and $b\bar{b}$ spectroscopy.

The third term in $V(r)$ is a confining potential with $a \simeq 0.2 \text{ GeV}^2$. The remaining term $V_I(r)$ parameterizes additional intermediate contributions. There are several potential parameterizations on the market; their parameters are fixed by $c\bar{c}$ and $b\bar{b}$ quarkonium data. Figure 10.1 shows a sketch of the potential and the regions probed by ψ and Υ states. In principle, toponium spectroscopy should probe the potential at smaller distances, but the energy levels are broadened by top decay (Figs. 3.19, 10.3) and hence not resolvable.

The one-gluon term alone with fixed α_s is exactly soluble, and will be of increasing importance for heavier quarkonia. However, the other terms are also important, and we shall see that the one-gluon approximation is not a reliable guide in $c\bar{c}$ and $b\bar{b}$ cases.

Exercise. From standard results for the hydrogen atom wave functions, show that the one-gluon potential alone with fixed $\alpha_s(m_Q^2)$ gives the $L = 0$ wave functions at the origin as

$$|\psi_n(0)|^2 = \left[\frac{2}{3} n^{-1} m_Q \alpha_s(m_Q^2) \right]^3 / \pi,$$

where $\psi_n(r)$ is the complete (not the radial) wave function and $n = 1, 2, \dots$ is the radial quantum number.

The short-distance structure of the wave function of a 3S_1 quarkonium state $V(Q\bar{Q})$ is represented by the matrix element

$$\langle 0 | \bar{Q} \gamma^\mu Q | V \rangle = \epsilon_V^\mu F_V,$$

where $\langle 0 |$ is the vacuum, ϵ_V is the V polarization vector and F_V is a constant with dimension $(\text{mass})^2$, related to the wave function at the origin by (see Appendix A.9)

$$|F_V|^2 = 12m_V |\psi_V(0)|^2.$$

Since the quarks $Q\bar{Q}$ are coupled to γ and Z^0 , V is coupled through them to fermion pairs $f\bar{f}$ via the effective matrix element

$$\mathcal{M}(V \rightarrow f\bar{f}) = -iF_V \epsilon_V^\mu \left[\bar{u}(f) \gamma_\mu (G_V^f + G_A^f \gamma_5) v(\bar{f}) \right],$$

where

$$G_V^f = \frac{e^2 e_f e_Q}{s} + \frac{8G_F M_Z^2}{\sqrt{2}} \frac{g_V^f g_V^Q}{s - M_Z^2 + i\Gamma_Z M_Z},$$

$$G_A^f = \frac{8G_F M_Z^2}{\sqrt{2}} \frac{g_A^f g_V^Q}{s - M_Z^2 + i\Gamma_Z M_Z},$$

and e_i, g_V^i, g_A^i are the electric charges and V, A couplings of basic fermions to Z^0 listed in §2.12. Hence the electromagnetic decay width to e^+e^- or $\mu^+\mu^-$ pairs is

$$\Gamma(V \rightarrow \gamma^* \rightarrow e^+e^-) = \frac{4\pi\alpha^2 e_Q^2}{3m_V^3} |F_V|^2 \left[1 - \frac{16}{3\pi} \alpha_s(m_Q^2) \right] \equiv \Gamma_\gamma,$$

where the QCD correction factor in square brackets will be common to many other decay modes, too. When $m_V \ll M_Z$, the virtual photon dominates the e^+e^- mode.

Exercise. By reference to particle data tables, show that the ϕ, ψ and Υ ground states have an empirical regularity

$$\Gamma(V \rightarrow e^+e^-) \simeq (11 \text{ keV}) e_Q^2$$

indicating that $|\psi_V(0)|^2 \sim m_V^2$ for these states. Show that the one-gluon exchange approximation above (with $|\psi_V(0)|^2 \sim m_V^3$ behavior)

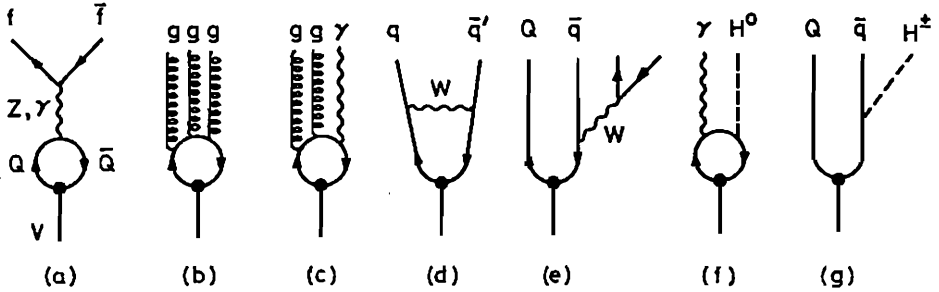


Fig. 10.2. Possible quarkonium decays discussed in the text.

underestimates $|\psi(0)|^2$ for these lighter quarkonia and predicts an n^{-3} dependence on the radial quantum number, compared to n^{-1} empirically.

The e^+e^- mode and other possible decays of the quarkonium ground state are illustrated in Fig. 10.2, that we now discuss.

- (a) $V \rightarrow f\bar{f}$ decays to fermion pairs via γ and Z^0 include the leptonic mode above. These are expected to be the most frequent final states of toponium decay for $m_V < 110$ MeV; see Fig. 10.3. Remember too that $\Gamma(V \rightarrow e^+e^-)$ governs the total integrated cross section.

Exercise. Show that the general formula for these decays is

$$\Gamma(V \rightarrow f\bar{f}) = C(m_V^2/e^2e_Q)^2(|G_V^f|^2 + |G_A^f|^2)\Gamma_\gamma,$$

where the color factor $C = 3$ (1) for quarks (leptons) and the expressions for G_V and G_A are evaluated at $s = m_V^2$.

- (b) Three-gluon decay is the dominant hadronic channel for ψ and Υ (two gluons are forbidden by C invariance):

$$\Gamma(V \rightarrow ggg) = \frac{10(\pi^2 - 9)}{81\pi e_Q^2} \frac{\alpha_s^3}{\alpha^2} \Gamma_\gamma.$$

- (c) Gluon-gluon-gamma decay is given by

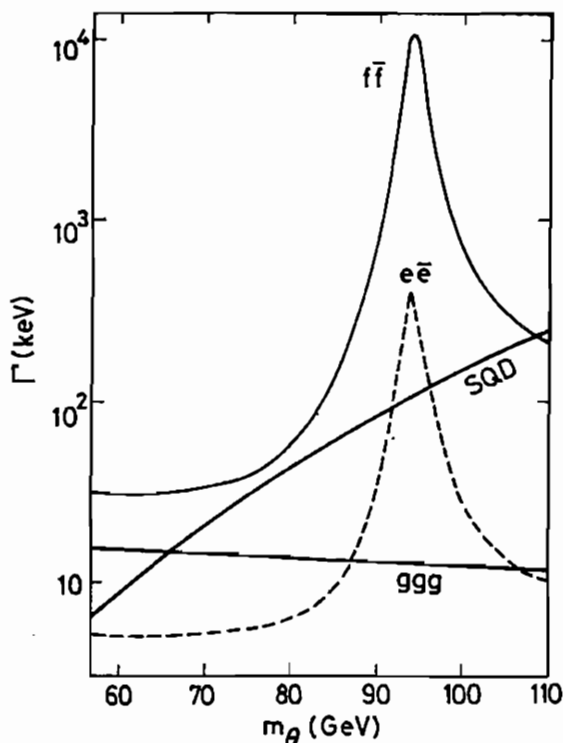


Fig. 10.3. Principal decay widths of toponium shown versus mass, neglecting possible charged-Higgs boson modes; $f\bar{f}$ denotes the sum of all fermion - antifermion channels, ggg is the three-gluon mode and SQD is single-quark decay.

$$\Gamma(V \rightarrow gg\gamma) = \frac{8(\pi^2 - 9)}{9\pi} \frac{\alpha_s^2}{\alpha} \Gamma_\gamma.$$

- (d) W -exchange contributions are mostly suppressed by small quark mixing matrix elements, but not in the case of toponium $\theta(t\bar{t}) \rightarrow b\bar{b}$ since $|V_{tb}| \approx 1$. In this case we have an additional contribution, interfering with that from process (a), giving

$$\Gamma(\theta \rightarrow b\bar{b}) = 3 \frac{m_\theta^4}{e^4 e_t^2} \Gamma_\gamma \left\{ |G_V^t|^2 + |G_A^t|^2 + \frac{1}{2} |G_W^t|^2 + G_W^t \operatorname{Re} [G_A^t - G_V^t] \right\}$$

with the definition

$$G_W^t = \frac{\sqrt{2} G_F}{3} |V_{tb}|^2 \frac{(M_W^2 + m_\theta^2/8)}{(M_W^2 + m_\theta^2/4)}.$$

- (e) Single-quark charged current decay can be calculated approximately as if the quark were free. The partial width increases like m_Q^5 (for $m_Q < M_W$), so this dominates over the previous

modes for $m_Q > 55$ GeV; see Fig. 10.3. For large mass m_Q the W -propagator factor must be included.

- (f) Radiative decay to the neutral Higgs boson is not a large channel but important for hunting the Higgs (the *Wilczek mechanism*):

$$\Gamma(V \rightarrow \gamma H^0) = \frac{G_F m_V^2 (1 - m_H^2/m_V^2)}{4\sqrt{2}\pi\alpha} \Gamma_\gamma.$$

QCD corrections to this decay rate are discussed in §12.4.1.

- (g) If there exist charged Higgs boson H^\pm with mass $m_H < m_Q$, single-quark decays via H^\pm will likely dominate over all other quarkonium modes; see §3.7.1 for examples of coupling schemes.

Exercise. Assuming an $H^+ \bar{t} b$ coupling of the form

$$\mathcal{L} = (2\sqrt{2}G_F)^{\frac{1}{2}} m_t H^+ \bar{t}_L b_R + \text{h.c.},$$

compare the relative strengths of channels (a), (b), (f), (g) for toponium decays with $m_t = 50$ GeV, $m_\theta \simeq 2m_t$.

Quarkonium production is usually signaled by narrow resonance peaks in total and partial e^+e^- cross section, but if such a resonance is close to the Z^0 mass important interference effects can be expected. For example, the production of $f\bar{f}$ fermion-antifermion pairs can proceed either directly via $e^+e^- \rightarrow (\gamma, Z) \rightarrow f\bar{f}$ or indirectly via $e^+e^- \rightarrow (\gamma, Z) \rightarrow (\text{quarkonium}) \rightarrow (\gamma, Z) \rightarrow f\bar{f}$. The corresponding amplitudes can be written

$$\mathcal{M}(e^+e^- \rightarrow \gamma \rightarrow f\bar{f}) = -\frac{4\pi\alpha e_Q}{s} [\bar{u}(f)\gamma_\mu v(\bar{f})] [\bar{v}(\bar{e})\gamma^\mu u(e)],$$

$$\begin{aligned} \mathcal{M}(e^+e^- \rightarrow Z \rightarrow f\bar{f}) &= \frac{8G_F M_Z^2/\sqrt{2}}{s - M_Z^2 + i\Gamma_Z M_Z} \\ &\times [\bar{u}(f)\gamma_\mu (g_V^f + g_A^f \gamma_5) v(\bar{f})] [\bar{v}(\bar{e})\gamma^\mu (g_V^e + g_A^e \gamma_5) u(e)], \end{aligned}$$

$$\begin{aligned} \mathcal{M}(e^+e^- \rightarrow V \rightarrow f\bar{f}) &= \frac{|F_V|^2}{s - m_V^2 + i\Gamma_V m_V} \\ &\times [\bar{u}(f)\gamma_\mu (G_V^f + G_A^f \gamma_5) v(\bar{f})] [\bar{v}(\bar{e})\gamma^\mu (G_V^e + G_A^e \gamma_5) u(e)], \end{aligned}$$

where g_V^i, g_A^i are the Z couplings (§2.12), G_V^i, G_A^i are the V couplings defined above, and s is the c.m. energy squared. Interference effects can be directly calculated from these formulas.

Exercise. At $s = m_\Upsilon^2$, show the direct $e^+e^- \rightarrow \gamma \rightarrow f\bar{f}$ amplitude does not interfere with the $e^+e^- \rightarrow \Upsilon \rightarrow f\bar{f}$ contribution.

Exercise. If $m_\theta = M_Z$, show there is destructive interference (a dip versus \sqrt{s}) between the broad dominant $e^+e^- \rightarrow Z \rightarrow f\bar{f}$ amplitude and the narrow $e^+e^- \rightarrow \theta \rightarrow f\bar{f}$ amplitude at $s = m_\theta^2$.

We have concentrated attention here on S -wave quarkonia (this includes $^3S_1 - ^3D_1$ mixtures). When these states are narrow, other quarkonium states are produced through their electromagnetic decays. Figure 10.4 shows how χ, η and h states arise in charmonium and bottomonium decays. As the number of narrow bound states increases, the spectroscopy becomes very much richer in the $t\bar{t}$ case. The many different transition rates are a challenge for potential models.

10.1.2. Open flavor production.

When a pair of produced heavy quarks Q, \bar{Q} end up in distinct heavy-flavored hadrons we speak of *open* (as opposed to *hidden*) flavor production. In e^+e^- annihilation the basic subprocess is $e^+e^- \rightarrow Q\bar{Q}$ and the charm threshold is at $\sqrt{s} = 2m_{D^0} = 3.73$ GeV. Section 4.6 gives the cross section formulas, including $\gamma - Z$ interference, threshold suppression factors and lowest order QCD corrections.

The simplest sign of open $Q\bar{Q}$ production is a step in the ratio $R = \sigma(e^+e^- \rightarrow \text{hadrons}) / \sigma(e^+e^- \rightarrow \mu^+\mu^-)$, as clearly seen in Fig. 4.10. Note that R is conventionally defined as the ratio with respect to the *theoretical* $e^+e^- \rightarrow \gamma^* \rightarrow \mu^+\mu^-$ QED cross section calculated to order α^2 . Well below the Z^0 resonance R changes little between quark thresholds and the step is simply $\Delta R(Q\bar{Q}) = 3e_Q^2$. Near the Z^0 peak however, the picture is much less simple; the fermion couplings to Z are quite different from their electric charges and as a result R changes strongly with energy even when there are no new thresholds.

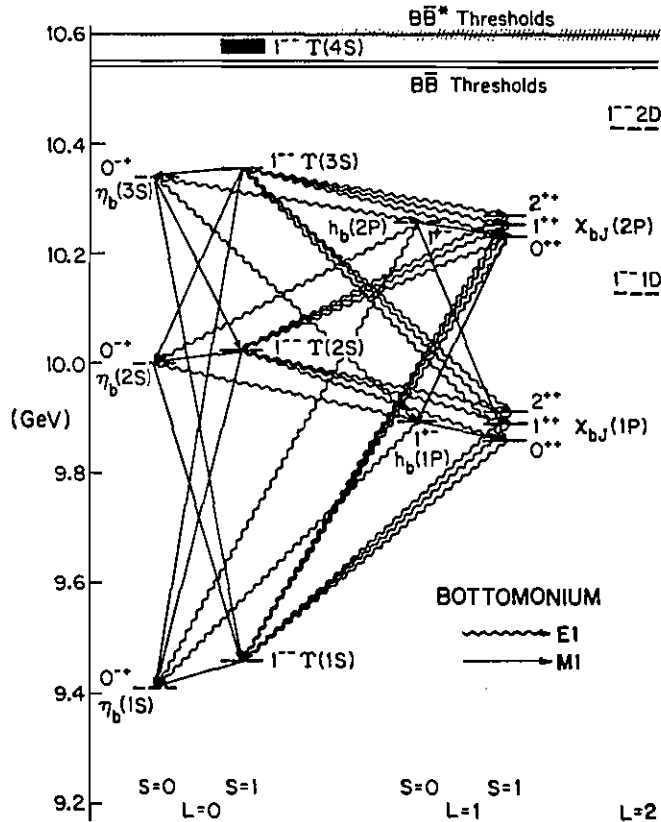
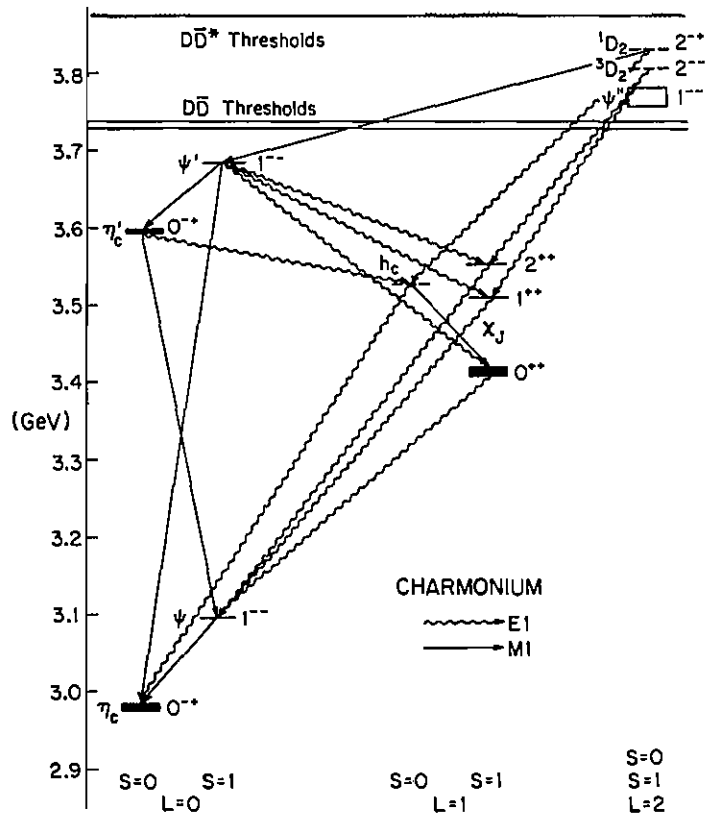


Fig. 10.4. Production of χ , η and h states from electromagnetic decays of ψ and Υ states. Wiggly lines (straight lines) denote E1 (M1) transitions.

Exercise. Show that with 5 flavors u, d, s, c, b only, R changes from about 3.8 at $\sqrt{s} = 40 \text{ GeV}$ to about 3×10^3 at $\sqrt{s} = M_Z$.

Hence any search for a step ΔR must take account of the changing base level of R , which requires a precise knowledge of M_Z, Γ_Z and $\sin^2\theta_w$.

Independent evidence of a $Q\bar{Q}$ threshold would be a step in the cross section for hadronic events with large sphericity (low thrust) and/or isolated leptons, since both properties are characteristic of heavy flavor (§3.7, §9.1). The background of spherical isolated-lepton events—which comes from fluctuations in the fragmentation of lighter $q\bar{q}$ pairs—will rise as the Z pole is approached but has no step behavior. If a sufficiently clean sample of low-thrust events can be found, the broadness of the jets can determine the mass m_Q and the number of events can in principle determine whether e_Q is $2/3$ or $-1/3$ (though there are ambiguous regions).

Measuring the total $\mu^+\mu^-$ and hadronic cross sections at the Z^0 resonance energy (or indeed integrating across the resonance) can determine the ratio $\Gamma(Z \rightarrow \text{hadrons})/\Gamma(Z \rightarrow \mu^+\mu^-)$. A positive excess over the theoretical expectation from u, d, s, c, b quarks might signal a new channel, but would not by itself establish that this channel is $Q\bar{Q}$ nor determine either m_Q or e_Q ; Fig. 4.13 shows that these questions are linked.

The identification of secondary b or c decay vertices by microvertex detectors can also help to determine the presence of new flavor production.

If the flavor of a heavy quark jet can be tagged (*e.g.* by the decay properties; §3.7) one can measure the left-right and forward-backward asymmetries in $e^+e^- \rightarrow \bar{Q}Q$ and investigate the electroweak couplings of Q .

Exercise. At the Z^0 resonance energy, show these asymmetries

are

$$A_{LR} = \frac{-2g_V^e g_A^e}{(g_V^e)^2 + (g_A^e)^2},$$

$$A_{FB} = \frac{4\beta g_V^e g_A^e g_V^Q g_A^Q}{[(g_V^e)^2 + (g_A^e)^2] \left\{ [(g_V^Q)^2 + (g_A^Q)^2] \left(1 + \frac{1}{3}\beta^2\right) + [(g_V^Q)^2 - (g_A^Q)^2] (1 - \beta^2) \right\}},$$

where β is the velocity of Q . Note that A_{LR} is the same as for $e^+e^- \rightarrow \mu^+\mu^-$ and contains no information about Q at this particular energy.

At other energies $\gamma - Z$ interference is important, too. There are QCD corrections for gluon emission and loops, that we do not give here. In the case of A_{FB} one must prescribe whether and how to include three-jet events.

The JADE collaboration measured the b -jet asymmetry at $Q = 34$ GeV. They used jet broadening, and the transverse momentum of decay muons and missing neutrinos to select $b\bar{b}$ events, and the sign of μ^\pm to discriminate b from \bar{b} jets. The result $A_{FB} = -0.228 \pm 0.060 \pm 0.025$ agrees well with the standard model prediction -0.252 for $\sin^2\theta_w = 0.23$, confirming that b belongs to a doublet and hence that t exists.

Another interesting possibility with tagged heavy quark events is to look for polarization effects, since $e^+e^- \rightarrow Q\bar{Q}$ creates quarks with correlated spins. With light quarks this information is usually lost; most of the quarks fragment to $(Q\bar{q})$ mesons that cascade down to the lightest spin-0 meson (which has no capacity for retaining spin information) before Q finally decays. With heavier quarks such as t the meson energy levels are closer together, many transitions can only go by photon emission and not by pion emission, and so the cascade process is slower; on the other hand, the quark lifetime is shorter. An increasing proportion of Q decays will therefore occur from excited meson states where Q is only partly depolarized. Angle and energy correlations between decay products of Q and \bar{Q} will

result, depending on the degree of Q and \bar{Q} depolarizations which is unfortunately hard to calculate.

To calculate three-jet production with heavy quarks we need the $e^+e^- \rightarrow Q\bar{Q}g$ matrix elements. The formulas are given in §10.2 for γ exchange only and in the literature for general γ and Z exchanges.

10.1.3. Flavor oscillations.

The pseudoscalar mesons $B_d^0(\bar{b}d)$ and $\bar{B}_d^0(b\bar{d})$ are eigenstates of the strong interaction Hamiltonian; they have the same J^{PC} quantum numbers and the same masses (*i.e.* same energy levels in the strong interquark potential) but are distinguished by their quark flavors. They are therefore the right basis for discussing the production of B -mesons by strong fragmentation, and also for discussing meson interaction or decay processes where the quark flavors are tagged.

Exercise. In the spectator decay approximation show that the decays $B \rightarrow e^\pm X$ (primary decay) and $B \rightarrow K^\pm X$ can be used to tag the flavor $b(\bar{b})$ of the constituent bottom quark. Identify some backgrounds in the kaon case, from unfavored decay modes, etc.

Weak interactions however do not conserve quark flavors and can mix B^0 with \bar{B}^0 states, for example by box diagrams like Fig. 10.5 and similar diagrams involving charged Higgs bosons H^\pm if they exist. We must therefore consider B^0 and \bar{B}^0 together as a coupled system with the possibility of transitions between them being detected by flavor-tagging. This phenomenon of $B^0 - \bar{B}^0$ oscillations (also known as $B^0 - \bar{B}^0$ mixing) occurs for other flavors, too; such oscillations were first found in the $K^0 - \bar{K}^0$ system. For the present discussion however we shall speak mainly of B mesons, including both the $B_d^0 - \bar{B}_d^0$ and $B_s^0 - \bar{B}_s^0$ systems.

In the rest-frame of an initial neutral B meson, we represent the coupled $B - \bar{B}$ system by a two-component wave function $[a(t), \bar{a}(t)]$ where $a(t)$ and $\bar{a}(t)$ are the amplitudes for finding B and \bar{B} , respectively, at time t . \bar{B} is the charge-conjugate of B so that $CP|B\rangle = -|\bar{B}\rangle$. The Hamiltonian in the B, \bar{B} sector is then a mass matrix and

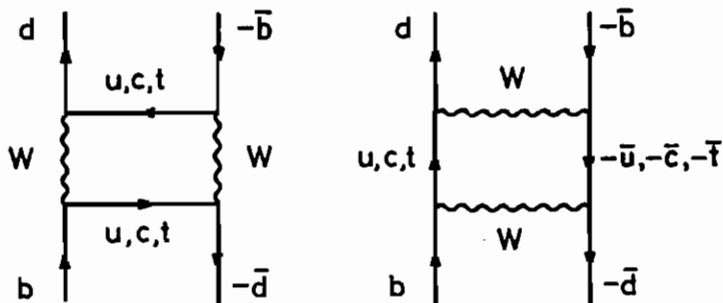


Fig. 10.5. Examples of weak processes that give $B^0 \leftrightarrow \bar{B}^0$ transitions.

the Schrödinger equation has the form

$$i \frac{d}{dt} \begin{pmatrix} a \\ \bar{a} \end{pmatrix} = \begin{pmatrix} m - \frac{1}{2}i\Gamma, & m_{12} - \frac{1}{2}i\Gamma_{12} \\ m_{12}^* - \frac{1}{2}i\Gamma_{12}^*, & m - \frac{1}{2}i\Gamma \end{pmatrix} \begin{pmatrix} a \\ \bar{a} \end{pmatrix}.$$

Here the quark rest-masses and the strong binding forces contribute to m ; $B \rightarrow X$ and $\bar{B} \rightarrow \bar{X}$ decays (with $X \neq \bar{X}$) contribute to Γ while such decays with $X = \bar{X}$ contribute to Γ_{12} . Diagrams like Fig. 10.5 contribute to the off-diagonal elements, the dispersive parts giving m_{12} and the absorptive parts (i.e. with on-shell real intermediate states) giving Γ_{12} ; box diagrams also contribute to the diagonal elements.

Exercise. Confirm from the structure of the box diagrams in Fig. 10.5 that the diagonal contributions are equal and the off-diagonal contributions are related by complex conjugation, as indicated in the mass matrix above.

The equality of the diagonal elements $m_{11} = m_{22} = m$, $\Gamma_{11} = \Gamma_{12} = \Gamma$ and the hermiticity of dispersive and absorptive parts $m_{21} = m_{12}^*$, $\Gamma_{21} = \Gamma_{12}^*$ can be shown to follow in general from TCP invariance.

Exercise. Show that the eigenvalues of the mass matrix are

$$m_j - \frac{1}{2}i\Gamma_j = m - \frac{1}{2}i\Gamma \pm [(m_{12} - \frac{1}{2}i\Gamma_{12})(m_{12}^* - \frac{1}{2}i\Gamma_{12}^*)]^{\frac{1}{2}}$$

with column eigenvectors

$$|B_j\rangle = \begin{pmatrix} (m_{12} - \frac{1}{2}i\Gamma_{12})^{\frac{1}{2}} / (m_{12} + m_{12}^* - \frac{1}{2}i\Gamma_{12} - \frac{1}{2}i\Gamma_{12}^*)^{\frac{1}{2}} \\ \pm (m_{12}^* - \frac{1}{2}i\Gamma_{12}^*)^{\frac{1}{2}} / (m_{12} + m_{12}^* - \frac{1}{2}i\Gamma_{12} - \frac{1}{2}i\Gamma_{12}^*)^{\frac{1}{2}} \end{pmatrix},$$

where $j = 1, 2$ labels the eigenvectors. Notice that the eigenvectors are not orthogonal in the most general case.

For a start let us neglect CP violation. In this case $m_{12} = m_{12}^*$, $\Gamma_{12} = \Gamma_{12}^*$ and the eigenvectors and eigenvalues are simply

$$|B_1\rangle = \frac{1}{\sqrt{2}} \begin{pmatrix} 1 \\ 1 \end{pmatrix}, \quad m_1 = m + m_{12}, \quad \Gamma_1 = \Gamma + \Gamma_{12},$$

$$|B_2\rangle = \frac{1}{\sqrt{2}} \begin{pmatrix} 1 \\ -1 \end{pmatrix}, \quad m_2 = m - m_{12}, \quad \Gamma_2 = \Gamma - \Gamma_{12}.$$

Notice that these eigenstates $|B_{1,2}\rangle = (|B\rangle \pm |\bar{B}\rangle)/\sqrt{2}$ are simply the eigenstates of CP with $CP = \mp 1$, as we should expect.

It may be surprising at first sight that a second-order weak process like Fig. 10.5 can bring about this large (indeed maximal) mixing between B^0 and \bar{B}^0 components in the mass eigenstates. This only happens because the diagonal mass matrix elements are exactly degenerate. The reader may have noticed that diagrams akin to Fig. 10.5 cause B_d, \bar{B}_d transitions to B_s, \bar{B}_s states too, making a four-fold coupled system. However the large inequality of diagonal elements suppresses $B_s \leftrightarrow B_d$ mixing, so that only $B_d \leftrightarrow \bar{B}_d$ and $B_s \leftrightarrow \bar{B}_s$ mixing need be considered.

Now that we have identified the eigenstates of propagation B_1 and B_2 , we can quantify flavor oscillation effects. Suppose a state $|B\rangle = (|B_1\rangle + |B_2\rangle)/\sqrt{2}$ is created initially and we work in the B rest frame. To discuss time evolution we must change to the B_1, B_2 basis and evolve each component independently. If after time t the flavor is probed, we must change back to the B, \bar{B} basis in order to

evaluate the decays. Algebraically, this is expressed as

$$\begin{aligned}
 |B\rangle &= \frac{1}{\sqrt{2}} [|B_1\rangle + |B_2\rangle], && \text{time } 0 \\
 &\rightarrow \frac{1}{\sqrt{2}} \sum_{j=1,2} \exp(-im_j t - \frac{1}{2}\Gamma_j t) |B_j\rangle, && \text{time } t \\
 &= a(t) |B\rangle + \bar{a}(t) |\bar{B}\rangle,
 \end{aligned}$$

where the amplitudes $a(t)$ and $\bar{a}(t)$ for $B \rightarrow B, \bar{B}$ transitions are

$$\begin{aligned}
 a(B \rightarrow B) &= \frac{1}{2} [\exp(-im_1 t - \frac{1}{2}\Gamma_1 t) + \exp(-im_2 t - \frac{1}{2}\Gamma_2 t)], \\
 \bar{a}(B \rightarrow \bar{B}) &= \frac{1}{2} [\exp(-im_1 t - \frac{1}{2}\Gamma_1 t) - \exp(-im_2 t - \frac{1}{2}\Gamma_2 t)].
 \end{aligned}$$

The probability of finding B or \bar{B} at time t is proportional to the squared modulus of the corresponding amplitude. Thus if B decays by a flavor-tagging channel such as $B \rightarrow e^+ X$, $\bar{B} \rightarrow e^- X$ semileptonic decays, the net probability that it does so via a B or \bar{B} mode is proportional to the time integral of $|a|^2$ or $|\bar{a}|^2$.

Exercise. Show that the time-averaged probabilities for an initial B to decay via a B or \bar{B} channel are

$$\begin{aligned}
 P(B \rightarrow \bar{B}) &= \frac{\frac{1}{2} [(\delta m)^2 + \frac{1}{4}(\delta\Gamma)^2]}{(\delta m)^2 + \Gamma^2} \equiv \chi, \\
 P(B \rightarrow B) &= \frac{\frac{1}{2} [(\delta m)^2 + 2\Gamma^2 - \frac{1}{4}(\delta\Gamma)^2]}{(\delta m)^2 + \Gamma^2} \equiv 1 - \chi,
 \end{aligned}$$

where $\delta m = m_1 - m_2 = 2m_{12}$, $\delta\Gamma = \Gamma_1 - \Gamma_2 = 2\Gamma_{12}$ and $\Gamma_1 + \Gamma_2 = 2\Gamma$.

The interesting case is $B \rightarrow \bar{B}$. Notice that the probability for flavor oscillations $\rightarrow 0$ if $\Gamma \gg |\delta m|$ and $|\delta\Gamma|$ (i.e. if the system decays before an appreciable phase difference between B_1 and B_2 states can build up) but $\rightarrow \frac{1}{2}$ if $|\delta m| \gg \Gamma$ or if $|\delta\Gamma| \sim 2\Gamma$ (i.e. if there are many phase oscillations during the lifetime).

The symbol χ introduced above is often used to denote the probability of an “oscillated” decay; subscripted symbols χ_d, χ_s distinguish the B_d, B_s cases. Another symbol often used is the ratio of “oscillated” to “normal” decays:

$$r = P(B \rightarrow \bar{B})/P(B \rightarrow B) = \chi/(1 - \chi).$$

We can estimate $\Gamma_1 \approx \Gamma_2 \approx \Gamma_b$ in the spectator decay model, from the $b \rightarrow cf\bar{f}'$ free quark decays. We can also estimate δm from the box diagrams like Fig. 10.5; in fact the diagram where both virtual quarks are t -quarks gives the dominant contribution. The result for the $B(\bar{b}q) - \bar{B}(b\bar{q})$ system is

$$\left(\frac{|\delta m|}{\Gamma}\right)_q = \left(\frac{2|m_{12}|}{\Gamma}\right)_q = \tau_{B_q} \frac{BG_F^2}{6\pi^2} f_{B_q}^2 m_{B_q} \eta_{\text{QCD}} |(V_{tq}V_{tb}^*)^2| I,$$

where $q = d$ or s , τ_{B_q} and m_{B_q} are the experimentally measured lifetime and mass of B_q , B is a confinement factor ($B \simeq 1$ commonly assumed), f_{B_q} is the decay constant ($f_B \simeq 0.09\text{--}0.13$ GeV estimated) and V_{ab} are quark mixing matrix elements. The short-distance factor η_{QCD} and box integral I are approximated by

$$\eta_{\text{QCD}} = X^{-6/23} \left[\frac{3}{2} Y^{-4/7} - Y^{-2/7} + \frac{1}{2} Y^{8/7} \right]$$

with $X = \alpha_s(m_b)/\alpha_s(m_t)$ and $Y = \alpha_s(m_t)/\alpha_s(M_W)$, and

$$I = \frac{1}{4} M_W^2 \left[x \left(1 + \frac{9}{1-x} - \frac{6}{(1-x)^2} \right) - \frac{6x^3}{(1-x)^3} \ln x \right],$$

where $x = m_t^2/M_W^2$. For $m_t^2 \ll M_W^2$, $I \approx m_t^2$.

For $K^0 - \bar{K}^0$ mixing there are similar box diagrams, but it is believed that long-distance contributions can also be significant here. For $D^0(c\bar{u}) - \bar{D}^0(\bar{c}u)$, $T_u^0(t\bar{u}) - \bar{T}_u^0(\bar{t}u)$ and $T_c^0(t\bar{c}) - \bar{T}_c^0(\bar{t}c)$ systems there are analogous box diagrams with intermediate d, s, b quarks exchanged; since none of these quarks is very massive, no single diagram dominates. Estimates of $\delta m/\Gamma$ for D^0 and T^0 systems are very small in the standard model; we do not pursue them here.

To estimate $\delta\Gamma = 2\Gamma_{12}$ we notice it arises from decay channels that are common to both B and \bar{B} and hence have no net flavor to distinguish them. Examples are $B_d(\bar{B}_d) \rightarrow c\bar{c}d\bar{d}$ and $B_s(\bar{B}_s) \rightarrow c\bar{c}s\bar{s}$ with $D(\bar{D}) \rightarrow s\bar{s}u\bar{u}$ in the case of charm; there are also annihilation modes $B(\bar{B}) \rightarrow c\bar{c}, u\bar{u}$ and $D(\bar{D}) \rightarrow s\bar{s}, d\bar{d}$.

Exercise. Show that all these modes are suppressed relative to the total decay rate, either by phase space or by small mixing matrix elements V_{ab} , so that $\delta\Gamma/\Gamma \ll 1$.

From these arguments $\delta\Gamma$ makes no substantial contribution to flavor oscillations and may be dropped from the analysis, leaving simply

$$\chi \simeq \frac{1}{2}(\delta m)^2 / [(\delta m)^2 + \Gamma^2], \quad r \simeq (\delta m)^2 / [(\delta m)^2 + 2\Gamma^2].$$

Any measurable oscillations would provide valuable information about the various factors that affect $\delta m/\Gamma$, especially the mixing matrix and the top quark mass.

As an illustration, Fig. 10.6 shows the values of r_d and r_s resulting from these formulas if we take $\eta_{\text{QCD}} = 0.84$, $m_{B_q} = 5.27$ GeV, $\tau_B = 1.11 \times 10^{-12}$ sec, $\sqrt{B} f_{B_q} = 0.10, 0.15, 0.20$ GeV, and choose the Kobayashi-Maskawa mixing angles (§2.10) to maximize r_d subject to the experimental constraints: $s_1 = 0.222$, $s_2 = 0.095$, $s_3 = 0.050$, $\delta = 168.5^\circ$. The results are displayed versus the top quark mass m_t . Both r_s and r_d may be substantial.

Evidence for flavor oscillations may be sought using flavor-tag decays like $B \rightarrow \ell^\pm$ semileptonic modes. In primary $b \rightarrow c\ell\nu$ decays the sign of the lepton's electric charge determines whether the decay quark was b or \bar{b} . In secondary $b \rightarrow c \rightarrow s\ell\nu$ decays the lepton has the opposite sign; the lepton acceptance must be chosen to disfavor them. Here are some examples:

- (i) Suppose $e^+e^- \rightarrow b\bar{b}$ at an energy high above threshold gives $B + \bar{B}$ jets, and that a muon with $p_T > 1$ GeV relative to the jet axis tags a primary $b \rightarrow c\mu\nu$ decay. If we observe one such muon in each jet, we have a sample of primary semileptonic decays of both quarks. Without flavor oscillations, only unlike sign pairs $\mu^+\mu^-$ should be seen. See Fig. 10.7.

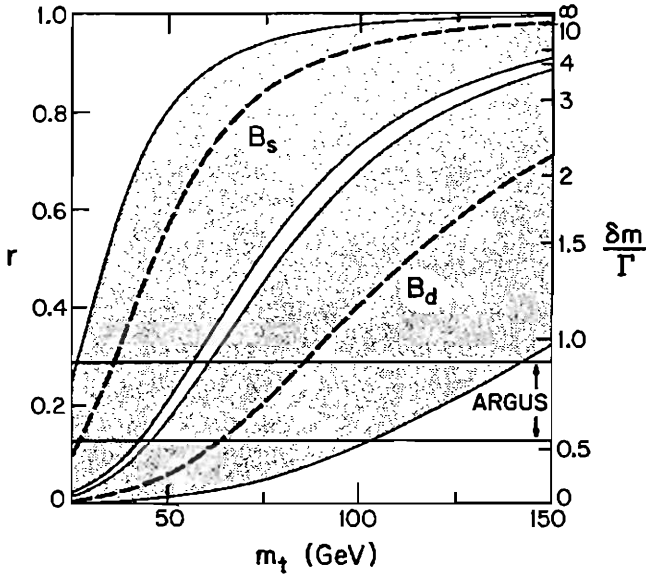


Fig. 10.6. Ranges of oscillation parameters r_d and r_s , corresponding to the region in mixing-parameter space that maximizes B_d^0 oscillations, plotted versus m_t ; the curves in each band correspond to the choices $f_{B_q}\sqrt{B_q} = 0.20, 0.15, 0.10$ GeV, respectively. The right-hand axis displays the corresponding values of $\delta m/\Gamma$. The ARGUS experimental result for r_d is shown.

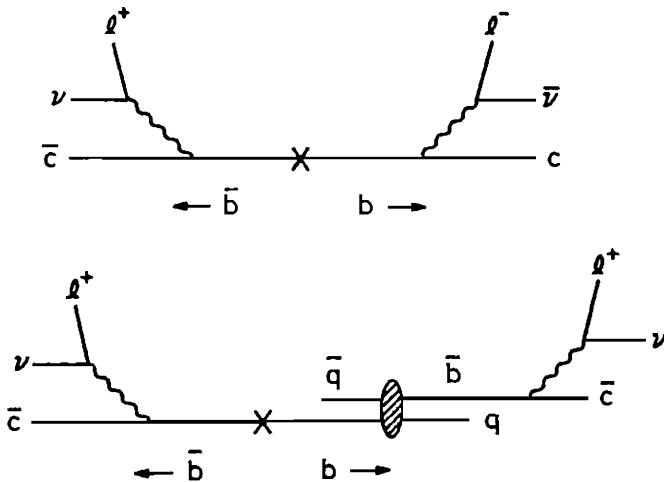


Fig. 10.7. Leptons from primary $b\bar{b}$ decays. (a) Normal decays give unlike-sign dileptons. (b) Flavor oscillations give like-sign dileptons.

Exercise. Assuming that initial b fragments to fractions f_u, f_d, f_s of $b\bar{u}, b\bar{d}, b\bar{s}$ mesons (and similarly for \bar{b}), that all mesons have similar semileptonic decays and baryons can be effectively lumped together with charged (non-oscillating) mesons, show that the ratio of like-sign to unlike-sign dimuons is

$$\frac{N(\pm\pm)}{N(\pm\mp)} = \frac{2\chi_d(1-\chi_d)f_d + 2\chi_s(1-\chi_s)f_s}{f_u + [\chi_d^2 + (1-\chi_d)^2]f_d + [\chi_s^2 + (1-\chi_s)^2]f_s}, \quad (a)$$

$$\text{or } \frac{2(\chi_d f_d + \chi_s f_s) [f_u + (1-\chi_d)f_d + (1-\chi_s)f_s]}{(\chi_d f_d + \chi_s f_s)^2 + [f_u + (1-\chi_d)f_d + (1-\chi_s)f_s]^2}, \quad (b)$$

depending whether the light quark flavors in the B, \bar{B} mesons are (a) correlated or (b) uncorrelated (more plausible at high energy).

In practice, corrections must also be made for $\pi, K \rightarrow \mu\nu$ decays, secondary $b \rightarrow c \rightarrow \mu$ decays, charm jets and misidentification. Notice that B_d and B_s oscillations are not separated.

Figure 10.8 shows results from the Mark II experiment at PEP, shown as 90% limits in the (r_s, r_d) plane for various assumed values of f_d and f_s . Since $B - \bar{B}$ oscillations would reduce the asymmetry A_{FB} observed for b -jets, the agreement of data with theory in §10.1.2 implies rather similar bounds, not plotted here.

- (ii) As a second example, consider $e^+e^- \rightarrow \Upsilon(4S)$ resonance production. $\Upsilon(4S)$ decays almost entirely to B^+B^- and $B_d^0\bar{B}_d^0$ states; subsequent electrons with energy $E_e > 1$ GeV then tag primary $B \rightarrow ce\bar{\nu}$ decays. Hence pairs of such electrons can only acquire opposite signs through $B_d^0 - \bar{B}_d^0$ oscillations (Fig. 10.7). The analysis differs from case (i) above, however, because of quantum correlations; the $B\bar{B}$ pair is produced via a virtual photon into a state with $C = -1$, namely

$$\Psi(x_1, x_2) = \frac{1}{\sqrt{2}} [B_d(x_1)\bar{B}_d(x_2) - \bar{B}_d(x_1)B_d(x_2)]$$

and the two components of this wave function contribute coherently.

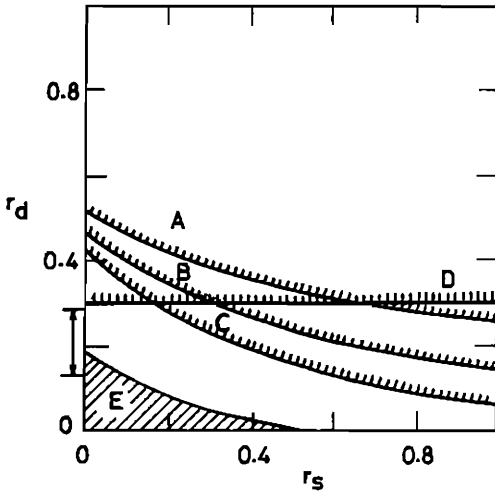


Fig. 10.8. Results for $B - \bar{B}$ mixing parameters r_s and r_d . Curves A-C are upper limits from the Mark II detector at PEP ($Q = 29$ GeV) with (A) $f_d = 0.35$, $f_s = 0.10$; (B) $f_d = 0.375$, $f_s = 0.15$; (C) $f_d = 0.40$, $f_s = 0.20$. Curve D is the CLEO upper limit at the $\Upsilon(4S)$ resonance. The shaded area E is excluded by UA1 measurements. The arrows denote a r_d result from the ARGUS collaboration at the $\Upsilon(4S)$.

To evaluate the interference effects we need expressions for transition amplitudes to given decay states. Suppose $|f_j\rangle$ denotes a set of final states with energies E_j into which only $|B\rangle$ can decay, with CP-conjugate states $|\bar{f}_j\rangle$ into which only $|\bar{B}\rangle$ can decay. Starting from initial $|B\rangle$, let the amplitudes for $|f_j\rangle$ and $|\bar{f}_j\rangle$ after time t be $c_j(t)$ and $d_j(t)$, respectively, while the amplitudes for $|B\rangle$ and $|\bar{B}\rangle$ are denoted $a(t)$ and $\bar{a}(t)$ as before.

Exercise. Show that the Schrödinger equations for the decayed-state amplitudes are

$$dc_j(t)/dt = \alpha_j a(t) - iE_j c_j(t), \quad dd_j(t)/dt = \bar{\alpha}_j \bar{a}(t) - iE_j d_j(t),$$

where $i\alpha_j$ ($i\bar{\alpha}_j$) is the matrix element for B (\bar{B}) to decay to f_j (\bar{f}_j).

Exercise. Show that the solutions (assuming CP conservation) are

$$\left. \begin{array}{l} c_j(t) \\ d_j(t) \end{array} \right\} = \frac{\alpha_j}{2i} \left[\frac{\exp(-i\mu_1 t) - \exp(-iE_j t)}{E_j - \mu_1} \pm \frac{\exp(-i\mu_2 t) - \exp(-iE_j t)}{E_j - \mu_2} \right]$$

(where $\mu_k = m_k - \frac{1}{2}i\Gamma_k$, $k = 1, 2$) with the asymptotic forms

$$\left. \begin{array}{l} c_j(t) \\ d_j(t) \end{array} \right\} = \frac{1}{2} i\alpha_j \exp(-iE_j t) [(E_j - \mu_1)^{-1} \pm (E_j - \mu_2)^{-1}].$$

The amplitudes to reach opposite-sign electron final states $(f_i \bar{f}_j - \bar{f}_i f_j)/\sqrt{2}$ and same-sign final states $(f_i f_j - \bar{f}_i \bar{f}_j)/\sqrt{2}$ therefore are

$$A(+ -) = A(- +) = (c_i c_j - d_i d_j), \quad A(+ +) = A(- -) = (c_i d_j - d_i c_j).$$

To get the net probabilities we must square these amplitudes, integrate over energies E_i , E_j and sum over channels i, j .

Exercise. By integrating over E_i and E_j , show that for each pair of channels i and j the probability of same-sign dileptons is

$$\frac{P(+ +) + P(- -)}{P(+ +) + P(- -) + P(+ -) + P(- +)} = \frac{1}{2} \frac{(\delta m)^2 + \frac{1}{4}(\delta \Gamma)^2}{(\delta m)^2 + \Gamma^2}$$

so that this ratio also describes the sum over channels. (Use Cauchy's formula).

Notice that this is precisely the probability χ for single uncorrelated B to decay in an oscillated mode. This also follows simply from the wave function (p. 350) which keeps this form for $t_1 = t_2$ by Bose statistics. If meson 1 decays first as \bar{B} (say), the $\bar{B}(x_1)B(x_2)$ component is selected, so meson 2 is pure B at this time and same-sign dileptons require $B \rightarrow \bar{B}$ decay, with probability χ .

Taking account of the $B^+ B^-$ modes we obtain in the present case

$$\frac{N(\pm\pm)}{N(\pm\mp)} = \frac{f_d \chi_d}{f_u + f_d(1 - \chi_d)},$$

where experimentally $f_u \simeq 0.59$, $f_d \simeq 0.41$ at $\Upsilon(4S)$. The difference between this and the previous example (setting $f_s = 0$) is due to quantum mechanical interference.

Let us now include CP violation. The relations between the CP-conjugate meson states B , \bar{B} and the mass eigenstates B_1 , B_2 can

be written

$$|B_1\rangle = \frac{|B\rangle + \eta|\bar{B}\rangle}{\sqrt{1+|\eta|^2}}, \quad |B\rangle = \frac{\sqrt{1+|\eta|^2}}{2} [|B_1\rangle + |B_2\rangle],$$

$$|B_2\rangle = \frac{|B\rangle - \eta|\bar{B}\rangle}{\sqrt{1+|\eta|^2}}, \quad |\bar{B}\rangle = \frac{\sqrt{1+|\eta|^2}}{2\eta} [|B_1\rangle - |B_2\rangle],$$

where η is a complex parameter

$$\eta = [(m_{12}^* - \frac{1}{2}i\Gamma_{12}^*) / (m_{12} - \frac{1}{2}i\Gamma_{12})]^{\frac{1}{2}}.$$

Any value $\eta \neq 1$ implies CP violation; assuming the effects are small, they are sometimes expressed by a small complex parameter ϵ ,

$$\epsilon = \frac{1-\eta}{1+\eta}, \quad \eta = \frac{1-\epsilon}{1+\epsilon} \simeq 1 - 2\epsilon.$$

In the $K^0 - \bar{K}^0$ system, the value $\mathcal{R}_e \epsilon = (1.621 \pm 0.088) \times 10^{-3}$ has been measured; in other $M^0 - \bar{M}^0$ systems it remains to be determined.

For semileptonic decay or any other flavor-tagging decay proceeding via a single weak-interaction diagram, TCP invariance relates the moduli of the transition matrix elements in CP-conjugate channels:

$$|\langle f_j | B \rangle| = |\langle \bar{f}_j | \bar{B} \rangle|.$$

Hence the factors $|\alpha_j|^2$ arising in $B \rightarrow f_j$ decay probabilities appear unchanged in $\bar{B} \rightarrow \bar{f}_j$ decays, under these conditions.

Exercise. Show that

$$\langle B_1 | B_2 \rangle = (1 - |\eta|^2) / (1 + |\eta|^2) \simeq 2\mathcal{R}_e \epsilon \simeq \frac{1}{2} \mathcal{I}m(\Gamma_{12}/m_{12})$$

assuming that $[\mathcal{R}_e(\Gamma_{12}/m_{12})]^2 \ll 4\mathcal{I}m(\Gamma_{12}/m_{12})$.

Exercise. Repeating the previous analysis with the present more general forms of B_1 and B_2 , show that the time-averaged probability ratio for initial B to decay into a \bar{B} rather than a B flavor-tagged state is

$$r = \frac{P(B \rightarrow \bar{B})}{P(B \rightarrow B)} = |\eta|^2 \frac{(\delta m)^2 + \frac{1}{4}(\delta\Gamma)^2}{(\delta m)^2 + 2\Gamma^2 - \frac{1}{4}(\delta\Gamma)^2},$$

whereas the corresponding ratio for initial \bar{B} is

$$\bar{r} = \frac{P(\bar{B} \rightarrow B)}{P(\bar{B} \rightarrow \bar{B})} = \frac{1}{|\eta|^2} \frac{(\delta m)^2 + \frac{1}{4}(\delta\Gamma)^2}{(\delta m)^2 + 2\Gamma^2 - \frac{1}{4}(\delta\Gamma)^2},$$

which differ by factors $|\eta|^2$, $|\eta|^{-2}$ from their common expression in the CP-conserving case. Show that the formulas for $P(B \rightarrow B)$ and $P(\bar{B} \rightarrow \bar{B})$ remain equal and unchanged. Hence show there will be an asymmetry A between the number of $++$ and $--$ muon pairs in example (i) above ($B\bar{B}$ pairs decaying independently) given by

$$A \equiv \frac{N(--)-N(++)}{N(--)+N(++)} = \frac{r-\bar{r}}{r+\bar{r}} = \frac{|\eta|^4-1}{|\eta|^4+1} \simeq -4\mathcal{R}e\epsilon.$$

Notice that this asymmetry could not arise without oscillations.

CP violating effects arise from m_{12} and Γ_{12} acquiring imaginary parts. The box diagrams of Fig. 10.5 give imaginary parts to m_{12} through complex phases in the quark mixing matrix. For example, if we take simply the dominant diagrams with intermediate t quarks on both internal quark lines, the $\bar{B}(b\bar{d}) \rightarrow B(\bar{b}d)$ transitions illustrated with t exchanges contain factors $V_{tb}^2 V_{td}^{*2}$ which have a complex phase in general. In cases of interest where $\delta m/\Gamma \sim 1$ and measurable oscillations occur, we expect that $\delta\Gamma/\Gamma$ is negligible and that any significant CP violation will come through $Im(m_{12})$. Estimates in the literature, based on the box diagram and limits on the mixing matrix, give rather small asymmetries however in the B_d and B_s cases;

$$|A_d| \lesssim 10^{-3}, \quad |A_s| \lesssim 5 \times 10^{-4}.$$

It would require very large numbers of same-sign dilepton events to establish asymmetries as small as these. However, there are other

possible origins of CP violating phases beside the quark mixing matrix (*e.g.* charged Higgs exchanges). We can also seek CP violation in exclusive B -decay channels (§10.3.5).

10.2 Leptoproduction

10.2.1 Introduction.

Heavy quarks can be produced by lepton-nucleon collisions in various ways. In early days this was an important area in which to search for new quarks and to study their decays. More recently, e^+e^- and $p\bar{p}$ colliders appear to offer cleaner signals and bigger cross sections for such studies while ep colliders may have advantages in searching for new gauge bosons and leptoquarks. In the future, the role of heavy quark production at ep colliders may be that of background rather than signal, but it cannot be ignored. We give the main features in this section.

The lowest-order contributing subprocesses are charged-current lepton-quark scattering, such as $\nu_\mu d \rightarrow \mu c$ or $e\bar{d} \rightarrow \nu_e \bar{c}$ (described in Chapter 5). In neutrino scattering, charm production with $c \rightarrow s\bar{\ell}\nu$ semileptonic decay gives opposite-sign dilepton events like $\nu d \rightarrow \mu^- c \rightarrow \mu^+ \mu^- \nu s$. Such events were among the earliest experimental indications of charm.

There are also lepton-quark scatterings via the electroweak neutral currents. Since flavor-changing neutral currents are absent, heavy flavors are produced only when the struck quark is a heavy component of the quark-antiquark sea. For example, muon scattering $\mu c \rightarrow \mu c$ gives $c\bar{c}$ production, since the presence of a charmed quark c implies a spectator \bar{c} in the incident hadron wavefunction. To calculate such $c\bar{c}$ production requires a realistic model of the $c\bar{c}$ sea dynamics; we return to this question below.

We must also consider higher-order $2 \rightarrow 3$ subprocesses. The most important class of these is current-gluon fusion, described below; see

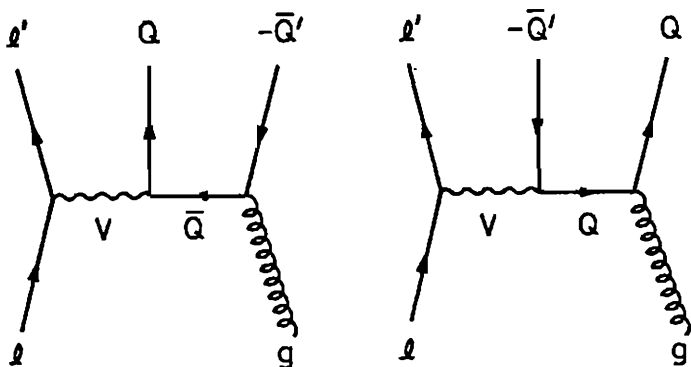


Fig. 10.9. Heavy quark production by current-gluon fusion.

Fig. 10.9. This gives a more complete picture when the struck quark is heavy; since it provides a dynamical model of the heavy quark sea, we regard this as essentially the leading process for scattering from heavy non-valence quarks.

Another class of $2 \rightarrow 3$ subprocesses is gluon bremsstrahlung (see Fig. 10.12). Although it gives much smaller cross sections to $O(\alpha_s)$, it contributes in a different way, producing low-mass $Q\bar{Q}$ pairs of the same flavor. In particular, since c and \bar{c} are produced symmetrically, it gives equal numbers of same-sign and opposite-sign dileptons in neutrino scattering. We describe this process in §10.2.5.

Finally, in §10.2.6 we describe some salient features to be expected for leptoquark production in ep collisions.

10.2.2 Current-Gluon fusion.

In this class of $2 \rightarrow 3$ subprocesses, the incident lepton emits a virtual boson $V = \gamma, Z$ or W^\pm , which fuses with an incident gluon to produce a $Q\bar{Q}'$ quark-antiquark pair; see Fig. 10.9. We are interested in cases where at least one of the produced quarks is heavy.

These subprocesses effectively describe lepton scatterings from sea quarks Q and \bar{Q}' in the incident hadron, but they also contain more information than the simple lowest-order $2 \rightarrow 2$ scattering calculation

would provide. Here are some examples.

- a) $eg \rightarrow \nu_e s \bar{c}$ via W^-g fusion. This can be viewed as the sum of charged current processes $e\bar{s} \rightarrow \nu\bar{c}$ plus $ec \rightarrow \nu s$. However, in the current-gluon fusion picture neither the initial \bar{s} nor c distribution needs to be input, both being determined by the gluon distribution through an intermediate $g \rightarrow s\bar{s}$ or $g \rightarrow c\bar{c}$ step. The interference effects are also included in this picture.
- b) $eg \rightarrow \nu_e b \bar{t}$ via W^-g fusion. This is the sum of $e\bar{b} \rightarrow \nu\bar{t}$ and $et \rightarrow \nu b$ processes.
- c) $eg \rightarrow e b \bar{b}$ via γg fusion. This can be seen as the sum of electromagnetic scatterings $eb \rightarrow eb$ and $e\bar{b} \rightarrow e\bar{b}$. (Zg fusion also contributes here and must be included at high Q^2 .)

As the quark mass increases, the virtual $Q\bar{Q}$ components in the incident nuclear wave function become progressively more off-shell and the standard treatment as on-shell incident partons becomes problematic. Current-gluon fusion explicitly solves this problem; it treats the heavy quark kinematics realistically throughout and includes interferences; as a bonus, it also tells us where *both* quarks have gone in the final state, so that all correlations can be calculated.

Current-gluon fusion thus replaces the calculation of heavy quark production from the quark-antiquark sea. But it does not include contributions from valence quarks such as $\nu_\mu d \rightarrow \mu c$ and $eu \rightarrow \nu_e b$, which depend on the quark mixing matrix elements V_{cd} and V_{ub} , respectively, and have to be calculated separately as described in Chapter 5 with the Q^2 -dependent distributions of Chapter 7.

Current-gluon fusion not only describes the continuum production of heavy quark pairs but also bound-state ($Q\bar{Q}$) or ($Q\bar{Q}'$) production—assuming the latter are approximated by constant, empirical fractions of the continuum near the bound state masses (as in §5.9). This approach has been used to extract the x -dependence of the gluon distribution from $\mu N \rightarrow \mu\psi X$ data (like the photoproduction case in §5.9).

In the following sections we give the complete current-gluon fusion cross section formulas. The expressions for structure functions F_1 , F_2 and F_3 are less interesting, because they average over all the details of the accessible $Q\bar{Q}'$ final states. The structure functions for heavy quark production cannot obey Bjorken scaling, since they contain nontrivial thresholds, but numerical studies show that current-gluon structure functions scale approximately with respect to a modified variable $x' = (Q^2 + (m_Q + m_{Q'})^2) / (2m_N\nu)$ instead.

10.2.3 Charged current cross section.

Consider the typical charged-current process $\ell g \rightarrow \nu Q\bar{Q}'$ with standard $V - A$ couplings. The differential cross section, summed (averaged) over final (initial) spins and colors, has the form

$$d\sigma = \frac{1}{4\ell \cdot g} |\mathcal{M}|^2 \prod_{i=\nu, Q, \bar{Q}} \left(\frac{d^3k_i}{2E_i} \right) \frac{\delta^4(\ell + g - \nu - Q - \bar{Q})}{(2\pi)^5},$$

where the corresponding squared matrix element is

$$|\mathcal{M}|^2 = 4\pi\alpha_s G_F^2 M_W^4 |V_{QQ'}|^2 L^{\alpha\beta} H_{\alpha\beta} / (q^2 - M_W^2)^2.$$

Here α_s is the gluon coupling evaluated at an appropriate scale such as $Q^2 = \hat{s} = (Q + \bar{Q}')^2$; $V_{QQ'}$ is the appropriate element of the quark mixing matrix describing the $WQ\bar{Q}'$ coupling; $q = \ell - \nu$ is the four-momentum transfer; ℓ, g, ν, Q, \bar{Q} denote the particle momenta (omitting the prime on \bar{Q}' for simplicity); $L_{\alpha\beta}$ and $H_{\alpha\beta}$ are tensors describing the lepton and hadron traces. These tensors differ from those defined in Chapter 5, in that here neither includes initial spin-averaging and the hadronic tensor is not integrated over final states.

It is convenient to use the square bracket symbol, (§3.1)

$$[A, B]_{\alpha\beta} = A_\alpha B_\beta + B_\alpha A_\beta - g_{\alpha\beta} A \cdot B - i\epsilon_{\alpha\beta\gamma\delta} A^\gamma B^\delta.$$

With this notation the lepton and hadron tensors can be written as

$$\frac{1}{2} L^{\alpha\beta} = [\ell, \nu]^{\alpha\beta},$$

$$\begin{aligned} \frac{1}{2}H_{\alpha\beta} &= (g \cdot Q)^{-1} \left\{ [\bar{Q}, g - Q]_{\alpha\beta} + [Q, Q]_{\alpha\beta} \right\} + Q^2 (g \cdot Q)^{-2} [\bar{Q}, g - Q]_{\alpha\beta} \\ &+ (g \cdot \bar{Q})^{-1} \left\{ [g - \bar{Q}, Q]_{\alpha\beta} + [\bar{Q}, \bar{Q}]_{\alpha\beta} \right\} + \bar{Q}^2 (g \cdot \bar{Q})^{-2} [g - \bar{Q}, Q]_{\alpha\beta} \\ &+ (g \cdot Q)^{-1} (g \cdot \bar{Q})^{-1} (Q \cdot \bar{Q}) \left\{ [\bar{Q}, Q - g]_{\alpha\beta} + [\bar{Q} - g, Q]_{\alpha\beta} \right\}. \end{aligned}$$

These tensors can be contracted using $[a, b]^{\alpha\beta} [c, d]_{\alpha\beta} = 4(a \cdot c)(b \cdot d)$ to give the final result:

$$\begin{aligned} \frac{L^{\alpha\beta} H_{\alpha\beta}}{8} &= 2(g \cdot Q)^{-2} Q^2 (\ell \cdot \bar{Q}) [\nu \cdot g - \nu \cdot Q] + 2(g \cdot \bar{Q})^{-2} \bar{Q}^2 (\nu \cdot Q) [\ell \cdot g - \ell \cdot \bar{Q}] \\ &+ (g \cdot Q)^{-1} (g \cdot \bar{Q})^{-1} \left\{ (Q^2 + \bar{Q}^2) [(\ell \cdot \bar{Q})(\nu \cdot \bar{Q}) + (\ell \cdot Q)(\nu \cdot Q)] \right. \\ &\left. - q^2 [(\ell \cdot \bar{Q})^2 + (\nu \cdot Q)^2 - \bar{Q}^2 (\ell \cdot \bar{Q}) + Q^2 (\nu \cdot Q)] \right\}, \end{aligned}$$

where $Q^2 = m_Q^2$, $\bar{Q}^2 = m_{\bar{Q}}^2$, $q^2 = (\ell - \nu)^2$ and the terms linear in lepton momenta come from using $\bar{Q} + Q - g = \ell - \nu$.

Figure 10.10 illustrates the energy-dependence of the charged-current cross section for top and bottom quark production in ep collisions, $ep \rightarrow \nu_e b \bar{t} X$, calculated with the Duke-Owens gluon distribution evolved up to $Q^2 = \hat{s}/4$.

For the crossed reaction $\bar{\nu} g \rightarrow \bar{\ell} Q \bar{Q}'$ the expression for $L^{\alpha\beta} H_{\alpha\beta}$ is unchanged, provided we make the identification of momenta $\nu = -\bar{\nu}$, $\ell = -\bar{\ell}$. But the expression for $|\mathcal{M}|^2$ is multiplied by 2, since we now have only one incident lepton helicity state to average over.

For the antilepton channel $\bar{\ell} g \rightarrow \bar{\nu} Q \bar{Q}'$ which is $W^+ g$ fusion, the lepton tensor becomes $L^{\alpha\beta} = 2[\bar{\nu}, \bar{\ell}]^{\alpha\beta}$ instead. The product of tensors is obtained by substituting $\ell \rightarrow -\bar{\nu}$, $\nu \rightarrow -\bar{\ell}$ in the expression for $L^{\alpha\beta} H_{\alpha\beta}$ above (the $-$ sign is needed to correct the linear terms). A certain symmetry between Q and \bar{Q}' is now apparent; our expression for $L^{\alpha\beta} H_{\alpha\beta}$ is invariant under substitutions $Q \leftrightarrow \bar{Q}'$, $\ell \leftrightarrow -\nu$. In other words, the dynamics of $Q(\bar{Q}')$ production by an ℓ beam is the same as that of $\bar{Q}'(Q)$ production by an $\bar{\ell}$ beam, as expected from the CP-invariance of $V - A$ couplings.

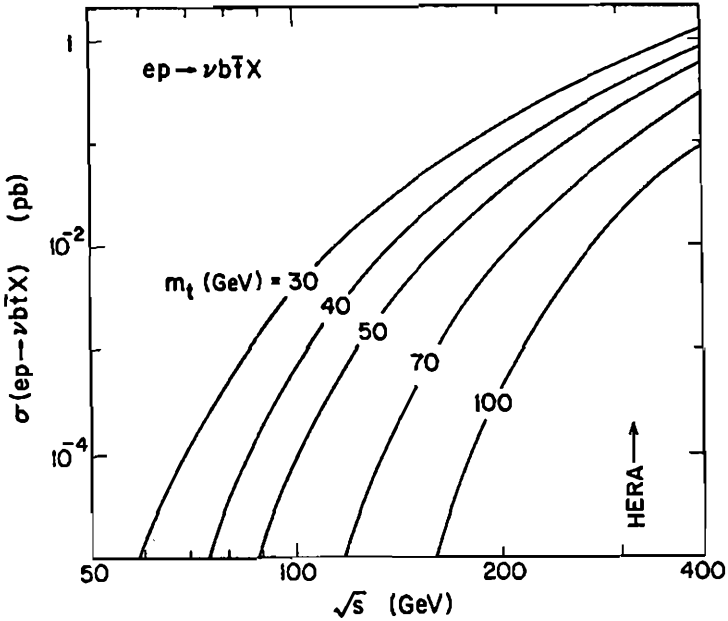


Fig. 10.10. Predicted cross section for $ep \rightarrow \nu_e b \bar{t} X$ production of bottom and top quarks, calculated from the $W + g$ fusion subprocess for $m_t = 30, 40, 50, 70, 100$ GeV.

Note incidentally that the same matrix element squared describes $\bar{Q}Q' \rightarrow Wg$ production with $W \rightarrow \bar{\ell}\nu$ decay, provided we take account of crossing by substituting $Q \rightarrow -\bar{Q}$, $Q' \rightarrow -Q'$, $\ell \rightarrow -\bar{\ell}$, $g \rightarrow -g$, also multiplying $|\mathcal{M}|^2$ by -1 for the reversed fermion lines and by $8/9$ for the changes in initial color averaging. In this case we are interested in light incident quarks, so $Q^2 = \bar{Q}^2 = 0$ and $L^{\alpha\beta} H_{\alpha\beta}$ becomes remarkably simple; the cross section formula has been given in §8.7.

10.2.4. Electromagnetic cross section.

The typical process here is $\ell g \rightarrow \ell' Q \bar{Q}$ by photon-gluon fusion. The differential cross section, summed over initial and averaged over final spins and colors has the same form as in the previous section, with squared matrix element

$$|M|^2 = 8\pi^3 \alpha_s \alpha^2 e_Q^2 L^{\alpha\beta} H_{\alpha\beta} / q^4,$$

where e_Q is the quark electric charge and $q = \ell - \ell'$ is the momentum transfer. The lepton and hadron tensors can be compactly written using the following curly bracket symbol,

$$\{A, B\}_{\alpha\beta} \equiv A_\alpha B_\beta + B_\alpha A_\beta - g_{\alpha\beta} A \cdot B$$

in terms of which

$$\frac{1}{4} L^{\alpha\beta} = \{\ell, \ell'\}^{\alpha\beta},$$

$$\begin{aligned} \frac{1}{4} H_{\alpha\beta} = & (g \cdot Q)^{-1} [\{\bar{Q}, g-Q\}_{\alpha\beta} + \{Q, Q\}_{\alpha\beta}] + Q^2 (g \cdot Q)^{-2} [\{\bar{Q}, g-Q\}_{\alpha\beta} + Q^2 g_{\alpha\beta}] \\ & + (g \cdot \bar{Q})^{-1} [\{g-\bar{Q}, Q\}_{\alpha\beta} + \{\bar{Q}, \bar{Q}\}_{\alpha\beta}] + Q^2 (g \cdot \bar{Q})^{-2} [\{g-\bar{Q}, Q\}_{\alpha\beta} + Q^2 g_{\alpha\beta}] \\ & + (g \cdot Q)^{-1} (g \cdot \bar{Q})^{-1} (Q \cdot \bar{Q}) + [\{\bar{Q}, Q-g\}_{\alpha\beta} + \{\bar{Q}-g, Q\}_{\alpha\beta} - 2Q^2 g_{\alpha\beta}]. \end{aligned}$$

We note that in the limit of zero quark mass, where $Q^2 = \bar{Q}^2 = m_Q^2 = 0$, the tensors $L^{\alpha\beta}$ and $H_{\alpha\beta}$ are simply related to their charged-current counterparts by changing square brackets to curly bracket symbols and multiplying by 2.

To contract these tensors we use the identities

$$\begin{aligned} \{A, B\}^{\alpha\beta} \{C, D\}_{\alpha\beta} &= 2(A \cdot C)(B \cdot D) + 2(A \cdot D)(B \cdot C), \\ \{A, B\}^{\alpha\beta} g_{\alpha\beta} &= -2A \cdot B, \end{aligned}$$

and obtain

$$\begin{aligned} \frac{L^{\alpha\beta} H_{\alpha\beta}}{16} = & Q^2 (g \cdot Q)^{-2} \{4(\ell \cdot \bar{Q})(\ell' \cdot \bar{Q}) + q^2 (q \cdot \bar{Q}) + q^2 Q^2\} \\ & + Q^2 (g \cdot \bar{Q})^{-2} \{4(\ell \cdot Q)(\ell' \cdot Q) + q^2 (q \cdot Q) + q^2 Q^2\} \\ & + (g \cdot Q)^{-1} (g \cdot \bar{Q})^{-1} \{4Q^2 [(\ell \cdot Q)(\ell' \cdot Q) + (\ell \cdot \bar{Q})(\ell' \cdot \bar{Q}) - (\ell \cdot g)(\ell' \cdot g)] \\ & - q^2 [(\ell \cdot Q)^2 + (\ell \cdot \bar{Q})^2 + (\ell' \cdot Q)^2 + (\ell' \cdot \bar{Q})^2] \\ & + q^2 Q^2 [q \cdot Q + q \cdot \bar{Q} - 2Q \cdot \bar{Q}]\}. \end{aligned}$$

This expression is symmetrical between Q and \bar{Q} , as expected. It equally describes the crossed lepton process $\bar{\ell}g \rightarrow \bar{\ell}'Q\bar{Q}$.

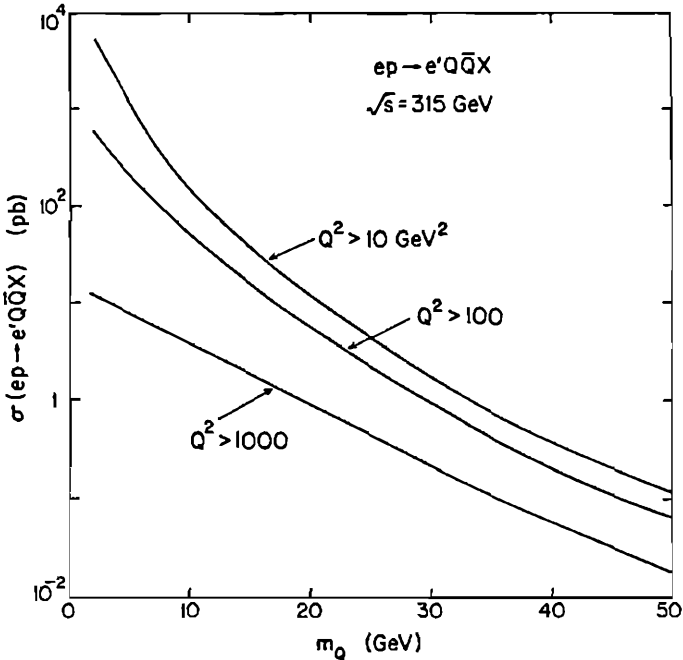


Fig. 10.11. Predicted cross sections for electromagnetic heavy quark production in $ep \rightarrow e'Q\bar{Q}X$ collisions at $\sqrt{s} = 315$ GeV, the HERA energy, via photon-gluon fusion. Various cuts on the momentum transfer squared are illustrated: $Q^2 > 10, 100, 1000$ (GeV^2).

Figure 10.11 illustrates the electromagnetic cross section for producing $Q\bar{Q}$ heavy quark pairs at HERA ($\sqrt{s} = 315$ GeV) through photon-gluon fusion, plotted versus mass m_Q , with various cuts on the momentum transfer to the electron. The Duke-Owens gluon distribution was used, evolved to $Q^2 = \hat{s}/4$.

The electromagnetic matrix element above also describes the process $\bar{Q}Q \rightarrow \bar{\ell}\ell g$ where quark-antiquark fusion gives a Drell-Yan lepton pair plus a radiated gluon. We have to make the substitutions $Q \rightarrow -\bar{Q}$, $\bar{Q} \rightarrow -Q$, $g \rightarrow -g$, $\ell \rightarrow -\bar{\ell}$ and multiply $|M|^2$ by $-8/9$ for fermion line reversal and the change in initial color averaging. In this case we are interested in light quarks, so $Q^2 = 0$ and the expression for $L^{\alpha\beta}H_{\alpha\beta}$ becomes very simple; (the cross section formula is given in §7.11).

The same matrix element also gives $e^+e^- \rightarrow Q\bar{Q}g$, the one-photon contribution to the 3-jet production of heavy quarks in e^+e^- annihilation. We have to substitute $\ell \rightarrow e^-$, $\ell' \rightarrow -e^+$, $g \rightarrow -g$ and multiply $|\mathcal{M}|^2$ by -8 .

At large momentum transfers $|q|^2$ of order M_Z^2 the weak neutral current process (Z^0 -gluon fusion) also contributes significantly. The matrix elements for this case are more complicated. Formulas for general V, A couplings are given in the literature.

10.2.5 Gluon bremsstrahlung.

Figure 10.12 shows the Feynman diagrams for the subprocess

$$\ell q \rightarrow \ell' q' Q \bar{Q},$$

where gluon radiation from the struck quark materializes a $Q\bar{Q}$ heavy quark pair. The exchanged boson can be $V = W, Z$ or γ .

This is a higher order $2 \rightarrow 4$ particle process. It is generally less important than current-gluon fusion as a source of heavy quarks. However, for charged current scattering it has some interest because it produces $Q\bar{Q}$ pairs of the same flavor. For example, it can give $ep \rightarrow \nu c \bar{c} X$ and hence charm particles decaying into either μ^- or μ^+ , whereas Wg fusion can only give $ep \rightarrow \nu s \bar{c} X$ with charm particles decaying to μ^+ . For neutrino beams, gluon bremsstrahlung can give $\nu N \rightarrow \mu c \bar{c} X$ and hence both same-sign and opposite sign dileptons (one lepton from c or \bar{c} decay), or even tripletons; lower order

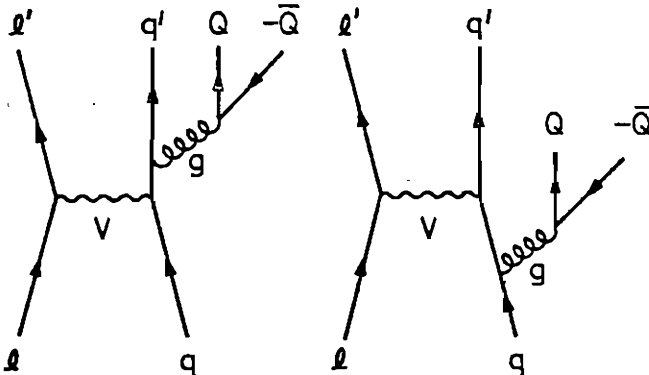


Fig. 10.12. Heavy quark leptoproduction by gluon bremsstrahlung.

subprocesses only give $\nu N \rightarrow \mu c X$ with only opposite sign dileptons.

The cross section for the charged-current case $\nu d \rightarrow \ell u c \bar{c}$ is

$$d\sigma = \frac{2}{3} \frac{16G_F^2 \alpha_s^2 C T(\nu, \ell, d, u) \delta^4(\nu + d - \ell - u - c - \bar{c})}{\pi^6 \hat{s} (g \cdot g)^2 (1 - q^2/M_W^2)^2} \prod_{k=\ell, u, c, \bar{c}} \frac{d^3 k}{2E_k},$$

where

$$\begin{aligned} T(\nu, \ell, d, u) = & \nu \cdot d (g \cdot g + 2g \cdot u)^{-2} [-(g \cdot g + 2g \cdot u)(c \cdot \ell \bar{c} \cdot u + \bar{c} \cdot \ell c \cdot u + c^2 \ell \cdot u) \\ & + (\ell \cdot g + \ell \cdot u)(4c \cdot u \bar{c} \cdot u + g \cdot g g \cdot u + 2c^2 g \cdot u - g \cdot g u^2)] \\ & + (g \cdot g + 2g \cdot u)^{-1} (g \cdot g - 2g \cdot d)^{-1} \left\{ g \cdot g [c^2 (\ell \cdot \nu u \cdot d - u \cdot \nu \ell \cdot d) \right. \\ & + \ell \cdot u (d \cdot u g \cdot \nu - \nu \cdot u g \cdot d - \nu \cdot d u \cdot d)] + 4\nu \cdot d \ell \cdot u \bar{c} \cdot d c \cdot u \\ & + 2\bar{c} \cdot c [c \cdot u (\nu \cdot \ell \bar{c} \cdot d - \ell \cdot d \bar{c} \cdot \nu) + c \cdot \nu (u \cdot d \bar{c} \cdot \ell - \ell \cdot d \bar{c} \cdot u)] \\ & + 2[c \cdot u (\bar{c} \cdot \ell + u \cdot \ell) - \bar{c} \cdot u (c \cdot \ell + u \cdot \ell)] (\bar{c} \cdot \nu c \cdot d - c \cdot \nu \bar{c} \cdot d) \\ & \left. - c^2 [\nu \cdot \ell (c \cdot u c \cdot d + \bar{c} \cdot u \bar{c} \cdot d) - 2\ell \cdot d (c \cdot \nu c \cdot u + \bar{c} \cdot \nu \bar{c} \cdot u) \right. \\ & \left. + u \cdot d (c \cdot \nu c \cdot \ell + \bar{c} \cdot \nu \bar{c} \cdot \ell)] \right\} + [u \leftrightarrow -d \text{ and } \ell \leftrightarrow \nu \text{ simultaneously}]. \end{aligned}$$

Here \hat{s} is the subprocess invariant energy-squared, α_s is the QCD coupling constant and $C = |V_{ud}|^2$. The symbols denote the particle four-momenta with $g = c + \bar{c}$ and $q = \nu - \ell$; the factor $\frac{2}{3}$ is for color.

The same formula describes the CP-conjugate process $\bar{\nu} \bar{d} \rightarrow \bar{\ell} \bar{u} \bar{c} \bar{c}$, substituting momenta $k \leftrightarrow \bar{k}$. It also describes the incident electron process $eu \rightarrow \nu d c \bar{c}$ if we substitute $\ell \rightarrow -e$, $u \rightarrow -u$, $d \rightarrow -d$, and divide by 2 for the change in initial spin averaging.

Gluon bremsstrahlung is essentially a perturbative contribution to the fragmentation of the struck quark into heavy flavors. In the case of $c\bar{c}$ production, some neutrino experiments reported prompt same-sign dileptons in approximately 10^{-3} of charged-current events with $E_\nu > 100$ GeV. This same-sign rate was more than an order of magnitude above that expected from gluon bremsstrahlung and suggested some additional soft $c\bar{c}$ contributions in quark fragmentation. However, the most recent Fermilab results (CCFR collaboration) indicate an upper limit 1.1×10^{-4} on same-sign dileptons for events with visible energy from 30-600 GeV, consistent with gluon bremsstrahlung alone.

10.2.6. Leptoquarks.

The symmetry between leptons and quarks in the standard model—their appearance in generations and their conspiracy to cancel anomalies—suggest they are related. It is then conceivable that there exist particles that carry both quark and lepton quantum numbers, *leptoquarks*. In superstring models with E_6 symmetry, the [27] multiplet of basic fermions contains a color-triplet fermion h , a singlet of $SU(2)_L$ with electric charge $-1/3$, that can also carry lepton number (§14.8). The spin-0 superpartner of h would be a scalar leptoquark, coupling directly to lepton-quark pairs; h itself would be a sleptoquark, coupling to slepton-quark and lepton-squark pairs. In certain Technicolor models too there appear composite bosons (composed of technileptons and techniquarks) that decay into lepton-quark pairs; the lightest of these are expected to have spin-0. Rather than specializing to a particular model, we briefly discuss some general properties that may be expected if color-triplet leptoquarks exist.

We assume first that they couple only to lepton-quark pairs. Because they have non-zero color and electric charge, they necessarily have gluon and photon gauge couplings and can be produced in e^+e^- , ep and hadron-hadron collisions at high enough energies. The strength of their couplings to leptons and quarks is not known a priori, but is also important. In the standard $SU(2) \times U(1)$ symmetry context, leptoquarks could have weak isospin 0, $1/2$, or 1. Initially we take the example of a scalar ($J = 0$) isoscalar ($T = 0$) color antitriplet (3^*) leptoquark S with charge $-1/3$. Its gauge-symmetric couplings to the quarks and leptons have the general form

$$\mathcal{L} = \sum_{i,j} \left\{ \lambda_L^{ij} \left[\overline{u_{Li}^c} e_{Lj} - \overline{d_{Li}^c} \nu_{Lj} \right] S + \lambda_R^{ij} \overline{u_{Ri}^c} e_{Rj} S \right\} + \text{h.c.},$$

where u, d, e, ν denote generic quarks and leptons, u_L^c denotes $(u_L)^c$ and $i, j = 1, 2, 3$ are generation labels (so that $u_1 = u, u_2 = c, u_3 = t$, etc.). λ_L^{ij} and λ_R^{ij} are dimensionless coupling strengths. The minus sign arises because the charge-conjugate doublet corresponding to (u, d) is $(d^c, -u^c)$.

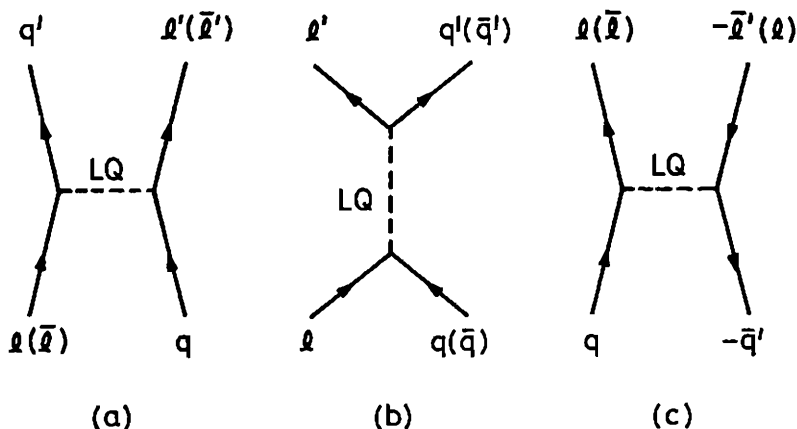


Fig. 10.13. Typical leptoquark exchange processes between leptons and quarks. The leptoquark LQ may have fermion number 0 or ± 2 .

Leptoquark exchanges, like those in Fig. 10.13, will generally contribute to lepton-nucleon scattering and to hadron decays. They have different systematics from gauge boson exchanges (no GIM mechanism, no helicity conservation). The experimental upper limits on various small cross sections and rare decay modes then force us to make many of the couplings $\lambda_{L,R}^{ij}$ very small; if the leptoquarks have observable masses of order 100 GeV, the mass suppression alone is inadequate in many cases.

Exercise. Show that leptoquark contributions to $\mu N \rightarrow eN$ coherent conversion, and to $\pi^0 \rightarrow \mu^\pm e^\mp$ and $D^0 \rightarrow \mu^+ \mu^-$ decays are suppressed if we forbid generation mixing λ^{ij} with $i \neq j$.

Exercise. Show that leptoquark contributions to $\pi^0 \rightarrow e^+ e^-$, $\pi^\pm \rightarrow e\nu$, $K^\pm \rightarrow e\nu$ and $D^0 \rightarrow \mu^\pm e^\mp$ are suppressed if a given leptoquark has only λ_L or only λ_R type couplings.

Exercise. Show that leptoquark contributions to $K^+ \rightarrow \pi^+ \nu \bar{\nu}$ are suppressed if a given leptoquark has couplings to only one generation.

All experimental constraints are satisfied if we restrict the couplings as suggested in the exercises, *i.e.* (i) no generation mixing ($i \neq j$ forbidden), (ii) a given leptoquark couples only via λ_L or only via λ_R ,

(iii) a given leptoquark couples only to one generation of fermions. Such restrictions apparently arise naturally in some E_6 -based superstring models. The leptoquark masses can then be relatively light, of order 100 GeV say, with coupling strengths λ of order 0.1.

One experimental signature of a leptoquark would be its decay, e.g. into charged lepton plus quark jet plus no missing energy, or into neutrino plus quark jet plus no charged lepton. Leptoquark pairs would be produced in e^+e^- collisions, with electromagnetic cross section (§4.4) and a factor 3 for color,

$$\sigma(e^+e^- \rightarrow \gamma^* \rightarrow S\bar{S}) = \frac{3}{4} \beta^3 e_S^2 \left(\frac{4\pi\alpha^2}{3s} \right),$$

to which we must in general add contributions from virtual Z^0 exchange (and also from quark q exchange if S couples to eq). The non-appearance of anomalous lepton events at PEP and PETRA excludes leptoquark masses below 20 GeV. Leptoquark pairs could also be produced at hadron colliders through QCD couplings, via $q\bar{q} \rightarrow S\bar{S}$ or $gg \rightarrow S\bar{S}$ subprocesses, just like heavy quark pairs (see §10.3). Limits on anomalous high- p_T lepton plus jet events at the CERN $p\bar{p}$ collider are said to exclude leptoquark masses below about 50 GeV (the two-body decay $S \rightarrow \ell q$ gives a harder lepton spectrum than the three-body decay of heavy quarks $t \rightarrow b\ell\nu$).

The most spectacular leptoquark signature however is to be found in lepton-nucleon scattering. The s -channel pole diagram Figure 10.13(b) gives a resonance in the subprocess $e^-u \rightarrow S \rightarrow e^-u$ and hence a peak in the inclusive x -distribution.

Exercise. Derive the subprocess cross section

$$\frac{d\hat{\sigma}}{d\hat{t}}(e^-u \rightarrow e^-u) = \frac{\lambda^4}{64\pi} \frac{1}{(\hat{s} - m_S^2)^2 + (m_S\Gamma_S)^2},$$

where λ denotes the assumed λ_L^{11} or λ_R^{11} coupling of the scalar leptoquark S to ue^- . Hence (following §5.2) show the corresponding

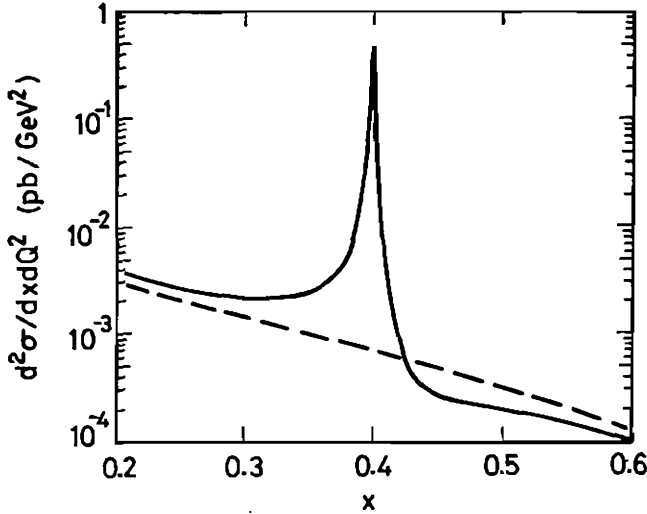


Fig. 10.14. Inclusive e^-p cross section $d\sigma/dx dQ^2$ plotted versus x at $Q^2 = 10^4 \text{ GeV}^2$, $\sqrt{s} = 315 \text{ GeV}$, showing the resonance effect from a leptoquark S with mass 200 GeV and coupling $\lambda_L = 0.3$. The dotted line is the standard model prediction. (From DESY-86-150.)

contributions to inclusive e^-p and e^+p deep inelastic scattering are

$$\frac{d\sigma}{dx dy}(e^-p \rightarrow e^-X) = \frac{\lambda^4 s}{64\pi} \frac{xu(x)}{(sx - m_S^2)^2 + (m_S \Gamma_S)^2},$$

$$\frac{d\sigma}{dx dy}(e^+p \rightarrow e^+X) = \frac{\lambda^4 s}{64\pi} \frac{x(1-y)^2 u(x)}{(sx(1-y) + m_S^2)^2},$$

based on u -quarks in the proton. For \bar{u} , change $u \rightarrow \bar{u}$, $e^+ \leftrightarrow e^-$.

Figure 10.14 shows the predicted resonance in $d\sigma/dx dQ^2(e^-p \rightarrow e^-X)$ at HERA energy at $Q^2 = 10^4 \text{ GeV}^2$, compared to the standard model prediction, assuming $\lambda_L = 0.3$ and $m_S = 200 \text{ GeV}$.

Thus far we have discussed only a scalar isoscalar leptoquark S with net fermion number -2 , coupling to $\bar{u}e^+$ and $d\bar{\nu}_e$ (and its charge conjugate to ue and $d\nu_e$). But there are other possibilities such as a vector isoscalar U with fermion number 0 , coupling to $d\bar{e}$ and $u\bar{\nu}$ via

$$\mathcal{L} = \lambda'_L (\bar{u}_L \gamma_\mu \nu_L + \bar{d}_L \gamma_\mu e_L) U^\mu \quad \text{or} \quad \lambda'_R \bar{d}_R \gamma_\mu e_R U^\mu.$$

Many other leptoquark assignments can be made, including isodoublets and isotriplets. Spin- $\frac{1}{2}$ sleptoquark superpartners couple to the corresponding lepton-squark and slepton-quark systems.

We have also assumed stringent constraints on the types of allowed leptoquark couplings. An alternative way to meet the experimental constraints is to assume that leptoquark couplings are related to the fermion masses, *e.g.* that the coupling to quark q and lepton ℓ contains a factor like $\sqrt{m_q m_\ell}$ or $(m_q + m_\ell)$. This happens in Extended Technicolor models, where leptoquarks and particle mass terms have a common origin. This would automatically suppress all couplings to light fermions but could leave couplings to heavy fermions unsuppressed. Leptoquark production would then proceed via heavy quarks in the nucleon sea, generated by a gluon as in Fig. 10.15. The diagrams where the leptoquark decays back to $e + t$ give a resonant contribution to the inclusive distribution $d\sigma/dx dQ^2$, but if the signal is small it will be easier to detect by looking for exclusive final states. Heavy flavor production via current-gluon fusion gives a background to such leptoquark signals.

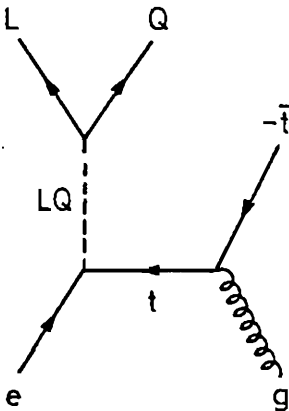


Fig. 10.15. Leptoquark production from electron-gluon fusion via couplings to heavy quarks such as t . L and Q denote the decay leptons and quarks, including e and t .

10.3 Hadroproduction

10.3.1 Quarkonia.

Both charm and bottom quarks were discovered by hadroproduction of the quarkonium states $\psi(c\bar{c})$ and $\Upsilon(b\bar{b})$ (simultaneously with $e^+e^- \rightarrow \psi$ in the case of charm), identified by their decays to $\mu^+\mu^-$ pairs.

Unlike e^+e^- collisions that only produce $J^P = 1^-$ states directly, hadron-hadron collisions can produce many quarkonium states directly through subprocesses such as

$$gg \rightarrow \eta, \chi_0, \chi_2, \quad gg \rightarrow \psi g, \quad q\bar{q} \rightarrow \psi.$$

These production subprocesses, shown in Fig. 10.16(a), are directly related by crossing to the corresponding decay processes

$$\eta, \chi \rightarrow gg, \quad \psi \rightarrow ggg, \quad \psi \rightarrow q\bar{q},$$

shown in Fig. 10.16(b). The production cross sections are fully determined by the decay widths,

$$\begin{aligned} \Gamma(\eta \rightarrow gg) &= (8/3)\alpha_s^2 |R_S(0)|^2 / (m_\eta)^2, \\ \Gamma(\chi_0 \rightarrow gg) &= 96\alpha_s^2 |R'_P(0)|^2 / (m_{\chi_0})^4, \\ \Gamma(\chi_2 \rightarrow gg) &= (128/5)\alpha_s^2 |R'_P(0)|^2 / (m_{\chi_2})^4, \\ \Gamma(\psi \rightarrow ggg) &= 40(\pi^2 - 9)\alpha_s^3 |R_S(0)|^2 / (81\pi m_\psi^2), \\ \Gamma(\psi \rightarrow q\bar{q}) &= 12\alpha^2 e_Q^2 e_q^2 |R_S(0)|^2 / (m_\psi)^2. \end{aligned}$$

Here $R_S(0)$ is the S -wave quarkonium radial wavefunction and $R'_P(0)$ is the radial derivative of the P -wave function at the origin, α_S is evaluated at the quarkonium mass scale, e_Q and e_q are the electric charges of the heavy initial quark and light decay quark. We have given only the virtual photon contribution to $\psi \rightarrow q\bar{q}$ (neglecting $\psi \rightarrow ggg \rightarrow q\bar{q}$ contributions); see §10.1.1 for the $\gamma + Z$ formula. $R(0)$ is related to the total wave function at the origin $\psi(0)$ by $|R(0)|^2 = 4\pi|\psi(0)|^2$.

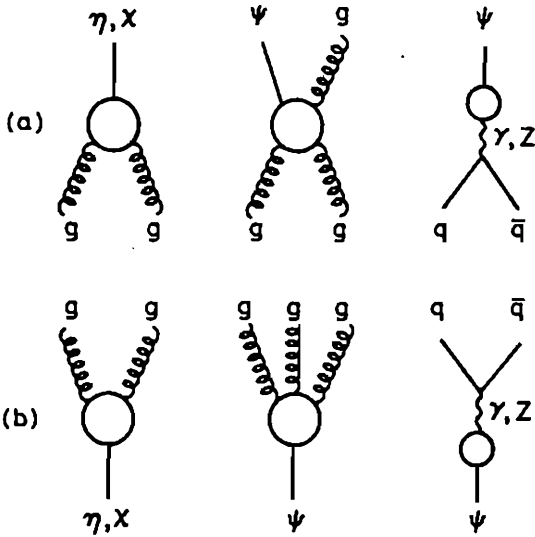


Fig. 10.16. (a) Parton subprocesses for producing quarkonia; (b) related quarkonium decays to gluons and quarks.

Exercise. Using crossing arguments, derive the formula for the $gg \rightarrow O$ spin- and color-averaged subprocess cross section, where O denotes a generic quarkonium state of spin J and mass m :

$$\hat{\sigma}(gg \rightarrow O) = (2J + 1)\pi^2(8m^3)^{-1}\Gamma(O \rightarrow gg)\delta(1 - \hat{s}/m^2).$$

(Remember that gluons are indistinguishable particles here).

Yang's theorem (that two massless spin-1 particles cannot have angular momentum $J = 1$ for a state symmetric in their space and spin variables) plus Bose statistics and color symmetry (a color-singlet state of two gluons is symmetric in their color variables) together forbid $gg \rightarrow \psi$ transitions. Thus the lowest order gg subprocess is $gg \rightarrow \psi g$ where a "bleaching gluon" carries off color in the final state. The cross section is given by

$$\hat{\sigma}(gg \rightarrow \psi g) = \frac{9\pi^2}{8m^3(\pi^2 - 9)} \Gamma(\psi \rightarrow ggg) I\left(\frac{\hat{s}}{m^2}\right),$$

where \hat{s} is the c.m. energy squared, m is the ψ mass and

$$I(x) = \frac{2}{x^2} \left[\frac{x+1}{x-1} - \frac{2x \ln x}{(x-1)^2} \right] + \frac{2(x-1)}{x(x+1)^2} + \frac{4 \ln x}{(x+1)^3}.$$

$I(x)$ is not singular at $x = 1$. 3S_1 states can similarly be produced by $q\bar{q}$ fusion, the inverse of $\psi \rightarrow q\bar{q}$ decay.

Exercise. Derive the spin- and color-averaged cross section

$$\hat{\sigma}(q\bar{q} \rightarrow O) = 4\pi^2(2J+1)(9m^3)^{-1}\Gamma(O \rightarrow q\bar{q})\delta(1 - \hat{s}/m^2).$$

For very heavy 3S_1 quarkonia, the widths $\Gamma(O \rightarrow gg)$ and $\Gamma(O \rightarrow q\bar{q})$ are comparable; in this case the superior flux of gluons at small x favors the $gg \rightarrow O$ mechanism at high energies. But for energies near threshold or for quarkonium masses near M_Z (see Fig. 10.3) the $q\bar{q} \rightarrow O$ mode may not be negligible. There are also contributions to 3S_1 and other states from the radiative decays of higher levels such as $\psi' \rightarrow \chi\gamma$, $\chi \rightarrow \psi\gamma$.

Hadronic cross sections are found by folding the subprocess cross sections with parton distributions as usual.

Exercise. Derive the formula

$$\sigma(AB \rightarrow OX) = K \int_{\tau}^1 dx \tau x^{-1} f_{g/A}(x, Q^2) f_{g/B}(\tau/x, Q^2) \hat{\sigma}_0(gg \rightarrow O)$$

for quarkonium O production via the dominant $gg \rightarrow O$ subprocess, where $\tau = m^2/s$, m being the O mass, K is an enhancement factor for non-leading QCD effects, $\hat{\sigma} = \hat{\sigma}_0\delta(1 - \hat{s}/m^2)$ and $Q^2 \simeq m^2$ is the scale at which the parton distributions are evaluated.

Figure 10.17 illustrates the predicted cross sections for various quarkonia up to $\sqrt{s} = 2$ TeV. Figure 10.18 shows predictions at $\sqrt{s} = 40$ TeV, the SSC energy, for heavy quarkonium production versus mass. In both figures the dominant gluon-gluon processes are used; shaded regions represent the range of uncertainty resulting from different choices of potential model to evaluate $R_S(0)$ and $R'_P(0)$; the most recent and realistic models give predictions near the lower limits shown. Clearly $\eta(^1S_0)$ states are the most strongly produced, one or two orders of magnitude above $\psi(^3S_1)$ states. The latter can be identified most easily as peaks in $\ell^+\ell^-$ mass distributions; however, there is no simple signature for η states, unless they are superheavy (§13.8).

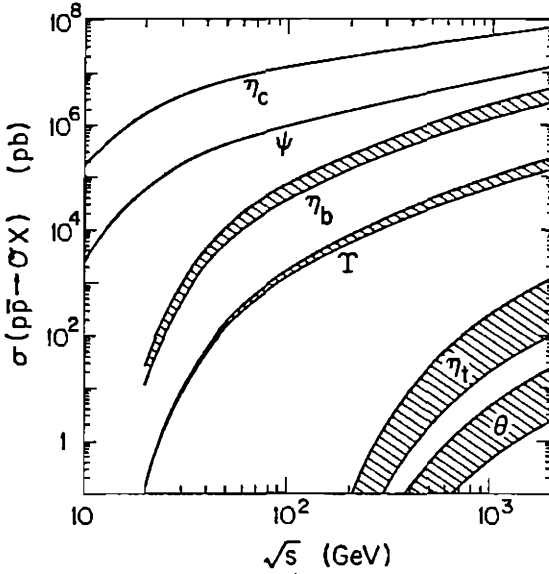


Fig. 10.17. Predicted quarkonium production cross sections in $p\bar{p}$ (or pp) collisions, resulting from $gg \rightarrow O$ subprocesses with enhancement $K = 2$, using Duke-Owens distributions. $\chi_J \rightarrow \psi\gamma$ decays are included. Shaded areas represent ranges of uncertainty from potential models. $m_t = 40$ GeV is assumed here.

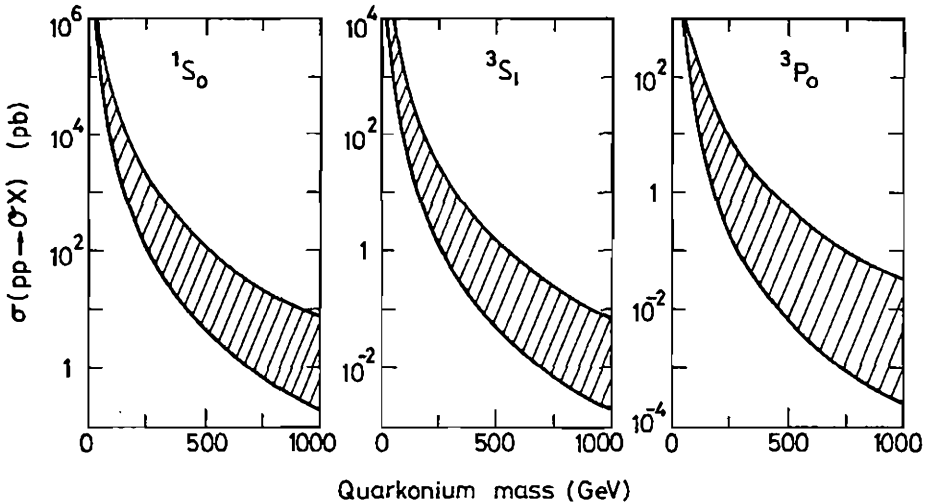


Fig. 10.18. Predicted cross sections for the production of 1S_0 , 3S_1 and 3P_0 heavy quarkonia in pp collisions at $\sqrt{s} = 40$ TeV, versus quarkonium mass (with $K = 1$).

10.3.2 Open flavor production.

The lowest order parton subprocesses producing heavy quark $Q\bar{Q}$ pairs are quark-antiquark and gluon-gluon fusion,

$$q\bar{q} \rightarrow Q\bar{Q}, \quad gg \rightarrow Q\bar{Q},$$

illustrated in Fig. 10.19.

Exercise. Derive the $q\bar{q} \rightarrow Q\bar{Q}$ cross section formula

$$\frac{d\hat{\sigma}}{d\hat{t}}(q\bar{q} \rightarrow Q\bar{Q}) = \frac{4\pi\alpha_s^2}{9\hat{s}^4} [(m^2 - \hat{t})^2 + (m^2 - \hat{u})^2 + 2m^2\hat{s}],$$

where $\hat{s} = (q + \bar{q})^2$, $\hat{t} = (q - Q)^2$, $\hat{u} = (q - \bar{Q})^2$.

For the other subprocess we have

$$\begin{aligned} \frac{d\hat{\sigma}}{d\hat{t}}(g_1g_2 \rightarrow Q\bar{Q}) &= \frac{\pi\alpha_s^2}{8\hat{s}^2} \left[\frac{6(m^2 - \hat{t})(m^2 - \hat{u})}{\hat{s}^2} - \frac{m^2(\hat{s} - 4m^2)}{3(m^2 - \hat{t})(m^2 - \hat{u})} \right. \\ &+ \frac{4}{3} \frac{(m^2 - \hat{t})(m^2 - \hat{u}) - 2m^2(m^2 + \hat{t})}{(m^2 - \hat{t})^2} + \frac{4}{3} \frac{(m^2 - \hat{t})(m^2 - \hat{u}) - 2m^2(m^2 + \hat{u})}{(m^2 - \hat{u})^2} \\ &\left. - 3 \frac{(m^2 - \hat{t})(m^2 - \hat{u}) + m^2(\hat{u} - \hat{t})}{\hat{s}(m^2 - \hat{t})} - 3 \frac{(m^2 - \hat{t})(m^2 - \hat{u}) + m^2(\hat{t} - \hat{u})}{\hat{s}(m^2 - \hat{u})} \right], \end{aligned}$$

where $\hat{s} = (g_1 + g_2)^2$, $\hat{t} = (g_1 - Q)^2$, $\hat{u} = (g_1 - \bar{Q})^2$. Notice that the \hat{t}^{-2} and \hat{u}^{-2} singularities of $gg \rightarrow q\bar{q}$ massless quark production (Table 9.1) have been removed by the presence of $m_Q = m$, since $\hat{t} < 0$ and $\hat{u} < 0$ by kinematics here. The running coupling $\alpha_s(Q^2)$ is evaluated at an appropriate scale, usually chosen to be $Q^2 = p_T^2$ or $\hat{s}/4$ or \hat{s} ; with the latter choices $\alpha_s(Q^2)$ remains finite at small p_T .

In lowest order QCD there are also *flavor-excitation* subprocesses in which a heavy quark Q is scattered out of the sea in one of the

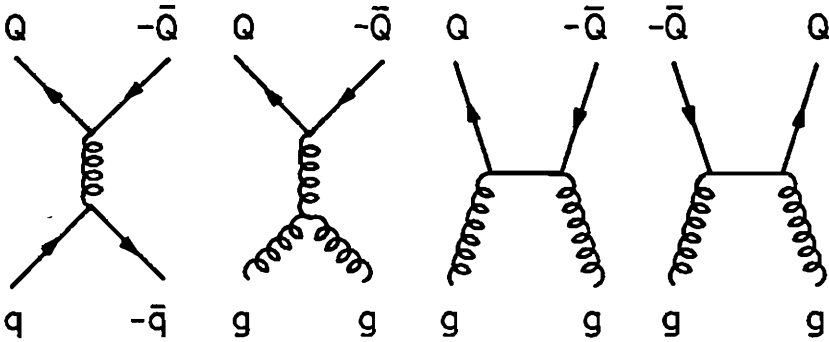


Fig. 10.19. Lowest-order QCD subprocesses producing heavy quark pairs $Q\bar{Q}$.

incident hadrons:

$$qQ \rightarrow qQ, \quad gQ \rightarrow gQ,$$

(similarly with initial \bar{q} and/or \bar{Q}) illustrated in Fig. 10.20. The corresponding cross section formulas are

$$\frac{d\hat{\sigma}}{d\hat{t}}(qQ \rightarrow q'Q') = \frac{4\pi\alpha_s^2}{9\hat{s}^2} \left[\frac{(m^2 - \hat{u})^2 + (\hat{s} - m^2)^2 + 2m^2\hat{t}}{\hat{t}^2} \right],$$

where $\hat{s} = (q + Q)^2$, $\hat{t} = (q - q')^2$, $\hat{u} = (q - Q')^2$ and

$$\begin{aligned} \frac{d\hat{\sigma}}{d\hat{t}}(gQ \rightarrow g'Q') &= \frac{\pi\alpha_s^2}{\hat{s}^2} \left[\frac{2(\hat{s}^2 - m^2)(m^2 - \hat{u})}{\hat{t}^2} + \frac{m^2(4m^2 - \hat{t})}{9(\hat{s} - m^2)(m^2 - \hat{u})} \right. \\ &+ \frac{4}{9} \cdot \frac{(\hat{s} - m^2)(m^2 - \hat{u}) + 2m^2(m^2 + \hat{u})}{(m^2 - \hat{u})^2} + \frac{4}{9} \cdot \frac{(\hat{s} - m^2)(m^2 - \hat{u}) + 2m^2(\hat{s} + m^2)}{(\hat{s} - m^2)^2} \\ &\left. + \frac{(\hat{s} - m^2)(m^2 - \hat{u}) + m^2(\hat{s} - \hat{u})}{\hat{t}(\hat{s} - m^2)} + \frac{(\hat{s} - m^2)(m^2 - \hat{u}) + m^2(\hat{u} - \hat{s})}{\hat{t}(\hat{u} - m^2)} \right] \end{aligned}$$

where $\hat{s} = (g + Q)^2$, $\hat{t} = (g - g')^2$, $\hat{u} = (g - Q')^2$, with $m = m_Q$ as before.

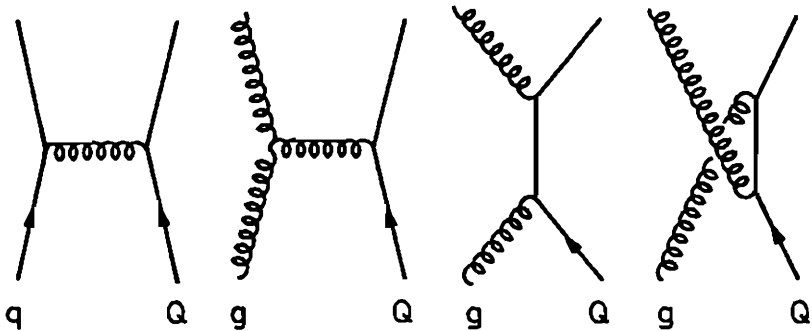


Fig. 10.20. Flavor-excitation subprocesses producing heavy quarks Q (and \bar{Q}).

These flavor-excitation subprocesses present some difficulties, however, when we try to calculate realistic final states from them.

- (i) It is not possible to arrange realistic kinematics to allow both the struck quark Q and its partner \bar{Q} to come on-shell in a single collision, when \bar{Q} is unseen and unspecified.
- (ii) It is unsatisfactory not to know what happened to \bar{Q} . We may want to include its decay products in the final state.
- (iii) The subprocess cross sections have soft and collinear divergences at $\hat{t} = 0$, where the exchanged gluon comes onto its mass shell, seeming to require an arbitrary cut-off.

Difficulties (i) and (ii) resemble the problems of exciting heavy sea quarks in electroweak lepton scattering, discussed in §10.2.2. The solution there was to go to higher order in QCD, where explicit $g \rightarrow Q\bar{Q}$ vertices provide a dynamical model of the $Q\bar{Q}$ sea; a similar step is helpful here.

The $2 \rightarrow 3$ parton subprocesses that produce $Q\bar{Q}$ pairs are

$$q\bar{q} \rightarrow Q\bar{Q}g, \quad gq(\bar{q}) \rightarrow Q\bar{Q}g(\bar{q}), \quad gg \rightarrow Q\bar{Q}g.$$

The lowest order contributions are $O(\alpha_s^3)$ tree graphs; Fig. 10.21 illustrates just two of very many possible graphs, including for clarity the incident hadrons, too. The cross section formulas are too lengthy

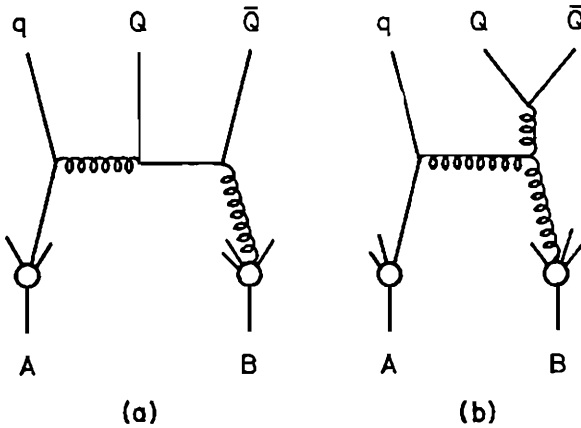


Fig. 10.21. Examples of $2 \rightarrow 3$ parton processes producing $Q\bar{Q}$ heavy quark pairs in the collision of hadrons A and B : (a) flavor excitation of the sea, (b) gluon fragmentation.

to reproduce here but relatively simple forms are given by Ellis and Sexton (Nucl. Phys. B282, 642 (1987)). An excellent approximation is obtained if we simply use the massless formulas of Table 9.2 for the matrix elements, inserting momentum vectors $k_1 \dots k_5$ with correct kinematics. This procedure correctly introduces masses into propagator denominators that have been written as $k_i \cdot k_j$ in terms of external momenta; $-2k_i \cdot k_j = (k_i - k_j)^2$ for massless particles but becomes $(k_i - k_j)^2 - m_j^2$ when final particle j is massive. The approximation works quite well for the dominant gg and gq channels but gives negative $|M|^2$ in limited parts of phase space for $q\bar{q} \rightarrow Q\bar{Q}g$ near threshold.

Returning to Fig. 10.21, we notice several interesting points

- (iv) These diagrams include flavor excitation; Fig. 10.21(a) shows $qQ \rightarrow qQ$ scattering from a $Q\bar{Q}$ pair explicitly generated by a gluon; this solves (i) and (ii) of the previous difficulties, since heavy quark kinematics are specifically put in and we know exactly what happened to the spectator \bar{Q} .
- (v) They have soft and collinear divergences when $p_T(Q\bar{Q}) \rightarrow 0$ and the momentum of an exchanged gluon goes on-shell (this is point (iii) above, encountered once again in this wider context). However, when this happens in Fig. 10.21(a) we can see that the on-shell gluon is simply part of the empirical parton distribution in hadron A , so this configuration is already included in

the gluon fusion cross section $gg \rightarrow Q\bar{Q}$ of Fig. 10.19. Thus the major (singular) part of flavor excitation is already included in the $gg, q\bar{q} \rightarrow Q\bar{Q}$ calculation and it would be double-counting to add it on separately. This solves the difficulty (iii) above; the cut-off should be at the scale of evolution of the parton distribution.

- (vi) Figure 10.21(b) illustrates gluon fragmentation as a source of $Q\bar{Q}$ pairs. Although soft fragmentation is not expected to give heavy quark pairs (§6), hard contributions from highly virtual gluons are certainly allowed; they first appear explicitly in order α_s^3 as shown here. Higher orders can be calculated by Monte Carlo shower techniques (§9.4). Gluon fragmentation is expected to be a major source of $c\bar{c}$ and $b\bar{b}$ production at the SSC.

Exercise. Using the leading-log approximation [§9.4],

$$\sigma(gg \rightarrow Q\bar{Q}g) \simeq 2\sigma(gg \rightarrow gg) \int \frac{dt}{t} \frac{\alpha_s(t)}{2\pi} P_{Qg}(z) dz,$$

where $t = (Q + \bar{Q})^2$ is the virtuality of the gluon that splits $g \rightarrow Q\bar{Q}$, and taking for simplicity the massless form of $P_{Qg}(z)$ (§7.7), show that

$$\frac{\sigma(gg \rightarrow Q\bar{Q}g)}{\sigma(gg \rightarrow Q\bar{Q})} \simeq \frac{\sigma(gg \rightarrow gg)}{\sigma(gg \rightarrow Q\bar{Q})} \frac{\alpha_s(4m_Q^2)}{3\pi} \ln \left(\frac{\hat{s}}{4m_Q^2} \right).$$

Hence show that gluon fragmentation dominates over gluon fusion as a $Q\bar{Q}$ source when the subprocess c.m. energy squared $\hat{s} \gg 4m_Q^2$.

How are we to combine the various subprocesses without double-counting? We first set on one side the question of final state showers, which are to be added in any case, and concentrate attention on the $2 \rightarrow 2$ and $2 \rightarrow 3$ channels for $Q\bar{Q}$ production. It appears that the total cross section is approximately given by the $2 \rightarrow 2$ subprocesses of Fig. 10.19, evolved up to an appropriate scale $Q^2 = p_T^2 + m_Q^2$

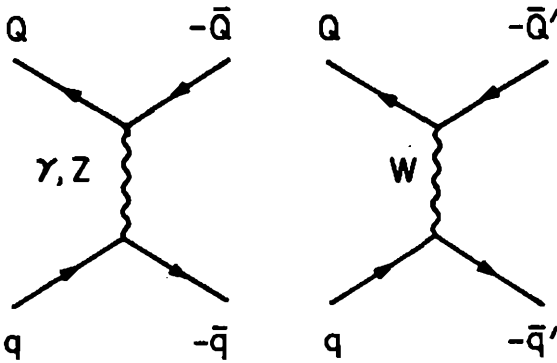


Fig. 10.22. Electroweak contributions to heavy quark hadroproduction.

or $\hat{s}/4$. The major contributions from flavor-excitation and $2 \rightarrow 3$ channels occur when an exchanged gluon nears the mass shell, and these contributions are already included in the diagrams of Fig. 10.20; according to this argument, the diagrams of Fig. 10.21 do not give large additional contributions. In effect we assume that the $Q\bar{Q}$ pair was born from two gluons (one from each hadron) or else from one gluon (in which case the two parents of this gluon came from different hadrons). This includes all the $O(\alpha_s^3)$ quark-excitation type processes and some of the gluon fragmentation, excepting gluons in initial or final state showers.

There are also electroweak channels to be added:

$$q\bar{q}' \rightarrow W^\pm \rightarrow Q\bar{Q}', \quad q\bar{q} \rightarrow \gamma, Z \rightarrow Q\bar{Q},$$

shown in Fig. 10.22. Their contributions are very small compared to QCD, except for t -quarks: $W \rightarrow t\bar{b}$ is competitive with $t\bar{t}$ hadroproduction for $m_t \sim 20\text{--}70$ GeV.

Heavy Q production calculations depend on several ingredients:

- (i) parton distribution parameterizations;
- (ii) choice of scale $Q^2 = p_T^2 + m_Q^2$ or $\hat{s}/4$ or whatever;
- (iii) α_s : choice of Λ , number of active flavors N_f , 1st/2nd order formula;
- (iv) quark mass;

(v) K factor from non-LLA corrections not included in $\alpha_s(Q^2)$.

Hence QCD calculations are uncertain by a factor of about 2. Electroweak calculations can however be normalized to the $W \rightarrow e\nu$ and $Z \rightarrow e^+e^-$ data. Typical predictions at $\sqrt{s} = 630$ GeV (2 TeV) using DO parton distributions, $Q^2 = \hat{s}/4$, $\Lambda = 0.2$ GeV, $N_f = 5$, 1st order α_s formula and $K = 1$ are as follows:

$$\begin{array}{ll} \sigma(\text{QCD} \rightarrow c\bar{c}) = 140 \text{ (300)} \mu\text{b} & m_c = 1.5, \\ \sigma(\text{QCD} \rightarrow b\bar{b}) = 6 \text{ (25)} \mu\text{b} & m_b = 5.0, \\ \sigma(\text{QCD} \rightarrow t\bar{t}) = 0.6 \text{ (10)} \text{ nb} & m_t = 40. \end{array}$$

The electroweak cross sections, normalized to W and Z data, are

$$\begin{array}{ll} \sigma(Z \rightarrow c\bar{c}) = 0.2 \text{ (0.8)} \text{ nb}, \\ \sigma(Z \rightarrow b\bar{b}) = 0.3 \text{ (1.0)} \text{ nb}, \\ \sigma(Z \rightarrow t\bar{t}) = 0.04 \text{ (0.14)} \text{ nb}, \\ \sigma(W^\pm \rightarrow tb) = 1.2 \text{ (3.8)} \text{ nb}, \\ \sigma(W^\pm \rightarrow cs) = 1.7 \text{ (5.8)} \text{ nb}. \end{array}$$

Figure 10.23 shows the energy-dependence of these calculations compared with some selected data points in the case of charm; the total W^\pm and Z^0 production are also shown (normalized to data). Notice that lowering the c and b quark masses would raise the corresponding QCD cross sections. In fixed-target experiments, the most reliable results are those where the charm particle tracks are detected; the πp and pp data points at $\sqrt{s} \simeq 25$ GeV are of this kind (high-resolution bubble chamber), and agree semiquantitatively with the calculations. The pp data near $\sqrt{s} = 60$ GeV are from the ISR; they differ widely among themselves but broadly suggest some large additional contributions (tentative $b\bar{b}$ production results, not shown, are also well above perturbative QCD). However a cautionary note should be added: the ISR results are extrapolated from a very small fraction of the total charm and beauty production in a small part of phase space and a few decay channels; corrections of order 10^6 have been applied to obtain the final cross sections.

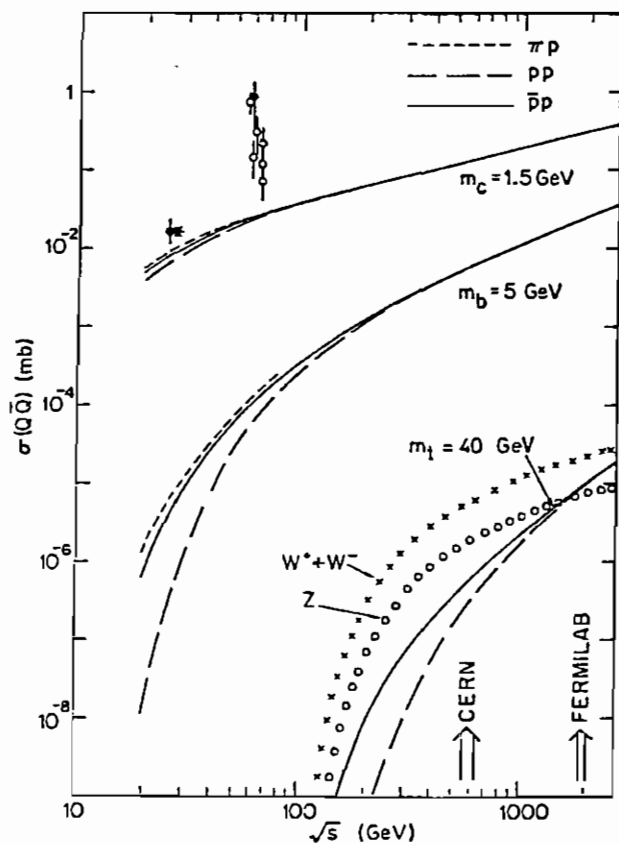


Fig. 10.23. Calculations of heavy flavor production based on $2 \rightarrow 2$ subprocesses for πp , pp and $p\bar{p}$ collisions, compared to a few selected data points. Data at $\sqrt{s} \approx 60$ GeV are for pp . Data at $\sqrt{s} \approx 25$ GeV are for πp (star) and pp (circle). The cross sections for W^\pm and Z^0 production are also shown.

Beside perturbative QCD and electroweak production, two other mechanisms have been mooted. One is *Recombination*: a heavy quark Q (production unspecified) may be picked up by one or more fast valence quarks and form a fast baryon qqQ or meson $\bar{q}Q$ state. This is a form of final state interaction that would give fast Q -flavored hadrons; it is not clear whether it should affect the total production cross section. The other is *Diffraction*: the incident p (say) is excited by vacuum-exchange to a high mass N^* state with essentially unchanged energy; this state can decay into Q -flavored hadrons, one of which can be fast; this process is distinct from perturbative QCD and gives an addition to the cross section. Both Recombination

and Diffraction are characterized by low- p_T and high x_F for heavy hadrons, but are not reliably predicted; we look to experiment to see if they are present.

Present data are contradictory. In the $\pi p \rightarrow DX$ charm measurements near $\sqrt{s} = 25$ GeV, there is a 20% diffractive component; fitting to a longitudinal distribution $d\sigma/dx_F \sim (1 - |x_F|)^n$, where $x_F = p_{DL}/p_{\max}$ in the c.m. frame, most of the cross section is fitted by $n \simeq 6-8$ in agreement with QCD fusion but a diffractive component with $n \simeq 1-2$ remains; see Figure 10.24(a). There is also a corresponding excess of those D -meson states that share a valence quark with the incident pion, as one would expect for diffraction or recombination (*e.g.* $\pi^+ \rightarrow D^+, D^0$; $\pi^+ \not\rightarrow \bar{D}^0, D^-$). In contrast, some ISR data at $\sqrt{s} \simeq 60$ GeV suggest an overwhelming diffractive contribution: Fig. 10.24(b) shows the x_F distribution reported for $pp \rightarrow \Lambda_c^+ X$ production. A large diffractive component would explain the large cross section values, but such a strong onset of diffraction over a relatively small change of energy regime seems surprising. The question still remains to be resolved.

The basic $2 \rightarrow 2$ fusion subprocesses produce $Q\bar{Q}$ pairs with zero net p_T . To get their p_T -dependence, we may take $2 \rightarrow 2$ fusion to define the central hard collision and add initial and final state Monte Carlo showers. The leading logarithm shower approximations are unsatisfactory near threshold, however. When typical subprocess energies are not so high that multiple $Q\bar{Q}$ production in the showers is likely, we can make a Poor Mans Shower Model based purely on the $2 \rightarrow 3$ subprocesses, which have realistic threshold dynamics and are expected to dominate at large $p_T(Q\bar{Q})$. In this approach (similar to that in §8.7) we put empirical $p_T(Q\bar{Q})$ cutoffs in the otherwise divergent $2 \rightarrow 3$ subprocess cross sections, adjusted to give the correct total cross section and invariant mass $m(Q\bar{Q})$ distribution (defined by $2 \rightarrow 2$ fusion folded with evolved parton distributions). This gives the correct cross section for each $m(Q\bar{Q})$ plus the correct $p_T(Q\bar{Q})$ -dependence at large p_T ; it is inexact at small $p_T(Q\bar{Q})$ but the details

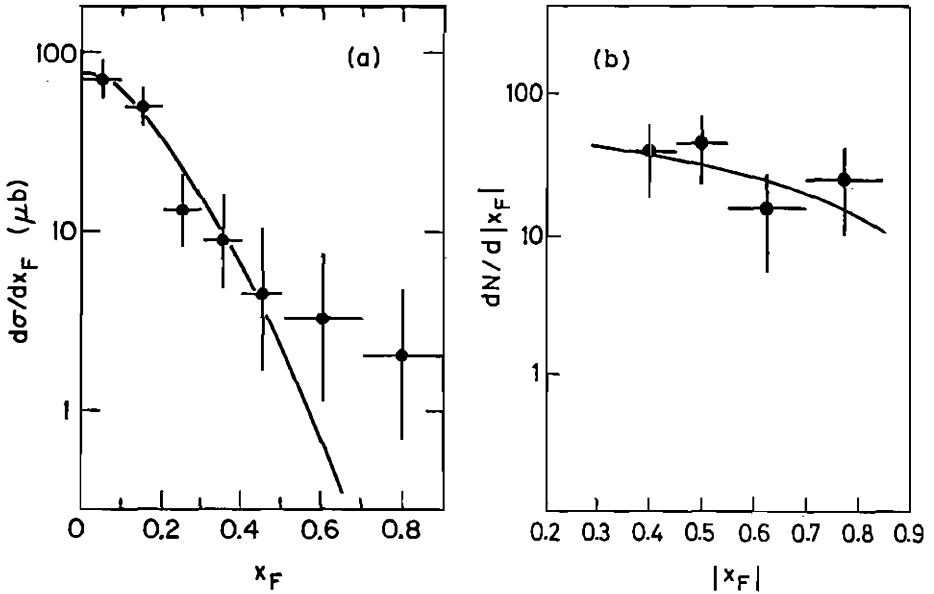


Fig. 10.24. (a) x_F dependence of inclusive $\pi p \rightarrow D$ production with $x_F > 0$ at $\sqrt{s} = 26$ GeV (NA27 experiment, Phys. Lett. **161B**, 400 (1985)); the curve is a $2 \rightarrow 2$ QCD calculation with δ -function fragmentation, normalized to the data. (b) x_F dependence of inclusive $pp \rightarrow \Lambda_c$ production at $\sqrt{s} = 63$ GeV (CERN-Bologna group, Nuovo Cim. **65A**, 408 (1981); the curve is an empirical fit $\sim (1 - |x_F|)^{0.9}$.

here are smoothed away by fragmentation and experimental resolution.

10.3.3 Lepton signals.

Leptons are a popular way to tag heavy quarks (§3.7). For c and b quarks the decay leptons are usually in or near jets: it is then easier to identify muons than electrons. Isolated leptons are characteristic of heavier quarks (assuming there is no charged Higgs decay channel); then either e or μ can be used. Tagging b via $B \rightarrow \psi X$ decays with $\psi \rightarrow e^+e^-$ or $\mu^+\mu^-$ is interesting too, in spite of the small branching fractions ($1.1 \pm 0.2\%$ for $B \rightarrow \psi X$, $6.9 \pm 0.9\%$ for $\psi \rightarrow e^+e^-$, $\psi \rightarrow \mu^+\mu^-$), because of the expected prodigious production of B -mesons

at future hadron colliders.

Consider first single-lepton detection. Figure 10.25 shows typical calculations of the inclusive single-muon p_T distribution from QCD and electroweak sources, for $p\bar{p}$ collisions at $\sqrt{s} = 540$ GeV. In these calculations the heavy quarks are produced via the Poor Mans Shower and fragmented into heavy hadrons using the Peterson model (§6.3); weak decays are followed through the complete cascades (§3.7.2), so secondary and tertiary decay muons are included. Mass $m_t = 40$ GeV is illustrated. UA1 data points are shown for comparison; at smaller p_T they may contain some background from $\pi, K \rightarrow \mu\nu$. Notice the following points:

- i) b decays give more muons than c -decays at large p_T , although $b\bar{b}$ and $c\bar{c}$ production are approximately equal at large p_T (where their masses do not matter). This is because b -fragmentation is harder than c -fragmentation (§6.3). Also $b \rightarrow c\mu\bar{\nu}$ has a harder muon spectrum than $c \rightarrow s\bar{\mu}\nu$, because of $V-A$ coupling (§3.6). b decays have additional secondary $b \rightarrow c \rightarrow \mu$ contributions too, but these are relatively soft and unimportant at large p_T .
- ii) The small- p_T peak in top-quark channels comes from secondary and tertiary decay muons.
- iii) Top-quark muons are nowhere dominant, not even at very large p_T . Extra conditions like muon isolation are needed to extract a top signal.
- iv) The agreement with experiment at large p_T is encouraging (this calculation used $K = 1$). At smaller p_T there may be backgrounds in the data.

Dilepton events have a lower rate (two semileptonic decays now required) but give cleaner signals, with relatively smaller backgrounds. Figure 10.26 shows calculations of unlike-sign $\mu^+\mu^-$ and like-sign $\mu^\pm\mu^\pm$ pair production versus dilepton mass $m(\mu\mu)$, from various sources. Drell-Yan $q\bar{q} \rightarrow (\gamma, Z) \rightarrow Q\bar{Q}$ and charm pair production give $\mu^+\mu^-$ only, neglecting very small $D^0 - \bar{D}^0$ oscillations; $b\bar{b}$

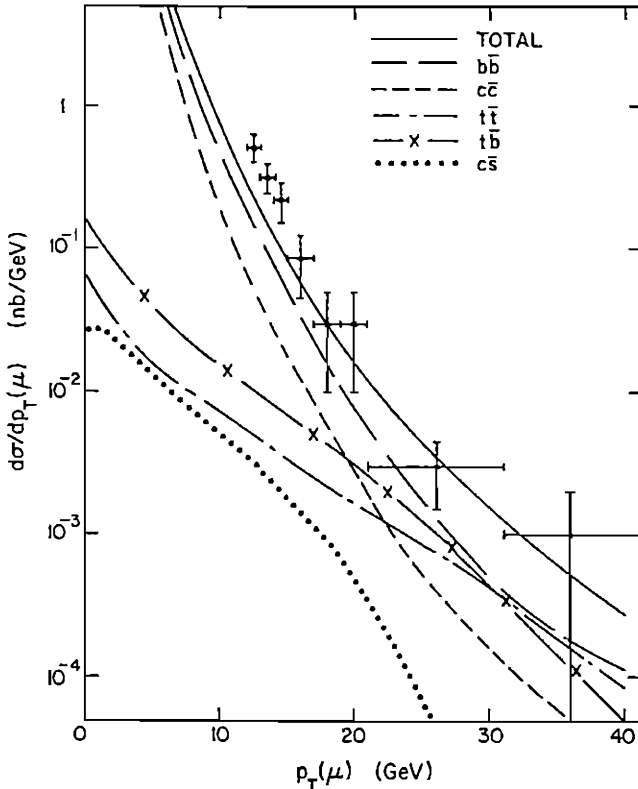


Fig. 10.25. Inclusive single-muon p_T spectrum. Typical calculations of heavy quark contributions from various sources (with hypothetical $m_t = 40$ GeV), are compared to UA1 data at $\sqrt{s} = 540$ GeV.

production gives both $\mu^+\mu^-$ and $\mu^\pm\mu^\pm$. Top-quark signals are much smaller but interesting, especially in same-sign events; one can suppress the $b\bar{b}$ and $c\bar{c}$ contributions by requiring one muon to be isolated and also by rejecting back-to-back dimuons (with relative azimuth $\Delta\phi \sim 180^\circ$), but through 1986 the statistics have been inadequate for a top search here.

Isolation criteria for dileptons can be defined in various ways. The UA1 collaboration selected muons with $p_T(\mu) > 3$ GeV and invariant mass $m(\mu\mu) > 6$ GeV, and measured the scalar sum of E_T in calorimeter cells within a cone $\Delta R = [(\Delta\eta)^2 + (\Delta\phi)^2]^{1/2} < 0.7$ around

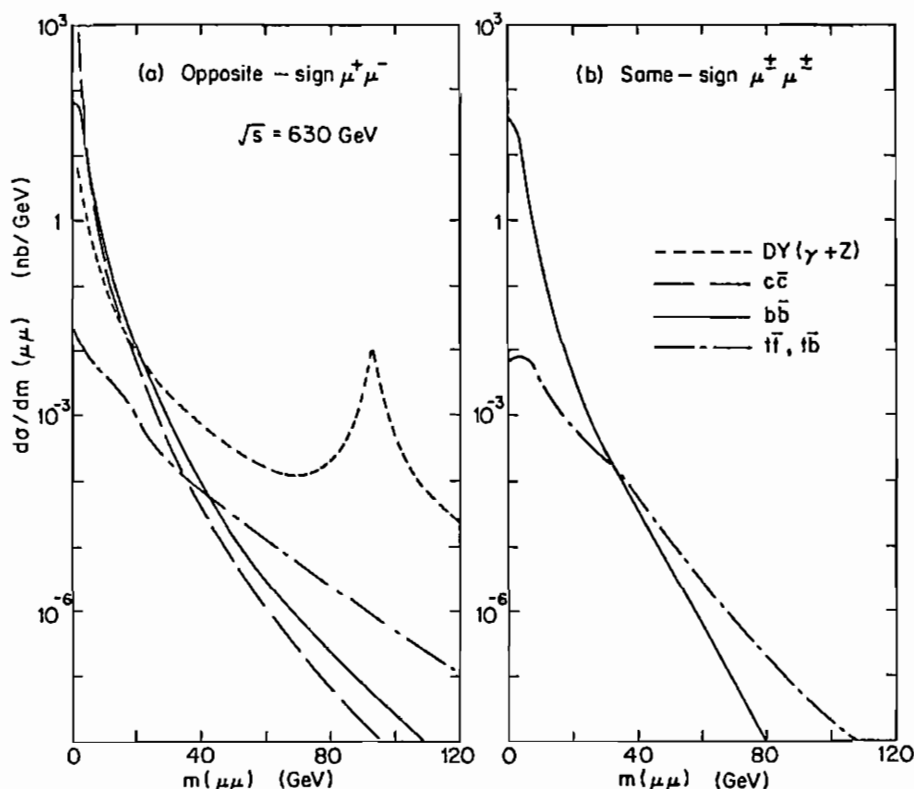


Fig. 10.26. Calculated invariant mass distributions for (a) unlike-sign dimuons and (b) like-sign dimuons from various sources in $p\bar{p}$ collisions at $\sqrt{s} = 630$ GeV. The ψ and Υ peaks are not shown.

each muon direction. They took the sum of squares

$$S = \left[\sum E_T(\mu_1) \right]^2 + \left[\sum E_T(\mu_2) \right]^2$$

and defined dimuons to be isolated if $S < 9$ GeV², non-isolated otherwise. With this criterion, most Drell-Yan events are isolated (and furthermore have little jet activity) while most $c\bar{c}$ and $b\bar{b}$ events are non-isolated, according to Monte Carlo simulations.

The important question of $B^0 - \bar{B}^0$ oscillations (§10.1.3) now can be addressed. With non-isolated dimuons, $b\bar{b}$ pairs are the dominant source. With a cut like $p_T(\mu) > 3$ GeV, soft secondary $b \rightarrow c \rightarrow \mu$

contributions are disfavored and primary b decays predominate. The situation is now exactly like example (i) of §10.1.3. If we neglect $c\bar{c}$ contributions, secondary b -decays, top decays and other backgrounds, the like-sign/unlike-sign ratio is once more

$$\frac{N(\pm\pm)}{N(\pm\mp)} = \frac{2\chi(1-\chi)}{\chi^2 + (1-\chi)^2}, \quad \chi = f_d\chi_d + f_s\chi_s,$$

for uncorrelated light quark flavors. Here $\chi_q = r_q/(1+r_q)$ is the parameter for $B(\bar{b}q) - \bar{B}(b\bar{q})$ oscillations and f_q is the fragmentation fraction leading to $B(\bar{b}q)$ states. For a realistic analysis all backgrounds must be included in a complete Monte Carlo simulation. In a total sample of 512 dimuon events, including isolated Drell-Yan and Υ events, the UA1 collaboration found an overall ratio $R = (\text{like-sign})/(\text{unlike-sign}) = 0.42 \pm 0.07 \pm 0.03$ whereas calculations with no oscillations gave 0.26 ± 0.03 . The enhancement of like-sign dimuons is attributed to oscillations. Defining an effective χ parameter as the overall probability that an initial $b(\bar{b})$ first fragments and then oscillates to $\bar{b}(b)$ before decaying, the UA1 group determined

$$\chi = 0.121 \pm 0.047.$$

If all B -hadrons have the same semileptonic branching fraction, then $\chi = f_d\chi_d + f_s\chi_s$ as defined above: assuming $f_d = 0.40$, $f_s = 0.20$, this gives a lower bound on r_s and r_d (90% CL), shown as the shaded area E in Fig. 10.8.

Though one might have imagined that the cleaner environment of $e^+e^- \rightarrow Q\bar{Q}$ production would be a better place to study heavy quark physics, this $B - \bar{B}$ oscillation example illustrates what may be done with the large cross sections and luminosities at hadron colliders.

Exercise. Using standard model cross sections and the luminosities in Table 1.4, compare the rate of production of $b\bar{b}$ events in e^+e^- and hadron colliders (at $\sqrt{s} = 40$ TeV, $\sigma(p\bar{p} \rightarrow b\bar{b}) \sim 0.1\text{-}1$ mb).

From a peak in isolated $\mu^+\mu^-$ pairs at the Υ mass, a cross section was found in good agreement with theory:

$$\begin{aligned} B\sigma(p\bar{p} \rightarrow \Upsilon, \Upsilon', \Upsilon'' \rightarrow \mu^+\mu^-) &= 0.98 \pm 0.21 \pm 0.19 \text{ nb} && \text{(UA1)} \\ &= 0.9 - 1.8 && \text{(theory)} \end{aligned}$$

where the theoretical number is based on Fig. 10.17.

Finally trileptons are another potentially interesting signal for heavy quarks, but with smaller rate (*three* semileptonic decays needed).

Exercise. Of the first three generations of quark, show that only $t\bar{b}$ and $t\bar{t}$ production can give same-sign trimuons ($\pm\pm\pm$) or mixed-sign trimuons in which all pair invariant masses exceed 5 GeV.

10.3.4 Signatures for top.

Top searches at the CERN $p\bar{p}$ collider were based on a single-lepton tag (to get adequate event rate); this assumes from the start that the charged Higgs decay channel (§3.7.1) does not dominate. Minimum p_T and isolation cuts are made on the lepton, to suppress charm and bottom backgrounds. Isolation is defined by requiring summed E_T to be less than some critical value, for calorimeter cells in a cone around the direction of the lepton, with parameters optimized to reject b and c .

These cuts represent a compromise: if minimum lepton p_T is set very high (say $p_T > 20$ GeV) then the kinematics constrain any contributing b or c decays to have highly collimated decay products and very few of their leptons will be isolated. Also at high p_T the b and c backgrounds are relatively smaller; on the other hand, the top signal itself is very small. With a lower p_T cut the signal is bigger but the backgrounds are more problematical.

Particular attention was focussed on the $W \rightarrow t\bar{b}$ production channel, both because its rate is reliably calculable given m_t and because it has many nice features that could help to identify it. Figure 10.27 shows a $W \rightarrow t\bar{b}$, $t \rightarrow be^+\nu$ event schematically.

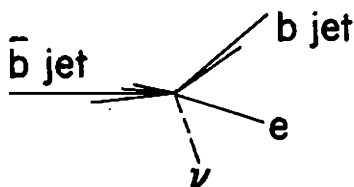


Fig. 10.27. Topology of a typical $W \rightarrow t\bar{b}$ event with $t \rightarrow be^+\nu$ decay.

We notice that:

- i) It gives mostly high- p_T isolated $e + 2$ jets: *1st signature*.
- ii) Kinematics: the recoil \bar{b} jet has a Jacobian peak.

Exercise. Neglecting $p_T(W)$, show this peak occurs at

$$p_T(\bar{b}, \text{peak}) = \left[(M_W^2 + m_b^2 - m_t^2)^2 / (4M_W^2) - m_b^2 \right]^{1/2} \\ \simeq (M_W^2 - m_t^2) / (2M_W) .$$

If $m_t < 50$ GeV, the \bar{b} jet nearly always has bigger p_T than the b , so we can tell which is which. This peak, which gets smeared by $p_T(W)$, is both a measure of m_t and a *2nd signature*. If we define a “recoil transverse mass” by

$$m_T^2(\text{recoil}) = M_W^2 - 2M_W p_T(\bar{b})$$

then the Jacobian peak of $p_T(\bar{b})$ translates into a peak in $m_T(\text{recoil})$ near the value m_t .

- iii) The invariant mass of e, ν, b is m_t . We cannot get this directly, but if the missing $p_T(\nu)$ is measured we can construct the transverse mass of $e + \nu$ (as in the $W \rightarrow e\nu$ analysis of §8.6)

$$m_T^2(e, \nu) = (|\mathbf{p}_{eT}| + |\mathbf{p}_{\nu T}|)^2 - (\mathbf{p}_{eT} + \mathbf{p}_{\nu T})^2$$

or, better still, the transverse mass of ν plus the “cluster” $c = (e + b)$ defined in a similar way

$$m_T^2(c, \nu) = \left(\sqrt{\mathbf{p}_{cT}^2 + m_c^2} + |\mathbf{p}_{\nu T}| \right)^2 - (\mathbf{p}_{cT} + \mathbf{p}_{\nu T})^2 ,$$

where \mathbf{p}_c and m_c are the total cluster momentum and invariant mass. This cluster transverse mass peaks sharply near its upper

limit value m_t . It is another independent measure of m_t and provides a *3rd signature*.

- iv) The invariant mass of e, ν, b, \bar{b} is M_W and unmeasurable. But the cluster transverse mass m_T ($c = e + b + \bar{b}, \nu$) peaks sharply near its upper limit M_W . This is a cross-check on the W -origin of the event and a *4th signature*. Figure 10.28 illustrates the various transverse mass peaks expected for $p\bar{p} \rightarrow W \rightarrow t\bar{b} \rightarrow \bar{b}be\nu$ events. The ideal signature for an event would be that it lay in all peaks simultaneously.

In real life there are complications: there may be additional semi-leptonic decays in the b and \bar{b} jets with extra neutrinos that smear $p_{\nu T}$; there may be extra hadrons or jets accompanying W production; there are experimental uncertainties in jets and in missing p_T . The solution is to include these complications in a Monte Carlo. There are also backgrounds, of which the most dangerous is $2 \rightarrow 3 b\bar{b}x$ production where $x = q, \bar{q}, g$; here it is possible for \bar{b} and x to provide

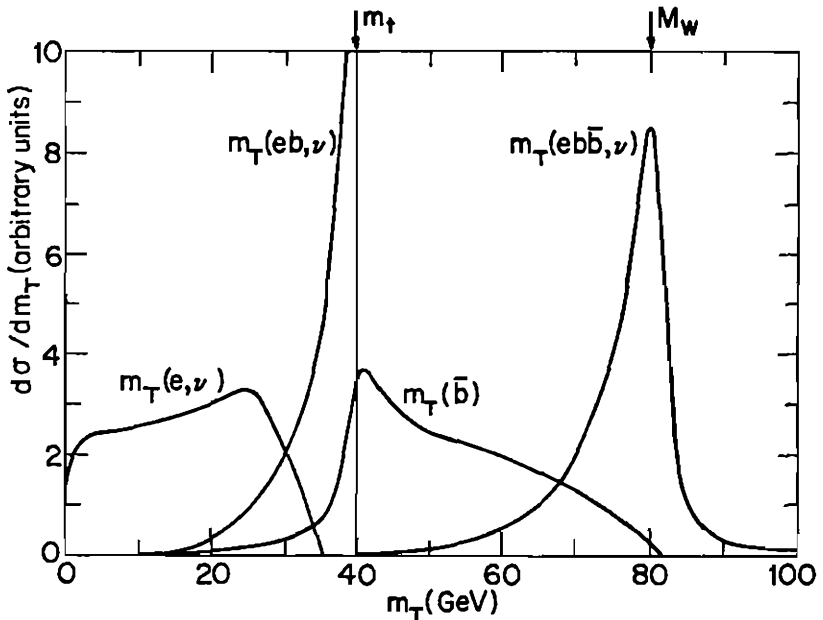


Fig. 10.28. The various transverse mass peaks expected in $p\bar{p} \rightarrow W \rightarrow t\bar{b}$ events, calculated at $\sqrt{s} = 630$ GeV but rather insensitive to energy, for assumed mass $m_t = 40$ GeV.

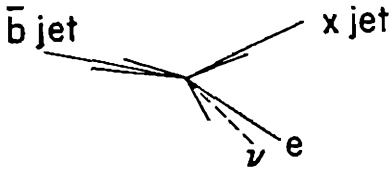


Fig. 10.29. A background to the $W \rightarrow t\bar{b} \rightarrow b\bar{b}e\nu$ signal from $b\bar{b}x$ events.

the two jets while b may decay $b \rightarrow ce\nu$ giving most of its energy to e which may then look isolated; see Fig. 10.29. These backgrounds can be suppressed by severe isolation criteria however.

Hadroproduced $t\bar{t}$ events have the signature “isolated high- p_T lepton plus jets,” but fewer other signatures. If a $b(\bar{b})$ jet can be identified in the event with e^+ (e^-), then we can form the $be\nu$ cluster transverse mass and look for a peak as before (where ν means missing p_T). Also the $e\nu$ transverse mass differs from $W \rightarrow e\nu$ background, if $m_t < M_W$.

In a study of isolated lepton plus jet(s) at the CERN $p\bar{p}$ collider, the UA1 collaboration reported some evidence of $W \rightarrow t\bar{b}$ and $t\bar{t}$ events, lying in the expected $be\nu$ and $b\bar{b}e\nu$ transverse mass peaks and suggesting m_t in the range 30-50 GeV [but top was eventually discovered in 1994, with $m_t \simeq 175$ GeV, at the Fermilab Tevatron collider].

If microvertex detectors can be used to pick out c , b and τ decay vertices and trace back to the vertices where they were born, top events may be distinguished by their multi-branch cascade decay modes such as $t \rightarrow bc\bar{s}$ or $t \rightarrow b\nu\bar{\tau}$. In these decays both b and c (or b and $\bar{\tau}$) emanate from a single point, unlike any $b\bar{b}$ or $c\bar{c}$ events. There may be a background from events with double-heavy-flavor production, like $p\bar{p} \rightarrow b\bar{b}c\bar{c}X$, but they are interesting too and differ in various details.

Finally, diffractive triggers have been suggested for top searches; if the large charm cross sections reported from the ISR have a diffractive origin, a typical event $p\bar{p} \rightarrow N^{**}\bar{N}^*$ might have low-mass \bar{N}^*

production with little high- p_T activity in one hemisphere, while in the other hemisphere (along the p direction) a high mass N^{**} decays into a fast Λ_t baryon and a slower T meson. Λ_t would be faster because it could contain two out of three of the original proton's valence quarks while T could have at most one. Semileptonic Λ_t decay would give high- p_T high- y leptons ℓ^+ near the p direction, while charge-conjugate processes with $\bar{\Lambda}_t$ would give ℓ^- near the \bar{p} direction. This lepton charge asymmetry would be evidence of a diffractive $t\bar{t}$ origin.

Exercise. Show that $b\bar{b}$ diffractive production would give a similar asymmetry but with opposite sign and smaller p_T of the leptons.

10.3.5 CP violation.

CP violation in b -decay can be investigated through the asymmetry of $++$ and $--$ like-sign dileptons in $b\bar{b}$ events, exactly as described for e^+e^- production in §10.1.3. Very large numbers of events are needed to overcome the small branching fractions and small asymmetries in these and other CP violating effects (estimates indicate that of order 10^8 $b\bar{b}$ events would be required) so we look initially to hadroproduction. However there are also proposals to build high-luminosity e^+e^- linear colliders to act as "B-factories".

Beside the same-sign lepton asymmetry, there are interesting effects for decays into final states common to both B^0 and \bar{B}^0 .

Exercise. Show that $D^+\pi^-$, $D^-\pi^+$, ψK^0 , $D\bar{D}$ are decay channels common to B^0 and \bar{B}^0 .

Exercise. Using the formulas in §10.1.3 show that the amplitudes for an initial B^0 or \bar{B}^0 to decay into a state f after time t are

$$A(B^0 \rightarrow f; t) = \frac{\alpha(f)}{2} [e^{-i\mu_1 t} + e^{-i\mu_2 t}] + \frac{\eta \bar{\alpha}(f)}{2} [e^{-i\mu_1 t} - e^{-i\mu_2 t}],$$

$$A(\bar{B}^0 \rightarrow f; t) = \frac{\bar{\alpha}(f)}{2} [e^{-i\mu_1 t} + e^{-i\mu_2 t}] + \frac{\alpha(f)}{2\eta} [e^{-i\mu_1 t} - e^{-i\mu_2 t}],$$

where $\alpha(f)$, $\bar{\alpha}(f)$ are the matrix elements for $B^0 \rightarrow f$, $\bar{B}^0 \rightarrow f$ and $\mu_j = m_j - \frac{1}{2}i\Gamma_j$ as before. Neglecting $\delta\Gamma/\Gamma$ for convenience (reason-

able for B decays) show that the time-integrated decay probabilities are

$$P(B^0 \rightarrow f) = \frac{|\alpha(f)|^2}{2\Gamma} \left\{ 1 + |\xi|^2 + \frac{1 - |\xi|^2 + 2x \operatorname{Im}\xi}{1 + x^2} \right\},$$

$$P(\bar{B}^0 \rightarrow f) = \frac{|\alpha(f)|^2}{2\Gamma|\eta|^2} \left\{ 1 + |\xi|^2 - \frac{1 - |\xi|^2 + 2x \operatorname{Im}\xi}{1 + x^2} \right\},$$

where $x = \delta m/\Gamma$ and $\xi = \eta \bar{\alpha}(f)/\alpha(f)$. Note that the limit $\xi = 0$ corresponds to the flavor-tagging decays that we studied previously.

We can look for CP violation in comparisons between $B^0 \rightarrow f$ and $\bar{B}^0 \rightarrow \bar{f}$ decays, but the situation is specially simple when the final state f is CP-self-conjugate ($\bar{f} = \pm f$), as with $f = \psi K_S$ or $D\bar{D}$. Then CP conservation would require $\bar{\alpha}(f) = \alpha(f)$ with $\eta = \xi = 1$; any departure from equality between $B^0 \rightarrow f$ and $\bar{B}^0 \rightarrow f$ decays would signal CP violation. Experimentally, one possibility is to select $B\bar{B}$ events in which one B is charged and flavor-tagged, establishing the initial flavor of a companion neutral $B^0(\bar{B}^0)$ whose decay to f is observed. Another possibility is that both B -mesons are neutral, in which case the oscillations of both must be taken into account.

If microvertex detectors are eventually able to measure the proper time t at which a B decay occurs, it will be possible to extract δm and perhaps $\delta\Gamma$ directly from the time-dependence of decays, and also to look for CP violation by comparing the time-dependence of CP conjugate channels (see the formulas above).

We can also look for CP violation in the decays of charged B mesons, where oscillations play no part. Interference effects are crucial here. If two different weak amplitudes contribute to $B^+ \rightarrow f^+$ decay, then by TCP invariance the contribution to the CP conjugate $B^- \rightarrow f^-$ channel is related by

$$M^+ \equiv \langle f^+ | \mathcal{L} | B^+ \rangle = g_1 M_1 \exp(i\delta_1) + g_2 M_2 \exp(i\delta_2),$$

$$M^- \equiv \langle f^- | \mathcal{L} | B^- \rangle = g_1^* M_1 \exp(i\delta_1) + g_2^* M_2 \exp(i\delta_2),$$

where g_1 and g_2 are the weak couplings (including complex mixing

matrix elements), δ_1 and δ_2 are the appropriate strong or electromagnetic phase shifts due to CP invariant final state interactions and M_1, M_2 are real. The difference of decay rates will then be proportional to

$$|M^+|^2 - |M^-|^2 = 4(M_1 M_2) \text{Im}(g_1 g_2^*) \sin(\delta_2 - \delta_1),$$

showing that an effect requires (a) more than one channel, (b) a complex coupling and (c) a final state phase. (In B^0 decays (a) and (c) are supplied by oscillations.)

Exercise. Show that $B^- \rightarrow K^- K_S^0 \pi^+ \pi^-$ can be produced via two different decay chains and fulfils the conditions for a possible asymmetry from CP violation.

Experimentally the study of rare B -decays involves several practical questions. Firstly we need a tag or trigger to select interesting events and suppress the huge backgrounds; we may for example tag and reconstruct $B \rightarrow \psi X$ decays. We then have the option to study these tagged B decays or to look for the decays of the other B in the same event (assuming pair hadroproduction). In the case of neutral decays like $B \rightarrow \psi K_S$ we need to find the other B anyway, to establish the initial flavor (B^0 or \bar{B}^0) of the first B ; if the other B is B^\pm we have an immediate answer, if it too is neutral we have to take account of possible oscillations of both. There is also a question of normalization, in establishing relative decay rates for B and \bar{B} channels. With $p\bar{p}$ colliders, the strong production and fragmentation processes are symmetrical between particles and antiparticles, but in pp colliders baryon production is favored over antibaryons and hence $\bar{B}(b\bar{q})$ mesons are somewhat depleted relative to $B(\bar{b}q)$ mesons. One possibility is to normalize the B/\bar{B} ratio by measuring final states like $B_d^0 (\bar{B}_d^0) \rightarrow \psi K^\pm \pi^\mp$, that are flavor-tagging decays and have no CP violating asymmetry in the standard model. However, it is undesirable to rely on the standard model entirely, since there may be non-standard contributions waiting to be found.

Table 10.2. Examples of B decays with CP violation. The asymmetry is $\frac{\Gamma(B^0 \rightarrow f) - \Gamma(\bar{B}^0 \rightarrow \bar{f})}{\Gamma(B^0 \rightarrow f) + \Gamma(\bar{B}^0 \rightarrow \bar{f})}$.

		Asymmetry	BF
$B_d^0 \rightarrow \psi\phi$	vs $\bar{B}_d^0 \rightarrow \psi\phi$	8%	10^{-5}
$B_d^0 \rightarrow \psi K_S^0$	vs $\bar{B}_d^0 \rightarrow \psi K_S^0$	8%	5×10^{-4}
$B_s^0 \rightarrow \psi\phi$	vs $\bar{B}_s^0 \rightarrow \psi\phi$	-2%	3×10^{-3}
$B_d^0 \rightarrow D^+\pi^-$	vs $\bar{B}_d^0 \rightarrow D^-\pi^+$	-60%	10^{-5}
$B_d^0 \rightarrow K^+K^-$	vs $\bar{B}_d^0 \rightarrow K^+K^-$	10%	$< 10^{-4}$
$B_d^0 \rightarrow D^-\pi^+$	vs $\bar{B}_d^0 \rightarrow D^+\pi^-$	-0.2%	2×10^{-2}
$B_s^0 \rightarrow K^+K^-$	vs $\bar{B}_s^0 \rightarrow K^+K^-$	38%	10^{-5}
$B_s^0 \rightarrow D^+\pi^-$	vs $\bar{B}_s^0 \rightarrow D^-\pi^+$	56%	2×10^{-4}
$B_s^0 \rightarrow D^-\pi^+$	vs $\bar{B}_s^0 \rightarrow D^+\pi^-$	23%	10^{-3}

Table 10.2 shows examples of B^0 and \bar{B}^0 decays that could be studied for CP violation at the SSC. Notice that the cases with large expected asymmetries unfortunately have small branching fractions.

10.3.6 W^+W^- signals.

When a heavy quark mass exceeds M_W , real W modes will dominate the decays (§3.8); for example

$$t\bar{t} \rightarrow (bW^+)(\bar{b}W^-)$$

$$\rightarrow \begin{cases} b\bar{b} + \text{jets} & (\sim 53\%) \\ b\bar{b} + \ell + \nu + \text{jets} & (\sim 40\%) \\ b\bar{b} + \ell^+ + \ell^- + \nu + \bar{\nu} & (\sim 7\%) \end{cases}$$

where $\ell = e, \mu$ or τ ; the b and \bar{b} (listed separated because they may be identified) also give jets. At $\sqrt{s} \sim 600$ GeV, this mechanism is already competitive with standard electroweak mechanisms for producing W^+W^- and $W^\pm Z$ pairs, for $m_t \sim 80$ -90 GeV. The UA1 and

UA2 groups have actually reported a few events which could be interpreted as W^+W^- pairs with one W decaying leptonically, one hadronically.

At higher energies the heavy quark mechanism totally dominates over electroweak W pair production. Figure 10.30 shows the energy dependence of the cross sections from various possible sources in $p\bar{p}$ collisions. At $\sqrt{s} = 2$ TeV, corresponding to the Tevatron, the heavy quark mechanism dominates over electroweak contributions for masses as large as 200 GeV.

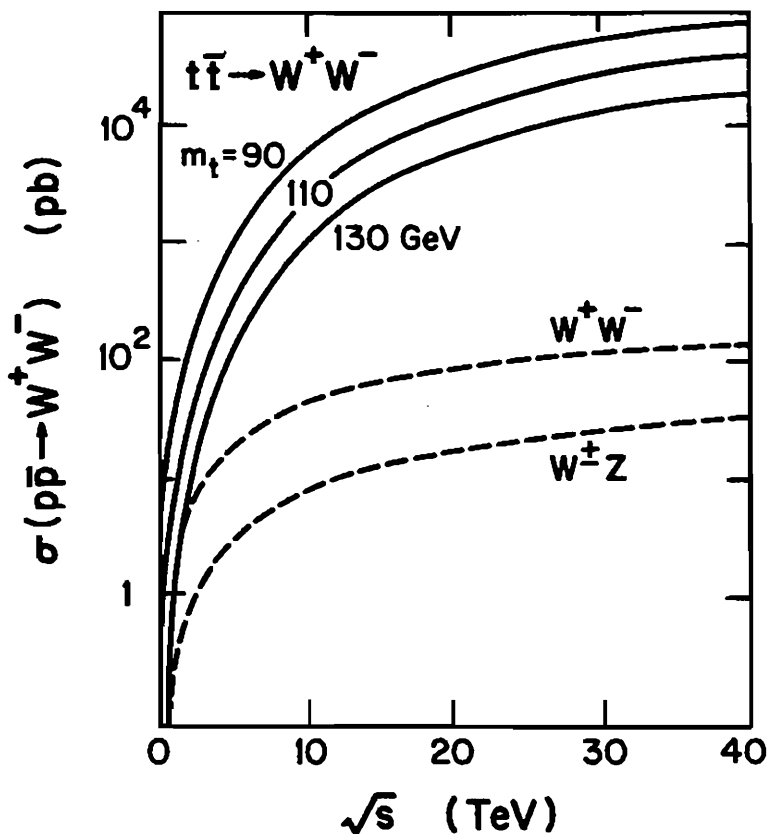


Fig. 10.30. Energy dependence of $p\bar{p} \rightarrow W^+W^-X$ production from heavy quark pairs $t\bar{t}$, for $m_t = 90, 110$ or 130 GeV, compared with electroweak W^+W^- and $W^\pm Z$ production. Results for pp collisions are similar above 2 TeV.

Chapter 11

Monte Carlo Simulations

11.1 Introduction

Monte Carlo is a way of calculating difficult integrals that may be intractable by ordinary numerical interpolation methods. The difficulty may come from a large number of integration variables; this is usually the way theorists get involved. Difficulties may also come from folding a predicted cross section with complicated geometrical factors representing detectors, a routine situation for experimenters.

Many interesting calculations have too many degrees of freedom for direct numerical integration. For example, if we take 10 interpolation points in each independent variable, a d -dimensional integration will require 10^d evaluations of the integrand; the practical limit is something like $d = 6$ with this approach. But n -body phase space gives $(3n - 4)$ -dimensional integrals: even if some of these integrals can be done exactly, we quickly get into deep water as n increases.

Monte Carlo methods offer a rescue. As the name suggests, they depend on random sampling. An n -fold integral over the range $(0, 1)$ can be approximated by sampling the integrand N times and taking the average:

$$\bar{f} = \int_0^1 dx_1 \dots \int_0^1 dx_n f(x_1 \dots x_n) \approx \frac{1}{N} \sum_{i=1}^N f(x_1(i), \dots, x_n(i)).$$

Here $x_1(i)$ is the i th sample of a random variable x_1 uniformly dis-

tributed over the range (0, 1), *etc.* This equation is intuitively obvious. We are just defining the mean value of the function f ; on the left-hand side the definition is mathematical, on the right-hand side it is statistical (or if you like, experimental: Monte Carlo can be described as a branch of experimental mathematics).

Each single evaluation of $f(x_1(i) \dots x_n(i))$ is a crude statistical estimator of \bar{f} . It is a random variable, call it f_1 ; its mean is precisely \bar{f} and its accuracy as an estimator is measured by its standard deviation σ_1 (defined by the variance $= \sigma_1^2 = \text{mean value of } (f_1 - \bar{f})^2 = \int dx_1 \dots \int dx_n (f - \bar{f})^2$). The average of N such evaluations, which appears on the right-hand side above, is a much better statistical estimator of \bar{f} . It is a random variable (call it f_N) with the same mean \bar{f} but smaller standard deviation $\sigma_N = \sigma_1/\sqrt{N}$. As N becomes large its probability distribution approaches Gaussian shape

$$P(f_N) \simeq \frac{1}{\sqrt{2\pi\sigma_N^2}} \exp [-(f_N - \bar{f})^2 / (2\sigma_N^2)]$$

by the Central Limit Theorem.

Thus the error in estimating \bar{f} goes down like $1/\sqrt{N}$. This rate of convergence versus N may seem rather slow, compared to the crudest numerical integration (the "trapezoid rule" for N equally-spaced points in a one-dimensional integral) where the numerical error goes down like $1/N^2$ or the m -point Gaussian formula which converges as $1/N^{(2m-1)}$. However, the crunch comes when we go to n -dimensional integrals; here Monte Carlo still converges as $1/\sqrt{N}$ while the trapezoid and Gauss prescriptions converge more slowly than before ($1/N^{2/n}$ and $1/N^{(2m-1)/n}$, respectively). Most important of all, Monte Carlo still works for large n while the others become unmanageable.

The best way to learn Monte Carlo is to do some examples—see

the following sections—but first, here are some practical remarks:

- (1) In elementary particle applications, Monte Carlo is usually a direct simulation of what happens physically. For instance, the quantity of interest \bar{f} may be a cross section or a decay width. The multiple integrations then arise from final phase space plus other continuous variables (*e.g.* momentum fractions of incident partons or of fragmentation products) and the integrand f may include not only a theoretical cross section but also geometrical acceptance and efficiency factors for specific detectors. Mathematically \bar{f} is an integral of a weight function $f(x_1 \dots x_n)$ over variables $x_1 \dots x_n$ that parameterize the possible physical configurations. Monte Carlo calculates this integral by generating a random sample of configurations and averaging the integrand, *i.e.* by generating a random sample of “real” events and averaging their weights.
- (2) During the calculation we can also collect these weighted events in bins, summing the weights in each bin, for each interesting observable quantity—just like collecting experimental data in fact. This gives a histogram of the event distribution versus each observable. These observables can be single variables (*e.g.* an angle or momentum component) or two-dimensional arrays (*e.g.* an energy-angle correlation) or what we please. Little extra effort is needed to add an extra distribution. Monte Carlo has an advantage here over numerical integration, where each fresh distribution needs a fresh calculation. (In effect each bin describes a partial cross section; the corresponding integrand $f_{\text{bin}} = f$ inside the bin, $f_{\text{bin}} = 0$ outside it.)
- (3) The limits of integration $(0, 1)$ are convenient. Computer systems have library subroutines that generate pseudo-random numbers uniformly in this range (sufficiently random for present purposes). The integration volume is conveniently 1. Physical variables usually have different limits, but we can easily re-scale them to fit the standard range $(0, 1)$.

- (4) For $f = \text{constant}$, the Monte Carlo approximation is exact. In this case, of course the integral is trivial and we do not need Monte Carlo, but it illustrates a general principle: the flatter the integrand, the better the approximation. (Put another way, the flatter the integrand, the smaller the standard deviation of the $N = 1$ case—single-shot sampling—and hence, the smaller the standard deviation for general N .)
- (5) Hence, we should avoid singular or near-singular integrands (even if they are formally integrable) by suitable changes of variable. For instance, if the physical problem includes integrating a squared energy s over a relativistic Breit-Wigner resonance factor, the latter can be absorbed as follows,

$$\dots \int \frac{ds}{(s - M^2)^2 + (M\Gamma)^2} = \dots \int \frac{d\theta}{M\Gamma}$$

putting $s - M^2 = M\Gamma \tan \theta$, $ds = M\Gamma \sec^2 \theta d\theta = M\Gamma(1 + \tan^2 \theta)d\theta$, and finally θ can be scaled to the range $(0, 1)$. In this example the offending factor has been removed exactly; in general, it may only be possible to take out part of a bump—but this will still improve the accuracy. This kind of adjustment is called *Importance Sampling* (see more below).

- (6) Avoid δ -functions. Monte Carlo cannot handle them. Integrate them out by hand.
- (7) Avoid discontinuities of f if possible. Try to arrange physical limits to fall at the limits $(0, 1)$ of an integration variable. Some discontinuities may however be inevitable, e.g. acceptance cuts in observables and the edges of bins in distributions.

Exercise. Consider the one-dimensional integral $\int_0^1 f(x)dx$ for the two cases (a) f is a step function, $f = 0$ for $x < 0.5$, $f = 2$ for $x > 0.5$; (b) f is linear, $f = 2x$. In both cases the mean is $\bar{f} = 1$. Show that the one-shot standard deviations are $\sigma_1 = 1$ and $\sigma_1 = 1/\sqrt{3}$, respectively, confirming that smoother integrands give higher accuracy.

- (8) Keep the number of Monte Carlo integrations to a minimum; each is an independent source of fluctuations. If any can be integrated out by hand without losing physics (*e.g.* integrations over unobserved particles), get them done first.
- (9) We can discover the accuracy achieved with N shots by comparing several independent runs. Better still, we can directly calculate the variance of the 1-shot and N -shot estimators by accumulating the statistical averages of both f and f^2 at the same time. The variance σ_1^2 of the 1-shot estimator is then given by

$$\sigma_1^2 = \frac{1}{N} \sum (f - \bar{f})^2 = (\overline{f^2}) - (\bar{f})^2$$

and the accuracy of the N -shot estimator is given by its standard deviation

$$\sigma_N = \sigma_1 / \sqrt{N}.$$

This is of course just a Monte Carlo calculation of σ_1 and σ_N , with some uncertainty of its own.

- (10) Any calculation is ultimately a compromise between accuracy and economy.
- (11) Reproducible computer-generated random numbers have some advantages over genuinely random numbers that are different every time. When developing or copying a program it is helpful to check against previous runs using the identical random numbers. When studying the effect of changing a particular physical parameter (*e.g.* the shape of a fragmentation function), it is best to compare a series of runs in which only this parameter is changed while all other inputs—including the random numbers—are unchanged. We then see the effect of the parameter changes on a fixed sample of events, without the extra fluctuations that would come from letting the event sample change, too.

- (12) There are also disadvantages. Pseudo-random number generators repeat themselves after a certain (very long) period: make sure this period is bigger than the sample you want. Also, there are correlations between numbers in the sequence that can sometimes produce bogus effects.
- (13) Weighted and unweighted events. Monte Carlo programs generate random events which correspond to the x_i coordinate values. These events are uniformly distributed in x_i space. An event's contribution to the sum is then weighted by $f(x_1 \dots x_n)$ which is just \bar{f} times the probability density for such an event to occur in x_i -space. Unless f is constant these uniformly distributed events in x_i space do not occur with the same frequency as events in the real world and are called "weighted" events. An alternate approach is to incorporate the probability of an event's occurrence into the event generation procedure to get Monte Carlo events with the same relative frequency as real events. Such "unweighted events" are generated in each region of phase space with a frequency determined by the function f in that region. Very few events are generated where f is small and many events are generated where f is large. Unweighted events are useful for making typical scatter plots, for confronting detector designs, or just for getting a feel for a new type of physics. The simplest way to convert weighted to unweighted events is the acceptance-rejection method. First find the maximum weight f^{\max} (if necessary, an upper bound will do). Then for each event $(x_1 \dots x_n)$ in a weighted sample, use the ratio $f(x_1 \dots x_n)/f^{\max}$ as the acceptance probability; generate an auxiliary random number y in the range $(0, 1)$, and accept the event if $y < f/f^{\max}$.

The approach described above may be called crude Monte Carlo. It contains the bare bones of the idea but many elegant improvements have been invented to give greater accuracy, faster convergence. The name of the game is *Variance Reduction*.

One area of improvement is *Importance Sampling*. There are computer programs that automatically take note of regions where the integrand f is biggest, from some initial set of random shots; in subsequent running, they adjust the sampling to emphasize these more important regions. The adjustment can be made by changing variables (cf. remark (5) above):

$$\int f dx_1 \dots dx_n = \int \frac{f}{g} g dx_1 \dots dx_n = \int \frac{f}{g} dy_1 \dots dy_n$$

provided $g = \partial(y_1 \dots y_n) / \partial(x_1 \dots x_n)$ is a Jacobian factor. The program chooses g such that f/g is much flatter than f , and then proceeds with Monte Carlo simulation of the y -integrations instead. This kind of “intelligent Monte Carlo” program is helpful if we want the most likely events calculated most accurately, but not necessarily if we want to calculate very unlikely events—such as the extreme tail of some distribution.

There are also classes of computer-generated quasi-random numbers (*e.g.* so-called Halton sequences and scrambled Halton sequences) which give faster Monte Carlo convergence than true random numbers, apparently because they provide a more uniform coverage of the interval $(0, 1)$ in some sense. This is an esoteric question beyond our present scope, but it works and is worth trying, especially in cases where large numbers of events are needed.

Another approach is *Stratified Sampling*. For a 1-dimensional integral, we get a more uniform distribution of samples—and hence better accuracy—if the integration range is subdivided into p equal parts and each part is sampled an equal number of times. For n -dimensional integrals, this means subdividing the integration into p^n equal hypercubes, so p cannot be large. If the integrand is bigger in certain hypercubes, we can arrange to sample the latter more frequently—adjusting the Monte Carlo formula accordingly. We can also adjust the formula for unequal subdivisions. The bookkeeping may be messy but the principle is simple.

Exercise. Consider the effect of stratified sampling on the one-dimensional examples (a) step-function and (b) linear, as in the preceding exercise. Show that with two equal subranges (0, 0.5) and (0.5, 1) the two-shot estimator, with one shot in each subrange, gives $\sigma_2 = 0, \sigma_2 = 1/\sqrt{24}$, respectively; these compare favorably with $\sigma_2 = 1/\sqrt{2}, \sigma_2 = 1/\sqrt{6}$ for the two-shot estimators without stratified sampling.

Exercise. Write and run a Monte Carlo program to calculate π using $\pi = \text{area of unit circle} = \iint dx dy f(x^2 + y^2)$ where $f(z) = 1$ for $z < 1$ and $f(z) = 0$ otherwise. See for yourself how slowly it converges. Do one of the integrals by hand and see how much better the approximation becomes. Alternatively, try Stratified Sampling. This is a poor way to calculate π but instructive about Monte Carlo.

11.2 First Example: $c \rightarrow se\nu$ Decay

Let us calculate the semileptonic decay of a charmed hadron in the spectator approximation (§3.4.1), where the charmed quark decays as if it were free. The $c \rightarrow s$ mode is favored by the Cabibbo mixing. We shall retain explicit e and ν masses in this example, so that it can be adapted to related processes like $b \rightarrow c\tau\bar{\nu}, b \rightarrow cs\bar{c}$ with two or three massive final particles.

The partial width for $c \rightarrow se\nu$ decay is

$$\Gamma = \frac{1}{2m_c} \int |\mathcal{M}|^2 \prod_{i=1}^3 \frac{d^3 p_i}{2E_i} (2\pi)^{-5} \delta^4(p_c - p_1 - p_2 - p_3)$$

where momenta p_1, p_2, p_3 refer to s, e, ν , respectively; $|\mathcal{M}|^2$ is the matrix element squared and spin-averaged. It is convenient to evaluate the invariant $d^3 p_1/E_1$ in the c -rest frame where it can be written

$$d^3 p_1/E_1 = p_1^2 dp_1 d\phi_1 d\cos\theta_1/E_1 = (2\pi p_1 p_{1\max}^2/E_1) dx_1 dx_2 dx_3$$

where x_1, x_2, x_3 are integration variables scaled to the range (0, 1)

as follows:

$$p_1^2 = x_3 p_{1\max}^2, \quad \cos \theta_1 = 1 - 2x_2, \quad \phi_1 = 2\pi x_1$$

and $p_{1\max}$ is the maximum accessible value of p_1

$$p_{1\max}^2 = \lambda(m_c^2, m_s^2, (m_e + m_\nu)^2) / (4m_c^2)$$

with λ the usual triangular function, familiar in kinematics,

$$\lambda(a, b, c) = a^2 + b^2 + c^2 - 2ab - 2bc - 2ca.$$

The $e\nu$ invariant mass m_{23} is related to $E_1 = (p_1^2 + m_s^2)^{1/2}$ by

$$m_{23}^2 = (p_c - p_1)^2 = m_c^2 + m_s^2 - 2m_c E_1.$$

We evaluate the remaining invariant phase space factors in the $e\nu$ rest-frame. The total energy in this frame is m_{23} and the momenta are $p_2^2 = p_3^2 = \lambda(m_{23}^2, m_e^2, m_\nu^2) / (4m_{23}^2)$. After integrating out the δ -function, we can write

$$\frac{d^3 p_2 d^3 p_3 \delta^4}{E_2 E_3} = \frac{p_2^2 d \cos \theta_2 d\phi_2}{E_2 E_3} \frac{dp_2}{d(E_2 + E_3)} = \frac{4\pi p_2}{m_{23}} dx_4 dx_5$$

where $\cos \theta_2 = 1 - 2x_5$, $\phi_2 = 2\pi x_4$ and x_4, x_5 run from 0 to 1.

The spin- and color-averaged matrix element squared is

$$|\mathcal{M}|^2 = 64 G_F^2 (p_c \cdot p_e)(p_s \cdot p_\nu) M_W^4 / \left[(m_{23}^2 - M_W^2)^2 + \Gamma_W^2 M_W^2 \right].$$

The W -propagator factor will be important if we use these formulas for heavier quarks like t . $|\mathcal{M}|^2$ can be evaluated in the $e\nu$ rest frame, where c, s have the same collinear 3-momentum p_c given by

$$p_c^2 = \lambda(m_{23}^2, m_c^2, m_s^2) / (4m_{23}^2).$$

Let us pause for a moment to think about Importance Sampling and the best choice of integration variables. The matrix element is innocuous in the present case, so we concentrate on the

phase space factors. The angular parts $d \cos \theta_1 d\phi_1 d \cos \theta_2 d\phi_2 = 16\pi^2 dx_2 dx_3 dx_4 dx_5$ are straightforward and introduce no variable factors in the integrand. The variable factor p_2/m_{23} above reduces to $1/2$ in the massless limit $m_2 = m_3 = 0$; we do not attempt to absorb this factor into the integration variables. There remain the factors $p_1^2 dp_1/E_1$; if we simply choose dp_1 as the integration variable, the factors p_1^2/E_1 remain in the integrand. A better choice is $d(m_{23}^2) = 2m_c dE_1 = 2m_c p_1 dp_1/E_1$ which absorbs all the variable factors except p_1 . Alternatively, we can choose the variable $d(p_1^2) = 2p_1 dp_1$ which absorbs p_1 but leaves p_1/E_1 ; the latter is unity for $m_1 = 0$, making this an ideal choice in the massless limit. This is precisely what we did above, in introducing x_3 .

We can now write a Fortran subroutine that will sample the integrand of Γ with respect to the integration variables $x_1 \dots x_5$. We can use it simply to evaluate Γ , or to study the distributions of decay products, or—as part of a bigger program—to generate $c \rightarrow se\nu$ decay (or other decays with similar matrix elements) when required. The program is written using the FORTRAN-77 standard with the extension of allowing lower-case letters. The notation is fairly transparent. We declare `m` to be floating-point, and `mc, ms = mc, ms`, etc. denote masses; `pie = π` ; `pmax2 = p12max`; the electron four-momentum is written `ee, ex, ey, ez` and similarly for other particles; ν is labeled `g` (for `gnu`) since we want `n` for integer use. We suppose the random number generator is called `rand(0)` and add a function subroutine `alam(a,b,c)` for $\lambda(a,b,c)$. Double precision is desirable in some applications with high-energy kinematics but is omitted here for speed and simplicity.

```

subroutine cdec (mc, ms, me, mg, w, se, sx, sy, sz,
*              ee, ex, ey, ez, ge, gx, gy, gz)
implicit real(m)
c generates c to s + e + gnu (denoted g) in c rest frame,
c weight w
Gf = 1.166*0.1**5
pie = 3.14159
```

```

mw = 81
gw = 2.5
c start in c rest frame
  pmax2 = alam(mc**2, ms**2, (me+mg)**2)/(4*mc**2)
  plsq = pmax2*rand(0)
  p1 = sqrt(plsq)
  e1 = sqrt(plsq + ms**2)
  m23 = sqrt(mc**2 + ms**2 - 2*mc*e1)
c now work in eg rest frame; assume boosted along z-axis.
  pesq = alam(m23**2, me**2, mg**2)/(4*m23**2)
  pe = sqrt(pesq)
  ee = (m23**2 + me**2 - mg**2)/(2*m23)
  costh = 1 - 2*rand(0)
  sinth = sqrt(1 - costh**2)
  phi = 2*pie*rand(0)
  ex = pe*sinth*sin(phi)
  ey = pe*sinth*cos(phi)
  ez = pe*costh
  ge = m23 - ee
  gx = - ex
  gy = - ey
  gz = - ez
  pcsq = alam(m23**2, mc**2, ms**2)/(4*m23**2)
  ce = (mc**2 - ms**2 + m23**2)/(2*m23)
  cz = sqrt(pcsq)
  se = ce - m23
  sz = cz
c matrix element squared and averaged
c Gf in units gev**(-2)
  msq = 64*Gf**2*(ce*ee - cz*ez)*(se*ge - sz*gz)
c for very heavy mc, include w-propagator, too
  msq = msq*mw**4/((m23**2 - mw**2)**2 + (mw*gw)**2)
  w = msq*p1*pmax2*pe/(64*pie**3*mc*e1*m23)
c boost back to c rest frame.
    
```

```
c b. g, bg = beta, gamma, beta*gamma
```

```
g = ce/mc
```

```
bg = - cz/mc
```

```
b = bg/g
```

```
ee = ee*g + ez*bg
```

```
ge = ge*g + gz*bg
```

```
ez = ee*b + ez/g
```

```
gz = ge*b + gz/g
```

```
c randomize orientation in c-restframe
```

```
ct = 1 - 2*rand(0)
```

```
st = sqrt(1 - ct**2)
```

```
phi = 2*pie*rand(0)
```

```
cp = cos(phi)
```

```
sp = sin(phi)
```

```
ez = ez*ct - ey*st
```

```
gz = gz*ct - gy*st
```

```
ey = (ez*st + ey)/ct
```

```
gy = (gz*st + gy)/ct
```

```
ex = ex*cp - ey*sp
```

```
gx = gx*cp - gy*sp
```

```
ey = (ex*sp + ey)/cp
```

```
gy = (gx*sp + gy)/cp
```

```
se = mc - ee - ge
```

```
sx = -ex - gx
```

```
sy = -ey - gy
```

```
sz = -ez - gz
```

```
return
```

```
end
```

```
c
```

```
function alam(a,b,c)
```

```
alam = a**2 + b**2 + c**2 - 2*a*b - 2*b*c - 2*c*a
```

```
return
```

```
end
```

This program simply calculates the integrand in the decay width formula, plus the four-momenta for each random point. The boosts and angular rotations may look strange at first; this is because we retain the same symbols for the boosted (rotated) components. Thus, for example, the first boost transformation $E' = \gamma E + \beta \gamma p_z$ looks standard, but the second transformation $p'_z = \beta \gamma E + \gamma p_z$ has to be written in terms of the new boosted E' and comes out as $p'_z = \beta E' + p_z/\gamma$. The last 24 lines which boost back to the c rest-frame and randomize orientation are needed if we want to generate real events, but not if we simply want to integrate Γ .

Suppose now that we just wish to calculate Γ by Monte Carlo. Here is a main routine to do this. It begins by defining masses and the number of shots n . We choose here m_c, m_s to equal the D, K meson masses, so that we have the correct kinematics (though not necessarily the exact width) for $D \rightarrow Ke\nu$ decay. It then calls `cdec` n times, generating random events with weights W , and calculates the average. As an embellishment, this particular program also calculates the n -shot standard deviation. The print-out is minimal.

```

implicit real(m)
mc = 1.87
ms = 0.50
me = 0
mg = 0
n = 1000
print 1, mc, ms, me, mg, n
1 format(' mc, ms, me, mg, n = ', 4f5.2, i6)
gamma = 0
var = 0
do 2 j = 1,n
call cdec(mc, ms, me, mg, w, a, b, c, d, e, f, g,
*          h, p, q, r, s)
gamma = gamma + w/n
2 var = var + w**2/n
var = var - gamma**2

```

```

sd = sqrt(var/n)
print 3, gamma, sd
3 format(' gamma, sd = ', 2e12.4, ' gev ')
stop
end

```

Now suppose we want distributions of decay particles from $D \rightarrow K e \nu$ in the laboratory, where D has momentum components dx , dy , dz . The previous subroutine generates decay momenta in the D rest frame, so we now need a subroutine to boost a typical 4-momentum ee , ex , ey , ez from here to the lab.

```

subroutine boost (md, dx, dy, dz, ee, ex, ey, ez)
real*4 md
c boost e-mom from d-rest to lab; pd=dx,dy,dz
c rotate z-axis to d-direction, boost, rotate back
c define boost and angles; avoid theta = 0 ambiguities;
c ct = cos(theta), cps = cos(phi)sin(theta), etc.
  bg = sqrt(dx**2 + dy**2 + dz**2)/md
  g = sqrt(1 + bg**2)
  ct = dz/(md*bg)
  cps = dy/(md*bg)
  sps = dx/(md*bg)
  rz = ex*sps + ey*cps + ez*ct
  ee = ee*g + rz*bg
  rz = ee*bg/g + rz/g
  rx = ex*(1-sps**2)-ey*sps*cps-ez*sps*ct+rz*sps
  ry = -ex*sps*cps+ey*(1-cps**2)-ez*cps*ct+rz*cps
  ez = -ex*sps*ct-ey*cps*ct+ez*(1-ct**2)+rz*ct
  ey = ry
  ex = rx
return
end

```

A main routine to calculate the energy-distributions of K , e and ν from the decay of an initial D with momentum 20 GeV/c could

be as follows. We set up a 3×25 array of bins; the first index labels the particle (1, 2, 3 = K, e, ν) and the second labels its energy in 1 GeV bins going from (0-1 GeV) up to (24-25 GeV). Bins are initially set to zero. We then generate decay events, boost them to the lab frame, and accumulate their weights in the appropriate bins. Finally we normalize each distribution such that the sum of bin weights is unity, and print them out in columns. For good measure, we also calculate the n -shot standard deviation on each bin (calling it *err*) and print it next to the bin value.

```

dimension bin(3,25), err(3,25), nb(3)
real*4 ke, kx, ky, kz, md, mk
c calculate energy distributions from d - k, e.
c gnu decay in flight
md = 1.87
mk = 0.50
dz = 20
n = 10000
print 1, md, mk, dz, n
1 format (' md, mk, dz, n = ', 2f5.2, f5.1, i6)
gamma = 0
do 2 i = 1,3
do 2 j = 1,25
err(i,j) = 0
2 bin(i,j) = 0
do 4 i = 1,n
call cdec (md, mk, 0.0, 0.0, w, ke, kx, ky, kz,
*          ee, ex, ey, ez, ge, gx, gy, gz)
call boost (md, 0.0, 0.0, dz, ke, kx, ky, kz)
call boost (md, 0.0, 0.0, dz, ee, ex, ey, ez)
call boost (md, 0.0, 0.0, dz, ge, gx, gy, gz)
c possible acceptance cuts can be inserted here
c sort each event into appropriate bin numbers nb(i),
nb(1) = ke + 1
nb(2) = ee + 1

```

```

nb(3) = be + 1
do 3 j = 1,3
bin(j,nb(j)) = bin(j,nb(j)) + w/n
3 err(j,nb(j)) = err(j,nb(j)) + w**2/n
gamma = gamma + w/n
4 continue
do 6 j = 1,25
do 5 i = 1,3
err(i,j) = err(i,j) - bin(i,j)**2
err(i,j) = sqrt(err(i,j)/n)/gamma
5 bin(i,j) = bin(i,j)/gamma
6 print 7, j, (bin(i,j), err(i,j), i = 1,3)
7 format (i4, 6e12.4)
stop
end

```

If there are experimental acceptance cuts to insert (*e.g.* requiring one of the particles to hit a given detector) they can go in as if statements at the place indicated. If a given shot fails the cut, go to 4 and do not accumulate its weight; gamma will not then be the true width but simply a normalizer.

11.3 $B\bar{B}$ Production with Cascade Decays

For another example, consider an e^+e^- collider such as CESR running on the $\Upsilon(4S)$ resonance, producing pseudoscalar B^+B^- and $B^0\bar{B}^0$ meson pairs almost at rest; for simplicity take them exactly at rest. We can use *cdec* and *boost* to simulate the $\bar{B} \rightarrow D$ decays by effective $b \rightarrow ce\bar{\nu}$, $b \rightarrow c\mu\bar{\nu}$, $b \rightarrow cd\bar{u}$, *etc.* transitions (assuming the spectator decay model); the difference in decay matrix element is compensated if we interchange the $e, \bar{\nu}$ 4-momenta compared to the $c \rightarrow s\bar{e}\nu$ case and adjust the masses. Subsequent D -decay can be simulated as before. There is no spin correlation between \bar{B} and D

decays, since in each case it is the lightest (pseudoscalar) state that undergoes weak decay, so they can be treated as independent steps.

Consider the electrons from semileptonic decays. There are four principal sources of electrons that we characterize by

$$\begin{aligned} \bar{B} &\rightarrow D e^{-} \bar{\nu}, & B &\rightarrow \bar{D} e^{+} \nu, \\ \bar{B} &\rightarrow D \rightarrow \bar{K} e^{+} \nu, & B &\rightarrow \bar{D} \rightarrow K e^{-} \bar{\nu}, \end{aligned}$$

(neglecting the $b \rightarrow c\tau\bar{\nu}$, $cs\bar{c}$ and all $b \rightarrow u$ channels for simplicity). A Monte Carlo simulator can start with \bar{B} at rest, make $\bar{B} \rightarrow DEG$ and $D \rightarrow \bar{K}QR$ successive decays; here E, G can stand either for $e, \bar{\nu}$ or for d, \bar{u} —the kinematics and the matrix elements are the same (within a constant color factor); similarly Q, R can stand either for e^{+}, ν or \bar{d}, u . If we require two-lepton correlations, a simultaneous decay chain for the B meson must be generated, but if we simply want the single-lepton spectrum it is enough to look at \bar{B} —since B decays on average will just be the same (charge-conjugate counterpart). Here is a main routine to get the single-electron spectrum, summing over e^{+} and e^{-} , assuming semileptonic branching fractions 10% and 12% for D and B decays, respectively.

```

dimension bin(20)
real*4 ke, kx, ky, kz, mb, md, mk
c electron spectrum from b decay at rest
mb = 5.27
md = 1.87
mk = 0.50
n = 10000
sum = 0
do 1 i = 1,20
1 bin(i) = 0
do 2 i = 1,n
call cdec (mb, md, 0.0, 0.0, wb, de, dx, dy, dz,
*          ge, gx, gy, gz, ee, ex, ey, ez)
call cdec (md, mk, 0.0, 0.0, wd, ke, kx, ky, kz,
```

```

*          qe, qx, qy, qz, re, rx, ry, rz)
  call boost (md, dx, dy, dz, qe, qx, qy, qz)
  w = wb*wd
c collect weights in bins and sum for normalization
  sum = sum + 0.22*w
  ne = ee/0.25 + 1
  nq = qe/0.25 + 1
  bin(ne) = bin(ne) + 0.12*w
2 bin(nq) = bin(nq) + 0.10*w
  do 3 i = 1,20
  bin(i) = bin(i)/sum
3 print 4, i, bin(i)
4 format (i4, e12.4)
  stop
end

```

This program collects e -energies in 20 bins of 0.25 GeV going from 0-0.25 up to 4.75-5.0 GeV; those of B -decay and D -decay origin are weighted accordingly and the whole distribution is normalized to unity. This is an inclusive distribution, which means that events with n electrons are counted n times.

A physics remark. In the program above, the c -quark coming from $b \rightarrow c$ decay has essentially turned into a D -meson with the same momentum vector as the quark, i.e. it has a hard fragmentation function $D(z) \approx \delta(1-z)$. This actually seems to be indicated by data. It is unlike deep inelastic scattering, where c -fragmentation is softer and the momentum fraction carried by the D -meson would be only 60% on average; b -decay is apparently not a deep inelastic situation.

Exercise. Devise instructions to generate the electron spectra from $b \rightarrow cs\bar{c}$, $c \rightarrow s\nu\bar{e}$, $\bar{c} \rightarrow \bar{s}e\nu$ and from $b \rightarrow c\tau\bar{\nu}$, $c \rightarrow s\nu\bar{e}$, $\tau \rightarrow e\nu\bar{\nu}$ decay chains. Subroutines `cdec` and `boost` and the $\tau \rightarrow e\nu\bar{\nu}$ branching fraction 0.18 are all we need, so long as we assume the spectator picture for decays.

11.4 Stratified Sampling

In the examples above, the random numbers corresponding to x_1, \dots, x_n have been generated independently by `rand` one at a time. If, however, we wish to use an external Importance Sampling program, it will be necessary to generate all x_i together to keep track of which is which. Similarly with Stratified Sampling; with p subdivisions we would have p^n hypercubes in x_i space to be sampled in succession, requiring an x_i -generator that follows a p^n -shot cycle.

It is simple but instructive to illustrate such a Stratified Sampling generator. We suppose that $ne =$ (event number), $nx =$ (number of x_i required) and $p =$ (number of subdivisions) are specified, and that the random variables $x(1), \dots, x(nx)$ are to be transferred via a common block. The strategy is to put $x(1)$ in the 1st, 2nd, ..., p th subdivision of the range (0, 1) according to whether $ne \bmod p$ is 0, 1, ..., $(p-1)$. Similarly we put $x(2)$ in the 1st, 2nd, etc. subdivision if $[ne \bmod p^2]/p$ has integral part 0, 1, ..., etc. For $x(nx)$ we subdivide according to the integral part of $[ne \bmod p^{nx}]/p^{nx-1}$. The instruction call `strat (ne,nx,p)` will suffice, with the following subroutine which gets its input random numbers from an assumed source `rand` as before.

```
subroutine strat (ne, nx, p)
integer p
common/xvar/x(10)
```

`c` generates nx stratified random variables, $nx \leq 10$

`c` with p equal subdivisions in each $x(i)$

```
dx = 1./p
do 1 i = 1, nx
ic = mod(ne, p**i)/p**(i-1)
1 x(i) = dx*(rand(0)+ic)
return
end
```



With such a generator, we call strat at the beginning of each event and simply replace the individual rand(0) factors in the Monte Carlo by the appropriate x(i) variables remembering to include the common/xvar/block where the x(i) are used. Remember also that the total number of events should be a multiple of p**nx.

11.5 Many-Body Phase Space

The methods above for 3-body decays can be generalized to handle n -body integrals such as

$$I_n = \int I \prod_{j=1}^n \frac{d^3 p_j}{(2\pi)^3 2E_j} (2\pi)^4 \delta^4 \left(p_0 - \sum_{j=1}^n p_j \right).$$

Here I is some unspecified integrand which for the present we ignore. It is convenient to evaluate the invariant $d^3 p_j/E_j$ in the c.m. frame of the particles $j, j+1, \dots, n$, and to evaluate the last two momenta plus the δ -function $d^3 p_{n-1} d^3 p_n \delta^4/(E_{n-1} E_n)$ all together in the c.m. frame of particles $n-1, n$. We can set up a simple iterative procedure to do this, accumulating the appropriate weight factors along the way, as follows.

- (1) Start in the c.m. frame of $1, 2, \dots, n$: call this Frame 1. Denote the invariant mass of $1, 2, 3, \dots, n$ by \tilde{m}_1 ; it is their overall c.m. energy. Similarly denote the invariant mass of $2, 3, \dots, n$ by \tilde{m}_2 ; its kinematic limits are $\tilde{m}_1 - m_1 > \tilde{m}_2 > m_2 + m_3 + \dots + m_n$. The corresponding value of p_1 in Frame 1 is

$$p_1 = \lambda^{1/2} (\tilde{m}_1^2, m_1^2, \tilde{m}_2^2) / (2\tilde{m}_1)$$

The choice of angular integration variables is obvious but the momentum variable is not: it could be p_1^2 or p_1 or $\tilde{m}_2 \dots etc.$ For n -body phase space it turns out that \tilde{m}_2 (and in general \tilde{m}_{j+1} for the $d^3 p_j/E_j$ integration) is a happy choice, because

the integrand stays relatively smooth and the limits of integration are easy to handle—thanks to a simple trick. We scale the momentum and angle variables to the range $(0, 1)$ by defining

$$\phi_1 = 2\pi x_1, \quad \cos \theta_1 = 1 - 2x_2, \quad \tilde{m}_2 = \sigma_2 + (\tilde{m}_1 - \sigma_1) x_3,$$

where $\sigma_i = m_i + m_{i+1} + \dots + m_n$. The invariant becomes

$$\frac{d^3 p_1}{(2\pi)^3 2E_1} = \frac{dx_1 dx_2 dx_3 p_1 (\tilde{m}_1 - \sigma_1) \tilde{m}_2}{4\pi^2 \tilde{m}_1}.$$

- (2) Now go on to the next factor, in precisely the same way. For the j th factor we are in Frame j , the c.m. frame of $j, j+1, \dots, n$ with total c.m. energy \tilde{m}_j . We define \tilde{m}_{j+1} to be the invariant mass of $j+1, j+2, \dots, n$ with kinematical limits $\tilde{m}_j - m_j > \tilde{m}_{j+1} > \sigma_{j+1}$. The corresponding momentum p_j is

$$p_j = \lambda^{1/2} (\tilde{m}_j^2, m_j^2, \tilde{m}_{j+1}^2) / (2\tilde{m}_j)$$

and we can rescale variables by

$$\begin{aligned} \phi_j &= 2\pi x_{3j-2}, & \cos \theta_j &= 1 - 2x_{3j-1}, \\ \tilde{m}_{j+1} &= \sigma_{j+1} + (\tilde{m}_j - \sigma_j) x_{3j}. \end{aligned}$$

to express the j th invariant factor as

$$\frac{d^3 p_j}{(2\pi)^3 2E_j} = \frac{dx_{3j} dx_{3j-1} dx_{3j-2} p_j (\tilde{m}_j - \sigma_j) \tilde{m}_{j+1}}{4\pi^2 \tilde{m}_j}.$$

- (3) Finally, for the last two factors we find ourselves in Frame $n-1$, the c.m. frame of particles $n-1, n$ with invariant mass \tilde{m}_{n-1} . The momenta are uniquely defined by

$$p_{n-1} = p_n = \lambda^{\frac{1}{2}} (\tilde{m}_{n-1}^2, m_{n-1}^2, m_n^2) / (2\tilde{m}_{n-1})$$

with corresponding energies E_{n-1}, E_n . The δ -function removes 4 degrees of freedom leaving purely an angular integration, just

as in the final stage of the $c \rightarrow se\nu$ example above. Rescaling the angular variables by

$$\phi_{n-1} = 2\pi x_{3n-5}, \quad \cos \theta_{n-1} = 1 - 2x_{3n-4},$$

we obtain the final factors

$$d^3 p_{n-1} d^3 p_n \delta^4 / [(2\pi)^2 4E_{n-1} E_n] = dx_{3n-5} dx_{3n-4} p_{n-1} / (4\pi \tilde{m}_{n-1}).$$

We have thus re-expressed the n -body phase space integral I_n as an integral over $dx_1 \dots dx_{3n-4}$ multiplied by a product of weight factors, which reduces to

$$I_n = \left(\frac{\tilde{m}_1 - \sigma_1}{4\pi^2} \right)^{n-2} \frac{1}{4\pi \tilde{m}_1} \int_0^1 dx_1 \dots dx_{3n-4} I \prod_{j=1}^{n-1} p_j.$$

All that remains is to ensure that the \tilde{m}_j variables above obey the chain of kinematic constraints (for $j = 1, 2, \dots, n-1$)

$$\tilde{m}_j > \tilde{m}_{j+1} + m_j.$$

The alert reader may have noticed that the relationship above between \tilde{m}_j and the random variable x_{3j} automatically satisfies the extreme upper and lower bounds $\tilde{m}_1 - \sigma_1 + \sigma_j > \tilde{m}_j > \sigma_j$ but does *not* necessarily satisfy the chain constraints. The latter are satisfied if and only if the x_{3j} values are ordered:

$$x_3 > x_6 > \dots > x_{3n-6}.$$

We could therefore generate sets of random numbers x_k but keep only that fraction (namely $1/(n-2)!$) of sets that satisfy the constraint. Or, much better, we can take whatever random numbers we get and simply reorder the subset x_{3j} ($j = 1, \dots, n-2$) to satisfy this criterion. This is much more economical, but we must then divide the weight factor by $(n-2)!$ to compensate.

A Monte Carlo program can be set up to generate random events in phase space, with their appropriate weight factors, following the iterative approach above. For initial conditions, we need to know the invariant mass \tilde{m}_1 of the system $1 + 2 + \dots + n$, its net momentum \vec{K}_1 and hence its energy \tilde{E}_1 in the lab frame. Random choices of x_1, x_2, x_3 define the momentum of particle 1 in Frame 1, and equally give the mass \tilde{m}_2 and momentum of the recoiling system $2 + 3 + \dots + n$ in this frame. A Lorentz boost defined by $\vec{\beta} = \vec{K}_1 / \tilde{m}_1$ converts these momenta to the lab frame. We now have \tilde{m}_2, \vec{K}_2 , and \tilde{E}_2 which are the required initial conditions to evaluate what happens in Frame 2. And so on up to Frame $n - 1$ where finally \vec{p}_{n-1} and \vec{p}_n are chosen and boosted back to the laboratory.

In the following Fortran subroutines we suppose that an external program has already defined the number of particles n , their masses m_i , their overall invariant mass \tilde{m}_1 , their overall energy \tilde{E}_1 and lab momentum \vec{K}_1 . For convenience, the kinematical quantities $\text{pie} = \pi, n = n, \text{m}(i) = m_i, \text{mt}(i) = \tilde{m}_i, \text{ms}(i) = \sigma_i, \text{p}(i, j) = (E_i, p_{ix}, p_{iy}, p_{iz})$, and $\text{k}(i, j) = (\tilde{E}_i, K_{ix}, K_{iy}, K_{iz})$ are held in a common block. We start with a controlling subroutine **phase**; it calls **xvalue** to provide $3n - 4$ random numbers $x(i) = x_i$ in the range $(0, 1)$, which are stored in common block, and then calls **order** to place the subset $x_{3j}, j = 1, 2, \dots, n - 2$ in descending order; these two subroutines are best handled by invoking library subroutines, different for each computer, so we do not specify them here. Then for successive steps $j = 1, 2, \dots, n - 2$, **phase** calls a subroutine **gen(j)** to generate random \tilde{m}_{j+1} and hence \vec{p}_j in Frame j , followed by subroutine **boo(j)** to boost \vec{p}_j to the lab frame and to calculate E_j and the lab recoil momentum \vec{K}_{j+1} . For the final step $j = n - 1$, **gen** generates the fixed final momentum p_{n-1} with random orientation in Frame $n - 1$, followed by **boo(n - 1)** to boost it to the lab and calculate \vec{K}_n —which is precisely \vec{p}_n in the lab. At each step the appropriate factors are added to the phase-space weight **wps** with a piece of the re-ordering normalization $1/(n - 2)!$. The necessary mass sub-sums $\text{ms}(i)$ are computed in **phase**. The subroutines **gen** and

boo contain instructions to make the necessary adjustments on the final step.

```

subroutine phase
  implicit real*4(k,m)
  common/kin/wps, pie, n, m(10), mt(10), ms(10),
*      p(10,4), k(10,4)
c generates n-body events (n.le.10)
c with phase space weight = wps
  ms(1) = 0
  do 1 i = 1,n
1  ms(1) = ms(1) + m(i)
  call xvalue
  call order
  jmax = n - 1
  wps = jmax*((mt(1)-ms(1))/(4*pie**2))**(n-2)/
*      (4*pie*mt(1))
  do 2 j = 1, jmax
  wps = wps/j
  ms(j+1) = ms(j) - m(j)
  call gen(j)
2  call boo(j)
  return
end

```

```

subroutine gen(i)
  implicit real*4(k,m)
  common/kin/wps, pie, n, m(10), mt(10), ms(10),
*      p(10,4), k(10,4)
  common/xvar/x(30)
c generates p(i,j) and mt(i+1) in frame i.
  if (i.eq.n-1) then
    mt(i+1) = m(n)
  else
    mt(i+1) = ms(i+1) + (mt(1)-ms(1))*x(3*i)

```

```

end if
psq = alam(mt(i)**2, m(i)**2, mt(i+1)**2)
ei = sqrt(psq+m(i)**2)
pi = sqrt(psq)
cost = 1-2*x(3*i-1)
sint = sqrt(1-cost**2)
phi = 2*pie*x(3*i-2)
p(i,1) = ei
p(i,2) = pi*sint*sin(phi)
p(i,3) = pi*sint*cos(phi)
p(i,4) = pi*cost
wps = wps*pi
return
end

```

```

subroutine boo(i)
implicit real*4(k,m)
common/kin/wps, pie, n, m(10), mt(10), ms(10),
*      p(10,4), k(10,4)
c boosts p(i) from frame i to lab, given mt(i) and k(i,...)
c successive x,y,z boost parameters
bg1 = k(i,2)/mt(i)
g1 = sqrt(1 + bg1**2)
bg2 = k(i,3)/(mt(i)*g1)
g2 = sqrt(1 + bg2**2)
bg3 = k(i,4)/(mt(i)*g1*g2)
g3 = sqrt(1 + bg3**2)
e = g1*g2*g3*p(i,1) + bg1*g2*g3*p(i,2)
*   + bg2*g3*p(i,3) + bg3*p(i,4)
x = bg1*p(i,1)+g1*p(i,2)
y = bg2*g1*p(i,1)+bg2*bg1*p(i,2)+g2*p(i,3)
z = bg3*g2*g1*p(i,1) + bg3*g2*bg1*p(i,2)
*   + bg3*bg2*p(i,3) + g3*p(i,4)
p(i,1) = e

```

```

p(i,2) = x
p(i,3) = y
p(i,4) = z
c defines k(i+1) in lab = p(n) on final step
  if (i.eq.n-1) go to 2
  do 1 j = 1,4
1 k(i+1,j) = k(i,j) - p(i,j)
  return
2 do 3 j = 1,4
3 p(n,j) = k(i,j) - p(i,j)
  return
end

```

To summarize, the command call phase will generate one random n -body event with phase space weighting wps . But π and the number n , the masses m , the overall invariant mass $mt(1)$ and net lab momentum $k(1, \dots)$ must first be specified in the common block.

Exercise. Write a program to calculate the decay of a particle of mass 1 GeV, moving with lab energy 20 GeV, into n zero-mass particles with pure phase-space distribution. Study the lab energy of a decay particle near the maximum energy $E_{\max} = 10(1 + \sqrt{399/400})$ GeV and see if it obeys a power law $dN/dx \sim (1-x)^\alpha$ where $x = E/E_{\max}$. We expect the power α to increase with n , because achieving large x requires the $n-1$ other particles to have small x simultaneously, which becomes more unlikely as n increases.

11.6 $p\bar{p} \rightarrow e^+e^- X$ Drell-Yan Pair Production

The lowest-order parton subprocess $q\bar{q} \rightarrow e^+e^-$ has cross section

$$d\hat{\sigma}(q\bar{q} \rightarrow e^+e^-) = \frac{\alpha^2 e_q^2}{12\hat{s}} (1 + \cos^2\theta) d\cos\theta d\phi$$

where θ and ϕ are c.m. scattering angles, e_q is the quark charge, after summing final spins and averaging initial spins and colors. The

corresponding $p\bar{p}$ cross section is found by integrating over the distributions of quarks and antiquarks in the incident hadrons:

$$d\sigma(p\bar{p} \rightarrow e^+e^-X) = \int d\xi_1 d\xi_2 \sum_q [(q_1(\xi_1)\bar{q}_2(\xi_2) + \bar{q}_1(\xi_1)q_2(\xi_2))] d\hat{\sigma}(q\bar{q} \rightarrow e^+e^-).$$

Here the indices $i = 1, 2$ refer to proton, antiproton, respectively; ξ_i are the parton momentum fractions and q_i, \bar{q}_i are the quark, antiquark distributions in hadron i , summed over flavors q .

The quark distributions peak approximately like ξ^{-1} at small ξ ; also, the subprocess cross section contains $\hat{s}^{-1} = (\xi_1 \xi_2 s)^{-1}$. Together these give a factor $(\xi_1 \xi_2)^{-2}$ that can conveniently be absorbed by choosing integration variables $d(\xi_i^{-1}) = -d\xi_i/\xi_i^2$. (This is for the case of low-mass pairs; for high masses the Z pole contribution should be added to $d\hat{\sigma}$ and then $\ln \xi_i$ or even plain ξ_i would be better integration variables; for emphasizing the Z pole, an arctan variable is best—see below.) Similar methods can be used to calculate cross sections with an extra parton, such as $q\bar{q} \rightarrow e^+e^-g$, but here we illustrate the lowest-order $2 \rightarrow 2$ case for simplicity.

A Monte Carlo calculation of low-mass Drell-Yan pairs can proceed as follows. First define s and choose a minimum e^+e^- pair mass m_0 (to avoid the singularity in $d\hat{\sigma}$). Then choose random ξ_1^{-1}, ξ_2^{-1} in the ranges

$$1 \leq \xi_1^{-1} \leq s/m_0^2, \quad 1 \leq \xi_2^{-1} \leq \xi_1 s/m_0^2.$$

by setting

$$\begin{aligned} \xi_1^{-1} &= 1 + \Delta_1 x_1, & \Delta_1 &= s/m_0^2 - 1, \\ \xi_2^{-1} &= 1 + \Delta_2 x_2, & \Delta_2 &= \xi_1 s/m_0^2 - 1. \end{aligned}$$

This fixes a dilepton mass squared $m^2 = \hat{s} = \xi_1 \xi_2 s$ and longitudinal momentum $p_L = \frac{1}{2}(\xi_1 - \xi_2)\sqrt{s}$ along the proton direction (assuming

collinear colliding beams). Choose random $\cos \theta$ and ϕ in the c.m. frame by $\cos \theta = 1 - 2x_3$, $\phi = 2\pi x_4$ as usual and finally boost the event momenta to the lab frame. This configuration has net weight in the cross section integral

$$W = \frac{\pi\alpha^2}{3s} (1 + \cos^2\theta) \xi_1 \xi_2 \Delta_1 \Delta_2 \sum_q e_q^2 [q_1(\xi_1) \bar{q}_2(\xi_2) + \bar{q}_1(\xi_1) q_2(\xi_2)] .$$

The following main routine will do all this, integrate the total cross section, divide it into mass bins for the pairs and lab energy and angle bins for the single electrons. We suppose that for given ξ and QCD scale Q^2 the u , d , s , \bar{u} , \bar{d} , \bar{s} distributions in the proton are given by a subroutine `prot(xi, qsq, u, d, s, ub, db, sb)`; we choose $Q^2 = \hat{s} = m^2$. The boost subroutine boosts to the lab. For illustration we take $n = 10^4$ shots with $\sqrt{s} = 2000$ GeV, $m_0 = 1$ GeV for the cutoff, 40 mass bins 1 GeV wide, 40 p_e bins 10 GeV wide, 40 θ_e bins 5° wide (of which only 36 get used); p_e and θ_e are averaged over e^\pm ; events with bin number > 40 are assigned to bin number 40. The (ee, ex, ey, ez) and (pe, px, py, pz) are electron and positron energy-momentum vectors.

```

      implicit real*4(m)
c Drell-Yan pair production cross section
      dimension bin (3,40), nbin(5)
      alpha = 1./137
      pie = 3.14159
      rts = 2000
      mzero = 1
      n = 10000
      do 1 i = 1,3
      do 1 j = 1,40
1 bin(i,j) = 0
      sigma = 0
      del1 = (rts/mzero)**2 - 1
c generate n events; start in pair cm frame

```

```

do 4 i = 1,n
xi1 = 1/(1 + del1*rand(0))
del2 = xi1*(del1 + 1) - 1
xi2 = 1/(1 + del2*rand(0))
m = sqrt(xi1*xi2)*rts
cost = 1 - 2*rand(0)
sint = sqrt(1 - cost**2)
phi = 2*pie*rand(0)
ee = m/2
ex = ee*sint*cos(phi)
ey = ee*sint*sin(phi)
ez = ee*cost
pe = ee
px = -ex
py = -ey
pz = -ez
c calculate weight of event
qsq = m**2
call prot(xi1,qsq,u1,d1,s1,ub1,db1,sb1)
call prot(xi2,qsq,u2,d2,s2,ub2,db2,sb2)
w =
* pie*alfa**2*(1+cost**2)*xi1*xi2*del1*del2/rts**2/3
* *(4*(u1*u2+ub1*ub2)+d1*d2+db1*db2+s1*s2+sb1*sb2)/9
c boost to lab frame
pl = rts*(xi1-xi2)/2
call boost(m,0.0,0.0,pl,ee,ex,ey,ez)
call boost(m,0.0,0.0,pl,pe,px,py,pz)
c collect events in bins(i,j):i = 1,2,3 for mass, elab,
c thetalab
c bin sizes 1 gev, 10 gev, 5 degrees, respectively
c bin number nbin(i) runs up to 40 at most
nbin(1) = m + 1
nbin(2) = ee/10 + 1
nbin(3) = arcos(ex/ee)*36/pie + 1

```

```

nbin(4) = pi/10 + 1
nbin(5) = arcos(pz/pe)*36/pie + 1
do 2 j = 1,5
2 nbin(j) = min(nbin(j), 40)
bin(1, nbin(1)) = bin(1, nbin(1)) + w
do 3 j = 2,3
bin(j, nbin(j)) = bin(j, nbin(j)) + w/2
3 bin(j, nbin(j+2)) = bin(j, nbin(j+2)) + w/2
4 sigma = sigma + w
c normalize distributions to sum unity, express sigma in mb
do 5 i = 1,3
do 5 j = 1,40
5 bin(i,j) = bin(i,j)/sigma
sigma = sigma/n*0.389
print 6, sigma
6 format(' sigma = ', e12.4, 'mb')
print 7
7 format(' bin '.6x, ' mass/1 '.4x,
*       ' pelab/10 '.2x, ' thetalab/5 ')
do 8 j = 1,40
8 print 9, j, (bin(i,j), i = 1,3)
9 format(i4, 3e14.4)
stop
end

```

If we wish to emphasize the Z^0 pole in Drell-Yan pairs, we must first put in the complete $\hat{\sigma}$ (see §4.6) which contains a factor $[(\hat{s} - M_Z^2)^2 + \Gamma_Z^2 M_Z^2]^{-1}$. This factor can be removed by choosing integration variables $\ln \xi_1$ and θ where

$$\tan \theta = (\xi_1 \xi_2 s - M_Z^2) / (\Gamma_Z M_Z),$$

$$d\xi_1 = \xi_1 d(\ln \xi_1),$$

$$\xi_1 d\xi_2 = d\theta [(s - M_Z^2)^2 + \Gamma_Z^2 M_Z^2] / (s \Gamma_Z M_Z).$$

With m_0 the minimum mass, we can relate these variables to x_1, x_2 in the range (0, 1) by defining

$$\xi_1 = \exp [x_1 \ln(m_0^2/s)]$$

$$\theta_{\min} = \arctan [(m_0^2 - M_Z^2)/(\Gamma_Z M_Z)]$$

$$\theta_{\max} = \arctan [(\xi_1 s - M_Z^2)/(\Gamma_Z M_Z)]$$

$$\theta = \theta_{\min} + x_2(\theta_{\max} - \theta_{\min})$$

$$\xi_2 = (\Gamma_Z M_Z \tan \theta + M_Z^2)/(\xi_1 s)$$

$$d\xi_1 d\xi_2 = \frac{[(\hat{s} - M_Z^2)^2 + \Gamma_Z^2 M_Z^2]}{s\Gamma_Z M_Z} \cdot \ln(s/m_0^2) \cdot (\theta_{\max} - \theta_{\min}) dx_1 dx_2$$

With this choice, the previous weight factor must be divided by $\xi_1^2 \xi_2^2 \Delta_1 \Delta_2$ and multiplied by the coefficient of $dx_1 dx_2$ in the last line.

Chapter 12

Higgs Boson

12.1 Renormalizability

The standard $SU(2)_L \times U(1)_Y$ gauge model provides a remarkably successful description of the observed weak interactions. An essential component of the model is the $SU(2)$ scalar doublet which is responsible for the spontaneous breakdown of the gauge symmetry. After electroweak symmetry breaking, there remains a single neutral scalar particle—the Higgs boson—as discussed in Chapter 2. The search for this elusive Higgs boson is one of the most important efforts for present and future accelerators, since its discovery would be the definitive confirmation of the model.

Renormalizability of the electroweak theory requires the existence of the Higgs boson. In a renormalizable theory the scattering amplitudes calculated in a perturbation expansion do not violate unitarity bounds at high energies.

Exercise. Neglecting spin for simplicity, show that unitarity for the $L = 0$ partial wave amplitude requires

$$\int_0^s dt \left| \left[\frac{1}{4\pi} \frac{d\sigma}{dt} \right]^{\frac{1}{2}} \right| < 1,$$

for any inelastic $2 \rightarrow 2$ cross section, if the amplitude has constant phase and does not change sign. Hence show that unitarity is

violated if $d\sigma/dt$ falls more slowly than s^{-2} at large t .

For example, in quantum electrodynamics, which is a renormalizable theory, the differential cross section for $e^+e^- \rightarrow \gamma\gamma$ at high energy-squared s and high momentum transfer-squared t is

$$\frac{d\sigma}{dt}(e^+e^- \rightarrow \gamma\gamma) \sim \frac{\alpha^2}{s^2}, \quad (\text{for } |t| \sim s),$$

as can be deduced from dimensional considerations. However, for a theory with massive vector bosons the contributions from longitudinally polarized vector bosons give amplitudes that grow unacceptably fast with energy. This growth arises from the appearance of E/M_V in the longitudinal polarization vector

$$\epsilon_\mu^L = \left(\frac{p}{M_V}, 0, 0, \frac{E}{M_V} \right).$$

As an illustration, consider the diagrams for $e^+e^- \rightarrow ZZ$ in Fig. 12.1. The contributions of the first two diagrams give a differential cross section at high s ,

$$\frac{d\sigma}{dt} \sim \frac{m_e^2 s}{M_Z^4} \frac{1}{s^2}, \quad (\text{for } |t| \sim s),$$

which violates the unitarity requirement at high s .

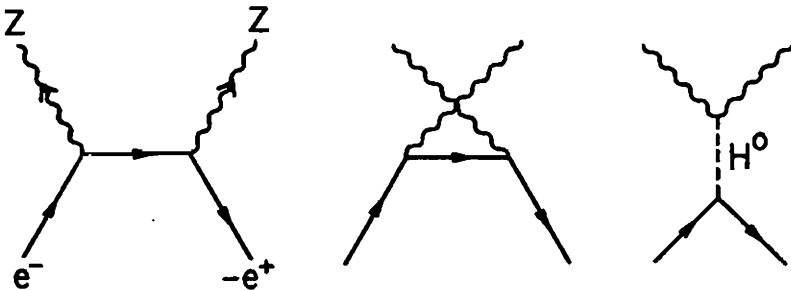


Fig. 12.1. Diagrams contributing to the process $e^+e^- \rightarrow ZZ$.

Exercise. For axial vector couplings to electrons of longitudinally polarized Z bosons, show that the sum of amplitudes for the first two diagrams in Fig. 12.1 is proportional to $m_e \bar{v}_e v_e$ in the limit that the momenta satisfy $k_1, k_2 \gg M_Z$.

The third diagram in Fig. 12.1 with the Higgs boson intermediate state is needed to cancel the inadmissible growth with energy of the other diagrams. (Note that in Chapter 8, we set $m_e = 0$ and this difficulty was not apparent.) The cancellation requires that the product of the Higgs boson couplings is $\sqrt{s} G_F m_e M_Z^2$, which is exactly the standard model strength. By considering the high energy behavior of other processes it is possible to establish that that all Higgs boson couplings must be proportional to the masses of the particles to which it couples.

12.2 Mass Bounds

The mass of the Higgs boson in the standard model is given by $m_H = (2\lambda)^{1/2} v$ where λ is a dimensionless coupling constant of the scalar potential and $v = (\sqrt{2} G_F)^{-1/2} = 246$ GeV is the vacuum expectation value. Since λ is a free parameter, the Higgs boson mass is arbitrary. However there is a lower limit on λ due to effective self-interactions from diagrams containing virtual gauge fields, such as in Fig. 12.2, which exist in addition to the bare $\lambda\phi^4$ interaction term. The coupling of the scalar field to the virtual gauge fields is fixed and a lower limit on the effective λ of order $\lambda \gtrsim \alpha^2$ is obtained. Taking into account vector ($V = W^+, W^-$ and Z), scalar (S) and fermion (f) loop diagram contributions to the effective potential, and requiring the minimum of this potential to be stable, leads to the condition

$$m_H^2 \geq \frac{3 \sum_V M_V^4 + \sum_S m_S^4 - 4 \sum_f m_f^4}{16\pi^2 v^2}.$$

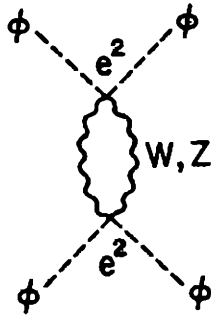


Fig. 12.2. Diagram which leads to an effective ϕ^4 self-interaction.

With $m_S = M_W$ and neglect of m_f contributions, this gives

$$m_H > 7 \text{ GeV} .$$

This lower bound would be weakened, however, if there exist fermions with mass of order M_W , such as a heavy t or fourth generation fermions. Moreover, in models with two Higgs doublets, there is no lower bound on the lightest Higgs boson mass since one of the vacuum expectation values could be very small compared to M_W .

There is no rigorous upper bound for the Higgs boson mass. If it is assumed that lowest order diagrams in the coupling λ should not violate unitarity then the condition

$$m_H < \left(\frac{8\pi\sqrt{2}}{3 G_F} \right)^{\frac{1}{2}} \approx 1 \text{ TeV}$$

is obtained. However, for large m_H the coupling λ is also large and higher order diagrams must be summed.

In GUT models the requirement that the couplings remain perturbative up to the GUT scale typically implies that the upper bound on the Higgs mass is in the range 100-200 GeV.

In the absence of theoretical predictions for the Higgs boson mass, it is necessary that all mass regions be explored for its detection.

12.3 Decays of the Higgs Boson

12.3.1 Higgs decays to fermions.

The coupling of the Higgs boson H to a fermion f (either lepton or quark) is given by

$$\mathcal{L} = -(\sqrt{2} G_F)^{\frac{1}{2}} m_f H \bar{f} f .$$

Hence, the decay amplitude is

$$\mathcal{M} = (\sqrt{2} G_F)^{\frac{1}{2}} m_f \bar{u}(p_1) v(p_2) .$$

This yields a partial decay width of

$$\Gamma(H^0 \rightarrow f\bar{f}) = c_f \frac{G_F m_f^2 m_H}{4\pi\sqrt{2}} \left[1 - \frac{4m_f^2}{m_H^2} \right]^{3/2} ,$$

where $c_f = 1$ for leptons and $c_f = 3$ for quarks. Because of the mass dependence of the coupling the dominant fermionic decays will usually be to final states with the maximum fermion masses allowed by kinematics.

12.3.2 Higgs decay to gluons.

The decay of the Higgs boson into two gluons occurs through the quark loop diagram of Fig. 12.3. Using a low-energy theorem, the amplitude for $g \rightarrow gH$ with the emission of a zero momentum Higgs can be determined from the amplitude of the diagram for $g \rightarrow g$

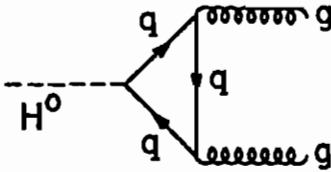


Fig. 12.3. Quark loop diagram for decay of a Higgs boson to gluons.

shown in Fig. 12.4 by differentiation with respect to the fermion mass

$$\mathcal{M}(g \rightarrow gH) = (\sqrt{2} G_F)^{\frac{1}{2}} \sum_q m_q \frac{\partial}{\partial m_q} \mathcal{M}(g \rightarrow g).$$

This relation is due to the fact that the Higgs interaction is equivalent to a mass insertion on the virtual quark lines, for which

$$-\frac{1}{\not{p} + m_q} (\sqrt{2} G_F)^{\frac{1}{2}} m_q \frac{1}{\not{p} + m_q} = (\sqrt{2} G_F)^{\frac{1}{2}} m_q \frac{\partial}{\partial m_q} \frac{1}{\not{p} + m_q}.$$

The one-loop diagram for $g \rightarrow g$ is divergent, but can be regularized by a cut-off parameter which does not enter the result for $g \rightarrow gH$. The effective Lagrangian found for $H \rightarrow gg$ has the form

$$\mathcal{L} = -(\sqrt{2} G_F)^{\frac{1}{2}} \frac{\alpha_s(m_H^2)}{12\pi} I G_{\mu\nu}^a G_a^{\mu\nu} H,$$

where $\alpha_s(m_H^2)$ is the strong coupling constant evaluated at m_H^2 and $G_{\mu\nu}^a = \partial_\mu g_\nu^a - \partial_\nu g_\mu^a$. The quantity I is given in terms of $\lambda_q = m_q^2/m_H^2$ by

$$I = \sum_q I_q, \quad I_q = 3 \int_0^1 dx \int_0^{1-x} dy \frac{1 - 4xy}{1 - xy/\lambda_q - i\epsilon}.$$

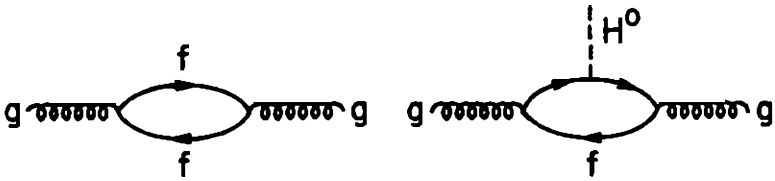


Fig. 12.4. Diagrams illustrating the relation between the fermion loop diagram and the $H \rightarrow gg$ diagram.

The evaluation of the integral gives

$$I_q = 3 [2\lambda_q + \lambda_q(4\lambda_q - 1)f(\lambda_q)],$$

where

$$f(\lambda) = -2 \left(\sin^{-1} \frac{1}{2\sqrt{\lambda}} \right)^2, \quad \text{for } \lambda > \frac{1}{4},$$

$$f(\lambda) = \frac{1}{2} \left(\ln \frac{\eta^+}{\eta^-} \right)^2 - \frac{\pi^2}{2} - i\pi \ln \frac{\eta^+}{\eta^-}, \quad \text{for } \lambda < \frac{1}{4},$$

with $\eta^\pm = \frac{1}{2} \pm \sqrt{\frac{1}{4} - \lambda}$. In the large m_q limit $\lambda_q \gg 1$, $I_q \rightarrow 1$. In the small m_q limit $\lambda_q \ll 1$, $I_q \rightarrow 0$.

Exercise. Show that partial decay rate is

$$\Gamma(H \rightarrow gg) = \frac{G_F m_H^3}{36\sqrt{2}\pi} \left[\frac{\alpha_s(m_H^2)}{\pi} \right]^2 |I|^2.$$

An example calculation of I is given in Fig. 12.5 summed over the five known quark flavors using $m_u = 3 \text{ MeV}$, $m_d = 8 \text{ MeV}$, $m_s = 180 \text{ MeV}$, $m_c = 1.25 \text{ GeV}$, $m_b = 4.5 \text{ GeV}$, $m_H = 100 \text{ GeV}$ and varying $\sqrt{\lambda_t} = m_t/m_H$. The value of $|I|^2$ peaks at $|I|^2 \simeq 3.2$ for $m_t/m_H \simeq 0.4$ and approaches unity for $m_t/m_H \gtrsim 0.7$. For most

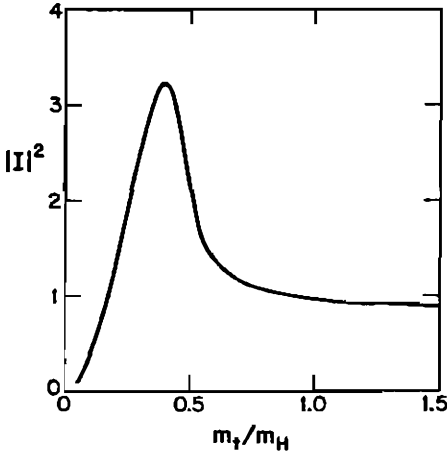


Fig. 12.5. Value of the factor I which appears in the $H \rightarrow gg$ amplitude versus the m_t/m_H .

discussions, the value $|I|^2 \simeq 1$ for one heavy quark is assumed. If there exist N quarks with $m_q > m_H$, then $|I|^2 \simeq N^2$.

12.3.3 Higgs decay to two photons.

The $H \rightarrow \gamma\gamma$ decay is similar to $H \rightarrow gg$ except that charged leptons, the W -boson and charged Higgs bosons also contribute to the loop. The low energy theorem is modified to

$$\mathcal{M}(\gamma \rightarrow H\gamma) = (\sqrt{2} G_F)^{\frac{1}{2}} \left(M_W \frac{\partial}{\partial M_W} + \sum_f m_f \frac{\partial}{\partial m_f} + m_{H^+} \frac{\partial}{\partial m_{H^+}} \right) \mathcal{M}(\gamma \rightarrow \gamma).$$

The resulting effective Lagrangian in the $m_f > m_H$ approximation is

$$\mathcal{L}_{\text{eff}} = -\frac{\alpha}{2\pi} (\sqrt{2} G_F)^{\frac{1}{2}} I F_{\mu\nu} F^{\mu\nu} H.$$

Exercise. Show that the $H \rightarrow \gamma\gamma$ decay rate is

$$\Gamma(H \rightarrow \gamma\gamma) = \frac{G_F m_H^3}{8\sqrt{2}\pi} \left(\frac{\alpha}{\pi} \right)^2 |I|^2.$$

The quark, lepton, W -boson and colorless charged scalar contribu-

tions are

$$I = \sum_q Q_q^2 I_q + \sum_\ell Q_\ell^2 I_\ell + I_W + I_S,$$

where Q_f denotes the charge of fermion f in units of e . Here

$$I_q = 3 [2\lambda_q + \lambda_q(4\lambda_q - 1)f(\lambda_q)],$$

$$I_\ell = 2\lambda_\ell + \lambda_\ell(4\lambda_\ell - 1)f(\lambda_\ell),$$

$$I_W = 3\lambda_W(1 - 2\lambda_W)f(\lambda_W) - 3\lambda_W - \frac{1}{2},$$

$$I_S = -\lambda_S [1 + 2\lambda_S f(\lambda_S)],$$

and $\lambda_i = m_i^2/m_H^2$. For all $\lambda_i \gg 1$, the above four contributions are

$$I \simeq \sum_q Q_q^2 + \frac{1}{3} \sum_\ell Q_\ell^2 - \frac{7}{4} + \frac{1}{12}.$$

Note that fermions and bosons contribute with opposite signs. In the limit that all $\lambda_i \ll 1$, only the W -loop contributes and the result for I is $I \simeq -\frac{1}{2}$.

12.3.4 Higgs decays to weak bosons.

The Yukawa couplings of the Higgs boson to the gauge fields are

$$\mathcal{L} = (\sqrt{2} G_F)^{\frac{1}{2}} (2M_W^2 H W_\mu^+ W^{-\mu} + M_Z^2 H Z_\mu Z^\mu).$$

The amplitude for $H \rightarrow W^+W^-$ decay is thus

$$\mathcal{M} = 2M_W^2 (\sqrt{2} G_F)^{\frac{1}{2}} \epsilon_\mu^*(p_1, \lambda_1) \epsilon^{\mu*}(p_2, \lambda_2).$$

Exercise. Show that the decay rate is

$$\Gamma(H^0 \rightarrow W^+W^-) = \frac{G_F}{8\pi\sqrt{2}} m_H^3 (1 - 4\lambda_W)^{\frac{1}{2}} (12\lambda_W^2 - 4\lambda_W + 1),$$

where $\lambda_W = (M_W/m_H)^2$.

In a similar calculation for $H^0 \rightarrow ZZ$, the different coupling in \mathcal{L} together with identical-particle symmetrization give an extra factor of 1/2. The partial width is

$$\Gamma(H^0 \rightarrow ZZ) = \frac{G_F m_H^3}{16\pi\sqrt{2}} (1 - 4\lambda_Z)^{\frac{1}{2}} (12\lambda_Z^2 - 4\lambda_Z + 1),$$

where $\lambda_Z = (M_Z/m_H)^2$. For $m_H \gg M_Z$ the ratio of ZZ to W^+W^- rates approaches 1/2.

Exercise. Show that the decay rates to transverse (\pm) and longitudinally (L) polarized W -bosons are

$$\Gamma(H \rightarrow W_+W_+) = \Gamma(H \rightarrow W_-W_-) = \frac{g^2}{16\pi} \frac{M_W^2}{m_H} \left(1 - \frac{4M_W^2}{m_H^2}\right)^{\frac{1}{2}},$$

$$\Gamma(H \rightarrow W_LW_L) = \frac{g^2}{64\pi} \frac{m_H^3}{M_W^2} \left(1 - \frac{2M_W^2}{m_H^2}\right)^2 \left(1 - \frac{4M_W^2}{m_H^2}\right)^{\frac{1}{2}},$$

$$\Gamma(H \rightarrow W_LW_{\pm}) = 0.$$

Hence for $m_H \gg M_W$ the W -bosons from Higgs decay are dominantly longitudinally polarized. Recall from Chapter 8 that the $q\bar{q} \rightarrow W^+W^-$ continuum background is dominantly W_TW_T .

Exercise. For $m_H \gg M_W$ show that the ratio of $\gamma\gamma$ to W^+W^- decay branching fractions is

$$\frac{\Gamma(H \rightarrow \gamma\gamma)}{\Gamma(H \rightarrow W^+W^-)} \simeq \frac{1}{4} \left(\frac{\alpha}{\pi}\right)^2 \simeq 10^{-6}.$$

12.3.5 Higgs branching fractions.

With the foregoing formulas for the partial decay rates, we can evaluate the branching fractions versus m_H into final state quarks, leptons and gauge particles. The results are shown in Figure 12.6. The decays $H^0 \rightarrow \tau^+\tau^-$ and $c\bar{c}$ dominate for $2m_c < m_H < 2m_b$, $H^0 \rightarrow b\bar{b}$ dominates for $2m_b < m_H < 2m_t$, and $H^0 \rightarrow W^+W^-$ and ZZ dominate for $m_H > 2M_W$ unless there is a very heavy fermion

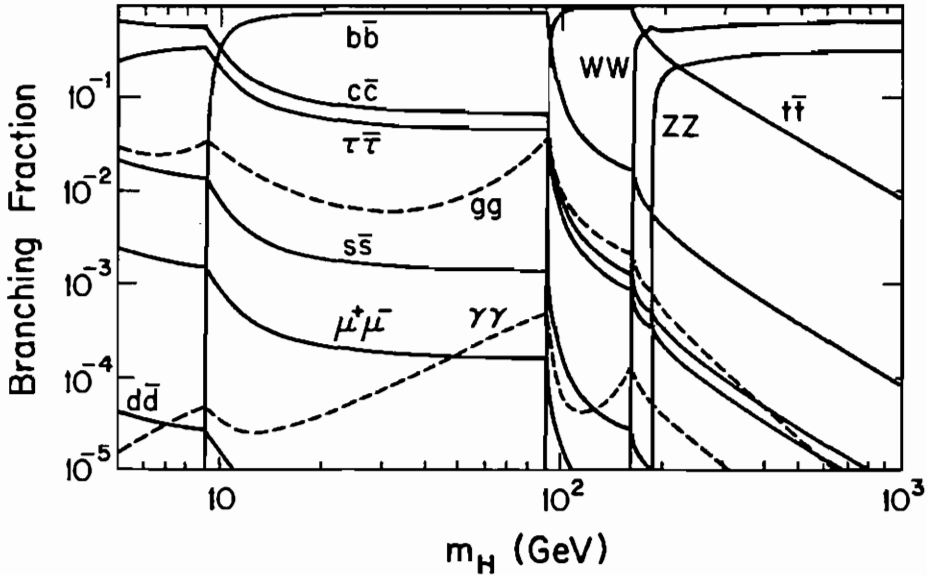


Fig. 12.6. Decay branching fractions of the Higgs boson of the standard model (assuming $m_t = 45$ GeV).

with $m_f > M_W$. These considerations enable us to identify the decay signatures of a Higgs boson of a given mass range. The decays $H \rightarrow \tau\bar{\tau}$, $c\bar{c}$, $b\bar{b}$ into particles with lifetimes of order 10^{-13} - 10^{-12} seconds may be identifiable using vertex detectors through their secondary vertices.

12.4 Higgs Boson Production

12.4.1 Heavy quarkonium decay.

Since the Higgs particle couples feebly to the constituent photons, electrons, muons, light quarks and gluons of particle beams, its production cross sections are quite small which makes systematic experimental Higgs searches exceedingly difficult. One of the most promising possibilities for Higgs production at colliders is via the

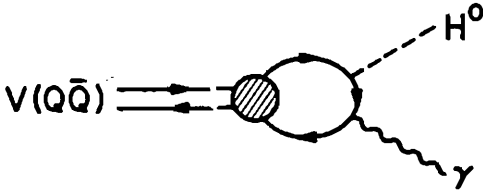


Fig. 12.7. Diagram for $V(Q\bar{Q}) \rightarrow H\gamma$ decay.

decays $V \rightarrow H^0\gamma$ of $J^{PC} = 1^{--}$ quarkonium bound states $V(Q\bar{Q})$ of heavy quarks $Q = c, b, t$.

The diagram for this decay is given in Fig. 12.7. In the non-relativistic approximation for the $Q\bar{Q}$ bound state, the decay rate for $V \rightarrow H\gamma$ relative to that for $V \rightarrow e^+e^-$ is given by

$$\frac{\Gamma(V \rightarrow H\gamma)}{\Gamma(V \rightarrow e^+e^-)} \simeq \frac{KG_F m_V^2}{4\sqrt{2}\pi\alpha} \left(1 - \frac{m_H^2}{m_V^2}\right) \approx 10^{-4} K \left(\frac{m_V}{1 \text{ GeV}}\right)^2 \left(1 - \frac{m_H^2}{m_V^2}\right).$$

The order α_s QCD correction factor K depresses the lowest order $V \rightarrow H\gamma$ decay rate by about a factor of 2. The expression for K is

$$K = \frac{1 - \frac{4\alpha_s}{3\pi} a(\kappa)}{1 - \frac{16\alpha_s}{3\pi}},$$

where $\kappa = m_H^2/m_V^2$ and the function $a(\kappa)$ can be approximated by the expression

$$a(\kappa) = \frac{\pi}{6} \left[\frac{8}{\sqrt{1-\kappa}} + 11(1-\kappa)^{\frac{1}{4}} \right].$$

For $m_H < 0.8 \text{ GeV}$, $K \simeq 0.5$. For the ψ and Υ vector resonances the predicted $H\gamma$ branching fractions, based on experimental e^+e^- branching fractions, are given in Table 12.1. For $m_V \gtrsim 150 \text{ GeV}$ the ratio $\Gamma(V \rightarrow H\gamma)/\Gamma(V \rightarrow e^+e^-)$ becomes of order unity. From toponium decays the Higgs boson could be found for m_H essentially up to m_V .

Table 12.1. Predicted branching fractions for $V \rightarrow \gamma H^0$, with $\kappa < 0.6$ taking $\alpha_s(m_\psi^2) = 0.2$.

Resonance	$B(V \rightarrow e^+e^-)$	$B(V \rightarrow \gamma H^0)/(1 - m_H^2/m_V^2)$
$\psi(3.097)$	6.9×10^{-2}	1.4×10^{-5}
$\psi(3.685)$	0.9×10^{-2}	3.2×10^{-6}
$\Upsilon(9.460)$	2.8×10^{-2}	9.3×10^{-5}
$\Upsilon(10.023)$	1.8×10^{-2}	6.8×10^{-5}
$\Upsilon(10.355)$	3.3×10^{-2}	1.4×10^{-4}

12.4.2 Bremsstrahlung from Z or W^\pm bosons.

Since the Higgs boson couples to the weak gauge bosons, it can be radiated from them, with the detection of the Z or W^\pm serving as a trigger. Here we discuss the rates and distributions in e^+e^- collisions of

$$Z \rightarrow Z^* H^0 \rightarrow \ell^+ \ell^- H^0,$$

where Z^* is virtual; see Fig. 12.8a. Similar considerations apply to pp and $p\bar{p}$ collisions. The $Z \rightarrow Z^* H^0$ process is the dominant H^0 production mechanism in e^+e^- collisions at the Z -resonance energy. In addition to $\ell^+\ell^-$ decays of the virtual Z^* one might also use $Z^* \rightarrow \nu\bar{\nu}$ and $Z^* \rightarrow q\bar{q}$ modes.

Exercise. Show that the differential decay rate for $Z \rightarrow \ell^+\ell^- H^0$ is

$$\frac{1}{\Gamma(Z^0 \rightarrow \ell\bar{\ell})} \frac{d\Gamma}{dx}(Z^0 \rightarrow \ell\bar{\ell} H^0) = \frac{\alpha(1-x + \frac{x^2}{12} + \frac{2}{3}y^2)(x^2 - 4y^2)^{\frac{1}{2}}}{4\pi x_w(1-x_w)(x-y^2)^2},$$

where $x = 2E_H/M_Z = (m_H^2 + M_Z^2 - m_{\ell\bar{\ell}}^2)/M_Z^2$ and $y = m_H/M_Z$.

Figure 12.9 shows the distribution in the variable $x = m_{\ell\bar{\ell}}/M_Z$. The distribution is sharply peaked towards high $\ell\bar{\ell}$ invariant masses,

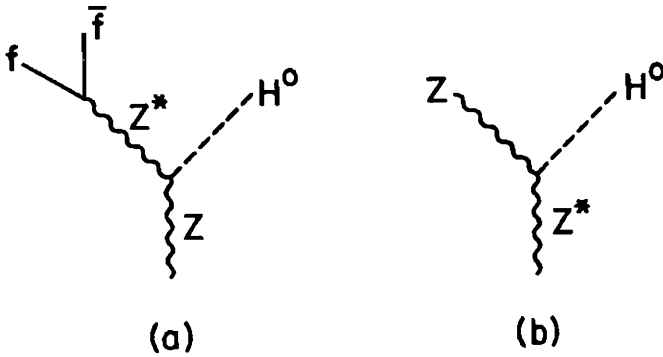


Fig. 12.8. Diagrams with a Higgs boson radiated from a real or virtual Z boson.

with the peak occurring at $m_{\ell\bar{\ell}} \simeq 0.95 m_H$. The rate for $Z \rightarrow \ell\bar{\ell}H$ relative to $Z \rightarrow \ell\bar{\ell}$ is shown in Figure 12.10 versus m_H/m_Z ; the ratio is about 0.3×10^{-2} for $m_H = 10$ GeV but decreases nearly exponentially with increasing m_H until close to the upper endpoint $m_{\ell\bar{\ell}} = M_Z - m_H$.

The bremsstrahlung process $Z^* \rightarrow ZH$, illustrated in Fig. 12.8(b), is similar to the one just discussed except that this time the produced Z is virtual and one must sit at c.m. energies above the Z^0 .

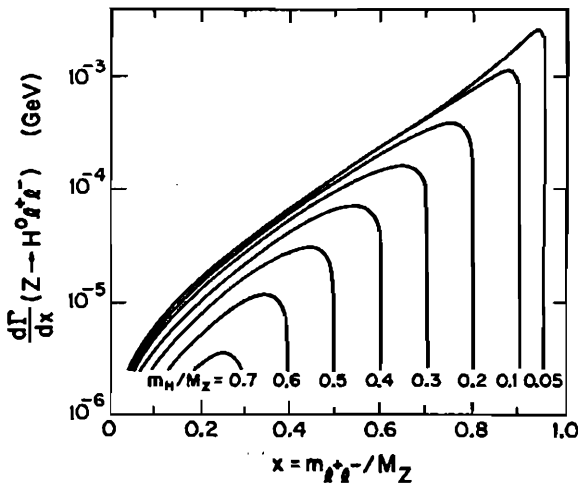


Fig. 12.9. Distribution in $x = m_{\ell\bar{\ell}}/M_Z$ from the $Z \rightarrow \ell^+ \ell^- H^0$ process.

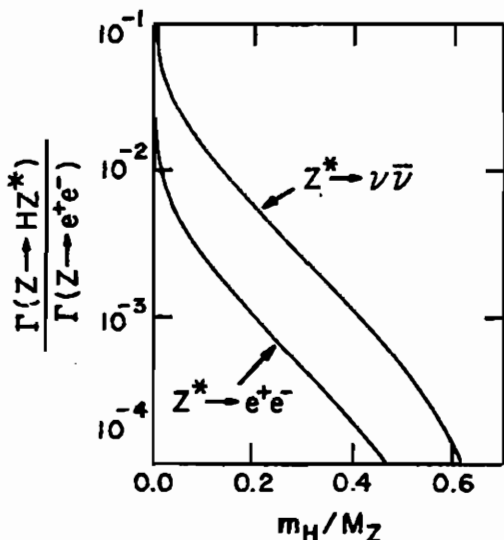


Fig. 12.10. Rates for $Z \rightarrow \ell\bar{\ell}H$ and $Z \rightarrow \nu\bar{\nu}H$ relative to $Z \rightarrow \ell\bar{\ell}$ at the Z resonance energy.

Exercise. Show that the $e^+e^- \rightarrow ZH$ cross section is given by

$$\sigma = \frac{G_F^2 M_Z^4}{96\pi} [1 + (1 - 4x_w)^2] \frac{8k}{\sqrt{s}} \left[\frac{k^2 + 3M_Z^2}{(s - M_Z^2)^2} \right],$$

where k is the c.m. momentum of the Higgs (or the produced Z).

This cross section peaks at c.m. energy $\sqrt{s} = M_Z + \sqrt{2}m_H$. Figure 12.11 gives representative values of $\sigma(e^+e^- \rightarrow ZH)$ versus \sqrt{s} .

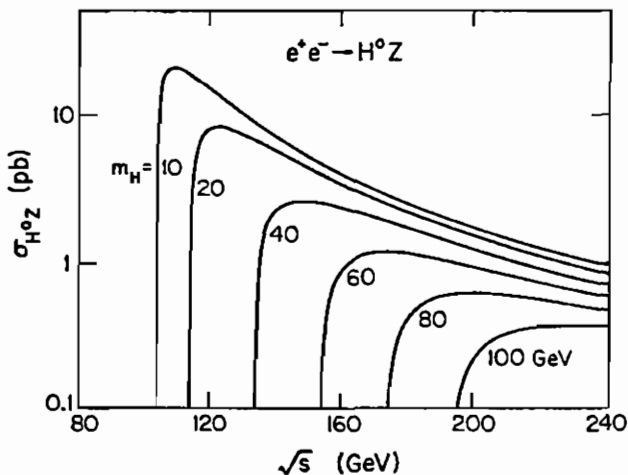


Fig. 12.11. Cross section for $e^+e^- \rightarrow ZH$ versus \sqrt{s} for various m_H .

At LEP II with $\sqrt{s} = 200$ GeV operating with an integrated luminosity of $1 \text{ pb}^{-1}/\text{day}$, it will be feasible to search for a ZH signal up to a mass $m_H = 100$ GeV.

12.4.3 Gluon fusion.

In pp or $p\bar{p}$ collisions the dominant Higgs production mechanism should be gluon fusion, shown in Fig. 12.12. Here gluons from the colliding beams couple to a heavy quark loop from which the Higgs boson is emitted. The general cross section expression for production of a single particle X of mass M , spin J and n_c color degrees of freedom ($n_c = 1, 3, 6, \dots$ for color singlet, triplet, sextet, ...) in hadronic collisions is

$$\sigma(AB \rightarrow X + \text{anything}) = \frac{16\pi^2(2J+1)n_c}{M^3} K \sum_{a,b} C_{ab} r_{ab} S \Gamma(X \rightarrow ab) \tau \times \int_{\tau}^1 \frac{dx}{x} [f_{a/A}(x, M^2) f_{b/B}(\tau/x, M^2) + (A \leftrightarrow B \text{ if } a \neq b)],$$

where S is a statistical factor ($S = 2$ for color singlet $X \rightarrow gg, \gamma\gamma, ZZ$, identical bosons; $S = 1$ otherwise) and K is a factor which represents non-leading QCD corrections. Here $\tau = M^2/s$ and $f_{a/A}(x, M^2)$ is the parton distribution evaluated at scale M . The r_{ab} is a spin average factor; for quarks or gluons $r_{ab} = \frac{1}{4}$. The factor C_{ab} depends on the colors of the partons: $C_{q\bar{q}} = \frac{1}{9}$, $C_{qg} = \frac{1}{24}$, and $C_{gg} = \frac{1}{64}$. In the case of Higgs production via gluon-gluon fusion we find

$$\sigma(pp \rightarrow H + \text{anything}) = \Gamma(H \rightarrow gg) \frac{\pi^2}{8m_H^3} \tau \int_{\tau}^1 \frac{dx}{x} g(x, m_H^2) g\left(\frac{\tau}{x}, m_H^2\right),$$

where $\tau = m_H^2/s$ and $g(x, Q^2)$ is the gluon distribution evaluated at $x = Q^2$. Substituting the expression for $\Gamma(H \rightarrow gg)$ from §12.3.2, in

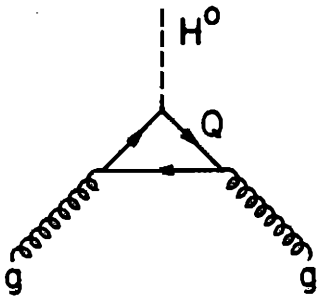


Fig. 12.12. Gluon fusion diagram for Higgs boson production.

the approximation that $I = N$ (the number of heavy quark flavors), one obtains

$$\sigma(pp \rightarrow H + \text{anything}) = \frac{G_F}{\sqrt{2}} \left(\frac{\alpha_s}{3\pi} \right)^2 \frac{\pi N^2}{32} \tau \int_{\tau}^1 \frac{dx}{x} g(x, m_H^2) g\left(\frac{\tau}{x}, m_H^2\right).$$

Figure 12.13 shows numerical evaluations of the exact cross section versus m_H at c.m. energies $\sqrt{s} = 2$ TeV, 17 TeV, and 40 TeV assuming that $m_t = 50$ GeV in the heavy quark loop.

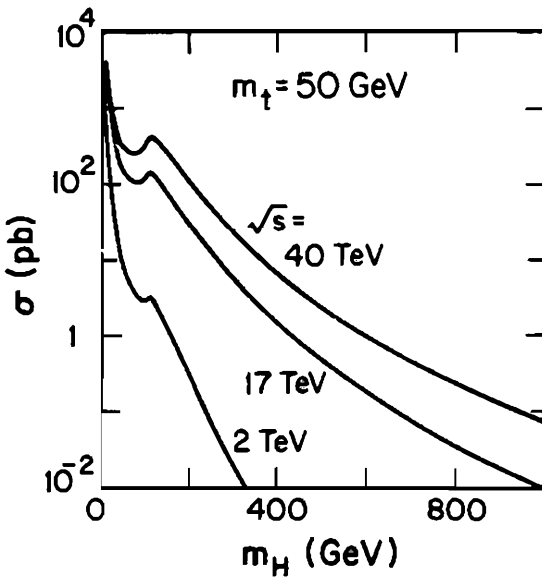


Fig. 12.13. Cross sections for Higgs boson production via gluon-gluon fusion. The maxima at $m_H \simeq 2m_t$ are related to the structure in I.

12.4.4 WW and ZZ fusion.

In WW and ZZ fusion the quarks in the colliding beams emit virtual W 's and Z 's which annihilate to form the Higgs boson. These subprocesses are illustrated in Fig. 12.14.

The matrix element for the subprocess $q_1 q_2 \rightarrow q'_1 q'_2 V_1 V_2 \rightarrow q'_1 q'_2 H$ is

$$\mathcal{M} = C_V \bar{u}(q'_1) \gamma^\mu (g_V^{q_1} + g_A^{q_1} \gamma_5) u(q_1) \bar{u}(q'_2) \gamma_\mu (g_V^{q_2} + g_A^{q_2} \gamma_5) u(q_2) D_1 D_2,$$

where, for W -bosons, $C_W = g^3 M_W$, $g_V^q = -g_A^q = \frac{1}{2\sqrt{2}}$, and for Z -bosons, $C_Z = g^3 M_W / (1 - x_w)^2$, g_V^q and g_A^q are given in §2.12, and $D_i = (V^2 - M_V^2 + iM_V \Gamma_V)^{-1}$, where the particle names are used to denote their momenta.

Then the squared matrix element, summed and averaged over the initial quark spins, is

$$\overline{|\mathcal{M}|^2} = 4C_V^2 [G_1 q_1 \cdot q_2 q'_1 \cdot q'_2 + G_2 q_1 \cdot q'_2 q'_1 \cdot q_2] |D_1|^2 |D_2|^2,$$

where $G_1 = (g_L^{q_1})^2 (g_L^{q_2})^2 + (g_R^{q_1})^2 (g_R^{q_2})^2$, $G_2 = (g_L^{q_1})^2 (g_R^{q_2})^2 + (g_R^{q_1})^2 (g_L^{q_2})^2$, with $g_{L,R} = g_V \mp g_A$.

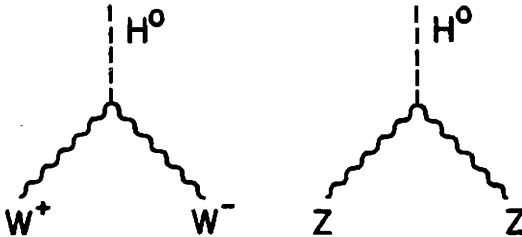


Fig. 12.14. WW and ZZ fusion production of the Higgs boson.

Thus the subprocess cross section for $qq \rightarrow q'q'VV \rightarrow q'q'H$ is given by:

$$\hat{\sigma} = \frac{1}{2\hat{s}} \frac{1}{(2\pi)^8} \int \sum |\mathcal{M}|^2 \delta^4(q_1 + q_2 - q'_1 - q'_2 - p_H) \frac{dq'_1}{2E_{q'_1}} \frac{dq'_2}{2E_{q'_2}} \frac{dp_H}{2E_H}.$$

Exercise. In the effective W approximation show that the subprocess cross section for $qq \rightarrow q'q'WW \rightarrow q'q'H$ is

$$\hat{\sigma} \simeq \left(\frac{\alpha}{x_w}\right)^3 \frac{1}{16 m_H^3} \left\{ \frac{m_H^3}{M_W^2} \left[(1 + \tau) \ln \frac{1}{\tau} - 2(1 - \tau) \right] + \frac{M_W^2}{2 m_H} \left[\ln \left(\frac{\hat{s}}{M_W^2} \right) \right]^2 \left[(2 + \tau)^2 \ln \frac{1}{\tau} - 2(1 - \tau)(3 + \tau) \right] \right\},$$

where $\tau = m_H^2/\hat{s}$ with \hat{s} the c.m. energy squared of the initial qq . Note that there is no integration over the phase space of the final state quarks in the effective W approximation where the W emission is collinear with the incident quark direction. The m_H^3/M_W^2 term in $\hat{\sigma}$ is from longitudinally polarized W bosons and the M_W^2/m_H term is from transversely polarized W 's. Give the appropriate modifications to the cross section formula for the effective Z approximation to $qq \rightarrow qqZZ \rightarrow qqH$.

12.5 Higgs Searches

Because the Higgs couples very feebly to light particles for which we now have beams, its production cross sections are tiny at existing machines. No experiment so far could have detected it if $m_H \gtrsim 7$ GeV as suggested above. A major goal of new machines is to find it if it exists. The physics of Higgs detection depends on its mass.

12.5.1 Low mass Higgs ($m_H < M_Z$).

If the Higgs boson is light, the best way of detecting it is at e^+e^- colliders because of low backgrounds. The H^0 can be radiated from a Z boson or appear with a hard photon in the decay of toponium (§10.1.1). The $Z \rightarrow Z^*H$ process is the dominant mechanism at the Z resonance energy. In addition to charged lepton pairs from the virtual Z^* one can also detect $Z^* \rightarrow \nu\bar{\nu}$, using a missing transverse momentum trigger in the latter case. At the SLC or LEP machines, with $\sqrt{s} \simeq M_Z$, it should be possible to find the Higgs boson in the $\ell\bar{\ell}H$ final state if $m_H < 40$ GeV and up to 50 GeV in the $\nu\bar{\nu}H$ channel.

At e^+e^- energies above the Z resonance the bremsstrahlung process $Z^* \rightarrow ZH$ with a virtual intermediate Z boson is relevant. This cross section peaks at energy $\sqrt{s} = M_Z + \sqrt{2}m_H$. At the future LEP II machine operating at $\sqrt{s} = 200$ GeV the Higgs boson could be found if $m_H < 85$ GeV.

Once Higgs boson candidate events are tagged by $Z^* \rightarrow e\bar{e}$, $Z^* \rightarrow \nu\bar{\nu}$ or a hard photon, microvertex detectors can provide evidence for $H \rightarrow \tau\bar{\tau}$ or $H \rightarrow b\bar{b}$ decays and the Higgs boson mass can be reconstructed from the recoil system.

12.5.2 Intermediate mass Higgs ($M_Z < m_H < 2M_W$).

A Higgs boson in this mass range is presumed to decay dominantly to a t -quark pair. It would be amply produced at a multi-TeV hadron collider via gluon fusion ($gg \rightarrow H$) but the continuum background from $gg \rightarrow t\bar{t}$ hopelessly obscures the signal. No way has been found to search for the intermediate mass Higgs at any presently proposed machine. However, this negative conclusion assumes that there are only three generations of quarks; in the case of a fourth generation another avenue of search exists that will be discussed in Chapter 13. Also in models with more than one Higgs multiplet it would be unlikely that all Higgs masses fell in this restricted range.

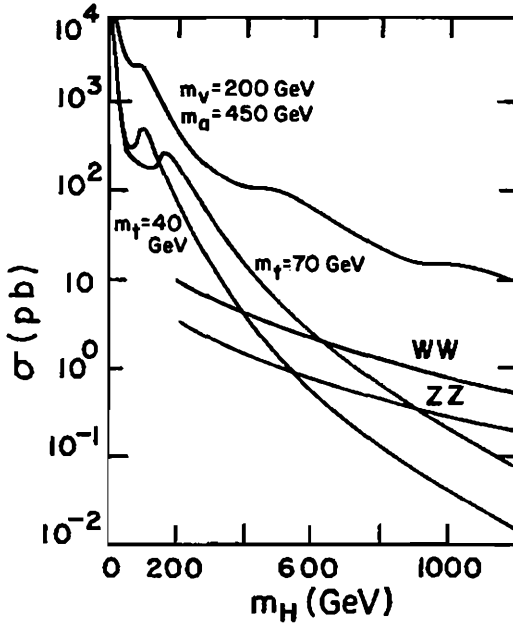


Fig. 12.15. Single Higgs production at the SSC from gluon-gluon, ZZ and WW fusion subprocesses. The top curve assumes a fourth generation quark doublet (a, v).

12.5.3 High mass Higgs ($2M_W < m_H < 1 \text{ TeV}$).

If the Higgs boson has mass greater than $2M_W$ or $2M_Z$, its dominant decays are $H \rightarrow W^+W^-$ and $H \rightarrow ZZ$, with branching fractions approximately in the ratio 2 to 1. At a multi-TeV hadron collider it can be produced via gluon-gluon or W^+W^- or ZZ fusion. Figure 12.15 compares these contributions at $\sqrt{s} = 40 \text{ TeV}$. For $m_H > 350 \text{ GeV}$, WW fusion dominates, assuming $m_t < 50 \text{ GeV}$ and no heavier quarks exist. The predicted Higgs boson cross sections are a few picobarns. For the design luminosity of $10^4 \text{ (pb)}^{-1}/\text{year}$ of the proposed Superconducting Supercollider (SSC) this gives tens of thousands of Higgs boson events.

Several signals may be used to identify a high mass Higgs boson produced in hadron collisions at SSC energies. The cleanest and most reconstructible is the decay mode

$$H \rightarrow ZZ \rightarrow (e^+e^-)(e^+e^-)$$

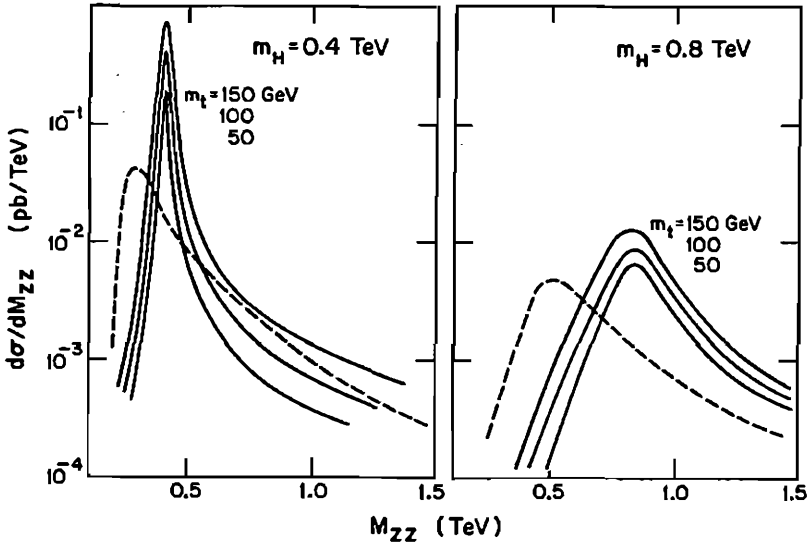


Fig. 12.16. The $pp \rightarrow H \rightarrow ZZ$ signal for leptonic decays of both Z 's, compared with the continuum ZZ -background (dashed curves).

but the branching fraction is small $BF \approx \frac{1}{3}(0.06)^2 \approx 10^{-3}$ giving few events. Nevertheless the $H \rightarrow ZZ$ signal is clearly identifiable above the $q\bar{q} \rightarrow ZZ$ background at least up to $m_H \simeq 1$ TeV, provided that at least one Z has high p_T . Figure 12.16 compares the double Z leptonic decay signal with the ZZ continuum background after cuts $p_T(\ell^\pm) > 20$ GeV, $\eta(\ell^\pm) < 3$, $p_T(Z) > m_H/4$ for one Z (with $m_t = 50, 100$ or 150).

The signal from the leptonic decay

$$H \rightarrow ZZ \rightarrow (\ell^+\ell^-)(\nu\bar{\nu})$$

occurs at six times the rate of two charged lepton pairs (for 3 neutrino species) and moreover has little background in the Standard Model. The Higgs signal and mass can be determined from the distribution in the transverse mass m_T given by

$$m_T^2 = \left[(p_T^2 + M_Z^2)^{\frac{1}{2}} + (\not{p}_T^2 + M_Z^2)^{\frac{1}{2}} \right]^2 - (p_T + \not{p}_T)^2,$$

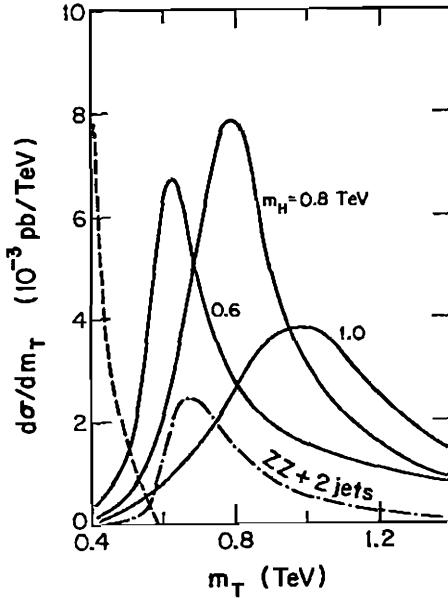


Fig. 12.17. Transverse mass distribution of Higgs boson signal in $pp \rightarrow ZZX \rightarrow (\ell\bar{\ell})(\nu\bar{\nu})X$ at $\sqrt{s} = 40$ TeV. The dashed curve is the Z + jets background with \cancel{p}_T coming from hadrons that are outside the acceptance region. The dash-dot curve is the ZZ + 2 jets background.

where $\cancel{p}_T = \cancel{p}_T(\ell\bar{\ell})$ and $\cancel{p}_T = \cancel{p}_T(\nu\bar{\nu})$; compare §8.6 and 10.3.4. The Higgs signal, coming largely from WW fusion, is enhanced relative to backgrounds by requiring two accompanying jets. Figure 12.17 compares the Higgs boson signal with backgrounds for several values of m_H in $pp \rightarrow \ell^+\ell^-\cancel{p}_T$ events with the cuts $p_T(\ell^\pm)$ and $p_T(j) > 20$ GeV, $\eta(\ell^\pm)$ and $\eta(j) < 3$, $p_T(\ell^+\ell^-) > 300$ GeV, $\cancel{p}_T > 120$ GeV.

Table 12.2 records the expected Higgs signals for an integrated luminosity of 10^4 pb^{-1} (standard expectation for one year of SSC running). Both signal and background are integrated over two full widths of the Higgs boson for the case $m_H = 600$ GeV, and over one full width for the heavier cases $m_H = 800, 1000$ GeV.

It is much more difficult to study the signal from one Z or W hadronic decay with the other decay leptonic. This has a much larger signal than the purely leptonic modes but encounters a larger background which can be reduced by requiring that the two additional jets in the events have substantial longitudinal and transverse momenta.

Table 12.2. Predicted event numbers for Higgs signal and backgrounds in $\ell^+\ell^-jj + \cancel{p}_T$ events at $\sqrt{s} = 40$ TeV for integrated luminosity 10^4 pb^{-1} .

m_H (GeV)		600	800	1000
Integrated range of m_T (GeV)		550 ~ 750	600 ~ 1100	700 ~ 1500
Number of events	Signal	11	24	21
	Backgrounds	4	7	5

It is important to note that the width of the Higgs boson grows rapidly with mass above $2M_W$, reflecting that the coupling to longitudinal W or Z becomes strong. For $m_H \gg 2M_W$ the total width is

$$\Gamma(H) \approx \frac{3G_F}{16\pi\sqrt{2}} m_H^3 \approx 0.48 \text{ TeV} \left(\frac{m_H}{1 \text{ TeV}} \right)^3.$$

The values of the width for some representative Higgs masses are given below:

m_H (GeV)	Γ_H (GeV)
200	2
400	25
600	100
1000	450

A very broad Higgs boson may be difficult to identify as a particle.

If Higgs bosons are not found below 1 TeV, it is argued that there will be enhanced WW , WZ , and ZZ yields in pp scattering which could be observed at the SSC. This would signal a new sector of strongly interacting particles at the 1 TeV scale or higher.

12.6 Two Higgs Doublet Model

The scalar sector of the standard model is not yet constrained by experiment and it is possible that the Higgs structure is more complicated. A strong motivation for extending the Higgs sector comes from supersymmetry, where two $SU(2)_L$ Higgs doublets

$$\Phi_1 = \begin{pmatrix} \phi_1^{0*} \\ -\phi_1^- \end{pmatrix}, \quad \Phi_2 = \begin{pmatrix} \phi_2^+ \\ \phi_2^0 \end{pmatrix},$$

are necessary to provide masses to the charged fermions. Here the Φ_1 doublet with hypercharge -1 gives mass to the $T_{3L} = -\frac{1}{2}$ quarks and the charged leptons while the Φ_2 doublet with hypercharge $+1$ gives mass to the $T_{3L} = +\frac{1}{2}$ quarks. With SUSY we need two doublets rather than the standard one doublet, in order to cancel out the corresponding Higgs fermion contributions to triangle anomalies. The neutral members of the doublets acquire vacuum expectation values v_1 and v_2 , respectively.

Exercise. Show that

$$\sqrt{2}(v_1^2 + v_2^2)^{\frac{1}{2}} = v = (\sqrt{2} G_F)^{-\frac{1}{2}}.$$

After shifting the neutral scalar fields by their vevs, diagonalization of the mass matrices gives the following physical Higgs boson states:

$$\begin{pmatrix} H_1^0 \\ H_2^0 \end{pmatrix} = \sqrt{2} \begin{pmatrix} \cos \alpha & \sin \alpha \\ -\sin \alpha & \cos \alpha \end{pmatrix} \begin{pmatrix} \text{Re } \phi_1^{0*} - v_1 \\ \text{Re } \phi_2^0 - v_2 \end{pmatrix},$$

$$H_3^0 = \sqrt{2}(\sin \beta \text{Im } \phi_1^{0*} + \cos \beta \text{Im } \phi_2^0),$$

$$H^- = -\phi_1^- \sin \beta + \phi_2^- \cos \beta = (H^+)^*.$$

Thus the physical spectrum of Higgs bosons in the two doublet model consists of two scalars, H_1^0 and H_2^0 , a pseudoscalar, H_3^0 , and a pair

of charged scalars, H^\pm . The angle α depends on parameters that appear in the Higgs potential and the angle β is given by

$$\tan \beta = \frac{v_2}{v_1}.$$

The angles α and β are chosen such that $-\pi/2 \leq \alpha \leq 0$ and $0 \leq \beta \leq \pi/2$. In the most general model these angles and the physical Higgs boson masses are all independent parameters. However in the minimal supersymmetric model the conditions on the potential imposed by supersymmetry reduces the number of parameters to three, which may be chosen to be M_W , v_2/v_1 and m_{H^\pm} . The other masses and the angle α are given by

$$m_{H_{1,2}}^2 = \frac{1}{2} \left\{ m_{H_3^0}^2 + M_Z^2 \pm \left[\left(m_{H_3^0}^2 + M_Z^2 \right)^2 - 4M_Z^2 m_{H_3^0}^2 \cos^2 2\beta \right]^{\frac{1}{2}} \right\},$$

$$m_{H_3^0}^2 = m_{H^\pm}^2 - M_W^2, \quad \tan 2\alpha = \tan 2\beta \left(\frac{m_{H_3^0}^2 + M_Z^2}{m_{H_3^0}^2 - M_Z^2} \right).$$

From these relations the Higgs boson masses satisfy the bounds

$$M_Z \leq m_{H_1^0} \leq \sec \theta_w m_{H^\pm}, \quad m_{H_2^0} \leq M_Z |\cos 2\beta|,$$

$$m_{H_3^0} \leq m_{H^\pm}, \quad m_{H^\pm} \geq M_W.$$

Since H_2^0 is lighter than the Z , it is a candidate for discovery at SLC or LEP. The mass of H_3^0 is not restricted and may be either lighter or heavier than the Z . The states H^\pm and H_1^0 are heavier than the Z and are of interest for a multi-TeV hadron collider, or for future e^+e^- machines of higher energies.

The Lagrangian for VHH interactions is

$$\begin{aligned} \mathcal{L} = & -\frac{ig}{2}W_{\mu}^{+}H^{-}\overleftrightarrow{\partial}^{\mu}\left[H_{1}^{0}\sin(\alpha-\beta)+H_{2}^{0}\cos(\alpha-\beta)+iH_{3}^{0}\right]+\text{h.c.} \\ & -\frac{ig}{2\cos\theta_{w}}Z_{\mu}\left\{iH_{3}^{0}\overleftrightarrow{\partial}^{\mu}\left[H_{1}^{0}\sin(\alpha-\beta)+H_{2}^{0}\cos(\alpha-\beta)\right]\right. \\ & \left.-(2x_{w}-1)H^{-}\overleftrightarrow{\partial}^{\mu}H^{+}\right\}, \end{aligned}$$

where $A\overleftrightarrow{\partial}^{\mu}B=A(\partial_{\mu}B)-B(\partial_{\mu}A)$. Bose statistics forbid a $ZH^{0}H^{0}$ vertex.

Exercise. Show that the partial width for $Z\rightarrow H_{2}^{0}H_{3}^{0}$ decay is

$$\Gamma=\frac{\cos^{2}(\alpha-\beta)G_{F}M_{Z}^{3}}{24\sqrt{2}\pi}\left[1-\frac{2}{M_{Z}^{2}}\left(m_{H_{2}^{0}}^{2}+m_{H_{3}^{0}}^{2}\right)+\frac{1}{M_{Z}^{4}}\left(m_{H_{2}^{0}}^{2}-m_{H_{3}^{0}}^{2}\right)^{2}\right]^{\frac{3}{2}}.$$

The VVH interaction terms are

$$\mathcal{L}=\left(gM_{W}W_{\mu}^{+}W^{-\mu}+\frac{gM_{Z}}{2\cos\theta_{w}}Z_{\mu}Z^{\mu}\right)\left[H_{1}^{0}\cos(\beta-\alpha)+H_{2}^{0}\sin(\beta-\alpha)\right].$$

Note that there is no tree level $W^{+}ZH^{-}$ vertex in the two doublet model. The interactions of the Higgs bosons with up and down type quarks are given by

$$\begin{aligned} \mathcal{L} = & -\frac{gm_{u}}{2M_{W}\sin\beta}\left[u\bar{u}\left(H_{1}^{0}\sin\alpha+H_{2}^{0}\cos\alpha\right)-i\cos\beta\bar{u}\gamma_{5}uH_{3}^{0}\right] \\ & -\frac{gm_{d}}{2M_{W}\cos\beta}\left[d\bar{d}\left(H_{1}^{0}\cos\alpha-H_{2}^{0}\sin\alpha\right)-i\sin\beta\bar{d}\gamma_{5}dH_{3}^{0}\right] \\ & +\frac{g}{2\sqrt{2}M_{W}}\left\{H^{+}V_{ud}\bar{u}\left[\left(m_{d}\tan\beta+m_{u}\cot\beta\right)\right.\right. \\ & \left.\left.+(m_{d}\tan\beta-m_{u}\cot\beta)\gamma_{5}\right]d+\text{h.c.}\right\}. \end{aligned}$$

The Higgs interactions with leptons are obtained by replacing (u, d) with (ν, e^{-}) . The factors $(\sin\beta)^{-1}$ and $(\cos\beta)^{-1}$ in the interaction can lead to enhancements or suppressions of neutral Higgs couplings.

There can be substantial changes in phenomenology relative to the standard model. The WW and ZZ couplings to H_3^0 are absent and these couplings to H_1^0 can be severely suppressed. It is likely that the WW and ZZ fusion mechanisms are essentially absent for all but the lighter neutral Higgs H_2^0 . Consequently H_1^0 and H_3^0 would be produced by gg fusion or $gg \rightarrow t\bar{t}H$. The decays of the heavy neutral Higgs would be dominantly to heavy quark pairs which is a difficult signature.

In the two doublet model the decay $\theta \rightarrow HZ$ of a heavy vector toponium state may be enhanced relative to the rate in the minimal standard model. In the standard model the $\theta \rightarrow HZ$ decay is suppressed due to a cancellation between a virtual Z diagram and a t -exchange diagram. The standard model predicts $\Gamma(\theta \rightarrow HZ)/\Gamma(\theta \rightarrow H\gamma) = \mathcal{O}(0.1)$ for $m_H \ll M_Z$. In the two doublet model values of this ratio larger than 1 are possible, especially for H_2 . Thus the $\theta \rightarrow HZ$ modes may be an important complement to the $\theta \rightarrow H\gamma$ process.

The charged Higgs boson can be singly produced in pp collisions via $gg \rightarrow \bar{t}bH^-$ subprocess of which one diagram is shown in Fig. 12.18(a). A good calculational approximation is given by the subprocess in Fig. 12.18(b) where the b quark distribution is generated by Altarelli-Parisi evolution. Fig. 12.19 gives the H^\pm production cross section versus m_H and $\sqrt{s} = 40$ TeV, assuming $\tan\beta = 1$. This cross section is substantial out to $m_{H^\pm} = 1$ TeV.

It is unlikely that the charged Higgs boson could be detected in the dominant $H^+ \rightarrow t\bar{b}$ decay mode because of enormous QCD backgrounds. However the rare mode $H^+ \rightarrow \tau^+\nu$ may give a viable signal at a hadron collider.

Exercise. Show that the $H^+ \rightarrow \tau^+\nu_\tau$ branching fraction is $B(H^+ \rightarrow \tau^+\nu_\tau) \approx 6 \times 10^{-4}$ for $m_t = 40$ GeV and $m_H > 100$ GeV, assuming $\tan\beta \simeq 1$.

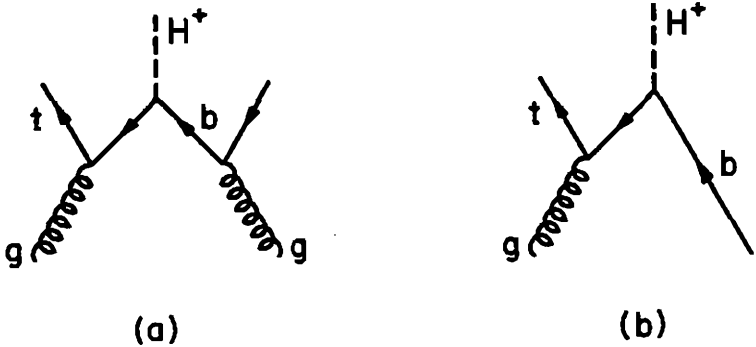


Fig. 12.18. Typical diagrams for charged Higgs production via (a) gluon-gluon fusion and (b) gluon-quark fusion.

If the top quark mass is larger than m_H , then the decay $t \rightarrow H^+ b$ is competitive with the $t \rightarrow W^+ b$ decay mode. Note that in the SUSY two doublet model it is not possible to have $m_{H^\pm} < m_t < M_W$ for which the $t \rightarrow H^+ b$ decay mode would completely dominate over virtual W -boson modes.

Exercise. Show that the ratio of partial widths is given by

$$\frac{\Gamma(t \rightarrow H^+ b)}{\Gamma(t \rightarrow W^+ b)} = \frac{p_H}{p_W} \frac{m_t^2(m_t^2 - m_H^2) \cot^2 \beta}{(m_t^2 + 2M_W^2)(m_t^2 - M_W^2)},$$

where p_H and p_W are the momenta in the t rest frame.

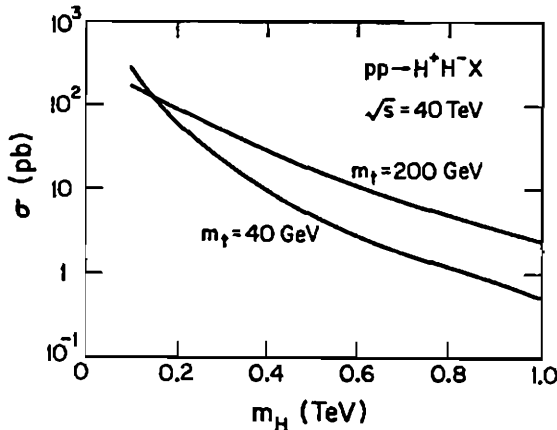


Fig. 12.19. Cross section for H^\pm production at $\sqrt{s} = 40$ TeV versus m_{H^\pm} .

12.7 Majorons

The question of small or vanishing neutrino masses has had many different explanations. In the standard model, with no right-handed neutrino states, no neutrino mass terms can be generated through Higgs doublet interactions. However we can generate a Majorana mass term of the form

$$\mathcal{L} = -m (\overline{\nu_R^c}) \nu_L + \text{h.c.}$$

through interaction with an $SU(2)$ triplet of scalar fields ϕ via the coupling

$$\mathcal{L} = -G_\nu \overline{L^c} \tau \cdot \phi L + \text{h.c.}, \quad \text{where } L = \begin{pmatrix} \nu_L \\ \ell_L \end{pmatrix}$$

and $\overline{L^c} = (\overline{\ell_R^c}, -\overline{\nu_R^c})$, provided that the neutral component of ϕ acquires a vev. The mass term does not conserve lepton number; the neutrino mass eigenstate is CP self-conjugate, a Majorana fermion.

Exercise. Show that the three components of ϕ have electric charges 2, 1, 0, so that it has $Y = 2$ and cannot couple to quark or antiquark pairs.

This idea, proposed by Gelmini and Roncadelli, introduces three new complex scalar fields leading to six new scalar bosons χ^{++} , χ^{--} , χ^+ , χ^- , χ^0 and M^0 . Of these M^0 is massless; it is a Goldstone boson, associated with the spontaneous breaking of lepton number (a global symmetry) and therefore called the *majoron*. The other new neutral scalar χ^0 has to be very light (of order 100 keV), from bounds on majoron emission in red supergiant stars. The charged scalar masses

are not determined, but are related by

$$m_{\chi^{++}} = \sqrt{2} m_{\chi^+}.$$

The gauge couplings to W and Z are given by

$$\begin{aligned} \mathcal{L} = & -ig \left[\chi^+ \overleftrightarrow{\partial}^\mu \chi^{--} + \frac{1}{\sqrt{2}} (\chi^0 - iM^0) \overleftrightarrow{\partial}^\mu \chi^- \right] W_\mu^+ \\ & - \frac{ig}{\cos \theta_w} \left[(1 - 2x_w) \chi^{--} \overleftrightarrow{\partial}^\mu \chi^{++} + x_w \chi^- \overleftrightarrow{\partial}^\mu \chi^+ - i\chi^0 \overleftrightarrow{\partial}^\mu M^0 \right] Z_\mu + \text{h.c.}, \end{aligned}$$

where $x_w = \sin^2 \theta_w$ and $g^2 = 4\sqrt{2} G_F M_W^2$.

Exercise. Derive the partial decay widths

$$\Gamma(W^+ \rightarrow \chi^{++} \chi^-) = \Gamma_W^0 (1 - 3w^2 + w^4/4)^{\frac{3}{2}},$$

$$\Gamma(W^+ \rightarrow \chi^+ M^0) = \Gamma(W^+ \rightarrow \chi^+ \chi^0) = \frac{1}{2} \Gamma_W^0 (1 - w^2/2)^3,$$

$$\Gamma(Z \rightarrow \chi^{++} \chi^{--}) = \Gamma_Z^0 (1 - 2x_w)^2 (1 - 4z^2)^{\frac{3}{2}},$$

$$\Gamma(Z \rightarrow \chi^+ \chi^-) = \Gamma_Z^0 x_w^2 (1 - 2z^2)^{\frac{3}{2}},$$

$$\Gamma(Z \rightarrow M^0 \chi^0) = \Gamma_Z^0,$$

where $\Gamma_W^0/M_W^3 = \Gamma_Z^0/M_Z^3 = G_F/(6\pi\sqrt{2})$, $w = m^{++}/M_W$, $z = m^{++}/M_Z$ and m^{++} is the mass of χ^{++} .

The heavy scalars χ^{++} and χ^+ have charged-current decay modes

$$\chi^{++} \rightarrow \chi^+ W^{*+}, \quad \chi^+ \rightarrow \chi^0 (M^0) W^{*+},$$

where W^* denotes a virtual boson going to $q\bar{q}'$ or $\nu\bar{\ell}$ pairs. They also have spectacular leptonic decay modes

$$\chi^{++} \rightarrow \ell^+ \ell^+, \quad \chi^+ \rightarrow \ell^+ \nu_\ell,$$

but the branching fractions depend on the masses and the Yukawa couplings that are unknown (though stringent upper limits are

known). These scalars are produced in e^+e^- collisions via γ^* or Z .

The majoron has interesting properties. The emission of a majoron flips neutrino helicity: $\nu_L \rightarrow \nu_R + M^0$. This has consequences in neutrino scattering (where $\nu_{\mu L} \rightarrow \mu^-$ but $\nu_{\mu R} \rightarrow \mu^+$ in charged-current interactions) and in double-beta decay (where $\nu_L\nu_L \rightarrow M^0$ vertices can appear). It can contribute to neutrino decays $\nu_1 \rightarrow \nu_2 + M^0$ in a general model with many Higgses but in the simple model above it couples to the mass matrix and gives no $\nu_1 \rightarrow \nu_2$ transitions.

The most immediate consequence however is the contribution to Z decay; $\Gamma(Z \rightarrow M^0\chi^0)$ is exactly twice the contribution from a simple neutrino species (compare §8.2). M^0 and χ^0 have neither strong nor electromagnetic interactions and escape undetected. Hence any experiment that counts the number of neutrinos by measuring $\Gamma(Z \rightarrow \text{invisible modes})$ automatically counts M^0 and χ^0 too, and must be interpreted accordingly. The 1986 upper limit

$$N_\nu \equiv (\text{Number of neutrinos} + M^0 + \chi^0) \leq 4.8 \quad (90\% \text{ CL}),$$

based on combining several experimental results from PEP and PETRA, for $e^+e^- \rightarrow \gamma + (\text{missing energy})$, is tantalizingly on the brink. If $N < 5$ is eventually established, or if a fourth generation of basic fermions is found, the majoron is excluded. Until then, the question of majorons versus more neutrinos remains open.

With the alternative approach to N_ν based on measuring the ratio Γ_Z/Γ_W (§8.2) charged scalar contributions can partly offset the majoron mode. For $m^{++} < 40$ GeV, the combined effect is less than one light neutrino, but for $m^{++} > 80$ GeV the charged scalar contributions are negligible.

A massless majoron also appears in a model where an additional

Higgs singlet breaks lepton number by giving Majorana mass to a singlet neutrino, but this does not have observable consequences.

12.8 The Technicolor Alternative

The $SU(2)_L \times U(1)$ electroweak model has many arbitrary parameters associated with the elementary Higgs field, in addition to the coupling constants of the gauge symmetry. These parameters are the Yukawa couplings of the Higgs boson to fermions and the self-couplings in the Higgs potential. Consequently, quark and lepton masses, quark mixing, $\sin^2\theta_w$, and the Higgs boson mass are not calculable, at least at this level. Technicolor models represent an attempt to avoid this arbitrariness by replacing the elementary Higgs scalar by composite ones. The composite scalars are meson bound states of a new strong interaction between new fermions. The low energy gauge group is

$$G_{TC} \times SU(3) \times SU(2)_L \times U(1)$$

where G_{TC} is the gauge group of the technicolor (TC) interaction. The usual quarks and leptons are TC singlets. The new fermions on which G_{TC} acts are called technifermions. Their TC singlet bound states are technimesons. G_{TC} is an asymptotically free unbroken gauge group analogous to QCD. The usual choice for G_{TC} is $SU(N)$ with the technifermions assigned to the fundamental N representation (*i.e.*, N is the number of technicolors). It is assumed that technicolor is confined with all physical states being technicolor singlets.

In the Farhi-Susskind model the chiral technifermions are

$$Q^i \equiv \begin{pmatrix} U^i \\ D^i \end{pmatrix}_L, \quad L \equiv \begin{pmatrix} N \\ E \end{pmatrix}_L, \quad U_R^i, D_R^i, N_R, E_R,$$

where $i = r, g, b$ is the ordinary $SU(3)$ color. The $SU(2)_L \times U(1)$

quantum numbers are the same as for the usual u, d quarks and ν_e, e leptons. The technicolor index is suppressed. In the absence of electroweak or strong interactions, there is a global $SU(8)_L \times SU(8)_R$ chiral symmetry of the eight flavors analogous to the chiral flavor symmetry of ordinary quarks. At energies below the scale Λ_{TC} at which G_{TC} becomes strong the technifermions acquire a dynamical mass associated with chiral symmetry breakdown. Following the QCD analogy, where the broken $SU(2)_L \times SU(2)_R$ flavor symmetry is invariant under $SU(2)_{ISOSPIN}$, it is assumed that the chiral symmetry is spontaneously broken to $SU(8)_{L+R}$ by eight equal condensates

$$\langle \overline{U}_L^a U_R^a \rangle = \langle \overline{D}_L^a D_R^a \rangle = \langle \overline{N}_L N_R \rangle = \langle \overline{E}_L E_R \rangle.$$

There is now less symmetry than in the original Lagrangian. The Goldstone theorem tells us that there will be a massless spin 0 boson for each broken generator. In the Farhi-Susskind model there are $8^2 - 1 = 63$ Goldstone bosons. The three Goldstone bosons

$$\phi^i \sim \bar{Q} \gamma_5 \frac{\tau^i}{2} Q + \bar{L} \gamma_5 \frac{\tau^i}{2} L, \quad i = \pm, 3$$

have couplings to the W^i and B^0 gauge bosons

$$\mathcal{L} = i\frac{1}{2}gFW^{i\mu}\partial_\mu\phi^i + i\frac{1}{2}g'FB^{0\mu}\partial_\mu\phi^3,$$

where F is a decay constant. The ϕ^i give masses to the gauge bosons. Consider the propagator

$$\Delta_{\mu\nu} = \frac{g_{\mu\nu} - q_\mu q_\nu / q^2}{q^2 [1 + \Pi(q^2)]},$$

where $\Pi(q^2)$ is the vacuum polarization. For a massless ϕ^\pm Goldstone

boson intermediate state the W^\pm vacuum polarization is

$$\Pi(q^2) = -\frac{1}{4}g^2 F^2/q^2$$

giving a W mass

$$M_W = \frac{1}{2}gF.$$

Similarly, the W^0, B^0 mass matrix is

$$\mathcal{M}^2 = \frac{1}{4}F^2 \begin{pmatrix} g^2 & gg' \\ gg' & g'^2 \end{pmatrix}$$

which has the eigenvalues

$$M_\gamma = 0, \quad M_Z = \frac{1}{2}(g^2 + g'^2)^{1/2} F.$$

The Standard Model result,

$$\frac{M_W}{M_Z} = \left(1 + \frac{g'^2}{g^2}\right)^{-1/2} \equiv \cos \theta_w,$$

follows as a result of isospin conservation. The ϕ^i Goldstone bosons are absorbed as the longitudinal components of the W^\pm and Z bosons. To get the W mass right, a technipion decay constant $F \sim 250$ GeV is required. This implies that Λ_{TC} is of order 1 TeV, since in QCD the pion decay constant $f_\pi \sim 93$ MeV is of the order of Λ_{QCD} .

In order to give masses to the quarks and leptons, the technifermions and ordinary fermions are placed in common multiplets of an *extended technicolor group* (ETC), which breaks down to technicolor at some large energy scale. In the ETC model problems were encountered with flavor-changing neutral currents. However, a resolution of this difficulty has been found in a class of models which effectively raise the mass scale of the condensates.

Table 12.3. Goldstone bosons of Farhi-Susskind model. The λ_a are $SU(3)$ color matrices and the τ^i are $SU(2)$ Pauli matrices, with $i = 0$ as the unit matrix. The ϕ^i states are absorbed by the W^\pm, Z bosons. The technicolor group is $SU(N)$.

color representation	boson	states	mass (GeV)
8	$(\pi_8)_a^i \sim \bar{Q}\gamma_5\tau^i\lambda_a Q$	$i = \pm, 3, 0$ $a = 1, \dots, 8$	$240\sqrt{\frac{4}{N}}$
$3, \bar{3}$	$(T)_a^i \sim \bar{L}\gamma_5\tau^i Q_a$	$i = \pm, 3, 0$ $a = 1, 2, 3$	$160\sqrt{\frac{4}{N}}$
1	$(P)^i \sim \bar{Q}\gamma_5\tau^i Q - 3\bar{L}\gamma_5\tau^i L$	$i = \pm, 3, 0$	< 100
1	$(\phi)^i \sim \bar{Q}\gamma_5\tau^i Q + \bar{L}\gamma_5\tau^i L$	$i = \pm, 3$	

The remaining sixty Goldstone bosons acquire mass from strong, electroweak, and extended technicolor forces to become pseudo-Goldstone bosons. These states and their expected masses in the simple model are given in Table 12.3. Higher masses are anticipated for the resolution of the flavor-changing neutral current problem.

At hadron colliders the color octet states π_8^i and the color triplet states T^i can be pair-produced by gluon-gluon fusion subprocesses. Also the states π_8^0 and P^3 can be singly produced through gluon-gluon fusion via a techniquark triangle diagram. Figure 12.20 shows these production diagrams for π_8^i and π_8^0 . The dominant decay modes of these particles, listed in Table 12.4, may not be easy in some instances to tag. For example, the technieta state η_8 of mass ~ 250 GeV has received considerable attention but its dominant gg and $t\bar{t}$ decays will be difficult to separate from QCD backgrounds.

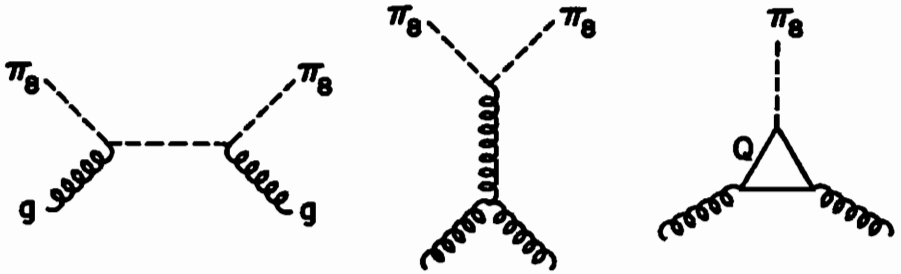


Fig. 12.20. Gluon-gluon fusion subprocesses for technihadron production at hadron colliders.

Table 12.4. Dominant decay modes of technicolor pseudo-Goldstone bosons.

π_8^0 (or η_8)	$t\bar{t}, gg$
π_8^3	$t\bar{t}$
π_8^+	$t\bar{b}, gW$
$T^{0,3}$	Dt, τ^+b
$T^{+(-)}$	$\tau^+t(Db)$
P^0	$b\bar{b}, \tau^+\tau^-$
P^3	$gg, b\bar{b}, \tau^+\tau^-$
P^+	$t\bar{b}, \tau^+\nu$

At e^+e^- colliders the charged technihadrons can be produced in pairs through the virtual photon. The cross section for P^+P^- production is

$$\sigma(e^+e^- \rightarrow P^+P^-)/\sigma(e^+e^- \rightarrow \mu^+\mu^-) = \frac{1}{4}(1 - 4M_P^2/s)^{3/2}.$$

The signals would be

$$e^+e^- \rightarrow P^+P^- \rightarrow (\bar{\tau}\nu)(\tau\nu), (\tau\nu)(t\bar{b}), (t\bar{b})(\bar{t}b).$$

At hadron supercolliders there is a promising signal of technicolor from the formation and decay of scalar bound states of technipions $\pi_8^+\pi_8^-$, $\pi_8^3\pi_8^3$ or $\pi_8^0\pi_8^0$ that may be bound together by the strong interaction similar to quarkonium. The technipionium state

$$\lambda = \frac{1}{2}[\sqrt{2}(\pi_8^+\pi_8^-) + \pi_8^3\pi_8^3 + \pi_8^0\pi_8^0]$$

can be produced via $gg \rightarrow \lambda$, as illustrated in Fig. 12.21. The production of λ is enhanced relative to quarkonium by orders of magnitude because of the larger color coupling. The cross section for λ production in pp collisions at 40 TeV is in the 100 pb range for $M_\lambda \sim \frac{1}{2}$ TeV. The decay of λ technipionium to W^+W^- , $\gamma\gamma$ and $Z\gamma$ with branching fractions of order 0.3 to 0.1%, would give thousands of gauge boson pairs a year.

Gauge models with more than one elementary Higgs multiplet have additional neutral H^0 and charged H^\pm , beyond the single H^0 of the standard model. For example, in supersymmetry two Higgs doublets are necessary to give masses to the fermions and there are three neutral and two charged Higgs bosons. These physical elementary bosons have decay modes similar to the P^0 , P^3 , P^\pm of the technicolor model. Thus the question naturally arises, if spin-0 states are discovered, how can we decide whether they are elementary Higgs bosons or technicolor composites. Fortunately there is

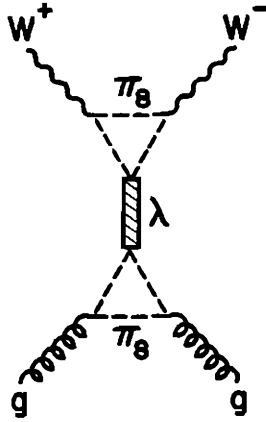


Fig. 12.21. Diagram illustrating production and decay to W^+W^- of the scalar technipionium bound state λ .

an easy resolution: only the elementary Higgs bosons have the tree level couplings to W and Z bosons. Thus the processes $Z \rightarrow ZH^0$ and $W^\pm \rightarrow W^\pm H^0$ exist but the corresponding technicolor processes $Z \rightarrow ZP^0$ and $W^\pm \rightarrow W^\pm P^0$ occur only through higher order diagrams and are suppressed.

Chapter 13

A Fourth Generation

13.1 Mass Bounds

The replication of fermion generations is one of the outstanding puzzles in particle physics. Could there also be a fourth generation of quarks and leptons? There is no convincing theoretical or experimental reason why not. In some grand unified schemes consistency with the evolution of masses and couplings may indicate only three generations, but these models are not uniquely established. Thus it is important for collider experiments to continue the search for new fermions that may belong to a fourth generation. We label the fourth generation leptons as (ν_L, L) and the fourth generation quarks by (a, v) where a and v have charges $(\frac{2}{3}, -\frac{1}{3})$. This notation for the quarks is suggested by the alphabetic labels used for the other quarks (*viz.*, $a, b, c, d, \dots, s, t, u, v$). The names *audio* and *video* have been proposed for these quarks, after the gods of the present generation!

Since the systematics of the masses of the known fermions are unexplained, there is no reliable extrapolation to masses of a possible fourth generation. However, a significant constraint is obtained on the mass splitting between doublet members from $\rho = G$ (neutral current)/ G (charge current) = $1 + \mathcal{O}(\alpha)$. The calculated value with one-loop radiative corrections is

$$\rho = 1.00 + \frac{G_F}{8\sqrt{2}\pi^2} [3(m_t - m_b)^2 + m_\tau^2 + 3(m_a - m_v)^2 + (m_L - m_{\nu_L})^2].$$

From the bound $\rho < 1.01$ at the one standard deviation level, $m_t < 160$ GeV if no fourth generation exists. In the case of a fourth generation, the mass splittings must satisfy

$$(m_a - m_\nu)^2 + \frac{1}{3}(m_L - m_{\nu_L})^2 < (160 \text{ GeV})^2 - (m_t - m_b)^2 .$$

When radiative corrections are included in a global fit to all neutral current data, preliminary results indicate that the 160 GeV mass limit above is improved.

If the absolute a and ν masses are sufficiently high, then the weak interaction among heavy particles becomes strong and perturbation theory breaks down. In order not to violate partial wave unitarity in perturbation theory, the masses must satisfy

$$m_a < 700 \text{ GeV} , \quad m_L < 1000 \text{ GeV} ,$$

but this is desirable rather than a necessary limit.

For heavy fermions the renormalization group equations of the Yukawa couplings converge at energies of order $v = 246$ GeV to fixed point values, assuming that the couplings remain perturbative up to grand unified scales $M_X \sim 10^{16}$ GeV. Then the masses satisfy the bound

$$\sum m_u^2 + \sum m_d^2 + \frac{1}{3} (\sum m_l^2 + \sum m_\nu^2) \leq 2v^2 ,$$

where the sums are over all quarks and leptons. Hence each fourth generation quark must be lighter than ≈ 200 GeV. Moreover, the heavy quark doublets are nearly degenerate

$$m_a^2 - m_\nu^2 \approx 0.02 v^2$$

or $m_a - m_\nu \approx \mathcal{O}(4 \text{ GeV})$ for $m_a \approx 200$ GeV. From the renormalization group equations of $N = 1$ supergravity the following upper bounds

were obtained

$$m_a \lesssim 140 \text{ GeV}, \quad m_\nu \lesssim 135 \text{ GeV}, \quad m_L \lesssim 70 \text{ GeV}.$$

All these bounds depend on the perturbative assumption, however.

13.2 Neutrino Counting

There is a cosmological bound on the number of light neutrino flavors. The amount of ${}^4\text{He}$ produced primordially in the standard big bang model increases with the addition of new species of particles that are relativistic during nucleosynthesis. Observations of ${}^4\text{He}$ abundance give the bound $N_\nu \lesssim 4.0$ on the number of equivalent left-handed neutrinos. If new neutrino flavors are heavy and unstable, this cosmological bound does not apply. In any case, there is no cosmology limitation on a fourth generation ν_L .

The process $e^+e^- \rightarrow \nu\bar{\nu}\gamma$ can be used to count the number of light neutrino species, both below the Z resonance and when a real Z is produced. The background from $e^+e^- \rightarrow e^+e^-\gamma$ when the final e^+ and e^- go down the beam pipe can be reduced by requiring that the photon have a minimum angle θ_γ^{\min} and a minimum transverse momentum $p_{\gamma T}^{\min}$ with respect to the beam axis. After integrating over the angle of the final state photon subject to these cuts, the E_γ distribution is

$$\frac{d\sigma}{dx}(e^+e^- \rightarrow \nu\bar{\nu}\gamma) = \hat{\sigma}(\sqrt{\hat{s}}, e^+e^- \rightarrow \nu\bar{\nu}) f(\sqrt{s}, x, \theta_\gamma^{\min}, p_{\gamma T}^{\min}),$$

where $x = 2E_\gamma/\sqrt{s}$, $\hat{s} = s(1-x)$ and f is the following function:

$$f = (\alpha/\pi x) \{ (2 - 2x + x^2) \ln [(1 + \delta)/(1 - \delta)] - x^2\delta \}.$$

The parameter δ is related to the acceptance:

$$\delta = \cos \theta_{\gamma}^{\min}, \quad \text{for } x > \frac{2p_{T\gamma}^{\min}}{\sqrt{s} \sin \theta_{\gamma}^{\min}},$$

$$\delta = \left[1 - \left(\frac{2p_{T\gamma}^{\min}}{x\sqrt{s}} \right)^2 \right]^{\frac{1}{2}}, \quad \text{for } \frac{2p_{T\gamma}^{\min}}{\sqrt{s}} \leq x \leq \frac{2p_{T\gamma}^{\min}}{\sqrt{s} \sin \theta_{\gamma}^{\min}}.$$

The $e^+e^- \rightarrow \nu\bar{\nu}$ subprocess cross section for N_{ν} light left-handed neutrinos is

$$\hat{\sigma} = \frac{G_F^2 \hat{s}}{6\pi} \left\{ 1 + (1 - 2x_w) \Re eR + \frac{N_{\nu}}{8} [1 + (1 - 4x_w)^2] |R|^2 \right\},$$

where $R = M_Z^2 / (\hat{s} - M_Z^2 + iM_Z\Gamma_Z)$. The three terms in $\hat{\sigma}$ are W -exchange, interference, and Z -pole contributions. The number of neutrinos is counted by comparing the calculated σ (integrated over the x -range allowed by the acceptance cuts) with the measured σ . Experiments by the ASP, MAC and CELLO collaborations at PEP and PETRA have placed a bound of $N_{\nu} < 4.8$ at 90% C.L. Future measurements on the Z -pole at SLC and LEP will measure N_{ν} to an accuracy of ± 0.3 .

Exercise. Generalize the $e^+e^- \rightarrow \nu\bar{\nu}$ cross section expression to include the effects of a heavy neutrino.

Exercise. Consider a generalized neutral current Lagrangian

$$\mathcal{L} = g_Z \sum_{\beta,j} Z_{\beta}^{\mu} \left[f_{\nu}^{\beta} \bar{\nu}_j \gamma_{\mu} (1 - \gamma_5) \nu_j + f_N^{\beta} \bar{N}_j \gamma_{\mu} (1 + \gamma_5) N_j \right. \\ \left. + \frac{1}{2} g_L^{\beta} \bar{e} \gamma_{\mu} (1 - \gamma_5) e + \frac{1}{2} g_R^{\beta} \bar{e} \gamma_{\mu} (1 + \gamma_5) e \right],$$

which has extra Z bosons and both left- and right-handed neutrinos. Here j is a generation index and the f and g are coupling coefficients.

Show that the $e^+e^- \rightarrow \nu\bar{\nu}, N\bar{N}$ cross section is given by

$$\hat{\sigma} = (G_F^2 \hat{s} / 6\pi) \left\{ 1 - 8 \sum_{\beta} f_{\nu}^{\beta} g_L^{\beta} \operatorname{Re}(R_{\beta}) + 16n(\nu) \left[\sum_{\alpha, \beta} f_{\nu}^{\alpha} f_{\nu}^{\beta} \left(g_L^{\alpha} g_L^{\beta} + g_R^{\alpha} g_R^{\beta} \right) \operatorname{Re}(R_{\alpha} R_{\beta}^*) \right] + 16n(N) [\nu \rightarrow N] \right\},$$

where $n(\nu)$ and $n(N)$ are the number of light left- and right-handed neutrinos, respectively, and

$$R_{\beta} = M_Z^2 / (\hat{s} - M_{Z\beta}^2 + iM_{Z\beta} \Gamma_{\beta}).$$

Measurements of the total visible and invisible Z widths constrain the number of new fermions. For $M_Z = 91.19$ GeV, $\alpha(M_Z) = 0.12$ and $x_w = 0.23$, the fermionic decay contributions are

$$\Gamma_Z = 2.49 + 0.16F_{\nu_L} + 0.08F_L + 0.30F_a + 0.38F_v \quad (\text{GeV}),$$

where 2.49 comes from the first 3 generations (0.50 from invisible neutrinos) and F_i are fourth-generation mass-dependent factors,

$$\begin{aligned} F_{\nu_L} &= [1 - m_{\nu_L}^2 / M_Z^2] (1 - 4m_{\nu_L}^2 / M_Z^2)^{\frac{1}{2}} \quad (\text{Dirac}), \\ &= (1 - 4m_{\nu_L}^2 / M_Z^2)^{\frac{3}{2}} \quad (\text{Majorana}), \\ F_L &= [1 - 3.96m_L^2 / M_Z^2] (1 - 4m_L^2 / M_Z^2)^{\frac{1}{2}}, \\ F_a &= [1 - 3.22m_a^2 / M_Z^2] (1 - 4m_a^2 / M_Z^2)^{\frac{1}{2}}, \\ F_v &= [1 - 2.05m_v^2 / M_Z^2] (1 - 4m_v^2 / M_Z^2)^{\frac{1}{2}}. \end{aligned}$$

Upper limits on Γ_Z , Γ_Z^{vis} and Γ_Z^{inv} impose upper bounds on the ν_L , L , a , v contributions, requiring all $F_i \simeq 0$ and hence $m_i \gtrsim \frac{1}{2} M_Z$ for any fourth-generation fermion. Figure 13.1 shows the sensitivity of Γ_Z to the number of light (essentially massless) neutrinos N_{ν} , given a hypothetical t -quark with $m_t = 40$ GeV or $m_t = M_W$ (i.e. essentially non-contributing).

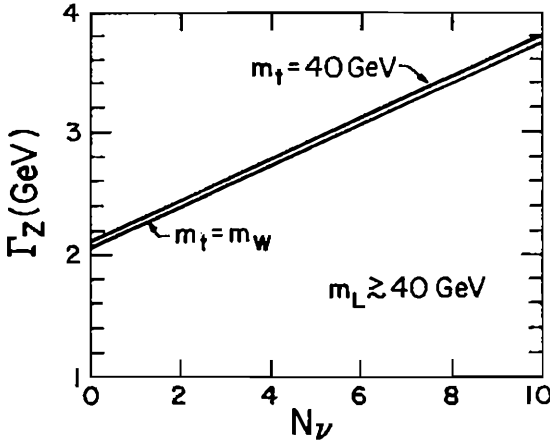


Fig. 13.1. Γ_Z versus N_ν for various m_t and m_L mass choices (assuming ν and a are too heavy to contribute).

The experimental upper bound on the ratio Γ_Z/Γ_W can be used to limit the contributions from fourth generation quarks and leptons (see the discussion of §8.2 where this ratio was used in connection with t -quark contributions). The fermion contributions to the W width are given by

$$\Gamma_W = 2.07 + 0.7H_t + 0.22H_L \quad (\text{GeV}),$$

where $m_a > M_W$ and $m_{\nu_L} = 0$ are assumed, and

$$H_i = \left[1 - \frac{3}{2}(m_i^2/M_W^2) + \frac{1}{2}(m_i^2/M_W^2)^3 \right]$$

for $i = t, L$.

Figure 13.2 shows the predictions of Γ_Z/Γ_W versus m_t for various illustrative examples with $N_\nu = 4$. Curve (a) shows the effect of a ν -quark ($m_\nu = 24 \text{ GeV}$) with no L contribution. Curve (b) shows the effect of an L -lepton with $m_{\nu_L} = 0$ ($m_L = 41 \text{ GeV}$) with no ν contributions. Curve (c) shows the effect of both these ν and L contributions together. The UA2 90% and 95% C.L. upper limits are also shown; by themselves, these allow a range of situations in which either ν or L or both are present with masses down to 24 GeV.

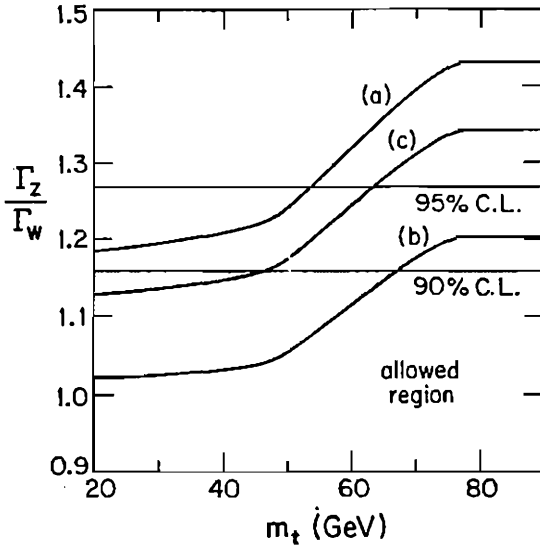


Fig. 13.2. Γ_Z/Γ_W predictions for several choices of ν -quark and L -lepton masses plotted versus the top quark mass.

13.3 Heavy Leptons from W -Decay

A new heavy lepton could be detected at the CERN or Fermilab $p\bar{p}$ colliders through the decay mode $W \rightarrow L\nu_L$ of real W bosons if $m_L + m_{\nu_L} < M_W$. We concentrate first on the case of ν_L essentially massless. The experimental signature depends on the decay mode of the charged heavy lepton. The leptonic and hadronic decay modes

$$L \rightarrow e\bar{\nu}_e\nu_L, \mu\bar{\nu}_\mu\nu_L, \tau\bar{\nu}_\tau\nu_L, d\bar{u}\nu_L, s\bar{c}\nu_L$$

have approximate branching fractions of $\frac{1}{9}, \frac{1}{9}, \frac{1}{9}, \frac{3}{9}, \frac{3}{9}$.

13.3.1 Leptonic signal.

For a leptonic decay chain such as

$$W \rightarrow L\bar{\nu}_L \rightarrow e\bar{\nu}_e\nu_L\bar{\nu}_L,$$

the signature is unfortunately the same as the direct and τ -initiated

decay modes of the W ,

$$W \rightarrow e\bar{\nu}_e, \quad W \rightarrow \tau\bar{\nu}_\tau \rightarrow e\bar{\nu}_e\nu_\tau\bar{\nu}_\tau,$$

namely, an isolated energetic electron accompanied by missing transverse momentum arising from the neutrinos. The W partial widths for these leptonic modes are in the approximate proportions

$$(W \rightarrow L \rightarrow e) : (W \rightarrow \tau \rightarrow e) : (W \rightarrow e) = \frac{1}{9}(1 - \frac{3}{2}r + \frac{1}{2}r^3) : 0.17 : 1,$$

where $r = m_L^2/M_W^2$. Thus the backgrounds are larger than the L -signal. However there is a restricted kinematic region of $8 < p_{eT} < 16$ GeV and $-0.9 < \cos\theta(\bar{p}, e^+) < 0.2$ where the L -signal for $m_L < 50$ GeV exceeds the direct $W \rightarrow e\nu_e$ background, as shown in Fig. 13.3. Even in this window the signal is about a factor of two below that from $W \rightarrow \tau \rightarrow e$. To identify such an L -signal at the 3 standard deviation level would require a data sample with more than 1000 $W \rightarrow e^+\nu$ events. This situation would be improved by the use of microvertex detectors that would help suppress the τ background by separating its production and decay vertices in these events. Since the discovery window above involves lepton transverse momenta of around 12 GeV, the observation of muons may be preferred from an experimental standpoint.

There is another background to the leptonic L -signal from $b\bar{b}$ production with $\bar{b} \rightarrow \bar{c}e^+\nu_e$ decay that must also be dealt with. In the above discovery window it is two orders of magnitude above the L -signal. However this background can be essentially eliminated by requiring little hadronic p_T in the events (*e.g.*, $\sum p_T < 10$ GeV from hadrons). The e^+ from $b\bar{b}$ events is accompanied by hadrons with substantial p_T from the b and \bar{c} decays.

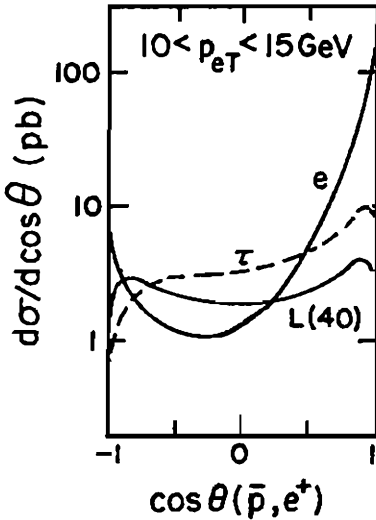


Fig. 13.3. The e^+ angular distribution for the interval $10 < p_{eT} < 15$ GeV from $W \rightarrow e$, $W \rightarrow \tau \rightarrow e$, and $W \rightarrow L \rightarrow e$ sources.

13.3.2 Missing p_T signal.

The hadronic decays of the charged heavy lepton provide its best potential signal at $p\bar{p}$ colliders. The relevant decay chains are

$$W \rightarrow \bar{L}\nu_L \rightarrow (u\bar{d} \text{ or } c\bar{s})\bar{\nu}_L\nu_L.$$

This has the distinctive signature in $p\bar{p}$ collisions of high missing transverse momentum (\cancel{p}_T) from $\nu_L\bar{\nu}_L$ balanced by hadron jets. For the \cancel{p}_T to be experimentally significant and not due for example to measurement errors on hadron momenta, it must be typically greater than 20 GeV. This L -signal is substantial for $m_L < 50$ GeV—it is roughly 10% of the rate for $W \rightarrow e\nu$. There are standard model backgrounds arising from $W \rightarrow \tau\nu$, $Z \rightarrow \nu\bar{\nu}$ and heavy quark decay processes that are comparable to the L -signal but can in principle be separated from it in various ways.

The jet structure of $W \rightarrow L\nu_L$ decay events is affected by additional gluons radiated from incident quarks, with the dominant

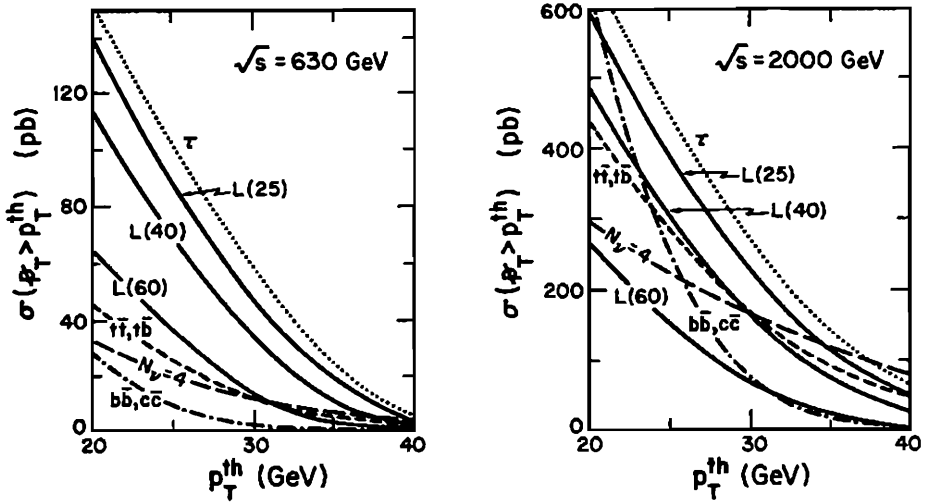


Fig. 13.4. The $p\bar{p} \rightarrow W \rightarrow L\nu_L \rightarrow \cancel{p}_T + \text{hadrons}$ cross section and backgrounds for \cancel{p}_T greater than a threshold p_T^{th} .

correction coming from $d\bar{u} \rightarrow Wg$ production. Also the $Z \rightarrow \nu\bar{\nu}$ background calculation requires gluon radiation since the Z must be produced at high \cancel{p}_T . The QCD radiation of gluons can be evaluated with Monte Carlo shower programs or by truncated shower calculations based on the dominant lowest order QCD radiative subprocess.

Representative evaluations of the L -signal and backgrounds are shown in Fig. 13.4 for CERN and Fermilab collider energies. The principal background comes from $W \rightarrow \tau\nu$ but this does not pose a serious problem. The hadron jets from $\tau \rightarrow \nu_\tau + \text{hadrons}$ have quite distinctive small angular spread and low charged particle multiplicity, so many of these events can be identified directly. Also the τ decay vertex can in principle be resolved by a microvertex detector.

The $Z \rightarrow \nu\bar{\nu}$ background in Fig. 13.4 assumes $N_\nu = 4$ neutrinos.

The heavy quark backgrounds assume $m_t = 40$ GeV. Even though these backgrounds are not small, various techniques can be used to separate them from the L -signal. The τ and Z backgrounds have lower mean jet multiplicity than the L -signal, whereas the heavy quark backgrounds have higher jet multiplicity than the signal. The quark jets from L decay contain a charm quark in 50% of the events but the jets associated with Z do not. In $\cancel{p}_T + 2$ jet events of $b\bar{b}$ or $c\bar{c}$ origin the two jets are nearly back-to-back in azimuth. Also heavy quark events will contain a large number of resolvable decay vertices which will distinguish them from the L -signal if a microvertex detector is available. Thus it appears that all standard physics backgrounds can be distinguished from the L -signal.

The UA1 collaboration investigated $\cancel{p}_T + \text{jet(s)}$ events at the CERN $p\bar{p}$ collider for possible evidence of W decay into heavy leptons. With selection criteria designed to suppress $W \rightarrow \tau \rightarrow \text{hadrons}$ events, 17 events remained compared to a calculated background of 17.8 ± 4.7 events (7.1 $W \rightarrow \tau \rightarrow \text{hadrons}$, 5.6 $Z \rightarrow \nu\bar{\nu}$ for $N_\nu = 3$, 5.1 other backgrounds; an additional 2.9 ± 1.5 events from heavy quarks were expected for $m_t = 40$ GeV). The predicted heavy lepton signal for mass $m_L = 25, 35, 45, 55$ GeV was 17.0, 12.3, 8.0, 3.9 events. On the basis of this comparison it was concluded that $m_L > 41$ GeV at 90% C. L. Also a limit $N_\nu < 10$ was deduced on the number of neutrino species.

13.4 $e^+e^- \rightarrow L\bar{L}$

Heavy lepton pairs would be produced at e^+e^- colliders via γ^* and Z intermediate states. The present limit on the L mass from e^+e^- experiments is $m_L > 22.7$ GeV at 90% C.L. Figure 13.5 shows the $L\bar{L}$ cross section relative to the $\mu\mu$ cross section versus the e^+e^- c.m. energy \sqrt{s} for different choices of heavy lepton mass. There is a dip

in the $\bar{L}L$ cross section at the Z resonance energy where the γ^*, Z interference goes to zero and the Z resonance contribution dominates. The production rate of $\bar{L}L$ pairs for e^+e^- machines operating at the Z resonance is very sensitive to m_L and can be used to determine m_L . An independent measurement of m_L can be made from the sharp rise in event rate as the c.m. energy is increased through the $\bar{L}L$ threshold.

The two primary classes of L decays $L \rightarrow \ell + \not{p}$ ($\ell = e$ or μ and \not{p} = missing energy-momentum of neutrinos) and $L \rightarrow \bar{q}_1 q_2 + \not{p}$ (q_1, q_2 = quark jets including $L \rightarrow \tau \rightarrow \bar{q}_1 q_2 \nu_\tau$ modes) are in the ratio 1 : 3. The resulting signatures for $\bar{L}L$ fall in the following three distinctive categories, in the approximate proportions 6 : 38 : 56,

- (i) $\ell_1 \bar{\ell}_2 + \not{p}$, a pair of opposite-sign leptons, which may have different flavors, along with missing energy-momentum from neutrinos,

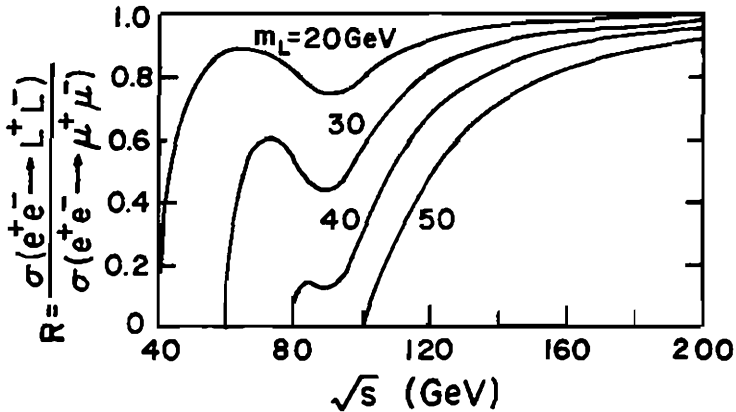


Fig. 13.5. Ratio of $L\bar{L}$ to $\mu\bar{\mu}$ cross sections versus the c.m. energy in e^+e^- collisions for various L masses.

(ii) $\ell q_1 \bar{q}_2 + \cancel{p}$, a single charged lepton with up to two hadronic jets plus missing energy-momentum,

(iii) $q_1 \bar{q}_2 q_3 \bar{q}_4 + \cancel{p}$, up to four jets and missing energy-momentum.

In the case of a c -quark jet from \bar{L} decay, semileptonic charm decay can give an additional lepton accompanied by hadrons. It is naturally understood that the hadronic jets arising from individual quarks may sometimes overlap to form broader jets; in the case of τ decay the $q_1 \bar{q}_2$ give a single narrow hadronic jet.

13.4.1 Dilepton signals from $\bar{L}L$.

An e^+e^- machine operating at the Z resonance could be a copious source of heavy leptons. The decay $Z \rightarrow \bar{L}L$ with each L decaying leptonically should provide a very clean signal. The expected rate of the leptonic channels into e and μ is about 5% of the total $\bar{L}L$ signal. The ee , $\mu\mu$, $e\mu$ opposite-sign dileptons would occur in the ratio of 1 : 1 : 2. There would be no accompanying hadronic activity. The leptons would be acollinear, with the shape of the opening angular distribution depending on the L mass as illustrated in Fig. 13.6. Dileptons from the $Z \rightarrow \bar{\tau}\tau$ background process will be nearly back to back.

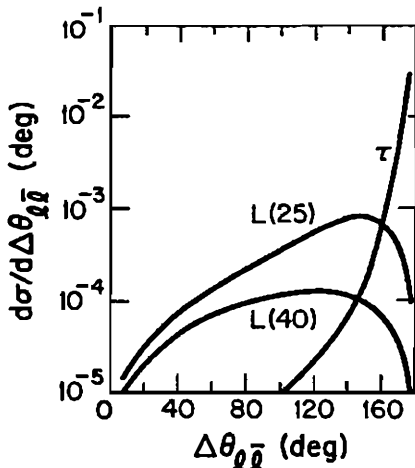


Fig. 13.6. Distribution in dilepton opening angle from leptonic decays of heavy lepton pairs produced in e^+e^- collisions at $\sqrt{s} = M_Z$.

13.4.2 Lepton + jets signals from $\bar{L}L$.

The decay $\bar{L} \rightarrow \bar{\nu}_L \nu_\ell \bar{\ell}$, $L \rightarrow \nu_L \bar{q}_1 q_2$ produces one or two jets. The invariant mass of these two jets can be used in determining the L mass, as the dijet mass is always bounded by m_L . A background process is $Z \rightarrow \bar{b}b$ or $\bar{c}c$ with one heavy quark decaying semileptonically; since the trigger lepton will be accompanied by hadronic debris, lepton isolation cuts can be used to suppress this background.

13.4.3 Four jet + missing energy signal from $\bar{L}L$.

The case that each L of the $\bar{L}L$ pair decays hadronically occurs half of the time. There are up to four jets accompanied by missing energy.

The various dilepton and lepton-plus-two-jet signals of heavy leptons at e^+e^- colliders would be easily recognizable against standard model backgrounds and heavy leptons will be discovered at SLC and LEP if their masses are less than $\frac{1}{2}M_Z$.

13.5 Unstable ν_4

Hitherto we have assumed the fourth generation neutrino is essentially massless. Should this not be the case, the previously considered signatures for L and ν_L may not apply, since a heavy neutrino will in general be unstable and could decay within the detector region. We now investigate the consequences of neutrino instability on experimental searches, assuming that ν_L is heavy but lighter than L .

In general ν_L is not a mass eigenstate. The neutrino flavors ν_ℓ which form left-hand doublets with the charged leptons $\ell = e, \mu, \tau, L$ are related to the mass eigenstates ν_j with $j = 1, 2, 3, 4$ by a unitary matrix V

$$\nu_\ell = \sum_j V_{\ell j}^\dagger \nu_j, \quad \nu_j = \sum_\ell V_{j\ell} \nu_\ell.$$

The elements $V_{4\ell}$ govern the couplings of W to $\nu_4 \bar{\ell}$. $V_{4e}, V_{4\mu}, V_{4\tau}$ are

expected to be small; $V_{4\tau}$ will be the largest if mixing occurs preferentially among nearest generations. The Z boson couples equally to the mass eigenstates $\bar{\nu}_j\nu_j$.

The ν_4 decays to a lepton ℓ and a virtual W boson with a decay amplitude proportional to $V_{4\ell}$. The partial decay widths for $\nu_4 \rightarrow \ell f \bar{f}'$ summed over final state fermions are

$$\Gamma_\ell = \frac{G_F^2 m_4^5}{192\pi^3} |V_{4\ell}|^2 \sum C_f |V_{ff'}|^2,$$

where the color factor is $C_f = 1$ for leptons and $C_f = 3$ for quarks. In this result the phase space suppression for massive final state particles has been neglected and $m_4 \ll M_W$ is assumed. In the case of a Majorana ν_4 the decays $\nu_4 \rightarrow \ell^-$ and $\nu_4 \rightarrow \ell^+$ occur equally and must be summed in Γ_ℓ . Assuming that $m_4 < m_L$, the ν_4 mean life is

$$\tau_4 = (\Gamma_e + \Gamma_\mu + \Gamma_\tau)^{-1}.$$

The corresponding mean decay length l is

$$l = \beta\gamma c\tau_4.$$

Depending on m_4 and V , the decay gap may be resolved or unresolvable from the production vertex or be long enough that ν_4 escapes from collider detectors unseen (see §3.3 for illustrative calculations). It is important that all possibilities be considered if we are to find or to exclude fourth generation neutrinos.

13.5.1 $W \rightarrow L\nu_L$ limit revisited.

The limit on m_L from $W \rightarrow L\nu_L$ applies only if all components of ν_L are light and undetected. If the main component ν_4 is heavy (but lighter than L), it will decay though lepton mixing

$$\nu_4 \rightarrow \ell(\nu_e\bar{e}, \nu_\mu\bar{\mu}, \nu_\tau\bar{\tau}, u\bar{d}, c\bar{s}).$$

If the ν_4 mixing elements and mass are such that the ν_4 decay length is short compared to the detector size, most of the ν_4 decay products

are detected and there is little if any missing p_T in a $W \rightarrow L\nu$ event. The UA1 limits on events with large p_T then have nothing to say about L .

13.5.2 $e^+e^- \rightarrow L^+L^-$ limit revisited.

If ν_4 decays, the e^+e^- limits on m_L are weakened since the most stringent limits have come from looking for acoplanar jets or acoplanar muon plus jets, assuming that $L \rightarrow \nu_4 f \bar{f}'$ decays have missing energy-momentum. However, $e^+e^- \rightarrow L^+L^-$ events will contribute about 0.5 to the ratio $R = \sigma(e^+e^- \rightarrow \text{hadrons})/\sigma(e^+e^- \rightarrow \mu^+\mu^-)$. The absence of an enhancement in R still allows one to exclude L^+L^- production up to $m_L \simeq 22$ GeV.

If ν_4 is stable or sufficiently long-lived to escape undetected from the apparatus, detecting L requires an appreciable mass difference between L and ν_4 to produce a measurable residue. With 0.14 GeV $m_L - m_4 \lesssim 3$ GeV a heavy charged lepton with mass $\gtrsim 4$ GeV would not yet have been discovered.

Exercise. Suppose that L^-, ν_4 have masses $m_L > m_4$ with $m_L - m_4 \ll m_L$. For $e^+e^- \rightarrow L^+L^-$ production at the Z resonance show that the charged particle emitted in the decay modes

$$L^- \rightarrow \nu_4 \ell^- \nu_\ell, \quad L^- \rightarrow \nu_4 \pi^-,$$

has maximum laboratory momentum

$$p_{\max} = \frac{1}{4} M_Z \left\{ 1 - (m_4/m_L)^2 \right\} \left\{ 1 + \left[1 - (2m_L/M_Z)^2 \right]^{\frac{1}{2}} \right\}$$

in the approximation that the masses of ℓ, ν_ℓ and π are neglected. For general $L \rightarrow \nu_4 X$ decays, show that the visible energy has the bound

$$E_{\text{vis}} < \begin{cases} M_Z/2 - m_4 & \text{if } M_Z m_4 \leq (m_L^2 + m_4^2) \\ p_{\max} & \text{if } M_Z m_4 > (m_L^2 + m_4^2) \end{cases}$$

Exercise. If $m_L - m_4 \lesssim m_\pi$ show that the L^- decay length becomes

of order of a meter or longer at $\sqrt{s} = 30 \text{ GeV}$. It would then have appeared in experimental searches for stable leptons and can be excluded.

13.5.3 Experimental limits on ν_4 .

Figure 13.7 summarizes experimental limits on the mass m_4 and mixing $|V_{4e}|^2$ of a fourth generation neutrino ν_4 . Similar limits exist for m_4 versus $|V_{4\mu}|^2$. The limits are obtained from searches for

- additional monochromatic peaks in electron or muon spectra in π , $K \rightarrow e\nu$ or $\mu\nu$ decays, curves labeled (1), (2), (3).
- downstream decays of ν_4 produced in π, K decays (4), (10) or charm decays, curves (5), (9), (11).
- monojet from decay of ν_4 produced via W exchange in $e^+e^- \rightarrow \nu_4\bar{\nu}_e$, curve (7).
- secondary decay vertices of ν_4 produced through a virtual Z in $e^+e^- \rightarrow \nu_4\bar{\nu}_4$, curve (8).
- deviations from e, μ universality, curve (6)

The continuation of e^+e^- searches at c.m. energies $\sqrt{s} < M_Z$ will probe the ranges

$$|V_{4e}|^2, |V_{4\mu}|^2 \gtrsim 10^{-6} \quad \text{for } m_4 \lesssim 20 \text{ GeV},$$

$$|V_{4e}|^2 \gtrsim 10^{-2} \text{ to } 10^{-3} \quad \text{for } m_4 \lesssim 30 \text{ GeV}.$$

In the $e^+e^- \rightarrow \nu_4\bar{\nu}_4$ process the $Z\nu_4\bar{\nu}_4$ couplings of the intermediate Z boson are $g_V = g_A = \frac{1}{4}$ for Dirac ν_4 and $g_V = 0$, $g_A = 1/2$ for Majorana ν_4 . Also the phase space for the identical particle Majorana case is $1/2$ that for Dirac ν_4 . Figure 13.8 illustrates the cross section dependence on \sqrt{s} in the two cases for several values of the ν_4 mass.

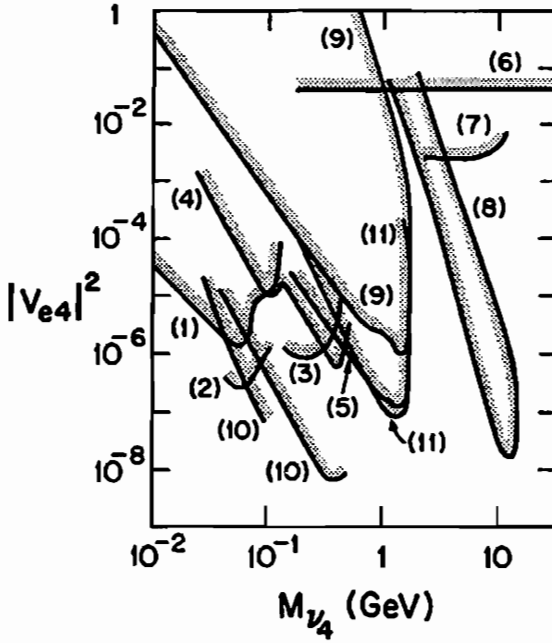


Fig. 13.7. Limits on $|V_{4e}|^2$ versus the ν_4 mass as summarized in Comm. Nucl. Part. Phys. 16, 231 (1986).

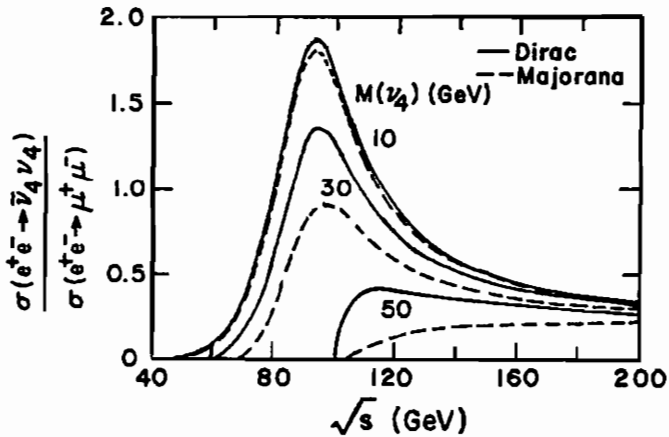


Fig. 13.8. Ratio of $\nu_4 \nu_4$ to $\mu^+ \mu^-$ events for Dirac or Majorana neutrinos versus the $e^+ e^-$ c.m. energy.

On the Z resonance the ratio of $Z \rightarrow \nu_4 \bar{\nu}_4$ to $Z \rightarrow e^+ e^-$ partial widths is

$$\frac{\Gamma(Z \rightarrow \nu_4 \bar{\nu}_4)}{\Gamma(Z \rightarrow e^+ e^-)} = \begin{cases} K(1-r)(1-4r)^{1/2}, & \text{Dirac} \\ K(1-4r)^{3/2}, & \text{Majorana} \end{cases}$$

where $K = (1 - 4x_w + 8x_w^2)^{-1} \simeq 2$ and $r = (m_4/M_Z)^2$. The use of vertex detectors will probe the region

$$|V_{4t}|^2 \gtrsim 10^{-10} \quad \text{for } m_4 \lesssim 40 \text{ GeV.}$$

Should no evidence for ν_4 be found by neutrino counting or unstable particle searches, the prospects for finding a fourth generation would be greatly diminished.

13.6 Quark Mixing and Decays

The phenomenology of fourth generation quarks depends on the a, v masses and on the quark mixing angles. We assume that $m_a > m_v$, following the pattern $m_c > m_s$ and $m_t > m_b$. The measurements of weak mixings, combined with unitarity constraints, suggest the following approximate form for the magnitudes of the elements of the 3×3 mixing matrix (§2.11)

$$|V_{nm}| = \begin{matrix} & \begin{matrix} d & s & b \end{matrix} \\ \begin{matrix} u \\ c \\ t \end{matrix} & \begin{pmatrix} 1- & \theta & \theta^3 \\ \theta & 1- & \theta^2 \\ \theta^3 & \theta^2 & 1- \end{pmatrix} \end{matrix}$$

where $\theta \simeq 0.23$ is the Cabibbo angle. Here the diagonal entries are slightly less than unity, as required by unitarity. The transitions

between different generations are increasingly suppressed as the generation separation increases and as the generation mass increases. A plausible extrapolation of this pattern to the fourth generation gives

$$|V_{nm}| = \begin{matrix} & d & s & b & v \\ \begin{matrix} u \\ c \\ t \\ a \end{matrix} & \begin{pmatrix} 1- & \theta & \theta^3 & \theta^5 \\ \theta & 1- & \theta^2 & \theta^4 \\ \theta^3 & \theta^2 & 1- & \theta^3 \\ \theta^5 & \theta^4 & \theta^3 & 1- \end{pmatrix} \end{matrix}.$$

For the weak decays of a and v , the principal decay branches, if energetically allowed, are then

$$\begin{aligned} a &\rightarrow v + W^+, & |V_{av}| &\sim 1 \\ v &\rightarrow t + W^-, & |V_{tv}| &\sim \theta^3 \end{aligned}$$

where the W bosons may be real or virtual, depending on the quark masses. An exception to this decay pattern occurs if $m_v < m_t$.

Light v -Quark

The possibility that $m_v < m_t$ leads to very interesting phenomena in the weak decays of v particles. The charged current $v \rightarrow a$ and $v \rightarrow t$ decays are then kinematically forbidden and the foregoing extrapolation of the mixing matrix suggests the $v \rightarrow c$ transitions dominate but are strongly suppressed,

$$v \rightarrow c + W_{\text{virtual}}^-, \quad |V_{cv}|^2 \sim \theta^8.$$

Consequently the v lifetime would be exceptionally long, possibly of order 10^{-13} s and measurable. Moreover flavor changing neutral current decays, that proceed via the virtual loop shown in Fig. 13.9, are enhanced, since the relevant mixing matrix elements $V_{tv}V_{tb}^*$ and $V_{av}V_{ab}^*$ are less suppressed than V_{cv} , and also because the loop amplitudes grow with the mass of the virtual quark (t or a) in the loop. For

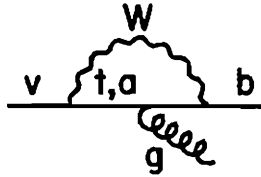


Fig. 13.9. Diagram for $v \rightarrow b + g$ decay.

a wide range of a, t masses the $v \rightarrow b + g$ mode may have a branching fraction as large as 5–10%.

The possibility that the v quark could be light received fresh stimulus from the suggestion that $e^+e^- \rightarrow v\bar{v}$ production might be the origin of an excess of low-thrust events containing muons seen with low statistics by the Mark J and JADE experiments at the highest PETRA energy ($\sqrt{s} = 46.3$ GeV). However, this suggestion has not been supported by data from the TRISTAN e^+e^- collider, nor from LEP and SLC operating on the Z resonance. Figure 13.10 compares the Z^0 resonance production cross section with that expected for other fermions, versus the fermion mass.

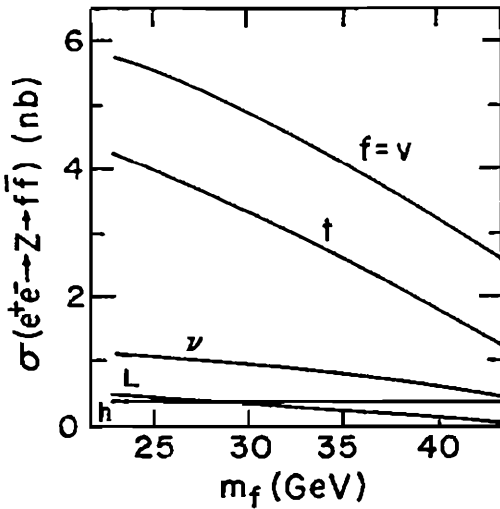


Fig. 13.10. Cross section for $e^+e^- \rightarrow Z \rightarrow f\bar{f}$ on the Z resonance for fermions $f = v, t, h, L, \nu$ versus the fermion mass; h is the isosinglet fermion in the 27-plet of E_6 symmetry, suggested by superstrings and ν, L are isodoublet heavy leptons for which the hadronic part of the cross section ($\approx 45\%$) is shown. For comparison $\sigma(e^+e^- \rightarrow Z \rightarrow \mu^+\mu^-) = 1.8$ nb.

There are several distinctive properties of $e^+e^- \rightarrow v\bar{v}$ events which can be used in their identification. First is the high multiplicity of charm particles, due to the $v \rightarrow c$ transition and the $v \rightarrow cs\bar{c}$ decay mode. The fractions of $\bar{v}v$ events containing 2, 3, 4 charm particles are $\sim 100\%$, 44% , 11% , unlike $\bar{b}b$ events with fractions $\sim 100\%$, 12% , $1/2\%$ because $b \rightarrow cs\bar{c}$ is phase space suppressed. Second the large energy release in v decay gives broad jets unlike most $\bar{q}q$ events with lighter quarks, except for $\bar{q}q + ng$ events with additional non-collinear gluons. The v -jet broadness measures m_v ; the sum of the momenta of the light final decay products normal to the v -jet axis is on average (§3.7.3)

$$\left\langle \sum_i p_T^i \right\rangle \simeq \frac{\pi}{4} m_v.$$

The distribution in $\sum_i p_T^i$ summed over visible particles (*i.e.*, excluding neutrinos) is shown in Fig. 13.11 for $Z \rightarrow \bar{v}v$ events including all cascade decays.

The transverse momenta of electrons or charm particles produced in v decay also reflect the energy release. The maximum p_T^c is

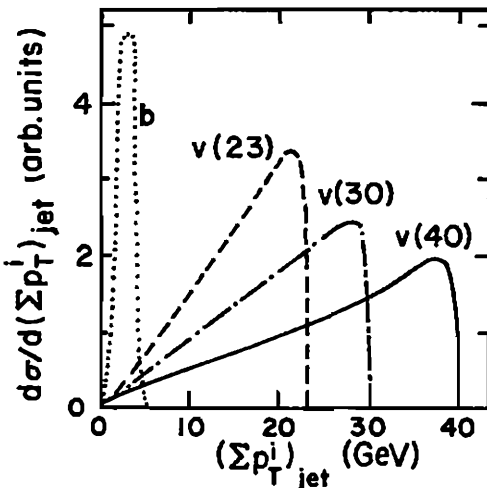


Fig. 13.11. Distribution versus $\sum_i p_T^i$ of momenta transverse to the jet axis for detectable particles in a v jet. The result for a b -jet is compared.

$(p_T^e)_{\max} = (m_b^2 - m_c^2)/(2m_b)$, allowing the electron to be isolated from the other decay products. In contrast the electron from b semileptonic decay is likely to be within the cone of the hadron fragments from the charm quark. In addition to the jet broadening and lepton isolation effects expected for any heavy quark, there will be extra signatures of the b quark including isolated c and $c\bar{c}$ and possibly the $b \rightarrow b\gamma$ two-body decay with distinctive kinematic features.

13.7 Decays to Real W -Bosons

At multi-TeV hadron colliders, such as the proposed proton-proton U. S. Superconducting Super Collider (SSC) with c.m. energy of 40 TeV, it will be possible to produce superheavy leptons and quarks, with masses exceeding 100 GeV. The decays of these particles will give real W -bosons. What are the prospects for detecting superheavy fourth generation fermions at supercolliders?

13.7.1 Superheavy leptons.

The dominant subprocesses for hadron production of superheavy charged leptons are shown in Fig. 13.12. Assuming $m_L > M_W$, the vector bosons in the intermediate state of these diagrams are virtual. The expected cross sections at the SSC are shown in Fig. 13.13 versus the L mass, assuming $m_{\nu_L} \approx 0$. For the design luminosity of 10^4 (pb) $^{-1}$ /year, these cross sections would yield substantial event rates. The signals for stable ν_L would be

$$W^* \rightarrow L\nu_L \rightarrow W\not{p}_T, \quad Z^* \rightarrow L\bar{L} \rightarrow WW\not{p}_T$$

with the missing p_T unaccompanied by jets.

The problem is that there are large backgrounds from the production of real W and Z bosons, both singly and in pairs, that submerge these heavy lepton signals. Figure 13.14 shows some typical back-

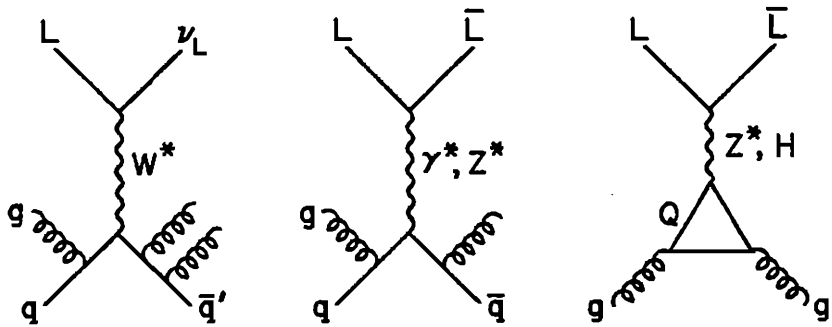


Fig. 13.12. Dominant diagrams for production of superheavy charged leptons.

ground subprocesses. Attempts to find ways of isolating the signal in theoretical simulations have proven unsuccessful. At the present time it seems unlikely that a sequential heavy lepton of mass greater than 100 GeV with a light neutrino companion could be detected at a hadron supercollider.

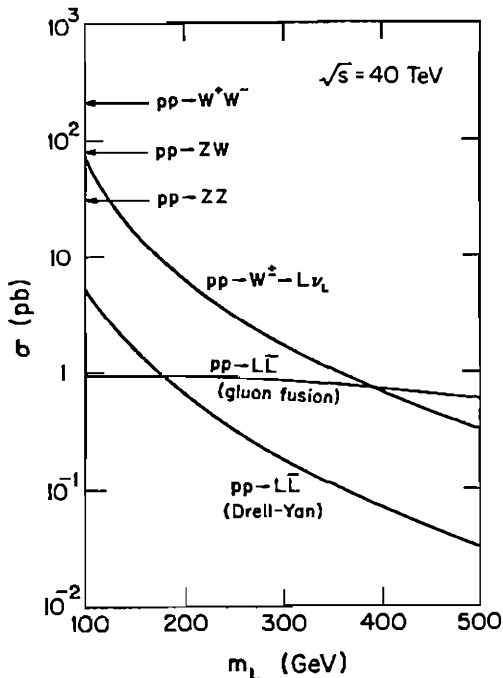


Fig. 13.13. Cross sections for charged superheavy lepton production at the SSC. The gluon-gluon fusion calculation assumes $m_H = 100$ GeV, $m_\nu = m_L$, and $m_a = m_L + 250$ GeV. The arrows on the left-hand side indicate the WW , ZZ and WZ background cross sections.

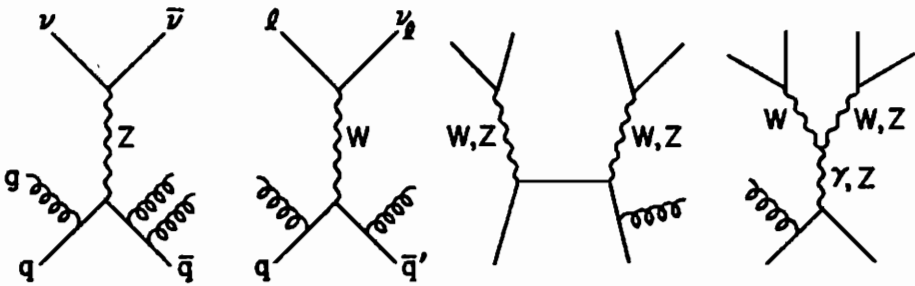


Fig. 13.14. Typical subprocesses that give backgrounds to a heavy lepton signal at the SSC.

13.7.2 Superheavy quarks.

The prospects for detecting fourth generation quarks that decay to W bosons are highly promising at the SSC because the cross sections from the QCD fusion subprocesses $gg \rightarrow Q\bar{Q}$, $q\bar{q} \rightarrow Q\bar{Q}$ are very large, as shown in Fig. 13.15. A quark of mass 500 GeV has a cross section ~ 100 pb. If the ν quark decays through the mode

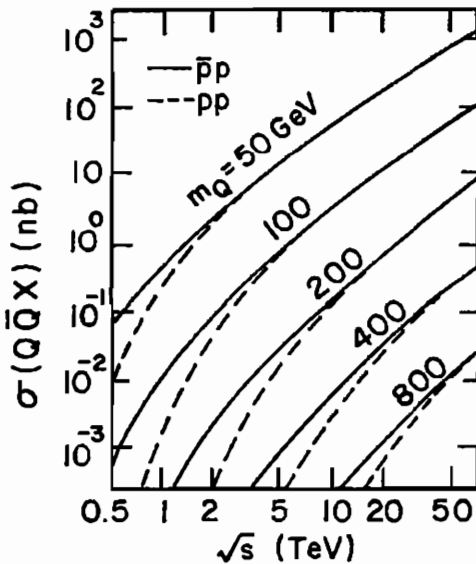


Fig. 13.15. QCD fusion $q\bar{q}, gg \rightarrow Q\bar{Q}$ cross sections for heavy quark production in pp and $p\bar{p}$ collisions.

$v \rightarrow tW^-$, and $m_a - m_v > M_W$ so that a decays as $a \rightarrow vW^+ \rightarrow tW^-W^+$, the events of interest are

$$pp \rightarrow v\bar{v} \rightarrow (tW^-)(\bar{t}W^+),$$

$$pp \rightarrow a\bar{a} \rightarrow (tW^-W^+)(\bar{t}W^+W^-).$$

The t , W^- , W^+ final state particles are on the mass shell so the v and a masses can in principle be reconstructed. With the enormous production cross section, a restrictive selection of leptonic and hadronic events together with severe acceptance cuts can be used to eliminate background processes which accidentally reconstruct the invariant masses of real W 's and real t 's. Monte Carlo studies for typical $v\bar{v}$ signatures bear out the discovery potential.

On dimensional grounds the p_T dependence of the v -quark in $v\bar{v}$ production is of the approximate form, neglecting scaling violations,

$$\frac{d\sigma}{dp_T^2} \sim \frac{1}{(p_T^2 + m_v^2)^2}$$

for p_T comparable with m_v . Hence events with $p_{vT} \gtrsim m_v$ can be selected without too high cost to the rate. In such events the decay products of v and \bar{v} will be largely in separate hemispheres and this helps in reconstructing the v mass.

A possible trigger is one semileptonic t -decay (e.g., $t \rightarrow b\mu^+\nu$) and one leptonic W -decay (e.g., $W^- \rightarrow e^-\nu$) with different lepton flavors to eliminate γ^* , $Z \rightarrow \ell\bar{\ell}$ backgrounds. Such an event is illustrated in Fig. 13.16. By requiring high p_T for the two leptons and high p_T , the v will also have high p_T . The \bar{v} mass can be reconstructed from the away side hadron jets.

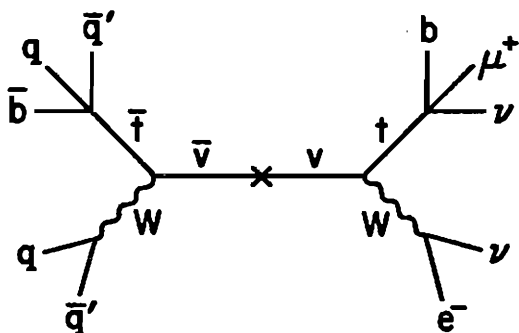


Fig. 13.16. A double lepton plus \cancel{p}_T trigger for $\nu\bar{\nu}$ events.

13.7.3 e^+e^- Supercollider search.

At a very high energy e^+e^- machine, fourth generation quarks and leptons that decay to W bosons would have promising signatures with a good signal to noise ratio. A distinctive signal for L production is a high p_T lepton plus missing energy from neutrinos, illustrated in Fig. 13.17; also shown is the W^+W^- background diagram. The W^- from L^- decay will be isotropically distributed while the W^- from the W -pair background will be forward peaked. An angular cut can therefore be used to suppress the background (e.g., $|\cos\theta| < 0.8$ at $\sqrt{s} = 200$ GeV or $\cos\theta < 0.85$ at $\sqrt{s} = 600$ GeV). Also, the visible energy on the hadronic side of the event will be approximately $\sqrt{s}/2$ for the W^+W^- background but will often be smaller for the L^+L^- signal. A cut $E_{\text{vis}} < 0.8(\sqrt{s}/2)$ on the measured energy in the hadronic hemisphere will further reject background events. The rates for the signal are sufficiently large that L -pair events can be detected for m_L almost up to $\sqrt{s}/2$ (e.g., $m_L = 90$ GeV for $\sqrt{s} = 200$ GeV or $m_L = 250$ GeV for $\sqrt{s} = 600$ GeV).

Exercise. Show that the cross section for $e^+e^- \rightarrow \nu_L\nu_L$ production via a virtual Z^0 at energies $\sqrt{s} \gg M_Z$ is

$$\sigma = 0.025 \text{ pb}/[s(\text{TeV}^2)].$$

Thus $\sigma \simeq 0.6 \text{ pb}$ at $\sqrt{s} = 200 \text{ GeV}$.

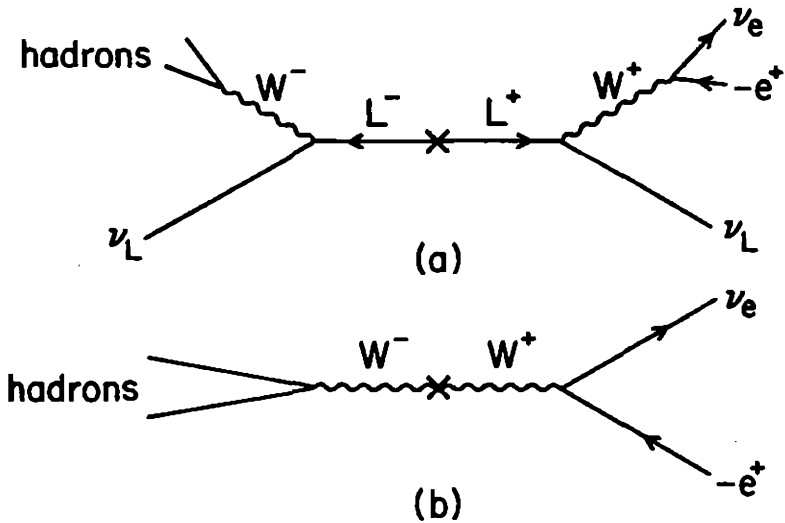


Fig. 13.17. Signal (a) from $e^+e^- \rightarrow L^+L^-$ with $L^\pm \rightarrow \nu_L^- W^\pm$, $W^- \rightarrow \text{hadrons}$, and $W^+ \rightarrow e^+\nu_e$. The background (b) from W^+W^- is also shown.

A good signature for fourth generation quarks produced at a high energy e^+e^- collider is isolated high p_T leptons (e^\pm, μ^\pm) from semileptonic decays. Figure 13.18(a), (b) show the topology of events resulting from $e^+e^- \rightarrow \nu\bar{\nu}$ production and backgrounds. The signal is characterized by high multiplicity and high aplanarity. Recall that aplanarity is a shape parameter which measures the momentum normal to the event plane; “fat” events have large aplanarity; see §9.1.1. The three backgrounds shown have, respectively, (c) relatively low multiplicity and low aplanarity (d) low aplanarity and relatively low p_T lepton (e) low multiplicity, low aplanarity and relatively low p_T lepton. Good rejection of background can be achieved by requiring an isolated lepton (*e.g.*, less than 100 MeV of energy within a 10° cone around the lepton), a charged multiplicity > 35 , and an aplanarity > 0.2 at $\sqrt{s} = 200$ GeV (> 0.15 at $\sqrt{s} = 600$ GeV).

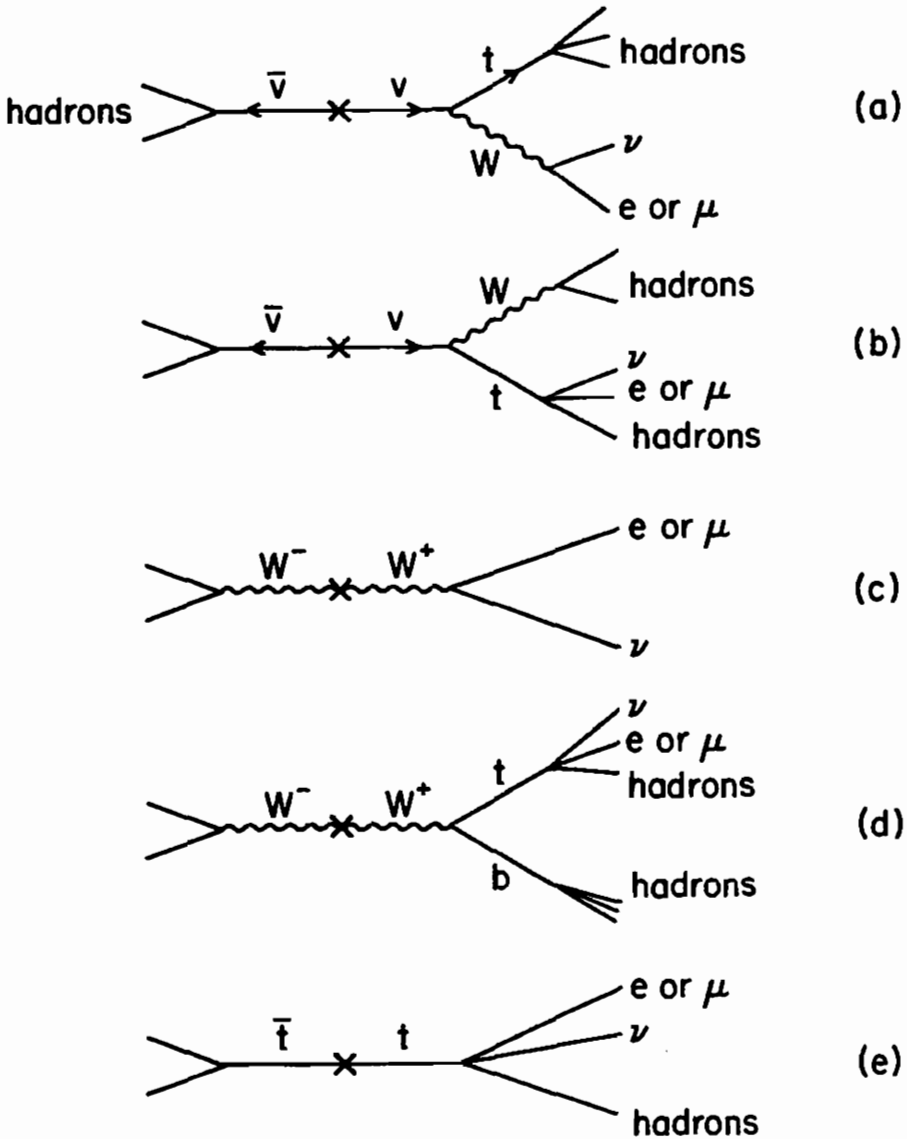


Fig. 13.18. Event topologies for $e^+e^- \rightarrow \nu\bar{\nu}$ production (a), (b) and backgrounds (c), (d), (e).

If a fourth generation quark is found, how can its mass be measured? One can fit the lepton p_T spectrum, measure the $\beta(3 - \beta^2)$ threshold dependence, or look for the quarkonium states. However, at a high energy linear collider with machine width $\Delta E/E \geq 10\%$ it would not be possible to detect quarkonium. At a high energy collider the a quark could be distinguished from the v quark by the rate at which it is produced and by the forward backward charge asymmetry, since the weak couplings are different.

Exercise. Compare the cross section and A_{FB} expectations for $\bar{a}a$ and $\bar{v}v$ production in e^+e^- collisions at $\sqrt{s} \gg M_Z$, for a given quark mass.

13.8 Superheavy Quarkonia

The first signals for charm and bottom quarks in hadronic collisions were the leptonic decays of their J/ψ and Υ bound states. Might superheavy quarks also be first discovered through the decays of their quarkonium bound states?

The partial widths for the decays of the S -wave states to gluons are

$$\Gamma(\eta \rightarrow gg) = C \frac{\alpha_s^2}{M^2} |\psi_S(0)|^2 \simeq 3 \text{ MeV} \left(\frac{M}{200 \text{ GeV}} \right),$$

$$\Gamma(\psi \rightarrow 3g) = C' \frac{\alpha_s^3}{M^2} |\psi_S(0)|^2 \simeq 20 \text{ KeV} \left(\frac{M}{200 \text{ GeV}} \right),$$

where M is the quarkonium mass, $M \simeq 2m_Q$, and C, C' are known dimensionless constants; see §10.3.1.

An important feature of superheavy quarkonia is the appearance of new decay modes involving weak bosons and Higgs bosons, enumerated below. The partial widths for these annihilation decays have

the generic forms

$$\Gamma = K \frac{\alpha^2}{M^2} \left(\frac{M^2}{M_W^2} \right)^x |\psi(0)|^2 \quad \text{for boson decay channels,}$$

$$\Gamma = K' \frac{\alpha^2}{M^2} \left(\frac{m_f^2}{M^2} \right)^y \left(\frac{M^2}{M_Z^2} \right)^x |\psi(0)|^2 \quad \text{for fermion-antifermion decays,}$$

with chirality suppression $y = 0, 1$ for ψ, η , respectively. Here K and K' are dimensionless factors that contain threshold and other mass dependence. The x -values for enhancement factors in the allowed η and ψ modes are as follows:

	$f\bar{f}$	$\gamma\gamma$	$Z\gamma, ZZ$	W^+W^-	γH	ZH
η	2	0	0	0	—	2
ψ	0	—	1	2	1	1

The enhancements originate from Higgs or longitudinal W, Z axial vector couplings to the superheavy quarks. The modes with $x = 2$ will be dominant, but in the case of $f\bar{f}$ only if m_f/M_W is not small.

In quarkonium decays it is necessary that the single quark decay to a real W -boson $Q \rightarrow q + W$ (leaving the other heavy quark as a spectator) be suppressed if the interesting modes above are to be detectable. The width for this decay grows like M^3 . If this spectator mode should dominate, the quarkonium decays would be indistinguishable from the continuum $Q\bar{Q}$ source. Fortunately, for the case of v -quark decays, the single $v \rightarrow t + W$ decay rate is likely suppressed by a factor of $|V_{tv}|^2 \sim 10^{-4}$. As Figure 13.19 shows this contribution is well below the total width expected for η and ψ from gluon and gauge boson final states, and can be neglected. For a -quark decays the $a \rightarrow v + W$ mode dominates the interesting decays unless m_a and m_v are closely degenerate.

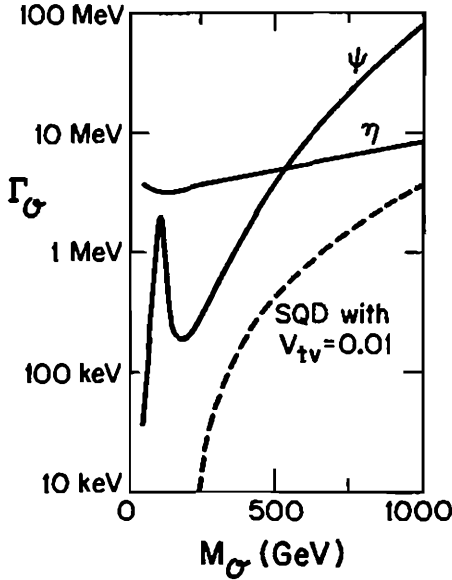


Fig. 13.19. Total widths for quarkonium $O = \eta(v\bar{v})$ and $\psi(v\bar{v})$ from gluon and gauge boson decays, compared with the widths from single quark decays $v \rightarrow t + W$.

The η and ψ states are produced in pp collisions via the gluon-gluon fusion subprocesses; see the diagrams and calculations in §10.3.1. The cross sections at $\sqrt{s} = 40$ TeV are shown in Fig. 10.18. Even for M_η as large as 700 GeV, the cross section is $O(1 \text{ pb})$ corresponding to 10^4 events/year at the SSC design luminosity. The cross-section for ψ production via the “bleaching gluon” subprocess is roughly two orders of magnitude below the η .

The dominant decay of η_v when $M_\eta > 400$ GeV and $M_H < M_\eta - 250$ GeV is $\eta \rightarrow ZH$ with a branching fraction approaching 100%. The large η event rate allows the use of the clean $Z \rightarrow \ell^+\ell^-$ decay modes as a trigger for these events. It may be possible to simultaneously discover the Higgs boson and the η_v by mass reconstruction of H^0 and $\ell^+\ell^-H^0$. Even for the elusive intermediate mass Higgs, with decay $H \rightarrow t\bar{t}$, the signal is greater than the background from $q\bar{q} \rightarrow Zt\bar{t}$ for reasonable experimental mass resolutions on M_{ZH} and M_H . Other η decay modes, such as $\eta \rightarrow ZZ, Z\gamma$ are not observable because of standard model backgrounds.

Chapter 14

Higher Symmetries

14.1 Grand Unification

Although the standard model is completely successful in accounting for low-energy phenomena, it leaves unexplained why the gauge group of strong and electroweak interactions is $SU(3) \times SU(2) \times U(1)$, with very different gauge couplings and why the fermion quantum numbers have their particular values. The idea of *Grand Unified Theories* (GUTS) is that the $SU(3)$, $SU(2)$ and $U(1)$ are subgroups of a larger gauge symmetry group G and that quarks and leptons belong to the same multiplets of G . This higher symmetry is unbroken above some very large mass scale M_X .

Above M_X all gauge couplings α_i are related by Clebsch-Gordan coefficients to a single gauge coupling α_G and evolve according to the β -function of G . Below M_X , G is supposed to be broken spontaneously and the α_i evolve separately according to the β -functions of their respective groups. A test of grand unification is that the evolution of the couplings from their known values at $\mu = M_W$ should meet at a common scale $\mu = M_X$.

The fermions must be assigned to representations of G . In any representation of a simple non-abelian group, the generators are traceless. Hence the sum of the eigenvalues of any diagonal generator is zero when this sum is taken over all the members of any representation. Since the charge operator Q is a linear combination of the

diagonal generators, the sum of charges of the fermions assigned to a representation must vanish. In most grand unification proposals, a given multiplet contains fermions of a single generation while replicas of this multiplet contain other generations. In G , a gauge boson links a fermion to another fermion in the same representation. Since quarks and leptons appear in a common representation (sometimes with antiquarks and antileptons, too), there are exotic gauge bosons with masses M_X that can both turn quarks into leptons and quarks into antiquarks thereby causing proton decay with a lifetime $\tau \sim \alpha_G^{-2} M_X^4 / m_p^5$. Since the limits on the proton lifetime are of order 10^{31} years, M_X must be at least of order $10^{16} \sqrt{\alpha_G}$ GeV.

An early attempt at grand unification was based on $G = \text{SU}(5)$. Here it is necessary to assign the first-generation fermions to two different representations, $5^*(d^c, e^-, \nu_e)$ and $10(e^{-c}, d, u, u^c)$; see Table 14.1. It is a remarkable fact that the standard model $\text{SU}(2) \times \text{U}(1)$ left-hand doublet and right-hand singlet fermion assignments are a natural consequence of the $\text{SU}(5)$ classification.

Table 14.1. *Assignment of left-handed fermions of the first generation to 5^* and 10 representations of $\text{SU}(5)$. The superscript c denotes the charge-conjugate state. Subscripts r, g, b denote the colors red, green, blue. The quintet 5^* can be represented as a vector V^c and the decuplet 10 as an antisymmetric tensor D_{ab} transforming like $\frac{1}{\sqrt{2}}(V_a V_b - V_b V_a)$:*

$$V^c = \left[(d_r)^c, (d_g)^c, (d_b)^c, e^-, \nu_e \right],$$

$$D = \frac{1}{\sqrt{2}} \begin{bmatrix} 0 & (u_b)^c & -(u_g)^c & -u_r & -d_r \\ -(u_b)^c & 0 & (u_r)^c & -u_g & -d_g \\ (u_g)^c & -(u_r)^c & 0 & -u_b & -d_b \\ u_r & u_g & u_b & 0 & -e^+ \\ d_r & d_g & d_b & e^+ & 0 \end{bmatrix}.$$

There are 24 generators in $SU(5)$. It has 4 commuting generators (rank 4) and contains $SU(3)_{\text{color}}$, $SU(2)_L$ and $U(1)_Y$ as subgroups; the breaking of $SU(5)$ to these subgroups is achieved through a Higgs multiplet in the adjoint **24** representation. It is convenient to pick the 4 commuting generators to be the $SU(3)$ color isospin and hypercharge operators T_3^c and Y^c , plus the weak isospin and hypercharge operators T_3^L and $\sqrt{\frac{3}{20}}Y$. The numerical factors here are needed to ensure that all generators have the same normalization, obeying

$$\text{Tr}_R(T_a T_b) = \delta_{ab} T(R),$$

where T_a is any generator and $T(R)$ is a constant depending on the representation R over which the trace is taken. The eigenvalues of these operators for the fermions in the 5^* representation are shown in Table 14.2; in this representation $T(R) = \frac{1}{2}$.

Table 14.2 Eigenvalues of the $SU(5)$ diagonal generators in the 5^* representation of left-handed fermions: subscripts r, g, b denote the colors red, green, blue. The generators T_3^c and Y^c are for $SU(3)_{\text{color}}$; T_3^L is for $SU(2)_L$ and $\sqrt{\frac{3}{20}}Y$ is for $U(1)_Y$. The charge operator is $Q = T_3^L + \frac{1}{2}Y$.

T_a	$(d_r)^c$	$(d_g)^c$	$(d_b)^c$	e^-	ν_e
T_3^c	$\frac{1}{2}$	$-\frac{1}{2}$	0	0	0
Y^c	$\frac{1}{2\sqrt{3}}$	$\frac{1}{2\sqrt{3}}$	$-\frac{1}{\sqrt{3}}$	0	0
T_3^L	0	0	0	$-\frac{1}{2}$	$\frac{1}{2}$
$\sqrt{\frac{3}{20}}Y$	$\frac{2}{3}\sqrt{\frac{3}{20}}$	$\frac{2}{3}\sqrt{\frac{3}{20}}$	$\frac{2}{3}\sqrt{\frac{3}{20}}$	$-\sqrt{\frac{3}{20}}$	$-\sqrt{\frac{3}{20}}$

Exercise. Evaluate $\text{Tr}(T_a^2)$ for the 10 representation of $SU(5)$, from the quantum numbers of the fermions in it.

Notice that the GUT symmetry has fixed the values of T_3^L and Y for each member of a multiplet, *i.e.* it has determined all charges relative to the electron charge. The assignment of Y values, which was arbitrary in the context of $SU(2) \times U(1)$ alone, is no longer free. These $SU(5)$ representations necessarily contain fractional charges; for example, since the sum of charges in 5^* vanishes, the three d^c quarks must balance the e charge and hence d has charge $-1/3$. Thus, GUTS explain charge quantization.

At the GUT scale, the covariant derivative is

$$D^\mu = \partial^\mu + ig_G \mathcal{G}_a^\mu T_a = \partial^\mu + ig_G \left[G_i^\mu T_i^c + \mathbf{W}^\mu \cdot \mathbf{T}^L + B^\mu \sqrt{\frac{3}{20}} Y + \dots \right],$$

where g_G is the unified gauge coupling, the \mathcal{G}_a^μ are the GUT gauge fields, and the GUT generators T_a have a common normalization as above. In the second equality above, we show explicitly the $SU(3) \times SU(2) \times U(1)$ content. Hence when the full GUT symmetry applies, the QCD coupling g_3 and the electroweak couplings g_2 and g_1 are equal,

$$g_3 = g_2 = g_1 = g_G,$$

and are related to the standard electroweak couplings g and g' of Chapter 2 by

$$g_2 = g, \quad g_1 = \sqrt{\frac{5}{3}} g'.$$

Hence $\tan \theta_w = g'/g = \sqrt{\frac{3}{5}}$ so that at the GUT scale

$$x_w = \frac{3}{8} = 0.375.$$

14.2 Running Couplings

All couplings evolve with the mass scale as discussed in Chapter 7. Only particles with mass $< \mu$ contribute to the evolution at any given mass scale μ . Hence below the GUT scale, g_3 , g_2 and g_1 evolve independently according to the β -functions of SU(3), SU(2) and U(1), respectively. The hope is that evolution from a common coupling at $\mu = M_X$ down to $\mu = M_W$ will bring these couplings into agreement with the experimentally measured strong and electroweak couplings. A complete analysis of this question should include two-loop contributions to the β -functions and radiative corrections to the low-energy couplings. For simplicity of presentation, however, we shall here make the one-loop approximation and neglect radiative corrections.

In the one-loop approximation $\beta(g) = -bg^3$, where the coefficient b is determined by gauge boson couplings to gauge bosons, fermions and Higgs fields, the solution to the evolution equations (§7.3) is

$$\alpha_N(\mu)^{-1} = \alpha_G(M_X)^{-1} + 8\pi b_N \ln(\mu/M_X).$$

Here $\alpha_N = g_N^2/4\pi$ and the β -function coefficients b_N are given by

$$\begin{aligned} 48\pi^2 b_3 &= 33 - 4n_f, \\ 48\pi^2 b_2 &= 22 - 4n_f - \frac{1}{2}, \\ 48\pi^2 b_1 &= -4n_f - \frac{3}{10}. \end{aligned}$$

On the right-hand side, the first terms in b_3 , b_2 are gauge boson contributions, the second terms are fermion contributions (with n_f the number of fermion generations) and the last terms in b_2 , b_1 are Higgs scalar contributions.

Starting from experimental values of the couplings at $\mu = M_W$,

$$\begin{aligned} \alpha_3(M_W)^{-1} &\simeq 8, \\ \alpha_2(M_W)^{-1} &\simeq x_w(M_W)/\alpha(M_W) \simeq 29, \\ \alpha_1(M_W)^{-1} &\simeq \left(\frac{3}{5}\right) [1 - x_w(M_W)]/\alpha(M_W) \simeq 59, \end{aligned}$$

based on $\Lambda_4 = 0.2$ GeV and $m_t = 40$ GeV, $x_w(M_W) = 0.23$ and

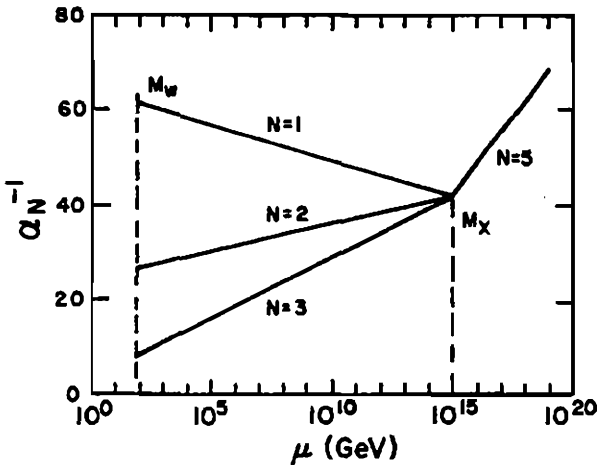


Fig. 14.1. Evolution of gauge couplings α_N with mass scale μ in SU(5). Above M_X , all couplings coincide. Below M_W , α_1 and α_2 are frozen but α_{em} evolves.

$\alpha(M_W)^{-1} = 128$, the evolved couplings should intersect approximately at a common value of $M_X \simeq 10^{15}$ GeV; see Fig. 14.1.

Exercise. Show that in the approximation of neglecting the Higgs terms in b_N , the couplings at scale μ are related by

$$2\alpha_3(\mu)^{-1} - 3\alpha_2(\mu)^{-1} + \alpha_1(\mu)^{-1} = 0.$$

Exercise. Show that requiring all three couplings to coincide at a single point M_X determines two quantities, for example $x_w(M_W)$ and M_X , via the relations (including Higgs terms)

$$x_w(M_W) = \left[(109/201)\alpha(M_W)/\alpha_3(M_W) + 23/134 \right] \simeq 0.205,$$

$$M_X = M_W \exp\{2\pi [3\alpha(M_W)^{-1} - 8\alpha_3(M_W)^{-1}]/67\} \simeq 0.9 \times 10^{15} \text{ GeV},$$

using the experimental $\alpha_N(M_W)$ values above. Notice that the number of fermion generations does not affect these relations.

Exercise. Show that this solution with $\alpha(M_W) = 1/128$ implies a value $\alpha_G(M_X) = 0.024$ for 3 generations.

It is remarkable that the x_w value above is not far from the experimental value $x_w = 0.23 \pm 0.01$ and that the mass M_X is approaching the right order for proton stability.

Table 14.3. Minimal $SU(5)$ model predictions for various values of the QCD scale parameter $\Lambda_{\overline{MS}}$, in GeV units.

$\Lambda_{\overline{MS}}$	M_X	$x_w(M_W)$	M_W	M_Z
0.1	1.3×10^{14}	0.216	82.8	93.6
0.2	2.7×10^{14}	0.212	83.5	94.3
0.4	5.5×10^{14}	0.208	84.6	94.9

Table 14.3 shows the results when two-loop and radiative corrections are included in the analysis, for a range of values of the QCD scale parameter $\Lambda_{\overline{MS}}$ defined in two-loop order for the modified minimal subtraction (\overline{MS}) renormalization scheme. The predicted x_w value is somewhat lower than the experimental value. The experimental couplings at M_W are not quite compatible with a common intersection at some M_X .

In the $SU(5)$ model, protons can decay via the exchange of virtual superheavy gauge bosons X , mediating for example $u \leftrightarrow \bar{u}$ and $d \leftrightarrow e^+$ transitions as illustrated in Fig. 14.2 where the final state is e^+ + meson(s). There are also decays to neutrino plus mesons. The predicted lifetime has some model-dependence; the results lie in the range

$$\tau_p = 2 \times 10^{29 \pm 1.7} \text{ years.}$$

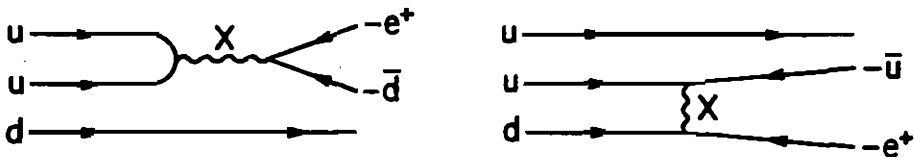


Fig. 14.2. Typical proton decay processes in $SU(5)$ GUT.

The predicted partial lifetime for the $p \rightarrow e^+\pi^0$ decay mode is

$$[\Gamma(p \rightarrow e^+\pi^0)]^{-1} = 4.5 \times 10^{29 \pm 1.7} \text{ years},$$

which now disagrees with the experimental bound

$$[\Gamma(p \rightarrow e^+\pi^0)]^{-1} > 10^{32} \text{ years}.$$

Although this and the x_w value exclude the minimal SU(5) model, we may nevertheless regard it as a near miss. The GUT idea is very attractive, since it explains the quantum number assignments of the known particles, and considerable interest remains in other possible GUT schemes. The predictions from evolution of couplings depend on the particle content, which may be larger than in the SU(5) model. Moreover, there may exist an intermediate symmetry breaking scale, although in conventional GUTS there is a desert between M_W and M_X .

14.3 Running Masses

Fermion masses are generated by Yukawa couplings to Higgs scalars. At the GUT scale, these couplings are invariant under the group G . In SU(5) for example, the left-handed fermions are in 5^* and 10 representations, so the possible representations for mass-generating Higgs scalars [coupled to two left-handed fields, *e.g.* $(d^c)_L d_L = (d_R)^c d_L$] are

$$5^* \times 5^* = 10^* + 15, \quad 5^* \times 10 = 5 + 45, \quad 10 \times 10 = 5^* + 45 + 50.$$

Since none of these contain a singlet, bare fermion mass terms are excluded. In the minimal SU(5) model there is a 24 Higgs multiplet H_{24} that breaks SU(5) at M_X and a 5 multiplet H_5 containing the isospin-doublet that breaks SU(2) \times U(1) at M_W . Fermion masses are generated by H_5 alone. It has two independent couplings to 10×10 and $5^* \times 10$ fermions, one involving H_5 and one involving its conjugate H_5^c , which generate masses for $T_3 = \frac{1}{2}$ quarks and $T_3 = -\frac{1}{2}$ fermions, respectively.

At the scale M_X , the GUT symmetry gives relations between Yukawa couplings and the resulting fermion masses. In $SU(5)$, if we order the members of a 5^* Higgs multiplet as in the vector Q^c in Table 14.1, then the corresponding H_5^c field can only acquire a vacuum expectation value in its fifth member,

$$\langle H_5^c \rangle = (0, 0, 0, 0, v)$$

(and similarly for H_5). Hence the mechanism for generating masses is completely symmetrical between the other degrees of freedom in the 5^* , and as a result the mass matrices for $Q = -\frac{1}{3}$ quarks and charged leptons are identical. This predicts

$$m_d = m_e, \quad m_s = m_\mu, \quad m_b = m_\tau, \quad (\text{at scale } M_X).$$

The fermion masses are products of the vacuum expectation value v and Higgs Yukawa couplings. These couplings evolve with mass scale, in order to absorb the effects of large logarithms in the theory. Consequently, the fermion masses also evolve and depend on the scale at which they are measured; the mass ratios depend only on the Yukawa couplings. In order to compare the GUT mass predictions with experimental masses at low energies, this evolution must be taken into account. In minimal $SU(5)$, the one-loop evolution equation is

$$\frac{d}{d \ln \mu^2} \left[\ln \frac{m_b(\mu)}{m_\tau(\mu)} \right] = -\frac{\alpha_3(\mu)}{\pi} + \frac{\alpha_1(\mu)}{4\pi}.$$

The evolution of the mass ratios is driven by the loop diagram in Fig. 14.3. There is no α_2 contribution because $SU(2)_L$ gauge bosons do not couple to right-handed fermions.

Exercise. Show that the solution of this equation for evolution between μ_1 and μ_2 is

$$\frac{m_b(\mu_1)}{m_\tau(\mu_1)} = \frac{m_b(\mu_2)}{m_\tau(\mu_2)} \left[\frac{\alpha_3(\mu_1)}{\alpha_3(\mu_2)} \right]^{\frac{1}{4\pi^2 b_3}} \left[\frac{\alpha_1(\mu_1)}{\alpha_1(\mu_2)} \right]^{-\frac{1}{16\pi^2 b_1}},$$

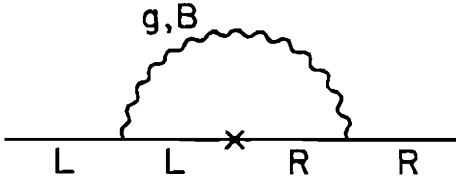


Fig. 14.3. Fermion self-energy diagram responsible for the evolution of fermion mass ratios. The cross is a mass insertion resulting from the Higgs Yukawa coupling with the Higgs field replaced by its vev.

where b_N are the β -function expansion coefficients in lowest order.

To accommodate changes of b_N at fermion thresholds $\mu = 2m_f$, this result can be applied sequentially. Since we estimate m_b experimentally from the Υ mass, it is appropriate to evaluate this ratio at $\mu \simeq m_\Upsilon \simeq 9.4$ GeV; the further evolution of m_τ down to $\mu = m_\tau$ is negligible, since the distance is short and lepton mass evolution does not involve the strong couplings α_3 in one-loop approximation.

Exercise. Using the formulas above, calculate the predicted ratio

$$\frac{m_b}{m_\tau} \simeq 2.5-3.0 \text{ for three generations,}$$

including a t quark threshold with $m_t = 175$ GeV.

This agrees with the experimental b/τ ratio of 2.65 estimating $m_b \simeq \frac{1}{2}m_\Upsilon = 4.7$ GeV. This was a success of minimal SU(5). Comparison with the experimental m_s/m_μ or m_d/m_e ratio is not practical, since the strong coupling becomes large at small mass scales and the RGE break down.

Exercise. Supposing that there is a fourth generation of fermions, degenerate in mass, with $m = 100$ GeV, calculate the predicted values of $\alpha_G(M_X)$ and the low-energy m_b/m_τ ratio.

14.4 SO(10) GUTS

Another proposed GUT symmetry group is SO(10). This is the group of orthogonal rotations in a space of 10 dimensions, with unimodular transformation matrices. It has rank 5 and contains $SU(5) \times U(1)$ as a subgroup. The **16** representation contains three SU(5) multiplets:

$$\mathbf{16} = \mathbf{10} + \mathbf{5}^* + \mathbf{1}.$$

Thus all the known fermions of one generation can be assigned to a single irreducible representation **16**. The SU(5) singlet is a new left-handed neutral fermion N^c which could be identified with the conjugate of a right-handed neutrino state, $(N^c)_L = (\nu_R)^c$; it has zero couplings to the SU(5) gauge bosons, which include those of $SU(3) \times SU(2) \times U(1)$.

There are different routes by which SO(10) can be broken to the low-energy gauge group. Figure 14.4 illustrates some possible evolution patterns of gauge boson couplings, corresponding to different symmetry breaking sequences. It is possible that some symmetry breaking occurs at intermediate mass scales between M_X and M_W ,

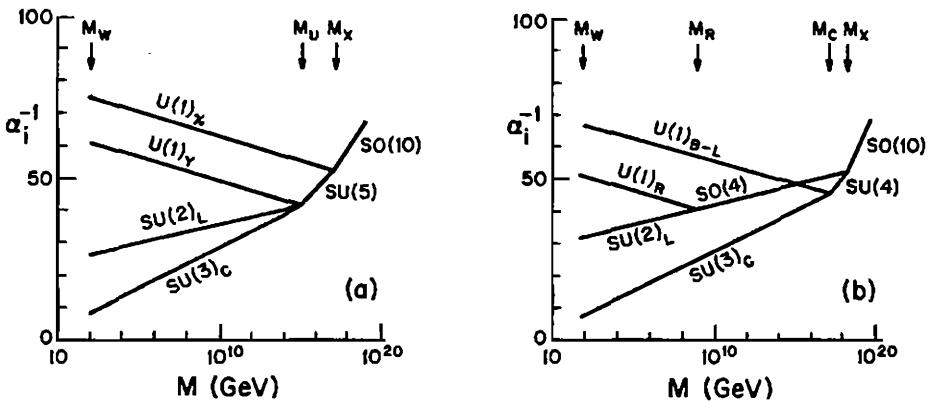


Fig. 14.4. Typical evolution of gauge couplings in SO(10) GUTS, for two symmetry breaking scenarios (a) $SO(10) \rightarrow SU(5) \times U(1)$, (b) $SO(10) \rightarrow SU(4) \times SO(4)$, $SO(4) \rightarrow SU(2) \times U(1)$, $SU(4) \rightarrow SU(3) \times U(1)$.

which will affect the evolution of the couplings. Moreover, it is possible that additional gauge bosons enter in electroweak interactions at low energy. Their masses are related to the scale at which the corresponding symmetry is broken; such bosons could be discovered at future colliders. In the symmetry-breaking cases shown, there is an additional U(1) gauge boson, which would mix with the Z boson.

It is convenient to discuss the particle assignments to group representations and the action of the generators upon them, in a Euclidean root space. For a group of rank r , we can choose r simultaneously diagonalized generators $\{H\}$ that form a Cartan subalgebra, e.g. T_3 and Y for SU(3). Each particle state $|p\rangle$ can be labelled by its eigenvalues, $H_i |p\rangle = p_i |p\rangle$; these p_i form a weight vector \vec{p} in an r -dimensional space. The generators H_i can be represented as unit coordinate vectors \vec{H}_i in this space, so that the particle eigenvalues are just the scalar products with the weight vectors, $p_i = \vec{p} \cdot \vec{H}_i$.

Of the remaining generators, we can choose a complete set $\{E\}$ analogous to isospin-raising and lowering operators, having commutation relations

$$[H_i, E_\alpha] = \alpha_i E_\alpha$$

with the Cartan subalgebra. α_i measures how much the H_i eigenvalue of a state is raised or lowered, when it is multiplied by E_α . These α_i form root vectors $\vec{\alpha}$ in the same r -dimensional space.

It can be convenient to represent the root vectors in a space of larger dimension; e.g. for SU(N) and SO($2N$) groups, the $\vec{\alpha}$ can be represented by combinations of unit vectors \mathbf{e}_i pointing along Cartesian axes in N dimensions, namely

$$\begin{aligned} \pm(\mathbf{e}_i - \mathbf{e}_j) & \text{ for SU}(N), \\ \pm(\mathbf{e}_i \pm \mathbf{e}_j) & \text{ for SO}(2N), \end{aligned} \quad \text{with } i < j = 1, 2, \dots, N.$$

For SU(N), $r = N - 1$, so the vectors $\vec{\alpha}$, \vec{p} , \vec{H}_i all lie in an $(N - 1)$ -dimensional subspace. Figure 14.5 illustrates the triplet representation in the root vector space of SU(3).

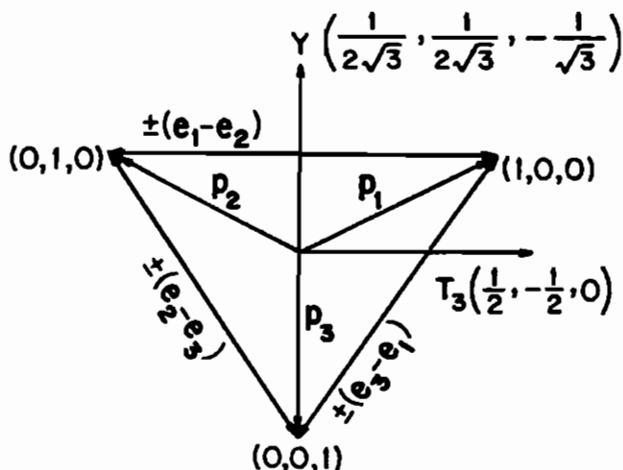


Fig. 14.5. Two-dimensional root vector space of SU(3), showing the particles in the triplet representation.

In SO(10) the states in the **16** representation of fermions can be written as weight vectors in the 5-dimensional root space as

$$p_i = (\pm \frac{1}{2}, \pm \frac{1}{2}, \pm \frac{1}{2}, \pm \frac{1}{2}, \pm \frac{1}{2})$$

with an odd number of $-$ signs occurring. Table 14.4 gives the identity of each particle in this representation. The vectors for the five diagonal generators of SO(10) are as follows:

SU(3) color	$T_3^c = \frac{1}{2}(1, -1, 0, 0, 0)$
	$Y^c = \frac{1}{2\sqrt{3}}(1, 1, -2, 0, 0)$
SU(2) _L	$T_3^L = \frac{1}{2}(0, 0, 0, 1, -1)$
U(1) _Y	$Y = \frac{1}{2\sqrt{15}}(-2, -2, -2, 3, 3)$
U(1) _χ	$\chi = \frac{1}{\sqrt{10}}(1, 1, 1, 1, 1)$

The product of each generator vector with a particle vector gives the corresponding coupling for that particle. Here and henceforth

Table 14.4. Classification of first generation fermions in a 16-plet of $SO(10)$.

SU(5) representation	Particle	weight vector $\frac{1}{2}(\pm 1, \pm 1, \pm 1, \pm 1, \pm 1)$	Q	T_3^L	$2\sqrt{10}\chi$
5^*	$(d^c)_L$	- + + + +	$\frac{1}{3}$	0	3
		+ - + + +			
		+ + - + +			
	e_L^-	+ + + - +	-1	$-\frac{1}{2}$	
	ν_{eL}	+ + + + -	0	$\frac{1}{2}$	
10	$(u^c)_L$	+ + - - -	$-\frac{2}{3}$	0	-1
		+ - + - -			
		- + + - -			
	u_L	+ - - + -	$\frac{2}{3}$	$\frac{1}{2}$	
		- + - + -			
		- - + + -			
	d_L	+ - - - +	$-\frac{1}{3}$	$-\frac{1}{2}$	
		- + - - +			
		- - + - +			
	$(e^c)_L$	- - - + +	1	0	
1	$(N^c)_L$	- - - - -	0	0	-5

we use Y to denote the correctly normalized generator, which in this case is $\sqrt{3/20}$ times the standard model hypercharge. χ is the extra generator of SO(10) beyond those of SU(5); it is the generator of the $U(1)_\chi$ group, arising in the $SO(10) \rightarrow SU(5) \times U(1)_\chi$ breaking illustrated in Fig. 14.4(a). The χ quantum numbers, which distinguish the different SU(5) multiplets in the **16**, are given in Table 14.4. The vectors for the generators of other U(1) groups occurring in the symmetry breaking pattern of Fig. 14.4(b) are linear combinations of T_3^L , Y and χ : $\mathbf{T}_3^R \propto \sqrt{\frac{3}{5}}\mathbf{Y} + \sqrt{\frac{2}{5}}\boldsymbol{\chi}$, $\mathbf{B} - \mathbf{L} \propto \sqrt{\frac{2}{5}}\mathbf{Y} - \sqrt{\frac{3}{5}}\boldsymbol{\chi}$.

With the extra neutral gauge boson of the SO(10) model, the covariant derivative in the electroweak sector is

$$D^\mu = \partial^\mu + i[g_2 \mathbf{W}^\mu \cdot \mathbf{T} + g_a B_a^\mu T_a + g_b B_b^\mu T_b],$$

where \mathbf{W}^μ , B_a^μ and B_b^μ are the SU(2), U(1)_a and U(1)_b gauge fields surviving at low energy. The couplings g_2 , g_a and g_b are all equal at the scale where SO(10) symmetry applies (the generators must all have the same normalization in representations of SO(10)), and their low energy values are related by the downward evolution. If g_a and g_b evolve from the same GUT scale, their values at low energy remain equal if full particle multiplets contribute. If \mathbf{W} and B_a are the gauge bosons of the standard model, then

$$g_a = g_b = \sqrt{\frac{5}{3}} e / \sqrt{1 - x_w}.$$

The T_a and T_b will in general be different for any particular fermion. The mass eigenstates in the neutral boson sector will be linear combinations of the standard model Z and a Z' boson.

In SO(10), the quantization of fermion charges is just like SU(5) and $x_w = 3/8$ at the GUT scale M_X . However, the evolution of couplings to low energies depends on the way in which the symmetry is broken, and differs from the SU(5) model in the case of Fig. 14.4(b).

14.5 The Hierarchy Problem

The hierarchy problem relates to the appearance of two very different mass scales, M_W and M_X , in a GUT theory. The physical Higgs scalar particle associated with electroweak symmetry breaking must have a mass of order M_W in order that the cancellation of diagrams in perturbation theory occurs at sufficiently low energy to satisfy unitarity; see §12.1. The Higgs bosons associated with GUT symmetry breaking on the other hand must have masses and vevs of order M_X , to give masses of this order to the GUT bosons which mediate proton decay. Hence the scalar potential must give a hierarchy of vacuum expectation values.

One could imagine adjusting the parameters of the scalar potential to give this hierarchy. However, the precision to which the scalar self-couplings can be specified is limited by radiative corrections. Figure 14.6 shows one-loop radiative corrections contributing to the mass renormalization of a Higgs boson. These contributions diverge quadratically and in the solution to the RGE equations the running mass square acquires a quadratic dependence on the scale μ of the form

$$M^2(\mu_2) = M^2(\mu_1) + Cg^2(\mu_2^2 - \mu_1^2) + g^2R + O(g^4),$$

where g is a coupling, C is dimensionless and R grows at most logarithmically as $\mu_1 - \mu_2 \rightarrow \infty$. Applied to the electroweak-breaking

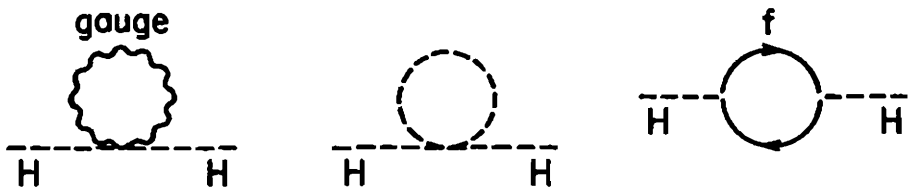


Fig. 14.6. Radiative corrections to a Higgs boson mass from gauge boson, scalar boson and fermion loops.

Higgs H , this equation gives

$$M_H^2(M_W) \simeq M_H^2(M_X) - Cg^2 M_X^2.$$

In order that the physical mass $M_H(M_W)$ be of order M_W , there would have to be a cancellation between the terms on the right-hand side. This would require a fine-tuning of parameters to an accuracy of order 10^{-26} in each order of perturbation theory, which is unnatural.

One way of bringing the radiative corrections under control is to postulate a cut-off $\Lambda \sim 1$ TeV in the loop integrals, by making the Higgs scalars effectively condensates of pairs of new fermions. This is the *Technicolor* approach, discussed in §12.8.

With elementary Higgs scalars, there is an elegant way of solving the hierarchy problem by introducing a boson-fermion symmetry (*supersymmetry*). If boson-fermion pairs have identical couplings, their contributions to the loop diagrams like Fig. 14.6 are of opposite sign and cancel against each other. Naturalness in the hierarchy problem requires that their masses satisfy

$$|m_B^2 - m_f^2| \lesssim O(1 \text{ TeV}^2).$$

The existence of an approximate supersymmetry would entail a complete doubling of the presently known particle spectrum.

14.6 Supersymmetry (SUSY)

14.6.1 Concept.

Hitherto we have encountered two kinds of symmetries in particle physics: the symmetry of space-time with generators P^μ of translations and $M^{\mu\nu}$ of rotations forming the Poincaré algebra and internal symmetries. The generators T_a of a non-abelian internal symmetry



form a Lie algebra,

$$[T_a, T_b] = i f_{abc} T_c,$$

and the T_a commute with the Hamiltonian and the Poincaré generators,

$$[T_a, H] = [T_a, P^\mu] = [T_a, M^{\mu\nu}] = 0.$$

Supersymmetry (SUSY) is a new kind of symmetry which interrelates fermions and bosons. The Lie algebra is extended to a *graded Lie algebra* with both commutation and anticommutation relations that connect the internal SUSY generators to the Poincaré generators. In its simplest form, the SUSY algebra has a self-conjugate spin- $\frac{1}{2}$ Majorana generator Q_α with the property that it changes the total angular momentum J by half a unit and turns boson fields into fermion fields

$$Q_\alpha |\text{boson}\rangle = |\text{fermion}\rangle$$

and vice versa, where $\alpha = 1, 2, 3, 4$ is a spinor index. The commutation [] and anticommutation { } rules are

$$\begin{aligned} [Q_\alpha, M^{\mu\nu}] &= i(\sigma^{\mu\nu} Q)_\alpha, & [Q_\alpha, P^\mu] &= 0, \\ \{Q_\alpha, \bar{Q}_\beta\} &= -2(\gamma_\mu)_{\alpha\beta} P^\mu, & \{Q_\alpha, Q_\beta\} &= \{\bar{Q}_\alpha, \bar{Q}_\beta\} = 0, \end{aligned}$$

where $\sigma^{\mu\nu} = \frac{1}{4}[\gamma^\mu, \gamma^\nu]$ and $\bar{Q}_\alpha = Q_\alpha^T \gamma^0$. The $[Q_\alpha, M^{\mu\nu}]$ commutation relation expresses that Q_α transforms as a spinor, while the $[Q_\alpha, P^0]$ commutation relation expresses that spinor charges are conserved. The $\{Q_\alpha, \bar{Q}_\beta\}$ anticommutation relation indicates that two successive SUSY transformations involve a space-time translation. Thus, supersymmetry involves the structure of space time. There could exist N different operators Q_α^i ($i = 1, \dots, N$) of this kind, but only $N = 1$ SUSY allows fermions in chiral representations, as observed.

The supermultiplets of $N = 1$ SUSY contain particles of different

spin as follows:

chiral	gauge	graviton/ gravitino
$f \begin{pmatrix} \frac{1}{2} \\ 0 \end{pmatrix}$	$\mathcal{G} \begin{pmatrix} 1 \\ \frac{1}{2} \end{pmatrix}$	$G \begin{pmatrix} 2 \\ \frac{3}{2} \end{pmatrix}$

A local gauge symmetry involves spin-1 gauge fields and a local symmetry for the Poincaré group involves spin-2 gravitons of general relativity theory.

In the spirit that all fundamental symmetries are local gauge symmetries, it is also possible to make supersymmetry local. Since the anticommutation relations of SUSY involve the Poincaré group generator P_μ , local supersymmetry involves both the supersymmetric partners of the graviton and the gauge bosons—the spin $\frac{3}{2}$ gravitino and the spin $\frac{1}{2}$ gauginos. A local supersymmetry is called *Supergravity* (SUGRA). In a global supersymmetric theory the gravitino would not be present. Henceforth we concentrate on the chiral and gauge supermultiplets, since the graviton couplings to particles are so feeble.

The masses of the SUSY partners of observed particles are unknown. It has been found phenomenologically that no known particle can be the spartner of any other known particle. Table 14.5 gives a commonly used notation for the SUSY particles. The SUSY partners of the W and B bosons are Majorana fermions \tilde{W} and \tilde{B} . The photino and zino are defined as linear combinations of gaugino fields \tilde{W}^3 and \tilde{B} analogous to the relation of the photon and Z to the gauge fields W^3 and B ;

$$\tilde{\gamma} = \sin \theta_w \tilde{W}^3 + \cos \theta_w \tilde{B}, \quad \tilde{Z} = \cos \theta_w \tilde{W}^3 - \sin \theta_w \tilde{B}.$$

In a supersymmetric world the number of fermion and boson degrees of freedom must match. For example for each quark chirality state, such as q_L , there is a boson supersymmetric partner, in this case \tilde{q}_L .

Table 14.5 Spectrum of SUSY particles.

Particle	Spin		Sparticle	Spin	
quark $q_{L,R}$	$\frac{1}{2}$		squark $\tilde{q}_{L,R}$	0, 0	
lepton $\ell_{L,R}$	$\frac{1}{2}$		slepton $\tilde{\ell}_{L,R}$	0, 0	
photon γ	1		gauginos {	photino $\tilde{\gamma}$	$\frac{1}{2}$
gluon g	1			gluino \tilde{g}	$\frac{1}{2}$
W	1			wino \tilde{W}	$\frac{1}{2}$
Z	1			zino \tilde{Z}	$\frac{1}{2}$
Higgs H	0	Higgsinos	{ shiggs \tilde{H}	$\frac{1}{2}$	

If the supersymmetry were unbroken, the sparticle states would have the same mass as their corresponding particle states.

In supersymmetry, two Higgs doublets are needed to give fermion masses and there are corresponding spin- $\frac{1}{2}$ shiggs partners:

$$\begin{array}{cc}
 \text{Higgs} & \text{shiggs} \\
 \text{doublets} & \text{doublets} \\
 \left(\begin{array}{c} H_1^0 \\ H_1^- \end{array} \right) \left(\begin{array}{c} H_2^+ \\ H_2^0 \end{array} \right) & \left(\begin{array}{c} \tilde{H}_1^0 \\ \tilde{H}_1^- \end{array} \right) \left(\begin{array}{c} \tilde{H}_2^+ \\ \tilde{H}_2^0 \end{array} \right)
 \end{array}$$

In supersymmetry, particles are assigned a quantum number known as R -parity defined by

$$R = (-)^{3B+L+2J}$$

where B is the baryon number, L is the lepton number, and J is the spin. R is $+1$ for the usual particles and -1 for their SUSY partners. R parity is not necessarily conserved, but is usually imposed as a discrete symmetry.

Exercise. Show that an R -violating vertex $dd \rightarrow \tilde{u}^c$ followed by $\tilde{u}^c \rightarrow u^c \tilde{\gamma}$ would allow nucleon decay unsuppressed by powers of M_X , if $m_{\tilde{\gamma}} < m_N$.

With R -conservation, SUSY particles are always pair produced and decay to the lightest SUSY particle which is stable.

Supersymmetry must be broken, because the observed particles do not exhibit boson-fermion degeneracy. However, if we assume the symmetry is broken spontaneously (at a scale $\lesssim 1$ TeV to solve the hierarchy problem) the mass degeneracy is removed but the predicted relations among couplings remain exact. For example, the fermion couplings to gauge bosons \mathcal{G} specify the couplings of the spin- $\frac{1}{2}$ gauge-fermions $\tilde{\mathcal{G}}$ (*gauginos*) to the fermions f and the scalar-fermion members \tilde{f} of the chiral multiplets (*sfermions*)

$$g \bar{f}_A \gamma_\mu f_A \mathcal{G}^\mu \rightarrow \sqrt{2} g \left[\left(\bar{f}_A \tilde{\mathcal{G}}_A \right) \tilde{f}_A + \text{h.c.} \right],$$

where $A = L$ or R labels the chirality. Note that the left and right chirality fermions have independent \tilde{f}_L and \tilde{f}_R sfermion partners, with different masses in general. Figure 14.7 shows some typical SUSY vertices.

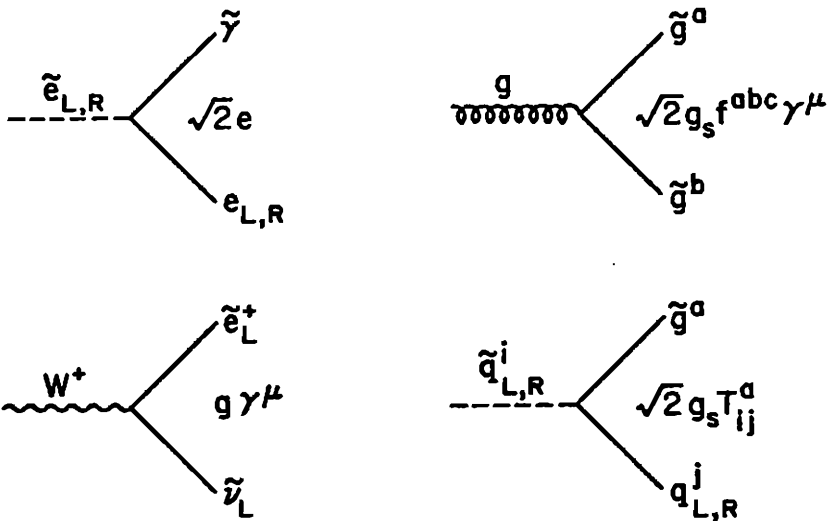


Fig. 14.7. Typical couplings of SUSY particles.

The strong interactions of squarks and gluinos are specified by

$$\begin{aligned}
 -i\mathcal{L}_{q\tilde{q}\tilde{g}} &= \sqrt{2}g_s \left(\tilde{q}_L^\dagger \tilde{g}_a T_a q_L + L \leftrightarrow R \right) + \text{h.c.}, \\
 -i\mathcal{L}_{\tilde{q}\tilde{q}g} &= -g_s \left[\tilde{q}_L T_a g_a^\mu \partial_\mu \tilde{q}_L - (\partial_\mu \tilde{q}_L)^\dagger T_a g_a^\mu \tilde{q}_L \right] \\
 &\quad + ig_s^2 \tilde{q}_L^\dagger T_a g_a^\mu T_b g_{b\mu} \tilde{q}_L + L \leftrightarrow R,
 \end{aligned}$$

where $T_a = \frac{1}{2}\lambda_a$ are the SU(3) color matrices and the gluino \tilde{g} is a Majorana fermion. The gauge interactions of the SUSY particles are

$$\begin{aligned}
 \mathcal{L} = e \bigg\{ & \left[-W_\mu^+ (\overline{\tilde{W}}^+ \gamma^\mu \tilde{\gamma}) - \cot \theta_w W_\mu^+ (\overline{\tilde{W}}^+ \gamma^\mu \tilde{Z}) \right. \\
 & - (\sqrt{2} \sin \theta_w)^{-1} W_\mu^+ (\overline{\tilde{H}}_1^{-c} \gamma^\mu \tilde{H}_{1L}^{0c} - \overline{\tilde{H}}_2^+ \gamma^\mu \tilde{H}_{2L}^0) + \text{h.c.} \bigg] \\
 & + \cot \theta_w Z_\mu (\overline{\tilde{W}}^+ \gamma^\mu \tilde{W}^+) \\
 & + (\sin 2\theta_w)^{-1} Z_\mu \left[(1 - 2 \sin^2 \theta_w) (\overline{\tilde{H}}_1^{-c} \gamma^\mu \tilde{H}_{1L}^{-c} + \overline{\tilde{H}}_2^+ \gamma^\mu \tilde{H}_{2L}^+) \right. \\
 & \left. - (\overline{\tilde{H}}_1^{0c} \gamma^\mu \tilde{H}_{1L}^{0c} + \overline{\tilde{H}}_2^0 \gamma^\mu \tilde{H}_{2L}^0) \right] \bigg\},
 \end{aligned}$$

where c denotes a charge-conjugate state, $\tilde{H}^c = C(\tilde{H}_i)^T$, with C the charge-conjugation matrix. The electroweak gaugino and Higgsino eigenstates which appear in this Lagrangian must be expressed in terms of the mass eigenstates. The couplings to sfermions are

$$\begin{aligned}
 \mathcal{L} = ie(2x_w)^{-\frac{1}{2}} W_\mu^+ \overline{\tilde{f}}_L \overset{\leftrightarrow}{\partial}^\mu \tau^+ \tilde{f}'_L - ie(x_w)^{-1/2} (\overline{\tilde{f}}_L \tilde{W}^-) \tilde{f}'_L + \text{h.c.} \\
 + ie2(\sin 2\theta_w)^{-1} Z_\mu \left[\overline{\tilde{f}}_L \overset{\leftrightarrow}{\partial}^\mu \left(\frac{1}{2} \tau^3 - x_w Q \right) \tilde{f}'_L - \overline{\tilde{f}}_R \overset{\leftrightarrow}{\partial}^\mu x_w Q \tilde{f}'_R \right] \\
 - i\sqrt{2} e Q_f \left[(\overline{\tilde{f}}_L \tilde{\gamma}) \tilde{f}'_L + (\overline{\tilde{f}}_R \tilde{\gamma}) \tilde{f}'_R + \text{h.c.} \right].
 \end{aligned}$$

Exercise. Show that the partial widths for W, Z decays to sfermions are, if kinematically allowed,

$$\begin{aligned}
 \Gamma(W^+ \rightarrow \tilde{a}\tilde{b}) &= c \frac{1}{2} \Gamma_W^0 \lambda^{\frac{3}{2}}(1, x_a, x_b), \\
 \Gamma(Z \rightarrow \tilde{a}\tilde{a}) &= c \frac{1}{2} \Gamma_Z^0 \lambda^{\frac{3}{2}}(1, y_a, y_a) (1 - 4|Q_a|x_w + 8Q_a^2 x_w^2),
 \end{aligned}$$

where Γ_W^0, Γ_Z^0 are defined in §8.1 and 8.2, $c = 1$ for sleptons, $c = 3$ for squarks and $x_a = m_a^2/M_W^2$, $y_a = m_a^2/M_Z^2$.

14.6.2 SUSY mass spectrum.

There are some stringent theoretical constraints on the SUSY mass spectrum from limits on flavor changing neutral current (FCNC) and on anomalous parity violation in nuclei. SUSY box diagrams can give potentially large contributions to the $K_L - K_S$ mass difference. These FCNC contributions are suppressed if the $\tilde{\gamma}$ and \tilde{g} couplings are flavor diagonal, the SUSY Kobayashi-Maskawa angles are identical to the conventional angles, and the squark masses of five flavors are nearly degenerate

$$m_{\tilde{u}} \simeq m_{\tilde{d}} \simeq m_{\tilde{s}} \simeq m_{\tilde{c}} \simeq m_{\tilde{b}}.$$

Parity violation in nuclear transitions can occur through penguin diagrams. The absence of anomalous parity violating effects requires

$$m_{\tilde{u}_L} \simeq m_{\tilde{u}_R}, \quad m_{\tilde{d}_L} \simeq m_{\tilde{d}_R}.$$

In phenomenological analyses this L, R squark mass degeneracy is often assumed to hold for all squark flavors.

Theoretical guidance on SUSY particle masses can be obtained from $N = 1$ supergravity models. Gaugino masses are induced by gauge interactions involving loops of superheavy fields, giving

$$\frac{\mu_1}{\alpha_1} = \frac{\mu_2}{\alpha_2} = \frac{\mu_3}{\alpha_3}$$

at any mass scale. Here the μ_i are the gaugino masses of the $U(1)$, $SU(2)$ and $SU(3)$ interactions and the $\alpha_i = g_i^2/4\pi$ are the couplings. The gluino mass is $m_{\tilde{g}} = |\mu_3|$. At the GUT scale there is a common gaugino mass μ and a common coupling g . In $SU(5)$ the above relation of μ_1 and μ_2 becomes

$$\frac{\mu_1}{\mu_2} = \frac{5}{3} \tan^2 \theta_w.$$

At scale M_W the $SU(2)$ and $U(1)$ gauginos mix with the Higgsinos and receive additional mass contributions from the Higgs vacuum

expectation values v_1, v_2 and from a supersymmetric Higgsino mixing mass term m_1 . The mass terms $\mathcal{L} = \frac{1}{2}\bar{\psi}M\psi$ of the Majorana fields in the neutralino sector are

$$(\tilde{H}_2^0, \tilde{H}_1^0, \tilde{W}_3, \tilde{B}) \frac{1}{2} \begin{pmatrix} 0 & -2m_1 & \frac{1}{\sqrt{2}}gv_2 & -\frac{1}{\sqrt{2}}g'v_2 \\ -2m_1 & 0 & -\frac{1}{\sqrt{2}}gv_1 & \frac{1}{\sqrt{2}}g'v_1 \\ \frac{1}{\sqrt{2}}gv_2 & -\frac{1}{\sqrt{2}}gv_1 & \mu_2 & 0 \\ -\frac{1}{\sqrt{2}}g'v_2 & \frac{1}{\sqrt{2}}g'v_1 & 0 & \mu_1 \end{pmatrix} \begin{pmatrix} \tilde{H}_2^0 \\ \tilde{H}_1^0 \\ \tilde{W}_3 \\ \tilde{B} \end{pmatrix}.$$

Here $\sqrt{2}(v_1^2 + v_2^2)^{1/2} = v = (\sqrt{2}G_F)^{-1/2}$.

Exercise. For $\mu_1 = \mu_2 = 0$ and $v_1 = v_2$ show that the absolute mass eigenvalues of the neutralino mass matrix M are $0, \mu_+, \mu_-$ and $2m_1$, respectively, where

$$\mu_- = (m_1^2 + M_Z^2)^{1/2} - m_1, \quad \mu_+ \mu_- = M_Z^2.$$

Note that $\mu_+ > M_Z$ and $\mu_- < M_Z$. Show that the massless state is the photino.

Exercise. In the limit in which μ_1, μ_2, m_1 are small compared to v show that the photino is an approximate eigenstate with mass given by

$$m_{\tilde{\gamma}} = |\sin^2 \theta_W \mu_2 + \cos^2 \theta_W \mu_1|.$$

Also show that the evolved symmetry relations yield

$$m_{\tilde{\gamma}} = \frac{8}{3} \frac{\alpha(M_W)}{\alpha_s(M_W)} m_{\tilde{g}} \simeq \frac{1}{6} m_{\tilde{g}}.$$

Exercise. For $v_1 = v_2$ show that $\frac{1}{\sqrt{2}}(\tilde{H}_1^0 + \tilde{H}_2^0)$ is an eigenstate of the mass matrix with eigenvalue $-2m_1$. Show that a γ_5 transformation converts a fermion state of negative mass to one of positive mass.

In the general case the neutralino mass matrix is difficult to diagonalize analytically, but the eigenvectors and eigenvalues can be obtained numerically for input values of μ_1 , μ_2 , v_2/v_1 and m_1 . The four neutralino mass eigenstates are then denoted by \tilde{Z}_1 , \tilde{Z}_2 , \tilde{Z}_3 and \tilde{Z}_4 , with $m_{\tilde{Z}_1} < m_{\tilde{Z}_2} < m_{\tilde{Z}_3} < m_{\tilde{Z}_4}$. Except for special situations such as small gaugino masses, these neutralinos are complex mixtures of the \tilde{H}_1^0 , \tilde{H}_2^0 , \tilde{W}_3 and \tilde{B} states in general and it is not possible then to think in terms of photino, zino and higgsino states.

In the chargino sector the mass matrix is of the form

$$(\tilde{W}, \tilde{H}_{1L} - \tilde{H}_{2R}) \left[\mathcal{M} \frac{1}{2} (1 - \gamma_5) + \mathcal{M}^T \frac{1}{2} (1 + \gamma_5) \right] \begin{pmatrix} \tilde{W} \\ \tilde{H}_{1L} - \tilde{H}_{2R} \end{pmatrix}$$

with

$$\mathcal{M} = \begin{pmatrix} \mu_2 & gv_1 \\ gv_2 & 2m_1 \end{pmatrix}.$$

The mass eigenstates are denoted by \tilde{W}_+ and \tilde{W}_- , where \tilde{W}_+ is the state of higher mass and \tilde{W}_- the state of lower mass.

Exercise. For $v_1 = v_2$ show that the mass eigenvalues are

$$m_{\pm} = \left[(m_1 - \frac{1}{2}\mu_2)^2 + M_W^2 \right]^{\frac{1}{2}} \pm (m_1 + \frac{1}{2}\mu_2),$$

where it is assumed that $m_1 + \frac{1}{2}\mu_2 > 0$. Show also that the eigenstates are given by

$$\begin{pmatrix} \tilde{W}_+ \\ \gamma_5 \tilde{W}_- \end{pmatrix} = \begin{pmatrix} -\cos \gamma & \sin \gamma \\ \sin \gamma & \cos \gamma \end{pmatrix} \begin{pmatrix} \tilde{W} \\ \tilde{H}_{1L} - \tilde{H}_{2R} \end{pmatrix},$$

where

$$\sin \gamma = \left(\frac{m_+ - \mu_2}{m_+ + m_-} \right)^{\frac{1}{2}}.$$

The γ_5 factor above is required to get positive mass. For $\mu_2 \ll 2m_1$ note that $m_- < M_W < m_+$, which is a general feature when the gaugino masses vanish ($\mu_1 = \mu_2 = 0$); see the preceding exercise on neutralino masses.

Exercise. In both the neutralino and chargino gauge-Higgs sectors verify that the number of fermionic and bosonic states is the same.

The squarks and sleptons have a common SUSY-breaking mass m_0 resulting from integrating out superheavy fields. In addition there are mass contributions from diagrams with a gaugino and a fermion in the loop. These are proportional to the gaugino masses, all of which can be expressed in terms of $m_{\tilde{g}}$. Finally there are scalar mass contributions from a supersymmetric “ D -term” in the potential that are proportional to $v_2^2 - v_1^2$ in the minimal Higgs model. The resulting masses at scale M_W , assuming 3 generations of standard-model quarks and leptons, are

$$m^2(\tilde{d}_L) = m_0^2 + 0.83 m_{\tilde{g}}^2 + 0.43 r M_Z^2,$$

$$m^2(\tilde{d}_R) = m_0^2 + 0.78 m_{\tilde{g}}^2 + 0.07 r M_Z^2,$$

$$m^2(\tilde{u}_L) = m_0^2 + 0.83 m_{\tilde{g}}^2 - 0.36 r M_Z^2,$$

$$m^2(\tilde{u}_R) = m_0^2 + 0.78 m_{\tilde{g}}^2 - 0.14 r M_Z^2,$$

$$m^2(\tilde{e}_L) = m_0^2 + 0.06 m_{\tilde{g}}^2 + 0.28 r M_Z^2,$$

$$m^2(\tilde{e}_R) = m_0^2 + 0.01 m_{\tilde{g}}^2 + 0.22 r M_Z^2,$$

$$m^2(\tilde{\nu}) = m_0^2 + 0.06 m_{\tilde{g}}^2 - 0.50 r M_Z^2,$$

where $r = (v_2^2 - v_1^2)/(v_1^2 + v_2^2)$. When $v_1 = v_2$ the squarks are nearly mass degenerate. The masses averaged over flavor and L, R satisfy

$$\langle m_{\tilde{q}}^2 \rangle - \langle m_{\tilde{\ell}}^2 \rangle = 0.77 m_{\tilde{g}}^2.$$

Thus squarks would be heavier than sleptons.

A schematic representation of SUSY particle masses that might be realized in a $N = 1$ supergravity model is shown in Fig. 14.8.

The general supersymmetric Lagrangian involves the mixing angles of the transformations that diagonalize the gaugino mass matrices. Thus although the fundamental interactions are simple in form,

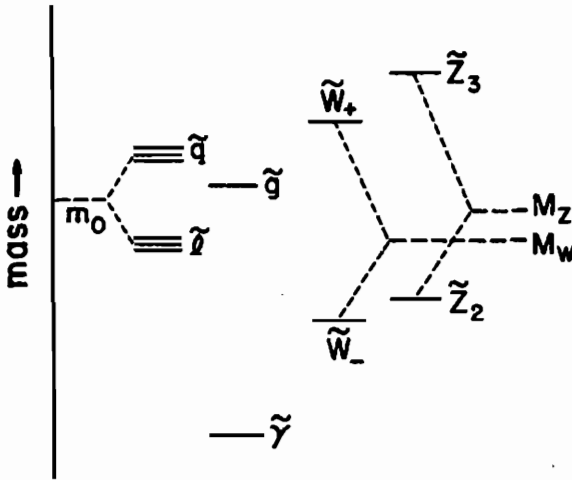


Fig. 14.8. Typical sparticle mass spectrum in $N = 1$ supergravity model assuming small gaugino masses.

the results including mixing can become rather complicated. The gaugino interactions have the general form

$$\mathcal{L} = ie \left[A \tilde{f}_L^\dagger \tilde{Z}_i \bar{f}_L + B \tilde{f}_R^\dagger \tilde{Z}_i \bar{f}_R + C \tilde{f}_L^\dagger \tilde{W}_i \bar{f}'_L + D \tilde{f}_L^\dagger \tilde{W}_i^c \bar{f}_R \right. \\ \left. + \tilde{W}_i (E + F \gamma_5) \gamma^\mu \tilde{Z}_j W_\mu + \tilde{W}_i (G + H \gamma_5) \gamma^\mu \tilde{W}_j Z + \text{h.c.} \right],$$

where A, B, \dots, G, H are complex coupling coefficients and $f = \ell, \nu, u, d$ are fermion fields and (f, f') are $T_3 = \frac{1}{2}, -\frac{1}{2}$ doublet members. The coefficients A, B, C, D have both flavor and gaugino indices; the coefficients E, F, G, H each have two gaugino indices i, j . All coefficients may depend on the mixing angles which diagonalize the gaugino mass matrices. For simplicity, in the present discussion we specialize to the case of a light photino and equal vevs, $v_1 = v_2$. Then two of the neutralino mass eigenstates are $\tilde{\gamma}$ and $(\tilde{H}_1^0 + \tilde{H}_2^0)/\sqrt{2}$, and the chargino mass eigenstates are \tilde{W}_-, \tilde{W}_+ . The coupling parameters of the gauginos $\tilde{\gamma}, \tilde{Z}_2$ and \tilde{W}_- are listed in Table 14.6.

Table 14.6.

(a) The non-zero coefficients that determine the neutralino couplings of $\tilde{\gamma}$ and \tilde{Z}_2 to $\tilde{f}f$. Here $N = M_Z/[2(M_Z^2 + \mu_-^2)]^{1/2}$ with μ_- the mass of \tilde{Z}_2 . The notation $t = \tan \theta_w$ and $c = \cot \theta_w$ is used.

	$A(\tilde{\gamma}) = B(\tilde{\gamma})$	$A(\tilde{Z}_2)/N$	$B(\tilde{Z}_2)/N$
ℓ	$-\sqrt{2}$	$c - t$	$2t$
ν	0	$[x_w(1 - x_w)]^{-1/2}$	0
u	$\frac{2}{3}\sqrt{2}$	$c - \frac{1}{3}t$	$-\frac{4}{3}t$
d	$-\frac{\sqrt{2}}{3}$	$-c - \frac{1}{3}t$	$\frac{2}{3}t$

(b) The non-zero coefficients of the chargino couplings.

$$C(\tilde{W}_-) = -ix_w^{-1/2} \sin \gamma \quad \text{for } T_3(\tilde{f}) = \frac{1}{2},$$

$$D(\tilde{W}_-) = ix_w^{-1/2} \sin \gamma \quad \text{for } T_3(\tilde{f}) = -\frac{1}{2}.$$

(c) The non-zero coefficients that determine the purely gaugino couplings.

$$\bar{\tilde{W}}_- \tilde{\gamma} W : E = \sin \gamma,$$

$$\bar{\tilde{W}}_- \tilde{Z}_2 W : E = \frac{N\mu_-}{\sqrt{2} x_w M_Z} (-\cos \gamma + 2 \sin \gamma \cos \theta_w M_Z^2 / \mu_-^2),$$

$$\bar{\tilde{W}}_- \tilde{W}_- Z : G = -\cot \theta_w (1 - \frac{1}{2} \sec^2 \theta_w \cos^2 \gamma).$$

14.6.3 SUSY searches.

In many phenomenological analyses the photino is assumed to be the lightest SUSY particle. The photino interacts feebly with matter through $\tilde{\gamma}q \rightarrow \tilde{q} \rightarrow \tilde{\gamma}q$, $\tilde{g}q$ and $\tilde{\gamma}e \rightarrow \tilde{e} \rightarrow \tilde{\gamma}e$. For example, with a light photino the $\tilde{\gamma}q$ subprocess cross section is of order

$$\hat{\sigma} \simeq \frac{\alpha^2}{(m_{\tilde{q}})^4} \hat{s},$$

assuming $\hat{s} \ll (m_{\tilde{q}})^2$, where \hat{s} is the subprocess c.m. energy squared.

With the present limits of $m_{\tilde{g}}, m_{\tilde{e}} \gtrsim O(50 \text{ GeV})$ the photino interaction cross sections are less than 10^{-32} cm^2 , on the order of neutrino cross sections. Thus a stable $\tilde{\gamma}$ will escape from collider detectors unseen and the characteristic signature for SUSY particle production is events with large transverse momentum imbalance due to the “missing” energy-momentum carried off by the photino. (Momentum considerations in the longitudinal direction are not possible in collider experiments due to the loss of particles down the beam pipe.)

e^+e^- colliders

SUSY searches have been made at e^+e^- colliders in the reactions (a) $e^+e^- \rightarrow \tilde{\gamma}\tilde{\gamma}\gamma$, (b) $e^+e^- \rightarrow e^\pm\tilde{e}^\mp\tilde{\gamma}$ and (c) $e^+e^- \rightarrow \tilde{e}^+\tilde{e}^-$. The Feynman diagrams for these processes are shown in Fig. 14.9. The experimental bounds obtained on the selectron and photino masses are shown in Fig. 14.10. Negative results from other sparticle searches at PETRA and PEP colliders put lower limits of about 20 GeV on $\tilde{\mu}, \tilde{\tau}, \tilde{H}^\pm, \tilde{W}^\pm$ and 25-30 GeV on the \tilde{Z} mass for $m_{\tilde{e}} < 60 \text{ GeV}$. More recently, the fact that visible and invisible Z decay widths are close to standard 3-generation non-SUSY predictions implies that the masses of $\tilde{H}^\pm, \tilde{W}^\pm$ and all sfermions must be $\gtrsim \frac{1}{2}M_Z$.

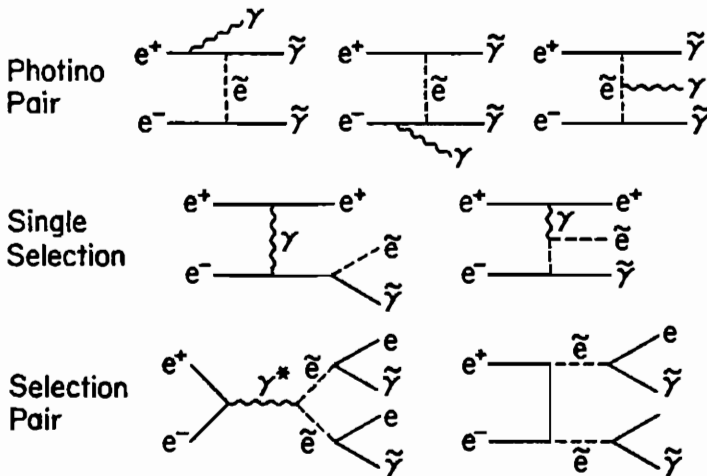


Fig. 14.9. Diagrams for SUSY particle production in e^+e^- collisions.

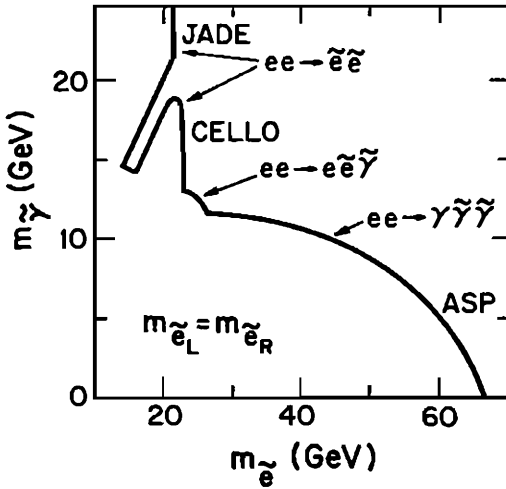


Fig. 14.10. Bounds on the selectron and photino masses from e^+e^- collider experiments.

$\bar{p}p$ colliders

In hadron-hadron collisions the strongly interacting SUSY particles \tilde{g} and \tilde{q} can be pair produced via the $O(\alpha_s^2)$ QCD fusion subprocesses

$$q\bar{q}, gg \rightarrow \tilde{q}\tilde{q}, \tilde{g}\tilde{g}; \quad qg \rightarrow \tilde{q}\tilde{g}.$$

Since the parton flux is dominantly at fractional momenta $x \lesssim 1/4$, the SUSY particle mass range that can be probed at a given collider energy \sqrt{s} is conservatively bounded by

$$2m_{\tilde{q},\tilde{g}}/\sqrt{s} \lesssim 1/4.$$

Thus at CERN collider energies, the accessible SUSY mass range is restricted to $\lesssim 80$ GeV. At the Tevatron, the range is extended to $\lesssim 250$ GeV and at the SSC searches for SUSY particles can be extended beyond masses of 1 TeV. By then the absence of signals would rule out supersymmetry as an answer to the hierarchy problem.

For the SUSY masses that can be probed at the CERN collider it

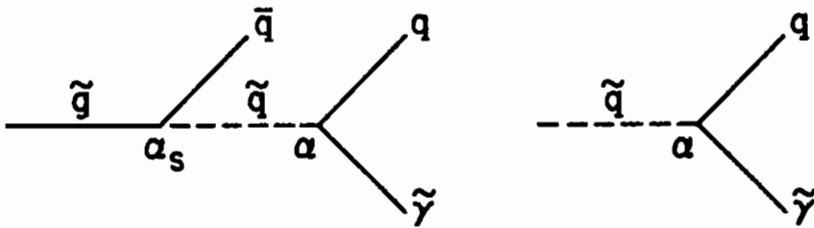


Fig. 14.11. Diagrams for \tilde{g} and \tilde{q} decays to $\tilde{\gamma}$.

is assumed that the dominant decays of gluinos and squarks are

$$\begin{aligned} \tilde{g} &\rightarrow q\bar{q}\tilde{\gamma}, & \tilde{q} &\rightarrow q\tilde{g}, & \text{if } m_{\tilde{g}} < m_{\tilde{q}}, \\ \tilde{q} &\rightarrow q\tilde{\gamma}, & \tilde{g} &\rightarrow q\bar{q}, \bar{q}\tilde{q}, & \text{if } m_{\tilde{q}} < m_{\tilde{g}}. \end{aligned}$$

The decay modes to photinos are illustrated in Fig. 14.11.

Exercise. For $m_{\tilde{g}} < m_{\tilde{q}}$ show that the $\tilde{g} \rightarrow q\bar{q}\tilde{\gamma}$ decay distribution is given by

$$\frac{d\Gamma}{dx dy} = \frac{e_q^2 \alpha \alpha_s m_{\tilde{g}}}{8\pi} \left[\frac{x(1-x)}{(\lambda-1+x)^2} + \frac{y(1-y)}{(\lambda-1+y)^2} \right],$$

where $x = 2\tilde{g} \cdot q/m_{\tilde{g}}^2$, $y = 2\tilde{g} \cdot \bar{q}/m_{\tilde{g}}^2$, and $\lambda = m_{\tilde{q}}^2/m_{\tilde{g}}^2$, assuming that \tilde{q}_L and \tilde{q}_R are degenerate. e_q is the quark charge.

Figure 14.12 shows a typical subprocess for the production and decays of gluino pairs in the case that $m_{\tilde{g}} < m_{\tilde{q}}$. The missing momenta carried by the two photinos add vectorially to give missing transverse momentum (\cancel{p}_T). By searching for events containing jet(s) + large \cancel{p}_T in excess of standard model backgrounds the UA1 collaboration concluded that

$$\begin{aligned} m_{\tilde{g}} &> 60 \text{ GeV}, & \text{(for } m_{\tilde{q}} \text{ large)}, \\ m_{\tilde{q}} &> 70 \text{ GeV}, & \text{(for } m_{\tilde{g}} \text{ large)}. \end{aligned}$$

Figure 14.13 shows the dependence of the gluino mass bound on the $\tilde{\gamma}$ mass assuming 5 flavors of degenerate squarks and a stable $\tilde{\gamma}$.

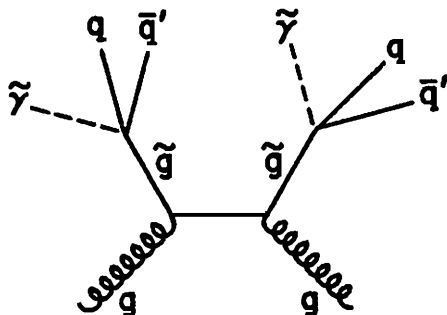


Fig. 14.12. Diagram illustrating $\tilde{g}\tilde{g}$ pair production with decays to photinos.

In supersymmetry models with $m_{\tilde{\gamma}} \ll M_W$ there are SUSY mass eigenstates \tilde{W} and \tilde{Z} in the gaugino-Higgsino sector that are lighter than the W and Z bosons. Then the weak boson decays

$$W \rightarrow \tilde{W}\tilde{\gamma}, \tilde{W}\tilde{Z}; \quad Z \rightarrow \tilde{W}\tilde{W}$$

are potential sources of gaugino pairs. These decays would increase the W and Z total widths. The winos and zinos decay via

$$\tilde{W} \rightarrow \ell\nu\tilde{\gamma} \text{ or } q\bar{q}'\tilde{\gamma}, \quad \tilde{Z} \rightarrow \ell\bar{\ell}\tilde{\gamma} \text{ or } q\bar{q}\tilde{\gamma},$$

giving characteristic n -jet + m -leptons + p_T signatures. Absence of the multilepton signals in the CERN collider data indicates that the decay $W \rightarrow \tilde{W}\tilde{Z}$ is kinematically suppressed and thus

$$M_{\tilde{W}}, M_{\tilde{Z}} \gtrsim 40 \text{ GeV}.$$

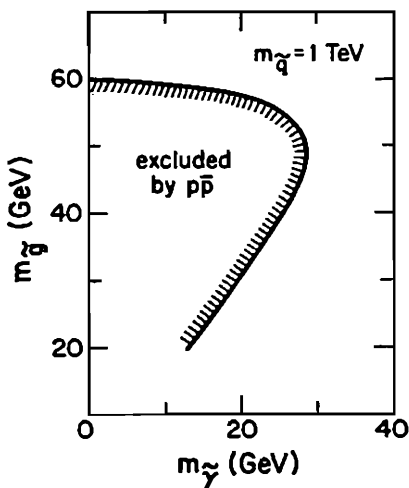


Fig. 14.13. Gluino mass limits versus the photino mass, from searches at the CERN $p\bar{p}$ collider.

Supercolliders

If the gluino mass exceeds 150-200 GeV (but is less than the squark mass), the weak decay modes

$$\tilde{g} \rightarrow q\bar{q}'\tilde{W}$$

account for about half of the gluino decays. Figure 14.14 illustrates representative expectations for heavy gluino decay branching fractions. Here the chargino states \tilde{W}_+ (heavy chargino) and \tilde{W}_- (light chargino) are the mass eigenstates of the charged wino-Higgsino sector. Similarly the neutralino states $\tilde{Z}_1, \tilde{Z}_2, \tilde{Z}_3, \tilde{Z}_4$ are the neutral mass eigenstates with \tilde{Z}_1 the lightest and \tilde{Z}_4 the heaviest. Only in special circumstances will the \tilde{Z}_1 correspond with the $\tilde{\gamma}$ gaugino eigenstate. Strictly speaking \tilde{Z}_1 is the photino only if it is massless. For small $M_{\tilde{Z}_1}$, \tilde{Z}_1 is nearly the $\tilde{\gamma}$ but for larger $M_{\tilde{Z}_1}$, the \tilde{Z}_1 also has substantial zino and higgsino components. The heavy gluino decays mainly to the heavier chargino, $\tilde{g} \rightarrow q\bar{q}'\tilde{W}_+$. The \tilde{W}_+ subsequently decays typically via $\tilde{W}_+ \rightarrow W\tilde{Z}_i$ to a W boson and one of the lighter neutralinos or via $\tilde{W}_+ \rightarrow Z^0\tilde{W}_-$. Thus a characteristic feature of a heavy gluino pair event would be W or Z bosons in the final state. The W, Z bosons, the \tilde{W}_- and possibly also the \tilde{Z}_i would further decay either leptonically or hadronically giving final states with several leptons, jets and p_T .

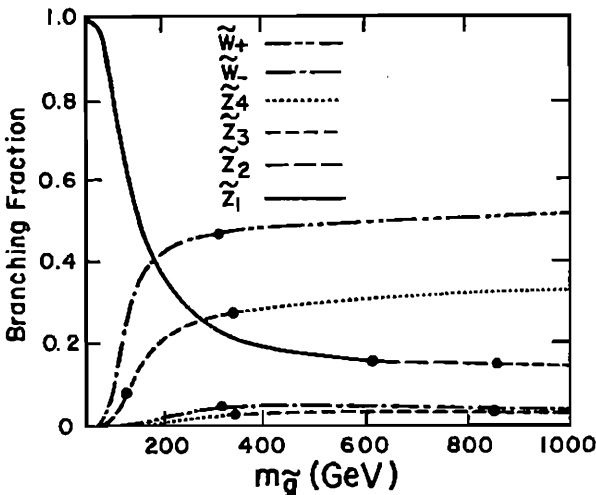


Fig. 14.14. Typical branching fractions of heavy gluino decay, assuming $m_{\tilde{q}} = 2m_{\tilde{g}}$.

The cross section for $\tilde{g}\tilde{g}$ production is large, ranging from $O(10 \text{ nb})$ for $m_{\tilde{g}} = 250 \text{ GeV}$ to $O(100 \text{ pb})$ for $m_{\tilde{g}} = 750 \text{ GeV}$ at the SSC energy of 40 TeV. Thus $\gtrsim 10^6$ gaugino pairs would be produced per year. Such large rates would permit a trigger on the rarer but cleaner leptonic decays of the gauge bosons and gauginos (there may be similar signals from superheavy quarks; see §10.3.6).

14.7 SUSY GUTS

In a supersymmetric SU(5) grand unified theory the beta function coefficients are given by

$$\begin{aligned} 48\pi^2 b_3 &= 27 - 6n_g, \\ 48\pi^2 b_2 &= 18 - 6n_g - 3, \\ 48\pi^2 b_1 &= -6n_g - \frac{9}{5}, \end{aligned}$$

where n_g is the number of generations. The changes in the b values from the non-SUSY SU(5) results are due to the loop contributions of the sparticles. The difference in the running of the gauge couplings α_N from M_W to M_{GUT} is depicted in Fig. 14.15. In SUSY SU(5) M_{GUT} is substantially larger than in non-SUSY SU(5). The larger value of M_{GUT} can give consistency with the proton lifetime. In SUSY GUTS there are additional nucleon decay diagrams with heavy fermion (rather than heavy vector) exchange; these have M_X^{-2} rather than $(M_X)^{-4}$ suppression factors, but in fact very small coupling constants keep the predicted lifetime long enough.

Exercise. Show that a $\tilde{u}u \rightarrow \tilde{H} \rightarrow \tilde{d}^c e^+$ process contributes to nucleon decay where \tilde{H} is a superheavy higgs.

The value of $\sin^2 \theta_w$ at scale M_W is given by

$$x_w(M_W) = \frac{b_3 - b_2 + \frac{5}{3}(b_2 - b_1)\alpha(M_W)/\alpha_3(M_W)}{b_3 - b_2 + \frac{5}{3}(b_3 - b_1)}.$$

The contributions of n_g cancel in the differences of the b coefficients. The difference in the gauge sector contributions in SUSY SU(5) as

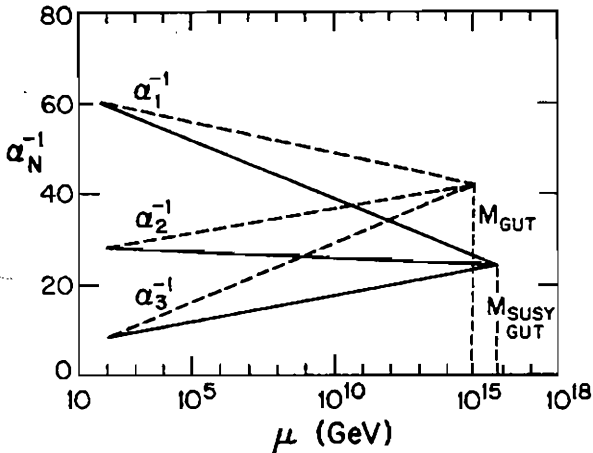


Fig. 14.15. Evolution of couplings in SUSY SU(5) compared with non-SUSY SU(5).

compared to non-SUSY SU(5) cancels in the ratio. Hence if the Higgs contribution were ignored the x_w prediction would be the same. Including the Higgs contributions and two loop corrections the results from the minimal supersymmetric extension of SU(5) are

$$x_w(M_W) = 0.233, \quad M_X = 7.7 \times 10^{15} \text{ GeV}.$$

This SUSY SU(5) prediction for x_w is in reasonable accord with the measured value. Also gauge coupling unification succeeds better with SUSY.

14.8 Superstrings

14.8.1 Strings as particles.

Superstring theory offers the exciting prospect of a possible ultimate unification of all the fundamental particles and forces, including a consistent quantum theory of gravity free of infinities. In the past the fundamental particles have been considered to be points in space. A point particle sweeps out a world-line in space time with trajectory $x(\tau)$. In string theory the fundamental objects are one-dimensional strings in space. A string sweeps out a world sheet in space-time with trajectory $x(\sigma, \tau)$, where σ is a string parameter that specifies the location of points along the string. In phenomenologically promising

string theories the ends of the string close to form a loop. A string has vibrational modes and each of these modes represents a particle. Thus a string describes an infinite number of particles—a finite number of massless particles and an infinite tower of massive particles. The fundamental scale of string theory is the string tension

$$T = \frac{1}{2\pi\alpha'}$$

where α' is the slope of the Regge trajectory with dimensions (mass) $^{-2}$. In superstring theory the massless modes of the string include gravity and $1/\sqrt{\alpha'}$ is taken to be the Planck mass $M_P = 1/\sqrt{G_N} \simeq 10^{19}$ GeV, where G_N is the gravitational constant. The length scale of the string is then of order 10^{-33} cm. All masses, couplings and other properties are in principle predictable, once the fundamental string theory is known. Only the zero-mass modes of the string can be excited at laboratory energies and these correspond to our elementary particles. At low energies, string theory looks just like a quantum field theory of point-like elementary particles, including a spin-2 graviton, except that in the string case the divergences associated with the graviton are cancelled by the massive modes (with masses $\sim M_P$).

The most promising candidate superstring theory (the *heterotic superstring*) is based on closed strings with the anomaly-free internal symmetry group $G = E_8 \times E_8$, where E_8 is the exceptional group of rank 8. The theory is formulated in 10 space-time dimensions. The six extra space dimensions are supposed to be *compactified* at the Planck scale (curled up into tubes with radii of order M_P^{-1} , too small to be observed) on a six-dimensional manifold.

A guiding principle followed in compactification is that a four-dimensional $N = 1$ supersymmetry be obtained in order that the hierarchy of the Planck and $\mathcal{O}(100 \text{ GeV})$ mass scales can be preserved. This is achieved if the six dimensional spaces K have an $SU(3)$ structure ($SU(3)$ holonomy); as a consequence one of the E_8 symmetries is reduced to an E_6 GUT symmetry group. The value

of x_w at the compactification scale is the same as in conventional GUTS. However the mass ratio m_b/m_τ is not predicted here.

The E_6 group contains the $SU(3) \times SU(2) \times U(1)$ of the standard model. The fermions belong to chiral families of this E_6 . The **27** representation of E_6 contains all the known quarks and leptons of one generation plus some exotics.

The E_6 is further broken down at the Planck scale by gauge fields winding around 'holes' in the spaces K , if K is not simply connected. Non-zero values of Wilson line integrals around loops act like symmetry-breaking fields in the adjoint representation. E_6 can be broken to a rank 6 group like $SU(3) \times SU(2) \times U(1)^3$ or to a rank 5 group like $SU(3) \times SU(2) \times U(1)^2$. Since E_6 has rank 6, and the standard $SU(3) \times SU(2) \times U(1)$ model has rank 4, the low-energy gauge theories resulting from E_6 breaking can contain additional gauge bosons, which can be searched for at colliders.

The right Higgs scalars are present for electroweak symmetry breaking. These Higgs fields are either the superpartners of the chiral **27** multiplets or arise from additional **27** + $\overline{\mathbf{27}}$ representations.

The gauge fields and gaugino partners of the other E_8 symmetry of the heterotic superstring interact with the E_6 sector only gravitationally. It has been speculated that these fields may form the *hidden sector* of supergravity models which breaks supersymmetry.

14.8.2 E_6 GUT classification symmetry.

The six-dimensional root space of E_6 is a subspace of the eight-dimensional root space of E_8 , which is spanned by eight unit vectors e_i . The $SU(3)$ subalgebra with which the E_6 commutes is spanned by e_1, e_2, e_3 and the non-zero root vectors of this $SU(3)$ may be chosen to be $\pm(e_1 + e_2), \pm(e_1 + e_3), \pm(e_2 - e_3)$. Since the unit vector $n = (-e_1 + e_2 + e_3)/\sqrt{3}$ has zero projection along these root vectors of the $SU(3)$, we may choose $n, e_4, e_5, e_6, e_7, e_8$ as unit vectors spanning the root space of E_6 . Then $e_4 \dots e_8$ span the root vector space

of an $SO(10)$ subgroup and the projection of a particle weight vector along \mathbf{n} corresponds to the $U(1)$ eigenvalue for $E_6 \rightarrow SO(10) \times U(1)$.

The **78**-plet of E_6 decomposes into $SO(10)$ multiplets as

$$\mathbf{78} = \mathbf{45} + \mathbf{16} + \mathbf{16}^* + \mathbf{1}$$

and the low-energy gauge bosons form a part of the broken **45**-plet. The **27** representation of E_6 has the $SO(10)$ decomposition

$$\mathbf{27} = \mathbf{16} + \mathbf{10} + \mathbf{1}.$$

The known fermions of one generation plus an extra neutrino N^c fill out the **16** and new quarks and leptons are required to fill the **10** and **1**. To classify the fermions in the **27**-plet, we can use the 6 dimensional root vector space. The particle quantum numbers will be specified by the diagonal generators of $SU(3)_{\text{color}} \times SU(3)_L \times SU(3)_R$ subgroups of E_6 : (the label L anticipates that the electroweak $SU(2)_L$ will be embedded in the $SU(3)_L$ group). The non-color diagonal generators are

$$\begin{aligned} T_{3L} &= (0 \mid 0, 0, 0, \frac{1}{2}, -\frac{1}{2}), \\ Y_L &= \frac{1}{2}\sqrt{3}(-\frac{1}{\sqrt{3}} \mid -\frac{1}{3}, -\frac{1}{3}, -\frac{1}{3}, 0, 0), \\ T_{3R} &= (0 \mid 0, 0, 0, \frac{1}{2}, \frac{1}{2}), \\ Y_R &= \frac{1}{2}\sqrt{3}(\frac{1}{\sqrt{3}} \mid -\frac{1}{3}, -\frac{1}{3}, -\frac{1}{3}, 0, 0). \end{aligned}$$

The electric charge is given by the linear combination

$$Q = T_{3L} + T_{3R} + \frac{1}{\sqrt{3}}(Y_L + Y_R).$$

Table 14.7 gives the members of the **27**-plet of fermions, with their weight vectors and classification under $SO(10)$, $SU(5)$ and $SU(3)_L \times SU(3)_R$ subgroups. The eigenvalues of the diagonal generators above are given by their scalar products with the weight vector of the particle in question.

Exercise. For the diagonal operators in Table 14.7, show that the normalizations are $\text{Tr}(T_a^2) = 3$ evaluated over the **27**.

For convenience we introduce the $\text{SU}(2)_L$ doublet notation

$$Q = \begin{pmatrix} u \\ d \end{pmatrix}_L, \quad L = \begin{pmatrix} \nu_e \\ e \end{pmatrix}_L, \quad L' = \begin{pmatrix} \nu_E \\ E \end{pmatrix}_L.$$

In terms of these the $\text{SU}(5)$ content of the first-generation **27** of left-handed fermions is

$$\begin{aligned} \mathbf{27} = & 5^* [d^c, L] + 10 [u^c, e^c, Q] + 1 [N^c] \\ & + 5^* [h^c, L'] + 5 [h, L'^c] + 1 [n]. \end{aligned}$$

The usual fermions of the **16** of $\text{SO}(10)$ appear on the first line while the second line has the exotic states needed for this E_6 multiplet.

The h state is a color triplet and $\text{SU}(2)_L$ singlet with electric charge $-\frac{1}{3}$; the accompanying L' is a color singlet and $\text{SU}(2)_L$ doublet. Thus far the baryon and lepton numbers of these states are unspecified; three possible assignments consistent with different choices of the superpotential are:

case	$B(h)$	$L(h)$	$B(L)$	$L(L)$
A	$\frac{1}{3}$	0	0	1
B	$\frac{1}{3}$	1	0	0
C	$-\frac{2}{3}$	0	0	0

In case A, h is an isosinglet quark and L is a lepton doublet. Mixing of the h quark with the d quark can occur. In case B, h is a leptoquark. In cases B and C, L has the quantum numbers of a Higgs superpartner and hence the Higgs bosons can belong to the same **27** as the supersymmetric partners of the known fermions. The production and decays of h and L depend on their quantum number assignments. The $\text{SO}(10)$ singlet state n is an additional neutral lepton.

Table 14.7. Classification of the first generation of fermions in a 27-plet of E_6 .

The symbols \pm in the root vectors in the top eight rows denote values $\pm 1/2$.

SO(10)	SU(5)	SU(3) _{color}	Weight	Left- Handed State	Q	T _{3L}	T _{3R}	$\frac{2}{\sqrt{3}}$ $\times Y_L$	$\frac{2}{\sqrt{3}}$ $\times Y_R$	$2\sqrt{15}$ $\times Q_n$	$2\sqrt{6}$ $\times Q_\psi$	$2\sqrt{10}$ $\times Q_x$
16	5*	3*	$(-\frac{1}{2\sqrt{3}} ++-++)$	d^c	$\frac{1}{3}$	0	$\frac{1}{2}$	0	$-\frac{1}{3}$	-1	1	-3
		1	$(-\frac{1}{2\sqrt{3}} +++-+)$	e^-	-1	$-\frac{1}{2}$	0	$-\frac{1}{3}$	$-\frac{2}{3}$			
		1	$(-\frac{1}{2\sqrt{3}} ++++-)$	ν_e	0	$\frac{1}{2}$	0	$-\frac{1}{3}$	$-\frac{2}{3}$			
	10	1	$(-\frac{1}{2\sqrt{3}} ---++)$	e^{-c}	1	0	$\frac{1}{2}$	$\frac{2}{3}$	$\frac{1}{3}$	2	1	1
		3	$(-\frac{1}{2\sqrt{3}} --+ -+)$	d	$-\frac{1}{3}$	$-\frac{1}{2}$	0	$\frac{1}{3}$	0			
		3	$(-\frac{1}{2\sqrt{3}} --+ +-)$	u	$\frac{2}{3}$	$\frac{1}{2}$	0	$\frac{1}{3}$	0			
		3*	$(-\frac{1}{2\sqrt{3}} +- - --)$	u^c	$-\frac{2}{3}$	0	$-\frac{1}{2}$	0	$-\frac{1}{3}$			
	1	1	$(-\frac{1}{2\sqrt{3}} - - - -)$	N^c	0	0	$-\frac{1}{2}$	$\frac{2}{3}$	$\frac{1}{3}$	5	1	5
10	5*	3*	$(\frac{1}{\sqrt{3}} -10000)$	h^c	$\frac{1}{3}$	0	0	0	$\frac{2}{3}$	-1	-2	2
		1	$(\frac{1}{\sqrt{3}} 000-10)$	E^-	-1	$-\frac{1}{2}$	$-\frac{1}{2}$	$-\frac{1}{3}$	$\frac{1}{3}$			
		1	$(\frac{1}{\sqrt{3}} 0000-1)$	ν_E	0	$\frac{1}{2}$	$-\frac{1}{2}$	$-\frac{1}{3}$	$\frac{1}{3}$			
	5	3	$(\frac{1}{\sqrt{3}} 100000)$	h	$-\frac{1}{3}$	0	0	$-\frac{2}{3}$	0	-4	-2	-2
		1	$(\frac{1}{\sqrt{3}} 00010)$	E^{-c}	1	$\frac{1}{2}$	$\frac{1}{2}$	$-\frac{1}{3}$	$\frac{1}{3}$			
		1	$(\frac{1}{\sqrt{3}} 00001)$	N_E^c	0	$-\frac{1}{2}$	$\frac{1}{2}$	$-\frac{1}{3}$	$\frac{1}{3}$			
1	1	1	$(-\frac{2}{\sqrt{3}} 000000)$	n	0	0	0	$\frac{2}{3}$	$-\frac{2}{3}$	5	4	0

14.8.3 Gauge Bosons from E_6 .

Since E_6 has rank 6, and the standard $SU(3) \times SU(2) \times U(1)$ model has rank 4, the low-energy gauge theory resulting from E_6 breaking can contain additional gauge bosons. In superstring theory the E_6 symmetry can be broken by a Wilson loop mechanism which involves path integrals of the gauge boson fields in the adjoint **78** representation of E_6 . This **78** decomposes with respect to the $SU(3)$ subgroups as follows

$$\begin{array}{rcccc}
 & & & SU(3)_{\text{color}}, & SU(3)_L, & SU(3)_R \\
 \mathbf{78} & \rightarrow & & (3, & 3, & 3^*) \\
 & & + & (3^*, & 3^*, & 3) \\
 & & + & (8, & 1, & 1) \\
 & & + & (1, & 8, & 1) \\
 & & + & (1, & 1, & 8)
 \end{array}$$

In order to preserve $SU(3)_{\text{color}}$ and break $SU(3)_L$ to $SU(2)_L$, the symmetry breaking must occur through the $SU(2)_L$ singlet member of $(1, 8, 1)$, which also preserves the $U(1)_{Y_L}$ symmetry. Since Y_L is not the standard model Y , there must be at least one extra $U(1)$ symmetry in order to get the fermion charges right.

If there is only one extra $U(1)$ symmetry (rank 5 low energy gauge group), its generator is uniquely specified for the Wilson loop mechanism.

Exercise. Show that if $SU(3)_R$ is broken to a $U(1)$ by a vev that is a member of an octet, the three possibilities for the $U(1)$ generator are $T_{3R} \pm \frac{1}{\sqrt{3}}Y_R$ and Y_R . Only $T_{3R} + \frac{1}{\sqrt{3}}Y_R$ enables one to construct the charge operator from it and T_{3L} , Y_L .

The $U(1)_{Y_L} \times U(1)_{T_{3R} + \frac{1}{\sqrt{3}}Y_R}$ group can be expressed as the product $U(1)_Y \times U(1)_{Q_\eta}$ where Y is the standard model hypercharge and Q_η is the generator coupled to a new vector boson Z_η orthogonal to the photon and standard model Z .

Exercise. Using the requirement that Q_η is orthogonal to the generators $Q = T_{3L} + \frac{1}{2}Y$ and $T_{3L} - x_w Q$ coupled to the photon and Z^0 , respectively, (where $Y = 2T_{3R} + \frac{2}{\sqrt{3}}(Y_L + Y_R)$) and that Q is a linear combination of the generators T_{3L} , Y_L and Q_η of the low-energy symmetry, show that

$$Q_\eta = -\sqrt{\frac{3}{5}} \left(\frac{1}{2}T_{3R} + \frac{1}{2\sqrt{3}}Y_R - \frac{2}{\sqrt{3}}Y_L \right)$$

with the weight vector

$$Q_\eta = -\frac{1}{4}\sqrt{\frac{3}{5}} \left(\frac{5}{\sqrt{3}} \mid 1, 1, 1, 1, 1 \right).$$

The Q_η values for the 27-plet fermions are given in Table 14.7. The couplings of the Z_η -boson to fermions are

$$g_{Z_\eta} Q_\eta = \sqrt{\frac{5}{3}} \frac{e}{\sqrt{1-x_w}} Q_\eta.$$

Here the factor $\sqrt{\frac{5}{3}}$ comes from the normalization at the GUT symmetry. The neutral current part of the covariant derivative in this model is thus

$$D_\mu = \partial_\mu + ieA_\mu Q + ig_Z Z_\mu Q_Z + i\sqrt{\frac{5}{3}} \sqrt{x_w} g_Z Z'_\mu Q_\eta,$$

where $g_Z = e[x_w(1-x_w)]^{-1/2}$ and $Q_Z = T_{3L} - x_w Q$.

Another possibility for the low-energy gauge group is the E_6 breakdown at the GUT scale to a rank 6 subgroup with three U(1) factors,

$$E_6 \rightarrow \text{SO}(10) \times \text{U}(1)_\psi, \quad \text{SO}(10) \rightarrow \text{SU}(5) \times \text{U}(1)_\chi, \quad \text{SU}(5) \rightarrow \text{SU}(3) \times \text{SU}(2) \times \text{U}(1).$$

Exercise. Show that the composition and weight vectors of the generators of $U(1)_\psi$ and $U(1)_\chi$ must be

$$Q_\psi = \frac{1}{\sqrt{2}} (Y_L - Y_R) = \frac{1}{\sqrt{2}} (-1 \mid 0, 0, 0, 0, 0),$$

$$Q_\chi = \frac{1}{\sqrt{10}} (\sqrt{3}Y_L + \sqrt{3}Y_R - 2T_{3R}) = \frac{1}{\sqrt{10}} (0 \mid -1, -1, -1, -1, -1).$$

These two generators are orthogonal to each other and to the stan-

standard model Z and γ generators. Thus there will be three massive neutral gauge bosons Z , Z_ψ , Z_χ and in general the mass eigenstates will be linear combinations of these. If only one of the extra two bosons is "light" ($\lesssim 1$ TeV), its generator $Z(\alpha)$ will be a linear combination

$$Q(\alpha) = Q_\psi \cos \alpha + Q_\chi \sin \alpha.$$

The rank 5 low-energy group with Z_η corresponds to $\tan \alpha = \sqrt{\frac{3}{5}}$.

14.8.4 Z' mass and mixing constraints.

The fields Z and Z' are in general not mass eigenstates. The real mass-squared matrix in the Z, Z' basis has the form

$$\mathcal{M}^2 = \begin{pmatrix} M_Z^2 & \delta M^2 \\ \delta M^2 & M_{Z'}^2 \end{pmatrix}.$$

This matrix can be diagonalized by an orthogonal rotation through an angle θ given by

$$\tan^2 \theta = \frac{M_Z^2 - M_{Z_1}^2}{M_{Z_2}^2 - M_Z^2},$$

where Z_1, Z_2 are the mass eigenstates. The effect of the mixing is to shift the mass of the Z downward from the standard model value and to shift the Z' mass upward

$$M_{Z_1}^2 \simeq M_Z^2 - \frac{(\delta M^2)^2 / M_Z^2}{M_{Z'}^2 / M_Z^2 - 1}, \quad M_{Z_2}^2 \simeq M_{Z'}^2 + \frac{(\delta M^2)^2 / M_Z^2}{M_{Z'}^2 / M_Z^2 - 1}.$$

The condition that M_{Z_1} be close to the standard Z mass M_Z , as required by measurements at the CERN $p\bar{p}$ collider, is illustrated in Fig. 14.16, where the region below the dash-dotted curve corresponds to $M_{Z_1} \geq 0.98 M_Z$. If future measurements of M_{Z_1} at the SLC and

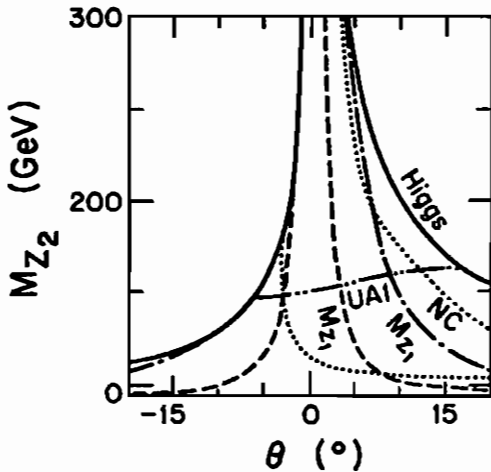


Fig. 14.16. Allowed regions in M_{Z_2}, θ parameter space from (a) $M_{Z_1} \geq 0.98 M_Z$, (b) $M_{Z_1} \geq 0.998 M_Z$, (c) low energy neutral current data, (d) CERN collider search for Z_2 , (e) **27** Higgs representation.

LEP colliders determine that $M_{Z_1} \geq 0.998 M_Z$ only the region below the dashed curves would be allowed.

The states Z and Z' in the neutral current Lagrangian are replaced by the mass eigenstates using

$$\begin{aligned} Z &= \cos \theta Z_1 - \sin \theta Z_2, \\ Z' &= \sin \theta Z_1 + \cos \theta Z_2. \end{aligned}$$

The effective neutral current Lagrangian at low energies is modified by this mixing and by the contributions of the extra Z . Assuming $x_w = 0.23$ a two parameter (M_{Z_2}, θ) fit to the low energy neutral current data allows the region within the dotted curves in Fig. 14.16.

Searches for an extra Z boson at the CERN $p\bar{p}$ collider also constrain the M_{Z_2}, θ parameters. If we assume that the Z_2 decays primarily into the known fermions, then only the region above the dash-dot-dot curve in Fig. 14.16 is allowed. This lower limit on M_{Z_2} is roughly 150 GeV.

Additional restrictions on the M_{Z_2}, θ parameter space follow from the **27** representation for the Higgs scalars that give the Z, Z' mass matrix. With the notation of Table 14.7 for the superpartners, the

possible neutral scalar vacuum expectation values and their T_{3L} quantum numbers are

vev	T_{3L}
$\langle \tilde{N}_E \rangle = v_1$	$\frac{1}{2}$
$\langle \tilde{\nu}_E \rangle = v_2$	$\frac{1}{2}$
$\langle \tilde{\nu}_e \rangle = v_3$	$\frac{1}{2}$
$\langle \tilde{N}^c \rangle = \chi_1$	0
$\langle \tilde{n} \rangle = \chi_2$	0

In the rank-5 breakdown of E_6 there is an ungauged $U(1)$ generator in the Cartan subalgebra and consequently there will be a Goldstone boson a_N corresponding to a global $U(1)$ invariance of the superpotential. This results in $K^+ \rightarrow \pi^+ a_N$ decay and present bounds on its absence require $\chi_1 < 40$ keV (hence $\chi_1 \approx 0$). With this constraint the quantum number assignments of case A can be excluded in the rank 5 breakdown by superpotential considerations. In the rank 5 model $\langle \tilde{\nu}_E \rangle$ and $\langle \tilde{\nu}_e \rangle$ contribute in exactly the same proportions to the mass matrix so we can set $v_3 = 0$ without loss of generality.

Exercise. From the kinetic term $|D_\mu \Phi|^2$ in the scalar Lagrangian show that the the Z, Z' mass matrix is

$$M^2 = g_Z^2 \begin{pmatrix} \frac{1}{2}(v_1^2 + v_2^2) & \frac{1}{6}\sqrt{x_w}(4v_1^2 - v_2^2) \\ \frac{1}{6}\sqrt{x_w}(4v_1^2 - v_2^2) & \frac{1}{18}x_w(16v_1^2 + v_2^2 + 25\chi_2^2) \end{pmatrix}.$$

The singlet vev χ_2 gives Z_2 its larger mass; the natural scale of χ_2 is $O(1 \text{ TeV})$. The region below the solid curves in Fig. 14.16 are allowed by this form of the mass matrix.

In the rank 5 low energy model, the renormalizable superpotential allows Dirac mass for neutrinos but not Majorana mass. Consequently the right-handed neutrino N^c has the same mass as the left-handed neutrino ν_e , which is very small or zero. There is no $Z \rightarrow N\bar{N}$ decay mode because N^c has no $SU(2)_L \times U(1)$ interactions.

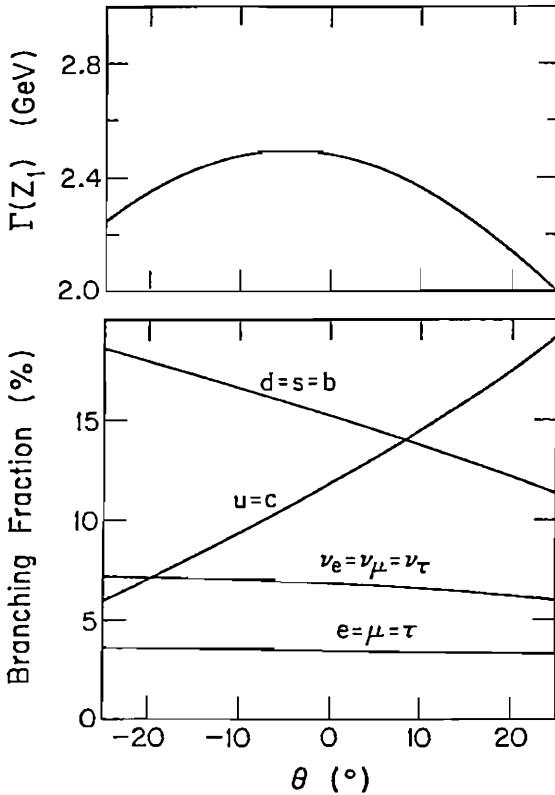


Fig. 14.17. Variations of Z_1 branching fractions and total width versus the Z, Z' mixing angle θ .

However, the presence of N^c in the early Universe would have affected primordial nucleosynthesis, which gives the bound $N_{\nu_L} < 4.6$ on the allowable number of equivalent left-handed neutrinos. The N^c density can be suppressed relative to ν_e if they decouple at higher temperature, which will be the case if the N^c interactions are weaker. This gives the mass bound

$$M_{Z_2} \gtrsim 0.4 \text{ TeV} .$$

The branching fractions and total width of the Z_1 are sensitive to the value of the mixing angle θ , as shown in Figure 14.17. These quantities will be measured to an accuracy of about 2-3% at SLC and LEP, and deviations from the standard model values along with a downward shift in mass would provide an indirect evidence for the existence of an extra Z boson.

The asymmetries in $e^+e^- \rightarrow \mu^+\mu^-$ are sensitive to deviations from the standard model. Figure 14.18 shows predictions for the asymmetries from Z, Z' mixing. Such measurements should determine the mixing angle θ to an accuracy of order 1° .

The Z_2 branching fractions and total width also depend on the mixing angle θ . Moreover the predictions depend on whether Z_2 decays to exotic fermions are kinematically suppressed. Representative results for the case that N_f generations of exotic fermions contribute fully are given in Table 14.8. The Z_2 may also decay to supersymmetric particles which would increase the total width and decrease the branching fractions to e^+e^- and $\mu^+\mu^-$. Other Z_2 decay channels of interest are W^+W^- and ZH .

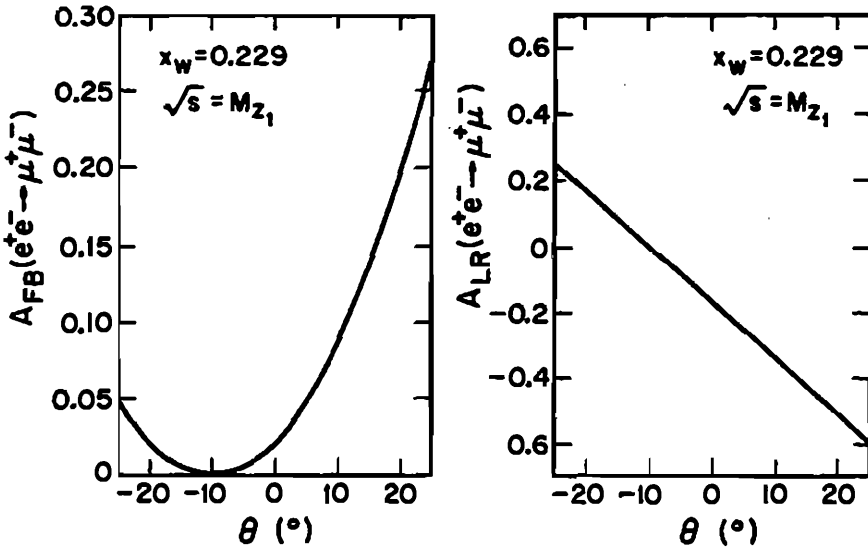


Fig. 14.18. Predictions for the integrated forward-backward asymmetry and the polarization asymmetry for $e^+e^- \rightarrow \mu^+\mu^-$ at $\sqrt{s} = M_{Z_1}$ versus the mixing angle θ .

Table 14.8. Partial and total widths in GeV for Z_1 and Z_2 decays for the rank 5 E_6 model with no mixing ($\theta = 0$), omitting QCD corrections and fermion mass corrections.

channel	Γ_{Z_1}	$\frac{M_{Z_1}}{M_{Z_2}} \Gamma_{Z_2}$
$\nu_e \bar{\nu}_e$.17	.005
$e \bar{e}$.09	.02
$u \bar{u}$.29	.11
$d \bar{d}$.38	.08
$h \bar{h}$.03	.23
$E \bar{E}$.09	.07
$\nu_E \bar{\nu}_E$.17	.005
$N_E \bar{N}_E$.17	.07
$N \bar{N}$	0	.11
$n \bar{n}$	0	.11

$$\Gamma_{Z_1} = 2.5 + 0.5 N_g$$

$$\Gamma_{Z_2} = (0.6 + 0.6 N_g) \frac{M_{Z_2}}{M_{Z_1}}$$

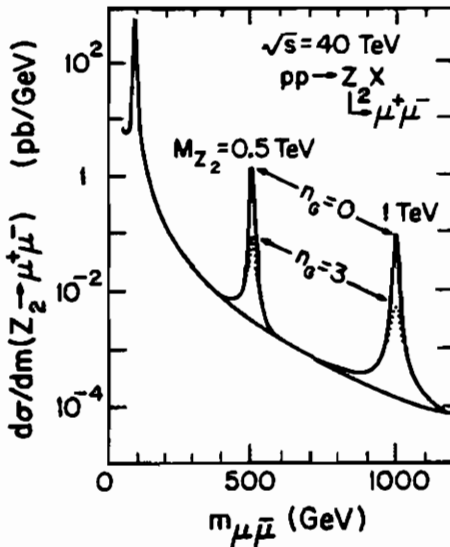


Fig. 14.19. Dilepton invariant mass distribution from Drell-Yan production of Z_2 in pp collisions at the SSC.

For a Z_2 of mass $M_{Z_2} = 1$ TeV produced in pp collisions at $\sqrt{s} = 40$ TeV the predicted properties are

$$\begin{array}{ll}
 N_g = 3 & N_g = 0 \\
 \Gamma_{Z_2} = 25 \text{ GeV} & 6 \text{ GeV} \\
 B(Z_2 \rightarrow e\bar{e}) = 1\% & 4\% \\
 \sigma B(Z_2 \rightarrow e\bar{e}) = .3 \text{ pb} & 1 \text{ pb}
 \end{array}$$

With an annual luminosity of 10^4 pb^{-1} at least 3000 $Z_2 \rightarrow e^+e^-$ events would be produced for a 1 TeV mass. Figure 14.19 shows the dilepton invariant mass spectrum for $M_{Z_2} = 0.5$ and 1 TeV. If a Z_2 were found in hadron collisions there would be a strong motivation to construct an $e^+e^- \rightarrow Z_2$ factory. The exotic fermions might well be produced in the Z_2 decays.

The isosinglet h can be strongly pair produced in hadron collisions via gluon-gluon fusion. The signatures depend on its quantum number assignments. In case A the decays proceed by mixing of h with the d quark,

$$A: \quad h \rightarrow \begin{cases} d^* \rightarrow uW \\ d^* \rightarrow dZ \\ h^* \rightarrow dZ \end{cases}$$

with W and Z branching fractions of about $2/3$ and $1/3$, respectively. The cross sections are sufficiently large that the Z 's can be observed in their leptonic decay modes. In cases B or C, which are necessary with the rank 5 model, h is expected to decay to an ordinary particle and a sparticle.

$$B: \quad h \rightarrow \begin{cases} d + \tilde{\nu} \\ u + \tilde{e} \\ \tilde{d} + \nu \\ \tilde{u} + e^- \end{cases}, \quad C: \quad h \rightarrow \begin{cases} \bar{u} + \tilde{d} \\ \bar{\tilde{u}} + \bar{d} \end{cases}.$$

These decay modes have distinctive signatures by which the h could be identified at a multi-TeV pp or $p\bar{p}$ collider.

Finally, in the context of no scale superstring models with a common gaugino mass as the source of supersymmetry breaking, the masses of the squarks and sleptons in the rank 5 model are given by

$$\begin{aligned}
 m_{\tilde{e}_R}^2 &= 0.14 m_{\tilde{g}}^2 + 0.22 r M_Z^2 + 0.2 M_{Z'}^2, \\
 m_{\tilde{e}_L}^2 &= 0.38 m_{\tilde{g}}^2 + 0.28 r M_Z^2 - 0.1 M_{Z'}^2, \\
 m_{\tilde{\nu}_L}^2 &= 0.38 m_{\tilde{g}}^2 - 0.5 r M_Z^2 - 0.1 M_{Z'}^2, \\
 m_{\tilde{q}}^2 &\approx 3.6 m_{\tilde{g}}^2,
 \end{aligned}$$

with r defined as in §14.6.2. Also, the lightest exotic h cannot be heavier than $2.1 M_{Z'}$ and the heaviest h must be lighter than $3.1 M_{Z'}$. In no scale models it may not be possible to allow a fourth generation.

Appendix A

Conventions and Feynman Rules

A.1 Four-Vectors and Scalar Product

Metric tensor:
$$g_{\mu\nu} = \begin{pmatrix} 1 & 0 & 0 & 0 \\ 0 & -1 & 0 & 0 \\ 0 & 0 & -1 & 0 \\ 0 & 0 & 0 & -1 \end{pmatrix}$$

Contravariant 4-vector: $a^\mu = (a_0, \vec{a})$

Covariant 4 vector: $a_\mu = g_{\mu\nu} a^\nu = (a_0, -\vec{a})$

Scalar products: $a^2 = a_\mu a^\mu = a_0^2 - |\vec{a}|^2$, $a \cdot b = a_\mu b^\mu = a_0 b_0 - \vec{a} \cdot \vec{b}$

Momentum 4-vector: $p^\mu = (E, p_x, p_y, p_z)$, where $E = (p^2 + m^2)^{\frac{1}{2}}$

Four-gradient: $\partial^\mu = \frac{\partial}{\partial x_\mu}$ or $\partial_\mu = \frac{\partial}{\partial x^\mu}$

Momentum operator in coordinate space:

$$p^\mu = i\partial^\mu = i \frac{\partial}{\partial x_\mu} = \left(i \frac{\partial}{\partial t}, -i\nabla \right),$$
$$p^\mu p_\mu = -\partial^\mu \partial_\mu = - \left[\frac{\partial^2}{\partial t^2}, -\nabla^2 \right] = -\square.$$

A.2 Gamma Matrices

Anticommutation relations:

$$\{\gamma^\mu, \gamma^\nu\} = \gamma^\mu \gamma^\nu + \gamma^\nu \gamma^\mu = 2g^{\mu\nu}, \quad \{\gamma^5, \gamma^\mu\} = 0$$

Definition of γ_5 : $\gamma_5 \equiv \gamma^5 \equiv i\gamma^0\gamma^1\gamma^2\gamma^3 = -i\gamma_0\gamma_1\gamma_2\gamma_3$

Hermitian conjugates:

$$\gamma^{0\dagger} = \gamma^0, \quad (\gamma^k)^\dagger = -\gamma^k, \quad (\gamma^5)^\dagger = \gamma^5, \quad (\gamma^\mu)^\dagger = \gamma^0\gamma^\mu\gamma^0$$

Squares: $(\gamma^0)^2 = -(\gamma^k)^2 = (\gamma_5)^2 = I, \quad k = 1, 2, 3$

Dirac representation:

$$\gamma^0 = \begin{pmatrix} I & 0 \\ 0 & -I \end{pmatrix}, \quad \vec{\gamma} = \begin{pmatrix} 0 & \vec{\sigma} \\ -\vec{\sigma} & 0 \end{pmatrix}, \quad \gamma_5 = \begin{pmatrix} 0 & I \\ I & 0 \end{pmatrix}$$

I is a 2×2 identity matrix; the 2×2 Pauli matrices are

$$\sigma_x = \begin{pmatrix} 0 & 1 \\ 1 & 0 \end{pmatrix}, \quad \sigma_y = \begin{pmatrix} 0 & -i \\ i & 0 \end{pmatrix}, \quad \sigma_z = \begin{pmatrix} 1 & 0 \\ 0 & -1 \end{pmatrix},$$

which satisfy $[\sigma_i, \sigma_j] = 2i\epsilon^{ijk}\sigma_k$, $\{\sigma_i, \sigma_j\} = 2\delta_{ij}$, $\text{Tr}(\sigma_i\sigma_j) = 2\delta_{ij}$, where ϵ^{ijk} is totally antisymmetric: $\epsilon^{ijk} = \epsilon_{ijk} = 1$ for an even permutation of 1, 2, 3.

A.3 Trace Theorems and Tensor Contractions

Some useful relations involving gamma matrices:

$$\begin{aligned} \gamma \cdot a &= \gamma_\mu a^\mu \equiv \not{a} = \gamma^0 a^0 - \vec{\gamma} \cdot \vec{a}, \\ \gamma_\mu \not{a} \gamma^\mu &= -2\not{a}, \quad \gamma_\mu \not{a} \not{b} \gamma^\mu = 4a \cdot b, \quad \gamma_\mu \not{a} \not{b} \not{c} \gamma^\mu = -2\not{a} \not{b} \not{c}, \\ \gamma_\mu \not{a} \not{b} \not{c} \not{d} \gamma^\mu &= 2(\not{a} \not{b} \not{c} \not{d} + \not{c} \not{b} \not{a} \not{d}), \end{aligned}$$

$\text{Tr}(ABC) = \text{Tr}(BCA) = \text{Tr}(CAB)$, A, B, C arbitrary matrices,

$\text{Tr} I = 4$, $\text{Tr} \gamma_\mu = 0$, $\text{Tr}(\text{odd \# of } \gamma \text{ matrices}) = 0$,

$\text{Tr}(\gamma_\mu \gamma_\nu) = 4g_{\mu\nu}$, $\text{Tr}(\gamma_\mu \gamma_\nu \gamma_\rho \gamma_\sigma) = 4[g_{\mu\nu}g_{\rho\sigma} - g_{\mu\rho}g_{\nu\sigma} + g_{\mu\sigma}g_{\nu\rho}]$;

$\text{Tr}(\not{a}_1 \not{a}_2 \dots \not{a}_{2n}) = \text{Tr}(\not{a}_{2n} \dots \not{a}_2 \not{a}_1) = a_1 \cdot a_2 \text{Tr}(\not{a}_3 \dots \not{a}_{2n})$

$- a_1 \cdot a_3 \text{Tr}(\not{a}_2 \not{a}_4 \dots \not{a}_{2n}) + \dots + a_1 \cdot a_{2n} \text{Tr}(\not{a}_2 \dots \not{a}_{2n-1})$,

$\text{Tr} \gamma_5 = 0$, $\text{Tr} \gamma_5 \gamma_\mu = 0$, $\text{Tr} \gamma_5 \gamma_\mu \gamma_\nu = 0$, $\text{Tr} \gamma_5 \gamma_\mu \gamma_\nu \gamma_\rho = 0$,

$\text{Tr} \gamma_5 \gamma_\mu \gamma_\nu \gamma_\rho \gamma_\sigma = -4i\epsilon_{\mu\nu\rho\sigma} = 4i\epsilon^{\mu\nu\rho\sigma}$,

$$\text{Tr } \gamma_5 \gamma_\mu \gamma_\nu \gamma_\rho \gamma_\sigma \gamma_\lambda \gamma_\tau = -4i [g_{\mu\nu} \epsilon_{\rho\sigma\lambda\tau} - g_{\mu\rho} \epsilon_{\nu\sigma\lambda\tau} + g_{\nu\rho} \epsilon_{\mu\sigma\lambda\tau} + g_{\sigma\lambda} \epsilon_{\mu\nu\rho\tau} - g_{\sigma\tau} \epsilon_{\mu\nu\rho\lambda} + g_{\lambda\tau} \epsilon_{\mu\nu\rho\sigma}],$$

$$\epsilon^{\mu\nu\rho\sigma} = -\epsilon_{\mu\nu\rho\sigma} = \begin{cases} 1, & \text{for even permutations of } 0, 1, 2, 3; \\ -1, & \text{for odd permutations;} \\ 0, & \text{otherwise;} \end{cases}$$

$$\epsilon^{\mu\nu\rho\sigma} \epsilon_{\mu\nu\rho\sigma} = -24, \quad \epsilon^{\mu\nu\rho\sigma} \epsilon_{\mu\nu\rho\sigma'} = 6g^{\sigma\sigma'},$$

$$\epsilon^{\mu\nu\rho\sigma} \epsilon_{\mu\nu}{}^{\rho'\sigma'} = -2(g^{\rho\rho'} g^{\sigma\sigma'} - g^{\rho\sigma'} g^{\rho'\sigma}),$$

$$\epsilon^{\mu\nu\rho\sigma} \epsilon_{\mu}{}^{\nu'\rho'\sigma'} = -\det(g^{\alpha\alpha'}), \quad \alpha = \nu, \rho, \sigma, \quad \alpha' = \nu', \rho', \sigma',$$

$$\epsilon^{\mu\nu\rho\sigma} \epsilon_{\mu'\nu'\rho'\sigma'} = -\det(g^{\alpha\alpha'}), \quad \alpha = \mu, \nu, \rho, \sigma, \quad \alpha' = \mu', \nu', \rho', \sigma'.$$

Summation of polarization states for real vector bosons:

$$\text{massless, } \sum_{\sigma} \epsilon_{\mu}^*(p, \sigma) \epsilon_{\nu}(p, \sigma) = -g_{\mu\nu}$$

$$\text{massive, } \sum_{\sigma} \epsilon_{\mu}^*(p, \sigma) \epsilon_{\nu}(p, \sigma) = -g_{\mu\nu} + \frac{p_{\mu} p_{\nu}}{M_V^2}$$

A.4 Dirac Spinors

Positive energy spinor $u(p, s)$: $(\not{p} - m)u(p, s) = 0$, $\bar{u}(p, s)(\not{p} - m) = 0$,
with adjoint spinor: $\bar{u}(p, s) = u^{\dagger}(p, s)\gamma^0$.

Negative energy spinor $v(p, s)$: $(\not{p} + m)v(p, s) = 0$, $\bar{v}(p, s)(\not{p} + m) = 0$,
with adjoint spinor: $\bar{v}(p, s) = v^{\dagger}(p, s)\gamma^0$.

Helicity basis spinors $u_{\lambda}(p)$, with $\lambda = \pm 1$ are eigenstates of the helicity operator.

$$\begin{aligned} \text{Normalization: } \quad \bar{u}_{\lambda}(p)u_{\sigma}(p) &= 2m\delta_{\lambda\sigma} \\ \bar{v}_{\lambda}(p)v_{\sigma}(p) &= -2m\delta_{\lambda\sigma} \\ \bar{u}_{\lambda}(p)v_{\sigma}(p) &= \bar{v}_{\lambda}(p)u_{\sigma}(p) = 0 \end{aligned}$$

$$\begin{aligned} \text{Projection operators: } \quad \sum_{\lambda} u_{\lambda}(p)\bar{u}_{\lambda}(p) &= \not{p} + m \\ \sum_{\lambda} v_{\lambda}(p)\bar{v}_{\lambda}(p) &= \not{p} - m \end{aligned}$$

Positive energy spinor with momentum $|\vec{p}|$ along the positive z -axis and with helicity $\lambda/2$ is

$$u_\lambda(p) = \sqrt{E+m} \begin{pmatrix} \chi_\lambda \\ \frac{2\lambda|\vec{p}|}{E+m} \chi_\lambda \end{pmatrix}, \quad \chi_+ = \begin{pmatrix} 1 \\ 0 \end{pmatrix}, \quad \chi_- = \begin{pmatrix} 0 \\ 1 \end{pmatrix}.$$

Antiparticle spinor: $v_\lambda(p) = -\lambda\gamma^5 u_{-\lambda}(p)$

Charge conjugation operator: $C = i\gamma^2\gamma^0 = -C^{-1} = -C^\dagger = -C^T$

Charge conjugate state: $\psi^c = C(\bar{\psi})^T$

$$C\bar{u}^T(p, s) = e^{i\theta(p, s)} v(p, s), \quad C\bar{v}^T(p, s) = e^{i\theta(p, s)} u(p, s)$$

A.5 Hermitian Conjugates of Matrix Elements

Generally: $[\bar{u}(p_1)\Lambda u(p_2)]^\dagger = \bar{u}(p_2)\bar{\Lambda} u(p_1), \quad \bar{\Lambda} = \gamma^0\Lambda^\dagger\gamma^0.$

Particular cases:

$$\begin{aligned} \bar{\mathbf{1}} &= \gamma^0\mathbf{1}^\dagger\gamma^0 = \mathbf{1} \\ \bar{\gamma}^\mu &= \gamma^0\gamma^\mu{}^\dagger\gamma^0 = \gamma^\mu, \\ \overline{\not{a}_1\not{a}_2\dots\not{a}_\mu} &= \not{a}_\mu\not{a}_{\mu-1}\dots\not{a}_1, \\ \bar{\gamma}^5 &= \gamma^0(\gamma^5)^\dagger\gamma^0 = -\gamma^5, \quad \overline{\gamma^\mu\gamma^5} = \gamma^0(\gamma^5)^\dagger(\gamma^\mu)^\dagger\gamma^0 = \gamma^\mu\gamma^5. \end{aligned}$$

A.6 Fierz-Michael Reordering Transformation

$$\bar{u}_3\Lambda_i u_2 \bar{u}_1\Lambda_j u_4 = \sum_{j=1}^5 \lambda_{ij} \bar{u}_1\Lambda_j u_2 \bar{u}_3\Lambda_i u_4,$$

where $\Lambda_i = (1, \gamma_\mu, \sigma_{\mu\nu}/\sqrt{2}, \gamma_\mu\gamma_5, \gamma_5)$ with $\sigma_{\mu\nu} = \frac{i}{2}[\gamma_\mu, \gamma_\nu]$,

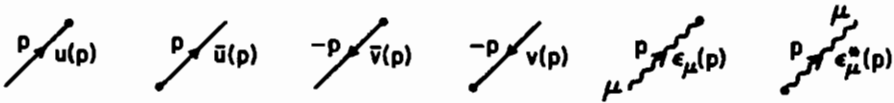
$$\lambda_{ij} = \frac{1}{4} \begin{pmatrix} 1 & 1 & 1 & -1 & 1 \\ 4 & -2 & 0 & -2 & -4 \\ 6 & 0 & -2 & 0 & 6 \\ -4 & -2 & 0 & -2 & 4 \\ 1 & -1 & 1 & 1 & 1 \end{pmatrix}$$

Under a Fierz transformation, a $V - A$ interaction remains $V - A$:

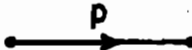
$$[\gamma^\alpha(1 - \gamma_5)]_{\lambda\rho} [\gamma_\alpha(1 - \gamma_5)]_{\mu\sigma} = -[\gamma^\alpha(1 - \gamma_5)]_{\mu\rho} [\gamma_\alpha(1 - \gamma_5)]_{\lambda\sigma}.$$

A.7 Feynman Rules for Tree Graphs

External lines

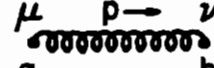


Propagators

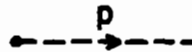
Fermion  $\frac{i}{\not{p} - m + i\epsilon}$

Photon  $\frac{-i[g_{\mu\nu} + (\xi - 1)p_\mu p_\nu / p^2]}{p^2 + i\epsilon}$

Massive Boson  $\frac{-i[g_{\mu\nu} + (\xi - 1)p_\mu p_\nu / (p^2 - \xi M^2)]}{p^2 - M^2 + i\epsilon}$

Gluon  $\frac{-i\delta_{ab}[g_{\mu\nu} + (\xi - 1)p_\mu p_\nu / p^2]}{p^2 + i\epsilon}$

ξ fixes the gauge: $\xi = \begin{cases} 1, & \text{Feynman gauge} \\ 0, & \text{Landau gauge} \\ \infty, & \text{Unitary gauge for massive bosons} \end{cases}$

Scalar  $\frac{i}{p^2 - m^2 + i\epsilon}$

Vertices

In the following, the $T^a = \frac{1}{2}\lambda_a$ are color matrices (the generators of the SU(3) group):

$$[T^a, T^b] = if^{abc} T^c, \quad a, b, c = 1, 2, \dots, 8.$$

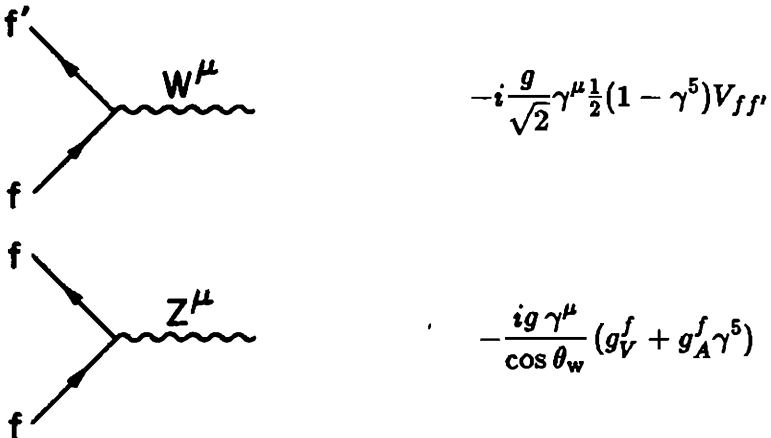
The f^{abc} are the structure constants of SU(3). They are antisymmetric under the interchange of two indices:

$$f_{123} = 1, \quad f_{147} = f_{246} = f_{257} = f_{345} = f_{516} = f_{637} = \frac{1}{2}, \quad f_{458} = f_{678} = \frac{\sqrt{3}}{2}.$$

Photon-Fermion



Weak Boson-Fermion

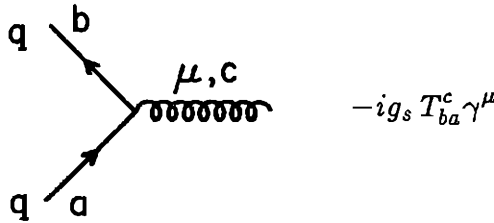


$$g^2 = \frac{8M_W^2 G_F}{\sqrt{2}}, \quad x_w = \sin^2 \theta_w = 0.23, \quad g \sin \theta_w = e,$$

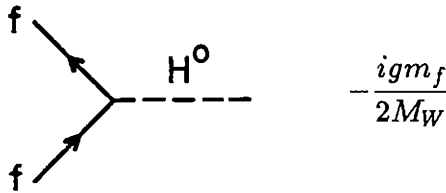
$$g_V^f = \frac{1}{2}(T_3^f)_L - \sin^2 \theta_w Q^f, \quad g_A^f = -\frac{1}{2}(T_3^f)_L,$$

f	Q^f	$(T_3^f)_L$	$(T_3^f)_R$
u, c, t	$\frac{2}{3}$	$\frac{1}{2}$	0
d, s, b	$-\frac{1}{3}$	$-\frac{1}{2}$	0
ν_e, ν_μ, ν_τ	0	$\frac{1}{2}$	-
e^-, μ^-, τ^-	-1	$-\frac{1}{2}$	0

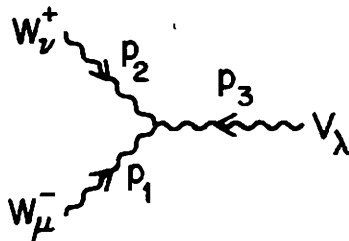
Gluon-Quark



Higgs-Fermion

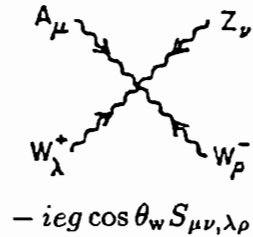
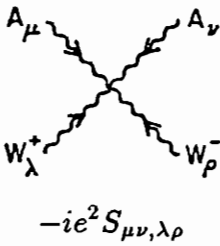
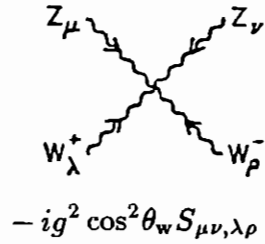
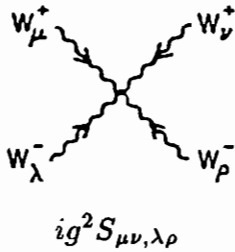


Gauge Boson Vertices



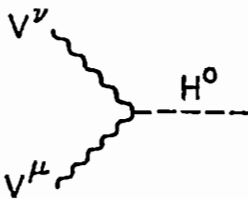
$$-ig_V [(p_1 - p_2)_\lambda g_{\mu\nu} + (p_2 - p_3)_\mu g_{\nu\lambda} + (p_3 - p_1)_\nu g_{\lambda\mu}]$$

$$g_V = \begin{cases} g \sin \theta_w, & \text{for } V = A \\ g \cos \theta_w, & \text{for } V = Z \end{cases}$$



$$S_{\mu\nu,\lambda\rho} = 2g_{\mu\nu}g_{\lambda\rho} - g_{\mu\lambda}g_{\nu\rho} - g_{\mu\rho}g_{\nu\lambda}$$

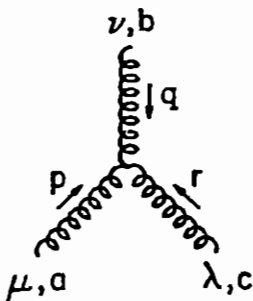
Gauge Boson-Higgs



$$iM_W g_{VH} g^{\mu\nu}$$

$$g_{VH} = \begin{cases} g & \text{for } V = W \\ g/(1 - x_w) & \text{for } V = Z \end{cases}$$

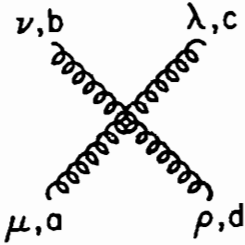
Gluon Triple Vertex



$$ig_s f^{abc} [(p-q)_\lambda g_{\mu\nu} + (q-r)_\mu g_{\nu\lambda} + (r-p)_\nu g_{\lambda\mu}],$$

$$\text{where } p + q + r = 0$$

Gluon Quartic Vertex



$$\begin{aligned}
 & -ig^2 \left[f^{abe} f^{cde} (g_{\lambda\nu} g_{\mu\rho} - g_{\lambda\rho} g_{\mu\nu}) \right. \\
 & \quad + f^{ace} f^{bde} (g_{\lambda\mu} g_{\nu\rho} - g_{\lambda\rho} g_{\mu\nu}) \\
 & \quad \left. + f^{ade} f^{bce} (g_{\lambda\mu} g_{\nu\rho} - g_{\lambda\nu} g_{\mu\rho}) \right]
 \end{aligned}$$

Color sums in $\sum |\mathcal{M}|^2$ can be evaluated by using these identities:

$$\begin{aligned}
 [T^a, T^b] &= i f^{abc} T^c, & \{T^a, T^b\} &= \frac{1}{3} \delta^{ab} + d^{abc} T^c, \\
 T^a T^b &= \frac{1}{2} (\frac{1}{3} \delta^{ab} + d^{abc} T^c + i f^{abc} T^c), & \text{Tr } T^a &= 0, & \text{Tr } T^a T^b &= \frac{1}{2} \delta^{ab}, \\
 \text{Tr } T^a T^b T^c &= \frac{1}{4} [d^{abc} + i f^{abc}], & \text{Tr } T^a T^b T^a T^c &= -\frac{1}{12} \delta^{bc}, \\
 T_{ij}^a T_{kl}^a &= \frac{1}{2} \delta_{il} \delta_{jk} - \frac{1}{6} \delta_{ij} \delta_{kl}, & f^{abb} &= 0, & f^{acd} f^{bcd} &= 3 \delta^{ab}, \\
 f^{abe} f^{cde} f^{acg} f^{bdg} &= 36, & f^{ace} f^{acg} f^{bde} f^{bdg} &= 72,
 \end{aligned}$$

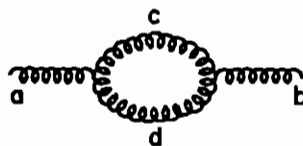
The f^{abc} are anti-symmetric under interchange of 2 indices; the d^{abc} are symmetric. The non-vanishing d_{abc} are

$$\begin{aligned}
 d_{118} &= d_{228} = d_{338} = -d_{888} = \frac{1}{\sqrt{3}}, \\
 d_{146} &= d_{157} = d_{256} = d_{344} = d_{355} = -d_{247} = -d_{366} = -d_{377} = \frac{1}{2}, \\
 d_{448} &= d_{558} = d_{668} = d_{778} = -\frac{1}{2\sqrt{3}}.
 \end{aligned}$$

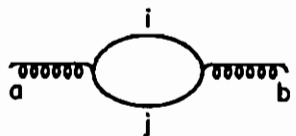
A conventional representation for the λ_α is

$$\begin{aligned}
 \lambda_1 &= \begin{bmatrix} 0 & 1 & 0 \\ 1 & 0 & 0 \\ 0 & 0 & 0 \end{bmatrix}, & \lambda_2 &= \begin{bmatrix} 0 & -i & 0 \\ i & 0 & 0 \\ 0 & 0 & 0 \end{bmatrix}, & \lambda_3 &= \begin{bmatrix} 1 & 0 & 0 \\ 0 & -1 & 0 \\ 0 & 0 & 0 \end{bmatrix}, \\
 \lambda_4 &= \begin{bmatrix} 0 & 0 & 1 \\ 0 & 0 & 0 \\ 1 & 0 & 0 \end{bmatrix}, & \lambda_5 &= \begin{bmatrix} 0 & 0 & -i \\ 0 & 0 & 0 \\ i & 0 & 0 \end{bmatrix}, & \lambda_6 &= \begin{bmatrix} 0 & 0 & 0 \\ 0 & 0 & 1 \\ 0 & 1 & 0 \end{bmatrix}, \\
 \lambda_7 &= \begin{bmatrix} 0 & 0 & 0 \\ 0 & 0 & -i \\ 0 & i & 0 \end{bmatrix}, & \lambda_8 &= \frac{1}{\sqrt{3}} \begin{bmatrix} 1 & 0 & 0 \\ 0 & 1 & 0 \\ 0 & 0 & -2 \end{bmatrix}.
 \end{aligned}$$

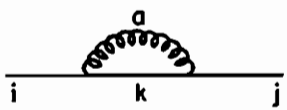
Color factors related to the following loops are



$$= \sum_{c,d=1}^8 f_{acd} f_{bcd} \equiv C_2(G) \delta_{ab},$$



$$= \sum_{i,j=1}^3 (T_a)_{ij} (T_b)_{ji} = \text{Tr}(T_a T_b) \equiv T(R) \delta_{ab},$$



$$= \sum_{a=1}^8 \sum_{k=1}^3 (T_a)_{ik} (T_a)_{kj}$$

$$= \sum_{a=1}^8 (T_a T_a)_{ij} \equiv C_2(R) \delta_{ij},$$

where R denotes the fundamental representation and an additional sum over flavors in the fermion loop is understood. For $G = \text{SU}(3)_c$ and for a flavor $\text{SU}(N_f)$ group, these color factors are

$$C_2(G) = 3, \quad C_2(R) = \frac{4}{3}, \quad T(R) = \frac{1}{2} N_f.$$

Additional Feynman rules for ghost contributions (that cancel unphysical degrees of freedom in loop diagrams), other Higgs boson interactions, Majorana particle interactions, and supersymmetric particle interactions can be found in other textbooks and literature.

A.8 Phase Space, Cross Sections, Decays

Define: $\lambda(x, y, z) = x^2 + y^2 + z^2 - 2xy - 2xz - 2yz.$

The cross section for $a + b \rightarrow n$ -final state particles can be expressed as

$$d\sigma = \frac{1}{2\lambda^{\frac{1}{2}}(s, m_a^2, m_b^2)(2\pi)^{3n-4}} \sum |\mathcal{M}|^2 \delta^4\left(p_a + p_b - \sum_{i=1}^n p_i\right) \prod_{i=1}^n \frac{d^3 p_i}{(2E)_i},$$

$s = (p_a + p_b)^2$ and m_a and m_b are the masses of the initial particles. The decay of particle a into n particles can be expressed as

$$d\Gamma = \frac{1}{2E_a(2\pi)^{3n-4}} \sum |\mathcal{M}|^2 \delta^4\left(p_a - \sum_{i=1}^n p_i\right) \prod_{i=1}^n \frac{d^3 p_i}{(2E)_i}.$$

To evaluate these expressions, one must first remove the constrained degrees of freedom by integrating over the delta functions. For example, for a 2-body final state,

$$\int \delta^4(a - b - c) \frac{d^3 b}{2b_0} \frac{d^3 c}{2c_0} = \frac{\lambda^{\frac{1}{2}}(a^2, b^2, c^2) d\Omega^*}{8a^2},$$

where $d\Omega^*$ is the c.m. solid angle.

Occasionally the matrix element is such that one can make use of the so-called vector and tensor integrals

$$\int \delta^4(M - p - b) b_\mu \frac{d^3 p}{2p^0} \frac{d^3 b}{2b^0} = \frac{\pi}{4M^4} \lambda^{\frac{1}{2}}(M^2, b^2, p^2) (M^2 + b^2 - p^2) M_\mu$$

and

$$\begin{aligned} \int \delta^4(M - p - b) p_\mu b_\nu \frac{d^3 p}{2p^0} \frac{d^3 b}{2b^0} &= \frac{\pi \lambda^{\frac{3}{2}}(M^2, b^2, p^2)}{24M^4} g_{\mu\nu} \\ &+ \frac{\pi \lambda^{\frac{1}{2}}(M^2, b^2, p^2)}{12M^6} [M^2(M^2 + p^2 + b^2) - 2(p^2 - b^2)] M_\mu M_\nu. \end{aligned}$$

Multi-particle phase space can be reduced to products of 2 particle phase space. For example, $a \rightarrow b + i \rightarrow b + c + d$ would yield

$$\delta^4(a - b - c - d) \frac{d^3 b}{2b_0} \frac{d^3 c}{2c_0} \frac{d^3 d}{2d_0} = \delta^4(a - i - b) \frac{d^3 i}{2i_0} \frac{d^3 b}{2b_0} \delta^4(i - c - d) \frac{d^3 c}{2c_0} \frac{d^3 d}{2d_0} d(i^2).$$

Subprocess differential cross sections can be expressed as

$$\frac{d\hat{\sigma}}{dt} = \frac{1}{16\pi \lambda(\hat{s}, m_a^2, m_b^2)} \sum |\mathcal{M}|^2,$$

where m_a and m_b are the initial particle masses.

A.9 Heavy Quarkonium Matrix Elements

Heavy quarkonium decay can be related to free $Q\bar{Q}$ annihilation. We give the relations for S-wave quarkonia in the usual approximation of zero binding energy ($2m_Q = M$). We denote the amplitude \mathcal{A} for free $Q\bar{Q}$ annihilation to a given final state by

$$\mathcal{A} = \bar{v}(\bar{Q}, \bar{s}) O_F u(Q, s) = \text{Tr}(O_F u \bar{v})$$

with $Q - \bar{Q} = (0, 2p)$ and $Q + \bar{Q} = (2m_Q, 0)$. The amplitudes for spins s, \bar{s} can be combined to represent 1S_0 and 3S_1 states of quarkonia. From the rest-frame spinors the appropriate combinations are

$$(u\bar{v})_{^1S_0} = \frac{1}{\sqrt{2}} \gamma_5 (\not{Q} - m_Q), \quad (u\bar{v})_{^3S_1} = \frac{1}{\sqrt{2}} \not{\epsilon} (\not{Q} - m_Q),$$

where ϵ_μ is the polarization of a 3S_1 state ($\epsilon \cdot Q = 0$). The quarkonium amplitudes \mathcal{M} are related to the free-quark Feynman amplitude \mathcal{A} by

$$\left[(2\pi)^{-3/2} (2M)^{-1/2} \right] \mathcal{M} = \left[(2\pi)^{-3/2} (2m_Q)^{-1/2} \right]^2 \int d^3p \phi(p) \mathcal{A}(p)$$

where the factors in square brackets give the correct normalization for the Feynman rules; $\phi(p)$ is the momentum-space wave function normalized by $\int d^3p |\phi(p)|^2 = 1$. Neglecting the momentum-dependence of $\mathcal{A}(p)$, the integral gives $\int d^3p \phi(p) = (2\pi)^{3/2} \Phi(0)$ where $\Phi(0)$ is the coordinate-space wave function at the origin. Thus the quarkonium decay amplitudes become

$$\mathcal{M}(^1S_0) = (2m_Q)^{-1/2} \Phi_S(0) \text{Tr} [O_F \gamma_5 (\not{Q} - m_Q)],$$

$$\mathcal{M}(^3S_1) = (2m_Q)^{-1/2} \Phi_S(0) \text{Tr} [O_F \not{\epsilon} (\not{Q} - m_Q)].$$

The S-wave bound state of two scalar constituents has amplitude

$$\mathcal{M}(S) = (m_Q)^{-1} \Phi_S(0) O_F.$$

Color factors remain to be included. Onium is a color singlet, with $Q\bar{Q}$ wave function $(r\bar{r} + g\bar{g} + b\bar{b})/\sqrt{3}$. Hence for example, onium \rightarrow color singlet amplitudes must be multiplied by $3/\sqrt{3} = \sqrt{3}$ on the right-hand sides above.

The same techniques can be applied to onium production.

Appendix B

Phase Space

B.1 Two-Body Phase Space

Consider a system X of two particles a and b , with four-momenta a_α and b_α . Since $a^2 = a^\alpha a_\alpha = m_a^2$, we can also use symbols a and b to denote the respective masses. Similarly, $X_\alpha = a_\alpha + b_\alpha$ and X denotes the momentum and invariant mass of the pair. The energies a_0 and b_0 of the individual particles in their c.m. frame are

$$a_0 = \frac{X^2 + a^2 - b^2}{2X}, \quad b_0 = \frac{X^2 + b^2 - a^2}{2X}.$$

The three-momenta \vec{a} and \vec{b} in the c.m. frame are oppositely directed but have the same magnitude p

$$p = \frac{1}{2} X \lambda^{\frac{1}{2}}(1, a^2/X^2, b^2/X^2),$$

where

$$\lambda(x, y, z) = x^2 + y^2 + z^2 - 2xy - 2yz - 2zx.$$

For particles a and b in an initial state before collision, the flux factor which appears in the denominator of the cross section formula can be expressed as an invariant quantity

$$2a_0 2b_0 |\vec{v}_a - \vec{v}_b| = 2X^2 \lambda^{\frac{1}{2}}(1, a^2/X^2, b^2/X^2).$$

In scattering processes X^2 is usually denoted by s .

For particles a and b in a final state, we define the invariant differential phase space $d_2(PS)$ as

$$d_2(PS) = \delta^4(X_\alpha - a_\alpha - b_\alpha) (d^3\vec{a}/2a_0) (d^3\vec{b}/2b_0) .$$

This reduces to a two-dimensional solid angle in the c.m. frame:

$$d_2(PS) = \pi (p/X) (d\Omega/4\pi) = \frac{1}{2}\pi\lambda^{\frac{1}{2}} (1, a^2/X^2, b^2/X^2) (d\Omega/4\pi) .$$

The following integrals are useful:

$$\begin{aligned} \int d_2(PS) a^\alpha b^\beta &= (\pi X^2/24) \lambda^{\frac{1}{2}} (1, a^2/X^2, b^2/X^2) \left\{ g^{\alpha\beta} \lambda (1, a^2/X^2, b^2/X^2) \right. \\ &\quad \left. + 2X^\alpha X^\beta / X^2 [1 + a^2/X^2 + b^2/X^2 - 2(a^2 - b^2)^2/X^4] \right\}, \\ \int d_2(PS) a^\alpha &= \frac{1}{4}\pi\lambda^{\frac{1}{2}} (1, a^2/X^2, b^2/X^2) (1 + a^2/X^2 - b^2/X^2) X^\alpha . \end{aligned}$$

For a decay $X \rightarrow ab$, the rest-frame decay width involves a phase space integration of the transition probability $|\mathcal{M}|^2$,

$$d\Gamma(X \rightarrow ab) = (1/2X) (1/4\pi^2) |\mathcal{M}|^2 d_2(PS) .$$

We illustrate fermion pair ab production via a vector coupling V and an axial vector coupling A to a spin-1 current. We assume a is a particle and b is an antiparticle. The transition amplitude is

$$\mathcal{M} = n_\alpha \bar{u}_a \gamma^\alpha (V + A\gamma_5) v_b .$$

The vector n_α depends on the nature of the parent X ; it could be a polarization or momentum vector. We sum $|\mathcal{M}|^2$ over all final state

helicities

$$\sum_{\text{spins}} |\mathcal{M}|^2 = n_\alpha n_\beta I^{\alpha\beta}$$

to obtain

$$\begin{aligned} n_\alpha n_\beta I^{\alpha\beta} &= n_\alpha n_\beta \text{Tr} \left[\gamma^\alpha (V + A\gamma_5) (\not{b} - b) \gamma^\beta (V + A\gamma_5) (\not{a} + a) \right] \\ &= n_\alpha n_\beta \left[4(V^2 + A^2)(a^\alpha b^\beta + b^\alpha a^\beta - g^{\alpha\beta} a \cdot b) - 4(V^2 - A^2) abg^{\alpha\beta} \right]. \end{aligned}$$

The integration over the two-body phase space

$$n_\alpha n_\beta T^{\alpha\beta} = \int n_\alpha n_\beta I^{\alpha\beta} d_2(PS)$$

gives

$$\begin{aligned} n_\alpha n_\beta T^{\alpha\beta} &= n_\alpha n_\beta \frac{1}{3} \pi X^2 \lambda^{\frac{1}{2}} (1, a^2/X^2, b^2/X^2) \left[(V^2 + A^2) \right. \\ &\quad \cdot \left\{ 2(-g^{\alpha\beta} + X^\alpha X^\beta/X^2) \left[1 + a^2/X^2 + b^2/X^2 - \frac{1}{2}(a^2 - b^2)^2/X^4 \right] \right. \\ &\quad \left. \left. - 3(a^2 - b^2)^2 X^\alpha X^\beta/X^6 \right\} + 3[V^2(a - b)^2 + A^2(a + b)^2] g^{\alpha\beta}/X^2 \right], \end{aligned}$$

and the decay width is

$$\Gamma(X \rightarrow ab) = n_\alpha n_\beta T^{\alpha\beta} / (8\pi^2 X).$$

This general formalism can be applied to special cases:

i) Pion and kaon decay ($m \rightarrow \ell\bar{\nu}$, $m = \pi, K$).

X_α is now the meson momentum m_α , and neutrino mass is neglected. The vector n_α is the meson momentum $n_\alpha = m_\alpha$, due to the scalar nature of pion and kaon. Also, we have $V^2 = A^2 = \frac{1}{2} G_F^2 f^2 V^2$ with $V = \cos \theta_c$ (or $\sin \theta_c$) for pion (or kaon). The term proportional to the projection $(-g^{\alpha\beta} + X^\alpha X^\beta/X^2)$ does not contribute. We obtain

$$\Gamma(m \rightarrow \ell\bar{\nu}) = G_F^2 f^2 V^2 m_\ell^2 (1 - \ell^2/m^2)^2 / (8\pi).$$

ii) Charged weak boson W -decay ($W \rightarrow f\bar{f}'$; $f\bar{f}' = \ell\bar{\nu}, \bar{u}d$, etc.).

In the standard model, the couplings are $A^2 = V^2 = G_F W^2 |V|^2 / \sqrt{2}$, with V the mixing matrix element between families. The vector n is the polarization of the W boson with the properties $n^2 = -1$ and $n_\alpha X^\alpha = 0$. We obtain

$$\Gamma(W \rightarrow f\bar{f}') = (G_F W^3 |V|^2 / 6\sqrt{2} \pi) \lambda^{\frac{1}{2}} (1, f^2/W^2, f'^2/W^2) \cdot \left[1 - \frac{1}{2} f^2/W^2 - \frac{1}{2} f'^2/W^2 - \frac{1}{2} (f^2 - f'^2)^2 / W^4 \right].$$

iii) Neutral weak boson Z -decay ($Z \rightarrow f\bar{f}$, $f = \ell, \nu, u, d$, etc.).

The calculation is similar to that of W -decay. The standard model couplings are

$$V^2 = \left(G_F Z^2 / (2\sqrt{2}) \right) (1 - 4|e_f| \sin^2 \theta_w)^2, \\ A^2 = G_F Z^2 / (2\sqrt{2}).$$

Using the previous equations, we obtain

$$\Gamma(Z \rightarrow f\bar{f}') = \left(G_F Z^3 / 24\sqrt{2} \pi \right) (1 - 4f^2/Z^2)^{\frac{1}{2}} \cdot \left[1 - 4f^2/Z^2 + (1 - 4|e_f| \sin^2 \theta_w)^2 (1 + 2f^2/Z^2) \right].$$

If the produced fermions are quarks in W and Z decays, a factor of 3 should be included in the $\Gamma(W \rightarrow f\bar{f}')$ and $\Gamma(Z \rightarrow f\bar{f}')$ equations for summing over all colored channels.

B.2 Three-Body Phase Space

We study a system Y of three particles a, b and c in the final state. The three-body phase space is

$$d_3(PS Y \rightarrow abc) = \delta^4(Y_\alpha - a_\alpha - b_\alpha - c_\alpha) \frac{d^3\vec{a}}{2a_0} \frac{d^3\vec{b}}{2b_0} \frac{d^3\vec{c}}{2c_0}.$$

It can be reduced by pairing two particles together, say a and b , as a subsystem X . The choice of pairing depends on convenience and the

physics. The previous equation becomes

$$d_3(PS Y \rightarrow abc) = (d^3\vec{c}/2c_0) d_2(PS X \rightarrow ab, X_\alpha = Y_\alpha - c_\alpha) .$$

The momentum \vec{c} in the c.m. frame of abc reaches its maximum magnitude when the recoiling pair ab have the lowest invariant mass $a+b$, so

$$|\vec{c}| \leq \frac{1}{2}Y\lambda^{\frac{1}{2}}(1, (a+b)^2/Y^2, c^2/Y^2) .$$

We can write this as a chain of two-body phase spaces,

$$d_3(PS Y \rightarrow abc) = d_2(PS Y \rightarrow Xc)dX^2 d_2(PS X \rightarrow ab) .$$

The chain is allowed for the following range of X

$$a + b \leq X \leq Y - c .$$

For the decay process $Y \rightarrow abc$, the decay width is

$$d\Gamma(Y \rightarrow abc) = \frac{1}{2Y} \frac{1}{(2\pi)^5} |\mathcal{M}|^2 \frac{d^3\vec{c}}{2c_0} d_2(PS X \rightarrow ab) .$$

We give examples of these reduction methods below.

B.2.1 $\pi^- \rightarrow e\bar{\nu}\pi^0$.

As the $e\bar{\nu}$ pair is coupled to a spin-1 current, the amplitude is given by the identification $a = e$, $b = \bar{\nu}$, $c = \pi^0$ and $Y = \pi^-$. From the CVC hypothesis, the vector n_α is the sum of π^0 and π^- momenta.

We have

$$n_\alpha = (p_{\pi^0} + p_{\pi^-})_\alpha , \quad A^2 = V^2 = G_F^2 \cos^2 \theta_c .$$

We then have

$$d\Gamma(Y \rightarrow abc) = \frac{1}{2Y} \frac{1}{(2\pi)^5} n_\alpha n_\beta T^{\alpha\beta} \frac{d^3\vec{c}}{2c_0} ,$$

with

$$T^{\alpha\beta} = (2/3)\pi X^2 (V^2 + A^2) \left(-g^{\alpha\beta} + X^\alpha X^\beta / X^2 \right) .$$

Here we have assumed zero masses for particles a and b , and summed

the helicities in the final state. Then

$$\begin{aligned}
 E_{\pi^0} d\Gamma/d^3\vec{p}_{\pi^0} &= (X^2/192\pi^4 m_{\pi^-})(V^2 + A^2) \\
 &\quad \times \left\{ -(p_{\pi^0} + p_{\pi^-})^2 + [(p_{\pi^0} + p_{\pi^-})(p_{\pi^0} - p_{\pi^-})]^2 / X^2 \right\} \\
 &= (G_F^2 \cos^2 \theta_c / 96\pi^4 m_{\pi^-}) \lambda(m_{\pi^-}^2, X^2, m_{\pi^0}^2) \\
 &= (G_F^2 \cos^2 \theta_c m_{\pi^-} / 24\pi^4) |\vec{p}_{\pi^0}|^2.
 \end{aligned}$$

Hence the integrated width is approximately

$$\begin{aligned}
 \Gamma &= \frac{G_F^2 \cos^2 \theta_c}{6\pi^3} \int_0^{(m_{\pi^-}^2 - m_{\pi^0}^2)/2m_{\pi^-}} |\vec{p}_{\pi^0}|^4 d|\vec{p}_{\pi^0}| \\
 &= G_F^2 \cos^2 \theta_c (m_{\pi^-} - m_{\pi^0})^5 / (30\pi^3).
 \end{aligned}$$

B.2.2 $\mu \rightarrow e\nu_\mu\bar{\nu}_e$.

The amplitude for this process is

$$M = -(G_F/\sqrt{2}) \bar{u}_{\nu_\mu} \gamma_\alpha (1 - \gamma_5) u_\mu \cdot \bar{u}_e \gamma^\alpha (1 - \gamma_5) v_{\bar{\nu}_e}.$$

After a Fierz transformation, it can be rewritten

$$M = (G_F/\sqrt{2}) \bar{u}_e \gamma_\alpha (1 - \gamma_5) u_\mu \cdot \bar{u}_{\nu_\mu} \gamma^\alpha (1 - \gamma_5) v_{\bar{\nu}_e}.$$

This can be identified with the amplitude in B.1 with the following substitutions:

$$\begin{aligned}
 a &= \nu_\mu, & b &= \bar{\nu}_e, & c &= e, & Y &= \mu, \\
 V &= -A = G_F/\sqrt{2}, & n_\alpha &= \bar{u}_e \gamma_\alpha (1 - \gamma_5) u_\mu.
 \end{aligned}$$

The calculation follows the same route as above except that $n_\alpha n_\beta$ is more complicated

$$n_\alpha n_\beta = \text{Tr} \left[(\not{p} + \mu) \frac{1}{2} (1 + \gamma_5 \not{S}) \gamma_\alpha (1 - \gamma_5) \cdot (\not{p} + e) \frac{1}{2} (1 + \gamma_5 \not{s}) \gamma_\beta (1 - \gamma_5) \right].$$

Here S and s are spin 4 vectors of muon and electron, respectively.

From the Dirac matrix properties,

$$\begin{aligned} n_\alpha n_\beta &= \frac{1}{2} \text{Tr} [(\not{\mu} - \mu \not{S}) \gamma_\alpha (\not{\epsilon} - e \not{S}) \gamma_\beta (1 - \gamma_5)] \\ &= 2 [(\mu_\alpha - \mu S_\alpha)(e_\beta - e S_\beta) + (\mu_\beta - \mu S_\beta)(e_\alpha - e S_\alpha) \\ &\quad - g_{\alpha\beta}(\mu_\gamma - \mu S_\gamma)(e^\gamma - e S^\gamma) - i\epsilon_{\alpha\beta\gamma\delta}(\mu^\gamma - \mu S^\gamma)(e^\delta - e S^\delta)]. \end{aligned}$$

Following the previous example, we construct

$$\begin{aligned} n_\alpha n_\beta T^{\alpha\beta} &= (4\pi G_F^2/3) [2(\mu_\alpha - \mu S_\alpha) \cdot (\mu^\alpha - e^\alpha)(\mu^\beta - e^\beta) \cdot (e_\beta - e S_\beta) \\ &\quad + (\mu_\gamma - \mu S_\gamma) \cdot (e^\gamma - e S^\gamma) \cdot (\mu_\alpha - e_\alpha) \cdot (\mu^\alpha - e^\alpha)]. \end{aligned}$$

Summing over the electron helicities, we obtain the decay width in the muon rest frame:

$$\begin{aligned} d\Gamma &= (G_F^2/48\pi^4)(d^3\vec{e}/2e_0) [3(\mu^2 + e^2)e_0 - 4\mu e_0^2 - 2\mu e^2 \\ &\quad + \vec{S} \cdot \vec{e}(\mu^2 + 3e^2 - 4\mu e_0)]. \end{aligned}$$

The allowed region of $|\vec{e}|$ is given by $|\vec{e}| \leq \frac{1}{2}(\mu^2 - e^2)/\mu$. After some analytic integration, the total decay width is

$$\Gamma = \frac{G_F^2 \mu^5}{192\pi^3} \left[1 - 8 \left(\frac{e}{\mu} \right)^2 + 8 \left(\frac{e}{\mu} \right)^6 - \left(\frac{e}{\mu} \right)^8 - 24 \left(\frac{e}{\mu} \right)^4 \ln \left(\frac{e}{\mu} \right) \right].$$

There is an alternative method to handle the three-body phase space integration. In the c.m. frame, the momenta of particles a , b and c in the final configuration lie on a plane. The integration of the orientation of this plane can be easily carried out, if the production rate depends only on the invariant dot products of momenta of a , b and c . For example, this happens when we study the unpolarized initial state and sum over final spins. Define scaling variables in the c.m. frame of Y ,

$$\begin{aligned} \mu_a &= a^2/Y^2, \\ x_a &= 2a_0/Y, \quad (\text{similarly for } b \text{ and } c) \\ x_a + x_b + x_c &= 2, \end{aligned}$$

we can express the production rate $|\mathcal{M}|^2$ as a function of x_i because

of the relation

$$a \cdot b = \frac{1}{2}Y^2(1 + \mu_c - \mu_a - \mu_b - x_c),$$

and similar relations from permutations of a , b and c . For three-body phase space, the spatial delta function is removed by integrating over $d^3\vec{c}$, and we write

$$\delta(Y_0 - a_0 - b_0 - c_0) \frac{d^3\vec{a}}{a_0} \frac{d^3\vec{b}}{b_0} = 4\pi|\vec{a}|da_0 \cdot 2\pi|\vec{b}|db_0 d(\cos\theta_{ab})\delta(Y_0 - a_0 - b_0 - c_0),$$

where θ_{ab} is the angle between \vec{a} and \vec{b} . Differentiating the equation

$$c_0^2 = c^2 + |\vec{a}|^2 + |\vec{b}|^2 + 2|\vec{a}||\vec{b}|\cos\theta_{ab},$$

we find

$$dc_0 = |\vec{a}||\vec{b}|d(\cos\theta_{ab})/c_0,$$

and integrate over dc_0 to remove the delta function,

$$d_3(PS \ Y \rightarrow abc) = \frac{1}{4}\pi^2 Y^2 dx_a dx_b.$$

The formula for the decay width becomes

$$d\Gamma(Y \rightarrow abc)/dx_a dx_b = (Y/256\pi^3)|M|^2.$$

Kinematics constrains the domain of x_a and x_b to be

$$\begin{aligned} 2\mu_a^{\frac{1}{2}} \leq x_a \leq 1 + \mu_a - \mu_b - \mu_c - 2(\mu_b\mu_c)^{\frac{1}{2}} \\ x_b \leq \frac{1}{2}(1 - x_a + \mu_a)^{-1} \left[(2 - x_a)(1 + \mu_a + \mu_b - \mu_c - x_a) \right. \\ \left. \pm (x_a^2 - 4\mu_a)^{\frac{1}{2}} \lambda^{\frac{1}{2}}(1 + \mu_a - x_a, \mu_b, \mu_c) \right]. \end{aligned}$$

These expressions simplify for the following special cases:

i) $\mu_a \neq 0$, $\mu_b = \mu_c = 0$. The domain of x_a and x_b is

$$2\mu_a^{\frac{1}{2}} \leq x_a \leq 1 + \mu_a, \\ x_b \leq \frac{1}{2} \left[(2 - x_a) \pm (x_a^2 - 4\mu_a)^{\frac{1}{2}} \right].$$

ii) $\mu_a = \mu_b = \mu_c = 0$. The allowed domain becomes

$$0 \leq x_a \leq 1, \quad 1 - x_a \leq x_b \leq 1.$$

We illustrate this method by the process $W \rightarrow H\ell\nu$. H is the Higgs boson in the standard model. The amplitude is

$$\mathcal{M} = 2G_F W^3 \bar{u}_\ell \not{\epsilon}_W (1 - \gamma_5) v_\nu / \left[(W - H)^2 - W^2 \right].$$

Summing over all spin states, the transition probability becomes

$$\sum |\mathcal{M}|^2 = \frac{4G_F^2 W^6 (W^\alpha W^\beta / W^2 - g^{\alpha\beta}) \cdot 8 \cdot (\ell_\alpha \nu_\beta + \ell_\beta \nu_\alpha - g_{\alpha\beta} \ell \cdot \nu)}{[(W - H)^2 - W^2]^2}.$$

In terms of scaling variables x_H , x_ℓ , x_ν and μ_H defined as above,

$$|\mathcal{M}|^2 = 16G_F^2 W^4 (1 + \mu_H - x_H + x_\ell x_\nu) / (x_H - \mu_H)^2.$$

The spin-averaged decay rate is

$$\frac{d\Gamma}{dx_H dx_\ell} = \frac{G_F^2 W^5}{48\pi^3} \frac{1 + \mu_H - x_H + x_\ell (2 - x_H - x_\ell)}{(x_H - \mu_H)^2},$$

with x_H , x_ℓ in the kinematic ranges,

$$2\mu_H^{\frac{1}{2}} \leq x_H \leq 1 + \mu_H, \\ x_\ell \leq \frac{1}{2} \left[(2 - x_H) \pm (x_H^2 - 4\mu_H)^{\frac{1}{2}} \right].$$

The integration over x_ℓ can be easily carried out. We have

$$\frac{d\Gamma}{dx_H} = \frac{G_F^2 W^5}{288\pi^3} \frac{(x_H^2 - 4\mu_H)^{\frac{1}{2}} (12 + 8\mu_H - 12x_H + x_H^2)}{(x_H - \mu_H)^2}.$$

B.3 Multiparticle Phase Space

Consider a system Z with particles of momenta p_1, p_2, \dots, p_n in the final state, with the invariant phase space

$$d_n(PS \ Z \rightarrow p_1 p_2 \dots p_n) = \delta^4(p_Z - p_1 - p_2 - \dots - p_n) \prod_{i=1}^n \frac{d^3 \vec{p}_i}{2E_i}.$$

To reduce it, we partition the final particles into two subsystems X and Y as follows:

$$Z \rightarrow X(p_1 p_2 \dots p_j) + Y(p_{j+1} \dots p_n).$$

The choice of the partition depends on convenience and interest.

$$d_n(PS \ Z \rightarrow p_1 p_2 \dots p_n) = d_2(PS \ Z \rightarrow XY) dm_X^2 dm_Y^2 \\ \cdot d_j(PS \ X \rightarrow p_1 p_2 \dots p_j) \cdot d_{n-j}(PS \ Y \rightarrow p_{j+1} \dots p_n).$$

The ranges of the invariant mass m_X and m_Y are

$$\sum_{i=1}^j m_i \leq m_X, \quad \sum_{i=j+1}^n m_i \leq m_Y, \quad m_X + m_Y \leq m_Z.$$

In the special case Y is a single particle p_n , the two previous equations are replaced by

$$d_n(PS \ Z \rightarrow p_1 p_2 \dots p_n) = d_2(PS \ Z \rightarrow XY) dm_X^2 \\ \cdot d_{n-1}(PS \ X \rightarrow p_1 \dots p_{n-1})$$

$$m_1 + m_2 + \dots + m_{n-1} \leq m_X \leq m_Z - m_n.$$

The subsystem X and Y can be further reduced recursively until we obtain a chain of products of two-body phase spaces.

Appendix C

Helicity Projection Techniques

C.1 Helicity Basis

The tree-level squared matrix element for a heavy-lepton production and decay sequence

$$ab \rightarrow Lx_1, \dots, x_n, \quad L \rightarrow \nu_L y_1 y_2,$$

where x_i and y_i denote additional particles, can be evaluated directly by gamma-matrix reduction routines. However this can lead to enormously complicated algebraic expressions that are very hard to simplify; great simplification can be achieved if we factor the amplitude into L -production and L -decay parts.

First let us decompose the amplitude \mathcal{M} for the complete process into factors describing L production, L decay as follows

$$\mathcal{M} = \sum_{\lambda} A_{\lambda}(ab \rightarrow Lx_1, \dots, x_n) B_{\lambda}(L \rightarrow \nu_L y_1 y_2) / D,$$

where $D = (L^2 - m_L^2 + im_L \Gamma_L)$ is a propagator denominator, and we keep track explicitly of the helicity $\lambda = \pm \frac{1}{2}$ of the intermediate heavy lepton L . This decomposition applies quite generally to *any* production and decay of L . We consistently use particle labels to denote their four-momenta. The squared matrix element, averaged

over initial and summed over final spins and colors, then takes the form

$$\begin{aligned} |\mathcal{M}|^2 &= \frac{1}{N_i} \sum_{\pi} \sum_{\delta} \sum_{\lambda, \mu} A_{\lambda} B_{\lambda} A_{\mu}^* B_{\mu}^* / |D|^2 \\ &= \frac{1}{N_i} \sum_{\lambda, \mu} \left(\sum_{\pi} A_{\lambda} A_{\mu}^* \right) \left(\sum_{\delta} B_{\lambda} B_{\mu}^* \right) / |D|^2. \end{aligned}$$

Here N_i is the number of initial spin/color states being averaged, while symbols π and δ denote the spin/color states of the external particles in the production and decay processes, respectively. The cross section is normalized as

$$d\sigma = \frac{1}{2s} |\mathcal{M}|^2 \prod_{\substack{\mathbf{k}=\nu_L, \nu_1, \nu_2, \\ x_1, \dots, x_n}} \frac{d^3 k}{(2\pi)^3 2E_k} (2\pi)^4 \delta^4(a+b-\nu_L-y_1-y_2-x_1-\dots-x_n).$$

The individual terms $\sum_{\pi} A_{\lambda} A_{\mu}^*$ and $\sum_{\delta} B_{\lambda} B_{\mu}^*$ are algebraically much less complicated than the complete amplitude squared; they are somewhat like the squared matrix elements for production and decay separately (actually they are proportional to elements of the density matrix for L production and decay). They can be calculated using the helicity spinors

$$\begin{aligned} u(p, +) &= (E+m)^{-1/2} (\boldsymbol{\gamma} \cdot \mathbf{p} + m) \begin{pmatrix} \cos \frac{1}{2} \theta \\ \exp[i\phi] \sin \frac{1}{2} \theta \\ 0 \\ 0 \end{pmatrix}, \\ u(p, -) &= (E+m)^{-1/2} (\boldsymbol{\gamma} \cdot \mathbf{p} + m) \begin{pmatrix} -\exp[i\phi] \sin \frac{1}{2} \theta \\ \cos \frac{1}{2} \theta \\ 0 \\ 0 \end{pmatrix}, \end{aligned}$$

labelled \pm for helicity $\pm\frac{1}{2}$, with the outer products

$$u(p, \pm)\bar{u}(p, \pm) = \frac{1}{2}(p \cdot \gamma + m)(1 \pm \gamma_5 \gamma \cdot S),$$

$$u(p, +)\bar{u}(p, -) = \frac{1}{2} \exp(i\phi) (p \cdot \gamma + m)\gamma_5 \gamma \cdot C,$$

$$u(p, -)\bar{u}(p, +) = \frac{1}{2} \exp(-i\phi) (p \cdot \gamma + m)\gamma_5 \gamma \cdot C^*.$$

(For the corresponding antiparticle $v\bar{v}$ -spinor outer products, put $m \rightarrow -m$ in the above equations.) Here S is the covariant spin vector

$$S_\mu = (|\vec{p}|/m, E\vec{p}/(m|\vec{p}|))$$

and C is defined as

$$C_\mu = (0, \cos\theta \cos\phi - i \sin\phi, \cos\theta \sin\phi + i \cos\phi, -\sin\theta),$$

where the polar angle θ and azimuthal angle ϕ define the direction of \vec{p} . The four vectors p, S, C, C^* obey orthogonality relations

$$p \cdot S = p \cdot C = p \cdot C^* = S \cdot C = S \cdot C^* = 0.$$

The summations over λ and μ in the expression for $|M|^2$ take particularly simple forms in a number of cases, thanks to algebraic identities.

Our discussion of production/decay helicity correlations applies formally to any spin- $\frac{1}{2}$ fermion L but is physically relevant only when L has no strong interactions: *e.g.* L is a lepton or wino of supersymmetry and ν_L is a neutrino or zino or photino. For strongly interacting fermions such as quarks or gluinos, there is an additional hadronization process between production and decay. Although the eventual heavy hadron decay may sometimes be approximated by a heavy quark or gluino decay process, the hadronization inevitably introduces some depolarization (for spinless hadrons the depolarization is complete) which has to be specified and is not included in our treatment.

We describe below the treatment of $V \pm A$ interactions. The techniques can be extended to general V and A interactions, too; see Phys. Rev. D35, 166 (1987).

C.2 $V \pm A$ Interactions

If $V-A$ coupling is assumed for both production and decay, there are effectively additional projection operators $\frac{1}{2}(1 - \gamma_5)$ on the left and $\frac{1}{2}(1 + \gamma_5)$ on the right in the expressions for the spinor outer products $u\bar{u}$. This greatly simplifies the algebra and the spinor outer products can be represented by the substitutions

$$\begin{aligned} u(p, \pm)\bar{u}(p, \pm) &\longrightarrow \frac{1}{2}(p \cdot \gamma \mp mS \cdot \gamma), \\ u(p, +)\bar{u}(p, -) &\longrightarrow -\frac{1}{2}m \exp(i\phi) C \cdot \gamma, \\ u(p, -)\bar{u}(p, +) &\longrightarrow -\frac{1}{2}m \exp(-i\phi) C^* \cdot \gamma. \end{aligned}$$

Since the spinor outer products are effectively of the form $u(\mu)\bar{u}(\lambda) = \gamma \cdot V_{\mu\lambda}$ where $V_{\mu\lambda} = \frac{1}{2}(p \mp mS)$, $-\frac{1}{2}mC \exp(i\phi)$ or $-\frac{1}{2}mC^* \exp(-i\phi)$ as determined by the above equations, it follows that the expressions for $\sum_{\pi} A_{\lambda} A_{\mu}^*$ are all of the scalar product form $X \cdot V_{\mu\lambda}$ where X is some 4-vector:

$$\begin{aligned} \sum_{\pi} A_{\pm} A_{\pm}^* &= \frac{1}{2} X \cdot (L \mp m_L S), \\ \sum_{\pi} A_{-} A_{+}^* &= -\frac{1}{2} X \cdot C m_L \exp(i\phi), \\ \sum_{\pi} A_{+} A_{-}^* &= -\frac{1}{2} X \cdot C^* m_L \exp(-i\phi). \end{aligned}$$

Here we explicitly specialize to L production, $p \rightarrow L$, $m \rightarrow m_L$; S , C , C^* are defined by the L kinematics. Similarly, the decay sums $\sum_{\delta} B_{\lambda} B_{\mu}^*$ are all described by the scalar products of a common 4-

vector Y and the same vectors $V_{\lambda\mu}$ (note that λ, μ are reversed here):

$$\begin{aligned}\sum_{\delta} B_{\pm} B_{\pm}^* &= \frac{1}{2} Y \cdot (L \mp m_L S), \\ \sum_{\delta} B_{+} B_{-}^* &= -\frac{1}{2} Y \cdot C m_L \exp(i\phi), \\ \sum_{\delta} B_{-} B_{+}^* &= -\frac{1}{2} Y \cdot C^* m_L \exp(-i\phi).\end{aligned}$$

The relevant vectors X, Y can be determined by evaluating particular cases. For example, they appear separately in the spin-averaged production and decay of L :

$$\begin{aligned}|\mathcal{M}(\text{production})|^2 &= \frac{1}{N_i} \sum_{\pi, \lambda} A_{\lambda} A_{\lambda}^* = N_i^{-1} X \cdot L, \\ |\mathcal{M}(\text{decay})|^2 &= \sum_{\delta, \lambda} B_{\lambda} B_{\lambda}^* = Y \cdot L,\end{aligned}$$

(note that the decay amplitude squared is *not* spin/color averaged in this definition). To extract X and Y from these simpler calculations, it is imperative to keep track throughout of the momentum vector L arising from the $u(L)\bar{u}(L)$ outer product and not to re-express it as a linear combination of other momenta.

Using the identity

$$\begin{aligned}2(X \cdot S)(Y \cdot S) + (X \cdot C)(Y \cdot C^*) + (X \cdot C^*)(Y \cdot C) \\ = 2(X \cdot L)(Y \cdot L)/m_L^2 - 2(X \cdot Y),\end{aligned}$$

the summation over λ and μ in the expression for $|\mathcal{M}|^2$ can now be performed:

$$\begin{aligned}|\mathcal{M}|^2 &= N_i^{-1} \sum_{\lambda, \mu} (X \cdot V_{\mu\lambda}) (Y \cdot V_{\lambda\mu}) / |D|^2 \\ &= N_i^{-1} [(X \cdot L)(Y \cdot L) - \frac{1}{2} m_L^2 (X \cdot Y)] / |D|^2.\end{aligned}$$

This complete result can thus be inferred directly from the easy-to-compute spin-averaged production and decay amplitudes squared, $|\mathcal{M}(\text{production})|^2$ and $|\mathcal{M}(\text{decay})|^2$.

Had we calculated the spin-averaged production of L multiplied by the spin-averaged (*i.e.* unpolarized) decay of L , we would have found $|\mathcal{M}|^2 = \frac{1}{2}N_i^{-1}(X \cdot L)(Y \cdot L)/|D|^2$ instead. This gives the correct total cross section, since the decay width of L is independent of helicity, but not the correct details since it omits the effects of L polarization on the decay distributions.

Similar results follow with $V + A$ couplings; in this case S , C and C^* appear with extra negative signs in the expressions for the spinor outer products. When both production and decay couplings are $V + A$, these negative signs occur squared in the result for $|\mathcal{M}|^2$ and the result is unchanged. When one coupling is $V + A$ and one is $V - A$, the bilinear S , C , C^* terms in the result for $|\mathcal{M}|^2$ change sign and the result becomes instead

$$|\mathcal{M}|^2 = N_i^{-1} \left[\frac{1}{2}m_L^2(X \cdot Y) \right] / |D|^2 .$$

Our discussion has referred to the production and decay of a particle, requiring positive-energy spinors u , \bar{u} . To describe antiparticles instead we use negative-energy spinors v , \bar{v} ; the m_L terms in the spinor outer products and the expressions for $\sum AA^*$ and $\sum BB^*$ then change sign but the final results are unchanged. These techniques can be applied successively to add in the sequential decay correlations of a number of particles, provided their production and decay couplings are always $V \pm A$.

C.3 Application: L Production via $d\bar{u} \rightarrow W^- \rightarrow L\nu_L$ with $L \rightarrow \nu_L e \bar{\nu}_e$

For a simple example, consider L production by the lowest order process $d\bar{u} \rightarrow L\nu_L$ followed by $L \rightarrow \nu_L e \bar{\nu}_e$ decay, with $V - A$ couplings throughout. There are $N_i = 36$ initial spin/color states to average over. The squared matrix elements for the spin/color-averaged production and decay of L corresponding to the expressions for

$|\mathcal{M}(\text{production})|^2$ and $|\mathcal{M}(\text{decay})|^2$ are then

$$N_i^{-1} \sum_{\pi,\lambda} A_\lambda A_\lambda^* = N_i^{-1} 384 G_F^2 M_W^4 (d \cdot \bar{\nu}_L)(\bar{u} \cdot L) / [(s - M_W^2)^2 + \Gamma_W^2 M_W^2],$$

$$\sum_{\delta,\lambda} B_\lambda B_\lambda^* = 128 G_F^2 M_W^4 (e \cdot \nu_L)(\bar{\nu}_e \cdot L) / [(s' - M_W^2)^2 + \Gamma_W^2 M_W^2],$$

where $s = (d + \bar{u})^2$ and $s' = (e + \bar{\nu}_e)^2$. We can immediately identify

$$X_\alpha = \left\{ 384 G_F^2 M_W^4 (d \cdot \bar{\nu}_L) / [(s - M_W^2)^2 + \Gamma_W^2 M_W^2] \right\} \bar{u}_\alpha \equiv F \bar{u}_\alpha,$$

$$Y_\alpha = \left\{ 128 G_F^2 M_W^4 (e \cdot \nu_L) / [(s' - M_W^2)^2 + \Gamma_W^2 M_W^2] \right\} (\bar{\nu}_e)_\alpha \equiv G (\bar{\nu}_e)_\alpha,$$

and hence construct the spin/color averaged matrix element for the complete process

$$|\mathcal{M}|^2 = N_i^{-1} F G [(\bar{u} \cdot L)(\bar{\nu}_e \cdot L) - \frac{1}{2} m_L^2 (\bar{u} \cdot \bar{\nu}_e)] / |D|^2.$$

It is straightforward to continue this analysis to include the decays of ν_L and $\bar{\nu}_L$, too, assuming they are massive.

Bibliography

For further reading we suggest a number of textbooks, some workshop reports on physics with future colliders, and a small selection of papers (including many review articles). We regret that only a small fraction of the relevant literature is listed here. For more complete coverage, see the references in recent reviews and conference reports.

Books:

- I. J. R. Aitchison, A. J. G. Hey: **Gauge Theories in Particle Physics**, (Hilger, Bristol 1982)
- J. D. Bjorken, S. D. Drell: **Relativistic Quantum Fields**, (McGraw-Hill, New York 1965)
- T. P. Cheng, L. F. Li: **Gauge Theory of Elementary Particle Physics**, (Oxford University Press, New York 1984)
- F. E. Close: **Introduction to Quarks and Partons**, (Academic Press, New York 1979)
- B. De Wit, J. Smith: **Field Theory in Particle Physics**, (North Holland 1986)
- R. P. Feynman: **Photon-Hadron Interactions**, (Benjamin 1972)
- H. Georgi: **Weak Interactions and Modern Particle Theory**, (Benjamin 1984)
- F. Halzen, A. D. Martin: **Quarks and Leptons**, (Wiley, New York 1984)
- J. M. Hammersley, D. C. Handscomb: **Monte Carlo Methods**, (Methuen, London 1964)
- C. Itzykson and J. Zuber: **Quantum Field Theory**, (McGraw-Hill 1980)

- C. Kounnas *et al.*: **Grand Unification with and without Supersymmetry and Cosmological Implications**, (World Scientific 1984)
- R. E. Marshak, Riazuddin, C. P. Ryan: **Theory of Weak Interactions in Particle Physics**, (Wiley-Interscience, New York 1969)
- T. Muta: **Foundations of Quantum Chromodynamics**, (World Scientific 1987)
- L. B. Okun: **Leptons and Quarks**, (North Holland, Amsterdam 1982)
- C. Quigg: **Gauge Theories of the Strong, Weak and Electromagnetic Interactions**, (Benjamin 1983)
- P. Ramond: **Field Theory, A Modern Primer**, (Benjamin 1981)
- G. G. Ross: **Grand Unified Theories**, (Benjamin 1984)
- J. C. Taylor: **Gauge Theories of Weak Interactions**, (Cambridge University Press 1976)
- J. Wess, J. Bagger: **Supersymmetry and Supergravity**, (Princeton University Press 1983)
- B. G. Wybourne: **Classical Groups for Physicists**, (Wiley, New York 1974)
- F. J. Yndurain: **Quantum Chromodynamics**, (Springer Verlag 1983)

Workshop Reports:

- Proceedings of the ECFA-CERN Workshop on a Large Hadron Collider in the LEP Tunnel*, CERN report 84-10
- Physics at LEP*, J. Ellis, R. Peccei, eds., CERN report 86-02
- Proceedings of 1984 Summer Study on the Design and Utilization of the SSC*, R. Donaldson, J. G. Morfin, eds., Fermilab 1985
- Proceedings of UCLA, Oregon, and Madison Workshops on Supercollider Physics*, (World Scientific 1986)
- Proceedings of 1986 Snowmass SSC Study*, (in press)
- Proceedings of Symposium on the Fourth Family of Quarks and Leptons*, (UCLA 1987)

Chapter 1. Introduction

- S. Glashow, *Partial Symmetries of Weak Interactions* Nucl. Phys. **22**, 579 (1961)
- C. Rubbia, *Experimental Observation of the Intermediate Vector Bosons W^+ , W^- and W^0* , Rev. Mod. Phys. **57**, 699 (1985)
- A. Salam, *Weak and Electromagnetic Interactions in Elementary Particle Theory*, W. Svartholm, ed., (Almquist and Wiksell, Stockholm 1968)
- S. Weinberg, *A Model of Leptons*, Phys. Rev. Lett. **19**, 1264 (1967)

Chapter 2. Standard Electroweak Gauge Model

- E. Abers, B. W. Lee, *Gauge Theories*, Phys. Rep. **9**, 1 (1973)
- L. L. Chau, *Quark Mixing*, Phys. Rep. **95**, 1 (1983)
- P. Q. Hung, J. J. Sakurai, *Structure of Neutral Currents*, Ann. Rev. Nuc. Part. Sci. **31**, 375 (1981)
- J. E. Kim *et al.*, *Review of the Weak Neutral Current*, Rev. Mod. Phys. **53**, 211 (1981)
- M. Kobayashi, M. Maskawa, *CP Violation in the Renormalizable Theory of Weak Interaction*, Prog. Theor. Phys. **49**, 652 (1973)
- W. J. Marciano, *Fourth Generation Physics*, in Proceedings of UCLA International Symposium for the Fourth Family of Quarks and Leptons (1987)
- W. J. Marciano, Z. Parsa, *Electroweak Tests of the Standard Model*, Ann. Rev. Nuc. Part. Sci. **36**, 171 (1986)
- Particle Data Group, Review, Phys. Rev. **D50**, 1173 (1994)
- E. A. Paschos, U. Türke, *The Mixing Matrix and its Implications*, Phys. Lett. **B176**, 185 (1986)
- L. Wolfenstein, *Status of CP Violation*, Ann. Rev. Nuc. Part. Sci. **36**, 137 (1986)
- C. N. Yang, R. Mills, *Conservation of Isotopic Spin and Isotopic Gauge Invariance* Phys. Rev. **96**, 191 (1954)

Chapter 3. Lepton and Heavy Quark Decays

- J. F. Donoghue *et al.*, *Low Energy Weak Interactions of Quarks*, Phys. Rep. **131**, 319 (1986)
- M. G. D. Gilchriese, *Weak Interactions of Leptons and Quarks*, Proc. Berkeley Conference (1986)
- F. Gilman, *Phenomenology of Heavy Quark Systems*, in Proceedings of SLAC Summer Institute on Particle Physics (1986)

Chapter 4. Basic e^+e^- and νe Processes

- B. Kayser, *Majorana Neutrinos*, Comm. Nucl. Part. Phys. **14**, 69 (1985)
- R. Marshall, *Hadron Production*, to appear in **Electron-Positron Physics**, A. Ali, P. Söding, eds., (World Scientific 1987)
- S. L. Wu, e^+e^- Physics at PETRA, Phys. Rep. **107**, 59 (1984)

Chapter 5. Partons and Scaling Distributions

- C. H. Llewellyn Smith, *Neutrino Interactions at Accelerators*, Phys. Rep. **3**, 261 (1972)

Chapter 6. Fragmentation

- B. Andersson *et al.*, *Parton Fragmentation and String Dynamics*, Phys. Rep. **97**, 31 (1983)
- X. Artru, *Classical String Phenomenology*, Phys. Rep. **97**, 147 (1983)
- R. D. Field, R. P. Feynman, *A Parametrization of Quark Jets*, Nucl. Phys. **B136**, 1 (1978)
- T. Gottschalk, *Hadronization in e^+e^- Annihilation*, Nucl. Phys. **B239**, 349 (1984)
- C. Peterson *et al.*, *Scaling Violations in Inclusive e^+e^- Annihilation Spectra*, Phys. Rev. **D27**, 105 (1983)
- D. H. Saxon, *Quark and Gluon Fragmentation*, to appear in **Electron-Positron Physics**, A. Ali, P. Söding, eds., (World Scientific 1987)

Chapter 7. QCD

- G. Altarelli, *Partons in QCD*, Phys. Rep. **81**, 1 (1982)
- A. J. Buras, *Asymptotic Freedom in Deep Inelastic Processes*, Rev. Mod. Phys. **52**, 199 (1980)
- S. J. Brodsky, G. P. Lepage, *Exclusive Processes in Quantum Chromodynamics*, Phys. Rev. **D22**, 2157 (1980)
- J. C. Collins, W. K. Tung, *Calculating Heavy Quark Distributions*, Nucl. Phys. **B278**, 934 (1986)
- D. W. Duke, J. F. Owens, *Q^2 -Dependent Parametrizations of Parton Distribution Functions*, Phys. Rev. **D30**, 49 (1984)
- D. W. Duke, R. G. Roberts, *Determination of QCD Coupling α_s and Scale Λ* , Phys. Rep. **120**, 275 (1985)
- E. Eichten *et al.*, *Supercollider Physics*, Rev. Mod. Phys. **56**, 579 (1984), erratum **58**, 1065
- F. Halzen, D. M. Scott, *Hadroproduction of Photons and Leptons*, Phys. Rev. **D18**, 3378 (1978)
- W. Marciano, H. Pagels, *Quantum Chromodynamics*, Phys. Rep. **36C**, 137 (1978)
- A. H. Mueller, *Perturbative QCD at High Energies*, Phys. Rep. **73C**, 237 (1981)
- H. D. Politzer, *Asymptotic Freedom*, Phys. Rep. **14**, 129 (1974)
- J. P. Ralston, *Pocket Partonometer*, Phys. Lett. **172B**, 430 (1986)
- E. Reya, *Perturbative QCD*, Phys. Rep. **69**, 195 (1981)
- F. Wilczek, *Quantum Chromodynamics*, Ann. Rev. Nuc. Part. Sci. **32**, 177 (1982)

Chapter 8. Weak Boson Production and Decay

- G. Altarelli *et al.*, *Vector Boson Production at Colliders*, Nucl. Phys. **B246**, 12 (1984)
- R. W. Brown *et al.*, *$W^\pm Z^0$ and $W^\pm\gamma$ Pair Production in νe , pp and $\bar{p}p$ Collisions*, Phys. Rev. **D20**, 1164 (1979)
- S. Dawson, *Effective W Approximation*, Nucl. Phys. **B249**, 42 (1985)

- K. Hagiwara *et al.*, Probing the Weak Boson Sector in $e^+e^- \rightarrow W^+W^-$, Nucl. Phys. **B282**, 253 (1987)
- M. A. Samuel and J. H. Reid, *Radiation Amplitude Zeros*, Prog. Theo. Phys. **76**, 184 (1986)
- UA1 Collaboration, (W, Z results) Phys. Lett. **166B**, 484 (1986); **185B**, 233 (1987); Europhys. Lett. **1**, 327 (1986)
- UA2 Collaboration, (W, Z results) Z. Phys. **C30**, 1 (1986); Phys. Lett. **186B**, 440, 452 (1987)

Chapter 9. Jets

- A. Bassetto *et al.*, *Jet Structure and Infrared Sensitive Quantities in QCD*, Phys. Rep. **100**, 201 (1983)
- F. A. Berends *et al.*, *Single Bremsstrahlung Processes in Gauge Theories*, Phys. Lett. **103B**, 124 (1981)
- B. L. Combridge, C. J. Maxwell, *Untangling Large- p_T Hadronic Reactions*, Nucl. Phys. **B239**, 429 (1984)
- L. DiLella, *Jet Production in Hadron Collisions*, Ann. Rev. Nucl. Part. Sci. **35**, 107 (1985)
- E. J. Eichten *et al.*, *Tests for Quark and Lepton Substructure*, Phys. Rev. Lett. **50**, 811 (1983)
- G. C. Fox, S. Wolfram, *A Model for Parton Showers in QCD*, Nucl. Phys. **B168**, 285 (1980)
- T. Gottschalk, *e^+e^- Annihilation Including Parton Bremsstrahlung*, Nucl. Phys. **B214**, 201 (1983); *Backwards Evolved Initial State Parton Showers*, Nucl. Phys. **B277**, 700 (1986)
- L. V. Gribov *et al.*, *Semihard Processes in QCD*, Phys. Rep. **100**, 1 (1983)
- F. Halzen, P. Hoyer, *Jets in $p\bar{p}$ Collider Events*, Phys. Lett. **130B**, 326 (1983)
- G. Marchesini, B. R. Webber, *Simulation of QCD Jets Including Soft Gluon Interference*, Nucl. Phys. **B238**, 1 (1984)
- B. Naroska, *e^+e^- Physics with the JADE Detector*, Phys. Rep. **148**, 67 (1987)

- B. Naroska, e^+e^- *Physics with the JADE Detector*, Phys. Rep. **148**, 67 (1987)
- R. Odorico, *Simulation of QCD in Hard Hadronic Processes*, Nucl. Phys. **B228**, 381 (1983)
- F. E. Paige, S. D. Protopopescu, *ISAJET, a Monte Carlo Event Generator for pp and $p\bar{p}$ Interactions*, Proc. UCLA Workshop, (World Scientific 1986)
- T. Sjöstrand, *A Model for Initial State Parton Showers*, Phys. Lett. **157B**, 321 (1985)
- G. Sterman, S. Weinberg, *Jets from QCD*, Phys. Rev. Lett. **39**, 1436 (1977)
- UA1 Collaboration: (jet results) Phys. Lett. **172** 461; **177** 244 (1986); Nucl. Phys. **B276**, 253 (1986); CERN-EP/85-196
- UA2 Collaboration: (jet results) Phys. Lett. **160B**, 349 (1985), Z. Phys. **C30**, 341 (1986)
- B. R. Webber, *Monte Carlo Simulations of Hard Hadronic Processes*, Ann. Rev. Nuc. Part. Sci. **36**, 253 (1986)

Chapter 10. Heavy Quark Production

- A. Ali, C. Jarlskog, *Signatures of $B_s^0 - \bar{B}_s^0$ Mixing in $p\bar{p}$ and e^+e^- Collisions*, Phys. Lett. **144B**, 266 (1984)
- V. Barger, A. D. Martin, *Quarkonium Production at $p\bar{p}$ Colliders*, Phys. Rev. **D31**, 1051 (1985)
- V. Barger, A. D. Martin, R. J. N. Phillips, *Sharpening up the $W \rightarrow t\bar{b}$ Signal*, Phys. Lett. **151B**, 463 (1985)
- V. Barger, R. J. N. Phillips, *Heavy Quark Production in $p\bar{p}$ Colliders with $B - \bar{B}$ Mixing*, Phys. Rev. Lett. **55**, 2752 (1985); *Trimuons in $p\bar{p}$ Collisions*, Phys. Rev. **D34**, 2727 (1986)
- K. Berkelman, *Upsilon Spectroscopy at CESR*, Phys. Rep. **98**, 145 (1983)
- J. Bernabeu, P. Pascual, *Neutral Current Effects for $e^+e^- \rightarrow \ell^+\ell^-$ Around Vector Resonances*, Nucl. Phys. **B172**, 93 (1980)

- I. I. Bigi, A. I. Sanda, *CP Violation in Heavy Flavor Decays*, Nucl. Phys. **B281**, 41 (1987)
- T. Brown, S. Pakvasa, *Mixing and CP Nonconservation in $K^0 - \bar{K}^0$ and $B^0 - \bar{B}^0$ Systems*, Phys. Rev. **D31**, 1661 (1985)
- W. Buchmüller, S. H. H. Tye, *Quarkonia and QCD*, Phys. Rev. **D24**, 132 (1981)
- W. Buchmüller, D. Wyler, *Constraints on $SU(5)$ Type Leptoquarks*, Phys. Lett. **177B**, 377 (1986)
- A. J. Buras *et al.*, *B-Decay, CP Violation and the Top Quark Mass*, Nucl. Phys. **B238**, 529 (1984)
- R. J. Cashmore *et al.*, *Exotic Phenomena in High Energy ep Collisions*, Phys. Rep. **122**, 275 (1985)
- I. Dunietz, J. Rosner, *Time-Dependent and CP-Violation Effects in $B^0 - \bar{B}^0$ Systems*, Phys. Rev. **D34**, 1404 (1986)
- J. Ellis *et al.*, *Phenomenology of the Next Left-Handed Quarks*, Nucl. Phys. **B131**, 285 (1977)
- J. Hagelin, *CP Violation in the $B^0 - \bar{B}^0$ System*, Nucl. Phys. **B193**, 123 (1981)
- K. Hagiwara *et al.*, *Probing QCD with Heavy Bound States*, Phys. Lett. **130B**, 209 (1983)
- A. Kernan, G. Van Dalen, *Charm and Beauty Production in Strong Interactions*, Phys. Rep. **106**, 297 (1984)
- J. H. Kühn *et al.*, *Annihilation of e^+e^- into Quarkonium*, Nucl. Phys. **B157**, 125 (1979)
- J. P. Leveille, T. Weiler, *Heavy Quark Lepton Production in QCD*, Nucl. Phys. **B147**, 147 (1979)
- C. Quigg, J. L. Rosner, *Counting Narrow Levels of Quarkonium*, Phys. Lett. **72B**, 462 (1978)
- L. M. Sehgal, P. Zerwas, *Electroweak $\gamma - Z - W$ Interference on Toponium*, Nucl. Phys. **B183**, 417 (1981)
- UA1 Collaboration, (heavy quarks) Phys. Lett. **147B**, 493 (1984), **186B** 237, 247 (1987)

Chapter 11. Monte Carlo Simulations

F. James, *Monte Carlo Theory and Practice*, Rep. Prog. Phys. **43**, 1145 (1980)

Chapter 12. Higgs Boson

V. Barger, W. Y. Keung, *Technipionium Bound State Formation and Decays*, Phys. Lett. **185B**, 431 (1987)

V. Barger *et al.*, *Decays of Weak Vector Bosons and t quarks into Doubly Charged Higgs Scalars*, Phys. Rev. **D26**, 218 (1982)

R. N. Cahn, S. Dawson, *Production of Very Massive Higgs Bosons*, Phys. Lett. **136B**, 196 (1984)

M. Davier, rapporteur talk, Proc. of Berkeley Conference (1986)

E. Eichten, *Theoretical Expectations at Collider Energies*, FERMI-LAB Conf-85/178-T (1986)

J. Ellis *et al.*, *A Phenomenological Profile of the Higgs Boson*, Nucl. Phys. **B106**, 292 (1976)

E. Farhi, L. Susskind, *Technicolor*, Phys. Rep. **74**, 277 (1981)

G. B. Gelmini, M. Roncadelli, *Left-handed Neutrino Mass Scale and Spontaneously Broken Lepton Number*, Phys. Lett. **99B**, 411 (1981)

H. M. Georgi *et al.*, *Unconventional Model of Neutrino Masses*, Nucl. Phys. **B193**, 297 (1981)

J. F. Gunion, H. W. Haber, *Higgs Bosons in SUSY Models*, Nucl. Phys. **278**, 449 (1986)

Z. Kunszt, *Associated Production of Heavy Higgs Bosons with Top Quarks*, Nucl. Phys. **B247**, 339 (1984)

G. Pocsik, G. Zsigmond, *On the Production of Neutral Higgs Bosons in the Weinberg-Salam Model with Two Higgs Doublets*, Z. Phys. **C10**, 367 (1981)

UA1 Collaboration, (neutrino counting), Phys. Lett. **185B**, 241 (1987)

UA2 Collaboration, (neutrino counting), Phys. Lett. **186B**, 440 (1987)

- A. I. Vainshtein *et al.*, *Higgs Particles*, Sov. Phys. Usp. **23**, 429 (1980)
- M. Vysotsky, *Strong Interaction Corrections to Semiweak Decays: Calculation of the $V \rightarrow H\gamma$ Decay Route to Order α_s* , Phys. Lett. **B97**, 159 (1980)
- F. Wilczek, *Decays of Heavy Vector Mesons into Higgs Particles* Phys. Rev. Lett. **39**, 1304 (1977)

Chapter 13. Fourth Generation

- H. Baer *et al.*, *Fourth Generation Charged Leptons and Neutrinos via Z^0* , Phys. Rev. **D32**, 688 (1985)
- V. Barger *et al.*, *Fourth Generation Quarks and Leptons*, Phys. Rev. **D30**, 947 (1984); *Possible v -quark Signatures at e^+e^- Colliders*, Phys. Rev. Lett. **57**, 1518 (1986)
- J. Dorfan, *Role of e^+e^- Colliders in the Search for New Quarks and Leptons* in Proc. of UCLA Symposium on the Fourth Family of Quarks and Leptons (1987)
- E. Ma and J. Okada, *How Many Neutrinos?* Phys. Rev. Lett. **41**, 287 (1978)
- S. S. D. Willenbrock and D. Dicus, *Production of Heavy Leptons from Gluon Fusion*, Phys. Lett. **156B**, 429 (1985)

Chapter 14. Higher Symmetries

- F. del Aguila *et al.*, *Superstring-Inspired Models*, Nucl. Phys. **B272**, 413 (1986)
- R. Arnowitt *et al.*, *Applied $N = 1$ Supergravity*, (World Scientific 1983)
- H. Baer, E. L. Berger, *Prospects for Supersymmetry at the Fermilab Collider*, Phys. Rev. **D34**, 1361 (1986)
- H. Baer *et al.*, *Can the Data from the CERN $p\bar{p}$ Collider Limit Gauginos Masses?* Phys. Rev. Lett. **57**, 296 (1986)
- V. Barger *et al.*, *Extra Fermions in E_6 Superstring Theories*, Phys. Rev. **D33**, 1912 (1986); *Phenomenological Mass Limits on Extra Z of E_6 Superstrings*, Phys. Rev. Lett. **56**, 30 (1986)

- P. Binetruy *et al.*, *Phenomenologically Viable Models from Superstrings?* Nucl. Phys. **B273**, 501 (1986)
- P. Candelas *et al.*, *Vacuum Configurations for Superstrings*, Nucl. Phys. **B258**, 46 (1985)
- S. Dawson *et al.*, *Search for Supersymmetric Particles in Hadron-Hadron Collisions*, Phys. Rev. **D31**, 1581 (1985)
- N. Deshpande *et al.*, *Number of Neutrinos in the Standard Model and its Extensions to Supersymmetry*, Phys. Rev. Lett. **54** 1757 (1985)
- J. Ellis *et al.*, *Aspects of the Superunification of Strong, Electroweak and Gravitational Interactions*, Nucl. Phys. **B276**, 14 (1986)
- M. B. Green, (*ed.*), *Superstrings*, (World Scientific 1985).
- H. Haber, G. Kane, *The Search for SUSY*, Phys. Rep. **117**, 75 (1985)
- I. Hinchliffe, *SUSY Models of Particle Physics and their Phenomenology*, Ann. Rev. Nuc. Part. Sci. **36**, 505 (1986)
- P. Langacker, *Grand Unified Theories and Proton Decay*, Phys. Rep. **72**, 185 (1981)
- D. V. Nanopoulos, *Applied Supersymmetry and Supergravity*, Rep. Prog. Phys. **49**, 61 (1986)
- E. Reya, D. P. Roy, *Constraints on Gluino and Squark Masses from the New Missing p_T Data at the $p\bar{p}$ Collider*, Phys. Lett. **223** (1986)
- R. W. Robinett, J. Rosner, *Prospects for a Second Neutral Vector Boson at Low Mass in $SO(10)$* , Phys. Rev. **D25**, 3036 (1982)
- J. Rosner, *E_6 and Exotic Fermions*, Comm. Nucl. Part. Phys. **15**, 195 (1986)
- J. Schwarz, *Superstring Theory*, Phys. Rep. **89**, 273 (1982); *An Update on Superstrings*, Comments on Nucl. and Part. Phys. **15**, 9 (1985)
- E. Witten, *Symmetry Breaking Patterns in Superstring Models*, Nucl. Phys. **B258**, 75 (1985)

Index

- acoplanarity 284
- Adler sum rule 154
- Altarelli-Parisi equations 215, 219, 229
- anomalies 15, 65, 452
- aplanarity 281
- asymmetry
 - forward-back 117, 120, 342
 - polarization 116, 120, 342
- asymptotic freedom 200
- b* quark (bottom quark) 5
 - asymmetry 342
 - decay 78, 82
 - production 331
- baryon 6
- BEPC 27
- beta function 196, 199, 202, 503, 532
- Bhabha scattering 118
- Bjorken limit 176
- Bjorken scaling 139, 153, 219
- box diagram 344
- Breit frame 209
- Breit-Wigner formula 115, 400-
- c* quark (charm quark) 5
 - decay 78, 80, 404
 - production 331
- Cabibbo angle 13, 58, 62
- Callan-Gross relation 153, 177
- calorimeter 30
- CESR 27
- charged current 13, 48, 56, 62, 143, 358
- chargino 523
- chiral 14, 65, 109
- colliders 22
- color 9, 193
 - flux lines 170, 183
- compactification 20, 534
- composite fermions 21, 308
- composite bosons 460
- confinement 9, 170
- covariant derivative 34, 38, 42, 193, 502, 513
- CP violation 57, 58, 353, 392
- cross sections 558
- current-gluon fusion 356
- decays 8, 18, 67, 558
- deep inelastic scattering 7, 134, 204
- diffraction 295, 318, 381, 391
- dileptons 112, 161, 355, 384, 479
- dimensional regularization 211
- DORIS 27
- Drell-Yan process 161, 230, 386
- electron 2, 5, 30
 - scattering 109, 136, 143, 279, 294
- energy-energy correlation 291
- E_6 GUT 535
- families 5
- Farhi-Susskind model 460
- Fermi coupling 49, 73
- Fermi momentum 82
- Feynman-Field model 180
- Feynman rules 553
- Feynman scaling 171
- Fierz-Michael transformation 68, 111, 552

- flavors 4
 - hidden flavor 331
 - open flavor 339
- flavor-changing neutral current 14, 63
- flavor excitation 374
- flavor oscillations 343, 386
- flavor-tag 91, 342, 346, 383
- fragmentation 169
 - fragmentation function 171, 175, 228
 - independent fragmentation 170, 180
 - string fragmentation 183
- gauge boson 3, 11, 500, 539, 553
- gauge field 35
- gauge group 11, 15, 37, 193, 499, 509, 535
- gauge invariance 34
- gauge theory 11
- gauge transformations 35, 37, 42
- gaugino 518
- generations 5
 - fourth generation 61, 67, 74, 467
 - generation mixing 53, 57, 60, 485
- GIM 14, 63
- gluino 20, 518
- gluon 3, 9, 193
 - couplings 194, 555-557
 - distribution 164, 225
 - fragmentation 188, 378
 - jets 188, 286, 307
 - fusion 165, 356, 374, 443
- Goldstone boson 46, 457, 461, 543
 - equivalence theorem 274
- Goldstone theorem 46
- graded Lie algebra 516
- graviton 3
- Gross-Llewellyn Smith sum rule 154
- GUTS 16, 499
- hadron 4
 - multiplicity 172
- hadronization 169
- heavy leptons
 - decay 74, 475
 - production 119, 240, 473, 477
 - superheavy 489
- heavy neutrinos
 - decay 75, 480
 - production 121, 493
- heavy quarks
 - decay 8, 67, 91, 485, 489
 - fragmentation 177
 - jets 97
 - production 125, 147, 239, 244, 331
 - superheavy 491
- HERA 27
- hierarchy problem 19, 514
- Higgs boson 16, 44, 428
 - charged 91, 452, 457
 - couplings 47, 52, 555, 556
 - decay 432, 464
 - mass 430
 - production 91, 278, 438, 497
 - search 446
 - two-doublet 452
 - width 451
- impact parameter 84
- importance sampling 400, 403
- impulse approximation 136
- infinite momentum frame 136
- infrared singularities 208, 211, 214
- isolation (see lepton isolation)
- ISR 26, 27
- Jacobian peak 257, 389
- jets 30, 279
 - see quark jets, gluon jets
 - minijets 315
 - multijets 318, 319
- jet algorithm 301
- K -factor 233, 248, 265, 315, 380
- Kobayashi-Maskawa matrix 58
- ladder graphs 216
- Landau gauge 198
- leading log approximation 202
- LEP 26, 27
- lepton 4, 53

- couplings 554, 555
- mass 52
- isolation 94, 385, 480
- leptoquark 365, 537
- LHC 27, 28
- luminosity 24, 27, 159
- Lund model 185
- Majorana fermion 77, 121, 457, 483, 517
- majorons 457
- mass singularities 208, 214
- meson 6
 - decay constant 106, 347
- Michel parameter 74
- microvertex detector 29, 84, 391
- minimal coupling 36
- minimum bias events 298
- missing p_T 31, 100, 258, 261, 389, 449, 475, 527
- mixing matrix 55, 57, 60, 75, 122, 144, 240, 247, 347, 358, 480, 485
- moment equations 223
- momentum sum rule 157, 218, 223, 224
- momentum tensor 280
- Monte Carlo methods 397
 - fragmentation 180, 187
 - shower models 319
- muon 5, 30, 31
 - decay 70
 - scattering 136, 294
- narrow width approximation 115
- neutral current 13, 49, 62, 149
- neutralino 522
- neutrino 4, 5
 - decay 75, 480
 - from colliders 100
 - heavy 75, 121, 480
 - left-handed 64
 - Majorana 77, 121
 - number of 246, 469
 - scattering 109, 130, 143, 149, 355
- non-abelian 37
- oscillations (see flavor oscillations)
- parton model 134
 - correlations 318
 - distributions 136, 155, 164, 225, 307
 - sum rules 141, 219
- PEP 27
- PETRA 27
- Peterson model 177
- phase space 70, 85, 87, 404, 406, 558, 561
- photino 20, 518
- photon 3
 - direct photons 235
- Planck mass 20, 534
- preons 21, 309
- proton decay 19, 500, 505
- QCD 9, 193
 - shower models 319
- QED 11, 34
- quark 4
 - couplings 554, 555
 - decays 67
 - distributions 136, 155, 225
 - masses 53
 - mixing 53, 57, 60, 485
 - sea 6, 141
 - valence 6, 10, 141
- quarkonium 331
 - decay 335, 370, 438
 - potential 333
 - production 332, 338, 370, 388
 - superheavy 496
- R 125
- rapidity 160
- recombination 381
- renormalizability 11, 34, 428
- renormalization group equations 195, 203, 468, 503
- root vectors 510
- running coupling 197, 503
- running mass 506
- scaling 134, 138, 144, 162
- shiggs 20, 518
- shower models
 - coherent 326

- final state 319
 initial state 328
 poor man's 265, 382
 SLC 26, 27
 slepton 20, 518
 soft singularity (see infrared)
 spectator approximation 78
 sphericity 281, 290
 spheriocity 286
 spherocity 286
 splitting functions 209-219
 spontaneous symmetry breaking 44
 SPS 26, 27
 squark 20, 518
 SSC 27
 Standard Model 15, 34, 193
 Sterman-Weinberg jet 283
 stratified sampling 403
 string effect 190
 string model 183
 structure constants 38, 193
 structure functions 150, 175, 204
 supergravity (SUGRA) 19, 517
 superstrings 20, 533
 supersymmetry (SUSY) 19, 515
 SUSY GUTS 532
 symmetry (see gauge group)
 t quark (top quark) 5
 decay 91
 signatures 91, 383, 388
 tau lepton 5
 decay 74
 identification 99
 production 120, 236, 242, 261
 Technicolor 21, 365, 460
 Tevatron 26, 27
 thrust 284, 290
 transverse energy 297
 transverse mass 259, 389, 390,
 449
 trigger 31
 trileptons 388
 triplicity 290
 TRISTAN 26, 27
 UNK 27, 28

 vacuum expectation value 45,
 430, 452, 457, 507
 valence quark (see quark)
 variance reduction 402
 virtual particles 2
 virtuality 320

 W -bosons 3, 41, 44
 couplings 38, 43, 62, 554-556
 decay 236, 266, 379, 473, 481
 effective W approximation 275
 from H decay 436, 448
 from Q decay 101, 395
 fusion 356, 445
 mass 47, 51
 production 247, 268, 448, 489
 width 240, 246, 472
 weak hypercharge 40, 41
 weak interactions 1, 3, 40
 weak isospin 40, 41
 weak mixing angle 43, 50, 504, 513,
 532
 Webber shower model 191, 326
 weight vectors 510
 weighted events 402
 wino 20, 518

 Yang's theorem 371
 Yang-Mills fields 37
 yo-yo modes 183
 Yukawa couplings 44, 52, 53, 436,
 458, 507

 Z -bosons 3, 41, 44
 additional Z' 510, 539
 couplings 38, 43, 64, 554-556
 decay 242, 379, 471
 effective Z approximation 275
 from H decay 436, 448
 fusion 356, 445
 mass 47, 51
 production 114, 128, 251, 268,
 436
 resonance 114, 124, 126, 338,
 447, 485
 width 245, 471, 485, 496
 zino 20, 518



“The extensive experience of Barger and Phillips is reflected in the breadth of coverage provided by *Collider Physics*.... [This book] makes an excellent reference source for experimenters and theorists alike.”

—*Physics Today*

This updated edition of *Collider Physics* surveys the major developments in theoretical and experimental particle physics and uses numerous illustrations to show how the Standard Model explains the experimental results. *Collider Physics* offers an introduction to the fundamental particles and their interactions at the level of a lecture course for graduate students, with emphasis on the aspects most closely related to colliders—past, present, and future. It includes expectations for new physics associated with Higgs bosons and supersymmetry. This resourceful book shows how to make practical calculations and serves a dual purpose as a textbook and a handbook for collider physics phenomenology.

Vernon D. Barger received his Ph.D. in Theoretical Physics from Pennsylvania State University in 1963. He is currently Vilas and J. H. Van Vleck Professor of Physics and Director of the Institute for Elementary Particle Physics Research at the University of Wisconsin. Dr. Barger's fellowships include the John Simon Guggenheim Memorial Foundation Fellow, Senior Visiting Fellow of the British Science-Engineering Research Council, and Fellow of the American Physical Society. Barger has coauthored three other books, *Phenomenological Theories of High Energy Scattering: An Experimental Evaluation*; *Classical Mechanics: A Modern Perspective*; and *Classical Electricity and Magnetism: A Contemporary Perspective*, and has published more than 350 scientific articles.

Roger J. N. Phillips received his Ph.D. in Theoretical Physics at Trinity College in Cambridge, England. He is currently Professor and Head of the Theoretical High Energy Physics Group at the University of Wisconsin-Madison. Dr. Phillips's honorariums include Fellow of the Institute of Physics and Visiting Fellow of the Japan Society for the Promotion of Science. Phillips has been a Visiting Scientist at CERN, at SLAC, and at the University of Hawaii. He has also been a Visiting Professor at the University of California, Riverside, and at the University of Wisconsin.

Find us on the World-Wide Web at:
<http://www.aw.com/gb/>



ADDISON-WESLEY PUBLISHING COMPANY, INC.



ISBN 0-201-14945-1